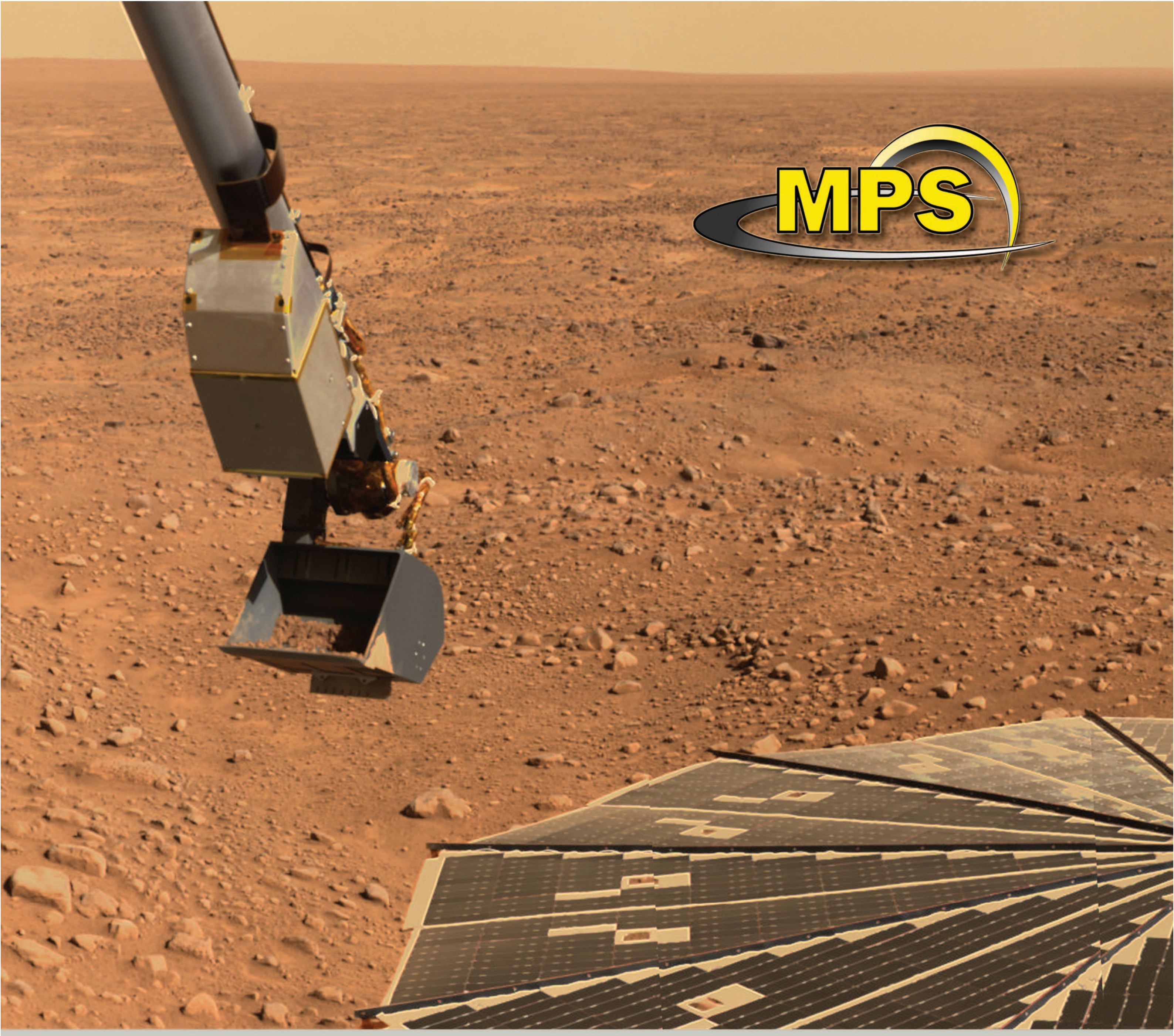

Max-Planck-Institut für Sonnensystemforschung Report 2008

MAX-PLANCK-GESELLSCHAFT

MAX–PLANCK–INSTITUT FÜR SONNENSYSTEMFORSCHUNG

KATLENBURG–LINDAU

Report 2008

Herausgegeben von der Institutsleitung:	*Prof. Dr. Sami K. Solanki*
	Prof. Dr. Ulrich R. Christensen
Redaktion:	*Dr. Johannes Wicht* *Dr. Patrick W. Daly* *Gerlinde Bierwirth* *Julia Müller*
Koordinatoren des wissenschaftlichen Teils:	*Prof. Dr. Jörg Büchner* *Dr. Norbert Krupp* *Dr. Laurent Gizon*

Abbildung auf dem Frontumschlag:

Das Titelbild zeigt den Landeplatz der Phoenix-Mission, aufgenommen mit der Stereokamera SSI. Links ist der Roboterarm mit der am MPS entwickelten und gebauten Kamera zu sehen.

Picture on the Cover:

The cover shows the landing site of the Phoenix mission recorded by the Surface Stereo Imager (SSI). The robotic arm with the arm camera which has been developed and build at the MPS can be seen at left.

Erschienen im September 2009.

Anschrift:

Max-Planck-Institut für Sonnensystemforschung
Max-Planck-Straße 2
37191 Katlenburg-Lindau
Deutschland
Tel.: +49-(0) 5556-979-0
Fax: +49-(0) 5556-979-240
http://www.mps.mpg.de

Inhalt / Contents

I Allgemeines zum Institut / Institute Overview

II Forschungshighlight / Research Highlight

III Sonne und Heliosphäre / Sun and Heliosphere

Übersicht der Projekte / overview of projects

Solar interior, photosphere and chromosphere

Solar-stellar connections, interstellar dust and cosmic rays

Fundamental science

IV Planeten, ihre natürlichen Satelliten und Kometen / Planets, their moons and comets

Übersicht der Projekte / overview of projects

Planetary interiors

Terrestrial planets research – Mercury

Terrestrial planets research – Venus

VI International Max Planck Research School

VII Elektroniklabor, Mechanik, Haustechnik, Ausbildung / Electronic Laboratory, Mechanics, Physical Plant Education

VIII Personelle Gliederung / Personnel

IX Wissenschaftliche Zusammenarbeit und Öffentlichkeitsarbeit / Scientific Collaboration and public relations

X Projektvorschläge, Lehrtätigkeit, Vorträge und Veröffentlichungen / Proposals, Teaching, Talks, and Publications

I. Allgemeines zum Institut / Institute Overview

Gegenstand und Methoden der Forschung / Subject and Methods of Research

Die verschiedenen Objekte des Sonnensystems bilden den Gegenstand der Forschung am MPS. Ein großes Forschungsgebiet betrifft die Sonne, ihre Atmosphäre, das vom Sonnenwind beeinflusste interplanetare Medium, sowie den Einfluss der schwankenden solaren Partikel- und Wellenstrahlung auf die Erde und auf andere Planeten. Das zweite große Forschungsthema befasst sich mit dem Inneren, den Oberflächen, Atmosphären, Ionosphären und Magnetosphären der Planeten, ihrer Monde, sowie von Kometen und Asteroiden.

Eine wichtige Rolle spielt die Auswertung von Bildern und Spektren, die mit Instrumenten auf Raumsonden oder von erdgebundenen Teleskopen gewonnen werden. Damit werden die Sonne, Planeten (insbesondere Mars und Venus), Monde (Titan), Kometen und andere Kleinkörper erforscht. Die Korona der Sonne wird mit optischen Instrumenten im gesamten Spektralbereich vom Sichtbaren bis zum weichen Röntgenlicht vom Weltraum aus beobachtet und ihre Plasmaeigenschaften werden mit spektroskopischen Methoden diagnostiziert. Die untere Atmosphäre der Sonne (die Photosphäre und Chromosphäre) wird anhand von spektropolarimetrischen Messungen sowohl vom Boden wie auch vom Weltraum aus untersucht. Dabei geht es vor allem um die Bestimmung des solaren Magnetfeldes, welches eine grundlegende Rolle für eine Vielzahl solarer Phänomene spielt. Ein neues Arbeitsgebiet ist die Untersuchung des Sonneninneren durch Analyse von beobachteten Schwingungen an ihrer Oberfläche (Helioseismologie). Geologische Vorgänge und die mineralogische Zusammensetzung an den Oberflächen planetarer Körper, sowie die Eigenschaften von Planetenatmosphären werden durch abbildende und spektrometrische Verfahren im sichtbaren Spektrum und nahen Infrarotbereich untersucht. In-situ-Methoden zur chemischen Untersuchung von Kometen- und Planetenoberflächen, sowie geophysikalische Untersuchungen des Planeteninneren werden in Zukunft eine Rolle spielen.

In den Magnetosphären der Erde und anderer Planeten, im Sonnenwind und in der Umgebung von Kometen werden Teilchen und Wellen von Instrumenten auf Raumsonden in-situ gemessen. Die chemische Zusammensetzung, die räumliche Verteilung der Teilchen sowie das Studium von Transportvorgängen und Beschleunigungsprozessen stehen dabei im Vordergrund.

Bei der überwiegend experimentell ausgerichteten Arbeitsweise des Instituts spielt die Entwicklung und der Bau von Instrumenten und die Gewinnung und Auswertung von Messdaten eine Hauptrolle. Diese Aktivitäten werden jedoch intensiv von theoretischen Arbeiten und der Bildung von physikalischen Modellen begleitet. Das Schwergewicht liegt hierbei auf der numerischen Simulation in den Bereichen planetare und solare Dynamos, atmosphärische Zirkulationsmodelle, MHD-Prozesse in der Konvektionszone und Atmosphäre der Sonne, Physik ionosphärischer und magnetosphärischer Plasmen, sowie Konvektionsströmungen im Gesteinsmantel terrestrischer Planeten und in den Gashüllen der Riesenplaneten.

The objects of the solar system are at the focus of research at MPS. One important area of research includes the Sun, its atmosphere, the interplanetary medium filled with and influenced by the solar wind, as well as the influence of the variable radiation of solar particles and waves on the Earth and other planets. The second major research field involves the interiors, surfaces, atmospheres, ionospheres, and magnetospheres of the planets and their moons, as well as those of comets and asteroids.

The analysis of images and spectra obtained from instruments on board spacecraft or from ground-based telescopes play an important role for the exploration of the Sun, the planets (especially Mars and Venus), moons (Titan), comets, and other small bodies. The solar corona is observed with optical instruments in space in the entire spectral range from visible to soft x-rays, and its plasma properties are analysed by spectroscopic methods. The Sun's lower atmosphere (the photosphere and chromosphere) is investigated by means of spectral polarisation measurements, both from the ground and from space. In this case, it is the solar magnetic field that is of key interest. It plays a fundamental role in a multitude of solar phenomena. A new field of endeavour is the study of the solar interior by analysing the observed oscillations on the *surface (helioseismology). Geological processes and mineralogical composition on the surfaces of planetary bodies, as well as the properties of the atmospheres of planets are investigated with imaging and spectrometric techniques in the visible and near infrared spectral regions. In-situ methods for chemical analysis of cometary and planetary surfaces, as well as geophysical investigations of the interiors of planets will play an important role in the future.*

In the magnetospheres of the Earth and other planets, in the solar wind and in the neighbourhood of comets, particles and waves are measured in-situ from space-borne instruments. The chemical composition, the spatial distribution of particles, and the study of transport mechanisms and energisation processes are at the forefront of the research into these topics.

As the Institute is primarily involved in experimental investigations, the development and construction of instruments together with the analysis of acquired data play a major role. These activities are accompanied by intensive theoretical efforts and the creation of physical models. The emphasis here lies on numerical simulations of the fields of planetary and solar dynamos, atmospheric circulation models, MHD processes in the convection zone and solar atmosphere, the physics of ionospheric and magnetospheric plasmas, as well as on convection currents in the solid mantle of terrestrial planets and in the gas envelopes of the giant planets.

Struktur und Leitung des Instituts / Structure and Management of the Institute

Das Institut ist in zwei Abteilungen gegliedert: der Abteilung Sonne und Heliosphäre unter den Leitung von Prof. Dr. S. K. Solanki und der Abteilung Planeten und Kometen unter der Leitung von Prof. Dr. U. R. Christensen. Am 1. September 2005 wurde das Institut um die Selbständige Nachwuchsgruppe Helio- und Asteroseismologie der MPG unter der Leitung von Prof. Dr. Laurent Gizon erweitert. Die im Jahr 2002 in Zusammenarbeit mit den Universitäten in Göttingen und Braunschweig gegründete "International Max Planck Research School on Processes in the Solar System and Beyond" bietet Promotionsausbildung an. Eine technische Abteilung und die Verwaltung sind zentral organisiert und stehen allen wissenschaftlichen Abteilungen zur Verfügung. Die zentralen technischen Einrichtungen umfassen eine Mechanische Abteilung, bestehend aus Konstruktion und Werkstätten, ein Entwicklungslabor für Elektronik, ein Rechenzentrum und eine Fachbibliothek.

Das Institut wird durch das Gesamtkollegium der Direktoren Prof. Dr. U. R. Christensen und Prof. Dr. S. K. Solanki gemeinschaftlich geleitet. Geschäftsführender Direktor ist seit 1. Januar 2008 Prof. Dr. S. K. Solanki.

Das Kollegium wird in seiner Arbeit durch einen Verwaltungsleiter (A. Poprawa) und einen Direktionsberaterkreis unterstützt. Letzterer besteht aus drei Mitarbeitern des wissenschaftlich-technischen Bereiches, die von allen Mitarbeitern des Instituts für eine einjährige Amtsperiode gewählt werden. Die technischen Vorhaben und Instrumententwicklungen der Abteilungen werden von zwei technischen Koordinatoren (P. Barthol (Sonne) und H. Boehnhardt (Planeten)) koordiniert.

Für die einzelnen Forschungsvorhaben werden innerhalb der Abteilungen jeweils Projektgruppen gebildet, die nach Abschluss des Projektes wieder aufgelöst werden.

The institute consists of two departments: the department Sun and Heliosphere, headed by Prof. Dr. S. K. Solanki, and the department Planets and Comets, headed by Prof. Dr. U. R. Christensen. In addition, the Independent Junior Research Group of the Max Planck Society "Helio- and Asteroseismology" was created on 1 September 2005 and is headed by Prof. Dr. L. Gizon. Since 2002, the "International Max Planck Research School on Processes in the Solar System and Beyond" offers doctorate education in collaboration with the universities in Göttingen and Brauschweig. A technical department and the administration are centrally organized and serve all research departments. The technical department comprises a mechanical department, including a design office and workshop, an electronics laboratory, a computing center, and a library.

The institute is jointly managed by the directors Prof. Dr. U. R. Christensen and Prof. Dr. S. K. Solanki who constitute the board of directors. Managing director since 1 January 2008 is Prof. Dr. S. K. Solanki.

The board of directors is assisted by the head of administration (A. Proprawa) and a director's advisory committee. The latter consists of three members of the scientific-technical staff who are elected for a one-year period by the complete staff. The technical projects and instrument development within each department is coordinate by two technical coordinators (P. Barthol (solar department) and H. Boehnhardt (planetary department)).

A dedicated project group is formed for the duration of each research project.

Das Kuratorium des Instituts / Board of Trustees of the Institute

Dem Kuratorium des Instituts gehörten im Jahr 2008 die folgenden Mitglieder an: /
The following were members of the board of trustees of the institute in 2008:

Prof. Dr. Stefan Dreizler, Institut für Astrophysik, Universität Göttingen;

Helge Engelhard, Ministerialdirigent im BMBF (Bundesministerium für Bildung und Forschung), Bonn;

Dr. Thomas Galinski, Raumfahrtmanagement Extraterrestrik, DLR, Bonn;

Prof. Dr. Jürgen Hesselbach, Präsident der Technischen Universität Braunschweig;

Dr. Hanna von Hoerner, Geschäftsführerin der von Hoerner und Sulger GmbH, Schwetzingen;

Markus Hoppe, Vizepräsident der Universität Göttingen;

Dr. Josef Lange, Staatssekretär im Niedersächsischen Ministerium für Wissenschaft und Kultur, Hannover;

Prof. Dr. Oskar von der Lühe, Kiepenheuer-Institut für Sonnenphysik, Freiburg;

Frau Erika Mann, Mitglied des Europäischen Parlaments, Hannover;

Dr. Fritz Merkle, OHB-System GmbH, Bremen;

Prof. Dr. Hermann J. Opgenoorth, Head, Solar System Mission Division, ESA-ESTEC, Noordwijk, The Netherlands;

Thomas Oppermann, Mitglied des Bundestags, Göttingen.

Das Kuratorium tagte am 4. November 2008 in Lindau. /
The board of trustees met on 4 November 2008 in Lindau.

Der Fachbeirat des Instituts / Scientific Advisory Board of the Institute

Im Jahr 2001 wurde vom Präsidenten der Max-Planck-Gesellschaft ein neuer Fachbeirat für das Institut berufen. In den Jahren 2001 -– 2008 gehören dem Fachbeirat die folgenden Mitglieder an: /
In 2001 a new advisory board for the institute was appointed by the President of the Max Planck Society. During the years 2001 -– 2008 the following were members of the scientific advisory board:

Prof. Dr. D. Crisp, Pasadena, CA, USA;
Prof. Dr. G. Hensler, Vienna, Austria;
Dr. L. J. Lanzerotti, Murray Hill, NJ, USA;
Prof. Dr. John W. Leibacher, Tucson, AZ, USA;
Prof. Dr. P. Lognonné, Saint Maur, France;
Prof. Dr. E. R. Priest, St. Andrews, UK;
Prof. Dr. R. Rosner, Chicago, IL, USA;
Prof. Dr. D. J. Southwood, Paris, France;
Prof. Dr. D. J. Stevenson, Pasadena, CA, USA.

Direktionsberaterkreis des MPS / „Direktionsberaterkreis“ at MPS

Gewählte Mitglieder des Direktionsberaterkreises für die Amtszeit 2008 waren: /
Elected members of the “Direktionsberaterkreis” for the period 2008:
Dr. Hermann Boehnhardt (Planeten / Planets), Ersatzmitglied / *substitute member Dr. Paul Hartogh, Dr. Udo Schühle (Sonne / Sun),* Ersatzmitglied / *substitute member Dr. Achim Gandorfer, Alexander Loose (Zentrale Dienste / Central Services),* Ersatzmitglied / *substitute member Dr. Peter Barthol.*

Personelle Entwicklung / Personnel Development

Im Jahr 2008 hat keine Veränderung der der Planstellen stattgefunden und beträgt weiterhin konstant 96. Davon waren 26 in der Kategorie Wissenschaftlern, 49 in der Kategorie Technik und 20 in der Kategorie Administration besetzt. Die Zahl der am Institut wissenschaftlich Tätigen war jedoch mit Einbeziehung der aus Mitteln Dritter finanzierten Wissenschaftler und Stipendiaten und Gästen beträchtlich größer und betrug am 31. Dezember 2008 etwa 140.

The number of 96 permanent positions has not changed during 2008. Of these, 26 were filled with scientists, 49 with technical staff, and 20 with administrational staff. The total number of scientific staff, however, was considerably higher at 140 (status 31 December 2008) due to a large number of PhDs, guests, postdocs, and non-permanent position payed by third-party funds.

In den Ruhestand traten: / The following have retired:

Dr. Jochen Kissel, Dr. Bernd Wöbke

40 Jahre in der MPG / 40 years at MPG

Werner Steinberg (30. April 2008)

Für das Institut aufgewendete Mittel / Institute Resources

Die vom Bund und den Ländern getragene und durch die Generalverwaltung der Max-Planck-Gesellschaft zugeteilte Grundausstattung des Instituts an Personal- und Sachmitteln betrug im Jahre 2008 7,6 Millionen Euro für Personal und Stipendien und 2,4 Millionen Euro für Sachausgaben. An Investitionsmitteln (Geräte mit Preisen über 5.000 Euro) wurden 0,5 Millionen Euro bewilligt.

Besondere Forschungsvorhaben sind durch das BMBF (Bundesministerium für Bildung und Forschung), die ESA (European Space Agency), die DFG, die EU und andere Drittmittelgeber gefördert worden. Insgesamt erhielt das Institut 2008 11,8 Millionen Euro.

Für diese Förderungen, ohne die viele experimentelle Forschungsvorhaben nicht durchführbar gewesen wären, möchten wir auch an dieser Stelle ausdrücklich danken.

The basic funding of the institute is secured by the german state and the Länder and is allocated through the administrative headquarters of the Max Planck Society. In 2008, it amounted to 7.6 million Euro for personnel and 2.4 million Euro for material. For capital investment funds (equipment over 5000 Euro) an additional amount of 0.5 million Euros was approved.

Special research project are funded by the BMBF (Federal Ministry for Education and Research), by ESA (European Space Agency), by the DFG (German Research Council), and by the EU (European Union). In 2008, the MPS recieved at total amount of 11.8 million Euro by these institutions.

Auszeichnungen / Awards

Prof. Dr. Ulrich R. Christensen
Preisträger der Augustus Love Medal der EGU, 2008. Die Medaille wird während der EGU-Generalversammlung in Wien im April 2009 überreicht.

Dr. Laurent Gizon
European Research Council (ERC) Starting Grant, 2008.

Prof. Dr. Eckart Marsch
Fellow der American Geophysical Union, 2008. Die Auszeichnung wird am 26. Mai 2009 in Toronto überreicht.

Prof. Sami K. Solanki
Bernard Price Lecturer, SAIEE (South African Institute of Electrical Engineering), 2008.

Prof. Vytenis Vasyliūnas
Van Allen Lecturer, AGU, 2008.
Bowie Lecturer für die Herbst-Tagung der AGU, 2008.

Nachruf / Obituary

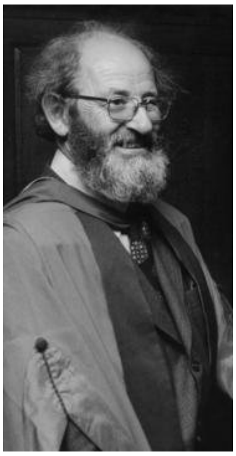

Professor W. Roy Piggott
International leader in ionospheric physics
18.07.1914 – 20.05.2008

Die Wurzeln des Instituts in Lindau reichen bis in das Jahr 1934 zurück, als in Rechlin am Müritzsee die sog. Sondergruppe "Funk" der Erprobungsstelle der Luftwaffe unter Leitung von Walter Dieminger gegründet wurde. Kriegsbedingt wurde diese Abteilung nach Leobersdorf und später nach Ried am Inn (Österreich) verlegt.
Englische Wissenschaftler unter Leitung des späteren Nobelpreisträgers Sir Edward Appleton hatten die wissenschaftlichen Erkenntnisse dieser Arbeitsgruppe über ionosphärische Untersuchungen und deren Bedeutung z.B. für die Funknavigation erkannt und empfahlen nach Kriegsende die Ausrüstung sowie das Personal in die britische Besatzungszone zu überführen. Dr. W. R. Piggott vom Department of Science and Industrial Research in London, ein enger Mitarbeiter Appletons, und der Luftwaffenleutnant Eric Ackerman wurden beauftragt, mit Dieminger Kontakt aufzunehmen und den Transport – gegen alle möglichen Widerstände – vorzubereiten.

Es ist W. R. Piggott zu verdanken, dass er die ursprünglich geringe Zahl von Transportfahrzeugen um ein Vielfaches erhöhte (über das wie gibt es diverse Vermutungen). Somit konnte ein Großteil der technischen Ausrüstung, der wertvollen Datensammlung sowie das Schicksal von vier Familien dem Zugriff von anderen "Interessenten" entzogen werden. Er war dafür verantwortlich, dass der riesige Konvoi (bis zu 80 Fahrzeuge) ohne Verluste durch die amerikanische Besatzungszone geschleust werden konnte. Durch sein Geschick auf dem Schwarzmarkt konnte er alle logistischen Probleme wie die Bereitstellung von Kraftstoff, Verpflegung und Unterkünften überwinden.
Am 3. März 1946 erreichten die ersten Fahrzeuge den kleinen Eichsfeldort Lindau, da dort – vermutlich auch auf Anweisung von Piggott – vorhandene Baracken zur Aufnahme des Transports geräumt wurden.

Somit ist es W. R. Piggott zu verdanken, dass Dieminger und einige Mitarbeiter hier einen Neubeginn starten konnten, der sich in den vergangenen 62 Jahren zu dem heutigen Institut entwickelt hat. W. R. Piggott wurde für sein Verdienste mit dem "Order of the British Empire" ausgezeichnet. Er hat Lindau des öfteren zu bedeutenden Veranstaltungen besucht und stets engen Kontakt zum Institut aufrechterhalten. Das gute und herzliche Verhältnis zu Dieminger hat all die Jahre überdauert. Er muss somit neben Dieminger zu den Vätern des Instituts gezählt werden.

W. R. Piggott war massgeblich an der Errichtung des britischen Ionosphären-Observatoriums in Halley Bay im internationalen Polarjahr 1957/58 beteiligt. Er leitete das britische Programm der arktischen Ionosphärenforschung über zwei Dekaden. Zusammen mit Karl Rawer verfasste er das definitive Handbuch zur Interpretation von Ionogrammen.

W. R. Piggott verstarb am 20. Mai 2008 im Alter von 93 Jahren. Wir werden ihm ein ehrendes Andenken bewahren und erinnern uns an ihn in Dankbarkeit.

The roots of the institute in Lindau reach back to the year 1934 when the "Sondergruppe Funk", headed by Walter Dieminger, was founded bei der german Luftwaffe in Rechlin at the Müritz lake. The group was moved to twice during the war, first to Leobersdorf and then to Ried at the Inn (Austria).

English scientists around the later Nobel prize winner Sir Edward Appleton recognized the relevance and importance of this ionosphere research group, for example for radio navigation. They recommended to secure its the equipment and staff for the british zone in Germany. Dr. William Roy Piggott of the Department of Science and Industrial Research in London and the Luftwaffen-officer Eric Ackerman were ordered to contact Dieminger and to prepare the move – against all odds. W. R. Piggott, a close collaborator of Sir Edward Appleton, was stationed in Slough at that time, instructing the military in radio communication during the day, while carrying out ionospheric research at night and during weekends.

He managed to organize many more vehicles than originally planned – nobody knows really how – so that the largest part of the technical equipment, the valuable data collection, and the fate of four families could be rescued from the hand of others. He conducted the large convoy of up to 80 vehicles through the american zone without any casualties. Thanks to a *mastership in the black-market subterfuge be managed to solve all problems regarding the supply of gasoline, food, and lodging. On 3 March 1946 the first trucks reaches the little Eichsfeld village Lindau were some barracks had already been cleared – likely due to Piggott's orders. It therefore was W. R. Piggott's foresight and commitment which allowed Dieminger and some of his employees to attempt a new start that has developed into today's MPS during the following 62 years. W. R. Piggott was rewarded with the "Order of the British Empire" for these wartime achievements. He visited Lindau several times to take part in conferences and meetings and kept a close contact. A good and affectionate relation with Dieminger survived all those years. Like Dieminger, W. R. Piggott has to be regarded as one of the institute's founders.*

W. R. Piggott was the prime mover in establishing the ionospheric observatory at Halley Bay in the International Polar Year, (1957 – 1958) and provided oversight of the programme for the next two decades. He teamed up with Karl Rawer to write the definitive handbook on the interpretation of ionogramms.

W. R. Piggott died on 20 May 2008 at the age of 93. We will always remember him with great gratitude.

(Peter Czechowsky, Johannes Wicht)

II. Forschungshighlight / Research Highlight

Phoenix / Phoenix

(English version see page 16)

Nachdem die Mars Polar Lander Mission (MPL) gescheitert war und Mars Surveyor 2001 (MS'01) Einsparungen zum Opfer gefallen war, gab es zunächst keine Aussicht auf eine polare Marsmission. Das änderte sich, als die Messungen der seit Anfang 2002 den Mars umkreisenden Sonde Odyssey große Wassereisvorkommen in den arktischen Regionen nahe legten – weniger als einen Meter unter der Oberfläche. Im Wassereis des arktischen Permafrosts könnten Spuren eventuellen Lebens aus den letzten Jahrmillionen konserviert sein. Die Gruppe um Peter H. Smith an der University of Arizona entwickelte die Idee für eine Mission, die auf die für arktische Missionen optimierte wissenschaftliche Nutzlast von MPL sowie das schon fertig gestellte MS'01 Landedeck aufbaute: ein Phoenix, der aus seiner eigenen Asche aufersteht! Der Raketenstart fand am 4. August 2007 statt und die Sonde landete bei 68,2° N, 234,3° E am 25. Mai 2008, dem Sol 0 (Marstag 0) der Mission.

Instrumente

Abb. 1 zeigt die Platzierung vieler Instrumente in einem Selbstportrait der Phoenix Sonde. Dazu gehören eine Reihe abbildender Systeme mit verschiedener Auflösung: Eine Panorama-Stereokamera (Stereo Surface Imager (SSI), Auflösung > 1 mm/Pixel), eine Roboterarmkamera (RAC, Auflösung > 24 μm/Pixel), ein Optisches Mikroskop (OM, Auflösung ∼ 4 μm/Pixel) sowie ein Rasterkraftmikroskop (AFM, Atomic Force Microscope, Auflösung ∼ 0.1 μm/Rasterpunkt). Darüber hinaus gab es ein Wet Chemistry Laboratorium (WCL), in dem Bodenproben mit flüssigem Wasser versetzt und mit ionenselektiven Elektroden (ISE) analysiert wurden. Die WCL Analysezellen geben Aufschluss über den in Wasser löslichen Anteil des Marsbodens, vor allem Salze. Ein weiteres zentrales Instrument erlaubt eine Erwärmung der Bodenproben auf bis zu 1000° C (TA, Thermal Analyzer) und die Analyse der freigesetzten Gase vermittels Massenspektroskopie (EGA, Evolved Gas Analyzer). TEGA (die aus TA und EGA bestehende Instrumentengruppe) sollte die

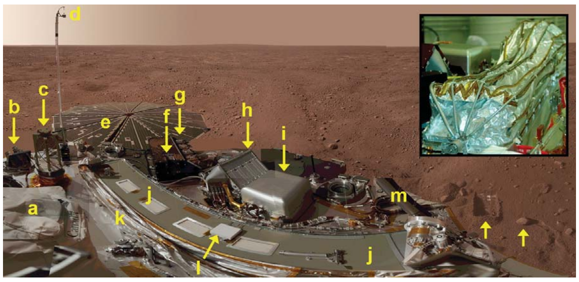

Abb. 1: Selbstbildnis der Phoenix-Landesonde und Umgebung (aufgenommen mit der Panoamakamera im ungefähren Zeitraum Sol 20 – 30). Die Mitte des Bildes zeigt etwa nach Nordwesten. a: LIDAR. b: Elektrische Anschlüsse für die Verbindung mit dem Kommandomodul während des Fluges. c: UHF Antenne. d: Wettermast mit Wetterhahn. e: Westliches Solarmodul. f: Schacht zur Überführung von Proben an das OM. g: Chemische Analysezellen (WCL). h: TA. i: EGA. j: Auflage des Auslegers während des Fluges (stark verzerrt). k: Biobarriere, eine faltbare Haube aus halbtransparentem Kunststoff zum Schutz des Auslegers und der Schaufel gegen biologische Verunreinigung. Das Bild (oben rechts) zeigt die Biobarriere in geschlossenem Zustand (Aufnahme im Labor). Nach der Landung wurde sie (zum Betrachter hin) geöffnet. l: Block aus reinem (absolut reinem, organik-freiem) Teflon. Bohrmehl aus diesem Block sollte – gemäß den ursprünglichen Plänen – dem TEGA Instrument (TA und EGA) zugeführt werden, um den Nullpunkt für die Detektion von potentiellen organische Verbindungen zu definieren. m: Das untere Ende des Greifarms. Die Pfeile rechts von der Sonde weisen auf einen ca. 20 cm breiten Graben (Abb. 6) und einen durch die Bremsraketen deplazierten Gesteinsbrocken hin.

Identifizierung von organischen Molekülen ermöglichen. Die Ofentemperaturen, bei denen Moleküle anorganischen Ursprungs freigesetzt werden, verraten deren mineralogische Herkunft, was gleichbedeutend ist mit dem Nachweis solcher Minerale. Während des Aufwärmens der Phoenix-Bodenproben wird die Temperaturzunahme als Funktion von der Zeit registriert. Wenn die Temperatur trotz andauernder Energiezufuhr konstant bleibt, lässt dies etwa auf einen endothermen Phasenübergang schliessen. Der Greifarm der Mission kann selbst als wissenschaftliches Instrument angesehen werden, denn er lässt Rückschlüsse auf die mechanische Beschaffenheit des Bodens zu. Die Schaufel am Ende des 2,30 m langen Arms erlaubte die Auswahl bestimmter Bodenproben und deren Überführung an diverse

Instrumente. Auf ihrer Rückseite sitzt ein Eisbohrer (Rapid Active Sampling Package, RASP). Hinter der Schaufel ist die RAC montiert, die das aufgesammelte Bodenmaterial mit hoher Auflösung (> 24 μm/Pixel) abbildet. Neben der Schaufel ist ein Bodensensor (Thermal and Electrical Conductivity Analyzer, TECP) montiert, der zwischen vier Probenadeln die elektrische und thermische Leitfähigkeit des Bodens messen kann. Darüber hinaus ist der TECP-Sensor in der Lage, vermittels eines zusätzlichen Sensors den atmosphärischen Wasserdampfdruck und die relative Feuchtigkeit der Atmosphäre zu messen. Zuletzt muss die kanadische Wetterstation erwähnt werden. Zu ihr gehören ein LIDAR-Gerät (Laser Detection And Ranging), welches durch Rückstreuung von Laserlicht an suspendierten Teilchen (Staub, Eis) Aufschluss über die vertikale Struktur der Atmosphäre gibt. Die täglichen Wetterstudien wurden durch Druck-/Temperaturmesser in drei verschiedenen Höhen (25, 50 und 100 cm) an einem Wettermasten ergänzt sowie durch einen von der Universität Aarhus (Dänemark) entwickelten Wetterhahn (TT, Telltale) am oberen Ende des Mastes. Die schon erwähnte Panoramakamera lieferte komplementäre Daten über atmosphärischen Staub und Wasserdampfgehalt durch Abbildung der Sonnenscheibe im sichtbaren sowie nah-infraroten spektralen Bereich. Abb. 2 zeigt die Instrumentanordnung (RAC, TECP) am Ende des Auslegers. Der Beitrag des MPS lag in Entwicklung und Bau der RAC sowie der Sensoreinheit des OMs.

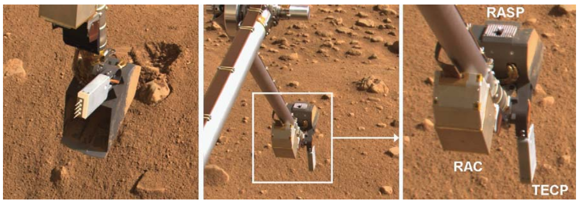

Abb. 2: Ende des Auslegers (SSI Bilder, Sol 49) mit Schaufel ($\sim$ 8 cm breit), RAC, TECP und Eisbohrer (RASP).

Geologie des Landeplatzes

Spektroskopische Daten sowie hochauflösende Bilder von verschiedenen Satellitenmissionen (Mars Global Surveyor, Odyssee, Mars Express, Mars Reconnaissance Orbiter) standen schon vor der Landung zur Verfügung und dienten der Auswahl geeigneter Landeregionen. Abb. 3 illustriert den geologischen Kontext des Phoenix Landeplatzes. Die Entfernung vom Landeplatz zum nördlichen Rand der vulkanischen Tharsisprovinz und zum nächstgelegenen Vulkan (Alba Patera) beträgt jeweils etwa 500 km und 1800 km. Die nordpolare Eiskappe und die dunklen zirkumpolaren Dünenregionen sind etwa 2000 km entfernt. Großflächig können wir also mit vulkanischer Asche aus der Tharsisprovinz sowie mit Sandkörnern der nordpolaren Dünen rechnen. Der Landeplatz liegt ferner etwa 20 km westlich des Heimdall Kraters mit einem Durchmesser von etwa 11 km und einer Tiefe von etwa 1 km (Abb. 3c). Wir müssen demnach am Landeplatz auch mit Material aus solchen Tiefen rechnen.

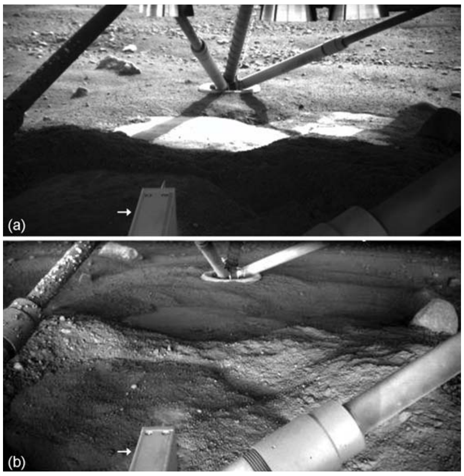

Abb. 4: Eisfläche Holy Cow: ‘Reingefegt’ durch Bremsraketen. Blick in südliche Richtung. Die RAC, die sich am Ende des Greifarms befindet, ist als einzige Kamera an Bord in der Lage, das Terrain unter der Sonde abzubilden. Der thermale und elektrische Sensor TECP (weiße Pfeile in a und b) ist stets im Gesichtsfeld der RAC, ausgenommenen bei RAC Bildern des Schaufelinneren (Abb. 8a). (a) Sol 5. Holy Cow sonnenbeschienen (etwa 15 Uhr). Bremsraketen am oberen Bildrand. Dieses frühe Bild war eine vorläufige Bestätigung des vorhergesagten Eisvorkommens in geringer Tiefe. (b) Sol 97. Holy Cow im Zwielicht (etwa 2 Uhr). Bemerke auch die Eisanlagerungen an einer der Verstrebungen (oben links) [Renno et al., Lunar Planet. Sci. Conf. XL, #1440, 2009]. Holy Cow hat eine glatte Oberfläche, und erscheint daher im Gegenlicht sehr hell (a). Im roten Zwielicht ist die Eisfläche kaum heller als das umgebende Bodenmaterial (b). Es handelt sich also nicht um reines Eis.

Wenige Tage nach der Landung wurde mit der RAC das Terrain unter der Sonde untersucht, um die Standsicherheit der Sonde zu bestätigen. Das erste Bild (Abb. 4a) zeigte (‘Holy Cow’ genannte) helles und glattes Material das offensichtlich durch den Schub der Bremsraketen freigelegt wurde. Das von Odyssey 2002 endeckte oberflächennahe Wassereis war also schnell gefunden, in nur wenigen Zentimetern Tiefe unter einer dünnen Staub-/Regolithschicht. Abb. 4b deutet an, dass es sich eher um eisreichen Regolith als um reines Eis handelt. Abb. 5 zeigt die benachbarte Eisfläche ‘Snow Queen’, die sich ebenfalls unter der Sonde befindet (die Namengebung der Lokalitäten sollte sich entsprechend den Richtlinien der Mission an Märchen orientieren). Das Eis arbeitet: Im Laufe von 52 Sols (Abb. 5b-c) haben sich zahlreiche Risse gebildet. Im Laufe der Phoenixmission wurden zwölf

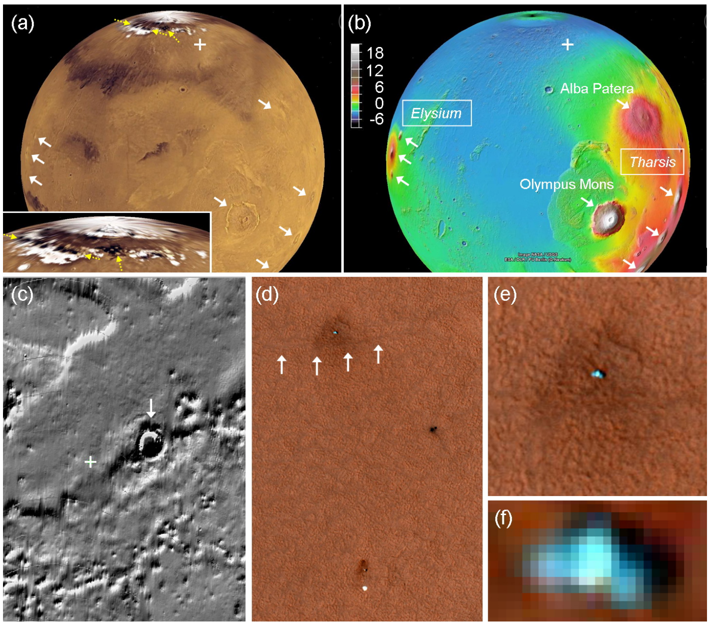

Abb. 3: Vom Planeten zur Landesonde. Alle Bilder sind eingenordet. (a) Viking Orbiter Echtfarben-Mosaik. Weißes Kreuz: Phoenix. Weiße Pfeile: Gößere Vulkane in der Elysium (links) und Tharsis Region (rechts). Gestrichelte gelbe Pfeile: Dunkle Sanddünen nahe der Polkappe (mit vergrößerter Darstellung unten im Bild). (b) Wie a, jedoch eine Höhenkarte basierend auf Mars Orbiter Laser Altimeter (MOLA) Daten. Die Legende gibt die Höhe in Kilometern an. (c) Satellitenbild (∼ 280 m von links nach rechts) der näheren Umgebung der Phoenix Sonde (weißes Kreuz). Auswurfmaterial von dem 20 km östlich gelegenen Heimdall Krater (weißer Pfeil) wird auch am Phoenix Landeplatz erwartet. (d) Hochauflösendes Bild (MRO, HiRISE) der Phoenix Sonde (oben), des Hitzeschildes (Mitte, rechts) und des Fallschirms mit hinterem Hitzeschild (unten), aufgenommen 22 Stunden nach der Landung. Die weißen Pfeile markieren einen Riss im Terrain. (e) Vergrößerter Ausschnitt von d. Bemerke die Unebenheit (polygonalen Konturen) der Oberfläche. Die Bremsraketen ließen in einem Umkreis von etwa 20 m von der Sonde grobkörnigeres (dunkleres) Material zum Vorschein kommen. (f) Vergrößerter Ausschnitt von e. Das näherungsweise kreisförmige Instrumentendeck (hellblau) wird flankiert von zwei (ebenfalls kreisförmigen) Solarmodulen (blau). Schattenbildung im Nordosten der Sonde. Auf eine Glättung des Bildes wurde verzichtet, so dass die einzelnen HiRISE Pixel sichtbar sind. Das Bild wurde aus etwa 300 km Höhe aufgenommen. Jedem Pixel entsprechen 33 cm der Sonde. Bilder: (a, b) Google Earth, (a, b, c, d, e) NASA.

Gräben mit einer maximalen Tiefe von 18.3 cm ausgehoben. Eisflächen, welche dadurch freigelegt wurden, haben sehr verschiedene Erscheinungsformen: Die Reflexionsspektren, die von der SSI Kamera im sichtbaren und nah-infraroten Bereich aufgenommen worden sind, lassen teilweise auf relativ reines Wassereis (Dodo Goldilock Graben, Abb. 6), teilweise auf eisreichen Regolith schließen. In manchen Gräben wurde überhaupt kein Eis angetroffen. Die Annahme, dass das helle Material in den oberflächennahen Schichten tatsächlich Wassereis darstellt, wird durch die beobachtete Sublimation zentimetergroßer, heller Klumpen über einen Zeitraum von vier Sols gestützt (Abb. 6a1 und b1). Es ist zum gegenwärtigen Zeitpunkt noch kein schlüssiges geophysikalisches Modell entwickelt worden, welches das Auftreten von unterschiedlichen Bodenstrukturen und Eis-Erscheinungsformen innerhalb von wenigen Metern erklären könnte. Das gängige Modell für die Bildung der Polygone ist von Sletten et al. (J. Geophys. Res., 108(E4), 8044, 2003) entwickelt worden (Abb. 7). Zyklische Ausdehnung und Kontraktion der oberflächennahen Bodenschichten im Rhythmus der Jahreszeiten erzeugt keilförmige vertikale Risse. Wenn sich diese Risse in der kalten Jahreszeit mit Lockermaterial füllen, dann können sie sich in der darauf folgenden warmen Jahreszeit nicht mehr vollständig schließen: Es kommt zu Spannungen und die zentralen Regionen des Polygons wölben sich auf. Das Resultat ist ein langsamer zyklischer Transport von Bodenmaterial, und stellt einen (auf der Erde als Kryoturbation bezeichneten) Erosionsprozess in arktischen und periglazialen Gegenden dar. Weiter oben hatten wir auf den nahe gelegenen Heimdall Krater hingewiesen, der auf der Grundlage von Kraterzählungen ein ungefähres Alter von 500 Millionen Jahren hat. Es scheint wahrscheinlich, dass Auswurfmaterial dieses Kraters den Phoenix Landeplatz mit geprägt hat. Damit wird angedeutet, dass das geologische (geomorphologische) Alter des Phoenix Landeplatzes diese 500 Mio. Jahre nicht überschreitet. Die oben beschriebenen Prozesse zur Bildung von Polygonen erfolgen über einen wesentlich kürzeren Zeit-

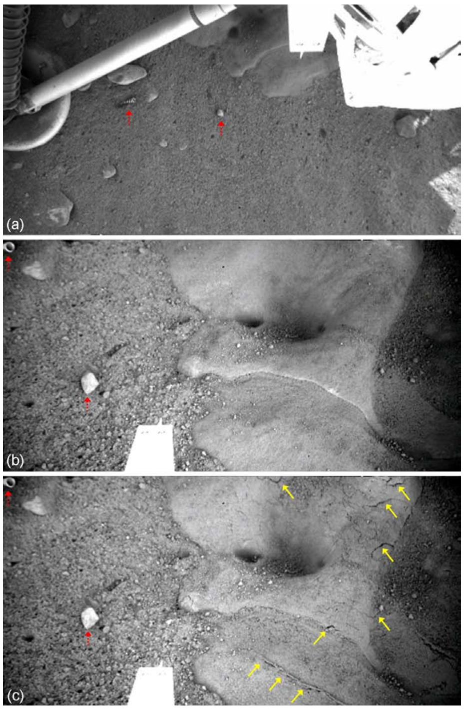

Abb. 5: Eisfläche ‘Snow Queen’, welche wie die benachbarte Region ‘Holy Cow’ (Abb. 4) durch die Bremsraketen von Staub und Bodenmaterial ‘reingefegt’ wurde. (a) Übersichtsbild, Sol 5. Blick nach unten, in leicht südliche Richtung. Links im Bild das nordöstliche der drei Sondenbeine (Diameter des Fußtellers = 29 cm). Die roten (gestrichelten) Pfeile markieren eine bei der Landung abgefallene Schraube (links) sowie durch Bremsraketen deplaziertes Geröll (Mitte) und dienen der Orientierung in b und c. (b) Vergrößerte Ansicht von Snow Queen, Sol 21. (c) Snow Queen (Sol 73) mit Rissen, die sich seit Sol 21 gebildet haben (gelbe Pfeile).

raum und sorgen daher für eine ständige Erneuerung der Landschaft, womit der Phoenix Landeplatz den jüngsten aller bisher besuchten Landeplätze (Viking, Mars Pathfinder, Mars Exploration Rovers) darstellt. Die bisher gezeigten Bilder (Abb. 1, 2, 3d und e, 4, 5, 7) bezeugen die Abwesenheit größerer Gesteinsbrocken am Landeplatz. Gibt es eine schlüssige Erklärung hierfür? Abb. 4 – Abb. 6 zeigen das reichhaltige Vorkommen von Wassereis nahe der Oberfläche in Übereinstimmung mit den Odyssey Daten von 2002. Vielleicht lässt sich die Abwesenheit der Gesteinsbrocken durch die hohe Konzentration an Volatilen (Wassereis) in den oberflächennahen Schichten erklären, die während des Heimdall-Einschlags erfasst wurden: Eine gewaltige Druckwelle mag die potentiellen (ursprünglich hier deponierten) Gesteinsbrocken weggesprengt und zertrümmert haben.

Eigenschaften des Bodenmaterials

Einige der Phoenix Instrumente haben neuen Einblick in die mikroskopische Struktur (AFM, OM, RAC) sowie die chemisch-mineralogische Zusammensetzung (TEGA, WCL) des Bodenmaterials verschafft. Abb. 8a zeigt eines der vielen RAC Bilder des Schaufelinneren, welche eine erste (visuelle) Charakterisierung des Bodenmaterials ermöglichte. Das Material (Abb. 8a) wurde dann noch am gleichen Tag (Sol 66) einer der WCL Zellen zugeführt (Abb. 8b). Nach dem Hinzufügen flüssigen Wassers (genauer: 25 cm^3 einer verdünnten wässrigen Lösung mit genau bekannter Zusammensetzung) zu 1 cm^3 Mars-Bodenmaterial entstand eine schwach basische Lösung (pH $\sim$ 8.3), welche – völlig unerwartet – beträchtliche Mengen an Perchlorat (ClO4-) enthielt. Überraschenderweise war das Perchloration das dominierende Anion. Daneben wurden v.a. Magnesium- und Natriumionen, aber auch Kalium- und Calciumionen nachgewiesen [Hecht et al., Lunar Planet. Sci. Conf. XL, #2420, 2009a and Science, 325, 64, 2009b]. Eine angenommene Gesamtmasse von $\sim$ 1 g analysierten Bodenmaterials entspräche etwa 1 Gew. % Perchlorat im Marsboden. Eine solche Konzentration übersteigt die Perchlorat-Konzentrationen, die in manchen terrestrischen Wüstengebieten gefunden werden, um mehrere Größenordnungen [Hecht et al., 2009a]. Der Nachweis von Chlor in der höchstmöglichen Oxidationsstufe beeinflusst unser Verständnis der chemischen Prozess, die in der Atmosphäre sowie den obersten Bodenschichten ablaufen. Es stellen sich eine Reihe von Fragen: Ist das Perchlorat eine exotische Erscheinung am Phoenix Landeplatz oder ist es an der Oberfläche des Planeten weit verbreitet? Und die daran anknüpfende Frage: Lag das an früheren Landeplätzen identifizierte Chlor (Viking Lander, Mars Pathfinder, MER) hauptsächlich als Perchlorat vor? Sogar die alte Frage nach Leben auf dem Mars muss neu formuliert werden: Welche Formen primitiven (terrestrischen) Lebens könnten angesichts der gemessenen Perchlorat-Konzentration im Marsboden gedeihen? Die für die Hofmeister-Ionenreihe (einschließlich Perchlorat und Nitrat) empfindliche ISE lieferte ein sehr starkes Signal, womit die Anwesenheit von Perchlorat eindeutig nachgewiesen war (die für dieses Signal erforderliche Nitratmasse wäre größer gewesen als die totale Masse der analysierten Bodenprobe). Im allgemeinen hat aber jede ISE eine stark variierende Empfindlichkeit für eine Reihe von Ionen. Daher ist die Konvertierung von ISE Daten in Ionenkonzentrationen nicht eindeutig. Einschränkungen durch andere Datensätze sind notwendig, um einige der mathematischen Lösungen auszuschließen. In dieser Hinsicht spielen TEGA Daten eine bedeutende Rolle. Thermische Zersetzungsprodukte von Per-

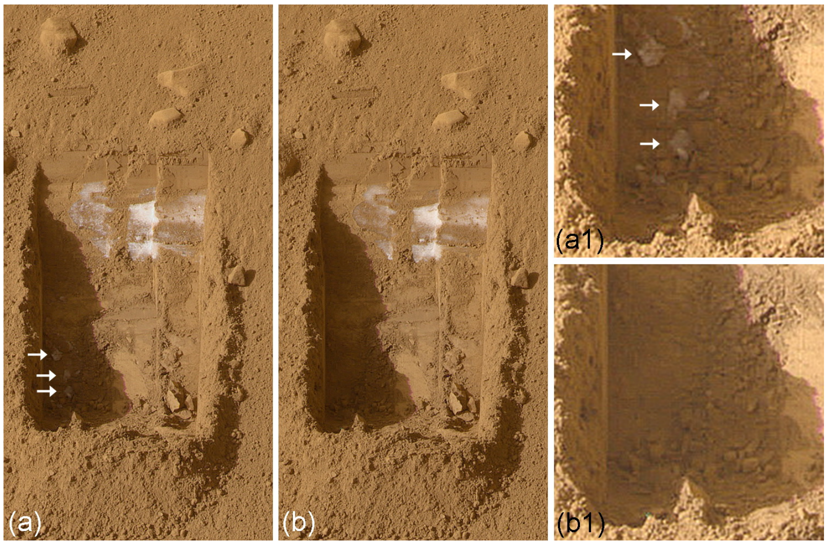

Abb. 6: Dodo Goldilock. (a) Sol 20. Dieser Graben (auch in Abb. 1 zu sehen) ist etwa 20 cm breit (entsprechend drei Schaufelbreiten, mit geringer Überlappung). Bemerke das freigelegte, (entsprechend gegenwärtiger Annahmen) mehr oder weniger reine Eis im oberen Teil des Grabens. (b) Wie a, jedoch vier Sols später aufgenommen. Die in a mit weißen Pfeilen gekennzeichneten Partikel ($\sim$2 cm im Diameter) sind am Sol 24 verschwunden entsprechend einer Sublimationsrate von $\sim$200 μm/Sol. Die Abbildungen a1 und b1 sind jeweils vergrößerte Ausschnitte von a und b.

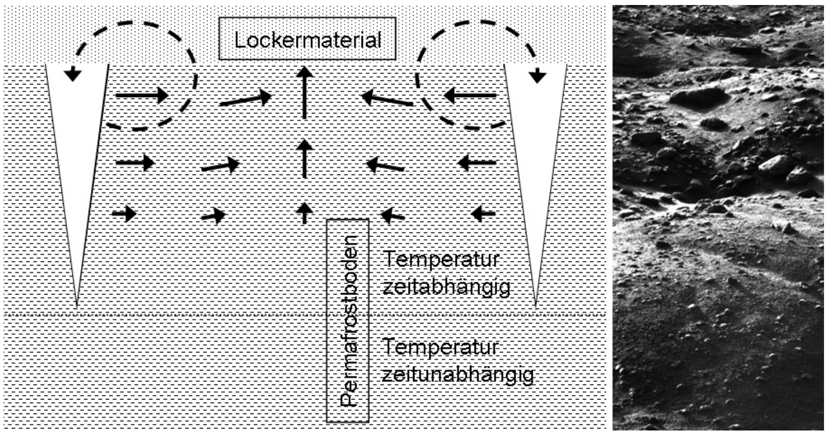

Abb. 7: Modell für die Entstehung der Polygone durch Kryoturbation [nach Sletten et al., 2003 (verändert)]: Bei der Kontraktion im Winter entstehen keilförmige Hohlräume, die sich mit Lockermaterial füllen. Im darauf folgenden Frühjahr und Sommer können sich die Sandkeile nicht mehr vollständig schließen: Es kommt zu Spannungen und die zentralen Regionen des Polygons wölben sich auf. Die gestrichelten Pfeile veranschaulichen den Langzeittransport von Bodenmaterial. Die durchgezogenen Pfeile stellen lokale Geschwindigkeitsvektoren dar. Unterhalb einer gewissen Tiefe (der Tiefe der Sandkeile) ist die Bodentemperatur nicht mehr den täglichen und jahreszeitlichen Temperaturschwankungen unterworfen, da die obere Bodenschicht thermisch isoliert. Eine aktive oberste Bodenschicht (mit Auftauphasen) gibt es auf dem Mars nicht. Die Permafrostzone erstreckt sich aufgrund des geothermischen Gradienten ($\sim 10°$ C/km, [Hoffman et al., Conference on the Geophysical Detection of Subsurface Water on Mars, 7044, 2001]) mindestens 5 km (je nach Breitengrad) in die Tiefe. Das noch tiefer liegende Grundgestein mag flüssiges Wasser enthalten, obgleich die Porosität des Grundgesteins in diesen Tiefen sehr klein ist. Das Gegenlicht im SSI Bild (rechts) vom Sol 61 (Blick nach ONO, 3:51 Uhr) hebt Relief und Konturen der Polygone besonders deutlich hervor. Die Polygone sind etwa 7 m von der Sonde entfernt.

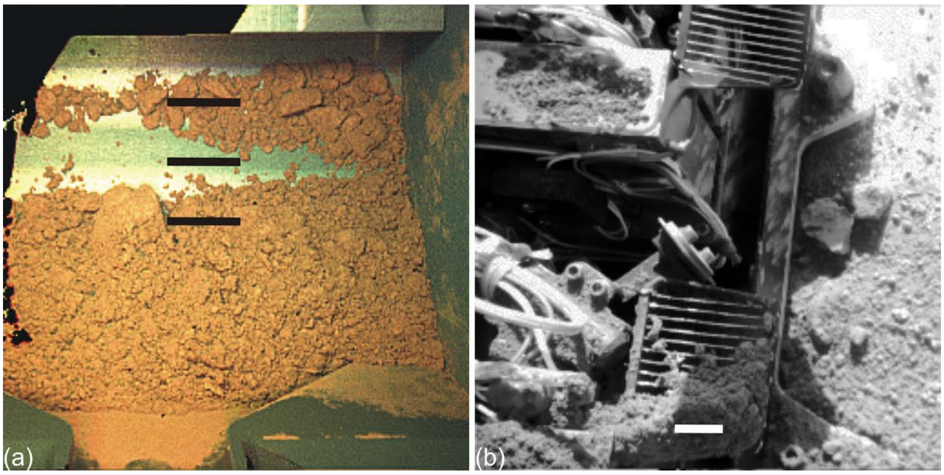

Abb. 8: (a) Marsbodenprobe in der Schaufel (RAC Bild, Sol 66). Ein RAC Farbbild entsteht durch das gewichtete Zusammenlegen von drei Bildern, die jeweils im roten, grünen und blauen Licht der RAC Leuchtdioden aufgenommen wurden. Die schwarzen Regionen in diesem Bild (oben links) sind direkt von der Sonne beschienene Regionen. Sie enthalten keine Farbinformation, da die Strahlungsintensität der Leuchtdioden wesentlich geringer ist als die direkten Sonnenlichts. (b) WCL Zelle #0, der dieses Material am Sol 66 zugeführt wurde. Die schwarzen und weißen Balken in den Bildern haben eine Länge von 10 cm. Sowohl in der Schaufel wie auch auf dem Gitter der WCL Zelle ist klumpiges Bodenmaterial erkennbar.

chloraten wurden in TEGA-Spektren im allgemeinen nicht nachgewiesen, was jedoch den WCL Nachweis dieser Ionen keinesfalls in Frage stellt. Immerhin wurde in einer der von TEGA untersuchten Bodenproben (Baby Bear, etwa Sol 25) die Freisetzung von Sauerstoff (O_2) beobachtet, welche kausal mit der Zersetzung eines Perchlorats zusammenhängen könnte [Lauer et al., Lunar Planet. Sci. Conf. XL, #2196, 2009; Hecht et al., 2009a, 2009b]. Ein wichtiger Fund des TEGA Instruments ist die Freisetzung von Kohlendioxid im Temperaturbereich 800 – 900° C, woraus auf die Gegenwart von 3 – 5 Gew. % Calciumkarbonat in den Phoenixböden geschlossen wurde [Boynton et al., Science, 325, 61, 2009]. Immerhin ist im vergangenen Jahrzehnt (insbesondere durch Fernerkundung aus der Umlaufbahn) gezielt nach diesem Mineral an der Oberfläche des Planeten gesucht worden [Ehlmann et al., Science, 322, 1828, 2008]: TEGA hat es gefunden, – und darüber hinaus in einer nicht vernachlässigbaren Konzentration! Das gefundene Karbonat ist auch mit WCL Daten vereinbar [Kounaves et al., Lunar Planet. Sci. Conf. XL, #2489, 2009] und erklärt z.T. den von WCL gemessenen basischen pH-Wert der wässrigen Lösungen. Auch die Abwesenheit von bestimmten Gasen kann kritische Informationen über die Mineralogie des Marsbodens liefern: In der Tat ist im gesamten Temperaturbereich (von Minusgraden bis zu 1000° C) kein Schwefeldioxid freigesetzt worden. Aber gerade die Abwesenheit des Gases ist überraschend: Immerhin haben bisher alle erfolgreichen Mars-Landesonden (Viking, Mars Pathfinder, Mars Exploration Rovers) wesentliche Mengen Schwefel (5 – 10 Gew. % SO_3) im Marsboden nachgewiesen. Die Gegenwart von Sulfationen ist vereinbar mit WCL Daten. Magnesiumsulfat würde sich bei Temperaturen unter 1000° C zersetzten und Schwefeldioxid freigeben. Die Abwesenheit dieses Gases beweist also die Abwesenheit von Magnesiumsulfat in Phoenix Bodenproben. Calciumsulfat (Gips, Anhydrit) würde sich unter Marsbedingungen (dem atmosphärischen Druck von 10 mbar) bei etwa 1400° C zersetzen, aber solche Temperaturen werden nicht erreicht. Die Vermutung liegt daher nahe, dass Calciumsulfat in Phoenix Bodenproben auftritt [Golden et al., Lunar Planet. Sci. Conf. XL, #2319, 2009]. Immerhin sind schon größere solcher Lagerstätten auf dem Mars durch Fernerkundung gefunden worden, eine davon zum Beispiel am Nordpol des Planeten [Langevin et al., Science, 307, 1584, 2005].

Abb. 9 zeigt mikroskopische Bilder sowie eine dreidimensionale Darstellung eines durch das AFM ‘abgetasteten’ Staubteilchens. Die unabwendbare Schwäche der AFM Daten liegt natürlich darin, dass aufgrund des hohen räumlichen Auflösungsvermögens (~ 0.1 μm/Rasterpunkt) nicht beurteilt werden kann, ob bestimmte morphologische Erscheinungsformen als repräsentativ gelten können. Der Leser bemerkt die ungeheure Teilchenvielfalt, wie sie in den mikroskopischen Farbbildern zutage tritt. Zunächst fällt der rötlich (orangefarbene) Staub auf, der in Abb. 9b dominiert. Die einzelnen Teilchen können durch das Mikroskop (4 μm/Pixel) nicht aufgelöst werden und müssen daher kleiner sein als ~ 10 μm sein. Eine vorläufige Klassifizierung der Siltkörner, die in Abb. 9a und 9b auftreten, unterscheidet zwischen rötlich-braunen bis farblosen Teil-

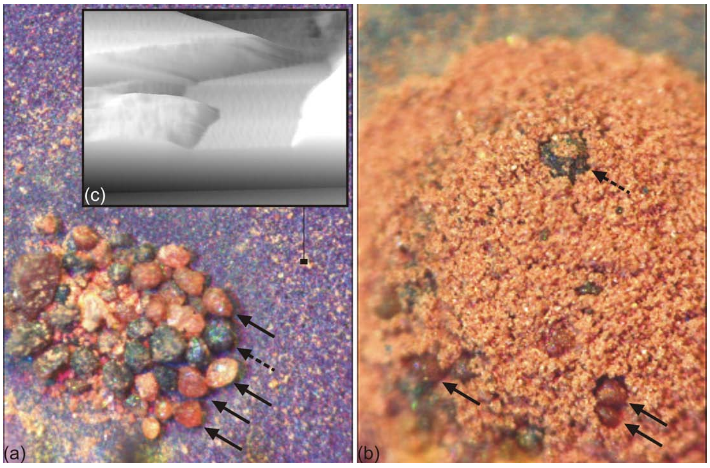

Abb. 9: Mikroskopische Aufnahmen von Marsbodenmaterial. (a) Sol 58. Etwa 60 μm große Siltkörner (Schluff) unterschiedlicher Farbe auf blau-violettem magnetischem Substrat. (b) Sol 122: Die gleichen Typen Siltkörner (wie in Abb. 9a) verteilt in einer 'Grundmasse' aus orangefarbenem klebrigen Marsstaub. Die Staubteilchen (Ø < 10 μm) sind in den Mikroskopbildern nicht einzeln erkennbar. Die weißlich-bis-bräunlichen Siltkörner (durchgezogene Pfeile) haben wahrscheinlich eine andere Entstehungsgeschichte als die dunklen (fast schwarzen) Siltkörner (gestrichelte Pfeile) [Goetz et al., Lunar Planet. Sci. Conf. XL, #2425, 2009]. Das Bodenmaterial in Abb. 9a-b ist magnetisierbar, da es im zentralen Bereich des vertikal (parallel zum lokalen Schwerefeld) orientierten Substrats zu liegen kommt. Die abgebildeten Flächen in Abb. 9a-b sind jeweils 1 mm breit. (c) Detailbild eines Staubteilchens (Sol 74, etwa 20 μm von links nach rechts), das aus AFM Daten generiert wurde. Ob es sich dabei um eine 'typische, repräsentative Morphologie' handelt, sei dahingestellt. Das kleine schwarze Rechteck deutet in Abb. 9a eine analoge Fläche an, die genauso groß wäre wie die in Abb. 9c abgebildete.

chen (durchgezogene Pfeile) und sehr dunklen (bisweilen schwarzen) Teilchen (gestrichelte Pfeile). Über den möglichen Ursprung beider Teilchentypen wird noch gerätselt [Goetz et al., 2009]. Nur der Vergleich mit zahlreichen terrestrischen Proben (z.B. palagonitischen Proben aus vulkanischen Regionen) kann die Szenarien eingrenzen, die möglicherweise zur Bildung der einzelnen Teilchentypen geführt haben. Hierbei muss der oben beschriebene geologische Kontext des Phoenixlandeplatzes in die Abwägung der einzelnen Entstehungsszenarien mit einfließen.

Wind und Wetter

Die Phoenix-Instrumente haben erstaunliche meteorologische Beobachtungen und Messungen am Landeplatz ermöglicht. Der überragende wissenschaftliche Erfolg dieser Daten hat folgende Ursachen: (a) Phoenix ist – wie schon weiter oben vermerkt – die erste Landesonde in den polaren Regionen des Planeten, wo Wetterphänomene (insbesondere Wolkenbildung) am stärksten ausgeprägt sind. Letzteres ist bekannt von Satellitenbildern. (b) Phoenix verfügt über eine durchdachte (hauptsächlich kanadische) meteorologische Messstation, die neben den üblichen (bei den Mars Exploration Rovers jedoch fehlenden) Druck-/Temperatursensoren ein LIDAR Instrument zum Nachweis von Wolken mit einschließt. Auch der (dänische) Wetterhahn (Telltale) hat – trotz seiner Einfachheit – gute Dienste geleistet. (c) Die Phoenix Wettermessungen konnten mit hervorragenden Instrumenten an Bord verschiedener Mars-Satelliten räumlich und zeitlich gut koordiniert werden, was die wissenschaftliche Aussagekraft aller Datensätze stärkt.

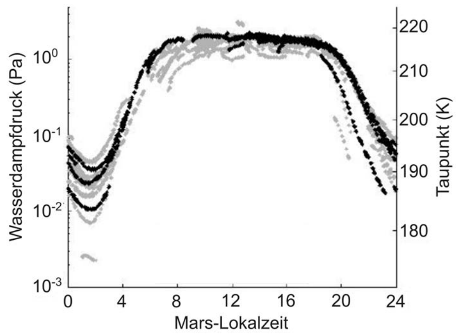

Abb. 10: TECP Messungen des atmosphärischen Wasserdampfdruckes $\sim$5 cm (schwarz) und $\sim$1 m (grau) über der Oberfläche. Jedem Druckwert entspricht ein Taupunkt (2. Ordinate), bei dem der Wasserdampf mit einem idealisierten Wassereisreservoir gleicher Temperatur im Gleichgewicht steht. Der Wasserdampfdruck steigt am frühen Morgen zu einem Plateauwert an ($\sim$1.8 Pa, 220 K) [Hudson et al., Lunar Planet. Sci. Conf. XL, #1804, 2009], der danach (trotz des weiteren Anstiegs der atmosphärischen Temperaturen auf mindestens 230 K) konstant bleibt. Der konstante Wasserdampfdruck ist vermutlich eine Folge der raschen Vermischung des zu Beginn des Tages neu gebildeten Wasserdampfes in der gesamten atmosphärischen Grenzschicht [Hudson et al., 2009].

Abb. 10 trägt den Wasserdampfgehalt der bodenna-

hen Atmosphäre (wie er durch den TECP Luftfeuchtigkeitssensor gemessen wurde) gegen die Tageszeit auf. Besonders deutlich ist das Wasserdampfplateau (∼ 1.8 Pa), welches sich zwischen 10 und 17 Uhr Mars-Lokalzeit bildet. Eigentlich sollte dieser Druck bis etwa 14 Uhr Mars-Lokalzeit andauernd steigen, – im Takt mit den atmosphärischen Temperaturen. Offensichtlich kommt es jedoch im Zeitraum von 10 bis 17 Uhr zu einem dynamischen Gleichgewicht der bodennahen Wasserdampfkonzentration, wobei Wasserdampf im Takt mit der Entstehungsrate nach oben abtransportiert und in der atmosphärischen Grenzschicht verteilt wird. In täglichen Zyklen wird der Wasserdampf zwischen der Atmosphäre und der festen Oberfläche ausgetauscht. Die Wasserdampfquellregionen könnten das bodennahe Wassereis am Landeplatz, adsorbiertes Wasser an Regolithkörnern oder Kristallwasser in Perchloraten sein (wie z.B. $Mg(ClO_4)2.6\, H_2O$; [Hudson et al., 2009]).

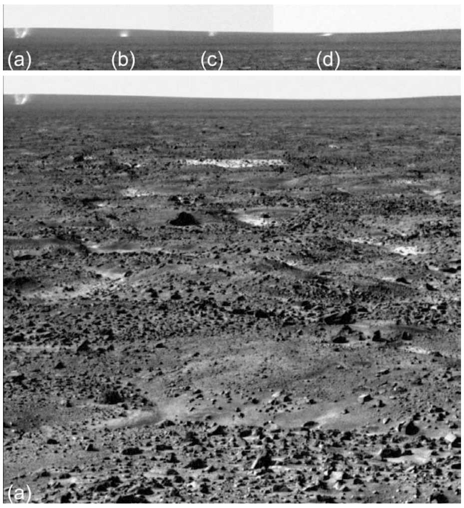

Abb. 11: Staubtornado (Sol 104, Blick nach Westen, ∼ 13.9° × 13.9°). (a) 11:53:50 Uhr Mars-Lokalzeit. (b) 51 Sekunden (Marssekunden). (c) 100 Sekunden. (d) 155 Sekunden nach (a). Der Tornado im Bild (a) ist etwa 1 km von der Phoenix Sonde entfernt und hat einen Durchmesser von etwa 5 m. Er bewegt sich von der Sonde weg (Abstand zur Sonde ∼ 1.7 km in Bild (d). Größere Staubwirbel wurden im Gusev-Krater beobachtet [Greeley et al., J. Geophys. Res. 111, E12S09, 2006; Landis et al., 7th Internat. Conf. on Mars, Pasadena, 2007].

Abb. 11 zeigt einen Staubtornado, der mit typischen Windgeschwindigkeiten (5 – 10 m/s) an der Sonde vorbeifegt. Systematische Studien der von der kanadischen Wetterstation gemessenen Drücke deuten darauf hin, dass solche Staubtornados mit kurzzeitigen Druckabsenkungen von 1 – 3 Pa korreliert sind [Ellehoej et al., Lunar Planet. Sci. Conf. XL, #1558, 2009]. Die LIDAR Daten, welche im späteren Teil der Phoenix Mission aufgesammelt wurden, sind von außerordentlicher Bedeutung [Whiteway et al., 2009]:

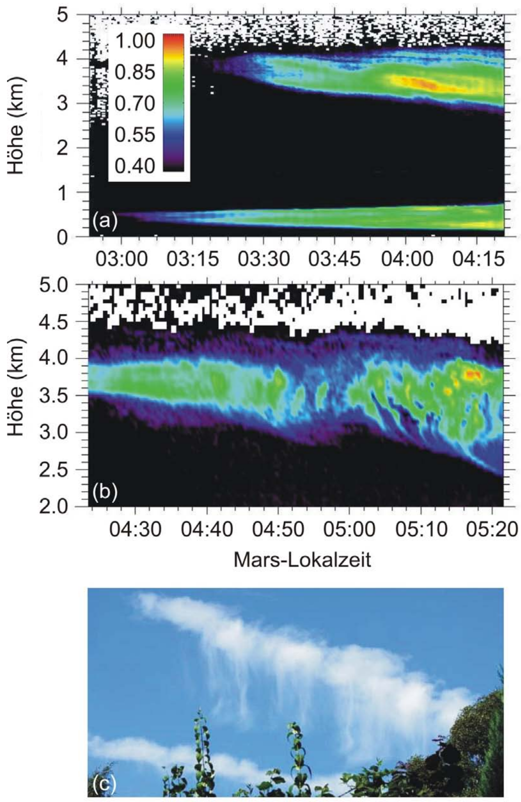

Arnsberg, Nordrhein-Westfalen, 8. Aug. 2007

Abb. 12: Charakterisierung von Nachtwolken durch LIDAR. Die Farben in a und b repräsentieren die LIDAR-Rückstreuintensität in relativen Einheiten. (a) Phoenix, Sol 98, 03:00-04:15 Uhr. Nach Sol ∼ 80 bilden sich täglich Bodennebel, sowie Eiswolken an der oberen Grenze der atmosphärischen Grenzschicht (∼ 4 km Höhe). (b) Phoenix, Sol 99, 04:20-05:20 Uhr. Eiswolke mit Fallschleppen (Virgas). Die Fallschleppen entstehen durch Sublimation ausfallender Eiskristalle und sind gekrümmt aufgrund unterschiedlicher Windgeschwindigkeiten in verschiedenen atmosphärischen Höhen. Die Wolke sinkt im Mittel um etwa 800 m nach unten im Zeitraum von 04:20-05:20 Uhr. Aus der Fallgeschwindigkeit ergibt sich gemäß der Stokes'schen Reibungsformel die durchschnittliche Größe der ausfallenden Eispartikel von etwa 60 μm. (c) Bild von analogen terrestrischen Fallschleppen (Quelle: M. Thiessenhusen).

Nach Sol ∼ 80 bildeten sich jede Nacht Bodennebel, sowie Eiswolken am oberen Rand der atmosphärischen Grenzschicht (∼ 4 km Höhe) (Abb. 12a). Die Eiswolken bildeten häufig Fallschleppen durch anfänglich wachsende, dann ausfallende und schließlich sublimierende Eiskristalle (Abb. 12b). Abb. 12c zeigt terrestrische Fallschleppen zum Vergleich. Hierzu muss bemerkt werden, dass LIDAR-Diagrammme (Abb. 12a-b) räumlich punktuelle Zeitdiagramme darstellen, welche nicht bedenkenlos mit gewöhnlichen Photos, i.e. räumlich ausgedehnten Momentanbildern (Abb. 12c) verglichen werden können. Am Tag aufgesammelte LIDAR-Daten waren geprägt durch Staub

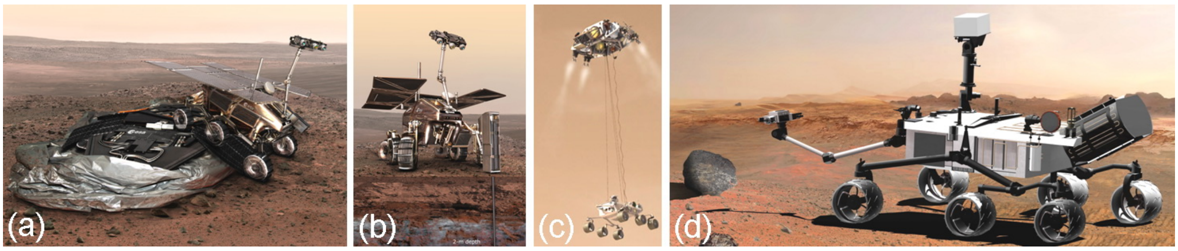

Abb. 13: Die nächsten Landemissionen auf dem Mars: (a), (b) ExoMars, ESA (Raketenstart 2018). (c), (d) Curiosity, NASA, Raketenstart im Herbst 2011. ExoMars soll auf Airbags landen (a), wohingegen Curiosity sich der neu entwickelten Sky Crane Technologie bedient, welche durch Herablassen des Rovers an einem Seil eine Präzisionslandung ermöglicht (c). Alle Bilder sind etwa im gleichen Maßstab (mit Ausnahme von c). Man bemerke den beachtlichen Größenunterschied zwischen ExoMars und Curiosity.

in der atmosphärischen Grenzschicht. Jedoch ist es gelungen, sublimierende Tagwolken mit Fallstreifen auch durch SSI Bilder zu dokumentieren [Whiteway et al., Science, 325, 68, 2009].

Gegenwärtiger Status der Phoenix Mission und Ausblick

Die Phoenix Mission lieferte wissenschaftliche Daten über einen Zeitraum von 152 Sols. Die letzte Datenübertragung erfolgt am 2. Oktober 2009. Im Zeitraum vom 1. April – 10. Juli 2009 herrschte die Polarnacht am Landeplatz. Seit Ende der Polarnacht steigt die Sonne wieder über den Horizont. Falls die Phoenix Sonde den Mars-Winter wider Design-anforderungen und wider Erwarten überlebt haben sollte, wird sie sich selbst vermöge des sogenannten Lazarus-Modus wiederbeleben. Mars Odyssey wird ab Mitte Oktober 2009 wieder nach einem Phoenix Signal suchen. Unbahängig von einer potentiellen Wiederbelebung der Phoenix Sonde, ist die Phoenix Mission als Geologie-, Geochemie- und Meteorologiemission hochgradig gelungen. Am Landeplatz wurden keine organischen Moleküle gefunden. Demnach gab es auch keine Spuren biologischer Aktivität. Die Suche nach organischen Molekülen ist den Nachfolgemissionen (Abb. 13) aufgetragen worden. Wegen des kontinuierlichen Zustroms organikreicher Meteoritentypen (CC-Meteoriten) sollte der Marsboden leicht nachweisbare organische Verbindungen enthalten. Die Tatsache, dass diese nicht gefunden wurden, legt die Vermutung nahe, dass es dort schnelle chemische Abbauprozesse gibt, so dass die Gleichgewichtskonzentration stets sehr klein bleibt. Die ständige Umwälzung von oberflächennahem Bodenmaterial (Kryoturbation) am Phoenix Landeplatz mag solche Abbauprozesse begünstigt haben (Abb. 7). Falls je organische Verbindungen im Bodenmaterial gefunden werden, stellt sich die schwierige wissenschaftliche Frage nach dem Ursprung dieser Verbindungen: Importiert durch einschlagende Kometen und Meteoriten oder die Entwicklung primitiven Lebens im Marsboden bezeugend? Obwohl bisher keine organischen Verbindungen im Marsboden gefunden wurden, macht die Suche danach weiterhin Sinn und muss als logische Konsequenz in besser geschützten Umgebungen, wie z.B. im Inneren sedimentärer Gesteine oder in tieferen Bodenschichten, fortgesetzt werden. Die nächsten Missionen, die für diese wissenschaftliche Aufgabe zur Verfügung stehen, sind die Rover Curiosity (NASA, Start 2012) und ExoMars (ESA, Start 2018), welche entsprechend ihrem gegenwärtigen Entwicklungsstand in Abb. 13 vorgestellt werden. Beide Rover enthalten komplexe Instrumente, die die TEGA Herausforderung wieder aufnehmen, und im nächsten Jahrzehnt in spezifischen, äquatorialen Regionen nach organischen Molekülen suchen werden: SAM (Sample Analysis at Mars/MSL) und MOMA (Mars Organic Molecule Analyzer/ExoMars). Das letztgenannte Instrument ist gegenwärtig in der Entwicklungsphase unter Leitung des Max Planck Instituts für Sonnensystemforschung. Das erstgenannte ist bereits fertig entwickelt und flugbereit (NASA Goddard Space Flight Center) und wird besonders niedrigen Konzentrationen an potentiellem organischem Material nachspüren können. Die besondere Aufmerksamkeit gilt hierbei dem Molekül Methan (CH_4), dessen Präsenz auf dem Mars unlängst nachgewiesen wurde [Mumma et al., doi:10.1126/science.1165243, 2009], und dessen Isotopenverhältnis 13C/12C noch bei minimaler Konzentration (< 1 ppb) gemessen werden kann [Mahaffy et al., Lunar Planet. Sci. Conf. XL, #1088, 2009].

Phoenix / Phoenix

After Mars Polar Lander (MPL) had crashed on 3 December 1999 and Mars Surveyor 2001 was canceled in 2000, there was no hope for a new mission to the Martian arctic regions. However, the situation changed early in 2002 when the Mars Odyssey orbiter discovered large amounts of near-surface hydrogen in exactly these regions. The hydrogen reservoir was interpreted as water ice – less than a meter below the surface, and it was argued that the arctic water ice might contain the long-searched for (and long-missed) organic compounds. These findings led a group around Peter H. Smith, University of Arizona, develop a mission that would build on the earlier designs (MPL) and use the already completed Mars Surveyor lander deck: Phoenix, a burned bird that resurrected from its ashes! The rocket was launched on August 4, 2007, and the spacecraft landed safely at 68.2° N, 234.3° E on 25 May 2008, sol 0 (Martian day 0) of the mission.

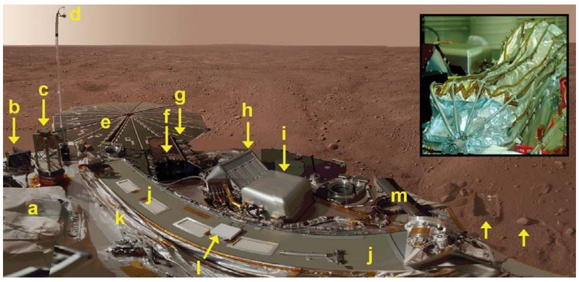

Fig. 1: Self-portrait of the Phoenix spacecraft and its surroundings (acquired by the SSI in the approximate time frame from sol 20 to 30). The center of the image corresponds to the north-western direction. a: LIDAR. b: Interface of the cruise stage. c: UHF antenna. d: Meteorological mast with weathercock (Telltale). e: Western solar panel. f: Chute for transfer of soil material to the OM. g: WCL. h: TA. i: EGA. j: Support to which the RA (in stowed configuration) was locked during flight (strongly distorted). k: Biobarrier, a foldable cover for protection of the RA and the scoop against biological contamination. The inset on the upper right shows the biobarrier in flight configuration. After landing it was opened towards the observer and stowed. l: Organic Free Blank (OFB). Drill dust from this teflon block was designed to serve as a zero reference for organic molecules. m: The first segment of the RA. The arrows to the right of the spacecraft point to a $\sim$20 cm wide trench (Fig. 6) and a small rock that was displaced by the thrusters.

Instruments

Fig. 1 shows the location of most of the instruments in a self-portrait of the spacecraft. These instruments include a number of imaging systems with varying resolution: A Stereo Surface Imager (SSI, resolution $>$ 1 mm/px), a Robotic Arm Camera (RAC, resolution $>$ 24 μm/px), an optical microscope (OM, resolution $\sim$ 4 μm/px), and an Atomic Force Microscope (AFM, resolution $\sim$ 0.1 μm/scan step). In addition, there is a Wet Chemistry Laboratory (WCL), where Martian soil was stirred up in liquid water. Four such cells were available and designed for single use. The resulting aqueous solution could be analyzed by means of ion-selective electrodes (ISE). The WCL cells thus provide information on the compounds in the soil (such as salts) which are soluble in liquid water. Another important instrument is designed to heat soil samples up to 1000° C (TA, Thermal Analyzer) and to analyze the evaporating gases by mass spectroscopy (EGA, Evolved Gas Analyzer). TEGA (the instrument group that is composed of TA and EGA) should be able to characterize the inventory of potential organics in the Martian soil by detecting the parent organic molecules or their thermally generated fragments. The temperatures, where specific gases are released, constrain the parent compound. The increase in temperature during the supply of known heat increments reveals phase transitions and their enthalpic characteristics.

The spacecraft's Robotic Arm (RA) is in itself a scientific instrument, as it allows to characterize the physical properties of the soil. The scoop at the end of the 2.3 m long arm allows to select and to transfer specific soil samples to the various instruments (in particular OM, WCL, TEGA). An ice drill (Rapid Active Sampling Package, RASP) is mounted to the backside of the scoop. The RAC is positioned on the RA, such that it can 'look' into the scoop and image the collected soil sample at high resolution ($>$ 24 μm/px). A soil sensor (Thermal and Electrical Conductivity analyzer, TECP) mounted next to the scoop can measure the soil's electric and thermal conductivity between four needles. An additional sensor (also incorporated into the TECP box) can measure the atmospheric water vapor pressure and the relative humidity of the atmosphere. Finally, the Canadian weather station must be mentioned. Its central instrument, the LIDAR (Laser Detection And Ranging), probes the vertical structure of the atmosphere by measuring the travel time of light that was backscattered by suspended particles (dust, ice). The daily weather studies were completed by pressure and temperature sensors that are mounted to a meteorological mast at three different heights above the deck (25, 50, and 100 cm) and by the Danish weathercock (Telltale) on top of that mast. The SSI provided complementary data on the atmospheric dust opacity and water vapor abundance by imaging the solar disk through specific visible and near-infrared filters. Fig. 2 shows the instruments (RAC, TECP) that are mounted at the end of the robotic arm. MPS contributed the RAC as well as the focal-plane assembly of the OM.

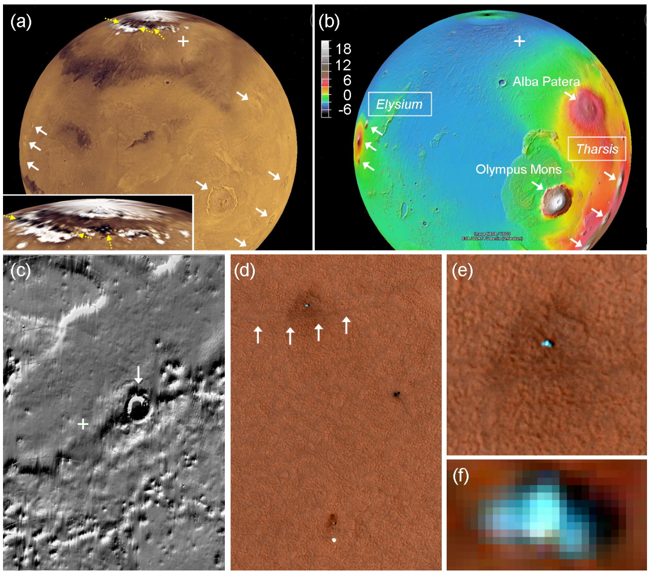

Fig. 3: From global to local scale. North is up in all images. (a): Approximate true-colour mosaic from Viking Orbiter, white cross = Phoenix, white arrows = major volcanoes in the Elysium (left) and Tharsis region (right), dotted yellow arrows = dark sand dunes near the polar ice cap (magnified in the inset). (b): Like (a), but an altitude map based on Mars Orbiter Laser Altimeter (MOLA) data. The legend specifies the height in kilometers. (c): Orbital image (280 m wide) of the surroundings of the Phoenix landing site (white cross) where ejecta from the nearby Heimdall crater (white arrow) are expected. (d): High-resolution image (MRO/HiRISE) of the Phoenix spacecraft (top), the heat shield (middle right), and the parachute with back shell (bottom), acquired 22 hours after landing. The white arrows mark a fissure in the terrain. (e): Enlarged section of (d). Note the surface roughness (polygons). As a result of thruster action, coarse-grained (darker) material showed up in the vicinity (< 20 m) of the lander. (f): Enlarged section of (e) showing the lander deck and the two solar panels. The location of the shadow (NE of the lander) confirm that this image has been acquired late in the afternoon, about one day after landing. This image has intentionally not been smoothed in order to show the individual HiRISE pixels (∼ 33 cm/px). Images: (a,b) Google Earth, (a, b, c, d, e) NASA.

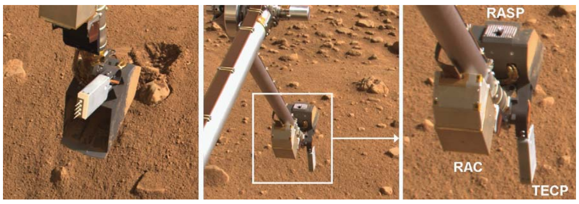

Fig. 2: End of the RA (SSI images from sol 49) with scoop (∼ 8 cm wide), RAC, TECP und ice drill (RASP).

Geology of the Landing Site

Spectroscopic data and high-resolution images from various orbiter missions (Mars Global Surveyor, Odyssey, Mars Express, Mars Reconnaissance Orbiter) were available prior to landing and were extensively used to select the best landing site from a safety and science perspective. Fig. 3 presents the geologic context of the Phoenix landing site. The distance to the northern border of the volcanic Tharsis region and to the nearest volcano (Alba Patera) is about 500 km and 1800 km, respectively. The north-polar ice cap and the circumpolar dunes are located about 2000 km north of the lander. On a large scale, we expect volcanic ashes from the Tharsis province as well as sand grains from the north-polar dunes. The landing site is also situated about 20 km west from the Heimdall crater with a diameter of 11 km and a depth of about 1 km (Fig. 3c). Ejecta from these depths may thus also be found at the landing site.

A few days after landing, the terrain below the spacecraft was examined by the RAC in order to confirm the stability of the spacecraft position. The first image (Fig. 4a) showed a bright, even surface (called 'Holy Cow') that was uncovered by the action of the descent thrusters. Apparently, the subsurface ice discovered by Odyssey in 2002 was already found – only a few centimeters below the surface.

Fig. 4(b) suggests that this is ice-rich regolith rather than pure water ice. Fig. 5 shows another icy soil patch called 'Snow Queen' (the nomenclature was supposed to follow fairy tale themes) that is located just next to Holy Cow: In the course of 52 sols (Fig. 5(b)–(c)) Snow Queen has developed numerous cracks after it had lost its thermally insulating blanket. During the Phoenix mission, 12 trenches were excavated. The deepest one has a depth of 18.3 cm. The appearance of the subsurface was different from trench to trench. In some trenches (such as Dodo Goldilock, Fig. 6) almost

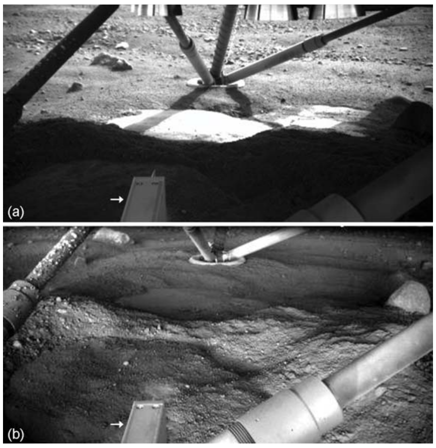

Fig. 4: Icy surface Holy Cow: 'Swept clean' by the descent thrusters. View towards south. The RAC is the only camera onboard that is able to image the terrain beneath the lander. The TECP (white arrows in a and b) is by hardware design always within the field of view of the RAC, except for images of the scoop interior (Fig. 8a). (a): Sunlit Holy Cow at Sol 5, about 3 pm. (b): Holy Cow in twilight at Sol 97, about 2 am. Note also the ice accumulations on one of the struts (top left) which may have been formed out of liquid brine droplets early in the mission. Holy Cow is very shiny in backlight (a) as a result of its even surface. However, in reddish twilight Holy Cow has about the same brightness as ordinary soil material nearby (b) indicating that its surface is not pure ice.

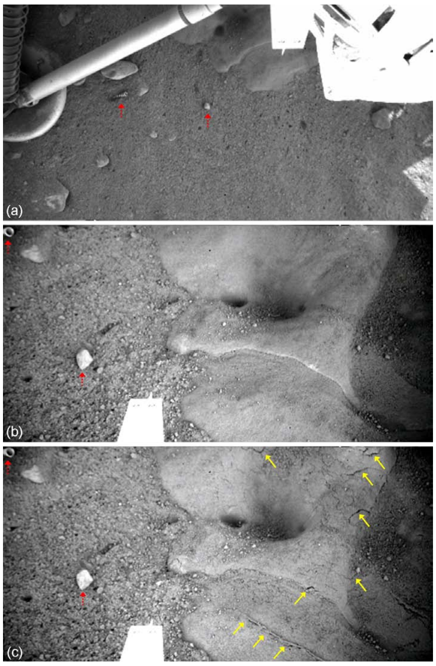

Fig. 5: Icy surface Snow Queen, 'swept clean' by the thrusters like the neighboring region Holy Cow (Fig. 4). (a): Overview, sol 5. View downwards and in southern direction. The northeastern leg (the one just cut off near the lower left corner of (Fig. 4b)) can be seen near the left end of the image (for scale, diameter of footpad is 29 cm). The red (dotted) arrows (denoting a screw and a small rock displaced by the thrusters) serve as reference in (b) and (c). (b): Enlarged view of Snow Queen, sol 21. (c): Snow Queen (sol 73) with fractures that have been formed since sol 21 (yellow arrows).

pure ice was found as testified by the VIS/NIR reflectance spectra acquired by the SSI. In other trenches ice-rich regolith was found, and sometimes no ice was found at all.

In the Dodo Goldilock trench, bright centimeter-sized clumps disappeared over the course of four sols (Fig. 6(a1) and (b1)). This observation suggests that the bright material in the shallow subsurface is indeed water ice. So far, no simple model has been developed that could explain the different ice/regolith mixing rates within a few meters. The current model for polygon formation has been developed by Sletten (Sletten at al, J. Geophys. Res. 108, 2003) and is illustrated in Fig. 7: Seasonal contraction and expansion of soil generates wedge-shaped fractures. During winter, some fine-grained debris moves into these wedges and prevents them from completely closing again during the next summer. The seasonal stress generated by these processes is relaxed by the formation of mounds ('polygons') at a certain spatial frequency. The net result is a slow cyclic transport of soil material. This erosional process is known as cryoturbation and occurs frequently in terrestrial periglacial environments.

The Heimdall crater was formed about 500 million years ago. Since excavations from this crater have likely contributed to the soil at the landing site signatures from this age should be expected. However, the above described cryoturbation processes occur over a much shorter time scale, continuously renew the landscape and made the Phoenix landing site the youngest among all Martian landing sites (Viking, Mars Pathfinder, Mars Exploration Rovers). The images shown above attest to the absence of larger rocks or boulders (say $>$ 20 cm) at the landing site. Do we have an easy explanation for this? Fig. 4 – 6 demonstrate the abundant occurrence of water ice near the surface in agreement with Odyssey 2002 data. Perhaps the absence of larger rocks can be explained by the high concentration of condensed volatiles (water ice) in the subsurface that were affected by the Heimdall impact: A violent explosion would have removed and crushed the rocks that may have been at the landing site in the first place. A systematic study (yet to be carried out) of the correlation between rock density and distance to nearest crater may provide further understanding of the rock size distribution at the landing site.

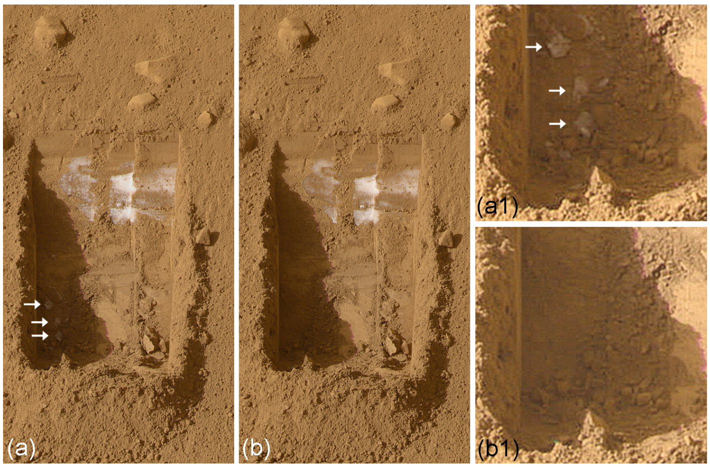

Fig. 6: Dodo Goldilock. (a): Sol 20. The trench (also visible in Fig. 1) is about 20 cm wide (corresponding to three scoop widths with little overlap). Note the uncovered (nearly pure) ice in the upper part of the trench. (b): As (a), but four sols later. The particles ($\sim$ 2 cm in diameter, marked in Fig. (a) by white arrows) have disappeared on sol 24 corresponding to a sublimation rate of $\sim$ 200 μm/sol. The figures (a1) and (b1) are enlarged sections of a and b, respectively.

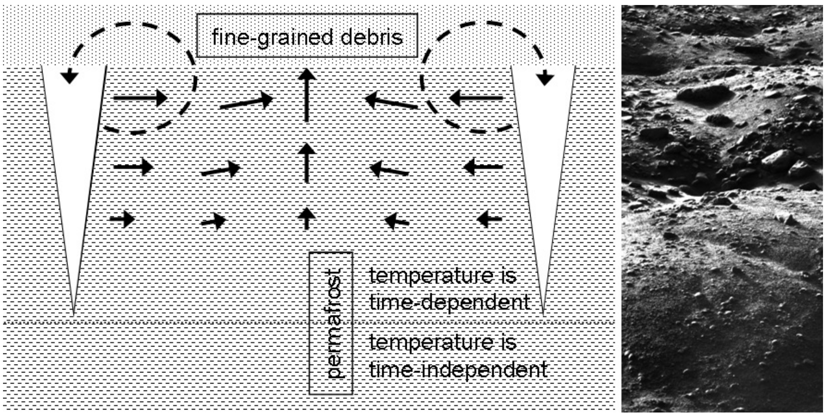

Fig. 7: The formation of polygons by cryoturbation (after Sletten): Wedge-shaped gaps form during winter and partially fill with fine debris which prevents a complete closure during summer. The resulting surface stress leads to the formation of several-meters large mounds ('polygons'). The dotted arrows illustrate the long-term motion of soil material. The solid arrows represent local velocity vectors. Below a certain depth (the depth of the sand wedges) the soil temperature is independent of seasonal variations as a result of thermal insulation by the material above. An active (uppermost) layer with temporal melting does not exist on Mars. Assuming abundant occurrence of water ice and a geothermal gradient of $\sim$10°C/km, the permafrost zone extends down to a few kilometers. Even deeper bedrock may contain liquid water, although the porosity of the rock is very small at such depths. The backlight in the SSI image (sol 61, view towards ENE, 3:51 am) enhances the three-dimensional shape of the polygons (about 7 m away from the lander).

Properties of Soil Material

Some of the Phoenix instruments have provided new insights into the microscopic structure (AFM, OM, RAC) as well as into the mineralogy (TEGA, WCL) of the soil material. Fig. 8(a) presents one of the many RAC images of the scoop interior that allowed a very first visual characterization of the soil material. The material shown in Fig. 8(a) was transferred on the same sol (sol 66) to one of the WCL cells (Fig. 8(b)). After addition of 25 cm^3 of a known aqueous solution (the leaching solution) to 1 cm^3 of soil material a weak alkaline solution (pH$\sim$ 8.3) was obtained that contained surprisingly large quantities of perchlorate (ClO_4-). The latter ion was by far the dominant anion in the solution. Among the cations magnesium, sodium, calcium, and potassium were found (here listed in sequence of decreasing concentration) (Hecht et al., Science, 325, 2009). An (assumed) sample mass of $\sim$ 1 g would imply a perchlorate abundance of about 1 wt% in the Martian soil. Such a concentration exceeds the one found in some terrestrial desert soils by orders of magnitude. Finding chlorine at the highest possible degree of oxidation has significant implications for our understanding of the chemical processes on the Martian surface as well as

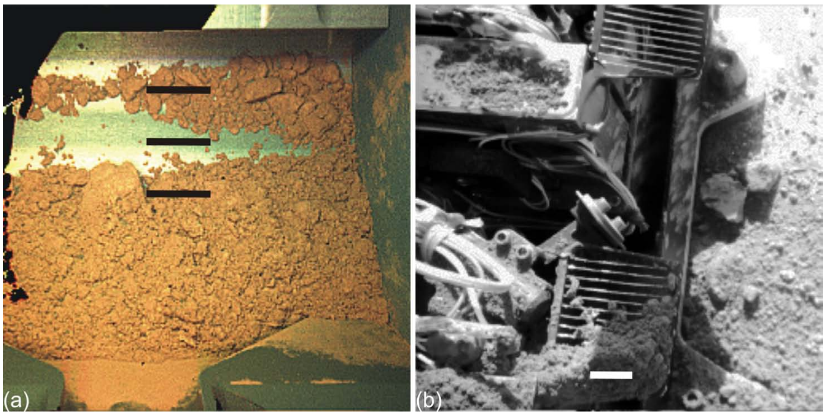

Fig. 8: (a): Soil sample in the scoop (RAC, sol 66). A RAC colour image is generated by combining three images (acquired during illumination by red, green and blue LEDs, respectively) into an RGB composite image. The black regions (upper left) correspond to sunlit regions and do not contain any colour information, as the radiant power of direct sunlight is significantly higher than that of the LEDs. (b): WCL cell #0, which the soil sample (shown in a) was transferred to. The black and white scale bars are 10 cm long. Cohesive soil material (organized into centimeter-sized clumps) is visible both in the scoop and on the grid of the WCL cell.

in the atmosphere and raises several important questions: Is the perchlorate just an exotic compound at the Phoenix landing site or is it wide-spread on the surface of the planet? And the corollary: Is the chlorine identified by all previously landed missions (Viking Landers, Mars Pathfinder, MERs) mostly present as perchlorate? Even the old question about life on Mars must be re-formulated: Which types of primitive (terrestrial) life forms could have evolved in the Martian soil, given the measured perchlorate concentration?

The ISE, which is sensitive to the Hofmeister series of ions (including perchlorate and nitrate), provided such a strong signal that the identification of perchlorate was unambiguous (the mass of nitrate needed to explain the ISE signal would have exceeded the total mass of the analyzed soil sample). However, any ISE (as used by WCL) is sensitive to a range of different ions with significantly different sensitivities. The conversion of ISE data into concentrations is therefore non-unique. Constraints by other data sets are needed and the TEGA data play an important role here. Thermal decomposition products of perchlorates were generally not detected in TEGA mass spectra, although this does not jeopardize in any way the WCL identification of perchlorate. At least in one of the samples analyzed by TEGA (Baby Bear, sol 25) some oxygen release (oxygen in molecular form, O_2) was observed that may be due to the decomposition of perchlorate (Hecht et al., Science 325, 2009). An important TEGA finding is the release of carbon dioxide in the temperature range 800 – 900°C that is diagnostic for the presence of 3 – 5 wt% calcium carbonate in the soil (Boynton et al., Science 325, 2009).

The result is remarkable, given that this mineral has been headhunted for many years: TEGA found it in the soil! The inferred presence of carbonates is also compatible with WCL results and explains e.g. the alkaline pH of the aqueous solutions. Also, the absence of certain gases can provide critical information on the mineralogy of the Martian soil: No sulfur dioxide has been released over the entire temperature range (from below 0°C and up to 1000°C). This is surprising, as all previous landed missions have identified substantial quantities of sulfur in the Martian soil (5 – 10 wt% SO_3). The presence of sulfate ions is compatible with WCL data. Magnesium sulfate would release SO_2 at temperatures below 1000°C. The absence of this gas therefore proves the absence of magnesium sulfate in the soil. In the Martian environment (atmospheric pressure of roughly 10 mbar), calcium sulfate (gypsum, anhydrate) would decompose at about 1400°C, but such temperatures are not reached by TEGA. All these facts taken together point towards the (likely) presence of calcium sulfate in Phoenix soils.

In fact, large deposits of calcium carbonate have been found on the surface of Mars, in particular adjacent to the north-polar ice cap (Langevin et al., Science 307, 2005). Fig. 9 shows microscopic colour images as well as a three-dimensional representation of a dust particle that was scanned by AFM. It is unclear how representative that latter particle may be for Martian dust in general. The microscopic images demonstrate the large diversity of particles. The reddish (orange) dust dominates (by volume) in Fig. 9(b). The individual dust particles cannot be resolved by the microscope and must therefore be smaller than $\sim 10\,\mu$m. According to a preliminary classification, two different types of grain are present in the soil (Fig. 9(a)–(b)): Reddish-brownish to colourless grains (solid arrows)

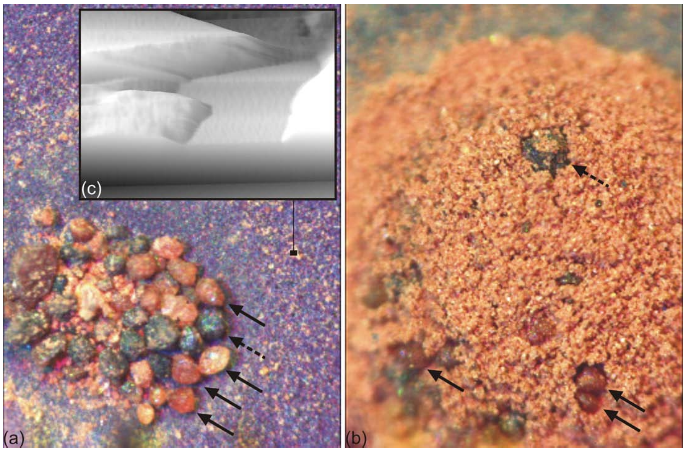

Fig. 9: Microscopic images of soil material. (a): Sol 58. About 60 μm large (silt- to sand-sized) grains of different colour on bluish magnetic substrate. (b): sol 122: The same types of grains (as in panel (a)) distributed throughout a matrix of orange-coloured cohesive dust. The dust particles (diameter¡ 10 μm) cannot be resolved by the microscope. The whitish-to-brownish grains (solid arrows) have likely been formed by a different process than the darker (almost black) ones (dotted arrows). The soil material in Fig. (a)–(b) is magnetizable, as it sticks roughly to the center region of the substrates that are oriented vertically in the local gravity field. The imaged areas in Fig. (a)–(b) are 1 mm wide. (c): Detail of a dust particle (sol 74, about 20 μm from left to right) that has been generated from AFM data. It is unknown if this is a representative morphology. The small black rectangle in Fig. (a) is an analogue area that would be as large as the one presented in Fig. (c).

and almost black grains (dotted arrows). The origin of these grains is uncertain, but careful comparison to terrestrial analogue soils (yet to be carried out) may constrain the potential scenarios for the formation of these grains.

Nice Weather

Phoenix instruments have enabled new types of meteorological measurements at the landing site. The success of the returned data has several reasons: 1) The polar regions exhibit strong weather phenomena, especially cloud formation (as known from orbital imagery). 2) The Phoenix meteorological station is a powerful instrument suite that includes a LIDAR instrument next to the usual pressure/temperature sensors (onboard the Viking Landers and Mars Pathfinder, but missing on MER). Also, the Telltale has returned data on wind velocity and direction throughout the mission enabling fruitful modeling. The meteorological station is highly synergetic with the TECP humidity sensor. 3) Phoenix weather measurements were coordinated with orbital observations (Odyssey, MRO) on a regular basis throughout the mission, strengthening the science return of all data sets.

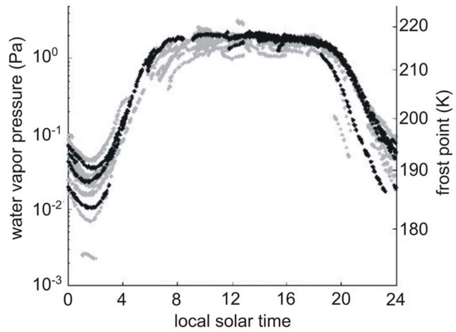

Fig. 10: The atmospheric water vapor pressure as measured by TECP about 5 cm (black) and 1 m (gray) above the surface. Each pressure value corresponds to a frost point (second ordinate), at which the water vapor would be in equilibrium with an idealized water ice reservoir at the same temperature. The water vapor pressure increases in the early morning hours and reaches a plateau value ($\sim$ 1.8 Pa, 220 K) by 10 am. Later on it remains constant throughout the day despite the further increase of the atmospheric temperature to at least 230 K. The constant water vapor pressure is likely caused by the fast mixing and re-distribution of newly formed water vapor throughout the atmospheric boundary layer.

Fig. 10 plots the atmospheric water vapor pressure (as measured by the TECP humidity sensor) against the local solar time. The water vapor pressure rises between about 2 am and 10 am, then reaching a plateau value ($\sim$ 1.8 Pa) that is maintained throughout most of the day, while atmospheric temperatures continue to rise until about 2 pm. Apparently, the atmospheric convection becomes very efficient and rapidly redistributes the newly formed water vapor after 10 am. Fig. 11 shows a dust devil that passed by the spacecraft on sol 104 with typical wind velocities (5 – 10 m/s). Analysis of the pressure data acquired throughout the mission show that such dust devils are correlated with brief pressure dips of 1 – 3 Pa.

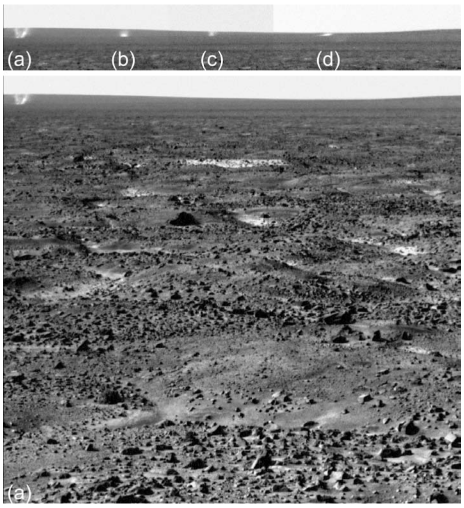

Fig. 11: Dust devil (sol 104, view towards west, the field of view is roughly 13.9°x13.9°). (a): Local time: 11:53:50 am. (b): 51 s after (a) (Martian seconds). (c): 100 s after (a). (d): 155 s after (a). The dust devil in Fig. (a) is about 1 km away from the Phoenix lander and about 5 m in diameter. It moves away from the lander (distance to the lander about 1.7 km in Fig. d). Larger dust devils have been observed in the Gusev crater (Greeley et al., J. Geophys. Res. 111, 2006).

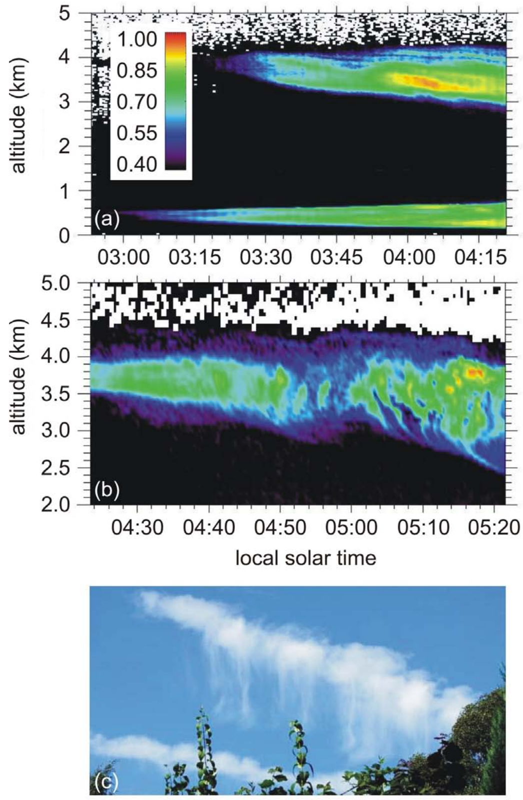

Arnsberg, Germany, 08-Aug-2007

Fig. 12: Night clouds as characterized by LIDAR. The colours in (a) and (b) are backscattering intensities in relative units. (a): Sol 98, 03:00-04:15 am. Ice clouds at the top of the atmospheric boundary layer (~ 4 km altitude) as well as ground fog formed every night after sol 80. (b): Sol 99, 04:20-05:20 am. Ice cloud with fall streaks. The latter ones form by sublimation of (freely falling) ice crystals and are bent as a result of different wind velocities at different altitudes. The cloud descends by about 800 m in the time frame 04:20-05:20 am. From the descent velocity (~ 0.2 m/s) the size of the ice particles is calculated to be about 60 μm according to using Stokes' formula. (c): Image of similar terrestrial fall streaks (Image: M. Thiessenhusen).

LIDAR data from the later part of the mission are particularly important (Whiteway at al., Science, 325, 2009): Ground fog as well as water ice clouds near the top of the atmospheric boundary layer (~ 4 km altitude) formed every night post sol 80 (Fig. 12(a)). Many of these clouds had fall streaks formed by initially growing, free-falling, and eventually sublimating ice crystals (Fig. 12(b)). Fig. 12(c) shows terrestrial fall streaks for comparison. Note that Fig. (a)–(b) are time diagrams of a fixed narrow sky sector overhead, while Fig. (c) is an ordinary photo (image of a spatially extended object at a given time). Thus, a direct comparison assumes a laterally homogeneous cloud layer that moves steadily through the LIDAR field of view. Day-time LIDAR data showed mostly dust in the atmospheric boundary layer. However, some SSI images documented sublimating day clouds with associated fall streaks.

In summary, Phoenix instruments were able to monitor the complete diurnal water cycle: During morning hours water vapor is released into the atmosphere. The sources for the water vapor include the shallow subsurface water ice, water adsorbed to soil grains, and (possibly) crystal water in perchlorates (such as $Mg(ClO_4)$ $2.6H_2O$). During the night, water vapor condenses and falls out by gravity. Most of these ice crystals sublimate again on their descent through the atmospheric boundary layer. In some cases snow fall was observed, as the fall streaks extended all the way down to the surface.

Present Status of the Phoenix Mission and Future Prospects

Phoenix surface operations lasted from late spring to late summer (26 May – 2 November 2008, 152 sols). The polar night started at the landing site on April 1 and ended on 10 July 2009. Since then the Sun has risen again above the horizon. If the spacecraft – contrary to all expectations – survived the low temperatures during winter (~ 150 K) and the dry-ice load on the solar panels, will be able to reanimate itself via the so-called Lazarus mode. Mars Odyssey is scheduled to search for Phoenix signals from mid-October 2009.

Independent of a potential reanimation, Phoenix was a highly successful mission that provided in-situ geo-

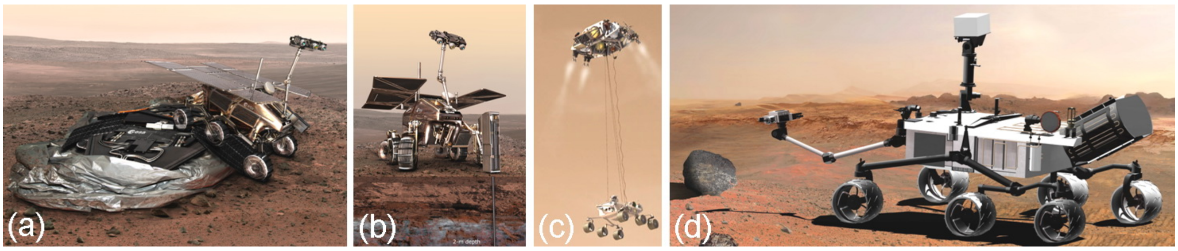

Fig. 13: The next lander missions to Mars: (a) and (b): ExoMars, ESA (launch 2016). (c) and (d): Curiosity, NASA, launch in fall 2011. ExoMars shall be landed on airbags (a). However, Curiosity will be using the new sky crane technology that allows for a precision landing by lowering the rover on a rope (c). All images are approximately at same scale (except for c). Note the significant difference in size between ExoMars and Curiosity.

chemical and atmospheric data and ground truth for the first arctic landing site ever explored. No organic molecules were found at the landing site. In particular, no traces of previous or present biological activity were found. Hence, the search for organic molecules is assigned to future missions (Fig. 13). It should be noted that organic molecules ought to be present in Martian soil due to the steady in-flux of certain types of meteorites (CC meteorites) that contain substantial quantities of organic material. The fact that no such molecules have been found in the soil indicates the occurrence of fast degradation processes that keep the equilibrium concentration very small. The ever continuing turnover of soil material (cryoturbation) at the landing site may have favored such degradation processes (Fig. 7). If organic molecules are ever detected, it will be a major scientific task to track down the origin of these molecules: Imported from outside by comets or meteorites, or attesting to primitive (extinct) life forms on the surface of Mars?

Although no organics have been found so far, it is essential to continue this exploration program and search for organic material in more protected environments, such as the interior of sedimentary rocks or deeper soil layers. The next missions that are available for this task are the rovers Curiosity (NASA, start 2012) and ExoMars (ESA, start 2018) (Fig. 13). They will carry complex TEGA follow-up instruments that will search for organic molecules in specific equatorial regions: SAM (Sample Analysis at Mars/MSL) and MOMA (Mars Organic Molecule Analyzer/ExoMars). The latter instrument is presently under development at the Max Planck Institute for Solar System Research. The former instrument is ready to go (NASA Goddard Space Flight Center) and will be able to detect particularly low concentrations of potential organic material. Special attention will be given to the molecule methane (CH_4) whose presence has recently been demonstrated (Mumma et al., Science 323, 2009), and whose isotope ratio C-13/C-12 will be measurable at extremely low methane concentrations ($<$ 1 ppb).

Further reading
Phoenix special issue, Science 325, 2008.
Many of the results described above were presented at the Lunar and Planetary Science Conference XL, The Woodlands, Texas, 2009.

(W. Goetz)

III. Sonne und Heliosphäre / Sun and Heliosphere

Übersicht der Projekte / overview of projects

Dargestellt ist die Dauer der verschiedenen Projektphasen (farbcodiert) einzelner Instrumente. Nähere Beschreibungen können den Jahres- bzw. Tätigkeitsberichten des MPS entnommen werden.

The different project phases of each instrument are shown colour-coded. Descriptions of these instruments can be found in the annual reports of the MPS.

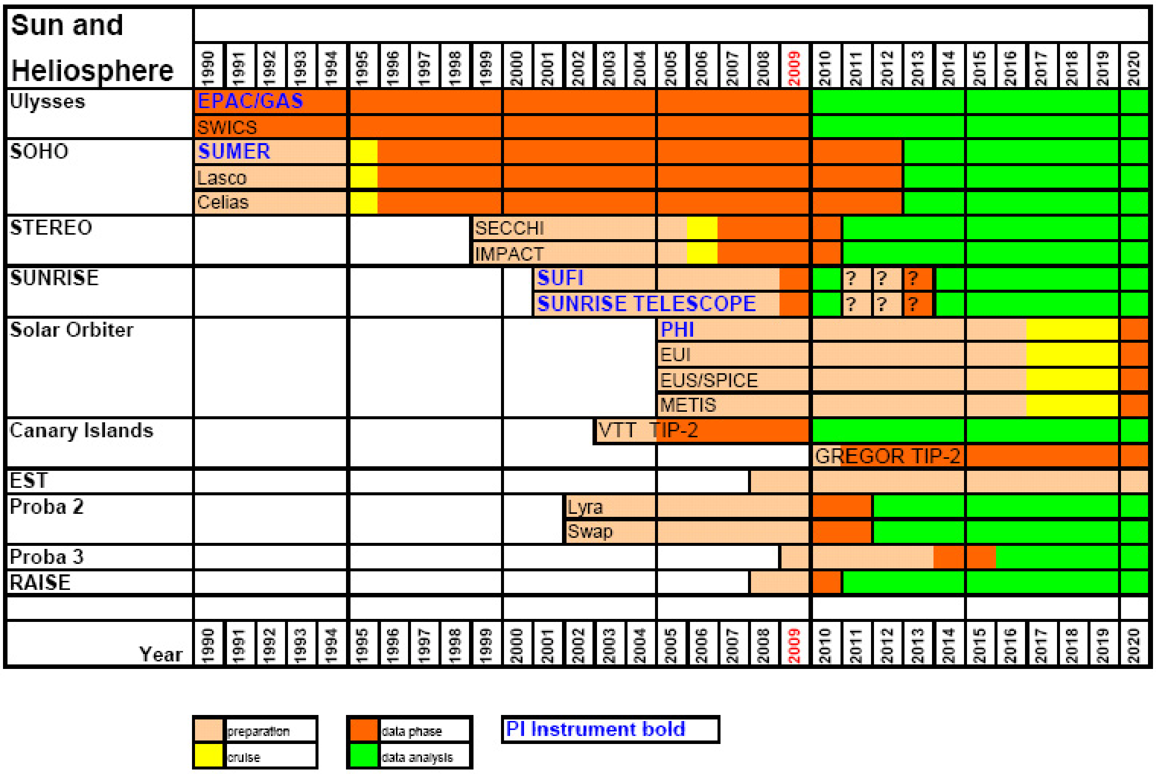

Solar interior, photosphere and chromosphere

Photospheric vortex flows at supergranular junction

It has been commonly acknowledged that the photospheric motions on the quiet Sun consist mainly in convection cells of different scales, starting from the granulation of 1 Mm up to the supergranulation of 30 – 40 Mm. At granulation scales, vortex flows were already reported. At larger scales, whirls and rotating sunspots were also observed.

With the use of a new efficient and noise-tolerant tracking technique called ball-tracking, we have revealed the existence of large vortex flows (see Fig. 14 formed in the quiet Sun, at the intersection of the supergranular network lanes. These junctions are the place where the downflow regions of neighbouring supergranules meet each other, creating a wide sink for the flows. The photospheric plasma is then entrained in a rotating motion like in a bath tub, forming vortices of ∼20 Mm typically, that also drive the magnetic flux at its center, and that can last several hours.

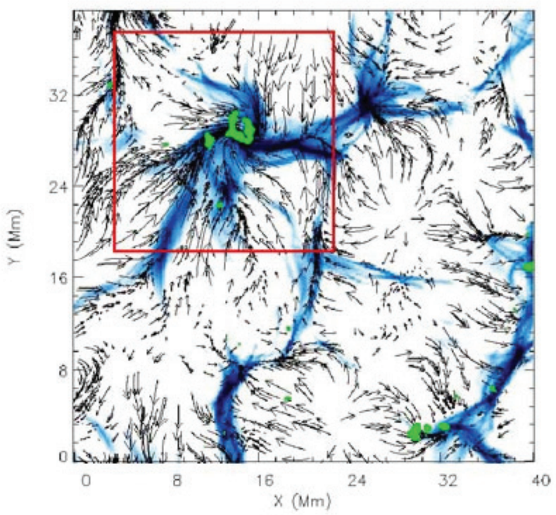

Fig. 14: Black arrows: velocity vector field near disk center on November 10, 2007. Green: filled contours of the maximum Ca II emission. The blue-shaded lanes in the background outline the network lanes, averaged over a few hours. The vortex flow is in the red square of sides ∼20 Mm.

(R. Attie and D. E. Innes in collaboration with H. E. Potts (Glasgow))

Expansion of magnetic flux concentrations

The appearance of network magnetic flux concentrations in circular polarization maps changes from unipolar at disk center to bipolar near the limb. This is consistent with network magnetic fields expanding and fanning out with height. To study the expansion properties we use circular polarization maps from the Solar Optical Telescope (SOT) on the Hinode *satellite. We do this by characterizing how the appearance of network flux concentrations changes from the solar disk center to the limb. The center-to-limb approach lets us examine the expansion of magnetic flux concentrations at different viewing angles and at different heights due to the shift in formation height of spectral lines as a function of μ ($\mu = cos(\theta)$, where θ is the viewing angle). To further expand the height coverage we use data from the narrowband filter imager (NFI) NaD_1 channel and spectropolarimeter (SP) observations of the Fe I 630 nm lines formed lower in the photosphere. We combine the observations with modeling the expansion of magnetic flux with height by using the thin flux tube approximation and realistic 3-dimensional magneto-convection simulations made with the MURaM code.*

Due to expansion of magnetic flux with height the appearance of magnetic features in NaD_1 filtergrams changes from unipolar at disk center to bipolar close to the limb (Fig. 15). As one moves away from the disk center towards the limb the circular polarization radial cuts change from having a single peak (unipolar cuts) to having two peaks with opposite signs (bipolar cuts). As expected based on geometrical considerations of a changing viewing angle of an expanding flux concentration, the ratio of the peaks ($|a_{center}|/|a_{limb}|$) decreases toward the limb. A similar trend is seen in the Fe 630 nm lines but, unlike the higher formed NaD_1, unipolar features are seen close to the limb as well.

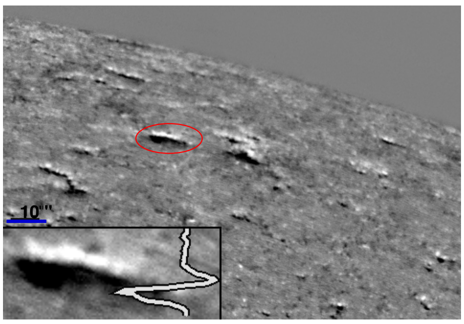

Fig. 15: Na D_1 circular polarization filtergram at the North pole. Left corner is a zoom-in of the circles feature. The white line is the radial profile of the feature. Blue line shows the spatial scale, $10''$.

Radial cuts based on synthetic spectra from thin flux tube models at varying viewing angles show a similar change from unipolar to bipolar, provided the tube radius is large enough, above ≈ 300 km. The bipolar features begin to emerge at $\mu \approx 0.5$ and the ratios

($|a_{center}|/|a_{limb}|$) decrease with decreasing μ. The synthetic ratios are similar to those observed. The MURaM simulations of an isolated magnetic flux concentration also show indications of the bipolar structures. The expansion of the field is strongly dependent on the upper boundary condition used for the magnetic field: a potential-field boundary condition creates a canopy-like structure close to the top of the simulation domain whereas a vertical boundary condition does not allow the field to expand as strongly.

(A. Pietarila, R. Cameron, and S. K. Solanki)

Evidence for convection in Sunspot penumbra

High-resolution observations provide evidence for convection in sunspot penumbrae, visible as twisting motions of bright filaments when observed perpendicular to their axes at intermediate heliocentric angles. However, as yet there is no knowledge whether these motions actually contribute to the heating of the penumbra, although estimates suggest that they have the potential to do so.

We used time series of blue continuum (4500 Å) images of sunspots located out of disk center observed with the Broadband Filter Imager (BFI) of the Solar Optical Telescope (SOT) onboard Hinode to study properties of the twisting motions in penumbral filaments, as shown in Fig. 16.

We analyzed twisting motions in different parts of penumbral filaments, in filaments located at different positions in sunspots and in sunspots at different heliocentric (viewing) angles. We found that these motions take place at rather different speeds, with the speed even varying along a single filament. Thus, in a statistical sense filaments display more rapid twisting in their inner than in their outer parts. The twist velocity is found to correlate best with the local intensity of the filament. The obtained correlation between intensity and horizontal twist velocity confirms their interpretation in terms of a manifestation of overturning convective flow perpendicular to the filament's major axes. This interpretation also suggests that they contribute significantly to energy transport in penumbra.

(L. Bharti, S. K. Solanki, and J. Hirzberger)

VFISV: Very Fast Inversion of the Stokes Vector

Inversion codes applied to the radiative transfer equation for polarized light allow us to infer the magnetic field on the solar surface from observations of the Stokes vector (I, Q, U, V; i.e: spectropolarimetry) in spectral lines. New space-borne instruments are delivering huge amounts of data that needs to be processed in real time.

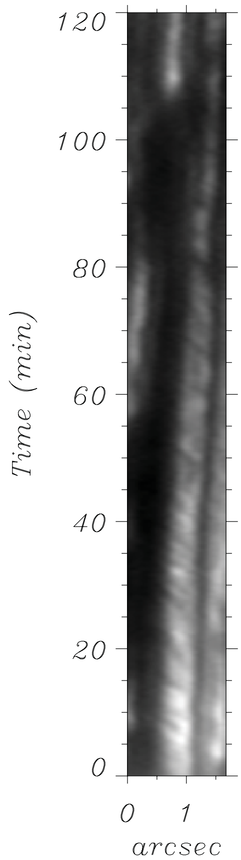

Fig. 16: Space-time plot for a penumbral filament along a line perpendicular to it's major axis. With time, the filament moves towards the umbra, so that this time slice samples different parts of the filament at different times. The slope of the dark stripes indicate horizontal velocity. More horizontal stripes imply more rapid twist while more inclined stripes imply slower twist. A correlation of filament brightness and horizontal velocity can be seen.

We have developed a new inversion code for the polarized radiative transfer equation (VFISV: Very Fast inversion of the Stokes vector). VFISV will routinely invert the Stokes vector in the Fe I 6173 Å spectral line recorded with the Helioseismic and Magnetic Imager (HMI) on-board of the Solar Dynamics Observatory (SDO) satellite. HMI will provide full-disk maps (4096×4096 pixels) of the Stokes vector in this spectral line every 10 minutes. For this reason VFISV is optimized to achieve an inversion speed that will allow it to invert 16 million pixels every 10 minutes, thus providing full-disk maps of the magnetic field vector on the solar surface with a cadence of 10 minutes. A map of the field strength in AR 10923 is shown as an example in Fig. 17.

(J. M. Borrero)

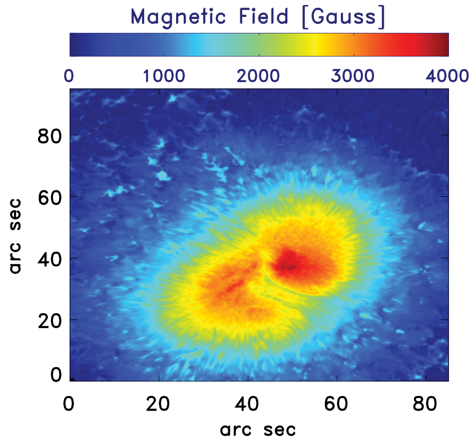

Fig. 17: Map of the Magnetic Field Strength in AR 10923. This region was observed with the spectropolarimeter onboard *Hinode* on 14 November 2006. This magnetic field was obtained through the inversion of the Stokes profiles of Fe I 630 nm. The inversions were carried with the VFISV inversion code and took only 227 seconds to be completed. This new ultra-fast inversion code shall be very usefull for the treatment of large data sets provided by new generation satellite instruments.

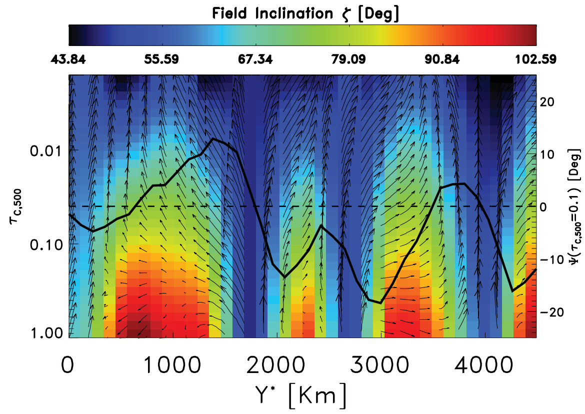

Fig. 18: Two dimensional slice perpedicular to the penumbral filaments showing the depth-dependence of the magnetic field inclination ζ (with respect to the vertical to the solar surface). The direction of the magnetic field vector in the Y-τ plane is indicated by the arrows. The solid black line indicates the value of the azimuthal angle of the magnetic field, Ψ, for a fixed optical depth $\tau_{c,500} = 0.1$. This figure shows that the penumbral magnetic field is formed by regions of highly inclined field ($\zeta \simeq 90°$, intraspines) surrounded by regions of more vertical field (spines, $\zeta \simeq 45°$). The change in the sign of the azimuthal angle Ψ denotes that the magnetic field in the spines wraps around the intraspines (see also arrows).

Evidence of magnetic field wrapping around penumbral filaments

The details of the small-scale magnetic structure of sunspot penumbrae continue to be largely unknown, with several models competing to explain it. In order to shed some light on this controversy, we have employed high-spatial-resolution spectropolarimetric observations from the Solar Optical Telescope onboard the Hinode *spacecraft to investigate the fine structure of the penumbral magnetic fields. The Stokes vector of two neutral iron lines at 630 nm is inverted at every spatial pixel to retrieve the depth-dependence of the magnetic field vector, line-of-sight velocity and thermodynamic parameters. We show in Fig. 18 that the azimuthal angle of the magnetic field vector has opposite sign on both sides above the penumbral filaments. This is consistent with the wrapping of an inclined field around the horizontal filaments. This large scale (hundreds of km) organization of the penumbral magnetic field seems to contradict a penumbra consisting of optically thin inhomogeneities (MISMA model).* Borrero et al. *(2008)*

(J. M. Borrero and S. K. Solanki)

Field-free gaps as the origin of Net Circular Polarization in Sunspot Penumbrae?

In a previous work we have ruled out the existence of optically thin inhomogeneities (MISMA model) in the penumbral magnetic field. In this work we focus on two other important models under consideration: embedded flux-tubes and field-free gaps models. To distinguish among these two we have employed a penumbral model that includes the Evershed flow and convective motions inside penumbral filaments, to reproduce the azimuthal Ψ-variation (Fig. 19) of the net circular polarization (NCP) in sunspot penumbrae at different heliocentric angles Θ. The theoretical (Fig. 20) net circular polarization fits the observations very satisfactorily. We have also found that, in order to fit the observed the NCP, the strength of the magnetic field inside penumbral filaments must be around than 1000 G. In particular, field-free or weak-field filaments fail to reproduce the correct sign and dependence of the net circular polarization with the azimuthal and heliocentric angles. These results rule out the existence of field-free gaps in the penumbra.

(J. M. Borrero and S. K. Solanki)

Contrasts of magnetic features from magneto-convection simulations

Solar irradiance changes on a wide range of time scales and is a key driver of the Earth's climate where secular variability in particular is relevant. This is, however, not well understood and our knowledge relies on reconstructions based on sunspot numbers and similar proxies.

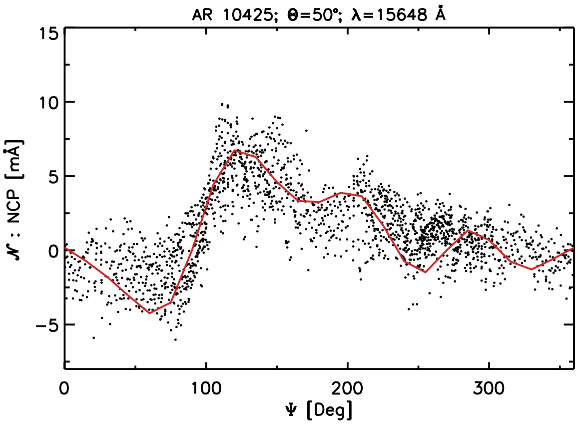

Fig. 19: Filled circles show the observed azimuthal (Ψ) variation of the Net Circular Polarization in penumbra of a sunspot at a heliocentric angle $\Theta = 50°$. The red solid line is the Net Circular Polarization reproduced by a penumbral model consisting of a penumbral filament with a magnetic field of 1000 gauss embedded in a penumbral surrounding field og 1000 gauss. Agreement is very satisfactorily.

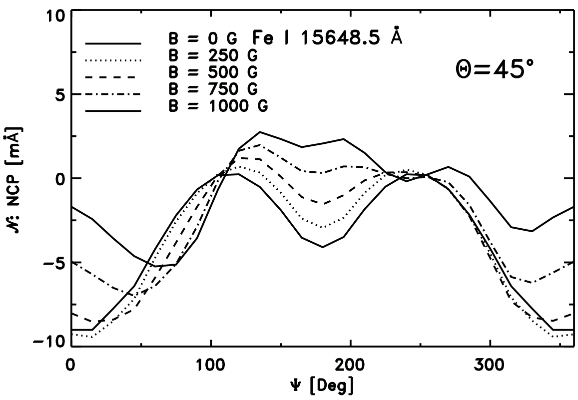

Fig. 20: Theoretical variations of the Net Cirular Polarization with the azimuthal angle Ψ in the penumbra of a sunspot at a heliocentric angle of $\Theta = 45°$. The different curves represent different field strengths inside the filament. For a magnetic field inside the penumbral filament of 1000 gauss (dashed-triple-dotted line) we obtain the same curve as in Fig. 19 (red solid line). For decreasing magnetic fields inside the filament the discrepancy between observations and theory grows, which indicates that the filaments cannot be field-free.

The prime candidate to produce secular variability is a change in the surface coverage of small-scale magnetic elements. Direct observational determination of the flux emitted by these magnetic elements is difficult, especially as information covering a large spectral range is needed. Here we present a theoretical approach to this problem using intensity calculations from 3-D simulations of solar magneto-convection and compare these with the intensity calculations used in the successful semi-empirical SATIRE models. Eventually, such a comparison should lead to the removal of the last free parameter from SATIRE-based irradiance reconstruction. In order to cover a broad wavelength range the ATLAS code of Kurucz is employed. As an important additional application of these computations, the output can be compared with high-resolution observations from Hinode and other sources, after the application of an appropriate point spread function.

(M. Schüssler and S. K. Solanki in collaboration with N. Afram, Y. C. Unruh (Imperial College London), and A. Vögler (Astronomical Institute Utrecht, The Netherlands))

A comparative study of radiative MHD modeling and Hinode observations of emerging flux regions

We have developed numerical models of emerging flux regions on the solar surface. To this end we have used the MURaM code to carry out 3-D radiative MHD simulations of the rise of buoyant magnetic flux tubes through the convection zone and into the photosphere. Owing to the strong stratification of the convection zone, the rise results in a lateral expansion of the tube into a magnetic sheet, which acts as a reservoir for small-scale flux emergence events at the scale of granulation. The interaction of the convective downflows and the rising magnetic flux tube undulates it to form serpentine field lines that emerge into the photosphere. The numerical results have been compared with new observations from the Hinode Solar Optical Telescope, including the pattern of the emerging flux regions (Fig. 21), the cancellation of surface flux and associated high-speed downflows, the convective collapse of photospheric flux tubes, the appearance of anomalous darkenings, the formation of bright points, and the possible existence of transient kilogauss horizontal fields.

(M. Schüssler in collaboration with M. C. M. Cheung, T. D. Tarbell, and A. M. Title (Lockheed Martin Solar and Astrophysics Laboratory, Palo Alto/California, USA))

Meridional flow and distribution of the polar magnetic field

The magnetic field near the solar poles plays an important role in solar and space physics. Its possible connection to the dynamo process has implications for predicting the solar cycle. It is related to the origin of the fast solar wind and is the dominant source of the interplanetary and heliospheric magnetic field. However, owing to the weakness of the polar field and the difficulty of observing the solar poles from the ecliptic, its structure is poorly known.

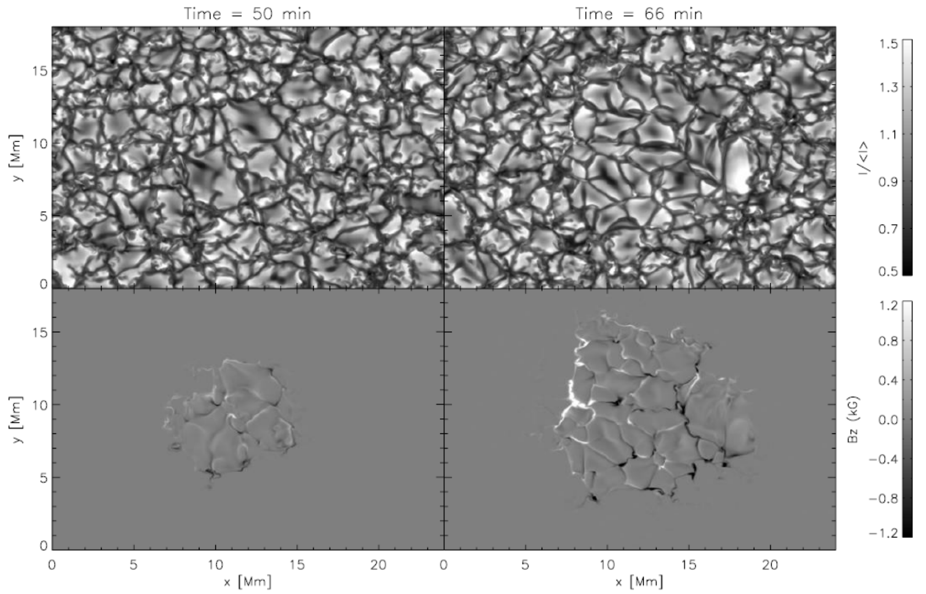

Fig. 21: Continuum intensity images (at 500 nm) and synthetic magnetograms of a simulated emerging flux region. The vertical component of the magnetic field (B_z) is sampled from the $\tau_{500} = 0.1$ surface along vertical lines of sight. The interaction of the flux tube with granular convective motions is clearly imprinted onto the surface flux pattern, which is far from a simple, tidy pair of opposite-polarity flux concentrations. Magnetic bright points in the intergranular lanes can be discerned in the snapshot at $t = 66$ minutes Cheung *et al.* (2008).

Recent observations indicate that the latitudinal profile of the magnetic field (Fig. 22) lux shows a pronounced decrease close to the solar north pole during the minimum phase of solar cycle 23. Using a surface flux transport model, which describes the redistribution of magnetic flux at the solar surface under the combined effects of differential rotation, supergranular diffusion and meridional flow, we have performed numerical experiments to study the conditions that could lead to such a latitudinal distribution. We find that a strong decrease of the magnetic field near the poles results if a weak countercell of the meridional flow at high latitudes with an equatorward speed of a few m s^{-1} is present. The existence of such a countercell has been suggested on the basis of results from helioseismology. The simulations also indicate that the total dipole moment of the solar magnetic field remains nearly unaffected by the presence of a polar countercell of the meridional flow.

(J. Jiang, R. Cameron, D. Schmitt, and M. Schüssler)

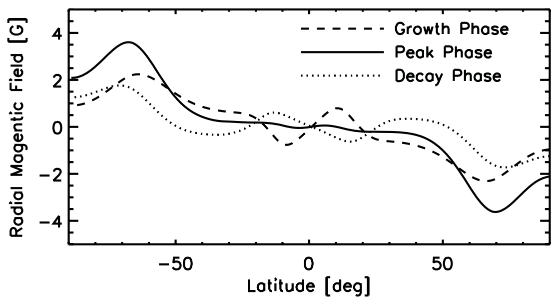

Fig. 22: Longitude-averaged surface magnetic field as a function of latitude for three phases of the polar field evolution (Jiang et al., doi:10.1088/0004-637X/693/2/L96, 2009).

Extended horizontal magnetic fields in the quiet Sun chromosphere

The combined action of the Hanle and Zeeman effect in the He I 10830 Å line offers a unique possibility to study chromospheric magnetic fields. Whereas the Zeeman effect allows reliable magnetic field measurements above ≈150 G, the Hanle effect grants access to the 1 G to 100 G regime. The proper treatment of the Hanle effect in the analysis of spectropolarimetric observations requires the solution of the radiative transfer equation by taking into account the impact of atomic level polarization. We implemented the forward calculation module of HAZEL (HAnle and ZEeman Light, Asensio-Ramos et al., 2008) into the MPS inversion code HELIX$^+$ *(**He**lium **L**ine **I**nformation **Ex**tractor, Lagg et al., A&A, 414, 1109, 2004). This improvement allowed us for the first time to quantitatively analyze the weak polarization signals above quiet Sun internetwork regions at chromospheric heights.*

Fig. 23 shows the linear polarization signal (Stokes Q) of a super-granular network cell, recorded in the He I 10830 Å line with the Tenerife Infrared Polarimeter 2

(TIP-2, Collados et al., Astron. Soc. Pacific Conf. Ser. 368, 611, 2007). Simultaneous measurements with the Hinode SOT/SP experiment confirmed the weak magnetization of the underlying photosphere (green rectangle). The formation process for the ground state of the He I *10830 Å transition involves ionization due to coronal UV radiation followed by recombination, making this transition free of any photospheric contribution. Therefore, the measured polarization signal exclusively stems from He atoms at chromospheric heights.*

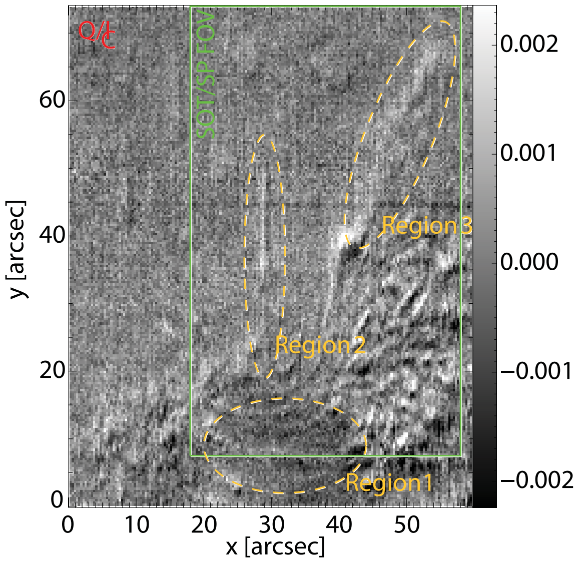

Fig. 23: Stokes Q map of a network region recorded with the Tenerife Infrared Polarimeter 2 (Collados et al., Astron. Soc. Pacific Conf. Ser. 368, 611, 2007). The orange ovals mark regions where linear polarization signal in He I 10830 Å was detected above weakly magnetized, photospheric areas.

The results of the inversions using the HeLIx$^+$ *code confirmed the presence of weak, horizontal magnetic fields at chromospheric heights above weakly magnetized, internetwork photospheric regions (see regions 1, 2, and 3 marked with orange ovals in Fig. 23). Field strengths in these region range from 20 G (region 3) to 200 G (region 1). The analysis shows that continuous, horizontal magnetic field structures at the height of the He* I *10830 Å line formation, resulting from the expansion of the network field, can exist above some parts of the quiet Sun photosphere. Obviously, the photospheric magnetic flux concentrations in the internetwork are not sufficiently strong to prevent the formation of canopy-like structures at chromospheric heights.*

(A. Lagg, L. Merenda, and S. K. Solanki)

The intensity oscillations in the chromospheric emissions

The role of dynamic processes in structuring the solar chromosphere remains a topic of intense debate. Most observations of such processes have been carried out in the visible and the ultraviolet. Millimeter wavelength radiation allows a different approach to studying the dynamics of the chromosphere, since it samples both hot and cool gas almost equally, unlike the observations at shorter wavelengths.

We searched for dynamic signatures in the intensities of the simultaneously observed chromospheric lines and continua. The data consist of radio images at 3.5 mm from the Berkeley–Illinois–Maryland Array (BIMA) and Ca II *K-line filtergrams from BBSO, analyzed together with MDI/SOHO photospheric dopplerograms. The interferometric millimeter data are obtained with the highest currently available spatial resolution of 12 arcsec.*

Several 30-minute duration time series of the best available quality were analyzed by means of the Fourier analysis techniques. We distinguish between the emission of the chromospheric network and its inner parts, applying the binary masks constructed from the calcium intensity distribution. In the chromospheric K-line emission and photospheric MDI velocities from the network locations most of the Fourier power is found at frequencies around 3.3 mHz, which is consistent with the classical picture of the 5-minute network oscillations. However oscillatory power in the mm data is distributed over a wider range of frequencies.

Chromospheric emission (both Ca II *K-line intensity and 3.5 mm brightness) from the internetwork shows significant 3-minute oscillations, together with oscillations at lower frequencies. We found low frequencies to be very prominent in the power spectra of the chromospheric data, especially in the mm data, which show oscillations with periods longer than 10 minutes both in the network and in the internetwork emission. The origin of these oscillations is not yet understood, although there is evidence that they are not instrumental. The discrepancy between the oscillatory behaviour of K-line and mm chromospheric emissions may be attributed to the difference in the resolutions of the analyzed observations and the difference in the heights of formation of these emissions.*

(M. Loukitcheva and S. K. Solanki in collaboration with S. White (University of Maryland, College Park, USA))

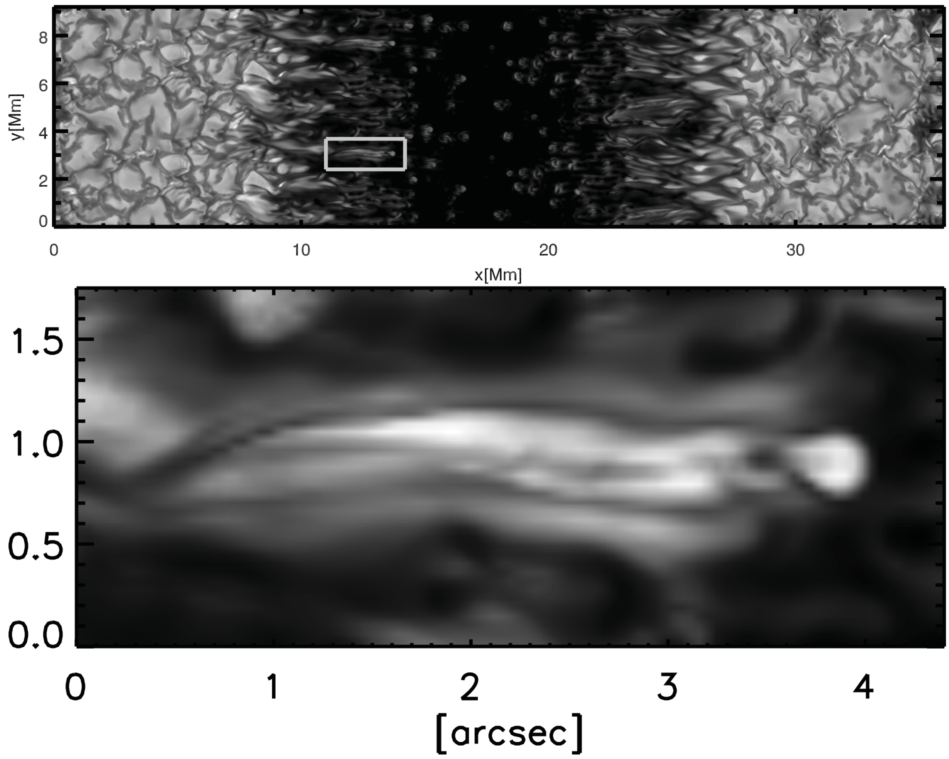

Fig. 24: Upper panel: Continuum intensity image at 630 nm of the simulated sunspot and its environment (doubled in the vertical direction). The bright umbral dots and penumbral filaments have peak intensities between 40 % and 90 % of the average value outside the spot. The penumbral filaments reach lengths of 2–3 Mm. Lower panel: detail of the penumbral filament outlined by the white frame in the upper panel (Rempel et al., Astrophys. J., 691, 640, 2009).

Radiative MHD simulation of sunspot structure

We have carried out a 3-D MHD simulation of a slab-like slice of a sunspot and the surrounding granular convection. The sunspot has a diameter of about 20 Mm, centered in a computational box spanning about 37 Mm × 4.6 Mm *in the horizontal directions and* 6.1 *Mm in depth. The simulation has been carried out with the MURaM code, which includes a realistic equation of state with partial ionization and radiative transfer along many ray directions. The simulated sunspot (Fig. 24) is divided in a central dark umbral region with bright dots and a penumbra showing bright filaments of about* 2 *to* 3 *Mm length with central dark lanes. By a process similar to the formation of umbral dots, the penumbral filaments are formed by magneto-convection in the form of upflow plumes, which become elongated by the presence of an inclined magnetic field: the upflow is deflected in the outward direction while the magnetic field is weakened and becomes almost horizontal in the upper part of the plume near the level of optical depth unity. A dark lane forms owing to the piling up of matter near the cusp-shaped top of the rising plume that leads to an upward bulging of the surfaces of constant optical depth. The simulated penumbral structure as shown in Fig. 24 corresponds well to the observationally inferred interlocking-comb structure of the magnetic field with Evershed outflows along dark-laned filaments with nearly horizontal magnetic field and overturning perpendicular ('twisting') motion, which are embedded in a background of stronger and less inclined field. Photospheric spectral lines are formed at the very top and somewhat above the upflow plumes, so that they do not fully sense the strong flow as well as the large field inclination and significant field strength reduction in the upper part of the plume structures.*

(M. Schüssler in collaboration with M. Rempel and M. Knölker (High Altitude Observatory, NCAR, Boulder/Colorado, USA))

Simulation of a flux emergence as seen by Hinode's SP/SOT and comparison with observations

We study the observational signature of flux emergence in the photosphere using synthetic data from a 3-D MHD simulation of a twisted flux tube emergence. Several stages in the emergence process are considered, starting from a relatively early appearance of the flux tube at the solar surface. At every stage *we compute the Stokes spectra of the two iron lines Fe I 6301.5 Å and Fe I 6302.5 Å, and degrade the data to typical spatial and spectral conditions of Hinode's SOT/SP. Then, following observational practice, we apply Milne-Eddington-type inversions to the synthetic spectra in order to retrieve different atmospheric parameters. We compare the results with observations (e.g. Okamoto et al. 2008, 2009). During the emergence sequence, the sepectral lines sample different parts of the rising flux tube, revealing its twisted structure. We infer the amount of twist in the field lines by studying the temporal evolution of the flux emergence. The horizontal component of the magnetic field retrieved from the simulations (Fig. 25) is similar to the observed one by Okamoto et al. (2008). We also observe a flattening of the flux tube above the $\tau_{5000} = 1$ level caused by radiative cooling, inhibiting the ascent of the tube to the upper solar atmosphere. Consistent with the observations, the overshooting magnetized plasma rising above the photosphere produces an apparent blue shift during a large fraction of the emergence sequence.*

(L. Yelles Chaouche, S. K. Solanki, M. Schüssler, and A. Lagg in collaboration with M. C. M. Cheung (Lockheed Martin Solar and Astrophysics Laboratory, Palo Alto, CA, USA))

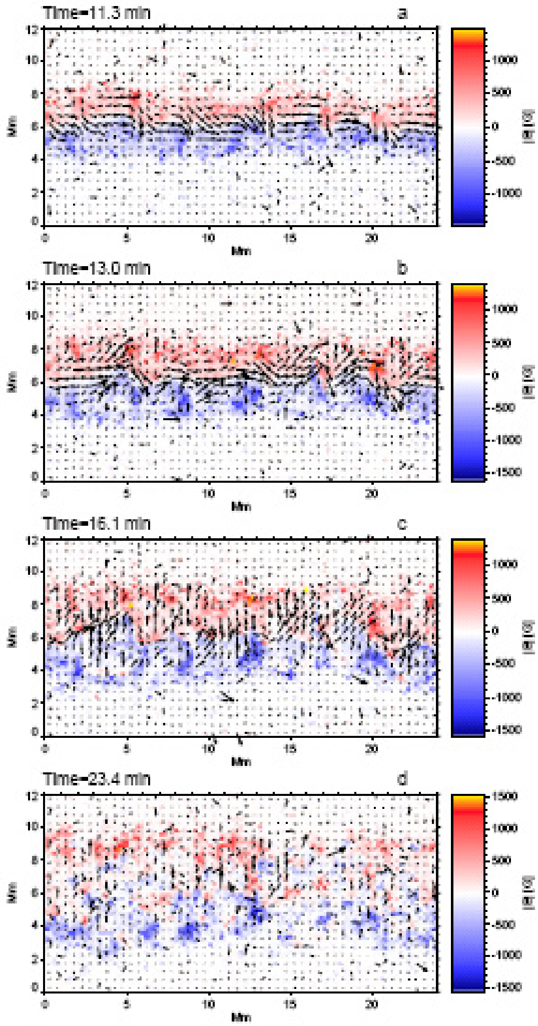

Fig. 25: Maps of the retrieved magnetic field vector from inversion of synthetic spectra. The colour code indicates the amplitude of the vertical (line-of-sight) component of the magnetic field. The orientation of the horizontal field components is shown by arrows. The maps correspond to (from top to bottom): $t = 11.3$, 13.0, 16.1 and 23.4 minutes.

Comparison of the thin flux tube approximation with 3-D MHD simulations

The structure and dynamics of small vertical photospheric magnetic flux concentrations has been very widely treated in the the thin flux tube approximation, based upon a low-order truncation of the Taylor expansions of all quantities in the horizontal direction, together with the assumption of instantaneous total pressure balance at the boundary to the non-magnetic external medium. Formally, such an approximation is justified if the diameter of the structure (a flux tube or a flux sheet) is small compared to all other relevant length scales (scale height, radius of curvature, wavelength, etc.). However, no reliable test of the validity of this approximation in a realistic situation dominated by turbulent magnetoconvection has so far been carried out. The advent of realistic 3-D radiative MHD simulations opens the possibility of checking the consistency of the approximation with the properties of the flux concentrations that form in the course of a simulation. We carry out a comparative analysis between the thin flux tube/sheet models and flux concentrations formed in a 3-D radiation-MHD simulation. In particular, we compare the distribution of the vertical and horizontal components of the magnetic field in a 3-D MHD simulation (Fig. 26) with the field distribution in the case of the thin flux tube/sheet approximation. We also consider the total (gas plus magnetic) pressure in the MHD simulation box. We find that above the solar surface flux concentrations with super-equipartition fields are reasonably well reproduced by the second-order thin flux tube/sheet approximation, even when their diameter exceeds the pressure scale height. The relatively small differences between approximation and simulation are due to the asymmetry and the dynamics of the simulated structures. Below the surface the approximation breaks down due to the strong influence of the convection on the magnetic structure.

(L. Yelles Chaouche, S. K. Solanki, and M. Schüssler)

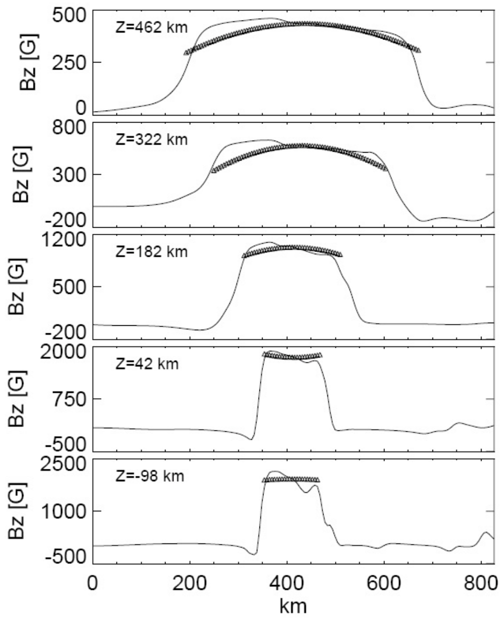

Fig. 26: Solid lines: vertical component of the magnetic field, B_z, along 5 horizontal locations (at different altitudes indicated in the upper left corner of each frame) across a thin flux sheet formed in the course of MHD simulations. The triangles represent B_z resulting from a second-order thin flux sheet model

Minimum height of chromospheric and coronal structures

Measurements of the magnetic field vector in the solar chromosphere and corona are of great importance, since the field controls the structure and dynamics of the Sun's upper atmosphere. One powerful diagnostic technique is based on the inversion of spectropolarimetric data obtained in the He I 10830 Å multiplet. This multiplet is sensitive to a large range of magnetic fields via the Hanle and Zeeman effects. The Zeeman effect has been widely used for measuring the strongest magnetic field of solar active regions while the Hanle effect has been used to measure weaker fields in a variety of structure, like prominences and spicules, observed off-limb. On-disk measurements using the Hanle effect have also been performed on filaments and regions of emerging magnetic flux, but in these cases the height of the He layer causing the absorption signature, a parameter necessary for the determination of the magnetic field vector, was arbitrarily set or estimated using different methods.

Since the height of the observed structure is also an important parameter to be determined in on-disk observations, we studied the possibility of using the Hanle effect in the saturation regime to determine at least a minimum height for these structures.

We make use of the fact that in the saturation regime of the Hanle effect the linear polarization depends in a complicated way on the geometry of the magnetic field and that it is proportional to the degree of anisotropy of the radiation field. The latter is a function of the height of the observed structure above the visible solar surface. By comparing the observed linear polarization profile with the maximum possible polarization signal obtained for each height, we can determine a lower limit of the observed He structure (see Fig. 27). Our analysis demonstrates that a minimum height of 5 Mm is required to produce the observed linear polarization signal, which in this case is consistent with the interpretation that the signal is from the top of an emerging magnetic loop, as originally proposed by Solanki et al. (2003).

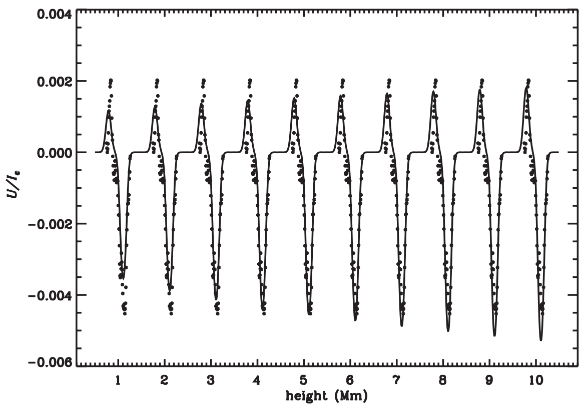

Fig. 27: Linear polarization profile observed on 13 May 2001 in an emerging flux region (Solanki et al., Nature, 425, 692, 2003). Comparisons with the maximum linear polarization signal from theoretical computations confirm a minimum height of 5 Mm for the observed He structure.

(L. Merenda, A. Lagg, and S. K. Solanki)

Spectropolarimetric investigations of the deep photospheric layers of solar magnetic structures

Solar surface magnetism manifests itself in a variety of structures with sizes often comparable to or even below our spatial resolution capabilities. Nevertheless, sub-resolution information about the intrinsic atmospheric structure can be obtained via indirect techniques. We use spectropolarimetric observations in carefully selected photospheric lines which include C I (5380.3 Å) as well as the strong Fe I (5379.5 Å), Fe I (5383.4 Å) and Ti II (5381.0 Å) lines to determine the temperature stratification of the deep photosphere with a technique independent of the spatial resolution [Solanki & Brigljević, 1992]. The decrease in ratio of the Stokes V amplitude [Solanki, 1987] of C I relative to the other lines with increasing Stokes V amplitude (Fig. 28) of those lines indicates that the magnetic fea-

tures in regions with little magnetic flux are on average hotter and brighter than in regions with higher flux. Inversions, done with the SPINOR code (Frutiger et al., Astron. & Astrophys., 358, 1109, 2000), provide quantitative support for a decrease in temperature from 6830 K to 6580 K from weak to strong signal. In Fig. 28, a_b and a_r represent the amplitudes in the blue and the red lobe of the Stokes V/I_c signal, respectively.

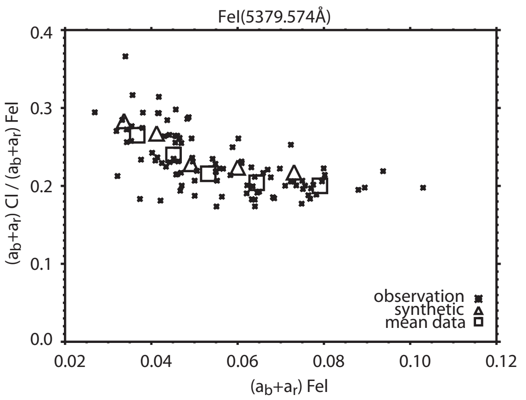

Fig. 28: Stokes V amplitude ratio of C I to Fe I. Stars indicate the amplitude ratios of each individual observed Stokes V/I_c profile, triangles represent the amplitude ratios of synthetic profiles while the amplitude ratios of the binned observed profiles are given by the open squares.

(N. Oklay, S. K. Solanki, A. Lagg, and A. Gandorfer)

Center-to-Limb Variation of the continuum contrast as a function of inferred magnetic parameters

The center-to-limb variation (CLV) of the continuum contrast of magnetic features represents a valuable constraint for flux tube models, as well as a useful input to reproduce the total solar irradiance. However, precise measurements are difficult because the contrast depends on the atmospheric and magnetic parameters of those features (field strength, amount of flux, surrounding granulation etc.), and is severely affected by the observing conditions (seeing).

Here, we present the first assessment of the dependence of the continuum contrast of magnetic features on both the heliocentric angle and on their magnetic properties. The magnetic parameters (field strength, filling factor and inclination) were inferred by Milne-Eddington inversions (VFISV) of seeing-free spectropolarimetric maps with high spatial resolution (Hinode/SP), covering a continuous range of μ between 1 and 0.2 in the quiet Sun.

The contrast was found to behave differently in two distinct regimes of magnetic flux (or "apparent flux density"), characterizing fields that are tied to granulation and strong network-like magnetic features, respectively (separated by the green dashed line in Fig. 29). The weak fluxes seem to be "wrapped" around granules: pixels with horizontal fields are on average located within granules and are brighter, while pixels with more vertical fields are preferably located in the intergranular lanes and are thus darker. For the stronger fields, the contrast CLV was found to depend essentially on the flux, with a rather symmetric dependence on the field strength and on the filling factor, while the fields are quasi-vertical (see Fig. 29). In particular, the pixels associated with such fields reach positive contrast values at disk center, in contradiction with previous studies performed at lower spatial resolution.

(P. Kobel and J. M. Borrero Santiago)

Magnetic field structure and plasma dynamics of a weak solar flare

Solar flares are most likely caused by a sudden release of magnetic energy due to plasma instabilities or magnetic reconnection. The dynamics of large X-class flares have been intensely studied in the last decades. The structure of smaller flares is much less clear since an in-depth study requires higher resolution observations, particularly, magnetograms.

A weak solar flare eruption (B7.8) as shown in Fig. 30 which was registered during a multi-channel polarimetry and imaging campaign at the Swedish Solar Telescope (SST) in La Palma, was studied in detail. Near-diffraction-limited blue continuum images, imaging polarimetric scans of the Fe I 6302 Å photospheric spectral line, as well as narrow band filtergrams of the Ca II H 3968 Å line made possible a reconstruction of the photospheric magnetic field and plasma flow structure. In addition, the chromospheric magnetic field structure could be guessed from the Ca II H observations.

The obtained structure can be fitted into a global picture of the flaring process as developed for larger flares. The observed region includes several islands of negative magnetic polarity in a positive polarity surroundings. According to this flare model the islands of negative polarity are connected to the adjacent regions by short loops leading to a closed core field enveloping the neutral line around the islands. Close to the magnetic neutral lines the fields are strongly sheared which is very often the case prior to a flare eruption. A separatrix surface encloses the islands. The footpoints of the separatrix surface enclose the entire region. In our case, this intersection of the separatrix with the surface marks the footpoints of the branches of Ca II H

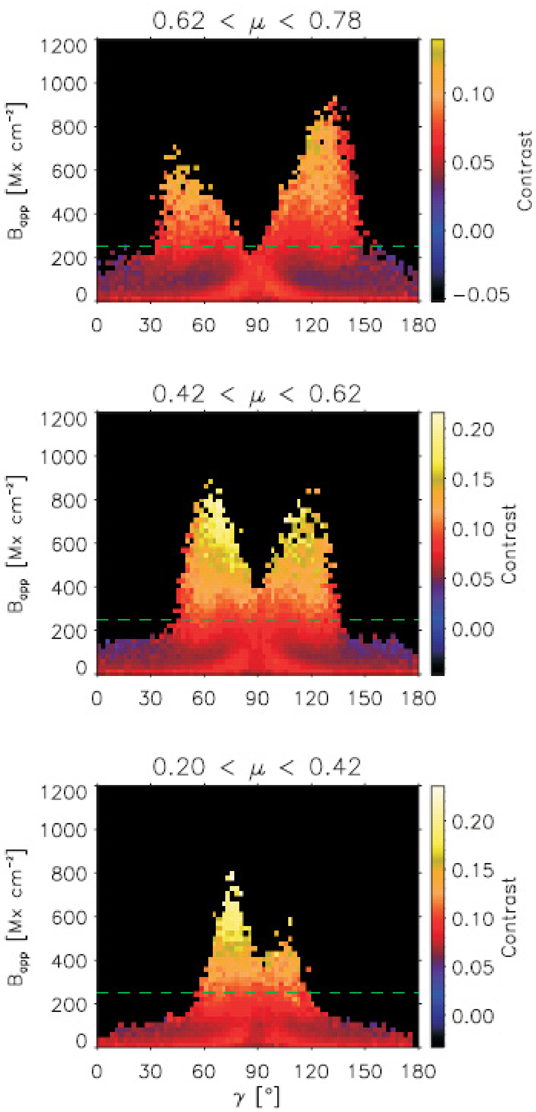

Fig. 29: Variation of the contrast as a function of both the "apparent flux density" B_{app} and γ in a 2-dimensional binning representation, in three different intervals of μ. The pixel contrast has been averaged into bins of 2.5° width in γ and 25 Mx cm^{-2} width in B_{app}. Dashed green: limit separating two distinct regimes of flux (see main text). Bins with less than 10 data points (pixels) are set to black. A common colour scale is used for the average contrasts in all μ intervals.

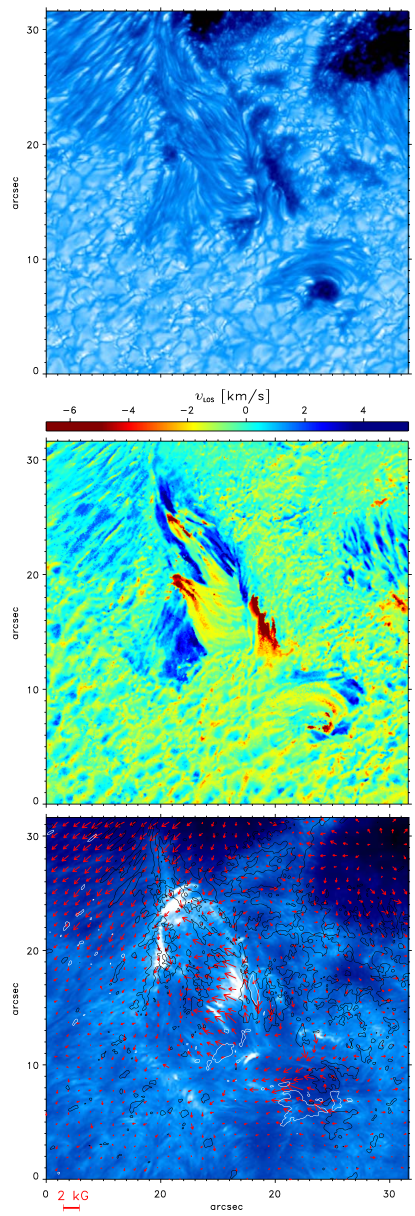

Fig. 30: Multi-channel observations of a weak solar flare. Upper panel: blue continuum image; middle panel: photospheric line-of-sight velocities; lower panel: Ca II H line core image overplotted by the photospheric magnetic field (contours are at -250 G and 750 G).

fibrils which are connected to the interior of the flaring region and can be easily identified by a continuous brightness enhancement prior to and after the flare.

Primarily, we found a sizable increase of the islands of inverse polarity during the flare. This is consistent with the long-term evolution of the sunspot. The evidence suggests that the sunspot was formed by a merger of two spots of the same polarity. The two spots achieved closest proximity about one day before the flare and started to re-split (and decay) in the following days. In the photosphere we observed a crossing of several penumbral branches of opposite horizontal field direction. This is due to the penetration of the penumbra of one spot into that of the other during the merger of the two spots. This penetration might also drive the emergence of reversed polarity magnetic flux during the flare eruption. The eruption might even have been triggered by this flux emergence.

(J. Hirzberger, T. Riethmüller, A. Lagg, S. K. Solanki, and P. Kobel)

Measuring turbulent magnetic field cancellation in the quiet Sun

Determining the strength of the magnetization of the "quiet" Sun is tied to the question of how much flux resides at small scales. This is important for determining the energy budget available for chromospheric (and coronal) heating. Interpretations of Hanle depolarization observations estimate the mean magnetic field strength as $\langle|B|\rangle \sim 100\,G$, but are dependent on assumptions about the probability distribution function (PDF) of the turbulent magnetic field. Interpretation of Zeeman-effect observations require no assumptions of the PDF and estimate the mean unsigned vertical field strength as $\langle|B_z|\rangle \sim 10\,G$. The order-of-magnitude discrepancy is not unexpected since non-uniformity of the magnetic field direction at sub-resolution scales leads to cancellation of the Zeeman signature.

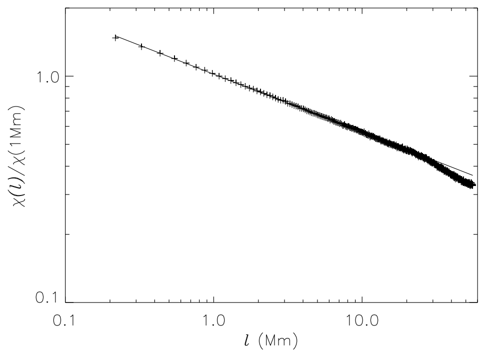

Fig. 31: Normalized cancellation function, $\chi(l)/\chi(1\,\mathrm{Mm})$, versus scale, l, from *Hinode* observation. A self-similar power-law is abundantly clear for 2 decades of length scales down to the resolution limit.

We employ the turbulent, fractal nature of the quiet Sun magnetic field to estimate the total Zeeman cancellation. We do this by measuring the cancellation function $\chi(l)$ – the portion of flux remaining after averaging over boxes of increasing size (see Fig. 31). We find a self-similar (fractal) power-law down to the observational resolution limit. From this, we can conclude that the scale of magnetic structuring in the photosphere must be 20 km or less. Estimating the magnetic dissipation scale as 80 m, we can extrapolate the power law to determine the true (resolution independent) unsigned vertical field strength $\langle|B_z|\rangle_{\mathrm{true}} > 46\,G$. This agrees with our MURaM simulation-based estimate of at least 80 % cancellation at 200 km resolution and (considering vector magnitudes) resolves the discrepancy between Hanle and Zeeman observations.

(J. Pietarila Graham, S. Danilovic, and M. Schüssler)

Solar transition region and corona

Origin of the solar wind in network funnel

The origin of the solar wind is a long standing issue in both observational and theoretical studies. To understand how and where in the solar atmosphere the mass and energy of the solar wind are supplied is very important. Previous observation suggests a scenario in which the fast solar wind originates at heights above 5 Mm in the magnetically open coronal funnel, a process that is accompanied by downward flow below 5 Mm, whereby mass and energy are supplied through reconnection between the open funnel and adjacent closed loops. Based on this scenario, we developed a new fluid model to study the solar wind generation under the assumption that mass and energy are deposited in the funnel at 5 Mm, which is illustrated in Fig. 32.

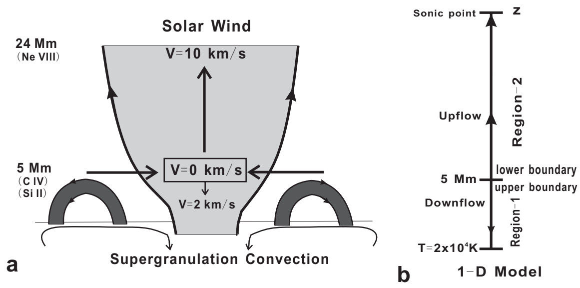

Fig. 32: (a) Sketch to illustrate the scenario of the solar wind origin and mass supply, and to show that supergranular convection can be the driver of solar wind outflow in coronal funnels. (b) Sketch of the two computational domains in the model. Region-2 ranges from its lower boundary at 5 Mm to its upper unfixed boundary at the sonic point. Region-1 ranges from its upper boundary at 5 Mm to its lower boundary with a temperature of 2×10^4 K where hydrogen atoms begin to become fully ionized. Mass flows upward in Region-2, and downward in Region-1.

The mass supply rate is estimated from the mass loss rate as it is given by emptying the side loops through their assumed reconnection with the funnel. Similarly, the energy input rate is consistent with the energy release rate as it is estimated from the energy flux associated with reconnection between the open magnetic funnel and the closed magnetic loops. Following the observations, we thus not only simulate the plasma flowing upward to form the solar wind, but also calculate the flow returning back to the lower atmosphere. Our model is a first attempt to study quantitatively this novel idea about the solar wind origin.

(E. Marsch in collaboration with C.-Y. Tu and J.-S. He (School of Earth and Space Sciences, Peking University, Beijing, China))

Coronal convection

Coronal convection is a generic term used here to emphasize that the plasma observed in the corona is not static but appears to flow everywhere, whereby it is strongly guided by the dominant magnetic field. The associated mass flux is likely supplied to, and lost from, the lower corona via various magnetic channels across the inner photosphere/chromosphere interface. Coronal convection presumably extends to the corona's outer interface, which is assumed to be located near the magnetic source surface at 2–3 solar radii, where the heliospheric field actually begins.

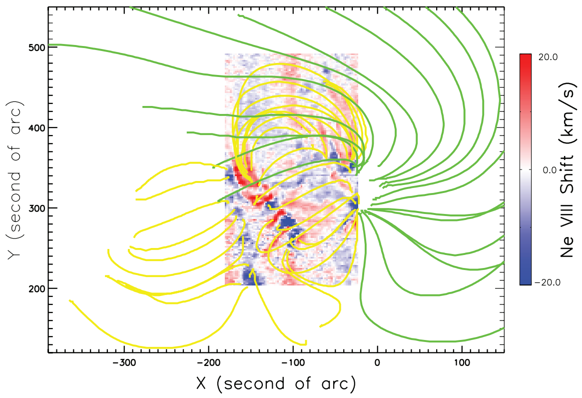

Fig. 33: SUMER Dopplergram of the Ne VIII line shift. The velocity scale is defined by the red/blue bar at the right side. Note that the magnetic field lines (closed, yellow, and open, green) start and end in patches of predominantly either red- or blue-shift, i.e., the legs of the magnetic field lines are associated with either up- or down-flows of plasma.

In this study new results are presented regarding the relationships between the coronal magnetic field and the intensities and Doppler shifts of ultraviolet emission lines. This combination of magnetic field and spectroscopic data (as shown in Fig. 33) is used to study material flows in association with the coronal field. The blueshifts and redshifts often seen in transition region and coronal ultraviolet emission lines are interpreted as upflows and downflows of the plasma on open (funnels) and closed (loops) coronal magnetic field lines, which tightly confine and strongly lead the flows in the low-beta plasma. Evidence for these processes exists in the ubiquitous redshifts mostly seen at both legs of loops on all scales, and the sporadic blueshifts occurring in strong funnels. Therefore, there is no static magnetically stratified plasma in the corona, but rather a continuous global plasma convection, being a natural perpetuation of the photospheric convection which ultimately is the driver.

(E. Marsch, H. Tian, W. Curdt, and T. Wiegelmann in collaboration with J. Sun (Mullard Space Science Laboratory, University College London, UK))

Drift instabilities in the solar corona

Recent observations revealed that the solar atmosphere is highly structured in density, temperature and magnetic field. The presence of these gradients may lead to the appearance of currents in the plasma, which in the weakly collisional corona can constitute sources of free energy for driving micro-instabilities. Such instabilities are very important since they represent a possible source of ion-cyclotron waves which have been conjectured to play a prominent role in coronal heating, but whose solar origin remains unclear.

Considering a density stratification transverse to the magnetic field, we studied the possible occurrence of gradient-induced plasma instabilities. We performed a Fourier plane waves analysis using the collisionless multi-fluid model. By neglecting the electron inertia, this model allows us to take into account ion-cyclotron wave effects that are absent from the magnetohydrodynamics. Realistic models of density and temperature, as well as a 2-D analytical magnetic-field model, are used to define the background plasma in the open-field funnel in a coronal hole.

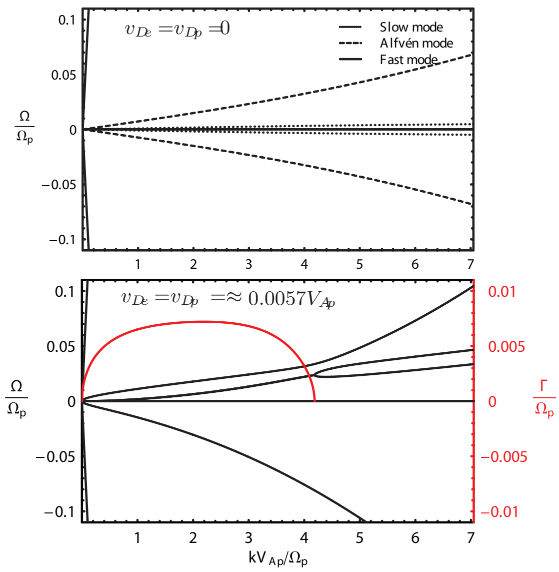

Fig. 34: Two-fluid (with $T_{0e} = T_{0p}$) dispersion curves in a funnel with a wave angle of propagation of $\theta = 85°$. Top: The case of a uniform plasma density, i.e. $v_{Dj} = 0$, with a plasma beta $\beta_e = \beta_p \approx 0.0097$. Bottom: Drift instability due to a density gradient with a small scale length of $L = 1$ km. Here ω and k are normalized, respectively, to the proton cyclotron frequency, Ω_p, and the proton inertial length, Ω_p / V_{Ap}, where $V_{Ap} = B_0/\sqrt{\mu_0 n_{0p} m_p}$ is the proton Alfvén speed (μ_0 is the magnetic permeability in vacuum).

We demonstrate in Fig. 34 that in such conditions, and when assuming a small transverse density length scale as suggested from radio observations, the current *generated by a relative electron-ion drift can provide enough free energy for driving waves unstable. This instability results from a coupling between oppositely propagating slow-mode waves. Thus drift currents caused by fine density structures in the corona can excite instabilities, which constitute a possible source of the sought after ion-cyclotron waves.*

(R. Mecheri and E. Marsch)

On the efficiency of nonresonant ion heating by coronal Alfvén waves

In the this parametric study, we discuss what is required for an efficient ion heating via nonresonant wave-particle diffusion without collisions. We consider a multi-ions, magnetized and homogeneous plasma, which consists of protons, helium and oxygen ions He^{2+} and O^{5+} (with the abundances $N_{\rm He}/N_p = 0.1$ and $N_{\rm O}/N_p = 10^{-3}$), and assume non-dispersive Alfvén waves propagating parallel to the magnetic field. Since we are interested in the nonresonant wave-particle interactions, the low-frequency Alfvén waves are assumed to have frequencies $|\gamma_k| < \omega_k \ll \Omega_i$.

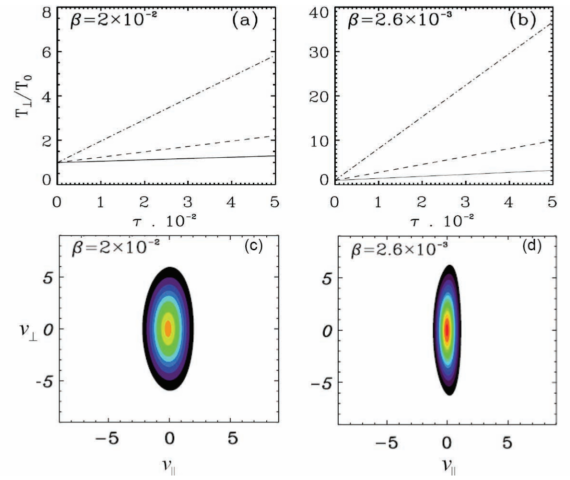

Fig. 35: (a) and (b): Perpendicular ion temperature normalized to the initial temperature, proton (solid), He^{2+} (dash line) and O^{5+} (dash-dot line). All temperatures are plotted versus the normalized wave energy τ. (b) and (c): The anisotropic velocity distribution function of O^{5+}.

As a result, the pitch-angle diffusion of ions leads to perpendicular heating. A closer inspection of the numerical values for different ions in Fig. 35 reveals in panel (a) and (b) that the perpendiculat ion temperature is inversely proportional to the plasma β, and proportional to the mass ratio m_i/m_p (with m_i and m_p being, respectively, the ion and proton mass). We find $(T_{i,\perp}/T_0 - 1) \propto (\tau/\beta\ m_i/m_p)$. The numerical results for the heating profiles of the ion species are plotted in Fig. 35 for $\beta = 2 \times 10^{-2}$ and 2.6×10^{-3}. It turns out that heating of the ions up to several million kelvin is in fact possible via nonresonant wave-particle interactions. But this heating requires a relatively large average wave amplitude and a small β.

(S. Bourouaine and E. Marsch)

Coronal loop model including ion kinetics

We have developed a semi-kinetic coronal loop model to study the mechanisms of loop heating. The model is based on a quasilinear treatment of the Vlasov equation for the reduced velocity distribution functions of the protons, which are the only ions considered in the loop plasma. For the energy input into the loop, we assume that linear Alfvén waves penetrate the loop from its footpoints and heat the protons via wave-particle interactions and wave absorption. Through Coulomb collisions between protons and electrons some thermal energy can be transferred to the electrons. The loop geometry is considered to be that of a semicircular cylindric and symmetric flux tube. The footpoints of the loop (where L is the loop length) are assumed to be emerging in the transition region, i.e., their height from the solar surface is about 2 Mm, and $s = 0$ refers to the left footpoint and $s = L$ to the right one. We simulate a static loop with symmetric heating and assume that Alfvén waves penetrate with the same wave-power density and wave energy flux ($F_0 \approx 7 \times 10^2$ J m^{-2} s^{-1}) the simulation domain from both footpoints and simultaneously heat the plasma. The final steady-state temperature profiles are presented in Fig. 36, for two values of the area expansion ratio Γ.

It turns out that in such a loop model protons are hotter than electrons, and in case of a nearly homogeneous flux-tube cross section, an almost flat temperature profile occurs along the major part of the loop with an enhanced plasma density. These plasma parameter profiles are consistent with those of loops having temperatures between 1 MK and 1.5 MK, as inferred from ultraviolet emission. However, if the magnetic field lines are more strongly diverging from the footpoints to the loop apex, the proton heating is found to be more uniform, resulting in a higher temperature and lower density along the loop. These profiles are similar to those observed in X-ray loops.

(S. Bourouaine and E. Marsch)

Multi-ions kinetic model for coronal loop

A multi-ions kinetic model for a coronal loop is presented, whereby ion heating in the magnetically confined plasma is achieved by absorption of ion-cyclotron waves. We assume that linear

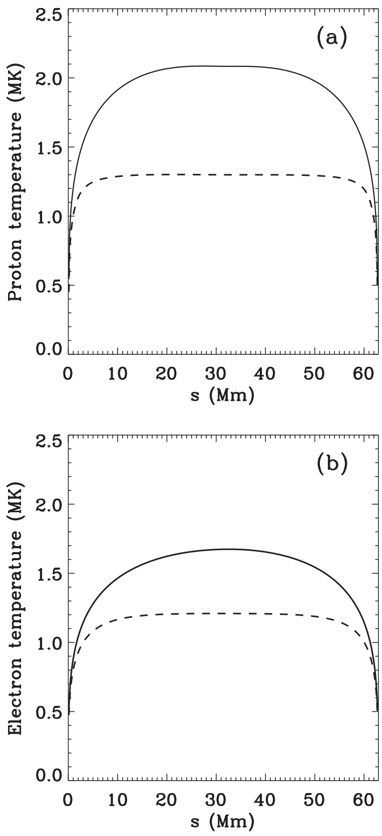

Fig. 36: (a): Proton temperature, (b): Electron temperature for $\Gamma = 1.48$ (line) and $\Gamma = 1.04$ (dashed line) versus distance along the loop.

Alfvén/cyclotron waves penetrate the loop from its footpoint and directly heat the ions. We model the coronal loop as a plasma column confined within a thin magnetic flux tube which has semicircular cylindrical geometry. The flux tube expands with height by a factor $\Gamma = 1.48$.

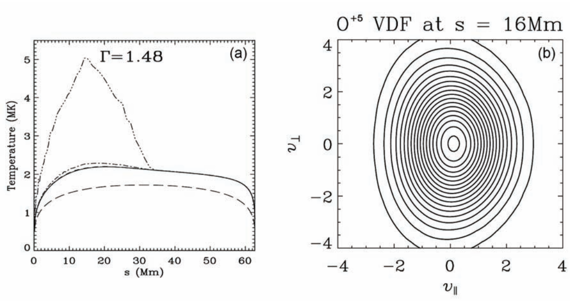

Fig. 37: (a): Proton and helium temperature (line), $T_{\parallel,O^{5+}}$ (dashed dotted line), $T_{\perp,O^{5+}}$ (dashed double-dotted line) and electron temperature (dashed line) as a function of distance s along the loop. (b): The velocity distribution function (VDF) of oxygen plotted for a loop with $\Gamma = 1.48$ at $s = 16$ Mm .

The kinetic temperature is plotted for each ion species in Fig. 37. It turns out that protons and He^{2+} *ions show the same isotropic temperature profiles along the loop. However, the heating of* O^{5+} *in the left part of the loop is higher in the perpendicular direction with respect to the mean magnetic field. This leads to a considerable temperature anisotropy, with* $T_\perp/T_\parallel > 1$. *The kinetic parallel temperature of* O^{5+}, $T_{\parallel,O^{5+}}$, *hardly differs from the temperatures of the other ion species. The perpendicular temperature* $T_{\perp,O^{5+}}$ *behaves differently, as it increases rapidly and then reaches values of up to 5 MK at* $s \approx 16$ *Mm, leading to a maximal temperature anisotropy. The electrons are found to be cooler than the ions. The electron thermal energy gained from ion-electron collisional heat exchange is reduced by the effects of the radiative losses and the strong heat conduction of the electrons. Therefore, this expanding coronal loop is far from local thermal equilibrium and shows remarkable temperature differences between electrons and ions.*

(S. Bourouaine and E. Marsch)

Cool and hot components of a coronal bright point

Coronal bright points (BPs) are small-scale phenomena in the solar corona and characterized by enhanced emission in X-ray, extreme-ultraviolet (EUV) and radio wavelengths. The energization of BPs may result from the interaction between two magnetic fragments of opposite polarities, magnetic reconnection along separator field lines or current sheets induced by photospheric motions. Recently, it was suggested that different processes may be responsible for the powering of the bright point at different heights.

By analyzing SUMER and EIS data, we performed a systematic study of the Doppler shifts (see Fig. 38) and the electron densities measured in an EUV bright point observed in more than 10 EUV lines with formation temperatures from $\log(T/\mathrm{K}) = 4.5$ *to 6.3. Those parts of a BP seen in transition region and coronal lines are defined as its cool and hot components, respectively. We found that the transition from cool to hot occurs at a temperature around* $\log(T/\mathrm{K}) = 5.7$. *The two components of the BP reveal a totally different orientation and Doppler-shift pattern, which might result from a twist of the associated magnetic loop system. The analysis of magnetic-field evolution and topology seems to favour a two-stage heating process, in which magnetic cancelation and separator reconnection are powering, respectively, the cool and hot components of the BP. We also found that the electron densities of both components of the BP are higher than those of the surrounding quiet Sun, and comparable to or smaller than active-region densities.*

(H. Tian, W. Curdt, E. Marsch, and J.-S. He)

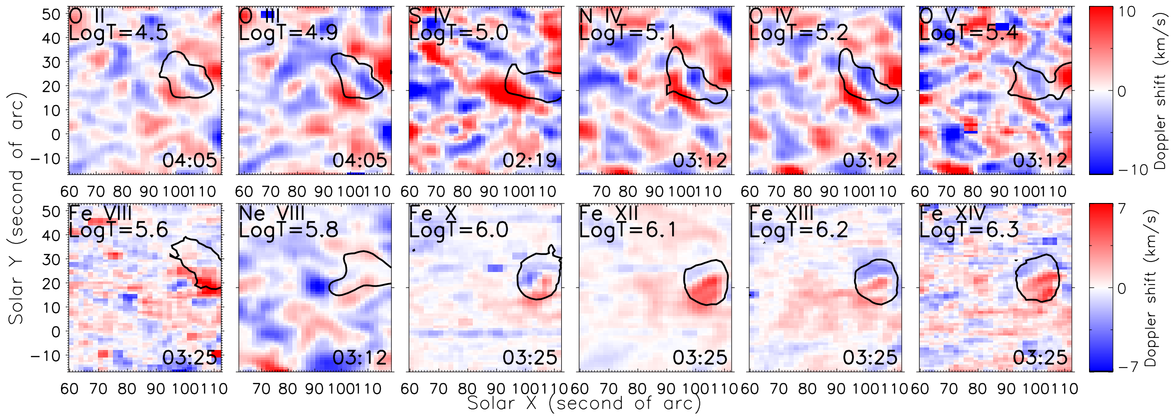

Fig. 38: Dopplergrams of different EUV lines indicated in the top left corners, together with the logarithms of their formation temperatures. The approximate time when the BP was scanned is shown in the lower right corner of each map. The black contours outline the positions of the BP as seen in different wavelengths.

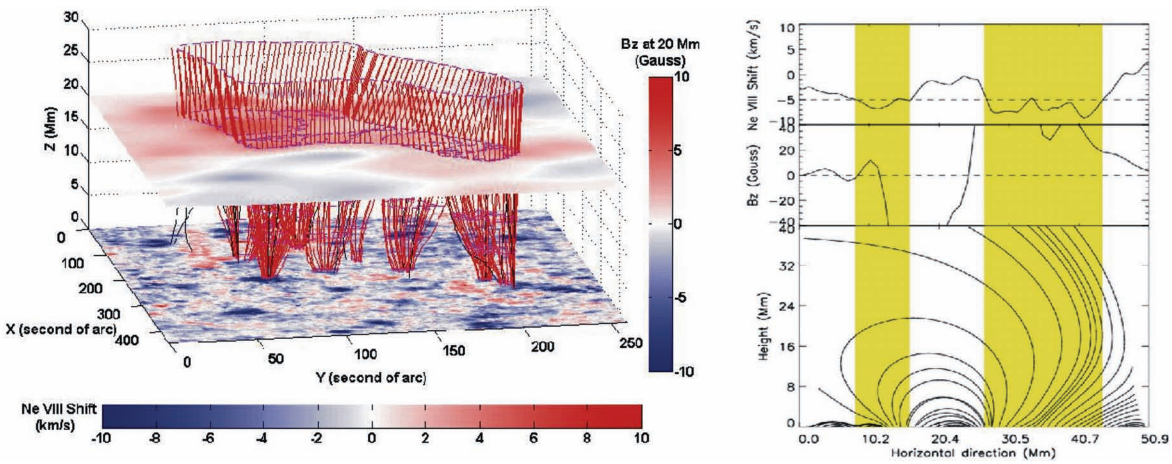

Fig. 39: Left: Magnetic funnels in a quiet sun region. The red lines are field lines originating from the funnel boundary, and the black ones are open field lines outside small funnels. Right: Ne VIII Doppler shift, line-of-sight component of the observed photospheric magnetic field strength along a horizontal cut, and magnetic field lines projected onto the vertical plane defined by the cut through the extrapolation box.

Signature of mass supply to quiet coronal loops

The blue shift of the Ne VIII line is considered to be a signature of solar-wind outflow in coronal holes. In the quiet Sun, large Ne VIII blue shifts were also found in the network junctions as shown in Fig. 39. This work attempts to understand this large quiet-Sun blue shift, by carefully checking the surrounding magnetic environment.

The significant Ne VIII blue shifts, which are visible as large blue patches on the Doppler-shift map of a middle-latitude quiet-Sun region observed by SUMER, were compared with the coronal magnetic-field structures as reconstructed from a simultaneous photospheric magnetogram by means of a force-free-field extrapolation. We show for the first time in Fig. 39 that coronal funnels also exist in the quiet Sun. The region studied contains several small funnels that originate from network lanes, expand with height and finally merge into a single wide open-field region. However, the large blue shifts of the Ne VIII line are not generally associated with funnels. A comparison between the projections of coronal loops onto the solar x-y-plane and the Ne VIII Dopplergram indicates that there are some loops that reveal large Ne VIII blue shifts in both legs, and some loops with upflow in one and downflow in the other leg.

The above results suggest that strong plasma outflow, which can be traced by large Ne VIII blue shift, is not necessarily associated with the solar wind originating in coronal funnels but appears to be a signature of mass supply to coronal loops. Under the assumption that the measured Doppler shift of the Ne VIII line represents the real outflow velocity of the neon ions being *markers of the proton flow, we estimate the mass supply rate to coronal loops to be about 10^{34} protons per second.*

(H. Tian, C.-Y. Tu (School of earth and space sciences, Peking University, Beijing, China), E. Marsch, J.-S. He, and G.-Q. Zhou)

Sizes of transition-region structures in coronal holes and in the quiet Sun

In order to estimate the characteristic sizes of the different features present in the chromosphere and transition region (TR), we have calculated the autocorrelation function for SUMER images (intensity, Doppler shift, and non-thermal width) as well as the corresponding extrapolated magnetic field at different heights. The Half Width at Half Maximum (HWHM) of the autocorrelation function is considered to be the characteristic size of the feature shown in the images.

The results are shown in Fig. 40 and indicate that, in both the coronal hole and quiet Sun, the HWHM of the intensity image is larger than that of the images of Doppler-shift and non-thermal width at any given altitude. The HWHM of the intensity image is smaller in the chromosphere than in the TR, where the sizes of intensity features of lines at different temperatures are almost the same. But in the upper part of the TR, the intensity size increases more strongly with temperature in the coronal hole (CH) than in the quiet Sun. We also studied the height variations of the HWHM of the magnetic field magnitude B and its component $|B_z|$, and found they are equal to each other at a certain height below 40 Mm in the CH. The height variations of the HWHM of $|B_z/B|$ seem to be consistent with the temperature variations of the intensity size.

The obtained results suggest that coronal loops are much lower, and that the magnetic structures expand through the upper transition region much more strongly with height in the CH than in the quiet Sun.

(H. Tian and E. Marsch in collaboration with C.-Y. Tu, J.-S. He (School of Earth and Space Sciences, Peking University, Beijing, China), and L.-D. Xia (School of Space Sciences and Physics, Shandong University, Weihai, China))

Multi-scale numerical simulation of cascading coronal magnetic reconnection

Magnetic field reconnection is a key physical process in the solar flares. Classical reconnection schemes with a single non-ideal plasma region at a X- or Null point suffer, however, by many problems. They cannot explain, e.g., the large fluxes of energetic electrons

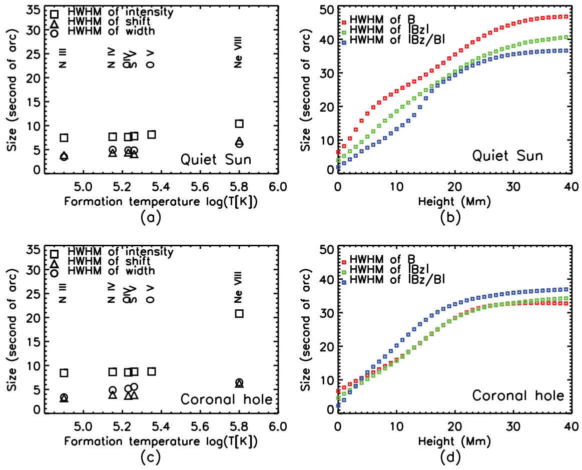

Fig. 40: Temperature/Height variations of the characteristic sizes of intensity, Doppler shift and non-thermal width (left), as well as of the extrapolated magnetic field (right) in the quiet Sun and CH.

needed to explain within the thick-target model the observed HXR. Also, there is a large scale-gap between the dimension at which the energy enters the corona from below the photosphere, the thickness of the current layer formed, e.g., behind ejected CMEs and the scale of the region of non-ideal plasma response.

Turbulent or cascading reconnection might solve these questions. In fact, subsequent tearing mode instabilities could create smaller and smaller magnetic islands until a microscopic dissipation scale is reached. Such a cascade of magnetic islands (flux-ropes/plasmoids) could bridge the scale gap in solar reconnection and reconcile the number problem accelerated particles: a large number of dissipative regions would naturally accelerate a larger number of particles.

Since the concept of nonlinearly interacting islands has not been quantitatively tested for the solar atmosphere we have developed a recursive numerical algorithm which, using the self-similarity of MHD processes, can describe the consequent fragmentation of current sheets (CS).

Applying our code we obtained both the global evolution of a reconnecting current sheet in a simulation domain large enough to minimise the influence of the outer boundary conditions and the small-scale structuring by the formation of micro-plasmoids and very narrow CS filaments as one can see in Fig. 41. While the upper plot depicts the resulting global structure of a vertical current sheet in a solar flare. Secondary plasmoids form (e.g. the one centered around $z = 70L_A$ and $z = 110L_A$ between the flare arcade (bottom) and the main plasmoid around $z = 160L_A$. The lower panel shows a zoomed-in view at the area indicated by a dashed-line rectangle in the top panel. Note that *between a secondary plasmoids near $z = 70L_A$ and the loop-top of the arcade at $z \approx 17L_A$ three even smaller magnetic islands are formed in the thinning current sheet.*

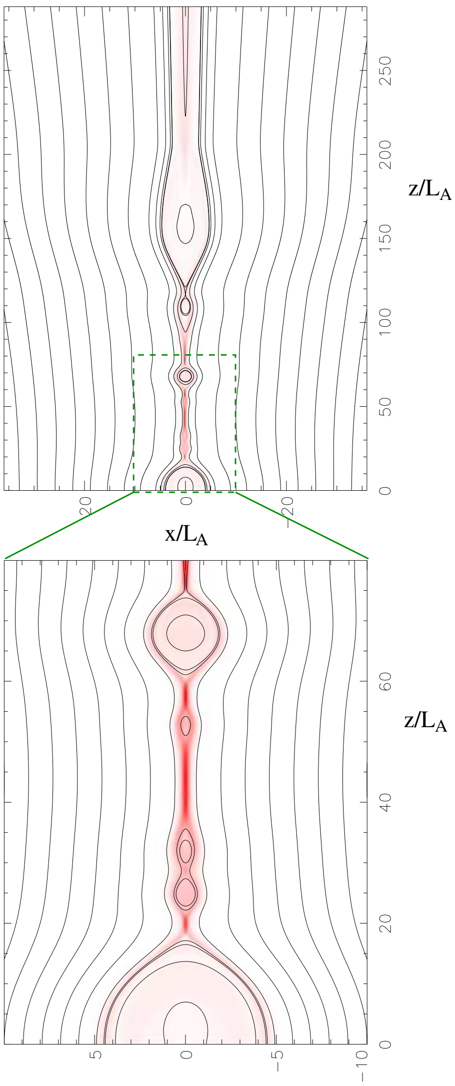

Fig. 41: Upper panel: global structure of a simulated solar flare-related vertical current sheet. The lower panel depicts a zoomed-in view at the region indicated by a dashed-line rectangle in the upper plot.

Thus, our new code effectively spans over a broader range of scales than previous models. Note that our simulations revealed, besides the current-sheet fragmentation, also the reverse process – the coalescence of plasmoids previously formed by tearing. A power-law spectral distribution is obtained by the dynamical balance of tearing and coalescence.

(M. Bárta and J. Büchner in collaboration with M. Karlický (Astronomical Institute of Czech Academy of Science, Ondřejov, Czech Republic))

A new, more realistic approach to coronal magnetic field extrapolation based on the principle of minimum dissipation rate

A new approach was developed to extrapolate solar coronal magnetic fields from photospheric vector magnetograms. Our approach is based on the principle of a minimum dissipation rate (MDR). The MDR system of equations is derived from a variational principle. For an open and externally driven system as the solar corona such variational approach seems to be more suitable than previously developed extrapolation methods. In particular, the resulting magnetic field solutions are more general than those restricted to the consideration of force-free currents. Instead, an approach based on the MDR principle allows to obtain also the location of current sheets, where currents flow perpendicular to the main coronal magnetic field direction.

In short, the MDR extrapolation method is based on the use of a superposition of two linear (constant-α) force-free fields (LFFFs) with distinct α parameters, and of one potential field. Thus, the original extrapolation problem is decomposed into three LFFF extrapolations, utilizing observed photospheric vector magnetic fields as boundary conditions. A full MDR-based approach requires the knowledge of two layers of vector magnetic fields in the photosphere. A slightly modified practical approach requires only one layer. Both approaches were tested against the results of Lindau-code based three-dimensional MHD simulations obtained in a finite volume above a well observed photospheric area. The analysis has shown that both approaches yield quantitatively good results. The errors in the determined magnetic field energy estimate are within a few percent. In particular, the main features of relatively strong perpendicular current sheets, representing non-force-free solutions, are well recovered. This can be seen in Figs. 42 – 44. The Figures depict contour plots of field-line-integrated parallel (force-free) and perpendicular (non force-free) current densities – the plots in the top row show for reference the values, obtained by simulating the MHD system, those in the middle row depict the field-line-integrated current densities obtained by the fully MDR-based approach and the bottom plots show the results obtained by the practical approach.

(J. Büchner in collaboration with Q. Hu, B. Dasgupta, and D. P. Choudhary (California State University, Northridge, USA))

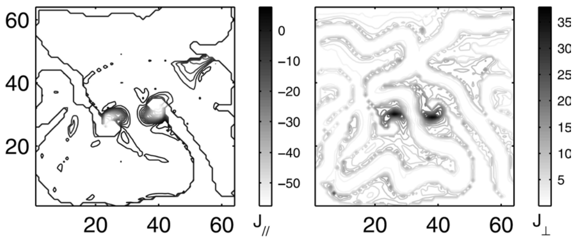

Fig. 42: Contour plots of field-line-integrated current densities from the exact solution. Left: The component parallel to the magnetic field. Right: The component perpendicular to the magnetic field. The gray colors show the levels of the contour lines, as indicated by the grey-scale bars to the right.

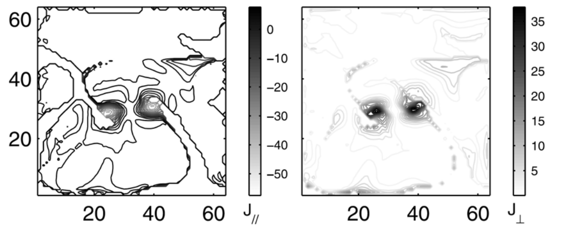

Fig. 43: Field-line-integrated current density distributions obtained by the full MDR-based approach depicted in the the same format as for the plots above.

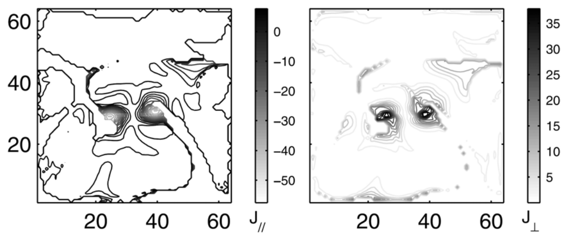

Fig. 44: Field-line-integrated current densities obtained by the practical approach depicted in the the same format as for the plots above.

Ab initio simulation of micro-turbulence using a 2D2V Vlasov code

The investigation of coherent phase space structures and other kinetic effects controlling the macroscopic dynamics of collisionless astrophysical plasmas requires the direct solution of the kinetic Vlasov equation. Often particle-in-cell-(PIC-) codes are too noisy to resolve fine phase-space structures. The investigation of the long-term nonlinear evolution of sufficiently large astrophysical plasma systems by directly solving higher dimensional Vlasov equations requires the development of optimum numerical schemes that allow a massive parallelization. For this sake a four dimensional (2D2V) unsplit conservative solution scheme was developed and optimized for the use on the ALTIX-4700 computer of the High Performance Leibnitz Rechenzentrum (HLRB) Garching in the course of the first phase of the High Permormance Supercomputing project h0842. For the cache-coherent Nonuniform-Memory Architecture (ccNUMA) of the ALTIX-4700 a satisfying performance was achieved only after optimizing the use of the processor-related caches. The achieved performance of the 2D2V Vlasov code running on 128 processors on the ALTIX-4700 allowed to simulate the nonlinear evolution of the two-dimensional instability of currents flowing in the solar corona.

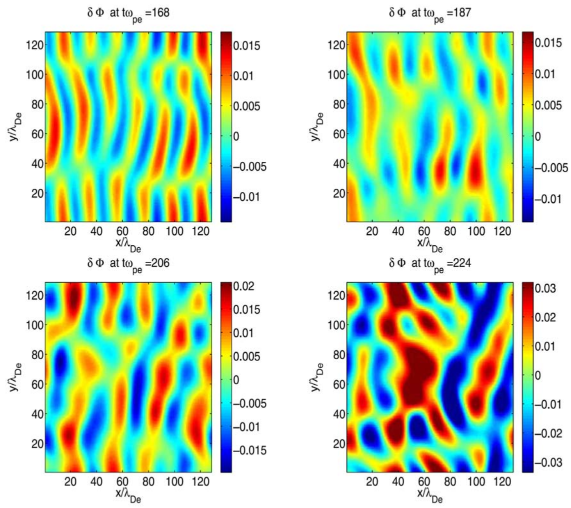

Fig. 45: Spatial x/λ_D vs. y/λ_D distribution of the amplitudes of the fluctuations of the electric potential $\delta\Phi$(x, y) given in in terms of k_BT (colorcoded – see colorbars to the right) at times $t\omega_{pe}$ = 168, 187, 206, 224.

Fig. 45 shows the resulting electric potential fluctuations obtained by simulating the instability of an electron beam. The drift velocity was $V_{de} = 4v_{te}$ in a 2D spatial simulation box of $Nx \times Ny = 128 \times 128$ grid planes in the X and Y directions, respectively. The spatial grid resolution was $\Delta x = \Delta y = \lambda_D$ the resolution of the velocity space was $N_{v_x} \times N_{v_x} = 128 \times 128$ grid points and, the simulation time was reduced by using an artificial ion-to-electron mass ratio of $M_i/m_e = 25$. During the initial evolution the simulation confirms the predictions of the linear instability theory: the fastest growing waves are sound waves excited by a Buneman instability at freqencies of about ω_{pi}. There is also a slower growing lower-hybrid instability which generates waves with frequencies about Ω_{lh} (the lower-hybrid frequency). This can be seen in Fig. 45 which illustrates how at later times, after the parallel propagating waves are saturated (by particle trapping in the potential wells of these waves) oblique modes become most significant. At this stage obliquely propagating waves cause a modulation in the transverse direction that results *in the formation of structures localized in two dimensions.*

(N. Elkina, J. Büchner, and J. Lee)

Magnetic helicity exchange between neighboring solar active regions

We addressed the long-lasting problem of the magnetic helicity distribution in the solar corona. In this context we looked for indications of magnetic helicity exchange between active regions (ARs). We found that when AR 9188 emerged it first started to accumulate positive helicity. Later the neighboring newly emerging AR 9192 accumulated negative helicity. We found a bright connecting loop between the two ARs that can be seen in Fig. 46.

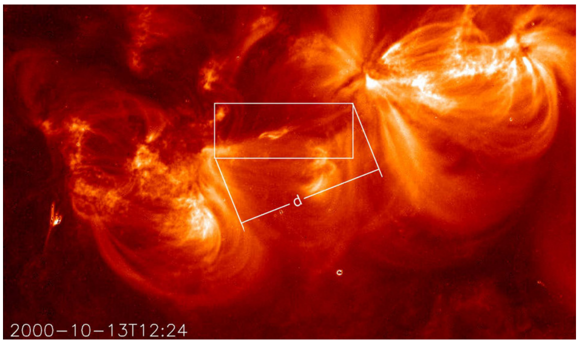

Fig. 46: Helical loop structure found between AR 9188 and AR 9192 on 13 October 2000; observation made by the TRACE spacecraft in EUV 17.1 nm

At a time, when the connecting loop was seen AR 9188 suddenly also started to gain negative helicity. At the same time AR 9192 started to loose negative helicity. We found that the magnetic helicity fluxes of the two ARs changed simultaneously by almost the same amount. At one instant it was possible to determine the helicity of the the connecting loop between the two ARs. It appeared to be negative. We could exclude the possibility that emerging magnetic flux was causing the observed variation of the magnetic helicity in the two ARs. Hence, we conclude that magnetic helicity was indeed transferred from the late emerging AR 9192 to AR 9188 via an unbalanced magnetic torque along a connecting loop.

We conjecture that our discovery of such kind of helicity transfer might indicate a common mechanism of redistribution of magnetic helicity in the solar atmosphere, which has just not been widely observed, yet Yang et al. (Astrophys. J., 695, L25, 2009).

(S. Yang and J. Büchner in collaboration with H. Zhang (Astronomical Observatory of the Chinese Academy of Sciences, Beijing, China))

Magnetic helicity accumulation and tilt angle evolution of newly emerging active regions

It has been known for years that there is a general dominance of negative (positive) helicity of active regions (ARs) in the northern (southern) solar hemisphere. However, different conclusions were drawn in the past, e.g., about the relationship between the accumulated helicity and the writhe of active regions. For a better understanding of the role of helicity in the evolution of active regions it is necessary to know more about the accumulation of helicity in the course of the emergence of active regions. We investigated the accumulation of helicity in newly emerging simple bipolar solar active regions. We also investigated the relation between the accumulated helicity and writhe. The helicity accumulation was obtained by applying Fast Fourier Transforms (FFT) and local correlation tracking (LCT) to photospheric magnetic fields obtained from the MDI onboard the SOHO spacecraft. We deduced the writhe of the active regions according to the evolution of the tilt angle between the connecting line of the weighting centers of opposite polarities in the AR. Fig. 47 depicts as an example the magnetic field evolution of AR 10569 – a simple bipolar active region. The top and bottom left images reflect the evolution of this active region at three different moments of time. The corresponding evolution of the tilt angle (Ta) is shown in the right lower panel as well as the evolution of the accumulated magnetic helicity.

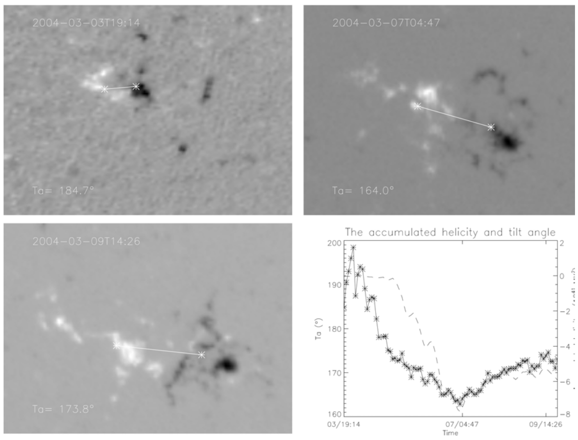

Fig. 47: Photospheric magnetic fields around AR 10569 at three instants of time between 3rd and 14th March 2004. The right lower panel depicts the evolution of the tilt angle (Ta) of the accumulated magnetic helicity – the ordinate corresponds to the tilt angle (asterisk) and the right to the accumulated helicity (dashed line).

We found that 72 % of 58 selected newly emerged simple ARs take negative (positive) helicity when the above defined tilt angle rotates clockwise (counterclockwise). We further found that the accumulated *helicity and writhe have the same sign for most of the investigated ARs. We also found that 57 % (66 %) of the selected active regions in the northern (southern) photosphere provide negative (positive) helicity to the corona in the course of the emergence of new magnetic flux.*

(S. Yang and J. Büchner in collaboration with H. Zhang (Astronomical Observatory of the Chinese Academy of Sciences, Beijing, China))

Influence of radiative cooling and heat conduction on the formation of an EUV bright point, observed by the Hinode spacecraft

We investigated the contribution of different physical effects to the formation and duration of an EUV bright point observed by the Hinode spacecraft. In particular, we investigated the balance between radiative cooling, heat conduction and heating due to current dissipation. For this sake we included radiative cooling and the heat conduction effects in the 3-D MHD simulation code developed in the Lindau group. The code starts with the magnetic fields extrapolated from the observed photospheric magnetic field. We used SOHO/MDI magnetograms for a region that includes a bright point observed on 19 December 2006 by the XRT telescope onboard the Hinode spacecraft. The photospheric plasma motion was inferred by applying the local correlation traccking (LCT) method to the magnetic fields changing in the course of the bright point evolution. The LCT technique was applied to the 5-min averaged MDI data. The obtained consequent motion patterns were included in the simulation model as boundary condition formulated in terms of a number of incompressible plasma vortices.

The resulting temperature variations and the consequences of heat conduction can be seen in Fig. 48. A temperature drop of approximately 2000 K is due to radiative cooling and heat conduction.

Comparing the time profile of the averaged currents we found an enhancement of the perpendicular, non-force-free current just below the transition region if the effects of radiative cooling and heat conduction are taken into account.

(S. Javadi, J. Büchner, and J. C. Santos)

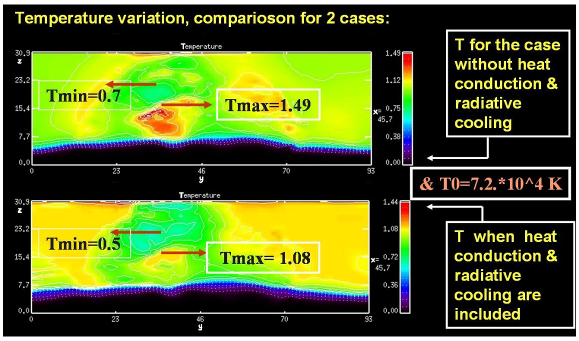

Fig. 48: Temperature variations in a plane that crosses the main polarities associated to this bright point shows a drop in temperature maximum for the case that includes the radiative cooling and heat conduction effects (lower panel).

On the relation between DC current locations and an EUV Bright Point: A case study.

Motion of the photospheric plasma can give rise to electric currents in the solar atmosphere. The dissipation of these electric currents and the consequent heating of the solar plasma may be responsible for the formation of Extreme-UltraViolet (EUV) and X-ray bright points.

We investigate the consequences of different patterns of horizontal photospheric plasma motion for the generation of electric currents (see Fig. 49) in the solar atmosphere and locate them with respect to an observed EUV bright point. To perform this study we use a 'data driven' three-dimensional magnetohydrodynamic model. The model solves an appropriate set of magnetohydrodynamic equations and uses, as initial condition, the magnetic field extrapolated from the line-of-sight component of the photospheric magnetic field observed by MDI/SOHO. We apply different patterns of horizontal photospheric plasma motion, derived from the temporal evolution of the photospheric magnetic structures in the course of the bright point lifetime, as boundary conditions of the model.

All applied patterns of horizontal photospheric plasma motion (shearing, convergence and fragmentation) lead to the formation of electric currents in the chromosphere, transition region and corona. Currents do not develop everywhere in the region where the motion is applied but in specific places where the magnetic field connectivity changes significantly. An important result is that the position where the electric currents develop is independent of the motion pattern used as boundary condition of the model. A comparison with data obtained by TRACE in the 1550 Å channel and by the EIT in the 195 Å channel shows that the region where the strongest current concentrations are formed coincides with the region where the EUV bright point appears.

(J. C. Santos and J. Büchner)

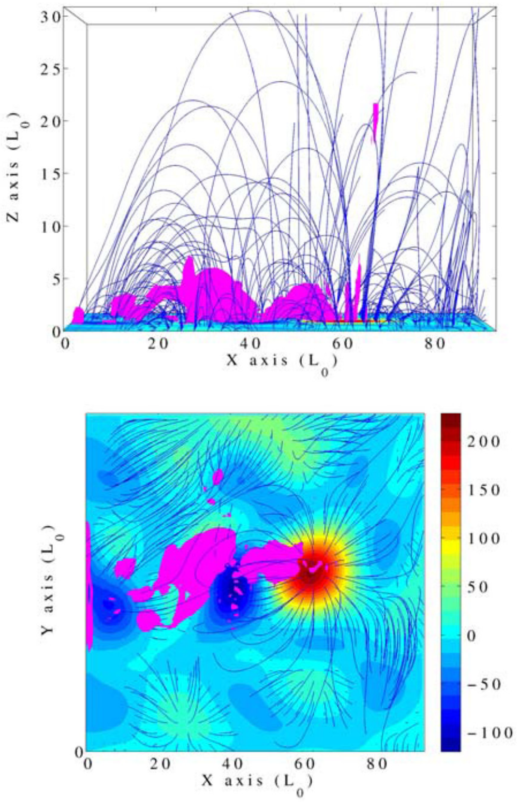

Fig. 49: Lateral view (top panel) and top view (bottom panel) of the isosurfaces of a parallel current $j_{\|} = 2j_0$ at the instant $t = 1300$ s, resulting from the application of the velocity pattern moving the negative polarity towards the positive polarity as boundary condition of the model. The colour code shows the vertical component of the photospheric magnetic field, with the magnetic field values given in gauss, and the lines correspond to the magnetic field lines of force. The isosurfaces of parallel current are shown in magenta.

Nonlinear force-free field extrapolations of SOLIS/VSM data

We study the coronal magnetic field structure inside active regions and its temporal evolution. We compare the magnetic configuration of an active region (AR) in a very quiet period with that during a flare.

We use Vector-SpectroMagnetograph (VSM) data from the Synoptic Optical Long-term Investigations of the Sun survey (SOLIS) to model the coronal magnetic field of active region NOAA 10960 as observed on 7 June 2007, as a sequence of nonlinear force-free (NLFF) equilibria. Three vector magnetograms with a time cadence of $\approx$ 10 minutes were available to investigate the magnetic energy content of the coronal field during a C1.0 flare and a simultaneously observed coronal mass ejection (CME), and six further snapshots were acquired to analyze a very quiet time about three hours after the flare.

Before as well as after the flare/CME, the total magnetic energy was approximately 3×10^{25} J. Before the flare the NLFF field had a free energy of $\approx 1.5 \times 10^{24}$ J which was ≈ 5 % of the potential field energy. A part of this excess energy was released during the flare/CME, reducing the free magnetic energy by almost a factor of 10 and producing an almost potential configuration at the beginning of the quiet period. Six snapshots acquired during this quiet period of 3 – 4 hours after the flare, showed again an increase in the free magnetic energy shown in Fig. 50. Since the estimated free magnetic energy remained only about 5 % of the total energy content, no large eruption was produced by AR 10960.

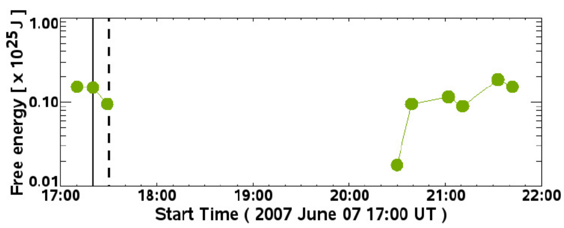

Fig. 50: Upper limit for the free magnetic energy (shown on logarithmic scale). Solid and dashed lines represent a recorded C1.0 flare and CME, respectively.

During the investigated period, the coronal magnetic energy was only a few percent higher than that of the potential field and consequently only a small C1.0 flare occurred. However, the accumulation of free magnetic energy before and its release during the flare is clearly observable also in small flares.

(J. K. Thalmann and T. Wiegelmann in collaboration with N.-E. Raouafi (National Solar Observatory, Tucson, Arizona, USA))

Study of magnetic channel structure in active region 10930

The concept of magnetic channel *was first introduced by Zirin and Wang. They were defined as a series of oppositely directed vertical-field inversions separated by extremely narrow elongated transverse fields. We utilized unprecedented filtergraph and spectropolarimetry observations from* Hinode*, and studied the evolution and physical properties of channel structure of AR 10930 in detail. We found the following: (1) Channels are associated with new flux emergence in the middle of existing penumbra connecting the δ sunspot. (2) The width of each channel is in the order of 1 arcsec or less. (3) The line-of-sight magnetic gradient is highest in the channel, 2.4 – 4.9 G km^{-1}. (4) The fields are highly sheared and inclined with a median shear angle around 64° degree and inclination* *angle around 25 degree. (5) Using nonlinear force-free field extrapolation, we derive a near surface current system carrying electric current in the order of* $5 \cdot 10^{11}$ *A. The corresponding 3-D visualization of the electric current density is shown in Fig. 51. (6) The X3.4 flare on 13 December 2006 occurred during the period that the channels rapidly formed, but a few hours before the maximum phase of channel structure development. Based on the observational evidence, we propose that the channels are formed during the emergence of a sequence of magnetic bipoles that are squeezed in the compact penumbra of the* δ *sunspot and they are highly nonpotential. Formation of channels might be a precursor of major flares.*

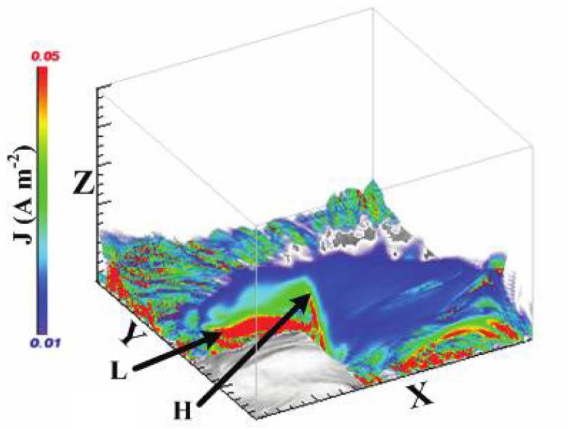

Fig. 51: 3-D visualisation of the electric current density in active region 10930. The arrows L and H indicate the low-lying and high-reaching strong current systems, respectively.

(T. Wiegelmann in collaboration with H. Wang, J. Jing, C. Tan (New Jersey Institute of Technology, Newark, USA), and M. Kubo (High Altitude Observatory, Boulder, USA))

Source region of the 18 November 2003 coronal mass ejection that led to the strongest magnetic storm of cycle 23

The superstorm of 20 November 2003 was associated with a high-speed coronal mass ejection (CME) which originated in the NOAA AR 10501 on 18 November. This coronal mass ejection had severe terrestrial consequences leading to a geomagnetic storm with Dst index of -472 nT, the strongest of the current solar cycle. In order to understand the factors that led to the coronal mass ejection on 18 November we studied the evolution of the photospheric magnetic field of NOAA AR 10501, the source region of this coronal mass ejection. For this purpose, the Michelson Doppler Imager line-of-sight magnetograms (One snapshot is shown shown in Fig. 52) and vector magnetograms from Solar Flare Telescope, Mitaka, obtained during 17–19 November 2003 were analyzed. In particular, quantitative estimates of the temporal variation in magnetic flux, energy, and magnetic field gradient were estimated for the source active region. The evolution of these quantities was studied for the 3-day period with an objective to understand the preflare configuration leading up to the moderate flare which was associated with the geoeffective coronal mass ejection. We also examined the chromospheric images recorded in H-alpha from Udaipur Solar Observatory (also shown in Fig. 52) to compare the flare location with regions of different magnetic field and energy. Our observations provide evidence that the flare associated with the CME occurred at a location marked by high magnetic field gradient which led to release of free energy stored in the active region.

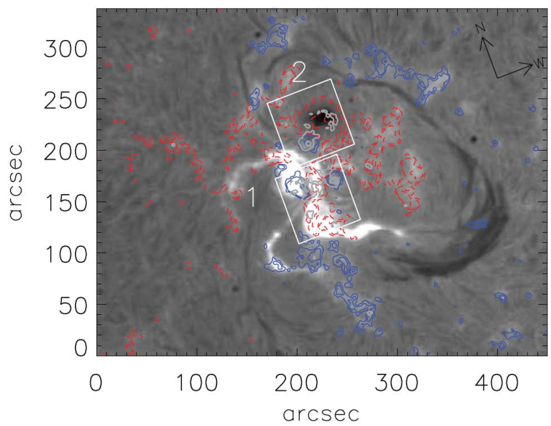

Fig. 52: Magnetic field contours (blue: positive, red: negative) from SOHO/MDI overlayed on an Hα image obtained from the Udaipur Solar Observatory. The white boxes locate subregions used to study the photospheric magnetic flux evolution.

(T. Wiegelmann in collaboration with N. Srivastava, S. K. Mathew, and R. E. Louis (Udaipur Solar Observatory, Physical Research Laboratory, Udaipur, India))

3-D magnetic field configuration of the 2006 december 13 flare

The photospheric vector magnetic field of the active region NOAA 10930 was obtained with the Solar Optical Telescope (SOT) on board the Hinode satellite. Observations of the two-ribbon flare on 2006 December 13 in this active region provide us a good sample to study the magnetic field configuration related to the occurrence of the flare. Using the optimization method for nonlinear force-free field (NLFFF) extrapolation, we derive the three-dimensional vector magnetic field configuration associated with this flare. The general topology can be described as a

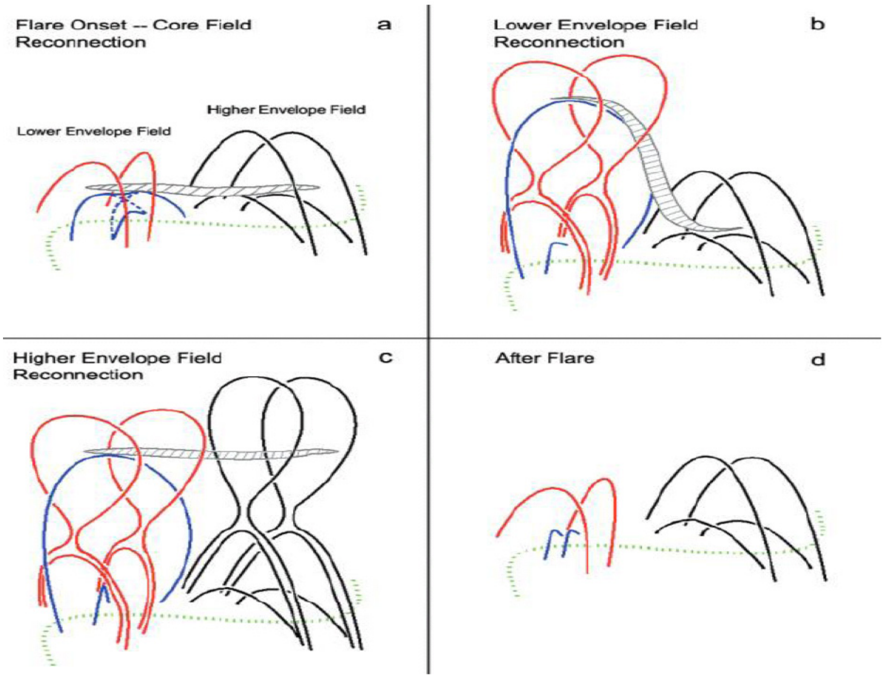

Fig. 53: Sketch of the magnetic field evolution during the 13 December 2006 flare. Green: polarity inversion line, hatched region: filament. During the evolution the filament passes through the envelope fields as a consequence of magnetic reconnection. The lower-envelope field reconnects first and the higher one thereafter. The core field becomes less sheared after the flare.

highly sheared core field and a quasi-potential envelope arch field. The core field clearly shows some dips supposed to sustain a filament. We find that the shear angles, defined as the angles between the NLFFF and potential field, become larger at some particular sites in the lower atmosphere, while they become significantly smaller in most places, implying that the whole configuration gets closer to the potential field after the flare. The Ca II *H line images obtained with the Broadband Filter Imager (BFI) of the SOT and the 1600 Å images with the Transition Region and Coronal Explorer (TRACE) show that the preflare heating occurs mainly in the core field. These results provide evidence in support of the tether-cutting model of solar flares as illustrated in Fig. 53. Before the flare the core field lines are originally almost horizontal and start to reconnect as response to photospheric foot point motion (Fig. 53a). This low-lying process triggers the two-ribbon flare starting from the upward rising of the filament (Fig. 53b–c) which is associated by further progressive reconnection events as observed with the X-Ray telescope XRT on* Hinode*. The high-energy particles accelerated in the reconnection area precipitate along the magnetic field lines into the lower atmosphere and form the two flare ribbons. After the flare (Fig. 53d) the magnetic field configuration becomes less sheared and more like a potential field.*

(T. Wiegelmann in collaboration with Y. Guo, M. D. Ding (Nanjing University, China), and H. Li (Purple Mountain Observatory, Nanjing, China))

Nonlinear Force-Free coronal magnetic field modeling and preprocessing of vector magnetograms in spherical geometry

Knowedge regarding the coronal magnetic field is important for the understanding of many phenomena, like flares and coronal mass ejections. Reliable measurements of the solar magnetic field are mainly available in the photosphere. To obtain the field in the higher layers of the atmosphere it is extrapolated from the measured photospheric field, mostly under the assumption that it is force-free. Unfortunately these data in the photosphere can not be directly used as boundary conditions for nonlinear force-free computations, because of inconsistencies and non-magnetic forces in the magnetograph data. We develop a preprocessing procedure in spherical geometry to derive suitable boundary conditions for a force-free extrapolation using force-free consistency criteria.
We test our newly developed method with a magnetogram derived from a known nonlinear force-free test field to which artificial noise had been added. The algorithm recovered all main structures of the magnetogram and removed small-scale noise. The main test was to extrapolate from ideal and noisy photospheric vector magnetogram with and without the preprocess-

ing (see Fig. 54). The preprocessing was found to significantly improve the agreement of the extrapolated with the exact field. We plan to apply our newly developed codes in spherical geometry to full-disk vector magnetograms from the forthcoming SDO (Solar Dynamic Observatory) mission.

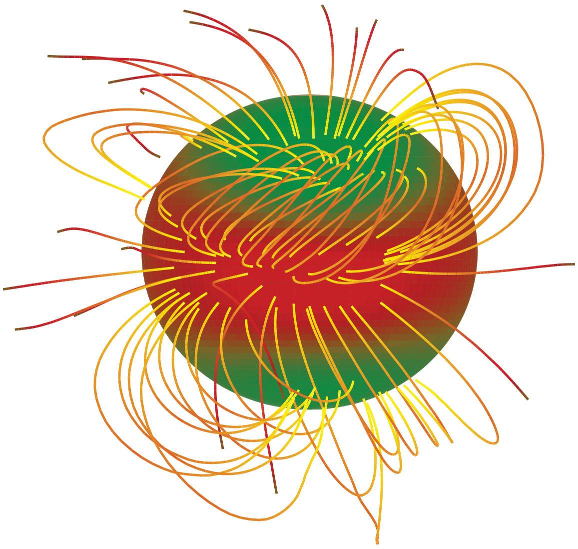

Fig. 54: Nonlinear force-free coronal magnetic field extrapolation from a noisy vector magnetogram after preprocessing.

(T. Tadesse, T. Wiegelmann, and B. Inhester)

Propagating waves in polar coronal holes as seen by SUMER and EIS

Propagating radiance oscillations were detected in polar plumes by different instruments aboard SOHO since the early phases of the mission and have since been identified as propagating slow magneto-acoustic waves.

Here, for the first time to our knowledge, we made simultaneous use of the SUMER/SOHO and EIS/Hinode spectrometer to study these propagating disturbances in the off-limb regions of the polar coronal holes. We construct time distance maps to study the properties of wave propagation and use wavelet analysis to establish their periods. Spectroscopic observations have the advantage of a narrow temperature response (by isolating specific spectral lines) and of allowing the study of resolved and unresolved plasma motions by measuring the Doppler shift and width of the observed profiles. These observables provide important constraints in establishing the nature of the observed oscillations.

From our data, we detect the presence of long period oscillations with periods of 10 to 30 minutes in polar coronal holes. The oscillations have an amplitude of a few percent in radiance and are not detectable in line-of-sight velocity. From the time distance maps we find evidence for propagating velocities from 75 km s^{-1} (Ne VIII, formed around 0.6 MK, see Fig. 55) to 125 km s^{-1} (Fe XII, formed around 1.3 MK). These velocities are subsonic and roughly in the same ratio as the respective sound speeds. We interpret the observed propagating oscillations in terms of slow magneto-acoustic waves. These waves can be important for the acceleration of the fast solar wind.

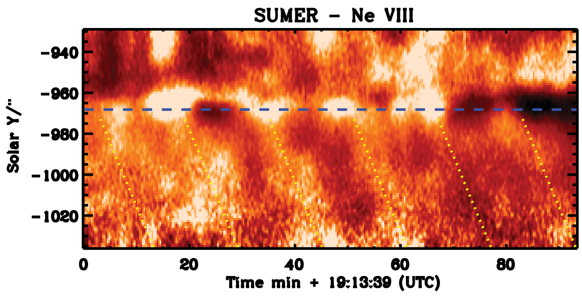

Fig. 55: Contrast enhanced map of the radiance variation along the slit (Solar Y direction) with time for Ne VIII as recorded by SUMER aboard SOHO on 8 April 2007. The slanted dotted yellow lines correspond to disturbances propagating with a speed of 75 km s^{-1} and a period of about 15 minutes. The horizontal dashed blue line marks the position of the solar limb.

(L. Teriaca and S. K. Solanki in collaboration with D. Banerjee (Indian Institute of Astrophysics, Bangalore), G. R. Gupta (Indian Institute of Science, Bangalore, India), S. Imada (National Astronomical Observatory of Japan, Tokyo), and G. Stenborg (Interferometrics, Inc., Herndon, USA))

SOHO-Lasco and SOHO-SUMER in the Bogart Phase

The SOHO mission, planned for a nominal duration of two years with an optional extension to six years, has completed its 12^{th} year of successfull operation. SOHO has seen a complete solar cycle. Since the spacecraft and several key instruments of the payload are still performing well, the idea came up to further extend the lifetime of this mission. A proposal was submitted to the NASA Senior Review panel by the SOHO SWT to present to the expected scientific merit, the relevance to the Heliospheric Physics Roadmap, the spacecraft and instrument health and status, data availability and accessibility, as well as the cost to NASA's Heliophysics Division. The main rationale behind this proposal was the potential role of SOHO as the 'third eye' for both STEREO spacecraft and, in particular, to have an overlap with the Solar Dynamics Observatory (SDO) mission to allow a comprehensive *cross-calibration with the major instruments on SDO. Among twelf science proposals for mission lifetime extension, the proposal 'SOHO in its Bogart Phase' – the actor Humphrey Bogart is well known as a person who smokes his cigarettes really up to the limit - was top ranked. NASA and consequently also ESA decided to continue SOHO operations for four more years, although with significantly reduced funding and downsizing of other resources.*

The two SOHO investigations on SOHO with major MPS contribution, SUMER and LASCO, are important for this mission phase: LASCO to complement STEREO and SUMER with its unique wavelength range to complement SDO, which does not have a spectrometer at all. Fig. 56 displays a record of the science return from both instruments. The chart is scaled in yearly peer-reviewed publications based on data obtained from SUMER and LASCO since the launch of SOHO. The figure demonstrates that the interest of the community in these instruments continues on a high level and that the expected merit seems realistic.

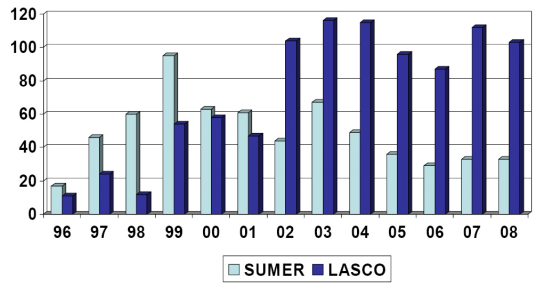

Fig. 56: Yearly publications in peer-reviewed journals

(W. Curdt, K. Wilhelm, and R. Schwenn)

Helium line formation and abundance during a C-class flare

Chemical composition is a key ingredient in understanding the physics of solar and stellar plasmas. An astrophysical plasma is subject to chemical fractionation processes of diverse nature (gravity, thermal diffusion, etc.) that can produce abundance "anomalies" between regions of different temperature and density. For the solar corona these anomalies are generally described in terms of the so-called FIP (First Ionization Potential) effect. Although the details are still debated, there is apparently consensus that the FIP effect should arise in the chromosphere.

Helium is one of the few elements that exhibits strong lines forming in the chromosphere, and thus, in principle at least, its abundance ([He/H] $\equiv \log A_{\rm He}$ (where $A_{\rm He} \equiv {\rm N_{He}/N_H}$, the ratio of number densities of He and H) could be estimated in that region. It is also the element with the highest FIP (24 eV). Furthermore, it is the second most abundant element in the Sun, and therefore must be included in any theoretical model of fractionation processes in the solar atmosphere.

In May 2001, a C-class flare was observed both with SOHO instruments and with the Dunn Solar Telescope at Sacramento Peak. Here we focus the analysis of the helium line formation to the later phases of the flare in two different locations of the flaring area. We have devised a new technique, exploiting all available information from various SOHO instruments, to determine the spectral distribution of the photoionizing EUV radiation produced by the corona overlying the two target regions. In order to find semiempirical models matching all of our observables, we analyzed the effect on the calculated helium spectrum both of $A_{\rm He}$ (the He abundance) and of the uncertainties in the incident EUV radiation (level and spectral distribution). We found that the abundance has in most cases (but not in all) a larger effect than the coronal back-radiation. The result of our analysis is that, considering the error of the measured lines, and adopting our best estimate for the coronal EUV illumination, the value $A_{\rm He} = 0.075 \pm 0.010$ in the chromosphere (for $T > 6300$ K) and transition region yields reasonably good matches for all the observed lines. This value is marginally consistent with the most commonly accepted photospheric value: $A_{\rm He} = 0.085$.

(L. Teriaca in collaboration with V. Andretta (INAF-Osservatorio Astronomico di Capodimonte, Italy), A. Falchi (INAF-Osservatorio Astrofisico di Arcetri, Italy), and P. J. D. Mauas (Instituto de Astronomía y Física del Espacio, Argentina))

Slow magnetoacoustic standing waves in a curved solar coronal slab

Standing slow magnetoacoustic waves have been regularly observed by the SUMER instrument onboard SOHO in active regions observed in an Fe XIX line. Remarkably, the observations show that a standing wave is set up within a single wave period of the initial pulse. Reproducing this with the help of numerical simulations had remained elusive. We consider a model of a two-dimensional solar coronal arcade to explore the effects of a curved magnetic field topology on excitation and attenuation of slow magnetoacoustic standing waves. The time-dependent ideal magnetohydrodynamic equations are solved numerically to find the spatial and temporal signatures of these waves. A pulse in gas pressure initially launched at a loop footpoint excites the fundamental mode of slow magnetoacoustic standing waves. The typical excitation time of such a wave mode is 2.5 wave periods, *with a similar attenuation timescale. These values are much closer to those recovered from observations by SOHO/SUMER than those obtained from previous computations. Consequently, we conclude that slow magnetoacoustic standing waves are excited and attenuated more efficiently in curved magnetic field lines than in a straight magnetic slab topology.*

(S. K. Solanki in collaboration with R. Ogrodowczyk (University of Chełm, Poland) and K. Murawski (University of Lublin, Poland))

Identification and misidentification of different types of kink modes in coronal loops

Oscillations of coronal loops are rapidly becoming an important new diagnostic of coronal parameters. In order to apply it properly it is important to correctly identify the observed oscillation mode. We explore the possible observational signatures of different types of kink modes (horizontal and vertical oscillations in their fundamental mode and second harmonic) that may arise in coronal loops, with the aim of determining how well the individual modes can be uniquely identified from time series of images. A simple, purely geometrical model is constructed to describe the different types of kink-mode oscillations. These are then "observed" from a given direction. In particular, we employ the 3-D geometrical parameters of 14 TRACE loops of transverse oscillations to try to identify the correct observed wave mode. We find that for many combinations of viewing and loop geometry it is not straightforward to distinguish between at least two types of kink modes just using time series of images. We also considered Doppler signatures and find that these can help obtain unique identifications of the oscillation modes when employed in combination with imaging. We then compare the modeled spatial signatures with the observations of 14 TRACE loops. We find that out of three oscillations previously identified as fundamental horizontal mode oscillations, two cases appear to be fundamental vertical mode oscillations (but possibly combined with the fundamental horizontal mode), and one case appears to be a combination of the fundamental vertical and horizontal modes, while in three cases it is not possible to clearly distinguish between the fundamental mode and the second harmonic of the horizontal oscillation. In five other cases it is not possible to clearly distinguish between a fundamental horizontal mode and the second harmonic of a vertical mode.

(S. K. Solanki in collaboration with T. J. Wang (Montana State University, Bozeman, USA) and M. Selwa (NASA Goddard Space Flight Center, Greenbelt, USA))

Evidence for polar jets as precursors of polar plume formation

Polar jets and polar plumes are two fascinating phenomena that until recently were not brought into connection with each other. Observations from the Hinode/XRT telescope and *STEREO*/SECCHI/EUVI are utilized to look for a connection between jets and plumes. The study focuses on the temporal evolution of both structures and their relationship. The data sample, spanning 7–8 April 2007, shows that over 90 % of the 28 observed jet events are associated with polar plumes. EUV images (*STEREO*/SECCHI) show plume haze rising from the location of approximately 70 % of the polar X-ray (*Hinode*/XRT) and EUV jets, with the plume haze appearing minutes to hours after the jet was observed. The remaining jets occurred in areas where plume material previously existed, causing a brightness enhancement of the latter after the jet event. Short-lived, jet-like events and small transient bright points are seen (one at a time) at different locations within the base of preexisting long-lived plumes. X-ray images also show instances (at least two events) of collimated thin jets rapidly evolving into significantly wider plume-like structures that are followed by the delayed appearance of plume haze in the EUV. These observations provide evidence that X-ray jets are precursors of polar plumes and in some cases cause brightenings of plumes. Possible mechanisms to explain the observed jet and plume relationship are discussed.

(S. K. Solanki in collaboration with N.-E. Raouafi, G. J. D. Petrie, A. A. Norton, and C. J. Henney (National Solar Observatory, Tucson, USA))

Quiet Sun mini-CMEs activated by supergranular flows

Images taken with the Extreme UltraViolet Imager (EUVI) on *STEREO* and MDI on SOHO are used to investigate the coupling between photospheric flows and coronal emission in the atmosphere of the quiet Sun. The photospheric flows are calculated by tracking granules in high-resolution MDI continuum images. These flows sweep up concentrations of mixed-polarity magnetic field to the supergranular lanes and junctions. In the EUVI images, we found eruptions with characteristics of small coronal mass ejections (CMEs) at supergranule junctions where converging and rotating supergranular flows, twist small concentrations of opposite polarity magnetic field, as in the example shown in Fig. 57 below. An estimate of the occurrence rate is about 1400 events per day over the whole Sun. One third of these events seem to be associated with waves. Typically, the waves last for about

30 min and travel a distance of 80 Mm, so at any one time they cover 1/50th of the lower corona.

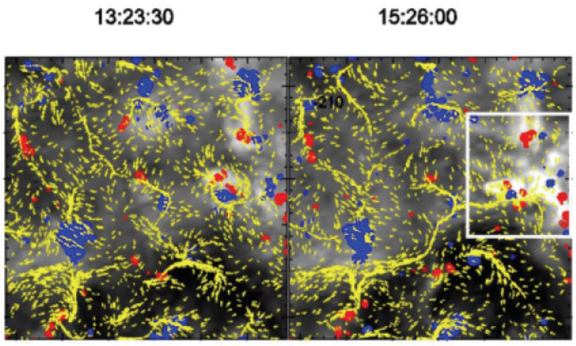

Fig. 57: A mini-CME. *STEREO* 171 images (greyscale) with regions of magnetic field greater (less) than 40 G (-40 G) coloured in blue (red), and the photospheric flows represented with yellow arrows. The FOV is 150 × 180 arcsec^2. The white box outlines the event.

(D. E. Innes, A. Genetelli, and R. Attie in collaboration with H. E. Potts (University of Glasgow))

EIS/Hinode observations of doppler flow seen through the 40 arcsec wide slit

The Extreme ultraviolet Imaging Spectrometer (EIS) on board *Hinode* is the first solar telescope to obtain wide slit spectral images that can be used for detecting Doppler flows in transition region and coronal lines on the Sun and to relate them to their surrounding small scale dynamics. We select EIS lines covering the temperature range 6×10^4 K to 2×10^6 K that give spectrally pure images of the Sun with the 40 arcsec slit. In these images Doppler shifts are seen as horizontal brightenings. Inside the image it is difficult to distinguish shifts from horizontal structures but emission beyond the image edge can be unambiguously identified as a line shift in several lines separated from others on their blue or red side by more than the width of the spectrometer slit (40 pixels). In the blue wing of He II, we find a large number of events with properties (size and lifetime) similar to the well-studied explosive events seen in the ultraviolet spectral range. Comparison with X-Ray Telescope (XRT) images shows many Doppler shift events at the footpoints of small X-ray loops. The most spectacular event observed showed a strong blue shift in transition region and lower corona lines from a small X-ray spot that lasted less than 7 min (see Fig. 58). The width of the emission implies a line-of-sight velocity of 220 km s^{-1}.

(D. E. Innes, R. Attie, and M. Madjarska in collaboration with H. Hara (National Astronomical Observatory, Tokyo, Japan))

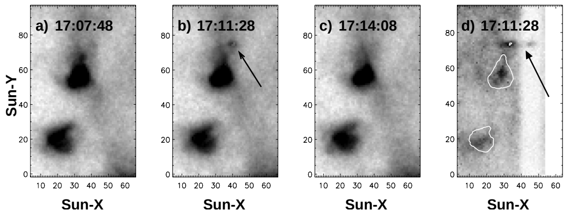

Fig. 58: (a–c) Time series of XRT Al-mesh intensity showing hot spot brightening (indicated with an arrow) and (d) the EIS Si VII image with XRT contours on 10 April 2007. The 220 km s^{-1} blue shift is indicated with an arrow. All intensities are represented as logarithmically scaled negatives.

Oscillations in the wake of a flare blast wave

An M2.5 flare and CME that occurred at the limb of the Sun on the 16 April 2002 produced high velocity blue and red shifts in the flare line Fe XIX 1118.1 Å across a 70 arcsec wide region of the slit for a period of about 15 min. The highest shifts coincided with the apex of a bright erupting loop seen in TRACE 195 Å filter images (Fig. 59). The sequence of TRACE 195 Å images are carefully co-aligned to structures seen in the SUMER Fe XIX emission line. TRACE image enhancement is performed using a wavelet-based algorithm. A large-scale oscillation in the TRACE intensity and SUMER Fe XIX line Doppler shift is observed over the entire region, suggesting heating and acceleration of hot plasma in the wake of a blast wave.

(D. Tothova and D. E. Innes in collaboration with G. Stenborg (Catholic University of America, Washington, USA))

A nanoflare model for active region radiance: application of artificial neural networks

Nanoflare heating of the solar corona was first proposed by Levine (1974). The idea is that current sheets arise spontaneously in coronal magnetic fields that are braided and twisted by random photospheric footpoint motions. These current sheets dissipate in many small-scale reconnection events (nanoflares), heating and accelerating plasma in the corona. Because the nanoflares would be the solar background emission, it is not possible to determine their energy input by measuring individual events. Instead, their energy can be estimated by extrapolating the energy frequency distribution of larger flares to lower energies. If the power law exponent is greater than 2 it is possible that nanoflares contribute significantly to the energy input.

In this work we modelled time sequences of ultraviolet line radiances observed in the corona of an active region with the aim of determining the power law exponent of the nanoflare energy distribution. A simple

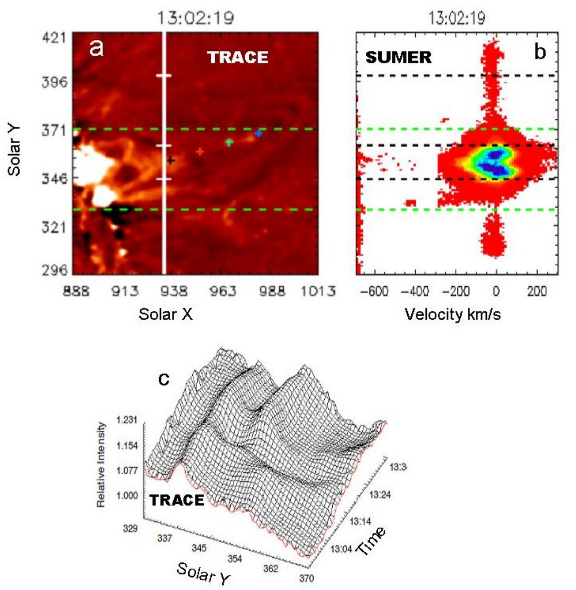

Fig. 59: Fe XIX line shifts and TRACE oscillation in the postflare corona. (a) TRACE 195 Å intensity, enhanced using the wavelet-based method. The white vertical line indicates the position of the SUMER slit. The green horizontal lines outline the spatial region of the oscillation shown below in c. (b) Fe XIX line showing a high blue shift just above the bottom green line and red shifts to the edge of the window near the image centre. (c) TRACE 195 Å intensity time series at the position of the SUMER slit and between the green lines in a.

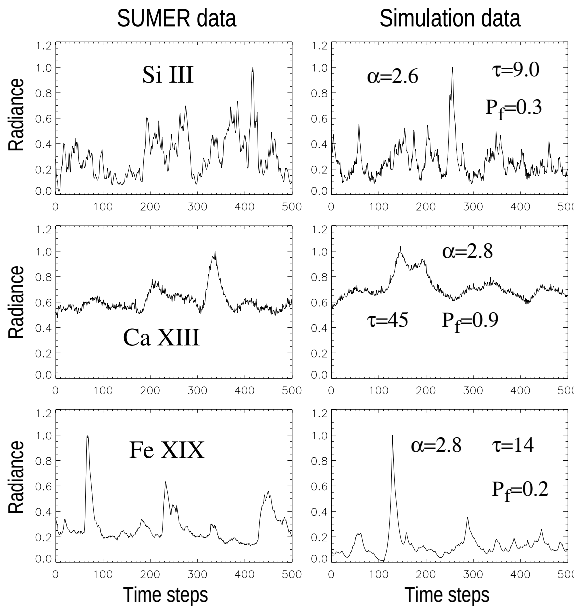

Fig. 60: Samples of the radiance time series: left panel: SUMER data, and right panel: simulation data.

nanoflare model based on three key parameters (the flare rate (P_f), the flare duration (τ), and the power law exponent (α) of the flare energy frequency distribution) is used to simulate emission line radiances from the ions Fe XIX, Ca XIII, and Si III, observed by SUMER in the corona of an active region Fig. 60.

Light-curve pattern recognition by an Artificial Neural Network (ANN) scheme is used to determine the values. The power-law exponents, $\alpha \approx 2.8$, 2.8, and 2.6 are obtained for Fe XIX, Ca XIII, and Si III respectively. Since they are all greater than 2, it implies that nanoflares could provide a significant contribution to the heating of active region coronae.

(D. E. Innes and S. K. Solanki in collaboration with M. Bazarghan and H. Safari (Zanjan University, Iran))

Stereoscopic reconstructions of polar plumes from EUVI/SECCHI images

We present stereoscopic reconstructions of the location and inclination of polar plumes of two data sets based on the two simultaneously recorded images taken by the EUVI telescopes onboard the *STEREO* spacecraft. The ten plumes investigated show a super-radial expansion in the coronal hole in 3-D which is consistent with the 2-D results. Their deviations from the local meridian planes are rather small with an average of 6.47°. By comparing the reconstructed plumes with a dipole field with its axis along the solar rotation axis, it is found that plumes are inclined more horizontally than the dipole field. The lower the latitude, the larger is the deviation from the dipole field. The relationship between plumes and bright points has been investigated and they are not always associated. For the first data set, based on the 3-D height of plumes and the electron density derived from SUMER/SOHO Si VIII line pair, we found that electron densities along the plumes decrease with height above the solar surface. The temperature obtained from the density scale height is 1.6 to 1.8 times larger than the electron temperature obtained from Mg IX line ratios. We attribute this discrepancy to a deviation of the electron and the ion temperatures. Finally, we have found that the outflow speeds studied in the O VI line in the plumes corrected by the angle between the line-of-sight and the plume orientation are quite small with a maximum of 10 km s^{-1}. It is unlikely that plumes are a dominant contributor to the fast solar wind (see Fig. 61).

(L. Feng, B. Inhester, S. K. Solanki, K. Wilhelm, T. Wiegelmann, and B. Podlipnik in collaboration with the SECCHI team R. A. Howard, S. Plunkett, and J.-P. Wuelser)

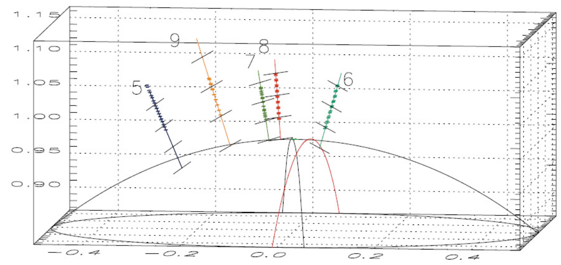

Fig. 61: Side view of the north polar cap on 1 June 200. The two *STEREO* satellites are on the right of the box. The long curve is a circular segment crossing the pole. The shorter black and red curves are the solar limbs as seen from *STEREO* A and B, respectively. The dotted points are the reconstructed 3-D plume axes. The solid lines are the extrapolations back to $r = 1\ R_\odot$. The uncertainties are indicated by the short black sticks.

Stereoscopic reconstruction and time series study of polar plumes from STEREO/SECCHI data using a wavelet-Hough transform

We developed a method to identify and determine the 3-D position of polar plumes in two corresponding images observed with the EUVI telescopes of *STEREO*/SECCHI.

The method is based on a combination of the Hough transform and the continuous wavelet transform. The Hough transform transfers a plume from an image into a single dot, defined by the Hough coordinates. The convolution of this Hough transform with the Mexican Hat wavelets at different scales yields a better localized dots with a good signal to noise ratio for plumes with different sizes and intensities (Fig. 62, top).

This method has two main aspects: The Wavelet-Hough space containts all the information from the original image. And the transform has the property of being invertible, which allows to have the backward projection into the image space (Fig. 62, bottom).

With this method, we are able to study the temporal evolution of plumes characterized by the intensity maxima in the Hough transform.

We applied this procedure to simultaneous *STEREO* images A and B at 171Å. Directly from the plumes coordinates the Wavelet-Hough space for the images A and B, we reconstruct their 3-D localizations and orientations on the Sun.

The capability of the method has been investigated with synthetic images built from a 3-D magnetohydrostatic coronal model.

We are working to automatize this procedure to scan longer time series. In future we will check whether the foot points of the detected plumes are correlated with

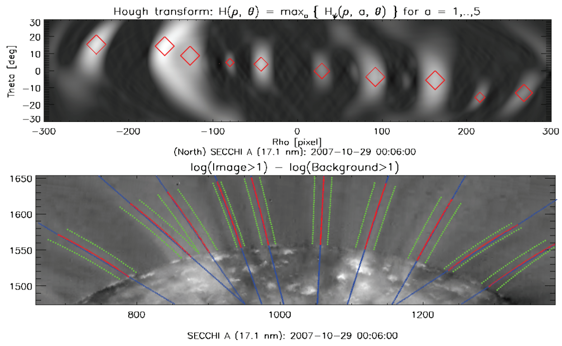

Fig. 62: Top: Red diamonds corresponds to intensity maximas at certain scales of plumes in the wavelet-Hough space. Bottom: The backward transformation of polar plumes on the coronal image. The red lines correspond to local maxima in the Hough space, and green lines indicate the computed width of the plume.

polar bright points.

(J. de Patoul, L. Feng, B. Inhester, and T. Wiegelmann)

The redshifted network contrast of transition region emission

The net redshift in the solar transition region (TR) emission lines has been known since the Skylab era. The reported peak downflow of 6 to 8 km/s in the quiet Sun (QS) at a temperature of around 10^5 K was well confirmed by high-resolution observations obtained by the SUMER spectrometer. To our knowledge, however, a satisfactory physical explanation of the net redshift has not yet been found. We aim at establishing a link with atmospheric processes and interpret the observed downflow as the most evident red branch of the prevailing global coronal mass transport. In this work we show that the spectrally resolved network contrast is offset in wavelength compared to the emission line itself (Fig. 63. This offset, if interpreted as redshift, peaks at middle transition region temperatures and is 10 times higher than the previously reported net redshift of transition region emission lines. We show that this effect can be reconstructed from the radiance distribution. We demonstrate that statistically the brighter pixels are more redshifted, and that this redshift-to-brightness relationship consequently causes both a significant shift of the network contrast profile and the well-known net redshift. This result is compatible with loop models, which assume downflows near both footpoints (cf., article on coronal convection by Marsch et al.; this volume). In contrast to earlier work, our new indirect method is unique in several ways, namely, it

· does not require an accurate wavelength calibration,

· does not require knowledge of the rest wavelength,
· closely relies on physical processes in the solar atmosphere.

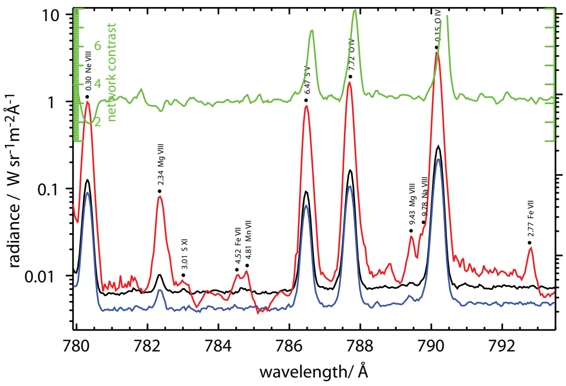

Fig. 63: Enlarged portion of the SUMER spectral atlas (Curdt et al. 2001) showing radiances of average QS (black), sunspot (red), and coronal hole (blue) regions. The network contrast (ratio bright network / cell interior in green), which is normally around 3, increases to values of 6 to 8 in TR lines, and the centroids of the contrast profiles are clearly redshifted.

(W. Curdt, H. Tian, and E. Marsch in collaboration with B. N. Dwivedi (Banares Hindu University, India))

The inverse assymetry of the H I Lyman-α and -β line profiles in the quiet Sun

Hydrogen is the most abundant element in the solar atmosphere. And thus its resonance lines, especially the Ly$-\alpha$ and Ly$-\beta$ lines, play an important role in the overall radiative energy transport of the Sun. Ly$-\alpha$ – by far the strongest line in the vacuum ultraviolet (VUV) spectral range – could, however, not be observed with the SUMER spectrograph because its enormous radiance would saturate the detectors. For the first time, a new method was applied, which employed the aperture door to reduce the incoming photon flux by a factor of $\approx$5 thus reaching a moderate level. A unique data set was acquired, where the full profiles of Ly$-\alpha$ and Ly$-\beta$ as well as the transition region lines λ 1206 Si III and λ 1032 O VI were recorded. The optically thin Si III line was employed to measure the Dopplershift in each pixel and to establish a velocity map. In a similar way to the radiance case, where we sorted the pixels of all observed locations on the disk by the total line radiance and defined six equally spaced radiance bins, we also define equally spaced velocity bins reaching from -3.0 km/s to 10.9 km/s for the scan at disk center. The profiles for these bins are displayed in Fig.64. A clear brightness-to-asymmetry relationship is evident; brighter features show a more asymmetric profile. It is most obvious that the asymmetries in the Ly$-\alpha$ and Ly$-\beta$ lines are reversed, and there is a clear correspondence between asymmetry and downflows for both lines. This surprising result is only poorly reproduced by static atmospheric models. From our work, we conclude that downflows must play a fundamental role in line profile formation. We plan further observations during the rise of solar cycle 24. These will reveal more details and indicate, whether there is an imprint of solar activity on the profile of these important lines.

(W. Curdt, H. Tian, L. Teriaca, and U. Schühle in collaboration with P. Lemaire (IAS Orsay, France))

Solar wind and heliosphere

Proton core heating and beam formation via parametrically unstable Alfvén-cyclotron waves

Numerical hybrid simulations were used to study the effects that compressible fluctuations, driven by parametric instabilities of Alfvén-cyclotron waves, have on solar wind proton velocity distributions (VDFs). Field-aligned proton beams are generated during the saturation phase of the wave-particle interaction, with a drift speed which is slightly greater than the Alfvén speed and is maintained until the end of the simulation. The main part of the distribution becomes anisotropic due to phase mixing, as is typically observed in the VDFs measured in the fast solar wind. We identified the key instabilities and also found that, even in the regime where fluid theory appears to be appropriate, strong kinetic effects still prevail.

Fig. 65 shows the contour plots of the proton VDF as obtained from the simulation at different normalized times. The apparent initial anisotropy is due to the overlapping of the particle transverse motion paths imposed by the slowly decreasing pump wave. By following the motion of individual protons, we found that this reshaping is due to pitch-angle scattering by the growing cyclotron daughter waves, leading to parabolic shell-like trajectories in velocity space as a dynamically stable final state.

(E. Marsch and Y. Maneva in collaboration with J. Araneda (University of Concepción, Chile))

Constraints on the temperature anisotropy of solar wind electrons

We have performed a statistical study of a substantial amount of electron data acquired in the solar

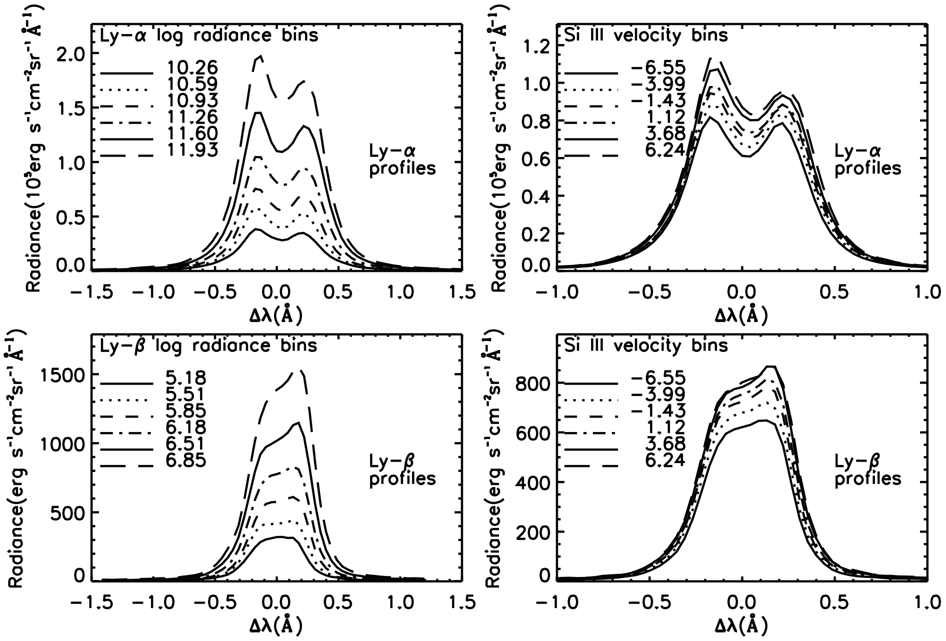

Fig. 64: Comparison of quasi-simultaneous line profiles of Ly$-\alpha$ and Ly$-\beta$ at disk center. We show the profiles for different radiance bins (left) and for different velocity bins as derived from line shifts in the Si III 1206 Å line (right). Negative values correspond to upflows, positive values to downflows.

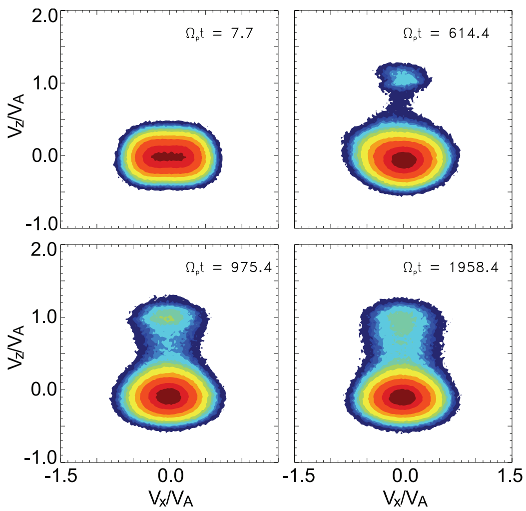

Fig. 65: Contour plots of the proton VDF in the (v_X, v_Z) plane at four instants of time. The colour coding of the contour lines corresponds, respectively, to 75 (dark red), 50 (red), 10 (yellow) % of the maximum, with a final density of about 7 % for the beam.

wind to understand the constraints imposed on electron temperature anisotropy by plasma instabilities and Coulomb collisions. We used a large data set of electron measurements from three different spacecraft (Helios 1, Cluster II, and Ulysses). The data were collected at low ecliptic latitudes and covered the radial distances from the Sun that range from 0.3 up to 4 AU.

We estimated the electron temperature anisotropy using fits of the measured electron velocity distribution functions as acquired in situ. We used the analytical model with two populations (core and halo), and the properties of both populations were studied separately. We examined all the acquired data in terms of temperature anisotropy versus parallel electron plasma beta, and then we related the measurements to the growth rates of unstable wave modes.

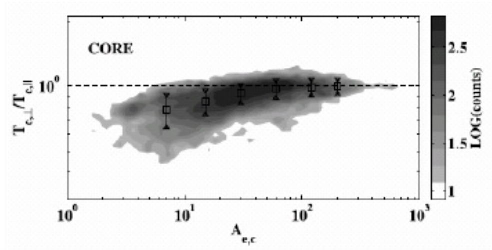

Fig. 66: Dependence of the electron temperature anisotropy of the core population on the Coulomb collisions represented by the collisional age $A_{e,c}$.

The effects of Coulomb collisions on the electron temperature anisotropy is shown in Fig. 66. They can be quantifed in terms of the collisional age $A_{e,c}$, defined as the number of collisions suffered by an electron during the expansion time of the solar wind. We showed that both instabilities and collisions are strongly related to the isotropisation process of the electron core population. In addition we examined the radial evolution of these effects during the expansion of the solar wind. We also showed that the bulk of the solar wind electrons is constrained by Coulomb collisions, while the large departures from isotropy are constrained and regulated by plasma instabilities.

(E. Marsch in collaboration mainly with Š. Štverák (Institute of Atmospheric Physics, Academy of Sciences of the Czech Republic, Prague, Czech Republic))

Heating of ions by parametrically unstable Alfvén-cyclotron waves in the extended solar atmosphere

Large-amplitude Alfvén/ion-cyclotron waves are normal modes of a hot collisionless homogeneous plasma. In situ measurements of particles and fields in high-speed solar wind show that large-amplitude Alfvén waves are intrinsic kinetic features of the plasma originating in coronal holes (CHs). Furthermore, recent analytical calculations and simulation works have shown that nonlinear circularly polarized electromagnetic (EM) waves are parametrically unstable, and that they couple to the thermal motion of the particles and generate a sequence of wave-wave interactions which result in the formation of both EM and acoustic micro-turbulent spectra. Those wave-wave processes can generate acoustic waves out of the thermal noise of the system, and thus give rise to "daughter" cyclotron waves. These in turn can fall in Landau and cyclotron resonance with the particles and thus deform their velocity distribution functions (see Fig. 67) and cause the appearance of strong ion anisotropies (conic features) and kinetic properties as observed in the fast solar wind.

By means of numerical 1-D hybrid simulations, we consider the parametric instabilities of large-amplitude Alfvén/ion-cyclotron waves and the consequent wave-particle interactions, and discuss their importance for modelling the evolution of ion velocity distribution functions in the tenuous and collisionless plasma of coronal holes and the fast solar wind. We study the nonlinear evolution of the parametric instabilities by analyzing the simulation results in terms of microinstabilities, and by discussing the influence of both Landau and cyclotron resonances on the evolution of the ion distributions. We demonstrate the origin of a relative drift between the protons and alpha particles, show the concurrent anisotropic ion heating and follow the simultaneous proton beam formation. Finally, we focus on the development and evolution of both electromagnetic and acoustic micro-turbulence, and we present indications for an inverse energy cascade from shorter to longer wavelengths.

(Y. Maneva and E. Marsch in collaboration with J. Araneda (University of Concepción, Chile))

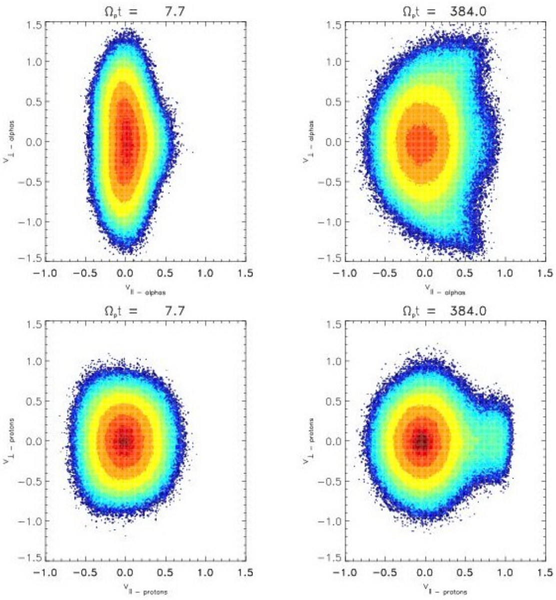

Fig. 67: Contour plots of the velocity distribution functions taken at two different times. The upper panels show the anisotropic wave heating of alpha particles, the lower ones illustrate the beam formation in the proton distribution. The x- and y-axes, respectively, refer to the parallel and perpendicular components of the velocity with respect to the external homogeneous magnetic field.

In situ observations of CIRs on STEREO during 2007 – 2008

During the 2007 – 2008 solar minimum period the *STEREO* spacecraft offered a new opportunity to study CIRs from spacecraft separated by up to five days of corotation. During this period there were numerous high speed solar wind streams and associated energetic particle increases from CIRs. Fig. 68 shows spectrograms of SIT-A and SIT-B CIRs for the month of August 2008, when the two spacecraft's angular separation corresponded to about five days of corotation. The figure shows that while some features are clearly seen by both SIT-B and SIT-A, this is not always the case. For example, the intense event starting around day 220 on SIT-B is clearly seen on SIT-A around day 225. However, the CIR related brief intensity increases on days 224 – 227 seen by SIT-B have no clear signature at SIT-A. While there is some temporal evolution of the CIRs over periods of days, the fact that many of the events are recurring indicates that the overall structures can be present for periods of several solar rotations. For this reason, it is likely that the bulk of the changes we observe were due to the relatively small and irregular coronal hole source sizes at the Sun, taken together with the different heliolatitude connections of the spacecraft connecting to different solar features.

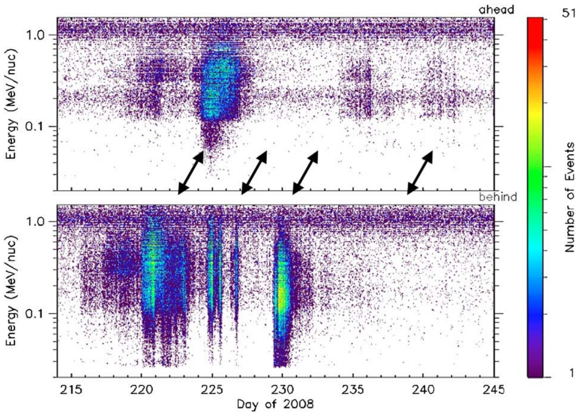

Fig. 68: Spectrograms of ion energy vs. arrival time for SIT-A (upper panel) and SIT-B (lower panel) for August 2008. During this period the angular separation of the two *STEREO* spacecraft increased from 65.4 ° to 71.2 °, or roughly five days of corotation. Double-ended arrows point to nominally associated features, or features that were observed on one spacecraft but not the other.

(R. Bučík, U. Mall, and A. Korth in collaboration with G. M. Mason (APL/JHU, Laurel, MD, USA))

Energetic ions from CIRs

Using SIT instrument on *STEREO* we have surveyed abundances and energy spectra of $\sim 0.1 - 1.0$ MeV/n heavy ions in two corotating interaction regions (CIRs) on 18 May (CIR1), and 24 May (CIR2) 2007, that occurred during two weak solar energetic particle (SEP) events. The ion intensity increases related to the CIR2 were much more pronounced compared with those associated with the CIR1, although the total pressure, the magnetic field magnitude and the speed difference between high and slow solar wind were less enhanced. We found that the ratio of He CIR2 and CIR1 fluence decreases with energy as a power-law below $\sim$ 1 MeV/n. The energy spectra of H and He inside the CIR2 are much softer compared to the spectra observed in the CIR1 region. Based on these findings, we argue the that larger intensities in the CIR2 could be due to an additional source population. Fig. 69 shows that the elemental abundances within the CIR2 (interval 6–7) and in the high speed streams of CIR1 (interval 3) have a SEP-like composition. The energy spectra of H and He inside the CIR2 were close to the preceding SEP event spectra. The similarity in the elemental composition and in the spectral slopes suggests that CIR2 has as seed population ions from the preceding SEP event. For the CIR1 event the ions seem to be contamined by SEPs.

(R. Bučík, U. Mall, and A. Korth in collaboration with G. M. Mason (APL/JHU, Laurel, MD, USA) and R. Gómez-Herrero (Universität Kiel, Kiel, Germany))

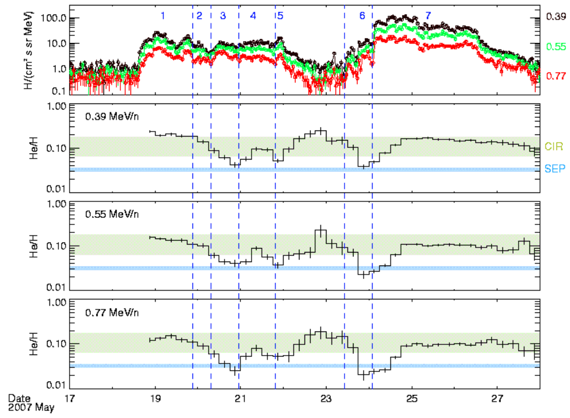

Fig. 69: Upper panel: hourly averaged proton intensities between 0.32 and 0.91 MeV. Panels 2-4: six-hour averaged He/H ratio. The green and blue bands show ranges of He/H ratios measured in CIR and SEP events. The dashed vertical lines mark intervals, where the SIT H intensities are believed to be dominated by contributions from different ion populations.

Simulation of SIT

A Monte Carlo simulation of a time-of-flight (TOF) Suprathermal Ion Telescope (SIT) aboard the *STEREO* spacecraft was performed by Geant. The instrument identifies the incident ion mass and the energy by measuring the TOF and the residual kinetic energy of the particle that enters the telescope through a thin nickel foil and stops in the silicon solid state detector (SSD) at the rear of the telescope. The TOF is determined by start and stop pulses from micro channel plates (MCPs) that detect secondary electrons that are emitted from the foil and the surface of the SSD. The simple mass model of the SIT telescope consists of four absorbers: nickel entrance foil, silicon SSD, and adjacent to the SSD an aluminum surface metallization, and a silicon junction dead layer. The simulated data in TOF-Energy plane are shown in Fig. 70. In the energy range of $0.1 - 1.0$ MeV/n the σ/m is $\sim$ 0.14 for six species, close to the calibration value of 0.10. In addition to the energy losses in the all absorbers, the system noise in the SIT instrument with FWHM of $\sim$ 50 keV and dispersion in TOF with FWHM of $\sim$ 1 ns were taken into account in the simulations. The simulations of angular scattering and energy losses in the SIT telescope show that: 1) angular scattering in the entrance foil of the telescope is responsible for intrinsic TOF dispersion, and for the increase of the nominal instrument field-of-view which leads to high energy losses in the foil, 2) Energy losses in both the SSD surface metallization and the junction dead layer contribute to the same amount to the mass resolution as the dispersion in energy and TOF measurements. Scattering in the entrance foil has a minor effect, about 30 % of the previous contributors, 3) penetrating particles do not form an identifiable component of the background in the simulated instrument.

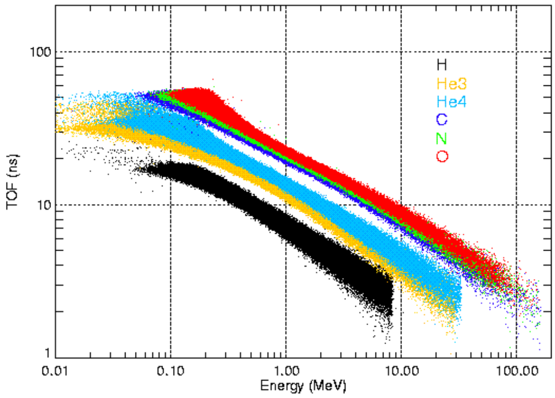

Fig. 70: Simulated data for different ions with a power-law energy distribution.

(R. Bučík, U. Mall, and A. Korth)

Observations of a flux rope in the solar wind

A flux rope is a helical magnetic structure, extending along its orientation in space. Though flux ropes in the magnetosphere have been widely studied, further observations about the flux ropes in the solar wind are still needed to clarify the basic characteristics, such as the length, the diameter, and the possible generation mechanism. Multiple-spacecraft observations are particularly demanded to study the space variation of the flux rope in the solar wind. On 15 January 2007, an extended magnetic structure (Fig. 71) was observed consecutively by five spacecraft (ACE, WIND, *STEREO* A and B, and Cluster) in the solar wind. The similar bipolar magnetic field variations from five spacecraft suggest a two-dimensional magnetic structure. The abrupt disappearance of the beam electrons in the structure core suggests the magnetic isolation of the structure core from the surrounding environment. The analysis shows that this magnetic structure is a flux rope, which extends over at least 180 R_E in space. The length and orientation of the flux rope was determined by a local Minimum Variance Analysis (MVA) from individual spacecraft observations of the magnetic field and a timing analysis based on the joint observations by all five spacecraft. The result shows that the orientation of the flux rope stays constant in space and time. The flux rope is embedded in a Corotating Interaction Region (CIR), which followed a magnetic cloud. The small scale and the possible reconnection signatures inside the flux rope suggested that the flux rope could be generated locally by magnetic reconnection in the solar wind.

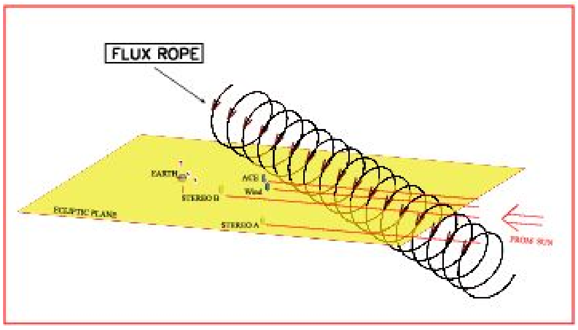

Fig. 71: Sketch of the flux rope being crossed by five spacecraft.

(P. Ruan, A. Korth, E. Marsch, B. Inhester, S. K. Solanki, T. Wiegelmann, and R. Bučík in collaboration with Q.-G. Zong (Center for Atmospheric Research, University of Massachusetts Lowelland, USA) and K.-H. Fornacon (Institut für Geophysik und Extraterrestrische Physik, Technische Universität Braunschweig, Germany))

Stereoscopic reconstructions of Coronal Mass Ejections (CME) from STEREO COR data

We have investigated in three consecutive papers different approaches to retrieve the main parameters of a CME plasma cloud (see Fig. 72) from *STEREO*/COR1 and 2 observations. As the main parameters, we extracted propagation direction and speed but also the CME shape for CMEs released both on the limb and on the front side of the Sun.
The methods comprised:

1. Center of mass reconstruction in a stacked epipolar planes
2. Height-time reconstruction of identifyable CME density irregularities
3. Reconstruction of the CME surface leading edge
4. Polarization ratio reconstruction of a mean meridional CME plane
5. Local correlation tracking of CME density irregularities
6. Forward modeling of an assumed class of CME shapes

From an intercomparison, we find that we can obtain the propagation longitude with a precision of ±10 degrees and the speed of CMEs approaching Earth to better than 10 %.

(B. Inhester and B. Podlipnik in collaboration with M. Mierla (Astr. Inst. Bucharest, Romania), N. Srivastava

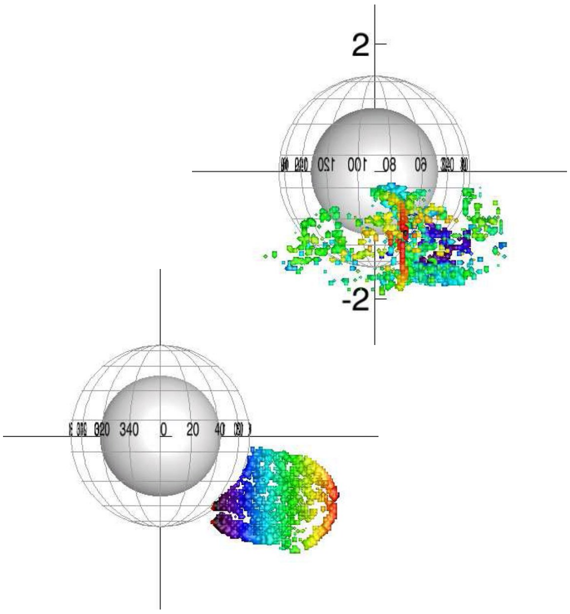

Fig. 72: Reconstruction of a CME cloud by the Local Correlation Tracking. The coloured dots all lie inside the CME cloud, their colour depending on the distance from the Sun's centre. The two plots show the results as viewed from approximately the propagation direction of the CME and a direction rotated by 90 degrees.

(Udaipur Solar Obs., India), J. Davila (GSFC Greenbelt, MD, USA), C. Marqué, L. Rodriguez, S. Gissot, A. N. Zhukov, and D. Berghmans (ROB Bruxelles, Belgium))

Solar activity and Sun-Earth relations

On the common solar signal in different cosmogenic isotope data sets

In this article, we aim to determine frequency ranges and intervals of time in which the solar signal dominates in different cosmogenic isotope data. From a ^{14}C-based reconstruction of cosmic ray intensity over the last millennia, we computed expected ^{10}Be variations in two Antarctic sites (Dom Fuji and South Pole) and two Greenland sites (Dye-3 and GISP-2) and compared them with the actually measured ^{10}Be abundance at the sites. By applying different methods of analysis, such as bivariate correlation, conventional FFT coherence, and wavelet coherence, we found the following: (1) The modeled series, on the basis of ^{14}C data, are in good agreement with the measured ^{10}Be data sets, on different timescales and at different locations, confirming the existence of a common solar signal in both isotope data. (2) The ^{10}Be data are driven by the solar signal on timescales from about 100 years up to 1000 years or even to multimillennial scales (at the longer scales, paleomagnetism plays an increasingly important role). (3) The local climate dominates the ^{10}Be data mostly on short ($<$ 100 years) timescales, but the solar signal becomes important even at short scales during periods of Grand minima of solar activity. (4) There is an indication of a possible systematic uncertainty in the early Holocene, likely due to a not-perfectly-stable thermohaline circulation, which requires additional studies. We have shown that both ^{14}C- and ^{10}Be-based records are consistent with each other over a wide range of timescales and time intervals. They form a robust basis for quantitative reconstructions of solar activity variations in the past.

(S. K. Solanki in collaboration with I. G. Usoskin (University of Oulu, Finland), K. Horiuchi (Hirosaki University, Japan), G. Kovaltsov (Ioffe Physical-Technical Institute, St. Petersburg, Russia), and E. Bard (Collège de France, Aix-en-Provence, France))

Correlation between growth rate and amplitude of solar cycles

We have considered the statistical relationship (Fig. 73) between the growth rate of activity in the early phase of a solar cycle with its subsequent amplitude on the basis of four datasets of global activity indices (Wolf sunspot number, group sunspot number, sunspot area, and 10.7-cm radio flux). In all cases, a significant correlation is found: stronger cycles tend to rise faster. This confirms that the essence of the Waldmeier effect, i.e., that stronger cycles tend to show a faster rise of activity levels during their ascending phase than weaker cycles, is a robust property present in all activity indices, refuting some claims in the literature.

Owing to the overlapping of sunspot cycles, this correlation leads to an amplitude-dependent shift of the solar minimum epoch. We show that this effect explains the correlations underlying various so-called precursor methods for the prediction of solar cycle amplitudes and also affects the prediction tool of Dikpati et al. (2006) based upon a dynamo model. Inferences as to the nature of the solar dynamo mechanism resulting from predictive schemes which (directly or indirectly) use the timing of solar minima should therefore be treated with caution.

For our understanding of the origin of the solar magnetic field, it is important to disentangle the effects of "real" physical precursors, i.e., properties of the old cycle directly affecting the flux generation for the next cycle or early high-latitude manifestations of the new cycle, from apparent precursors, which derive their

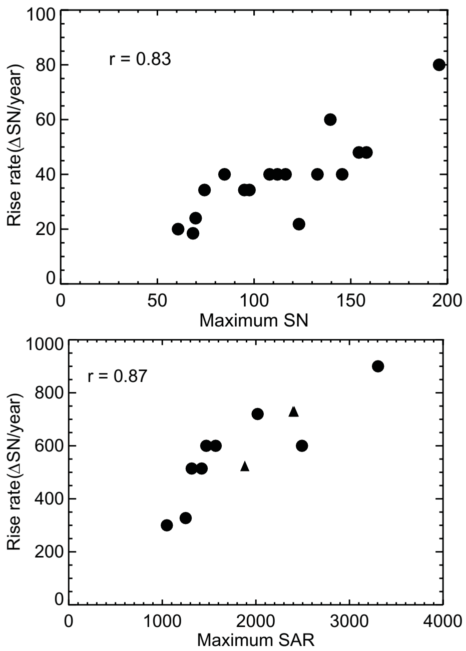

Fig. 73: Scatter diagrams of rise rates versus cycle amplitude for two sets of solar activity indices: Wolf sunspot number (top), and sunspot area (bottom). The corresponding linear correlation coefficients are indicated (after Cameron and Schüssler (2008)).

predictive power from the the amplitude-dependent shift of the minimum epoch.

(R. Cameron and M. Schüssler)

Total solar irradiance: Is there a secular trend between 1978 and 2003?

A gap in the total solar irradiance (TSI) measurements between ACRIM (Active Cavity Radiometer Irradiance Monitor) I and ACRIM II led to the ongoing debate on the presence or not of a secular trend between the minima preceding cycles 22 (in 1986) and 23 (1996). We have reconstructed the total solar irradiance between 1974 and 2003 using solar surface magnetic field distribution derived from Kitt Peak magnetograms and continuum images. We have then compared the model with three existing composites of solar irradiance measurements going back to 1978. A good correspondence is found with the TSI composite from PMOD/WRC, with no bias between the three cycles. The agreement with the other composites (the ACRIM composite mainly based on ACRIM I, II and III, and the IRMB composite from the Institut Royal Meteorologique Belgique) is less marked. In particular, a secular trend in the TSI exhibited by these composites is not present in the reconstructions. Hence any secular trend in TSI between 1978 and 2003 is not due to magnetic fields at the solar surface.

Recently, Scafetta-Willson (2009) proposed to use our model (Krivova et al., A&A, 467, 335, 2007) to bridge the ACRIM-gap by comparing the model directly to the ACRIM I and II data rather than to the composites. Unluckily, they have taken the model which was designed to give a good estimate of the secular variation in the TSI, but is less accurate on time scales of several months to years, i.e. exactly the time scales most critical for such an analysis. We have employed the model based on direct measurements of the solar photospheric magnetic field (magnetograms). The accuracy of this model on months to years timescales is significantly higher than that of the model developed for long-term reconstructions used by Scafetta-Willson (2009). The constructed 'mixed' ACRIM – SATIRE composite shows no increase in the TSI from 1986 to 1996 either, in contrast to the ACRIM TSI composite.

(N. A. Krivova and S. K. Solanki in collaboration with T. Wenzler (Hochschule für Technik, Zürich, Switzerland)))

Reconstruction of solar UV irradiance since 1974

Solar irradiance variations show a strong wavelength dependence. Whereas the total solar irradiance varies by about 0.1 % over the solar cycle, variations at wavelengths around the Ly-α emission line near 121.6 nm reach up to 100 %. At the same time, variations of the solar UV irradiance are an important driver of chemical and physical processes in the Earth's upper atmosphere and may also influence global climate. We have reconstructed solar UV irradiance in the range 115 – 400 nm over the period 1974 – 2007 by making use of the empirical extension of the SATIRE models employing SUSIM data (Krivova et al., A&A, 452, 631, 2006). The evolution of the solar photospheric magnetic flux, which is a central input to the model, is described by the magnetograms and continuum images recorded at the Kitt Peak National Solar Observatory between 1974 and 2003 and by the MDI instrument on SOHO since 1996. The reconstruction extends the available observational record by 1.5 solar cycles. The reconstructed Ly-α irradiance agrees well with the composite time series by Woods et al. (JGR, 105 (A12), 27, 195, 2000) (Fig. 74). The amplitude of the irradiance variations in the wavelength regions of special interest for studies of the Earth's climate (Ly-α and oxygen absorption continuum and bands between 130 and 350 nm) is one to two orders of magnitude stronger than in the visible or if integrated over all wavelengths (total solar irradiance).

(N. A. Krivova, S. K. Solanki, T. Wenzler, and B. Podlipnik)

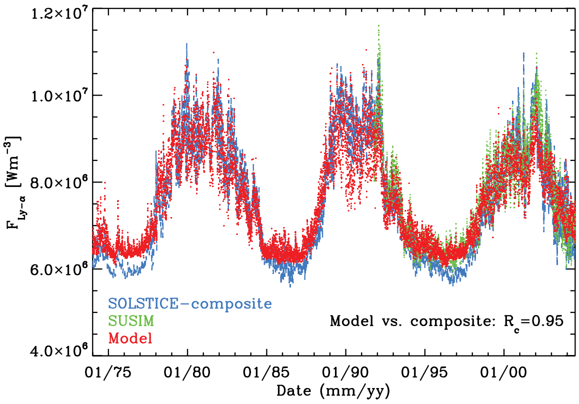

Fig. 74: Solar Ly-α irradiance since 1974: reconstructed (red), measured by the SUSIM instrument (green) and compiled by Woods et al. (blue). This latter record includes measurements by the space instruments AE-E, SME, UARS SOLSTICE and TIMED SEE, as well as proxy models based on Mg C/W and F10.7 indices, all adjusted to the absolute level of SOLSTICE.

Historical Ca spectroheliograms: making an old resource available for new studies

Various observatories around the globe started regular full-disc imaging of the solar atmosphere in the Ca II K line in the early decades of the 20th century. The archives made by these observations have the potential of providing far more detailed information on solar magnetism than just the sunspot number and area records to which most studies of solar activity and irradiance changes are restricted. We have analysed the image quality and content of three Ca II K spectroheliogram time series, specifically those obtained by the digitization of the Arcetri, Kodaikanal and Mt Wilson photographic archives, in order to estimate their potential value for studies focussing on time scales longer than the solar cycle. We have also compared the results to those obtained from similar present-day observations taken with the Meudon spectroheliograph and with the Rome-PSPT. We show that historic data suffer from stronger geometrical distortions and photometric uncertainties than the present-day observations. The photometric uncertainties mostly originate from the photographic calibration of the original data and from stray-light effects. We also show that the image contents of the three analysed series vary in time. These variations are due to instrumentation changes and aging, as well as changes of the observing programmes.

We have also investigated whether image-segmentation techniques, such as those developed for identification of plage regions on present-day Ca II K observations, could be used to process historic series. The segmentation technique we have tested gave reasonably consistent results for the three analysed series after application of a simple photographic calibration. Although the plage areas measured from the three analysed series differ somewhat (Fig. 75), the difference to previously published results is larger.

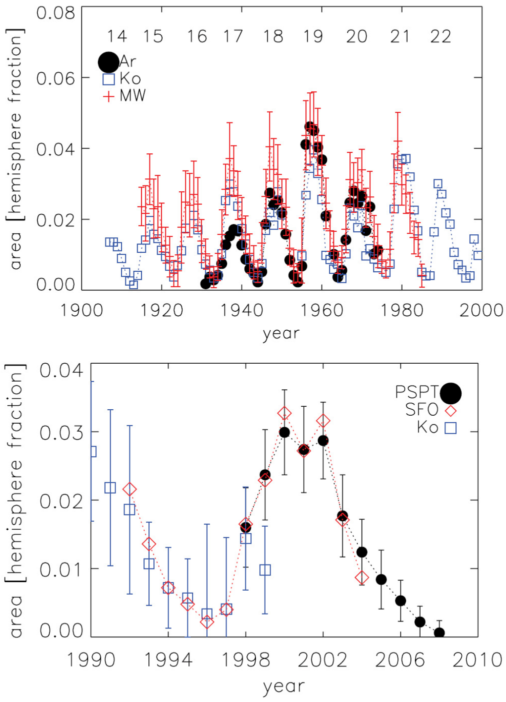

Fig. 75: Upper panel: Temporal variation of yearly median values of the plage coverage measured from the Arcetri, Kodaikanal and Mt Wilson series. The error bars represent the standard deviation of measured values over the annual interval: for clarity they are only shown for the Mt Wilson series. Cycle numbers are given at the top of each cycle. Lower panel: Same as in the top panel, but now for the Kodaikanal, PSPT and San Fernando Observatory (SFO) Ca II observations since 1990.

(S. K. Solanki and N. A. Krivova in collaboration with I. Ermolli (Rome Observatory, Italy) and A. Tlatov (Pulkovo Observatory, Russia))

Sunspot tilt angles and the strength of the solar cycle

It is well known that the tilt angles of active regions increase with their latitude (Joy's Law). It has never been checked before, however, whether the average tilt angles change from one cycle to another. We employ two data sets that cover the years 1917 – 1985 and 1913 – 1987 from the Mount Wilson and Kodaikanal observatories respectively. Since stronger cycles have sunspots in average at highter latitudes, Joy's law would suggest larger tilt angles during stronger cycles. In contrast, we find an anti-correlation between the mean tilt angle and the cycle strength, which becomes even stronger after removing the cycle-to-cycle variation due to Joy's law. We also find a strong correlation between the maximum smoothed tilt angle weighted by the area and latitude of sunspots and the amplitude of the next solar cycle (Fig. 76). It appears that tilt angles play an important role in the build up of magnetic field for the following cycle, which has important implications for the prediction of future solar activity.

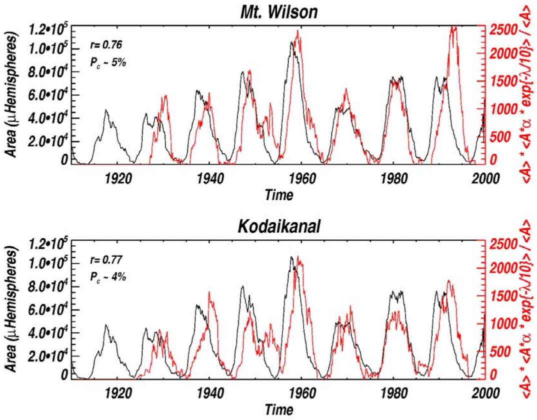

Fig. 76: Black curve is monthly means of sunspot area smoothed over 1 yr. Red curve is monthly means of sunspot area multiplied by monthly means of weighted sunspot tilt angle shifted by 11 years, smoothed over 2 years. The correlation coefficients (r) given in each frame are between the peaks of the red and black curves. Also given is the probability (P_C) that the correlation is due to chance.

(M. Dasi, S. K. Solanki, N. Krivova, R. Cameron, and T. Peñuela)

Ongoing and future solar missions and instruments

Solar Orbiter

Status and programmatic issues

The Solar Orbiter mission has existed for almost 10 years. It has been decribed extensively in previous annual reports. Presently, its main characteristics are the following: The spacecraft will reach an orbit with lowest perihelion at about 0.24 AU. By multiple Venus gravity assist manouvres (swing-bys) it will increase the inclination of its orbital plane with respect to the solar equator to 30° for the nominal mission, and 34° for the extended mission (goal) permitting polar observations. The launch is planned for 2017 (with 2018 as back up) by a NASA-provided launch vehicle (Atlas 5 or Delta 4), and as baseline still a Soyuz-Fregat 2-1b from Kourou as back-up. The science payload instruments and dedicated support elements will have a total mass of 180 kg requiring a power of 180° W. The three-axis stabilised spacecraft will be Sun pointing and equipped with a heatshield to protect the bus and payload. The overall mass is about 1320 kg. The solar arrays maximum power demand is 1100 W. A bi-propellant chemical propulsion system will be used. The ground station using X/Ka-band telemetry will be New Norcia in Australia.

After many political discussions and reconsiderations of the mission by the various committes of the ESA advisory structure, the Science Programme Committee (SPC) of ESA decided in late 2008, upon suggestion by the executive and director of the science programme, that Solar Orbiter should become an M-size candidate mission in the new Cosmic Vision (CV) programme. The consequence was that it would have to compete anew, but now with the other currently 6 M-size candidate missions proposed for CV. The final down-selection will occur by the end of 2009, whereby 2, 3 or 4 candidate missions may be down-selected. The results and the confirmation of the selected missions is expected in early 2010. The down-selection review will again examine the science case, the payload technological readiness and funding, spacecraft technical feasibility, programme cost and schedule. The CV competitors proposed for solar system mission are Cross-Scale, Marco-Polo and Solar Orbiter. Their industrial studies will end between June and September 2009, with techical reviews in October 2009. The final SPC downselection will only take place in February 2010.

Following the common announcement of opportunity (AO) for the Solar Orbiter by ESA and NASA in autumn 2007, the MPS responded with several proposals. The due date for proposal delivery was 15 January 2008. In late March 2008, the instrument selection was finally announced by the agencies. The MPS proposals were quite successful. MPS will participate in Solar Orbiter with key instrumentation for imaging and spectroscopy in the visible and extreme ultraviolet light. These instruments are the PHI (former VIM), EUI, SPICE (former EUS), and METIS (former COR), which are all by now well defined technically and scientifically. They are described in more detail in the sections below.

(E. Marsch)

The Multi Element Telescope for Imaging and Spectroscopy (METIS) instrument for the Solar Orbiter mission

METIS, the Multi Element Telescope for Imaging and Spectroscopy, is an instrument proposed to the European Space Agency to be part of the payload of the

Solar Orbiter mission. The instrument was designed by a consortium lead by E. Antonucci (INAF-Turin Astronomical Observatory, Italy) and comprising Institutes in Germany (MPS), Italy, France, the UK and in the United States.

The proposal submitted to ESA in January 2008 consisted of three different interconnected elements, COR, EUS and SOCS, sharing the same optical bench, electronics, and S/C heat shield aperture. COR is a visible-EUV multiband coronagraph based on a classical externally occulted design. EUS is the component of the METIS EUV disk spectrometer which includes the telescope and all the related mechanisms. Finally, SOCS is the METIS spectroscopic component including the dispersive system and the detectors. The capability of inserting a small telescope collecting coronal light was added to perform also EUV coronal spectroscopy. METIS/COR can simultaneously image the visible and ultraviolet emission of the solar corona and diagnose, with unprecedented temporal coverage and space resolution the structure and dynamics of the full corona in the range from 1.2 to 3.0 (1.6 to 4.1) solar radii at minimum (maximum) perihelion during the nominal mission. METIS could also perform spectroscopic observations of the solar disk and out to 1.4 solar radii within the 50 to 150 nm spectral region (EUS component), and of the geo-effective coronal region 1.7 to 2.7 solar radii within the 30 to 125 nm spectral band (SOCS component).

The METIS instrument was selected by ESA in March 2009 but without the SOCS and EUS components. However, the Payload Review Committee recommended retaining the full scientific capabilities of the COR component, including the VUV channels in the Lyman lines of H I 121.6 nm and He II 30.4 nm.

The MPS contribution consists in providing both the visible-light and VUV detector of METIS.

(L. Teriaca, U. Schühle, and S. K. Solanki)

The Solar Orbiter PHI instrument

A Visible Light Imager and Magnetograph (VIM) is a primary instrument of the remote-sensing package of ESA's Solar Orbiter mission. A consortium for implementation of such an instrument, led by the MPS, has been formed. This consortium has responded to the Announcement of Opportunity (AO) for the Solar Orbiter payload released by ESA in October 2007 with a proposal for a Polarimetric and Helioseismic Imager (PHI, see Fig. 77) as an implementation of the VIM instrument (submission January 2008).

The proposed design is based on two optical telescopes – a high-resolution Telescope (HRT) and a Full Disk Telescope (FDT) – as well as a Filtergraph coupled alternately to either telescopes. This concept allows measuring the full magnetic field vectors and the velocity fields at the photospheric level by scanning across a magnetically sensitive spectral line.

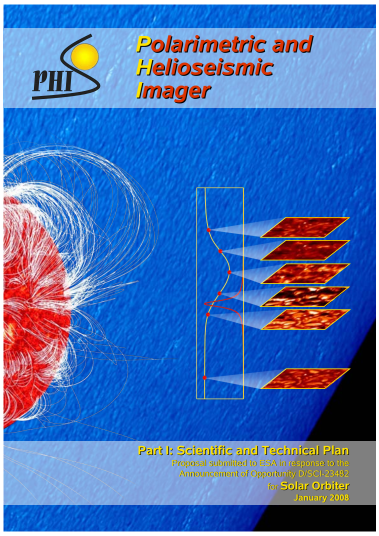

Fig. 77: Cover Page of the proposal for a Polarimetric and Helioseismic Imager (PHI) for Solar Orbiter.

In July 2008 the PHI instrument was conditionally selected as part of the SOLO payload. In an iterative process between the PHI team and the SOLO project team the instrument was successfully consolidated to match the constrained spacecraft resources.

Two Technology Development Activities (TDA) were initiated by ESA based on input from the PHI team. The TDAs are related to the crucial heat rejecting entrance windows of PHI and the PHI detector. The progress of the TDAs was monitored by the PHI team with respect to compliance with performance specifications. The TDAs showed promising initial results.

(J. Woch, A. Feller, A. Gandorfer, L. Gizon, J. Hirzberger, A. Lagg, U. Schühle, and S. K. Solanki in collaboration with V. Martínez Pillet (IAC, Tenerife), A. Alvarez (INTA, Madrid), T. Appourchaux (IAS, Paris), W. Schmidt (KIS, Freiburg) and others)

The Solar Orbiter EUI instrument

The Extreme-Ultraviolet Imager (EUI) is a suite of remote-sensing telescopes which will image at high-resolution the structures in the solar atmosphere, from the chromosphere to the corona.

In response to the call for proposals by ESA a consortium was formed to propose the EUI instrument package with one Principal Investigator and three Lead-Co-Investigators from MSSL (UK), IAS (F), and

MPS (G). The proposal was submitted to ESA on 15 January 2008 by J. F. Hochedez (ROB, Belgium) as Principal Investigator and six Co-investigators of MPS. Upon selection of the instrument package, a reduction of complexity was imposed by the Payload Review Committee, which requested the deletion of one of the high-resolution channels, namely the 19.5 nm EUV-telescope. A re-design of the entire package and a re-assessment of the mass budget was carried out and submitted to ESA. The resulting configuration is shown in Fig. 78.

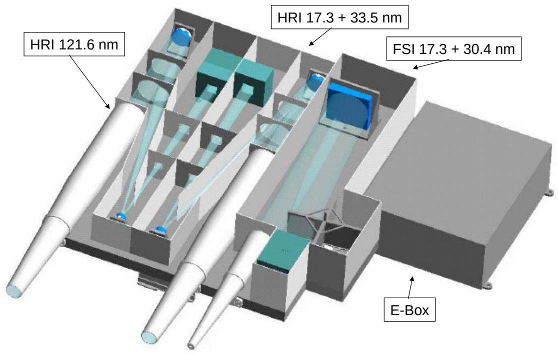

Fig. 78: Configuration of the EUI telescope suite

It consists of one dual-band EUV-HRI, one Lyman-Alpha HRI, and one dual-band FSI. The dual-band systems use a filter wheel for band selection. The preferred wavelength bands are 121.6 H I, 17.3 Fe IX/X, and 33.5 Fe XVI lines for HRIs, to cover the transition region and cool and hot coronal plasma, and the bands 17.3 Fe IX/X and 30.4 He II for the FSI.

The contribution of MPS, the Lyman-Alpha HRI, plays a key role in the suite of EUI telescopes. Future activities of the instrument design are the space-qualification of the Lyman-alpha narrow-band interference filter and the fabrication of a prototype camera system with image intensifier for 121 nm.

(U. Schühle, J. Büchner, W. Curdt, E. Marsch, S. Solanki, and L. Teriaca in collaboration with the team of EUI Co-Investigators)

SPICE – the EUV spectrograph for Solar Orbiter

During the past years several studies had been carried out in preparation of the proposal to NASA for the Extreme Ultraviolet Spectrograph, dubbed EUS in the Solar Orbiter model payload (cf., previous reports). Based on these studies, a mature design was developed and proposed to NASA by a proto-consortium, lead by Don Hassler (SWRI, USA) with contributions from GSFC (USA), MPS (Germany), RAL (UK), IAS (France) and ITA (Norway). The Spectral Imaging of the Coronal Environment (SPICE) investigation is a high-resolution, imaging spectrograph with a movable occulter to observe both on the solar disk and off-limb out to 3.0 solar radii. The solar occulter is used to reduce stray light for outer coronal observations by fully occulting the solar disk. The proposal was fully selected by NASA, the proposal assessment report mentions its high technology readiness level and only small weaknesses. NASA regards SPICE as key instrument of Solar Orbiter and requests no descope actions. The MPS work package *'Telescope main mirror with B_4C/Ir coating'* plays a key role in the SPICE optical and thermal design. It involves new technology and requires phase-A studies to demonstrate the long-term stability of the coating under environmental conditions with intense-UV and particle radiation and extreme temperature excursions.

(W. Curdt, U. Schühle, E. Marsch, and L. Teriaca)

Sunrise: A balloon-borne telescope for high-resolution observations of the Sun

Sunrise is a balloon-borne solar telescope with an aperture of 1 m, working in the UV and visible optical domain. The main scientific goal of Sunrise is to study the structure and dynamics of the magnetic field in the atmosphere of the Sun at high spatial resolution. Sunrise will provide diffraction-limited images of the photosphere and chromosphere with an unprecedented resolution down to 35 km at wavelengths around 220 nm. Focal-plane instruments are a UV filter imager (SUFI), a Fabry-Perot imaging magnetograph (IMaX), and a spectrograph/polarimeter (SUPOS). Stratospheric long-duration balloon flights of Sunrise over the North Atlantic and/or Antarctica are planned, starting in summer 2009. Sunrise is a joint project of the Max-Planck-Institut für Sonnensystemforschung (MPS), Katlenburg-Lindau, with the Kiepenheuer-Institut für Sonnenphysik (KIS), Freiburg, the High-Altitude Observatory (HAO), Boulder, the Lockheed-Martin Solar and Astrophysics Lab. (LMSAL), Palo Alto, and the Spanish IMaX consortium.

Project status:

Having successfully performed the test flight in October 2007, the project is now preparing for the first scientific flight in summer 2009 from ESRANGE, Kiruna, North Sweden. Negotiations with NASA and ESRANGE responsibles have lead to an agreement about conducting the upcoming flight with the support of the Columbia Scientific Ballooning Facility. Details and planning of the campaign were discussed during the Project Initiation Conference on 13 November 2008 in Washington.

The hardware development of Sunrise made good progress. The long lead item No. 1, the Sunrise primary mirror, was shipped on 2 June 2008 from SAGEM, France, to the telescope manufacturer Kayser-Threde, Munich. The 1-meter-aperture lightweighted Zerodur mirror was manufactured, polished and ion-beam figured and coated within 33 months (contract kick-off to delivery). A surface accuracy of better than 30,2 nm rms (@632,8 nm, 0° elevation) has been achieved. A map imprint provides even better performance at medium elevation angles. Assembly, integration and alignment of the telescope was performed in June and July 2008 (see Fig. 79), the optical end-to-end verification was done 12–13 August 2008 with a full aperture interferometrical test. After further integration and testing the telescope was delivered to MPS on 6 December 2008.

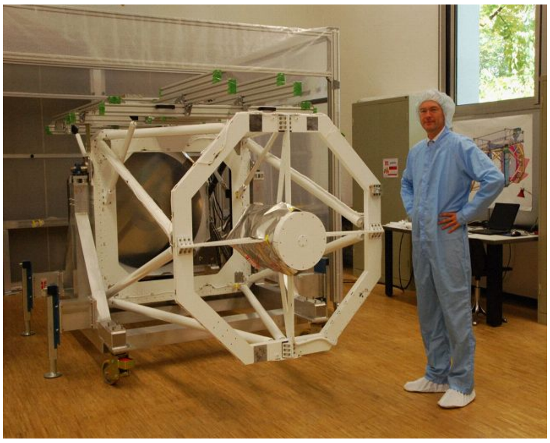

Fig. 79: Sunrise Telescope prior to delivery to MPS.

The carbon-fiber based honeycomb structural elements for the postfocus instrumentation (PFI) were delivered 6 May 2008 to MPS. The assembly, integration, alignment and characterization of the FM models of the Sunrise Filter Imager SUFI and the Image Stabilization and Light Distribution unit ISLiD were performed during the summer months (see Fig. 80). Integration into the PFI was finished 25 September 2008, see Fig. 81. As first external instrument, the Correlation tracker and Wavefront Sensor was integrated on 21 October 2008. Integration of the IMaX instrument was postponed to January 2009.

The flight hardware of the instrument control system, main-on-board computer, power distribution unit and data storage systems have been assembled and environmentally tested. Development of the on-board and ground segment software is ongoing.

(P. Barthol, A. Gandorfer, M. Schüssler, S. K. Solanki, and the MPS engineering team in collaboration with teams led by M. Knölker (High Altitude Observatory, Boulder, USA) V. Martínez Pillet (Instituto de Astrofisica de Canarias, La Laguna, Tenerife/Spain), W. Schmidt (Kiepenheuer-Institut, Freiburg, Germany), and A. Title (Lockheed Palo Alto Research Laboratory, USA))

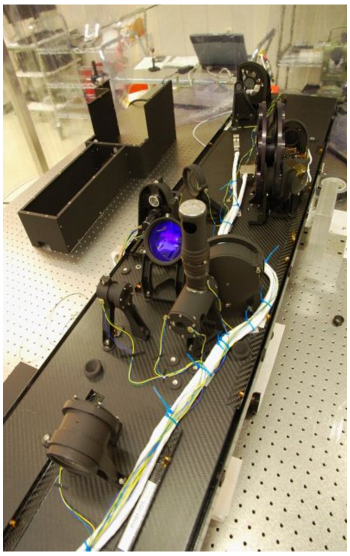

Fig. 80: ISLiD/SUFI Flight Model during assembly and alignment.

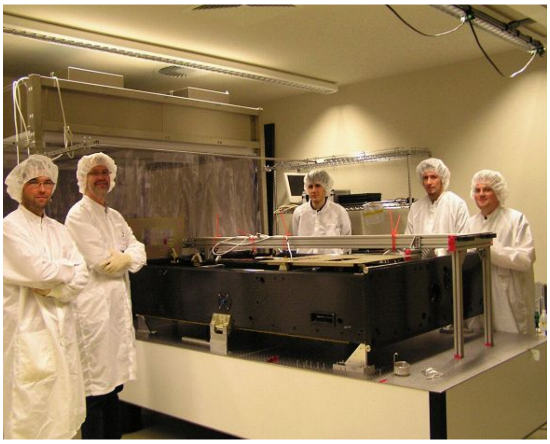

Fig. 81: ISLiD/SUFI intergrated in PFI support structure.

Optical verification and calibration of the SUNRISE instrument package

Sunrise is a balloon-borne solar observatory based on a 1-m-aperture solar telescope and a suite of post-focus instruments working in the UV/VIS spectral domain: SUFI, a near UV narrowband filter imager, IMaX, a tandem Fabry-Perot based imaging spectropolarimeter, and CWS, a correlation tracker/wavefront sensor. ISLID, the light distribution and image stabilisation unit serves as feed optics between the telescope and the instruments and distributes the light from the Sunrise telescope to these instruments. After the integration of the instruments into the instrumentation platform all instruments have been co-aligned. The coalignment has been verified by indirect methods using theodolite measurements in combination with mechanical 3-D measurements of the individual instruments using a Leica lasertracker, as well as by direct optical stimulation of the complete instrument package. For this task different optical ground suppport units have been developed. Besides the coalignment verification the optical quality of ISLID has been measured both, with interferometric methods, as well as with MTF measuring techniques. All relevant calibrations have been performed in the laboratory, like distortion, field rotation, plate scale, and internal magnification. The polarimetric calibration of the whole system was performed over the full science field of view of IMaX using the ZIMPOL II polarimeter from ETH Zurich.

(A. Gandorfer, B. Grauf, and A. Feller)

European Solar Telescope

The European Solar Telescope (EST) is a paneuropean project, presently in its conceptual design study phase. The study is financed by the European Union within the Seventh Framework Programme for research and technological development. MPS is one of the 29 partners in a consortium involving teams from 14 countries.

EST will be a 4-m-class solar telescope, located in the Canary Islands. Such a large aperture represents a true performance quantum leap compared to today's observing facilities which are in the 1-1.5 m range. The EST project is coordinated by the EAST consortium (European Association for Solar Telescopes), comprising representatives from 15 European countries, and managed by the Spanish Instituto de Astrofísica de Canarias.

EST will be optimised for studies of the magnetic coupling between the deep photosphere and the upper chromosphere. This will require diagnostics of the thermal, dynamic and magnetic properties of the solar plasma over a large range of scale heights. By using multiple wavelength imaging, spectroscopy and spectropolarimetry this goal can be achieved. The EST design will strongly emphasise the simultaneous use of several visible and near-infrared channels, thereby improving the overall photon efficiency and the diagnostic capabilities relative to other existing or proposed solar telescopes. Moreover EST must specialise in high spatial and temporal resolution using efficient post-focus instrumentation with large and fast detectors and so-called multi-conjugate adaptive optics which can correct image degradation by turbulences in the earth atmosphere at different altitude layers.

The design study has started in February 2008 and lasts for three years. It includes all aspects needed for a conceptual design of the whole telescope. During the first phase in 2008, different potential alternatives have been compiled for all systems and subsystems. During phase two, which has started by the end of 2008, the alternatives are further analysed and trade-off decisions are taken on the most adequate ones that are compatible with the scientific goals and the technical strategies. At the end of the design study, technical specifications will be given for all systems and subsystems which can then open out into future detailed engineering studies and finally the construction of the telescope.

In 2008 MPS has contributed to several work packages which are shortly outlined in the following paragraphs.

Optical coatings:

The aim of this work package under the responsibility of MPS, is the study of coating alternatives for the main 4-m mirror and the other reflective optics of the telescope. A demanding task, since a candidate should combine high reflectivity in the wide spectral region of 315 nm to 20 μm with good durability properties. The aluminum coating used so far in the majority of large astronomical optics, has high emissivity and low reflectivity, among the metals (see Fig. 82), which significantly lowers the throughput of telescopes. Recently, silver coating became a valuable alternative to aluminum. Among its advantages are its highest spectral reflectivity compared to other metals, low polarization and low infrared emissivity. Several coating alternatives are considered in the work package: aluminum, protected and enhanced silver and a combination of silver with aluminum. Within the durability study the samples, including commercial coatings, will be sent to the German VTT solar telescope on Tenerife, where they will be exposed to open air and solar radiation under typical observing conditions. After this test their performance will be investigated.

Polarisation optics:

This work package studies different types of polarisation modulation and demodulation concepts as well as the polarisation properties of the telescope optics. The

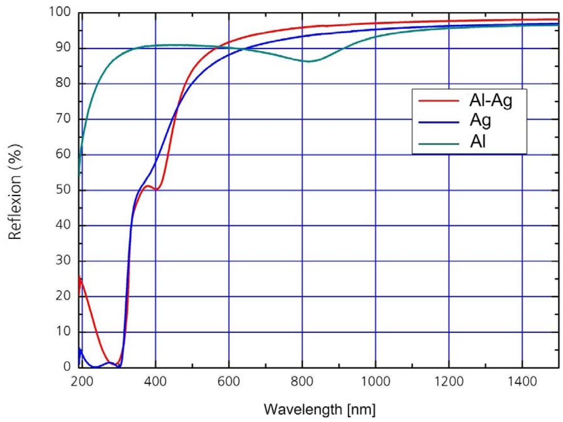

Fig. 82: Measured reflectivities of various metallic coating samples prior to the outdoor test in Tenerife.

goal is to devise for each polarimetric post-focus instrument the optimum modulator type and placement in the beampath which results in a high polarimetric efficiency and low instrumental polarisation. MPS is measuring, amongst others, the polarisation properties of different metallic mirror coatings which are then incorporated into a polarisation model of the telescope.

Tunable narrow-band filter:

Under study are different types of Fabry-Pérot filtergraphs with bandwiths of order 100 mÅ or below, which can be tuned to perform wavelength scans across a spectral line of interest. The main challenge is to accommodate a reasonably large field of view while maintaining the requirements on spatial and spectral resolution, homogeneity of the filter passband and straylight.

Grating spectrograph:

Different spectrograph configurations are thinkable: a long-slit standard configuration investigated by MPS, a fiber-optics-fed configuration, or a so-called multichannel subtractive double pass setup. Whereas the first two options produce a two-dimensional mixed image with one spectral and one spatial dimension, the latter results in two-dimensional solar images with the wavelength varying across one spatial axis. Moreover the grating spectrographs must simultaneously feed five spectral channels in the visible and three spectral channels in the near-infrared.

Data flow:

The multi-channel capabilities of the EST combined with its high spatial, temporal and spectral resolution requirements leads to an unprecedented high data volume per observing day. MPS contributes to the definition of an efficient and powerful data handling and storage system. The data flow work package identifies optimum solutions to handle data fluxes of 10 to 100 Gbyte per second, to pre-process the data (calibration and image reconstruction), to archive the data, and to provide the data to the scientific community in a user-friendly format.

(A. Feller, J. Hirzberger, A. Lagg, and O. Pleier)

The Gregor Telescope

Within the framework of a *Großgeräteantrag*, funded by the Max-Planck Society, the MPS is participating at the 20 % level in the Gregor project. In 2008 the fabrication of the 1.5 m Zerodur main mirror has been started. After the mounting of this mirror into the telescope structure in the beginning of 2010 (see Fig. 83), Gregor will belong to the largest solar telescopes world-wide. Spectro-polarimetric observations will reveal details of the convection processes and magnetic field structures on the Sun with a spatial resolution of 75 km. A multi-conjugate adaptive optic system will allow for diffraction-limited observations even when the sky quality is not ideal.

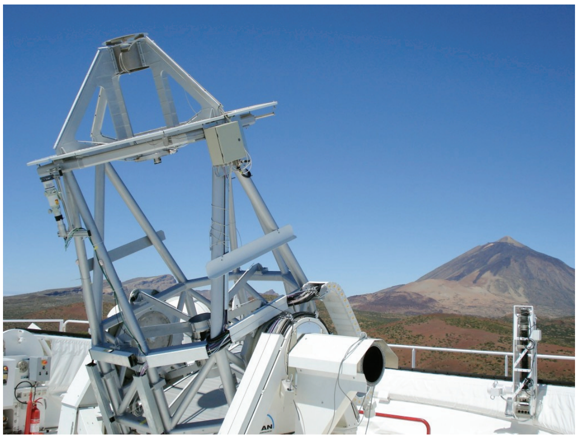

Fig. 83: Gregor telescope at the Tenerife Observatory, Spain.

The Tenerife Infrared Polarimeter 2 (TIP-2, Collados et al., Astron. Soc. Pacific Conf. Ser. 368, 611, 2007) will be one of the two first-light instruments. This infrared camera, currently mounted at the Vacuum Tower Telescope next to the Gregor building, has been the work horse for ground based solar observations at the MPS during the last years. With the large aperture of the Gregor telescope the performance of TIP-2 will be significantly improved.

The Gregor project is lead by the Kiepenheuer Institute für Sonnenphysik. Partner institutions are the Astrophysikalisches Institut Potsdam (IAP) and the Institut für Astrophysik (Göttingen, until end of 2008).

(A. Lagg, A. Feller, A. Gandorfer, J. Hirzberger, and S. K. Solanki)

The Kuafu space weather mission

The KuaFu mission is designed to explore the physical processes that are responsible for space weather and also to make an essential contribution to the space weather application. KuaFu encompasses three spacecraft. KuaFu-A will be located at the L1 libration point and have instruments to observe solar extreme ultraviolet and far ultraviolet emissions and white-light coronal mass ejections (CMEs), and to measure radio waves, the local plasma and magnetic field, and high-energy particles. KuaFu-B1 and KuaFu-B2 will be in elliptical polar orbits chosen to facilitate continuous (24 hours per day for 7 days per week) observation of the northern polar aurora oval and the inner magnetosphere. A heuristic illustration of the proposed configuration of the three spacecraft of the KuaFu mission is shown in Fig. 84.

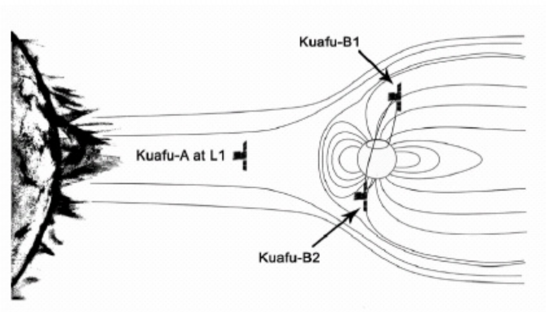

Fig. 84: Illustration of the three Kuafu spacecraft

Space weather refers to the conditions on the Sun, in the solar wind and geospace, that can influence the performance and reliability of space-borne and ground-based systems. Modern society is increasingly vulnerable to disturbances from outside our Earth system, and in particular to those initiated by explosive events on the Sun. Predicting space weather is important for space exploration, manned space flight, and economic exploitation of space.

The KuaFu mission will globally observe the complete chain of disturbances from the solar atmosphere to geospace, including solar flares, CME initiation, interplanetary clouds, shock waves, and their geo-effects, with a specific focus on such dramatic space weather events as magnetospheric storms. The mission start was targeted for the next solar maximum with launch hoped for in 2012, which presently seems unrealistic. The overall mission design and instrument complement will enable us to understand the multi-scale interactions of the Sun–Earth space system.

(R. Schwenn and E. Marsch in collaboration with C.-Y. Tu (Peking University, Beijing, China) and E. Donovan (Department of Physics and Astronomy, University of Calgary, Canada))

Solar-stellar connections, interstellar dust and cosmic rays

Simulations of gamma-ray response

The preliminary simulations of the response of the CsI scintillator detector to high-energy photons were performed by Geant. One of the basic measures of the instrument response is the detector effective area. Two kinds of gamma ray sources were chosen for simulation: an isotropic gamma-ray source evenly distributed in the upper hemisphere and a parallel gamma-ray beam. For each source configuration, the effective area was evaluated at 35 energy values between 30 keV and 100 MeV. Fig. 85 shows simulated effective area for CsI in 2-cm thick plastic veto as a function of incident photon energy for parallel beam. For isotropic source the effective area is lower since photons see lower projected area compared to the parallel incidence. The geometry with parallel particle beam, which is equivalent to isotropic source in infinity, can be used for solar energetic particle investigations. For the study of detector response to the local gamma rays produced in the Earth's atmosphere or in the satellite material we have used isotropic distribution of incident photons.

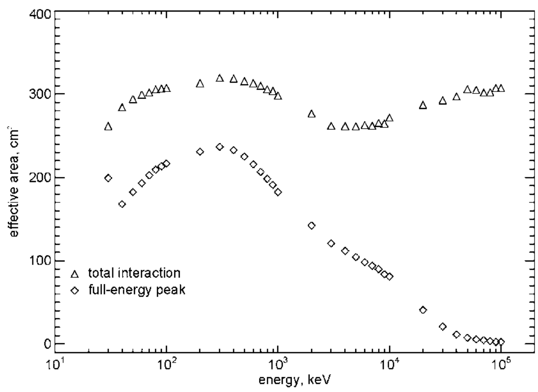

Fig. 85: Effective area vs energy for CsI in plastic veto.

(R. Bučík in collaboration with K. Kudela (IEP/SAS, Košice, Slovakia) and D. M. Smith (UC Santa Cruz, Santa Cruz, CA, USA))

Toroidal versus poloidal and radial magnetic fields in Sun-like stars: a rotation threshold

The Sun's magnetic field is mainly radial at the solar surface and near solar activity minimum is distributed poloidally on large spatial scales. With the help of Zeeman-Doppler Imaging it has become possible to image the large-scale magnetic flux distribution on rapidly rotating starts. The surprising result is that for these stars the magnetic structure is mainly toroidal. The question remains whether this is an artifact of the method or whether the large-scale magnetic structure for more rapidly rotating stars really differs so significantly from that of the Sun.

From a set of stellar spectropolarimetric observations, we report the detection of surface magnetic fields in a sample of four solar-type stars, namely HD 73350, HD 76151, HD 146233 (18 Sco) and HD 190771. Assuming that the observed variability of polarimetric signal is controlled by stellar rotation, we establish the rotation periods of our targets, with values ranging from 8.8 d (for HD 190771) to 22.7 d (for HD 146233). Apart from rotation, fundamental parameters of the selected objects are very close to the Sun's, making this sample a practical basis to investigate the specific impact of rotation on magnetic properties of Sun-like stars.

We reconstruct the large-scale magnetic geometry of the targets as a low-order ($\ell < 10$) spherical harmonic expansion of the surface magnetic field. From the set of magnetic maps, we draw two main conclusions. (i) The magnetic energy of the large-scale field increases with rotation rate. The increase in chromospheric emission with the mean magnetic field is flatter than observed in the Sun. Since the chromospheric flux is also sensitive to magnetic elements smaller than those contributing to the polarimetric signal, this observation suggests that a larger fraction of the surface magnetic energy is stored in large scales as rotation increases. (ii) Whereas the magnetic field is mostly poloidal for low rotation rates, more rapid rotators host a large-scale toroidal component in their surface field. From our observations, we infer that a rotation period lower than $\approx$ 12 d is necessary for the toroidal magnetic energy to dominate over the poloidal component. This also suggests that the toroidal fields found on more rapidly rotating late-type stars are not an artifact of the Zeeman-Doppler Imaging technique.

(S. K. Solanki in collaboration with P. Petit, B. Dintrans, J.-F. Donati, M. Aurière, F. Lignières, J. Morin, F. Paletou, R. Fares (Université de Toulouse, CNRS, France), J. Ramirez, and C. Catala (LESIA, Observatoire de Paris-Meudon, France))

The FeH $F^4\Delta$-$X^4\Delta$ system – creating a valuable diagnostic tool to explore solar and stellar magnetic fields

Lines of diatomic molecules are ideal tools for studying cool stellar atmospheres and the internal structure of sunspots and starspots, given their temperature and pressure sensitivities, which are typically higher than in atomic lines. The Wing-Ford FeH $F^4\Delta$-$X^4\Delta$ system represents such a diatomic molecule that is, in addition, highly sensitive to magnetic fields. The current theoretical description of those transitions that include the involved molecular constants, however, are only based on intensity measurements because polarimetric observations have not been available until now, which limits their diagnostic value. Furthermore, the theory has so far been optimized to reproduce energy levels and line strengths without taking magnetic sensitivities into account. The FeH $F^4\Delta$-$X^4\Delta$ system is produced by transitions between two electronic states with the coupling of the angular momenta that is intermediate between limiting Hund's cases (a) and (b). Our goal is to investigate the diagnostic capabilities of the current theoretical description of the molecule FeH.

Using the most precise available Hamiltonian, we carried out the perturbation calculation of the molecular Zeeman effect for this transition and computed the Landé factors of the energy levels and of transitions. We extracted Landé factors from a comparison of observed and calculated Stokes I and V profiles. Certain spectral lines, most frequently with high magnetic sensitivity, exhibited discrepancies between the theory and observations. We extended the theoretical model with a semi-empirical approach to obtain a diagnostic tool that is able to reproduce many of the interesting spectral lines.

We find that the current theory successfully reproduces the magnetic properties of a large number of lines in the FeH $F^4\Delta$-$X^4\Delta$ system and that the modified Hamiltonian allows us to synthesize and successfully reproduce the most sensitive lines. Thus, our observations have provided valuable constraints for determining empirical molecular constants and Landé factors.

The FeH $F^4\Delta$-$X^4\Delta$ system is found to be a very sensitive magnetic diagnostic tool. Polarimetric data of these lines, in contrast to intensity measurements, provide us with more direct and detailed information to study the coolest parts of sunspot and starspot umbrae, as well as cool active dwarfs.

(S. K. Solanki and A. Lagg in collaboration with N. Afram, S. V. Berdyugina, and D. M. Fluri, (ETH Zurich, Switzerland))

A coupled model of magnetic flux generation and transport in stars

We have developed a tripartite model of magnetic field generation and transport for the Sun and rapidly rotating Sun-like stars. A thin-layer dynamo model provides the latitude-time distribution (shown in Fig. 86) of the toroidal magnetic field at the bottom of the convection zone. The field strengths and latitudes of emerging flux tubes are determined by using the results of a linear stability analysis and setting the emergence probability proportional to the strength of the mean toroidal field. Following the rise of each unstable flux tube with a simulation code based on the thin flux tube approximation, the emergence latitudes and tilt angles are determined and used as input for a surface flux transport model. The properties for resulting activity patterns and cycles have been obtained for the case of the Sun and for rapidly rotating solar-type stars.

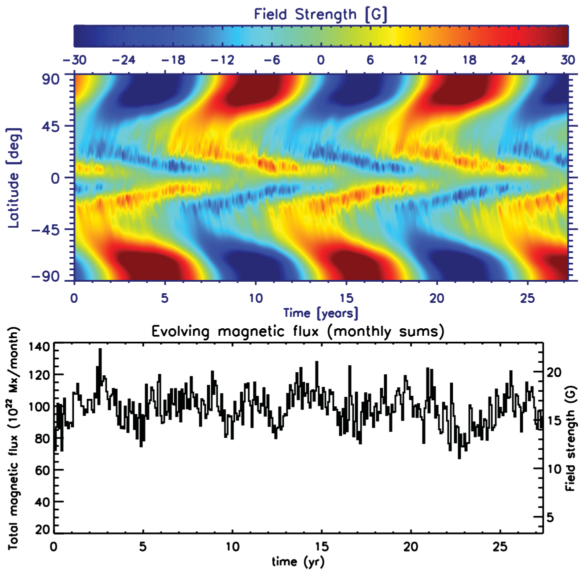

Fig. 86: Top: time-latitude diagram of the azimuthally averaged surface magnetic field for a solar-type star with a rotation period of 10 days. Bottom: time variation of the surface-integrated magnetic flux. Because of the overlapping of cycles, the cycle signal is almost not observable in the integrated surface flux (Isik et al., Astron. Nachr., 328, 1111, 2007).

(E. Işık, D. Schmitt, and M. Schüssler)

Imaging the heliosheath using SOHO CELIAS HSTOF

Voyager 1 and 2 LECP instruments measure the distributions of the heliosheath ions of energies greater than 40 keV. This threshold energy is an order of magnitude higher than the maximum energy (6 keV) of

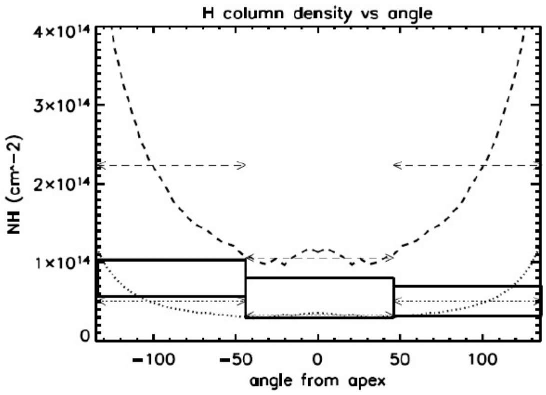

Fig. 87: Average column densities of neutral hydrogen (boxes) in the heliosheath forward and flank sectors, obtained from the fit to the HSTOF ENA data, compared to two gas-dynamical models of the heliosphere. For the models, the column density NH is plotted as a function of direction, with the NH averages over the sectors shown by horizontal line segments terminated by arrowheads (dashed or dotted, thin line).

the energetic neutral atoms (ENA) to be measured by the forthcoming IBEX mission. On the other hand, the energy range of SOHO CELIAS HSTOF ENA measurements overlaps with the energy range of Voyagers LECP. This offers a unique opportunity to combine HSTOF ENA measurements at 1 AU with LECP ion measurements in the heliosheath (see Fig. 87) and obtain information about the large-scale structure of the heliosphere.We use energetic neutral atoms data at 1 AU and a Voyager 1 spectrum in the heliosheath to estimate the average column density of neutral hydrogen in selected sectors of the forward heliosheath. We reanalyzed the energetic neutral hydrogen and helium data from HSTOF to identify the contribution to the neutral atoms flux originating in directions close to the apex of the Sun's motion relative to the local interstellar medium (LISM). We combine the data from HSTOF with the parent ion spectrum in the heliosheath measured by Voyager 1 to derive the background neutral hydrogen column density NH in the heliosheath and estimate the thickness L of the heliosheath from the apex direction and in the flank sectors. In the forward sector of the heliosheath the estimated thickness L is 42 ± 12 AU. This is within the range of values predicted by theoretical models, but suggests that the heliosheath is thinner than expected. The hydrogen column densities in the flank sectors are not symmetric relative to the apex, but the difference is within the statistical uncertainty. The H to He ratio measured by HSTOF is lower than the value following from Voyager 1 heliosheath spectra.

(M. Hilchenbach, A. Czechowski, and R. Kallenbach)

Rotation and variability of F stars in the CoRoT initial run

It is well known that as stars rotate faster their magnetic activity increases. This is best seen in primary activity indicators sampling the coronae or chromospheres of stars, such as X-rays or the cores of the Ca II H and K lines. In photospheric radiation, as sampled by CoRoT, the signal of magnetic activity is more hidden. CoRoT has opened the possibility to study the microvariability of stars, thus allowing techniques for determining the rotation period and rotational modulation of their lightcurves (here an indicator of the magnetic activity) so far limited to strongly variable stars, to be applied also to rather constant stars. In its initial run the satellite has observed three F stars that display rather different variability on different time scales, as seen in their power spectrum. We estimate the rotational period for these stars, and separate the contributions due to magnetic activity and non-magnetic processes (convection, oscillations). A similar analysis is also carried out for the Sun at activity minimum and maximum conditions using VIRGO/SOHO data. We then analyze the relative differences in power in relation to the spectral type, luminosity and rotation period of each star.

(M. Dasi, T. Stahn, S. K. Solanki, N. Krivova, and L. Gizon)

Fundamental science

Effective Dirac equation for a relativistic binary of fermions

The precise calculation of the energy spectra of relativistic binaries including their fine structure is a main topic of relativistic quantum mechanics. The state of this field has been described in a recent textbook by Pilkuhn (2005). The classical example of such a binary system is the hydrogen atom. If one only considers the static Coulomb coupling between the proton and electron but accounts for their spins, one can solve this problem exactly by using the so-called Dirac–Coulomb Hamiltonian (Marsch, 2005).

However, for this problem also an effective single-particle Dirac equation can be derived, which yet is applicable to any binary system of two fermions, whereby use is made of the original two-fermion Dirac-type Hamiltonian written in a 16-component spinor representation. For spherical interaction potential the spin dynamics in the product spin space and spatial dynamics in the particle–antiparticle state space can be fully decoupled and separated. The case of atomic hydrogen was solved again as an example, and the results obtained by various authors were retained, including the effects of the recoil through the reduced mass and the spectral fine structure induced by the joint spin–orbit coupling of the two fermions constituting the binary. The resulting fine-structure energy-level splitting remains the same for the binary as for the single Dirac electron, and it is independent of the mass ratio. However, this fine structure will by only revealed by the ortho-fermionium (triplet state) and not para-fermionium (singlet state), a prediction that could experimentally be tested with hydrogen.

(E. Marsch)

Validation of MHD large eddy simulation

Due to the high Reynolds numbers (Re) of solar plasmas, the degrees of freedom required to model all scales of the magnetic and velocity fields far exceed technological limits for computation. Assuming a doubling of computer power every 18 months, all scales of the magnetic field in a supergranule cannot be computed until the year 2040 and the velocity will remain unresolved until 2080. Scale truncation of a computation removes the important physics of multiscale interactions. The only viable approach is to employ subgrid modeling of the omitted scales – large eddy simulations (LES). Eddy-viscosity cannot be extended to magnetohydrodynamics (MHD) due to MHD's unknown (possibly non-universal) energy spectrum as well as its spectral non-locality.

One promising model is the Lagrangian-averaged MHD (LAMHD) equations. It separates fluctuations from the Lagrangian mean, retains multiscale interactions and Alfvén waves, and models unresolved dissipation with enhanced Ohmic losses. LAMHD and its equivalent hydrodynamic model (LANS) have reproduced well moderate Re (< 3000) flows with significantly reduced computational expense. For larger Re, LANS develops an artifact, a positive power-law spectrum at superfilter scales (see Fig. 88) due to the depletion of energy transfer at subfilter scales – greatly limiting LANS's use. Because of the interaction between large and small scales in MHD (Alfvén waves), the Lagrangian-averaged approach does not suffer this problem in the MHD case. We have also demonstrated a gain of a factor of 1300 in computation time using LAMHD for a $Re \approx 9200$ computation.

(J. Pietarila Graham in collaboration with P. Mininni and A. Pouquet (National Center for Atmospheric Research))

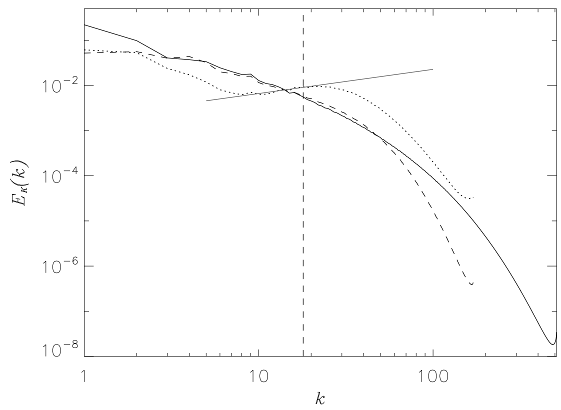

Fig. 88: Energy spectra for 3 similar (but not identical) flows: 1536^3 grid point MHD (solid line), 512^3 LAMHD (dashed), and 512^3 LANS (dotted). Vertical line is the filter scale. Gray line is positive slope, $k^{0.5}$.

Understanding the WMAP results: low-order multipoles and dust in the vicinity of the solar system

Analyses of the cosmic microwave background (CMB) radiation maps made by the Wilkinson Microwave Anisotropy Probe (WMAP) have revealed anomalies not predicted by the standard inflationary cosmology. In particular, the power of the quadrupole moment of the CMB fluctuations is remarkably low, and the quadrupole and octopole moments are aligned mutually and with the geometry of the solar system. It has been suggested in the literature that microwave sky pollution by an unidentified dust cloud in the vicinity of the solar system may be the cause for these anomalies. In this paper, we simulate the thermal emission by clouds of spherical homogeneous particles of several materials. Spectral constraints from the WMAP multi-wavelength data and earlier infrared observations on the hypothetical dust cloud are used to determine the dust cloud's physical characteristics. In order for its emissivity to demonstrate a flat, CMB-like wavelength dependence over the WMAP wavelengths (3 through 13 mm), its particles must be macroscopic. Silicate spheres from several millimetres in size and carbonaceous particles an order of magnitude smaller will suffice. Our preliminary estimates confirm that the solar system dust can potentially be visible to WMAP, although it is not clear at the moment whether special techniques should be applied to enhance the signal to noise ratio, or the emission from dust is indeed capable to explain some of the WMAP anomalies.

(V. Dikarev, O. Preuß, S. K. Solanki, and H. Krüger in collaboration with A. Krivov (University of Jena, Germany))

IV. Planeten, ihre natürlichen Satelliten und Kometen / Planets, their moons and comets

Übersicht der Projekte / overview of projects

Dargestellt ist die Dauer der verschiedenen Projektphasen (farbcodiert) einzelner Instrumente. Nähere Beschreibungen können den Jahres- bzw. Tätigkeitsberichten des MPS entnommen werden.

The different project phases of each instrument are shown colour-coded. Descriptions of these instruments can be found in the annual reports of the MPS.

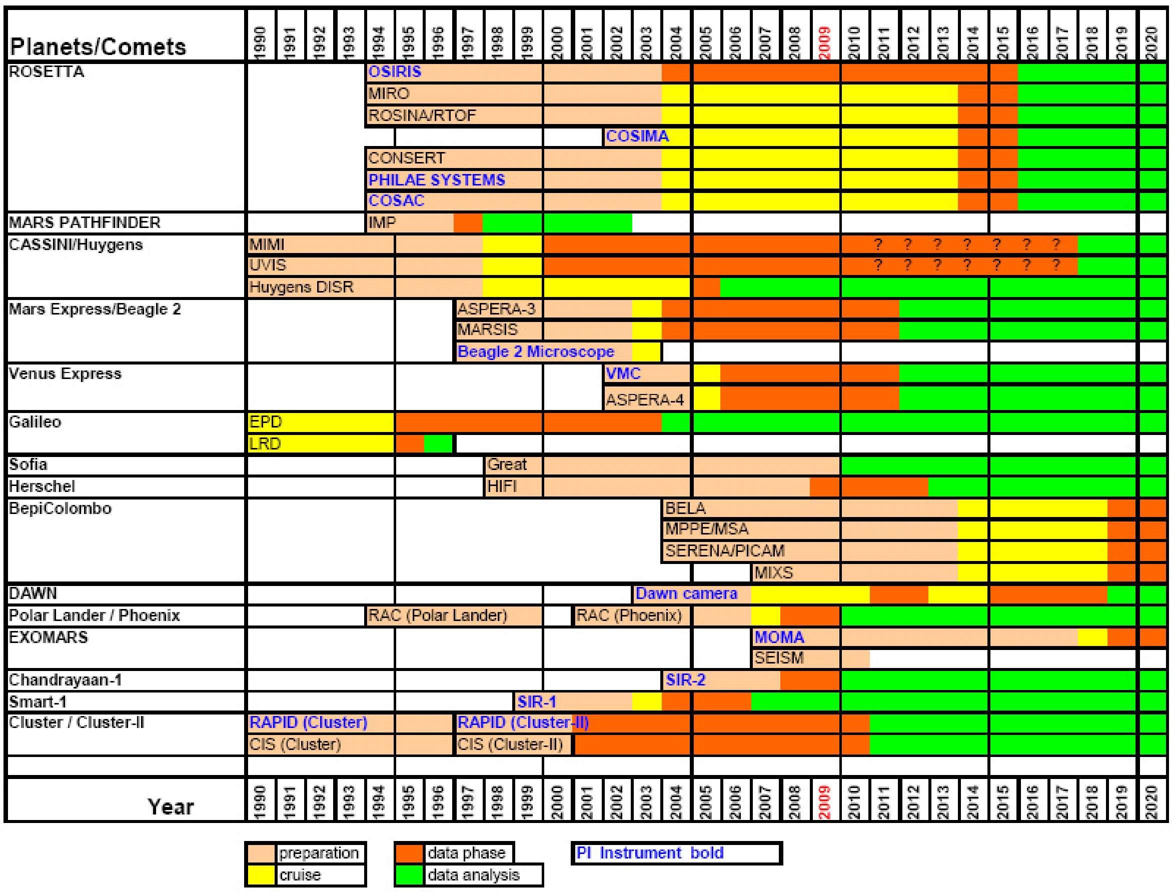

Planetary interiors

Magnetic field strength scaling of planets and stars

The magnetic fields of planets and many stars are generated by a dynamo process driven by convection. The solar dynamo is thought to operate rather differently from the geodynamo, for example the strong shear at the tachocline may play a fundamental role for magnetic field generation. Stars with less than 0.35 solar masses (M-dwarfs) are fully convective and often rotate rapidly. They boost strong magnetic fields at their surfaces. In a few cases their field morphology has been mapped and is found to be of large scale and often dominated by the axial dipole. This suggests that the dynamo in these objects may be more similar to planetary dynamos. From numerical simulations of planetary dynamos we had previously found a scaling law that predicts the magnetic field strength to vary primarily with the available energy flux (Christensen and Aubert, Geophys. J. Int., 166, 97, 2006). We now generalize it to make it applicable to objects with strong density stratification, such as stars (see Fig. 89). The following rule is found for the magnetic energy density in the dynamo: $B^2/(2\mu_o) = c f_{ohm} \rho^{1/3} (F q_o)^{2/3}$, where ρ is the mean density and q_o the heat flux out of the dynamo region. The constant of proportionality c, the relative fraction of ohmic dissipation f_{ohm} and the thermodynamic efficiency factor F are all numbers of order one. We compare the predictions of this scaling law with the observations for Earth, Jupiter, rapidly rotating M-dwarfs and young contracting T-Tauri stars. We find good agreement over six orders of magnitude for the energy flux and nearly three orders of magnitude for the magnetic field strength (see figure). This reconfirms the validity of the scaling law for planetary dynamos and suggests that it may apply rather universally for convection-driven dynamos in rapid rotators. More slowly rotating stars fall below the prediction. Uncertainties on the energy flux and the structure of the dynamo region make it difficult to test the rule for other solar system planets. Applying our rule to objects that are intermediate between planets and stars, we predict fields at the kGauss level for brown dwarfs and at the 0.1 kGauss level for massive extrasolar planets of several Jupiter masses. In the latter case this opens prospects for the detection of the field and determination of its strength by non-thermal radio-emissions. (Christensen et al., Nature, 457, 167, 2009).

(U. Christensen)

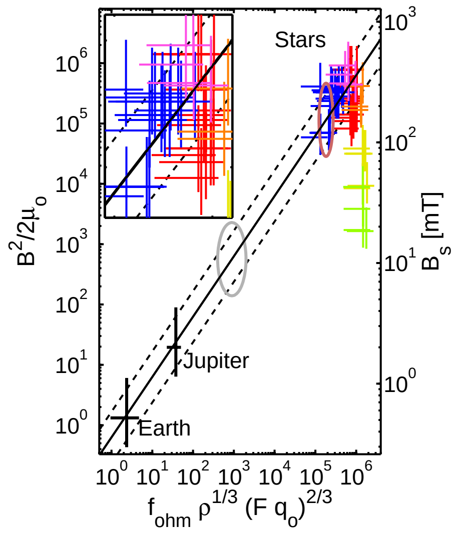

Fig. 89: Magnetic energy density in the dynamo versus a function of density and outer boundary heat flux q_o. The scale on the right shows r.m.s. field strength at the dynamo surface. T-Tauri stars are shown in blue, old-dwarfs where the total field is known are show in red, those where only the large scale field was observed are shown in pink. The bar lengths show estimated uncertainty rather than formal error. The stellar field is enlarged in the inset. Brown and grey ellipses indicate predicted locations of a brown dwarf with 1,500 K surface temperature and an extrasolar planet with seven Jupiter masses, respectively.

Core flow inversion from geomagnetic secular variation

The observed secular variation of the geomagnetic field has been used in many studies to infer the fluid motions at the top of Earth's core. Almost all used the frozen flux assumption which neglects magnetic diffusion. At long wavelength the contribution from horizontal diffusion is small. Radial diffusion could be much larger and contribute substantially to the secular variation, but cannot be inferred directly from observation. In numerical dynamo models we find that the pattern of radial diffusion is correlated with the tangential diffusion (which is obtained from the observed field at the core-mantle boundary in case of the Earth), but is larger in amplitude. From the numerical results we derive the relative scaling of radial and tangential diffusion as function of Rayleigh number. Extrapolating the result to the Earth suggests that radial diffusion may be several hundred times larger than horizontal diffusion at the core-mantle boundary. In core flow inversion models we parameterize the radial contribution by a strongly enhanced diffusivity for tangential diffusion. We obtain core flow patterns that are broadly similar to those obtained with the frozen flux assumption, but in some regions important differences arise. For example, the slow flow under the Pacific, which results in frozen-flux inversions from the weak secular variation in this region, is intensified when taking diffusion into account. This suggests that diffusive and advective contributions to the secular variation may cancel each other to a significant degree. (Amit and Christensen (2008)).

(U. Christensen in collaboration with H. Amit (Paris, France))

Librational flow instabilities in planetary and lunar cores

Mercury and several moons in our solar system undergo forced longitudinal librations. This is a variation in the planetary or lunar rotation due to non-axisymmetric gravitational interaction with the Sun or planet these bodies orbit. Few studies to date have investigated how longitudinal libration couples with the interior fluid dynamics of the planet or moon. We use laboratory experiments and numerical simulations to investigate the viscously driven flows in a spherical librating fluid cavity (Noir et al., Phys. Earth Planet. Inter., 173, 141, 2009). The focus lies on libration frequencies less than or equal to the planetary rotation frequency and a broad range of librational amplitudes. We also model three different core geometries: a full sphere, an aspect ratio of $r_i/r_o = 0.6$ and an aspect ratio of $r_i/r_o = 0.9$ where r_i and r_o are the radii of the inner and outer boundary, respectively. Direct flow visualization in the laboratory experiment and a comparison with the simulations allow to identify three distinct librationally driven flow regimes. The transitions between these regimes are governed by the value of the outer boundary layer Reynolds number $Re = u/d\Omega$, where u is the speed associated with the libration, d is the Ekman boundary layer thickness, and Ω is the rotation rate of the planet or moon. For $Re < 20$ the flow is dominated by inertial modes and develops transverse shear layers that radiate from the Ekman layer through the fluid volume. For $20 \leq Re \geq 120$ the system becomes unstable to longitudinal rolls that form around the equator beneath the outer boundary and travel towards the poles in each libration cycle. Fig. 90 shows numerical simulations of these two flow regimes. For $Re > 120$ the flow in the vicinity of the outer boundary becomes turbulent. These scenarios seem to be independent of the inner core size since the instabilities originate from the outer boundary. For several librating planets and moons Re lies in the range of values accessible in our laboratory experiment. Our results suggest that Mercury, Io, Europa and Titan may undergo boundary layer turbulence which can significantly enhance the viscous coupling of the fluid to the rigid part of the planet/moon. Earth's moon, Callisto and Ganymede may become unstable to laminar longitudinal rolls which provide a much weaker coupling (Noir et al., Phys. Earth Planet. Inter., 173, 141, 2009).

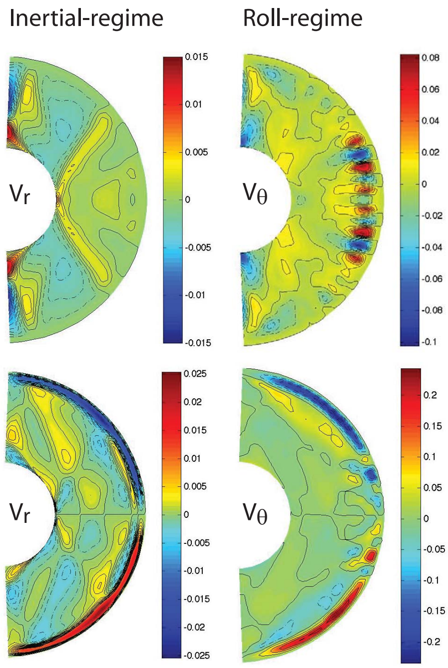

Fig. 90: Numerical simulations of the flow excited by libration in a spherical shell filled with fluid. The left column shows radial and meridional flow components in the inertial stable regime, the right column shows the respective components in the longitudinal role regime. Velocity is given in the Reynolds number scale.

(J. Wicht in collaboration with J. Noir, J. Aurnou, F. Hemmerlin, and S. M. Baca (UCLA, USA))

Statistical analysis of dipole moment variation in a numerical geodynamo model

The axial dipole moment in geomagnetic data and numerical dynamo simulations varies on many different time scales in an apparently stochastic fashion. We have analyzed the time evolution of the axial dipole moments (ADM) for three numerical geodynamo models by relating it to the Fokker–Planck equation governing the systematic and random ADM 'motion'. This allowed us to determine an effective ADM growth rate and a diffusion coefficient that both characterize the random fluctuations in the Focker-Planck equation. The analysis shows that the numerical ADM data exhibit a nonlinear quenching, i.e. the growth grate decreases with growing ADM. The quenching is only partly owed to the reduction of the rms flow amplitude and more subtle local effects must therefore also contribute. The diffusion coefficient is found to be independent of the ADM. Overall, these statistical properties agree with those found in geomagnetic field variations. The results allow us to derive a probability distribution for the ADM which deviates from the classically assumed Gaussian shape (see Fig. 91). Moreover, the reversal rate can be estimated to one reversal per Myr which nicely agrees with the reversal rate found in the simulations (Kuipers et al., Phys. Earth Planet. Inter., 173, 228, 2009).

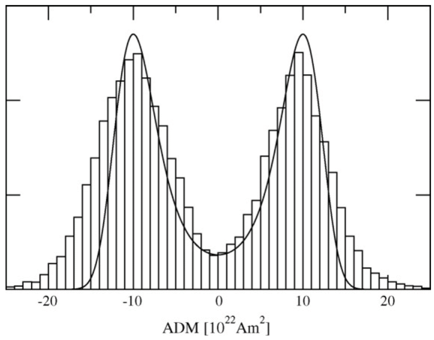

Fig. 91: Comparison of the axial dipole moment likelihood in a long numerical dynamo simulation (bars) with the theoretical distribution (line) derived from the statistical analysis.

(J. Wicht in collaboration with J. Kuipers, G. T. Brakema (University Utrecht, The Netherlands), and P. Hoyng (SRON, The Netherlands))

Statistical properties of the multipole coefficients of the geomagnetic field

The Earth has had a magnetic field for several billion years. The main component is the dipole, which is variable on all time scales from a few 100 yr and longer. A spectacular aspect of this variability are the sudden dipole polarity reversals, which occur on average every few 10^5 yr.

The magnetic field is generated by induction processes in the fluid outer core of the Earth. Because of the nonlinear interaction of the flow and the magnetic field, this dynamo action is a complex MHD problem. A self-consistent approach requires numerical solution of the MHD equations in a rotating and convecting spherical shell. The numerical dynamo models developed at the MPS exhibit many of the characteristics of the geomagnetic field.

The objective of the project is a systematic quantitative analysis of the output of these geodynamo models. To this end we extract the (first) multipole components of the magnetic field from the magnetohydrodynamical simulations of the geodynamo, and subsequently compare them with analytical theory.

The stochastic differential equations for the mode coefficients lead to a Fokker-Planck equation for the probability distribution of the multipole coefficients, from which the statistical properties such as the mean square amplitudes, the autocorrelation functions, cross correlations, the mean reversal rates of the axial dipole etc can be derived.

By comparing theory and numerical simulations we hope to gain insight in the inner working of the geodynamo, especially in the likelihood of polarity reservals.

(M. Schrinner, D. Schmitt, J. Wicht, and U. Christensen in collaboration with P. Hoyng (Utrecht, The Netherlands))

Saturation and time dependence of geodynamo models

Large-scale magnetic fields in planets, stars and galaxies are maintained by hydromagnetic dynamo action. A magnetic field builds up due to an appropriate motion of a conducting fluid and saturates with increasing field strength owing to the back reaction of the Lorentz force on the flow. In this study we focus on the latter and address the question under which conditions a saturated velocity field stemming from geodynamo simulations leads to an exponential growth of the magnetic field in a corresponding kinematic calculation. We performed global self-consistent geodynamo simulations and calculated the evolution of a kinematically advanced tracer field. The self-consistent velocity field enters the induction equation for the tracer field in each time step, but the tracer field does not contribute to the Lorentz force. This experiment has been established by Cattaneo and Tobias (2008) and is closely related to the test-field method (Schrinner et al. 2007).

We found two dynamo regimes in which the tracer field either grows exponentially or approaches a state aligned with the actual self-consistent field after a transition period. Both regimes can be distinguished by the Rossby number and coincide with the dipolar and multipolar dynamo regimes identified by Christensen and Aubert (2006) (Fig. 92). Dipolar dynamos with low Rossby number are kinematically stable whereas the tracer field grows exponentially in the multipolar dynamo regime (Fig. 93). This difference in the saturation process for dynamos in both regimes comes along with differences in their time variability. Within our sample of 20 models, solely kinematically unstable dynamos show dipole reversals and large excursions. The complicated time behaviour of these dynamos presumably relates to the alternating growth of several competing dynamo modes. On the other hand, an eigenmode computation suggests that dynamos with low Rossby number are dominated by only one fundamental mode, which is repeatedly quenched and rebuilt. All other modes in this case are clearly subcritical. In this sense, dynamo models in the low Rossby number regime, i.e. fast rotators, exhibit a simple time dependence and their saturation merely results in a fluctuation about their critical state.

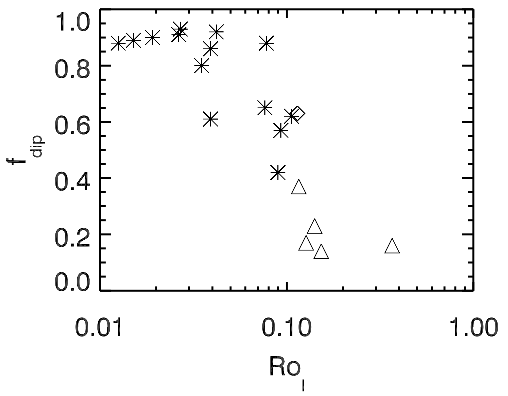

Fig. 92: Relative dipole field strength versus Rossby number Ro_l. Stars denote non-reversing dynamos which are kinematically stable, whereas triangles represent dynamos which do revers and are kinematically unstable. Both regimes coincide with the dipolar and multipolar dynamo regimes identified by Christensen and Aubert (2006). There is one example (diamond), which undergoes a transition between both regimes. Note that this example has a considerably lower relative dipole field strength in the second state.

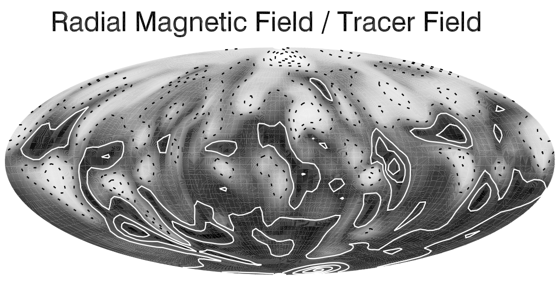

Fig. 93: Contour plot of the radial component of the actual magnetic field and the tracer field for a kinematically stable dynamo given at a certain snapshot in time after an intitial transition phase at $r = 0.62 r_0$. Note that the tracer field is totally aligned with the actual magnetic field. Both components are normalised due to their maxima and minima. Therefore the greyscale coding varies from -1, white, to $+1$, black, and the contour lines correspond to ± 0.1, ± 0.3, ± 0.5, ± 0.7, ± 0.9.

(M. Schrinner, D. Schmitt, R. Cameron, and U. Christensen in collaboration with P. Hoyng (Utrecht, The Netherlands))

A domino model for geomagnetic field reversals

One of the most exciting phenomenon of the geomagnetic field is its sporadic reversals. Such reversals have also been observed in large-scale simulations of the geodynamo. We here study a simplified model that exhibits the behaviour of the geomagnetic reversal record.

We consider a system of N spins aligned along a ring like in an one-dimensional Ising-Heisenberg model which is used in statistical mechanics to describe, for instance, ferromagnetism. Each spin has unit length and is described by its angle with respect to the rotational axis. The orientation of the spins can vary in time due to random forcing and spin-spin interaction of neighbouring spins. We assume that the geomagnetic field is made up of the aggregate of all spins. We compare the model results with the geomagnetic field reversals and find strikingly similar behaviour.

We solve the equations of motion of this Ising-Heisenberg model which has a number of parameters: besides the number of spins a parameter describing the preferred orientation along the rotational axis, a parameter describing the strength of the spin-spin interaction, a term of friction that retards the motion of the individual spins, and a term of a random pushing of the spins orientation updated after each time Δt.

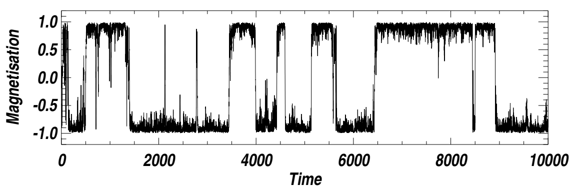

Fig. 94: The orientation of the sum of the spins as a function of time.

As a result, we get Earth-like behaviour of the sum of all spins (Fig. 94). They keep the same direction for a long time and, once in a while, begin flipping to change the orientation by almost 180 degrees (mimicking a geomagnetic reversal) or to move back to the original direction (mimicking an excursion). Most of the time the spins are aligned or anti-aligned and moving only slightly with respect to the rotational axis (mimicking the secular variation of the geomagnetic pole with respect to the geographic pole). A reversal is fast compared to the times in between and it occurs at random times, in the model as in the case of the Earth's magnetic field.

(D. Schmitt and J. Wicht in collaboration with N. Mori (Ochanomizu University Tokyo, Japan))

A new method for computing the eigenfunctions of the dynamo operator

We developed a new method to determine the eigensolutions of the induction and the dynamo equation in a fluid embedded into vacuum. The magnetic field is expanded in a complete set of functions. The new method is based on the biorthogonality of the adjoint electric current and the vector potential with an inner product defined by a volume integral over the fluid domain. The advantage of this method is that the velocity and the dynamo coefficients of the induction and the dynamo equation do not have to be differentiated and thus even numerically determined tabulated values of the coefficients produce reasonable results. We performed test calculations and compared with published results obtained by the classical treatment based on the biorthogonality of the magnetic field and its adjoint. We especially considered dynamos with mean-field coefficients determined from direct numerical simulations of the geodynamo and compare with initial value calculations and the full MHD simulations.

(M. Schrinner, D. Schmitt, and J. Jiang in collaboration with P. Hoyng (Utrecht, The Netherlands))

Terrestrial planets research – Mercury

Extraction of Mercury's tidal signal from synthetic BepiColombo laser altimeter (BELA) data sets by a local basis function expansion of the topography grid

Solar tidal forces generate elevation changes of Mercury's surface of the order 1 m within one Hermean year. Knowledge of the precise reaction of the planet to tidal forcing, expressed by the Love numbers h_2 and k_2 puts constraints on the internal structure, for example the state and the size of the core. We investigate if the Love number h_2 can simultaneously be determined together with the static topography of the planet from a global synthetic altimetry record of the BepiColombo Laser Altimeter BELA over the nominal mission duration of approximately 4 Mercury years. We find that for a precise determination of the tidal Love number h_2 the extracted topography grid must have a resolution similar to the resolution given by the spacing of spacecraft tracks on Mercury's surface. The tidal Love number is extrated with an accuracy of about 1 % (2σ-uncertainty) by using higher order interpolation methods such as cubic Spline interpolation for the idealized case of a resonant orbit of the spacecraft and without restricting the data coverage (Fig. 95). Restricting the data coverage in time or space or both leads to an increase of the uncertainty of the tidal Love number to about 14 % (2σ-uncertainty). The simulation results demonstrate that it seems feasible to test current models on Mercury's interior with sufficient precision using BepiColombo Laser Altimeter data.

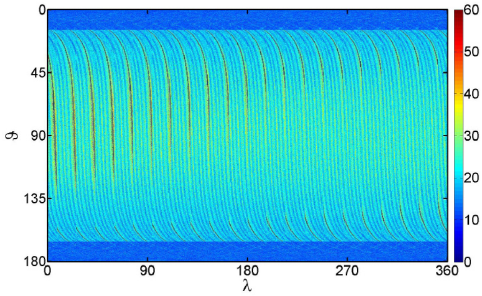

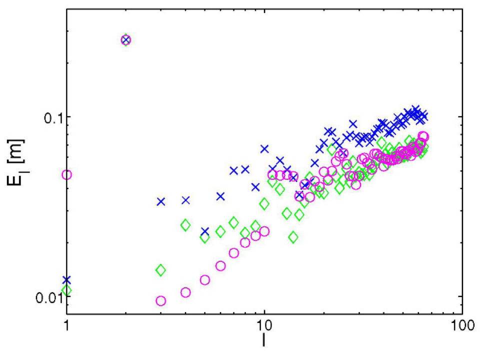

Fig. 95: *Upper panel:* Standard deviations of the extracted topography with respect to the input topography for the case of restricting the spatial coverage to locations where the spacecraft altitude is less than 1000 km. Step functions are used in longitude and latitude direction as local basis functions, and the input and output topographic grid are chosen to have the same resolution. Dark colours indicate areas with a lower number of observations or no observations at all. *Lower panel:* Mean degree error E_l of the transformed output topography in a spherical harmonic expansion for a non-resonant orbit without data restrictions ($\diamond$), for a non-resonant orbit with limiting measurements up to 1000 km spacecraft altitude ($\times$), and for a resonant orbit with 4 Mercury years ($\circ$), when cubic Splines are used as local basis functions and two grid points of the input topography are binned for the output topographic grid. The peak at degree 2 represents the retrieved tidal signal.

(C. Koch, U. R. Christensen, and R. Kallenbach)

The initial temporal evolution of a Hermean feedback dynamo

Various possibilities are currently under discussion explaining the observed weakness of the intrinsic magnetic field of planet Mercury. One of the possible dynamo scenarios is a dynamo with feedback from the magnetosphere. Due to its weak planetary magnetic field, Mercury exhibits a small magnetosphere whose sub-solar magnetopause distance is only about 1.7 Hermean radii. Hence, the magnetic field due to magnetopause currents cannot be disregarded in the dynamo region. Since the external field of magnetospheric origin is antiparallel to the dipole component of the dynamo field, a negative feedback results (Fig. 96).

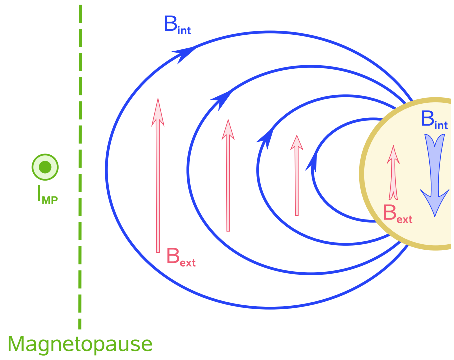

Fig. 96: Schematic illustration of the feedback mechanism. The planet's dynamo generates an internal field. The interaction with the solar wind causes a magnetopause current which itself induces an external field which is of opposite orientation to the internal field in the Hermean core.

For an $\alpha\Omega$-dynamo two stationary solutions of such a feedback dynamo emerge, one with a weak and another with a strong magnetic field. The question, however, is how these two stationary solutions can be realized. To address this problem, we discussed various scenarios for a simple dynamo model and the conditions under which either of the stationary situations evolves. We find that the feedback mechanism quenches the overall field growth to a low value of about 100 nT if the dynamo is not driven too strongly.

(D. Schmitt and J. Wicht in collaboration with D. Heyner, K.-H. Glassmeier and U. Motschmann (Braunschweig, Germany))

Terrestrial planets research – Venus

Venus Express extended mission

In 2008 Venus Express – the first ESA mission to Venus – continued global survey of the atmosphere, the plasma environment and the surface of Venus. The 1-st extended mission that began on 3 October 2007 is now approved until the end of 2009. Both the spacecraft and the payload are in good shape, continuing systematic monitoring of Venus that now is already the longest and most complete in many aspects. In June-August 2008 Venus Express performed pericenter lowering maneuver (to 180 km) to allow plasma sounding closer to the planet and to begin atmospheric drag experiment. MPS is deeply involved in many aspects of the mission: scientific support of the mission planning and operations, development of new observation modes, observations by Venus Monitoring Camera (VMC) (PI experiment), VIRTIS, and ASPERA-4 experiments and their data analysis. The 2-d Venus Express extension requested by ESA has several goals. 1). Extending the survey to study long term process in the Venus atmosphere and plasma environment in the period of increasing solar activity. 2). Joint observations with Planet-C – Japanese satellite scheduled to arrive at Venus in the end of 2010. 3). Further pericentre lowering and possibly aerobraking with the aim to circularize the orbit. MPS participates in the development of the future strategy for Venus exploration: D. Titov was the member of the Science and Technology Definition Team selected by NASA to define the future Flagship mission to Venus.
The paper "Highlights of the Venus Express mission" featured the MPG Jahrbuch-2008 and in the Annual MPS report to the German Astronomical Society. A special issue of the Journal Geophysical Research that includes about 40 original papers covering all science topics of Venus Express was published with D. Titov as Guest Editor (Titov et al., 2008b; Svedhem et al., 2009; Titov et al., 2009). Two PhD thesis based on the VMC data analysis were successfully defended by R. Moissl (IMPRS) and I. Khatuntsev (IKI, Moscow).

(D. Titov, W. J. Markiewicz, and M. Fränz)

Morphology of the Venus clouds

In 2008 VMC observations focused on more detailed study of meso-scale and small scale features and phenomena. These observations were made possible due to implementation of new modes of spacecraft pointing like spot tracking and close-up mosaics. These observations revealed various features on the cloud tops in unprecedented detail and resolution. Fig. 97a shows equatorial region in vicinity of sub-solar point. Deposition of solar energy in the clouds creates a dark wake in the afternoon. Figs. 97b,c show transition region between dark and turbulent low latitudes and bright and quiet mid-latitude zone. The transition is rather sharp and the reason maintaining it is not clear. Long cloud streaks seen in this region indicate that laminar flow dominates over turbulent eddies. Fig. 97d shows close-up snapshot of the "polar cap". Its bright and uniform cloud coverage is often broken by dark streaks and grooves. Dark oval is the feature almost permanently present in the polar regions (> 70° S) (Fig. 97b,c). The hot eye of the polar vortex observed by VIRTIS at thermal infrared wavelengths usually resides inside the dark UV

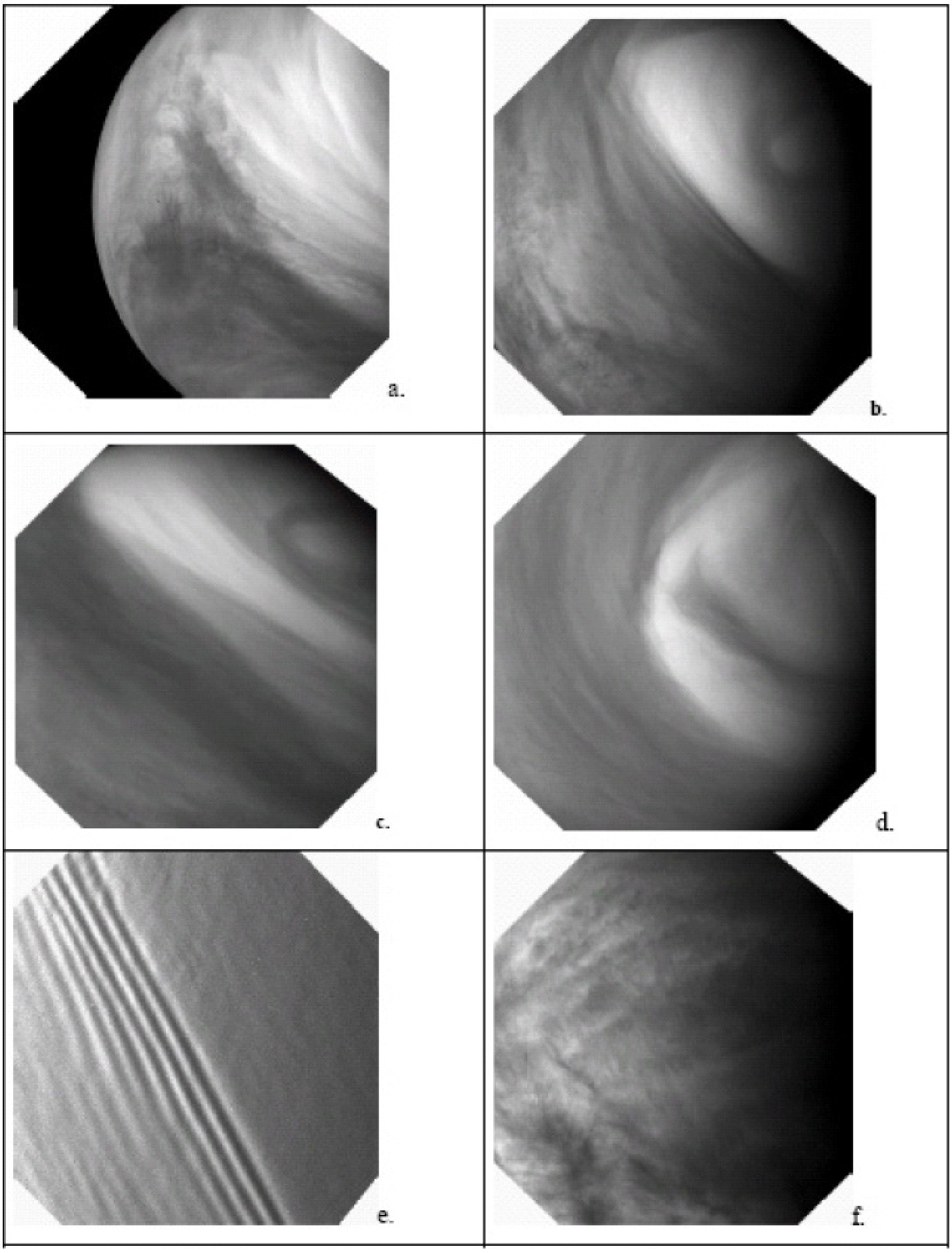

Fig. 97: VMC UV images of Venus: equatorial regions (a), transition zone and polar "cap" (b,c,d), long polar waves (e), and close-up view of the clouds at sub-solar point (f).

oval (Fig. 98) and is connected to it morphologically and dynamically. Waves on the cloud tops in the polar region are shown in Figure 1e with resolution of $\sim$ 500 meters. Fig. 97f is a close up snapshot of the sub-solar region (see Fig. 97a) showing details of the mottled clouds here. Comparison of the cloud morphology in the morning and afternoon sectors of the planet clearly shows significant influence of the solar heating (Fig. 99). Global cloud pattern at the middle and high latitudes resembles very much the structure of Earth hurricanes, but the Venus planetary vortex is 3 – 4 times larger (Fig. 100). Numerical modeling of the barotropic instability in the vortex managed to reproduce "fancy" and variable shape of the polar eye (Limaye et al., 2009).

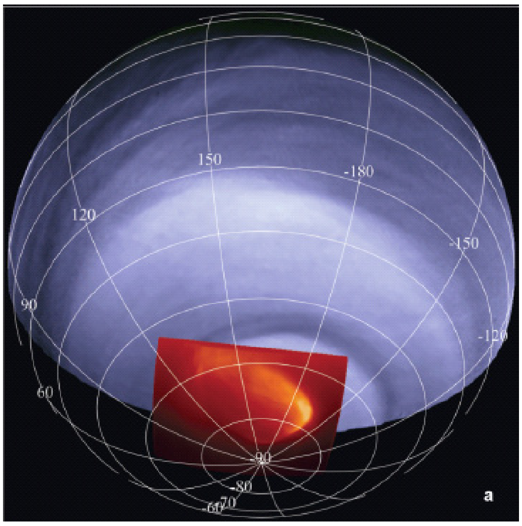

Fig. 98: Global view of Venus in UV (grey) with insert of VIRTIS thermal-IR image of the eye of polar vortex (red).

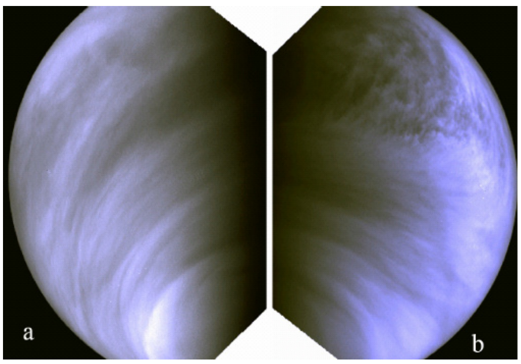

Fig. 99: Morning (left) and afternoon (right) sectors of Venus. Zonal super-rotation is from right to left.

(D. Titov, W. J. Markiewicz, S. Limaye, R. Moissl, M. Almeida, S. F. Hviid, and H. U. Keller)

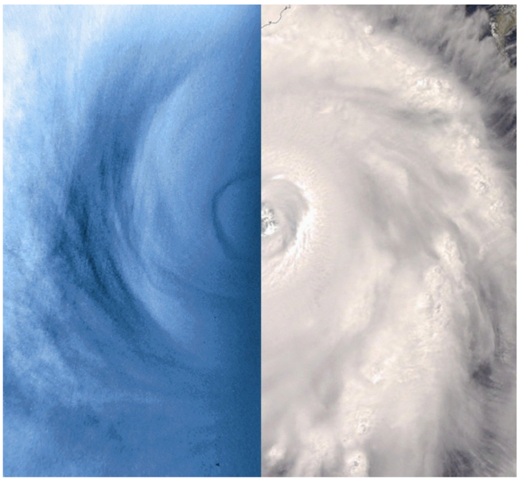

Fig. 100: Comparison of the cloud morphology in the Venus planetary vortex (VMC image on the left) and that of the Earth hurricane Frances.

Venus cloud altimetry

Knowledge of the altitude of the Venus cloud tops is important for the problems of cloud morphology, identification of the UV absorber, and assignment of the cloud tracked winds to a certain height. Earlier observations placed the cloud tops in the altitude range of 66 – 72 km and gave poor constrains on its variability over the Venus disc. Simultaneous observations by VIRTIS and VMC allowed us to map the cloud top altitude and to relate it to the UV markings. The cloud top altitude is retrieved from the depth of CO_2 absorption band at 1.6 m. In low and middle latitudes the cloud top is located at 74 ± 1 km. Its altitude decreases poleward from $\sim 50°$ and reaches 63 – 69 km in the polar regions (Fig. 101a). This depression coincides with the eye of the planetary vortex. Cloud top altitude experiences fast variations of about 1 km in tens of hours, while larger long-term variations of about several kilometers have been observed only at high latitudes. UV markings correlate with the cloud altimetry, however the difference between adjacent UV dark and bright regions do not exceed several hundred meters. Surprisingly, CO_2 absorption bands are often weaker in the dark UV features, indicating that the clouds may be located there even few hundred meters higher. Dark UV spiral arms, which are often seen at about 70°, thus formally correspond to higher altitudes or to the regions with strong latitudinal gradient of the cloud top altitude (Fig. 101b). Cloud altimetry in the polar region reveals the structure that correlates with the thermal emission maps but is invisible in UV images. This implies that the UV optically thick polar hood is transparent in the near IR.

(N. Ignatiev, D. Titov, W. Markiewicz, G. Piccioni, and P. Drossart)

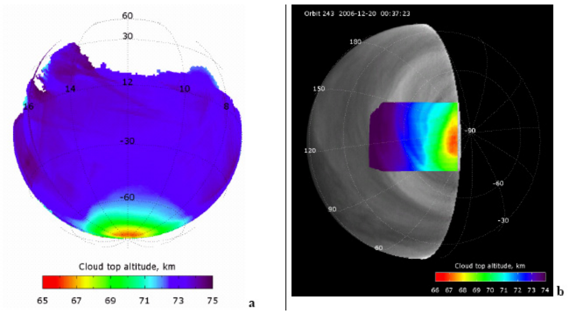

Fig. 101: Altimetry of the Venus cloud tops. a). Mean cloud top altitude as function of latitude and local time; b). Cloud altimetry map overplotted (colour) on the VMC UV image (grey).

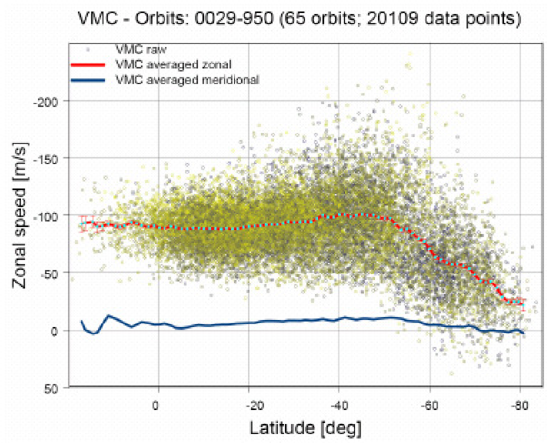

Fig. 102: Zonal and meridional winds measured by tracking cloud features in the VMC UV images.

Venus cloud top winds

The Venus Monitoring Camera continues to acquire imaging sequences with up to 8 hours duration and good temporal resolution down to few minutes between images. This data is being used to determine the winds at the cloud tops (∼70 km) by tracking UV markings on the Venus disc. Fig. 102 shows an overview of measurement points on zonal (longitudinal) winds. Latitudinal wind profiles show almost constant average mean velocity of 90 – 100 m/s at low latitudes (<40 deg) in agreement with the earlier measurements. Within the wide spread of measurement values in the steadily growing data set it was possible to identify several global wave modes in the lower mesosphere of Venus, such as a near-equatorial Kelvin-type wave with a periodicity of ∼ 4 days. Also the measurements are in agreement with the occurrence of planetary mode 1 and 2 waves, likely to be caused by the influence of thermal tides in the Venus atmosphere. Future investigations will focus also on high-resolution images with higher temporal resolution in order to resolve potential higher frequency variations and allow to study the relatively slow meridional wind component.

(R. Moissl, I. Khatuntsev, S. Limaye, W. J. Markiewicz, D. Titov, and N. Ignatiev)

Origin of UV markings and conditions at the cloud tops

When seen in ultraviolet light Venus has contrast features that arise from the non-uniform distribution of unknown absorbers within the sulphuric acid cloud and appear to trace dynamical activity in the middle atmosphere (Fig. 97). It has long been unclear whether the global UV pattern arises from differences in cloud top altitude, compositional variations, or temperature contrasts. A consistent picture of the global UV pattern of the cloud tops and its relation to the physical conditions and dynamics of the lower mesosphere is emerging from the multispectral imaging by VIRTIS and VMC onboard Venus Express. Three latitude zones can be distinguished on the planet (Fig. 103): UV-dark low latitudes (<50°S), a UV-bright mid-latitude band coinciding with the cold collar (50 – 70°S), and a polar "cap" (> 70°S) with embedded vortex eye. They differ significantly in cloud morphology, UV appearance, temperature structure and dynamics.

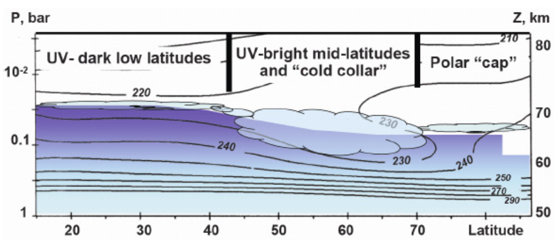

Fig. 103: Sketch of the global cloud top morphology. Isolines show the mesospheric temperature field derived from Venera-15 spectrometry in the northern hemisphere18. Conservatively scattering UV-bright cloud is shown in light blue, while the UV absorbing layer is in dark blue.

Strong convection induced by deposition of solar energy inside the main cloud dominates in low latitudes. We see its traces clearly in the cloud top morphology (Figs. 97, 99). Convective mixing brings UV absorbers from depth, making low latitudes appear relatively dark at these wavelengths. The situation changes dramatically at ∼50°S when we enter the cold collar, an annulus of cold air located right at the cloud tops. Strong temperature inversions found here by the Venus Express temperature sounding provide convective stability and suppress vertical mixing. Streaky clouds point to non-turbulent horizontal flow that dominates over convection (Fig. 97). Both zonal wind velocity and its vertical gradient quickly decrease with latitude, preventing development of shear instabilities (Fig. 102). All this suppresses the supply of absorbers from depth and explains the bright appearance and the paucity of UV features in middle latitudes. In addition, the cold temperatures in the collar region create favourable conditions for formation of bright sulphuric acid haze. This dense conservatively scattering aerosol masks the UV absorbing layer hidden deeper inside the cloud (Fig. 103). (Titov et al., 2008a)

(D. Titov, F. Taylor, H. Svedhem, N. Ignatiev, W. J. Markiewicz, G. Piccioni, and P. Drossart)

Thermal wind in the Venus mesosphere

Venus mesosphere (60 – 100 km altitude) is a transition region between strong super-rotation with zonal wind speed up to 100 $m\,s^{-1}$ in the troposphere and solar-antisolar circulation with wind speeds of $\sim$120 $m\,s^{-1}$ in the thermosphere. Previous studies showed that mesospheric dynamics is well described by the cyclostrophic approximation that allows one to derive zonal winds directly from the temperature field. The temperature structure is measured by VIRTIS thermal sounding and in VeRa radio-occultation experiment onboard Venus Express. Fig. 104 shows the zonal wind field derived from the VIRTIS temperatures. The main features of the wind field are: (1) the mid-latitude jet with a maximum speed of 90 ± 10 m/s located at $\sim$50° S latitude and 70 km altitude; (2) fast decrease of the wind speed from $\sim$60° S toward the pole; (3) the decrease of the wind speed with height above the jet. Comparison with the cloud tracked winds (Fig. 102) shows good agreement at middle latitudes.

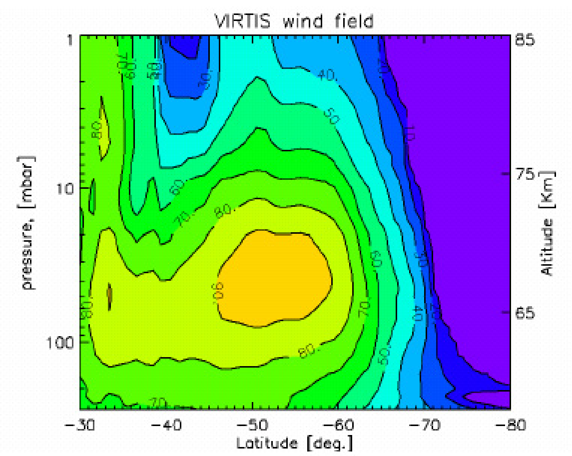

Fig. 104: Thermal wind field derived from the VIRTIS temperature sounding using cyclostrophic assumption.

(A. Piccialli, D. Titov, D. Grassi, and A. Migniorini)

Venus Monitoring Camera sees the surface through the thick cloud veil

Infrared radiation emitted by the hot (735 K) surface of Venus escapes to space after numerous scatterings in the 25 km thick cloud layer through narrow spectral "windows" between strong absorption bands of atmospheric gases. VMC uses 1 m "window" to map the planet on the night side. Fig. 105 a,b show Atahensik (a) ad Artemis (b) coronae -giant volcanic structures 1000 – 2000 km in diameter in the rift zone. Fig. 105c shows global view of Aphrodite Terra. Fig. 105d shows one-orbit mosaic of the Maat Mons vicinity. Surface images are currently used to study variation of mineralogical composition correlated with topography and radar reflectivity, and to search for volcanic activity (Basilevsky et al., 2008).

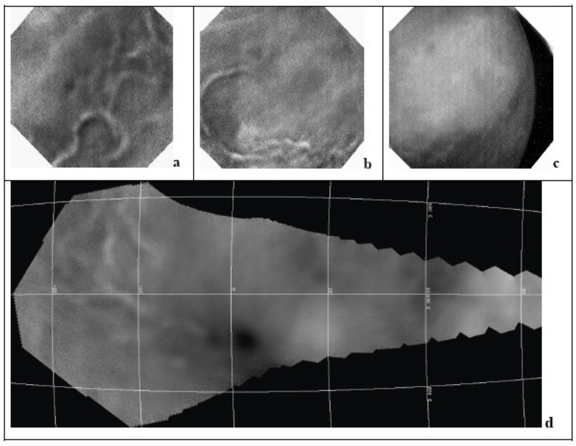

Fig. 105: VMC near IR images of the Venus surface: a, b). Coronae in the rift zone; c). Global view of Aphrodite Terra; c). mosaic of the Maat Mons region. Dark regions are higher than the bright ones.

(D. Titov, M. Almeida, F. Scholten, and W. J. Markiewicz)

O^+ ion flow below the magnetic barrier at Venus post terminator

Venus forms an obstacle in the streaming solar wind. Above the ionosphere the solar wind and its embedded magnetic field is deflected and a magnetic barrier is formed. Inside the barrier ions of planetary origin dominate the plasma. The objective of this study is to investigate the properties of the O^+ ions inside the obstacle boundary of Venus in the wake; we are especially interested in the characterization of the different plasma regions the O^+ ions occupy. The study is based on the data collected by the ASPERA 4 plasma analyzer flying onboard of the Venus Express mission in a region never explored before experimentally. The obstacle boundary was approximately identified from the dropout of magnetospheric electrons and the sharp decrease of the proton speed; the entry point correlated well with the location of the magnetic barrier derived by eyes from magnetometer data (Fig. 106). The most characteristic structures seen during the various flybys were (1) the tailward continuation of the mantle was evident; (2) in the mantle near Venus the O^+ ion flow was significantly intense in low-energy counts; (3) the inbound and outbound crossings of the tailward boundary were sharp, characterized by less intense but higher-energy O^+ beams; (4) the crossing of the central tail region (current sheet) was marked by the change of the sign of Bx and by an intense low-energy O^+ ion flux; (5) it is remarkable that the O^+ ion outflow was not confined to the central tail region; the intensity elsewhere was highly variable, resulting in a ray-like outflow pattern in most of the cases (Szego et al., JGR, E00B26, 2009).

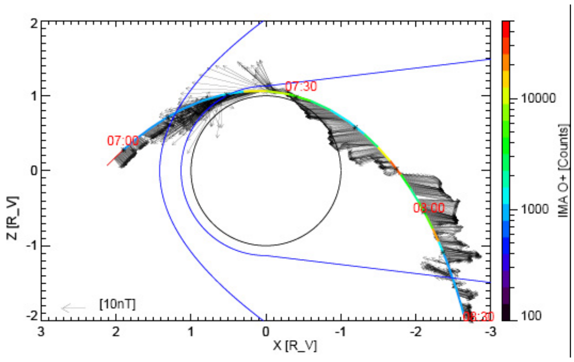

Fig. 106: The magnetic field vectors projected on the VSO y-z plane. The length of the vectors is proportional to Btot. The blue lines show the bow shock and magnetic pileup boundary. Along the orbit the O^+ ion counts are shown in colour. This shows how the ion outflow is organized by the global magnetic structure.

(M. Fränz, Z. Bebesi)

Contribution with the first and second coordinated campaigns of Venus ground-based observations in support of the Venus Express mission

We collaborated with the first world-wide coordinated campaign of Venus ground-based observations (23 May 2007 to 9 June 2007) in support of Venus Express and MESSENGER. Submillimetre observations of the ^{12}CO J=3-2 and 2-1, and ^{13}CO J=2-1 transitions of the Venusian atmosphere obtained with the Heinrich Hertz Submillimetre Telescope (HHSMT) in Arizona were used to carry out a complete retrieval analysis: mesospheric parameters such as the wind, vertical thermal structure, and CO abundance (Rengel *et al.* (2008)a, Rengel *et al.* (2008)b). Changes in the thermal structure of the Venusian mesosphere are detected: day-to-night small temperature variations and short-term (day-to-day) on a time scale as short as one day. This is consistent with the picture of dramatic variability of the Venus mesosphere with changes in temperature occurring on short time scales. Furthermore, retrieved winds show variations of around 100 m s^{-1} between the winds on 14 June and those on 15 June. We also found a temperature peak at 90 – 100 km which seems to support the finding of the extensive layer of warm air detected by SPICAV onboard Venus Express (Bertaux et al. 2007, Nature, 450, 646), Fig. 107.

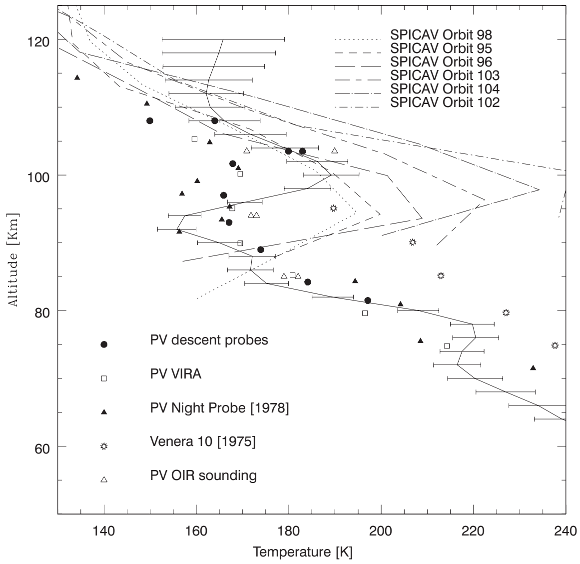

Fig. 107: Temperature profile retrieval (from a ^{12}CO J=2-1 line at the Venus center (18 LT) taken on 15 June 2007), solid line, compared to the profile from the stellar occultations with the SPICAV onboard Venus Express (Bertaux et al., 2007), PV descent probes (Seiff et al., 1980), from the OIR sounding measurements (Schofield and Taylor, 1983), and from the PV night probe (Seiff and Kirk, 1982).The SPICAV measurements were taken at latitude 39° N for orbits 95, 96, and 98, and latitude 4° S for orbits 102-104. The Pioneer-Venus derived VIRA reference profile for latitudes <30° are indicated by the squares. The anomalously warm temperatures returned by the Venera 10 probe in 1975 are shown as stars symbols. The absolute uncertainty for the temperatures derived here is ± 15K.

Since the success of the first world-wide coordinated campaign of Venus ground-based observations, a second campaign is organized by the Venus Express Science Working Team, extending from January to June 2009. During part of year 2008 we have actively prepared observational projects in order to participate with this second campaign. Our participation includes several observational facilities like the HHSMT, the Combined Array for Research in Millimeter-wave Astronomy (CARMA), and the Submillimetre Array (SMA), among others. This time, taking advantages of new instrumentation available and also the interferometric technique, the spatial resolution and accuracy of the temperature and wind retrieval is expected to be improved.

(M. Rengel, P. Hartogh, C. Jarchow, and H. Sagawa)

Terrestrial planets research – Mars

Microscopic views of soil and dust at the Phoenix landing site

The Phoenix Spacecraft landed on 25 May 2008 in Martian north-polar plains about 1800 km north of the shield volcano Alba Patera and about 20 km west-southwest of the 10 km diameter Heimdall crater. Based on remote sensing data from orbit the material at the Phoenix landing site is believed to be of multiple origin including ancient volcanic ash deposits (dating back to the Hesperian), impact ejecta from the 500 million years old Heimdall crater as well as aeolian material brought in from outside as saltation and suspension loads. The Phoenix lander provided ground truth by returning among many other data sets about 500 colour high-resolution images of soil material (4 micrometer/pixel) from the Optical Microscope. The figure (top part) shows a magnetic substrate (circular, 3 mm in diameter) before and after soil delivery that occurred on sol 75. The substrates are oriented vertically with the gravity vector (g) pointing downwards. All particles are noticeably magnetized, as they stick to the near-center of the substrate. The presence of particles prior to delivery (top left part of the figure) is due to (limited) redistribution of soil material due to motions and vibrations of the sample wheel translation stage. The bottom part of the figure shows a bimodal particle size distribution (silt-sized versus unresolved clay-sized particles) and a wide spectral range of silt-sized particles. Currently we believe that the reddish clay-sized fraction represents ordinary martian dust. Among the silt-sized fraction the brownish particles (marked by a 1 in the figure) might be impact glasses from Heimdall crater, while the black ones (marked by a 2) might be the result of wind abrasion of basaltic rocks. Comparison with images from the Microscopic Imager (MI) onboard the Mars Exploration rover Spirit in Gusev crater provides further clues on the nature of these particles. (see Fig. 108).

(W. Goetz, S. F. Hviid, M. R. El Maarry, H. U. Keller, and W. J. Markiewicz)

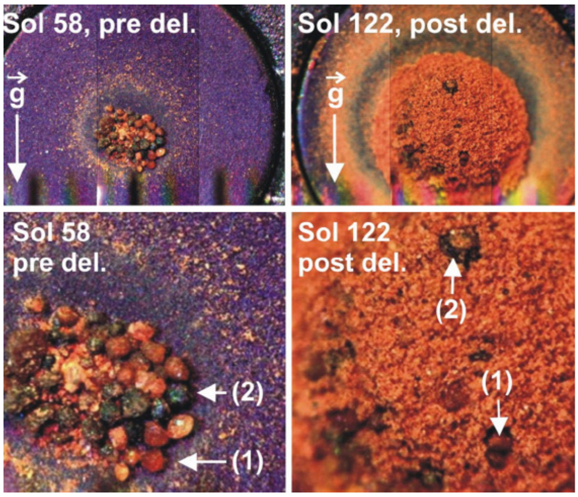

Fig. 108: Phoenix soil particles on microscope substrates. Top: The same substrate (circular, 3 mm in diameter) shown before and after soil delivery. The substrates are oriented vertically with the gravity vector (g) pointing downwards. Bottom: Zoom of the top images.

Atmospheric correction for Mars Express images

The High Resolution Stereo Camera (HRSC) on board Mars Express (MEX) has been delivering stunning images of the Martian surface for over five years (Neukum et al. 2004), and still remains in good shape. On Mars, the surface is protected from wind erosion neither by vegetation nor by oceans and thus the wind is able to transport large amounts of dust up into the thin atmosphere. As a result, the HRSC images show the surface through a haze of airborne dust. During large global storms this haze can become so thick that it renders the atmosphere completely opaque. However, in general the dust load is much lower, generally between $\tau = 0.3$ and $\tau = 1$, as measured by the Mars Exploration Rovers, and the surface is visible. These atmospheric contributions limit the use of HRSC images (and of all other remote sensing images from space) for e.g., photogrammetric and spectral analysis and for the mapping of the Martian surface.

However, if the amount of airborne dust and its optical properties are known it is possible to compensate for its contribution using radiative transfer models. From previous work on Mars Pathfinder and other landers we know the optical properties of the Martian red dust (Markiewicz et al., Adv. Space Res., 29(2), 175, 2002, Markiewicz et al., J. Geophys. Res., 104, 9009, 1999). For the derivation of the optical depth which accounts for the amount of dust in the atmosphere we are developing different methods that make use of the stereo channels of the HRSC, shadows on the surface and of known surface colours. Each of these methods has a different set of strengths and weaknesses and they are meant to supplement each other.

Fig. 109: Caldera of Pavonis Mons, mosaic of two images after atmospheric correction for red dust. Some minor additional colour corrections have been done afterwards. The boundary between both images lies at the western rim of the caldera.

Results show that in most cases the atmospheric correction, even when not very precise, can substantially improve contrast and colour of the images. Fig. 109 shows an example of atmospheric correction. Since illumination and dust-load of the atmosphere change between images, it is necessary to correct for these influences before fitting different images together into a single image. In the case presented here, illumination and optical depth did not vary much between the different orbits. While in cases were illumination and optical depth are largely different, the correction is less precise and the preparation of mosaics for maps becomes more difficult, atmospheric correction still improves the results.

(O. J. Stenzel, N. M. Hoekzema, W. J. Markiewicz, and H. U. Keller)

Simulations of the dust cycle on Mars

Airborne dust plays an important role in the Martian climate system. Aerosol particles absorb and scatter the solar flux, and therefore, atmospheric temperature is strongly affected by temporal and spatial distributions of dust. The latter is supplied from the ground, and especially strong dust lifting occurs during so-called dust storms. Depending on the size and duration of the storms, they can be divided into three types: local, regional and global (planet-encircling). Numerous observations show that dust storms are generated mainly in the southern hemisphere every Martian year, although not every dust storm develops into global one. Implementation of the dust cycle in general circulation models (GCM) is highly important for simulations of the Martian climate system. Many existing Martian GCMs employ the observational data in order to evaluate the seasonal dust distributions in the atmosphere. We developed a dust lifting scheme, and implemented in into the GCM. The scheme accounts for dust particles lifting if the near-surface wind exceeds a certain threshold, their transport by the local wind, and sedimentation. The scheme is interactive in the sense that the simulated dust distributions affect radiative calculations, and ,thus, provide the feedback to the atmospheric wind and temperature. The scheme currently undergoes an extensive validation and sensitivity tests. Fig. 110 shows the simulated vertical flux of dust particles on the surface. It is seen that strong dust lifting occurs near 30° S, in a good agreement with observations.

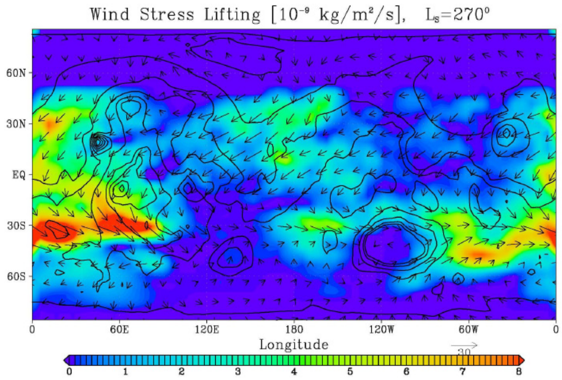

Fig. 110: The dust lifting flux on the surface simulated with the MGCM. Colour contours show the flux, and the arrows denote the surface wind.

(M. Kadowaki, A. S. Medvedev, and P. Hartogh in collaboration with M. Takahashi (Center for Climate System Research, University of Tokyo, Japan))

Martian water cycle from the OMEGA/Mars Express observations

In 2008 the imaging spectrometer OMEGA onboard Mars Express continued observations of Mars. Seasonal behaviour of atmospheric water vapor was monitored during more than one Martian year from the end of MY26 through the MY 27. The study covered all aspects of the water cycle: temporal evolution at seasonal and diurnal scales, lateral and vertical distribution. (Fig. 111). shows seasonal behaviour of the atmospheric water column density. The mean abundance during the year was ~ 10 pr. μm, with slightly higher value in the northern hemisphere. The peak of activity, up to 60 pr. μm, occurs at the edge of the northern polar cap during local summer. Southern summer peak is less pronounced. The global circulation affects the water cycle by transporting water to the equator. Comparison of the OMEGA and TES/MGS data sets limited diurnal water vapor exchange between the surface and the atmosphere to few pr. μm. Spatial distribution of the atmospheric water after correction for topography shows local maxima over Tharsis and Arabia Terra. The saturation height of water vapor is mainly governed by the varying insolation during the year. Water is confined to the lower 5 – 15 km near the surface at aphelion, while during perihelion it extends up to 55 km.

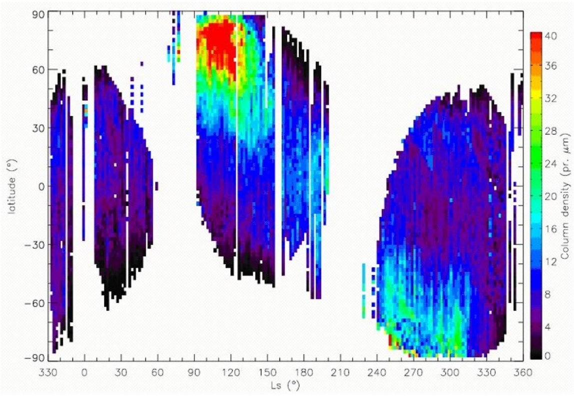

Fig. 111: Seasonal behaviour of the atmospheric water column density.

(L. Maltagliati, D. Titov, and H. U. Keller)

Submillimetre wavelength instrument on the Japanese Mars mission MELOS

A new Japanese Mars exploration mission is now planned by the Japan Aerospace Exploration Agency (JAXA). The mission is named MELOS which is an abbreviation of "Mars Exploration with a Lander and OrbiterS", a full explanation of how the mission looks like: it consists of a lander and two orbiters with different orbits. The launch is planned in 2017 or 2018. Now an official working group for this mission is established at JAXA, and the final implementation of the project will be decided in 2011. Two orbiters, which will be developed with the heritages of the past Japanese Mars orbiter NOZOMI and ongoing Japanese Venus orbiter Planet-C, explore the climate of Mars and more specific the water cycle, atmospheric circulations, atmospheric escape, photochemistry, and mechanism of dust storm development. Among others, a submillimetre wavelength instrument (SMM sounder) is one of the candidates of onboard instruments of these orbiters. The SMM sounder is a powerful and epoch-making remote sensing tool for Martian atmospheric science. Its high spectral resolution allows us to measure accurate line shapes of the molecular rotational tansitions. Their Doppler shift due to the winds on Mars can be also observed. Limb and nadir observations from an orbit close to Mars enables us to obtain the vertical profiles of temperature, winds, and other important chemical species such as CO, CO istopes, H_2O, HDO, and H_2O_2. In addition, Martian dust becomes almost transparent at the submillimetre wavelengths because the dust particles are small compared to the wavelength. This makes the SMM sounder unique in Martian atmospheric observations in that it can observe inside a dense dust storm while other optical instruments cannot.

The instrumental development of the SMM sounder is led by the group at National Institute of Information and Communications Technology (NICT), Japan, which have developed a submillimetre limb emission sounder for the Earth stratosphere (SMILES). We MPS researchers join the study with a simulation study of the observations and a design study of the instrument, in particular of the Chirp Transform Spectrometer.

(H. Sagawa, T. Kuroda, and P. Hartogh in collaboration with Y. Kasai (NICT, Japan) and T. Satoh (ISAS/JAXA, Japan))

Pressure broadening coefficients of H_2O in the atmosphere of Mars and Venus

Water vapor is of central importance in Mars' and Venus' atmosphere. Several millimeter and submillimetre observations of Martian and Venusian H_2O have been published (e.g., Encrenaz et al., 1991, 1995, 2001; Sandor and Clancy, 2005; Gurwell et al., 2000, 2007). The advantage of such microwave observations is that they are able to resolve the line shape of the water vapor transitions, and can retrieve an altitude profile information of the H_2O abundance from such high resolution spectra by using the pressure dependency of the line width. Using this approach, it is crucial to accurately know the spectroscopic parameters of H_2O like transition frequency, line intensity, collision-broadened half widths (expressed by the pressure broadening coefficient γ), lower state energy, etc. Since pressure broadening coefficients vary widely between different perturbing gases, it is essential to adopt those induced by CO_2 in the case of Mars and Venus. A number of laboratory and theoretical studies of N_2-, O_2-, and self-broadening coefficients of H_2O, as appropriate for Earth atmospheric conditions (γ_{air}), can be found (e.g., HITRAN database (Rothman et al., 2009)). However, CO_2 induced pressure broadening coefficients γ_{CO2} have not been studied sufficiently, in particular at millimeter and submillimetre wavelengths.

In this research project, we measured γ_{CO2} of H_2O rotational transitions at 0.5 – 3 THz for the first time using a Terahertz Time-Domain Spectrometer (TDS). Using the TDS allows one to measure absorption spectra with one order of magnitude better accuracy than

Fourier Transform Spectrometers in this frequency region. The precision of our measurements was 2.4 % in average. The measured γ_{CO2} are compared to those calculated by the complex Robert-Bonamy formalism (Bauer et al., 1996). The difference between the measurement and the theoretical estimation was in the range of $-13.5\,\%$ to $+20.1\,\%$ confirming the credibility of the theoretical approach.

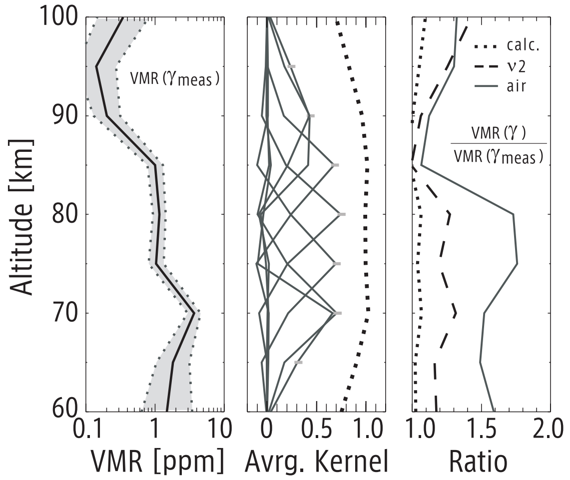

Fig. 112: Application of our measured γ_{CO2} to the retrieval analysis of Venus H_2O mixing ratios. The left and center panels show the retrieved H_2O profile with retrieval errors, obtained by using our measured γ_{CO2}, and their averaging kernels, respectively. The averaging kernels indicate that the retrieved H_2O profile has sensitivity at altitudes of 70 – 85 km with a vertical resolution of ~10 km. The right panel shows the difference in the retrieved H_2O profile under various γ conditions: "air" (solid line) represents the case using γ_{air} listed in the HITRAN database, and it introduces a critical difference in the retrieval results.

We examined the impact of our newly measured γ_{CO2} on application to the retrieval of H_2O abundance by performing an inversion analysis of the Venusian atmosphere obtained with the Submillimetre Wave Astronomy Satellite (Fig. 112). In this example, the retrieved H_2O mixing ratio reduces by half at the altitude region of 70 – 85 km when applying the newly measured γ_{CO2} compared to γ_{air}.

(H. Sagawa and P. Hartogh in collaboration with T. Seta, J. Mendrok, and Y. Kasai (NICT, Japan))

On forcing the winter polar warmings in the Martian middle atmosphere during dust storms

Using a Martian general circulation model, we investigated the changes in the meridional circulation during planet-encircling dust storms on Mars that produce strong temperature inversions in the middle atmosphere over winter polar regions. It is shown that vigorous poleward and downward transport (Fig. 113), and, consequently, the adiabatic heating are caused by dissipating thermal tides, planetary and resolved small-scale gravity waves and eddies to almost equal degree (Fig. 114). The increase of tidal forcing is mainly due a stronger excitation in the summer hemisphere. Contribution of the stationary planetary wave (SPW) with the zonal wavenumber s=1 increases during dust storms due to intensified generation in the lower atmosphere as well as due to more favorable vertical propagation. For the first time, we demonstrated a significance of small-scale gravity waves and eddies in maintaining the meridional circulation in the Martian middle atmosphere, at least in high winter latitudes during dust storms.

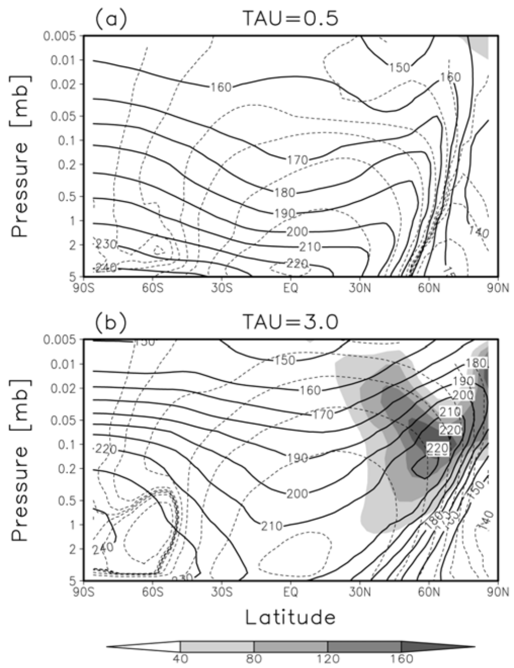

Fig. 113: The zonal-mean temperature [K] (solid lines), meridional mass stream function (dashed line), and adiabatic heating rate [K sol^{-1}] (shades) for (a) the "low dust" ($\tau = 0.5$) run and (b) the "dust storm" ($\tau = 3.0$).

(T. Kuroda, A. S. Medvedev, and P. Hartogh in collaboration with M. Takahashi (Center for Climate System Research, University of Tokyo, Japan))

Maintenance of zonal wind variability associated with the annular mode on Mars

Results from a Mars general circulation model (MGCM) were used to investigate the maintenance of the annular mode in the Martian atmosphere. Analysis of the Martian northern winter, as represented by the MGCM, revealed a prominent transient wave with zonal wave number 1 that had a baroclinic in-

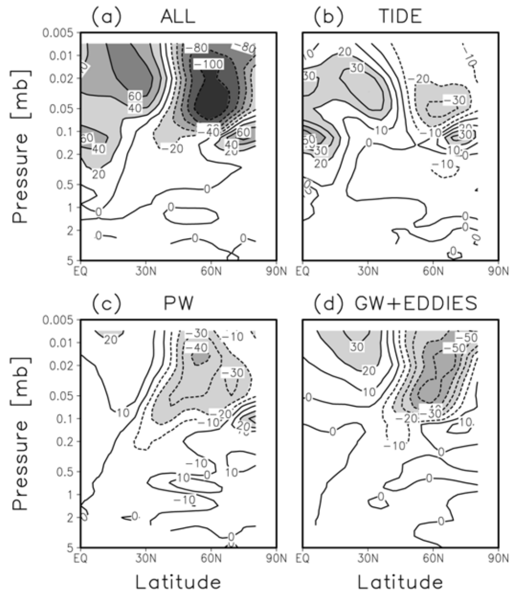

Fig. 114: EP flux divergence [m s^{-1} sol^{-1}] for the "dust storm" simulation: (a) The total values, (b) contribution of tides (the sum of the diurnal to quad-diurnal components with s=1 to 10), (c) contribution of planetary waves, and (d) contribution of gravity waves and eddies (with s>10 and periods less than a day).

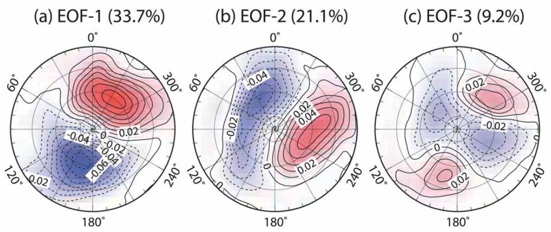

Fig. 115: The structures of EOF-1 to EOF-3 for the surface pressure (P_s) deviation on Mars. Each EOF ($\mathbf{e}_\mu$) was multiplied by the eigenvalue ($\lambda_\mu^{1/2}$), and each $\lambda_\mu^{1/2}\mathbf{e}_\mu$ is shown. Solid lines indicate positive values, and the broken lines indicate negative values. The area shown is north of 20°N, and latitude circles at 40, 60, and 80°N are shown. Note that the P_s was weighted by the cosine of latitude before EOF decomposition.

stability structure. An empirical orthogonal function (EOF) decomposition showed that the first two modes of the EOF contained features of the transient wave with wave number 1, and the third EOF mode had an annular structure about the Martian North Pole with an equivalent barotropic structure in the vertical (Fig. 115). Each term in the transformed Eulerian mean equation was estimated from the MGCM output to investigate the maintenance of the annular mode. Wave forcing (Eliassen-Palm flux divergence) played an important role in maintaining the mode. In the wave forcing term, contributions from transient baroclinic waves with wave numbers 1 and 2 were important.

(T. Kuroda in collaboration with Y. Yamashita and M. Takahashi (Center for Climate System Research, University of Tokyo, Japan))

The Mars express ionosphere and subsurface radar sounder

The MARSIS (Mars Advance Radar for Subsurface and Ionospheric Sounding) instrument on the Mars Express spacecraft is a powerful new tool for studying the ionosphere of Mars. The radar can perform two types of ionospheric sounding, remote and local. The remote radio soundings consist of transmitting a short pulse at a fixed frequency and measuring the time delay for the pulse to reflect from the topside of the ionosphere. By measuring the delay time as a function of frequency, the vertical profile of the electron density in the topside ionosphere can be determined. Vertical electron density profiles obtained using this technique are in general good agreement with similar electron density profiles determined earlier using radio occultations from spacecraft orbiting Mars, but extend to smaller and larger solar zenith angles. The main new result from the remote sounding measurements is the discovery of oblique echoes from localized density structures that occur over regions of strong nearly vertical crustal magnetic fields. In addition to the remote radar soundings, two types of local sounding measurement have been obtained, (1) from the excitation electron plasma oscillations at the local electron plasma frequency, and (2) from excitation of electron echoes at the local electron cyclotron frequency. Since the frequency of the electron plasma oscillations is proportional to the square root of the electron density, the frequency of these oscillations provides a very accurate measurement of the local electron density. Electron density measurements using this technique can be made at much higher altitude than can be obtained from the MARSIS remote radio soundings. This new capability for measuring the electron density at high altitude has revealed that the upper level of the Martian ionosphere, from about 300 km to 1200 km, is highly variable, with electron density fluctuations generally increasing in amplitude with increasing altitude, and often exceeding a factor of ten at high altitude. The spectrum of these fluctuations tends to follow the well known, Kolmogorov, $1/f^{5/3}$ spectrum that is characteristic of fully developed three-dimensional turbulence. Probably because of the high level of fluctuations well-defined ionopause crossings, such as are often observed in the ionosphere of Venus, are seldom observed in the ionosphere of Mars. The large density fluctuations observed at high altitudes are almost certainly due to an interaction with the solar wind, either caused by disturbances in the solar wind that propagate into the ionosphere, or by an instability, such as the Kelvin-Helmholtz instability, that is driven by the velocity shear between the solar wind and the ionosphere. In addition to the excitation of electron plasma oscillations, the excitation of electron echoes at the electron cyclotron frequency, which is proportional to the magnetic field strength, provides a powerful new tool for measuring the local magnetic field strength with high accuracy. Since no magnetometer is carried on Mars Express, the ability to measure the local magnetic field strength from the frequency of the electron cyclotron echoes has proven to be very valuable for analyzing various magnetic effects, such as the draping of the solar wind magnetic field around Mars and its interaction with the ionosphere.

The subsurface of Mars was unexplored territory. Only glimpses of the third dimension of Martian geology could be obtained by studying exposures on craters and valley walls. However, no direct measurements of the subsurface layers were possible before MARSIS started operations.

(E. Nielsen)

"Hook" structure in MARSIS ionogram

In general the echo trace observed by MARSIS is associated with reflections in nadir and indicates an ionosphere with a main maximum electron density at typically about 130 km altitude, and a monotonously decreasing density with increasing altitude. Another maximum is sometimes detected at higher altitudes, indicating a double layer in the vertical electron density distribution in the upper ionosphere, and occasionally there is even a third layer. Sometimes a special structure (here called a "hook") is observed at the low frequency end in the sounder data: a rapid increase of the delay time of the sounder signal with decreasing frequency. It is here proposed that this signature indicates a secondary maximum with densities which can only partly be resolved by the radar. The maximum is associated with too low densities on the topside to be fully resolved by the radar observations. An analytical inversion approach coping with the "hook" case is then proposed. It is further suggested that the "hook" is caused by vertical wavelike structures in the Martian topside ionosphere (and very large horizontal wavelength).

(X. D. Wang and E. Nielsen)

Martian dayside electron fluxes and boundaries

Electron fluxes on the dayside of Mars have been studied with the ASPERA instrument on board the MARS EXPRESS spacecraft for the purpose of determining boundary positions. The location of the Magnetic Pileup Boundary (MPB), as determined by these particle measurements, was found to be in good agreement with earlier estimates using Phobos-2 and MGS observations. Fluctuations of electron fluxes were observed over an altitude range with a mean width of ~ 0.07 Mars radii extending marsward from the MPB. The inner limit of the region of variable fluxes is located at an altitude which is consistent with the location of the Photo Electron Boundary. The MPB is primarily defined as a region of strong magnetic fields arising from the pile up of solar wind magnetic fields as the solar wind encounters the planet. MARSIS is not only a remote sounder experiment but make also local sounding measurement have been obtained from excitation of electron echoes at the local electron cyclotron frequency. The excitation of electron echoes at the electron cyclotron frequency, which is proportional to the magnetic field strength, provides a powerful new tool for measuring the local magnetic field strength. We could confirm that on the day side of Mars there is a region of strong magnetic fields located at the MPB, as determined by the particle measurements.

(E. Nielsen, H. Zou, M. Fraenz, and J. Woch)

Dielectric properties of the Martian South Polar layered deposits: MARSIS data inversion using Bayesian inference and genetic algorithm

MARSIS (Mars Advanced Radar for Subsurface and Ionosphere Sounding) is not only sounding the ionosphere but also the sugsurface layers of Mars. It has offered abundant data, which have been used to estimate dielectric properties of the South Polar Layered Deposits (SPLD) of Mars. This paper presents a new way to invert the data to estimate the dielectric properties of the SPLD. A total of 4364 measurements were analyzed. The received radar signals are controlled by the physical properties of the SPLD and its basal layer, and in addition by a number of factors including the transmitted wave properties, the satellite height, and the atmosphere/ionosphere environments. The received signals may also be influenced by surface clutter. Most of these factors are variable. This complexity causes the inversion to be difficult. To carry out the inversion it is therefore essential to define a reasonably simple model for the physics of the surface/subsurface layers where the radar signal is reflected. The top and bottom interfaces of the SPLD are observed by MARSIS as two reflection peaks of the radar signals. The intensity ratio between the two reflection peaks is observed to be a function of the time difference separating the two peaks. By modeling this dependency, the influences of the satellite position and the atmosphere/ionosphere environments are canceled. This is a major step towards carrying out the inversion. Nevertheless, the inverse problem remains ill-posed and highly nonlinear. Bayesian inference is employed to deal with the ill-posed aspect of the inversion, and genetic algorithm is introduced to deal with the nonlinearity. It is concluded that the most probable value of the relative dielectric constant of the SPLD lies in 3.0 – 5.0, conductivity $1.0 - 2.0\times10^{-6}$s/m, and the relative dielectric constant of the basal layer is 7.5 – 8.5 (The basal layer conductivity is assumed to be 1.0×10^{-7}s/m.) These results support a suggestion that the SPLD are water ice/dust mixtures with dust content varying from 0 to more than 75 %.

(Z. Zhang, T. Hagfors, and E. Nielsen)

Ionospheric corrections of MARSIS subsurface sounding signals with filters including collision frequency

Ionospheric corrections of MARSIS (= Mars Advanced Radar for Subsurface and Ionosphere Sounding) subsurface sounding signals are necessary before they can be further analyzed. Usually the ionosphere correction only considers the phase dispersion owing to electron densities. In this paper we show that if the electron-neutral collision frequency is included in the correction filter, the signal-to-noise ratio of the processed signal can be further maximized and the spatial resolution of the signal be improved. Three different models of the ionosphere profile have been studies, and it is shown that a uniform slab model, of both densities and collisions, is feasible and probably the best choice when implementing the correction filter including collisions. The physical significance of the parameters obtained with the uniform model (equivalent parameters) are discussed, and it is shown that they are useful for estimation of the real physical parameters of the ionosphere. We developed a recursive, random search algorithm to facilitate the realization of the correction process with the filter including collision frequency.

(Z. Zhang and E. Nielsen)

The scale-height of optical depth of the martian atmosphere from shadows in images taken by the High Resolution Stereo Camera of Mars Express

The optical depth of the martian atmosphere in the visible is mainly determined by the amount of aerosols it contains and is considerable. It is easily measured by robot explorers on the surface of Mars that can look into the Sun, but there are no well established ways yet to measure the optical depth from orbiter images. We tested an experimental method that estimates it from the brightness of shadows: the so called "shadow method". Our work also offers indications on how optical depth and aerosol distribution depend on altitude in the lower atmosphere.

It is not well known yet how the accuracy of the shadow method depends on optical depth, colour, and observing geometry. We therefore tested it by analyzing a set of stereo and colour images taken by the High Resolution Stereo Camera of the European orbiter Mars Express. It consists of five panchromatic (675 ± 90 nm) stereo images, four other images taken in colours between blue and near infra red, and a digital terrain model. The images were observed during orbit 1944 of Mars Express, and show a part of Valles Marineris that spans about ten kilometers in altitude which enabled us to study how the estimates of optical depth depend on altitude. We estimated the optical depth at more than 150 locations in each of the nine images. If the scale height of optical depth is close to that of the pressure scale-height of the air itself, then the accuracy with which our measurements can reproduce this value yields information about how the accuracy of the shadow method depends on altitude. Fig. 116 illustrates our results.

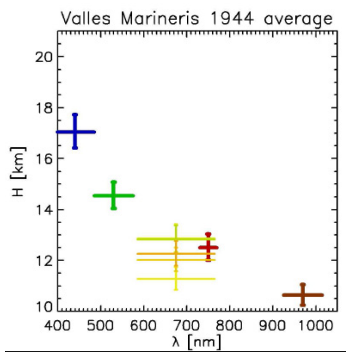

Fig. 116: The images taken during Mars Express orbit 1944 yielded nine estimates in five different colours of the scale-height of optical depth H. H is plotted as a function of colour with the vertical lines denoting the 1 sigma variaton from the average and the horizontal line denoting the wavelength range in which the image was observed. The five panchromatic images are all observed around 675 nm. The retrieved scale-heights clearly increase from near-infra-red towards the blue.

The panchromatic stereo images yielded five estimates of the scale height of optical depth with an average of 12.2 ± 0.7 km, which is close to the expected local pressure scale height. The red image yielded very similar results. Thus, for the panchromatics and for red there is no indication that any errors in estimates with the shadow method depend on altitude. Moreover, the phase angles under which the five panchromatic images were observed varied between 65° and 80°, and the relatively small spread of the results make it clear that the differences in phase angle only play a minor role in the accuracy of the shadow method.

The scale height derived from the near-infrared image is lower and we speculate that this is an indication that the airborne dust particles on average are larger in the lower than in the higher atmosphere. The scale heights that were derived from blue and green images were unrealistically high and this may be caused by thin white high altitude hazes, or indicate that the precision of the shadow method varies with optical depth in these colours.

(N. M. Hoekzema, O. J. Stenzel, W. J. Markiewicz, M. Garcia Comas, E. Petrova, K. Gwinner, A. Inada, H.U. Keller,)

A comet-like escape of ionospheric plasma from Mars

New measurements of the ion escape from Mars display a mantle of low-energy ionospheric ions swept from the dayside over the terminator, expanding into the tail in a comet-like fashion (Fig. 117). The finding is based on data obtained with new energy settings for the ASPERA-3 ion mass analyzer (IMA), enabling us to also measure cold ionospheric ions. By including the comet-like contribution of low-energy ions (<200 eV), we obtain a heavy ion escape rate of $3.3 \cdot 10^{24} (\pm 0.6 \cdot 10^{24})$/s. While a modest energization characterizes the draped comet-like outflow of low-energy ions, ion pickup and acceleration above magnetic anomalies leads to the energetic and structured ion fluxes observed in the Martian tail. Compared to the previous measurements, where the flow of accelerated ionospheric ions is asymmetric, controlled by the solar wind electric field, the low-energy ion escape is symmetric, emerging from the dayside and expanding towards the tail along the tail flank. An analysis of the escape rate versus tail distance from the planet displays a gradual energization of ions, yet maintaining an almost constant escape rate. We finally note that the planetary heavy ion escape rate is measured during solar minimum. The solar maximum value is yet to be determined, but it may very well exceed 10^{25} ions/s (Lundin *et al.*, 2008).

(M. Fränz, E. Dubinin)

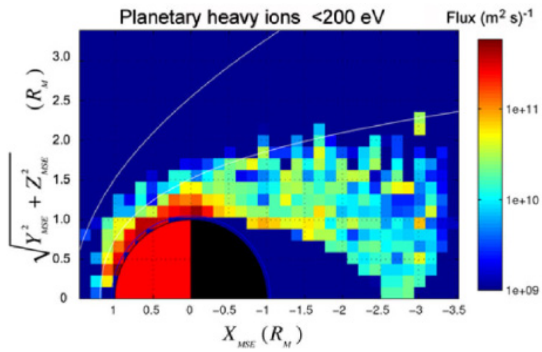

Fig. 117: Low-energy (<200 eV) planetary heavy ion (O^+, O_2^+, CO_2^+) fluxes near Mars. Colour scale represents average fluxes in the 500x500 km quadrants.

Ion acceleration in the Martian tail

Due to the absence of a magnetic obstacle at Mars the solar wind directly interacts with its upper atmosphere and ionosphere and induces a magnetosphere by the pile up of the interplanetary magnetic field. The draping magnetic field lines are slipping around the poles and push the ionospheric plasma into the plasma sheet. ASPERA-3 observations in the Martian tail clearly show this process of ion acceleration (Fig. 118) and allow to evaluate the efficiency of the momentum transfer. The momentum flux carried mainly by solar wind protons ($\sim n_{sw} m_{H^+} V_{sw}^2$) is transferred to the normal and tangential magnetic field stresses producing the stress balance in flow direction on the dayside. At the nightside, the magnetic tensions of the field lines ejected from the ionosphere pull the ions by means of the electric polarization field transferring their momentum to planetary ions ($\sim n_{O^+} m_{O^+} V_{O^+}^2$). As a result, $n_{sw} m_{H^+} V_{sw}^2 \approx k n_{O^+} m_{O^+} V_{O^+}^2$, where k is the efficiency of the momentum transfer. The measurements of the peak energy of oxygen ions in the central plasma sheet and the momentum flux carried by solar wind protons at different solar wind conditions provide us a test of this relationship. Top panels in Fig. 119 show variations of solar wind dynamic pressure for two one week intervals. Blue symbols on the bottom panels depict the energy gained by oxygen ions in the plasma sheet. It is observed that the efficiency of ion acceleration in the plasma sheet is controlled by the momentum carried by solar wind. Red symbols show the expected values of the peak energy evaluated from the solar wind parameters and the number density of oxygen ions in the plasma sheet assuming that $k = 0.7$. A reasonable agreement with observations implies very efficient momentum transfer from solar wind to plasma in the tail of the induced magnetosphere.

(E. Dubinin, M. Fränz, and J. Woch)

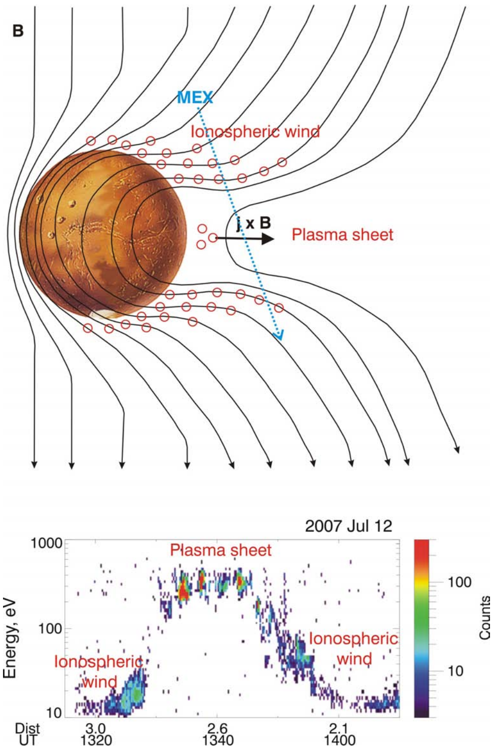

Fig. 118: (top) Cartoon of a draping of the IMF lines around Mars with subsequent acceleration of ionospheric ions by the magnetic field tensions. During convection of the field lines within the ionosphere some part of ionospheric plasma expands along the open field lines forming the ionospheric wind. Another ionospheric population is dragged by the field tensions, gains energy and forms plasma sheet. (bottom) Energy-time spectrogram of oxygen ions shows a transition from the ionospheric wind to plasma sheet along the MEX trajectory.

Ionospheric storms on Mars: Impact of the corotating interaction region

Measurements made by the ASPERA-3 and MARSIS experiments on Mars Express have shown, for the first time, that space weather effects related to the impact of a dense and high pressure solar wind (corotating interaction region) on Mars cause strong perturbations in the martian induced magnetosphere and ionosphere (Fig. 120). The magnetic barrier formed by pile-up of the draped interplanetary magnetic field ceases to be a shield for the incoming solar wind. Large blobs of solar wind plasma penetrate to the magnetosphere and sweep out dense plasma from the ionosphere. The topside martian ionosphere becomes very fragmented consisting of intermittent cold/low energy and energized plasmas. The scavenging effect caused by the intrusions of solar wind plasma clouds enhances significantly (by a factor of ≥ 10) the losses of volatile material from Mars (Dubinin et al., Geophys. Res. Lett., 36, L01105, 2009).

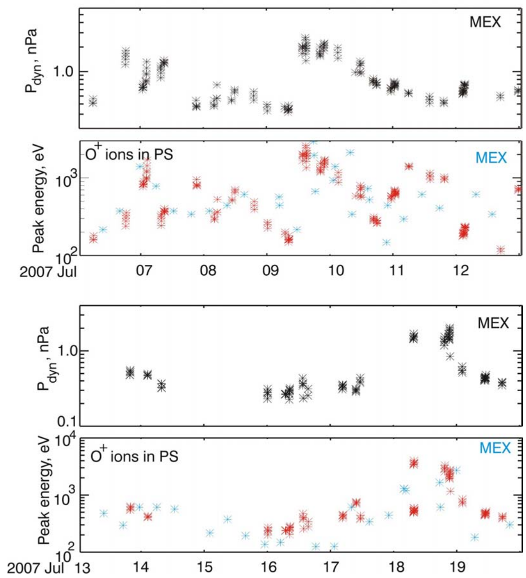

Fig. 119: Variations in solar wind dynamic pressure (top panels) and energy gained by oxygen ions in plasma sheet (bottom panels). Blue and red symbols show the observed and calculated values, respectively.

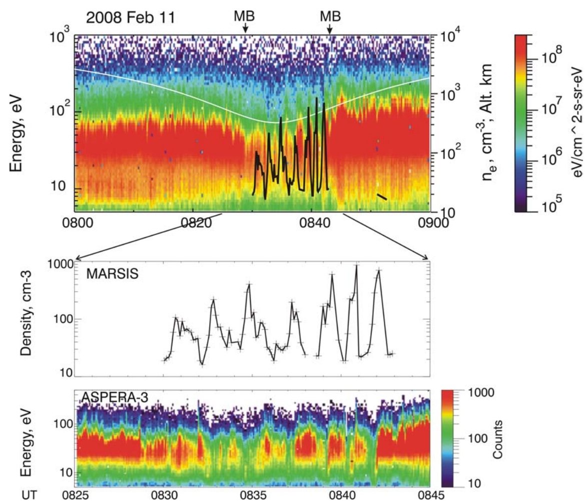

Fig. 120: Energy-time spectrogram of electron fluxes measured by ASPERA-3 during the CIR impact on Mars. The black curve shows the filamentary structure of the electron number density in the upper ionosphere inferred from the measurements by the sounding experiment MARSIS. The white curve depicts the altitude of the MEX spacecraft above the martian surface. The bottom panels show the ionospheric structure in more detail. Dips in the ionospheric density are measured at the times (or locations) when (or where) the intruded clouds of solar wind plasma are observed.

(E. Dubinin, M. Fränz, and J. Woch)

Modifications in martian ionosphere in crustal magnetic anomalies by solar wind

Mars presents a nonmagnetized, conducting (due to the presence of the ionosphere) obstacle to the solar wind. But it also has local magnetizations of the crust. As a result, the picture of interaction is rather complicated and variable – with main elements of induced and some of intrinsic magnetospheres. The field lines near Mars have different topology – closed field lines connected at both ends to Mars, field lines connected at both ends to the IMF, and open field lines connecting Mars and its ionosphere to the IMF. In this case of connection the ionospheric dynamics in the regions with strong crustal magnetization can be changed. Due to a direct access of solar wind electrons along the open field lines localized patches of enhanced ionization can appear. Fig. 121 compares the observations of precipitating solar wind electrons carried out by the ASPERA-3 experiment with MARSIS sounding observations of the total electron content (TEC) derived from radar echoes reflected from the surface. The spacecraft passed over a region with a strong magnetic anomaly at the nightside. Spikes of solar wind electrons well mark the open field lines generated by reconnection between the IMF and crustal fields. Peaks in the TEC observed in these spots correspond to the regions where the radial component of the crustal field dominates.

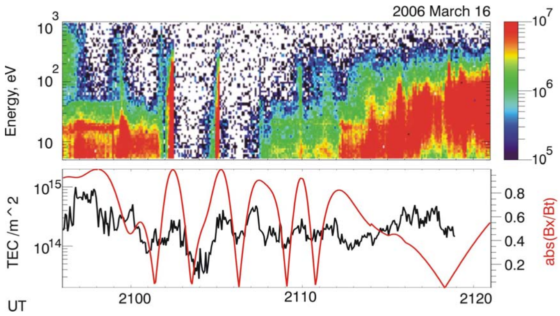

Fig. 121: (top) Energy time spectrogram of electron fluxes. Narrow spikes of solar wind electrons mark the appearance of open field lines. (bottom) Black curve shows the TEC value below the MEX spacecraft. Red curve depicts the ratio B_r/B, where B_r and B are the radial component and the total magnetic field strength.

On the other hand an open magnetic field topology allows planetary plasma from the top-side ionosphere to escape along the field lines. Fig. 122 presents the local observations of the electron number density in the martian ionosphere at the dayside derived from the resonant frequencies of plasma waves excited by the MARSIS radar sounder in the upper ionosphere over the strong crustal sources. Dips in the density coincide with the appearance of open field lines traced by the precipitating solar wind electrons.

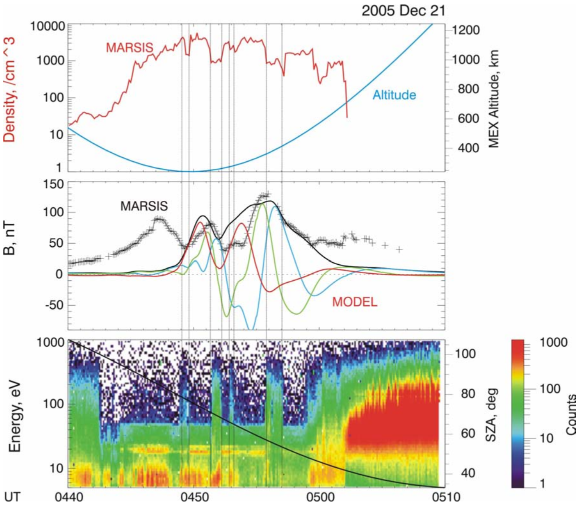

Fig. 122: (upper) Local electron number density inferred from the wave echoes. Blue curve shows the altitude of the MEX spacecraft. Dips in density reach a factor of more than 5. (middle) Black symbols show the magnetic field strength also derived from the wave echoes. Colour curves depict the components of the model crustal field. Black and blue curves show the total and radial magnetic fields, respectively. Red and green curves show the horizontal components. (bottom) Electron fluxes measured by ASPERA-3. The martian ionosphere is well traced by the characteristic spectral peaks at $\sim 20-30$ eV of CO_2 photoelectrons. Multiple spikes of the electrons of solar wind origin mark the appearance of open field lines. The local ionospheric plasma in these flux tubes is depleted. Black curve gives the solar zenith angle.

(E. Dubinin, M. Fränz, and J. Woch)

Long-lived auroral structures and atmospheric losses through auroral flux tubes on Mars

Although Mars presents a nonmagnetized conducting obstacle to solar wind the discovery of a strong localized crustal magnetic fields suggests that the martian magnetosphere comprises also some features typical for the Earth case. Reconnected with the IMF, the crustal magnetic field lines can be stretched in the antisunward direction producing an intricate magnetic field configuration. The ASPERA-3 observations of electron and ion fluxes over the regions dominated by crustal magnetic fields show the existence of long-lived and active aurora-type magnetic flux tubes with a width of $20-150$ km. The activity manifests itself by large electron energy fluxes ($\geq 10^{-4}$ W/m^2) and strong distortions in the upper ($350-400$ km) ionosphere. In some events the peaked electron energy distributions typical for Earth aurora are so pronounced that they are present in velocity distribution functions.

A significant depletion of such auroral flux tubes is accompanied by the appearance of oxygen beams and a heating of the ions of ionospheric origin. Auroral activity was observed on several subsequent orbits of the Mars Express spacecraft during more than two weeks implying a reactivation of auroral flux tubes on almost every planetary rotation. Atmospheric loss driven by energy deposition in the auroral flux tubes is estimated as $\sim 10^{23}\,\mathrm{s}^{-1}$ and can essentially contribute to the losses driven by other mechanisms (Fig.123) (Dubinin et al., Geophys. Res. Lett., 36, L08108, 2009).

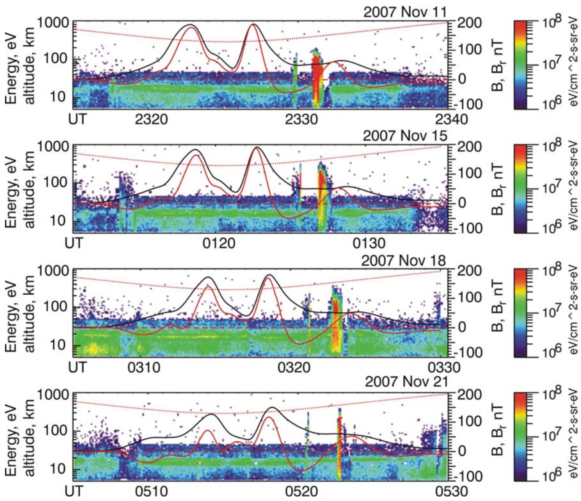

Fig. 123: Electron fluxes on the MEX orbits sequentially crossing the same altidude range ($\leq$ 1000 km) of the martian ionosphere/magnetosphere near the periapsis (see the red dotted curve showing the altitude of the spacecraft) over the same region of strong crustal fields in the southern hemisphere. The value and the radial component of the crustal field are shown by the black and red solid curves, respectively. The remarkable feature is a recurring doublet structure of electron intrusion into the martian ionosphere implying the recurrent reactivation of auroral flux tubes on Mars.

(E. Dubinin, M. Fränz, and J. Woch)

Project MOMA

MOMA (Martian Organic Molecule Analyser) is a gas-chromatograph, laser-desorption mass-spectrometer instrument for the ESA ExoMars mission. The purpose of the instrument is the detection and identification of organic molecules on Mars. The launch is scheduled for 2018. The team comprises an American group at Johns Hopkins University for the mass-spectrometer, a French group for the gas-chromatograph, and MPS for the laser, the pyrolysis ovens and the tapping station. The system lead and the team coordinator are located at MPS.

The central part of the instrument is an ion-trap mass-spectrometer. It is used for the identification and quantification of molecules. Two major ion sources for the MS are envisaged: The first is the classical gas-chromatography / mass-spectrometry (GC-MS) approach where solid soil samples are pyrolysed and the volatile fraction is separated by a GC and analysed by the MS. This channel also allows for chiral separation of enantiomers. The second is laser desorption (LD-MS) where larger and likely less volatile molecules are ionized via short laser flashes, transferred to the MS and analysed. In order to aid the identification of intricate molecular mixtures it is possible to run the ion-trap in an MS-MS mode where a particular mass can be pre-selected and its fragments investigated further. Direct atmospheric sampling is also intended.

DLR funding for four additional members of staff was secured at MPS. The project is funded under contract number 50QX0601.

In 2008 the main activities were directed at the production of instrument prototypes to reach the technical readiness level 5 (TRL5).

A laser prototype was produced by von Hoerner & Sulger (subcontracted to Laser-Zentrum Hannover) and is under test at MPS.

Several prototypes for ovens and the oven interface device (tapping station) were built at MPS. Fig. 124 shows the first oven prototype in three different views.

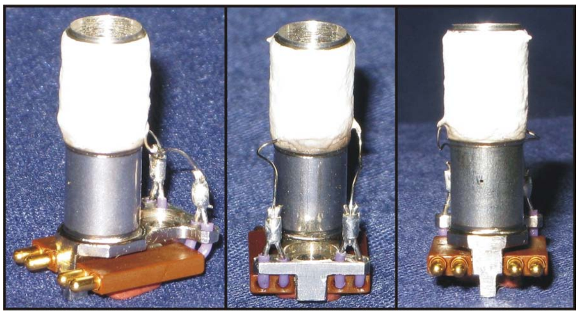

Fig. 124: Prototype oven for MOMA pyrolysis in three different views; the internal diameter is 6 mm, the overall height 22 mm.

On the administrational side the US Initial Design Review (IDR) in December 2008 and the ESA Preliminary Design Review (PDR) in January 2009 were completed successfully.

A new clean room compliant with Planetary Protection requirements was started to be built at MPS. Completion is scheduled for mid 2009.

(F. Goesmann)

The SEIS instrument for ExoMars

The SEIS instrument is an assembly of two very broad band seismometers (VBB) and two short period seismometers (SP) designed to study the seismic activity of the planet by interior processes. In addition it will detect the frequency of meteoritic impacts on the surface of Mars. Seismic events will be ranked according to their magnitude and the source location shall be determined by approximate distance and azimuth. No seismometer was yet operated successfully on the planet. SEIS is part of a suite of geophysical experiments on ESA's ExoMars mission. These instruments, the so called Humboldt payload, are located on the ExoMars Lander. The ExoMars mission will search for traces of past and present life, characterize Martian geochemistry and water distribution, identify possible surface hazards to future human exploration missions and improve the knowledge of the Mars environment including the deep interior. The launch is scheduled for January 2018. MPS is responsible for the deployment subsystem of SEIS, i.e. for the accommodation and levelling of the seismic sensors and the mechanical interface to the Lander platform. The measurements require levelling of the sensors and a good mechanical coupling to the ground. This will be achieved by a frame with a good seismic transfer function. Different deployment options are included in the design regarding terrain uncertainties. Baseline is a first measurement period with SEIS fixed in the Lander and a second measurement period after deployment to the ground. A levelling mechanism is connected to the VBB sensors to allow measurements in locked position at the Lander and in addition the deployment to ground shall be possible after launch lock release by three legs, adjustable in length for proper ground placement.

The SEIS instrument comprises contributions from five European countries:

- Team coordination, VBB sensors incl. sensor electronics and E-box design: IPGP, Institut de Physique du Globe de Paris, Saint Maur des Fossés, France; Project management: Institut Supérieur de l'Aéronautique et de l'Espace, Toulouse, France;
- SP sensors incl. sensor electronics: Imperial College, London and Oxford University, Dept. of Atmospheric, Oceanic & Planetary Physics, Oxford, Great Britain;
- SEIS acquisition electronics: Swiss Seismological Service, ETH, Zurich, Switzerland;
- ASIC: SRON Netherlands Institute for Space Research, Utrecht, Netherlands;
- Deployment systems incl. electronics: MPS, Katlenburg-Lindau, Germany;

The project started already in 2006 with a first three-leg model. However, the mission design was not in the state to do more than first breadboard proposals in 2006 and 2007. Detailed work started after selection as payload for ExoMars in the mentioned team configuration. A MPS team was settled with two MPS long-term specialists for electronics and mechanics to support the design and later on the commissioning and operation on Mars. DLR funding for four additional members gained the team in 2008, working in mechanics and electronics design, testing and management. A stiff frame (see Fig. 125) was designed to accommodate the mechanism for levelling and to connect the three legs. Two different designs for the levelling system were developed and built. In addition a base plate for accommodation of the whole assembly at the Lander including a launch lock system was developed and built, too. All breadboard hardware was vibration load tested. DC-motors with planet drives were selected for the leg drives and the levelling systems. A dedicated electronics including FPGA was designed and built. The preliminary design review (PDR) by ESA in fall 2008 showed all MPS contributions as well as the whole instrument well above the required technological readiness level TRL 5.

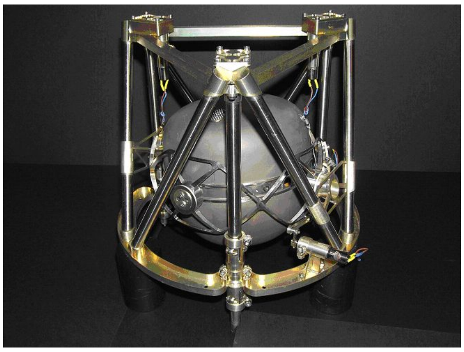

Fig. 125: The figure shows the stiff frame with one leg in front and a cardanic ring inside for levelling of the VBB sensors, located inside the sphere.

(R. Roll, M. Bierwirth, U. Christensen, J. Heise, A. Hilz, I. Krause, W. Kühne, D. Oberdorfer, and M. Wedemeier)

Project Phobos Grunt

Phobos Grunt is a Russian mission to the Mars moon Phobos. The launch is scheduled for October 2009. It is intended to land on Phobos, do some in-situ investigations and bring a sample back to Earth.

The MPS contributes to the gas-chromatograph on the lander, together with the French team already involved in Rosetta in the COSAC team.

The carrier gas tanks, the calibration gas tanks, and the pressure reduction valves were developed, built, and tested at MPS. The final hardware parts were delivered in February 2009.

(F. Goesmann)

Outer planets research – Jupiter and Saturn

Investigations in Jupiter's environment

Discontinuity in Jupiter's main auroral oval

On the basis of a series of FUV Hubble Space Telescope images obtained between 1997 and 2007 it is shown that there is a segment of the main auroral oval where the emission drops significantly from a few hundreds to a few tens of kiloRayleigh, forming a discontinuity in the oval. It is shown that the discontinuity is present in both hemispheres and confined in magnetic local time. Its equatorial source is located in the prenoon and early noon sector. The main auroral oval is associated with the ionosphere-magnetosphere coupling current system which is related to the breakdown of corotation in the middle magnetosphere. Necessary for the electron precipitation in the ionosphere and the formation of the main auroral oval is the presence of upward field-aligned currents, carried by downward moving electrons. Field-aligned currents inferred by Pioneer, Voyager and Galileo in situ observations in the near equatorial plane showed evidence of reduced or/and downward field-aligned currents in the prenoon and early afternoon sector, the location of the equatorial source of the discontinuity. Additionally, we estimate the precipitation energy flux in the ionosphere, for a typical reduced upward field-aligned current value at that region, which is found to be within the range of the observed brightness of the discontinuity. Field aligned current distributions in the ionosphere based on magnetohydrodynamic simulations of the interaction between the solar wind and the magnetosphere have predicted a region of downward currents implying a discontinuity at the main auroral oval emission, in very good agreement with the HST observations (see Fig. 126).

(N. Krupp and J. Woch in collaboration with LPAP (Belgium))

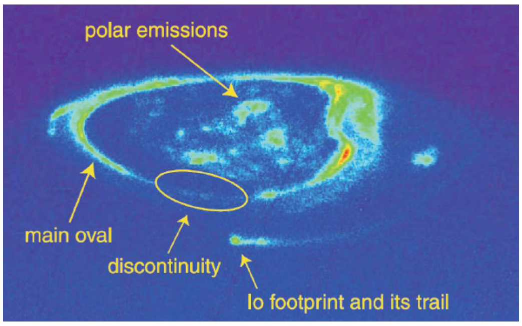

Fig. 126: Raw HST-STIS clear image showing the FUV auroral emission at the north pole of Jupiter, taken on 28 December 2000. The CML is 153$\mathcal{A}$. The arrows indicate the main auroral features: the main oval, the Io footprint and its trail and the polar emissions. The ellipse indicates the discontinuity in the main oval.

In-situ observations of the Saturnian magnetosphere and interaction of magnetospheric particles with moons

Transient radiation belt at Saturn

Data from Cassini's MIMI/LEMMS instrument have been used to identify for the first time, the two components of variability Saturn's ionic radiation belts: a stable inner belt, and a transient, and variable outer belt. The ionic radiation belts of Saturn usually contain considerable particle fluxes only inside the orbit of the moon Tethys, that resides almost 5 Saturn radii (Rs) away from the center of the planet. However, an extension of these radiation belts up to a distance of 8 – 10 Rs appeared twice within 2005 (Fig. 127). Each of these sudden intensifications in energetic ion intensity formed a transient radiation belt component, that was centered in the vicinity of the moon Dione at 6.3 Rs ("Dione belt") and that its intensity decayed for several weeks, before it disappeared. The appearances and the variability of the Dione belt coincided with three interplanetary events, triggered by solar eruptions and revealed that, as in the case of the Earth, solar storms also control (to some extent) the variability of Saturn's radiation belts. However, it was found that this variability is restricted in the Dione belt only: within the inner belts (inside the orbit of Tethys), MeV ion fluxes showed negligible response to the solar storm occurrence and almost no variability for a period of 4 years. As the transient Dione belt is separated from the inner belts by a permanent MeV ion depletion, all along the orbit of Tethys, it was inferred that the latter moon inhibits inward radial transport of energetic ions, shielding the planet's main, inner radiation belt from solar wind influences. It was also hinted that the source of the inner belt ions is almost certainly solely from the interaction of GeV cosmic rays with Saturn's main rings and atmosphere.

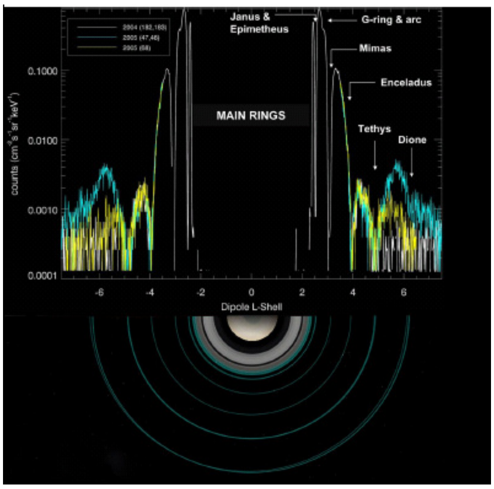

Fig. 127: Differential ion fluxes from the LEMMS P2 ion channel (2.28 – 4.49 MeV/nuc) as a function of dipole L-shell. Negative L denotes the inbound part of the orbit, positive outbound. The 2004 profile (white curve) is the most common, identified in 27 out of the 36 orbits considered in this study. Several moons' and rings' L-shells are indicated. The lowest background is measured above the main rings that absorb all energetic ions, while Saturn's volume and the strong dipole field "shadow" instrument-penetrating, galactic cosmic rays. The two 2005 profiles (yellow and turquoise), correspond to orbits with periapsis at L = 3.5 reveal a flux enhancement centered close to Dione's L-shell (the Dione belt). The enhancement exists only outside Tethys' L-shell.

(E. Roussos and N. Krupp in collaboration with JHUAPL (USA), UCL-MSSL (UK), FTECS (USA), Academy of Athens (Greece), Univ. of Athens (Greece), UoM (USA))

Injection events in the Saturnian magnetosphere

The Kronian magnetosphere represents a magnetosphere which is driven by internal processes as well as by solar-wind-related processes.
Voyager 1 and 2 data and current analysis of Cassini data have shown that the magnetospheric plasma does not rigidly corotate with the planet. At a distance of about 4 Saturnian radii, the azimuthal velocity profile shows clear breakdown of corotation.
The investigations of Energetic Particle Injection Events have turned out to be a new method to obtain a plasma flow profile. High energetic plasma is transported into the inner part of the magntosphere. Due to the magnetic drifts, the particles begin to disperse and leave an imprint in the spectrograms of the Magnetospheric Imaging Instument (MIMI) onboard the Cassini Spacecraft. The shape of these profiles depends strongly on the azimuthal velocity of the magnetospheric plasma and the age of the injection event.
To develop a model for the velocity profile we started by calculation of theoretical profiles to analyse how the shape of the dispersion profiles varies by changing the age of the injection as well as the free parameters of the velocity profile.
Since 2004 Cassini detected a few hundreds of these events. To realize a statistical analysis, 52 of these events have been automatically extracted from the data. Preliminary analysis showed that the magnetosphere is subcorotating. Our aim is to develop an azimuthal plasma flow profile by comparing the measured with the theoretically calculated dispersion profiles.

(A. Müller and N. Krupp in collaboration with Univ. of Cologne (Germany), JHUAPL (USA), UCL-MSSL (UK))

Tail reconnection

Five instances of tail reconnection events at Saturn involving the ejection of plasmoids downtail as identified in the MAG data by northward/southward turnings and intensifications of the field. These events have been analyzed with data from the magnetometer, plasma and energetic particle data. The northward/southward turnings of the field elucidate the position of the spacecraft relative to the reconnection point and passing plasmoids (Fig. 128), while the variability of the azimuthal and radial field components during these events indicates corresponding changes in the angular momentum of the magnetotail plasma following reconnection. Other observable effects include a reversal in flow direction of energetic particles, and the apparent evacuation of the plasma sheet following the passage of plasmoids.

(N. Krupp in collaboration with Imperial College London (UK), UCL-MSSL (UK), Univ. of Leicester (UK), JHUAPL (USA), UoM (USA), LANL (USA))

Dust halo around Saturn'n moon Rhea

Saturn's moon Rhea had been considered massive enough to retain a thin, externally generated atmosphere capable of locally affecting Saturn's magnetosphere. The Cassini spacecraft's in situ observations reveal that energetic electrons are depleted in the moon's vicinity (Fig. 129). The absence of a substantial exosphere implies that Rhea's magnetospheric interaction region, rather than being exclusively induced by sputtered gas and its products, likely contains solid material that can absorb magnetospheric particles. Combined observations from several instruments suggest that this material is in the form of grains

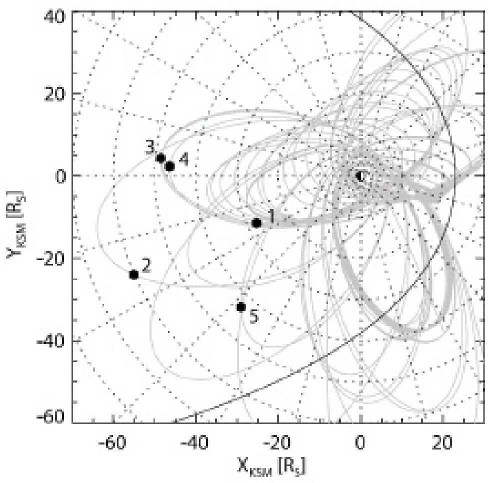

Fig. 128: Orbit of the Cassini spacecraft around Saturn shown in an equatorial projection in Kronocentric Solar Magnetospheric (KSM) coordinates, where X points from Saturn to the Sun and Z is north in the plane containing X and the Saturn rotation axis. The Sun is to the right of the diagram, and the magnetopause with subsolar standoff distance of 26 RS is shown in black . The location of the spacecraft at the onset of each of the five events is numbered and shown by the black hexagons. The dates of the events are (1) 6 September 2006, (2) 18 June 2006, (3) 4 August 2006, (4) 12 July 2006, and (5) 4 March 2006.

and boulders up to several decimetres in size and orbits Rhea as an equatorial debris disk. Within this disk may reside denser, discrete rings or arcs of material.

(G. H. Jones, E. Roussos, N. Krupp, A. Lagg, and J. Woch in collaboration with UCL-MSSL (UK), MPI-K (Germany), SWRI (USA), CESR (France), Astrn. Institute St. Petersburg (Russia), Imperial College London (UK), IRF-U (Sweden), JPL (USA), UIOWA (USA), Univ. of Virginia (USA), IGPP-UCLA (USA), JHUAPL (USA), Academy of Athens (Greece), Institut für Geophysik Cologne (Germany), Univ. Potsdam (Germany, JHU (USA, LANL (USA))

Electron population in Saturn's magnetosphere

Radial distribution of electron populations inside 20 Rs in Saturn's magnetosphere have been analyzed. We calculate moments for these populations by a forward modeling method using composite spectra produced by the CAPS/ELS (0.6 eV to 26 keV) and the MIMI/LEMMS (15 keV to 10 MeV) instruments on board Cassini (Fig. 130). We first calculate and harmonize both data sets in physical units and apply corrections taking into account biases introduced by spacecraft interaction with the magnetospheric environment. We then test different bimodal isotropic electron distribution models, deciding on a model

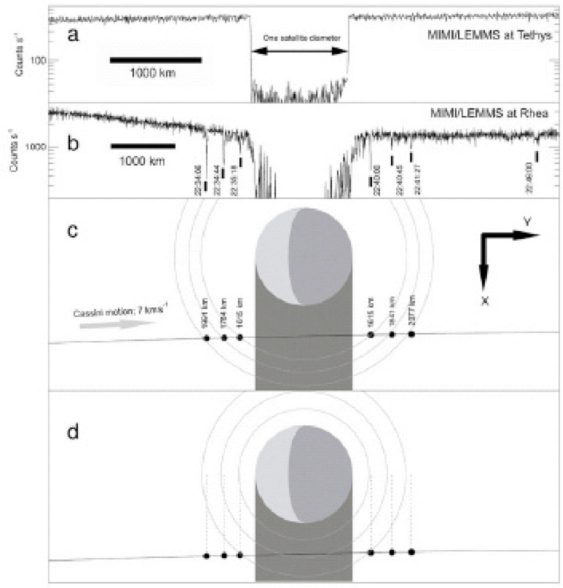

Fig. 129: Interpretation of electron flux dropouts as evidence of a ring system. (A) 28 to 49 keV electron fluxes at Tethys, demonstrating that moon's sharp, isolated absorption signature, in contrast to equivalent data from Rhea (B). The panels are scaled such that the relative size of the satellites' diameters is equal. Rhea's wake infills more rapidly because of the higher local plasma temperature. (C) Locations of some short-lived electron flux dropouts visible in the MIMI-LEMMS electron flux shown in (B). Their distances from Rhea's rotational axis are shown. Such absorptions, reminiscent of other planetary ring signatures, could be explained by the occultation of southward-traveling electrons before detection by Cassini. The signatures' spatial near symmetry may signal the presence of three near-circular rings or arcs of material ~ 230 km north, in Rhea's equatorial plane. (D) An alternative dropout formation scenario.

with two kappa distributions. We adjust our isotropic model to the flux composite spectra with a least square method to produce three sets of fluid parameters (density, temperature, spectral index) per electron population. The radial profiles are then analyzed, revealing a relevant boundary at 9 Rs in both thermal and suprathermal electron populations. Observed discontinuities in the moment profiles (sudden drop-off in cold density profile outside 9 Rs, hot electrons drop-off inside 9 Rs) coincide with the known outer edge of Saturn's neutral OH cloud. Farther out, thermal electrons disappear completely beyond 15 Rs while suprathermal electrons are still observed in the middle and outer magnetosphere.

(N. Krupp in collaboration with CESR (France, ESTEC (Netherlands), UCL-MSSL (UK), UIOWA (USA), JHUAPL (USA), SWRI (USA), Imperial College London (UK))

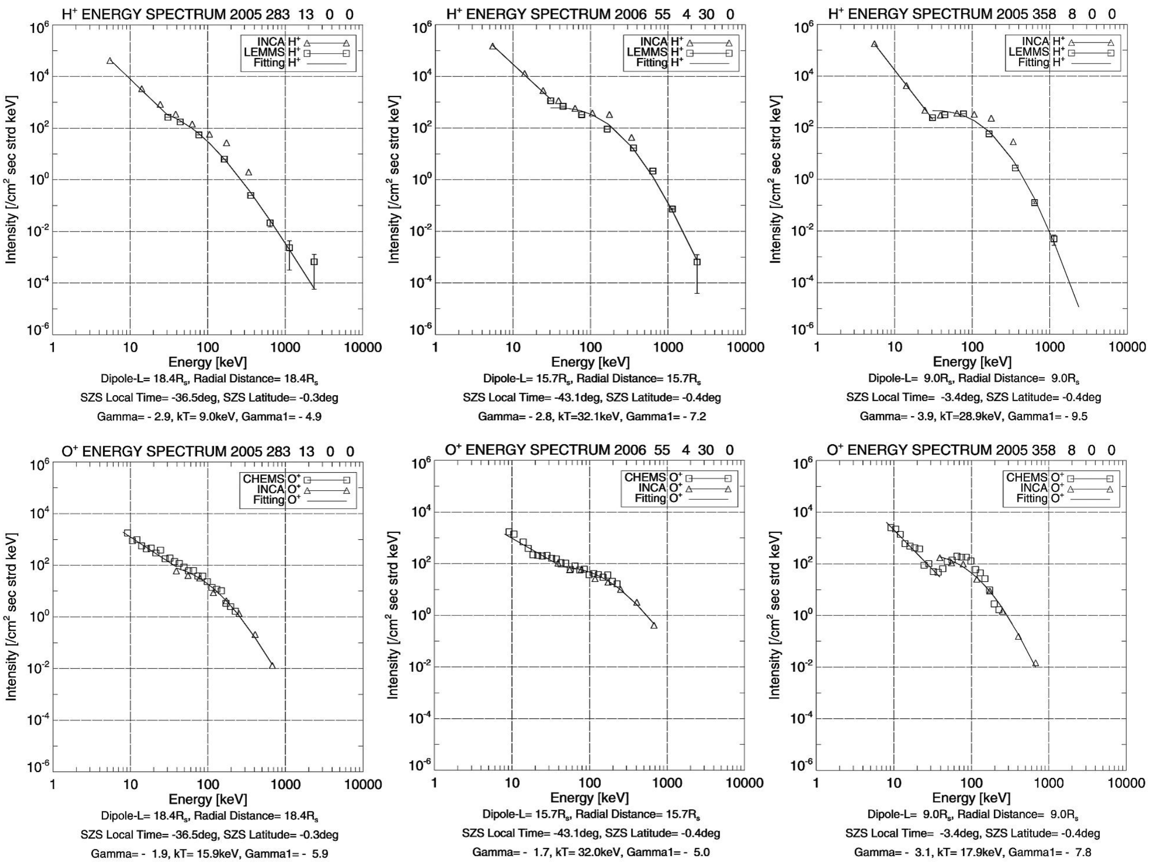

Fig. 130: Composite CAPS/ELS and MIMI/LEMMS (energy channels C0-C7) spectral plots of electron intensities versus energy, observed at (top) 2200 UT (R = 9 Rs, local time 18:32 h, latitude 0.23 degrees) and at (bottom) 07:27 UT (R = 12.8 Rs, local time 19:82 h, latitude 0.35 degrees) on days of year 142 and 143 of 2006 during Rev. 24, respectively. Original data are represented in black, our interpolated data are represented in red, and the results of our various models are represented in blue. (left) Model with 2 Maxwellian distributions. (middle) Model with one Maxwellian and one kappa distribution. (right) Model with two kappa distributions.

Sources and losses of energetic protons in Saturn's magnetosphere

Cassini data revealed that protons between a few keV and about 100 keV energy are not stably trapped in Saturn's inner magnetosphere. Instead these ions are present only for relatively short times following injections. Injected protons are lost principally because the neutral gas cloud converts these particles to energetic neutral atoms via charge exchange. At higher energies, in the MeV to GeV range, protons are stably trapped between the orbits of the principal moons because the proton crosssection for charge exchange is very small at such energies. These protons likely result from cosmic ray albedo neutron decay (CRAND) and are lost principally to interactions with satellite surfaces and ring particles during magnetospheric radial diffusion. A main result of this work is to show that the dominant energetic proton loss and source processes are a function of proton energy. Surface sputtering by keV ions is revisited based on the reduced ion intensities observed. Relatively speaking, MeV ion and electron weathering is most important closer to Saturn, e.g. at Janus and Mimas, whereas keV ion weathering is most important farther out, at Dione and Rhea.

(E. Roussos and N. Krupp in collaboration with JHUAPL (USA), UCL-MSSL (UK), Univ. of Virginia (USA), UoM (USA), FTECS (USA))

Energetic neutral atoms absorption and imaging at Titan

The Saturn magnetosphere interacts with the Titan atmosphere through various mechanisms. One of them leads, by charge exchange reactions between the energetic Saturnian ions and the exospheric neutrals of Titan, to the production of energetic neutral atoms (ENAs). The Ion and Neutral Camera (INCA), one of the three sensors that comprise the Magnetosphere Imaging Instrument (MIMI) on the Cassini/Huygens mission to Saturn and Titan, images the ENA emissions in the Saturnian magnetosphere. This study focuses on the ENA imaging of Titan (for 20 – 50 keV H ENAs), with the example of the Ta Titan flyby (26 October 2004): our objective is to understand the positioning of the ENA halo observed around Titan. Thus we investigate the main ENA loss mechanisms, such as the finite gyroradii effects for the parent ions, or the charge stripping with exospheric neutrals. We show that multiple stripping and charge exchange reactions have to be taken into account to understand the ENA dynamics (Fig.131). The use of an analytical approach, taking into account these reactions, combined with a reprocessing of the INCA data, allows us to reproduce the ENA images of the Ta flyby and indicates a lower limit for ENA emission around the exobase. However, the dynamics of energetic particles through the Titan atmosphere remains complex, with an inconsistency between the ENA imaging at low and high altitudes.

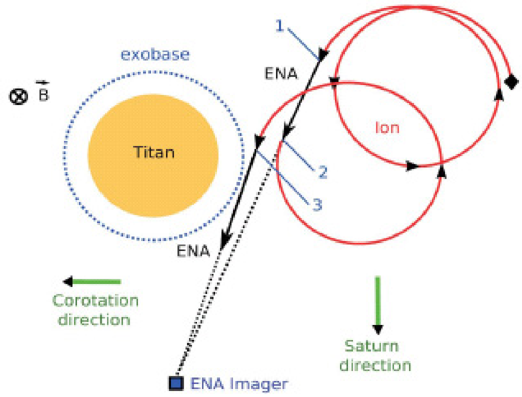

Fig. 131: This figure gives a schematic view of the dynamics of an energetic particle in the Titan atmosphere, with the directions of the corotation, Saturn, and the magnetic field indicated. An energetic ion, with a large gyroradius, has a cycloidal motion, is then neutralized (process no. 1 at point 1), the produced ENA is later ionized (process no. 2, at point 2), before the new ion finally leads to an ENA (process no. 3, at point 3) which is detected by the ENA imager. The length scales and the number of collisions used in the figure are chosen for a better understanding.

(N. Krupp in collaboration with CESR (France), JHUAPL (USA), UoM (USA), IRF-U (Sweden), LPG (France))

The mass-release process in the Jovian magnetosphere: statistics on particle burst parameters

The Jovian magnetosphere undergoes periodic reconfiguration processes mainly driven by the fast planetary rotation and mass-loading from the moon Io. These reconfiguration processes of the Jovian magnetosphere are associated with the release of plasmoids discernible as ion flow bursts associated with bipolar magnetic signatures. We investigate these plasma flows statistically using data from the Energetic Particles Detector (EPD) and from the Magnetometer (MAG) onboard Galileo. The plasma flows are observed in different magnetospheric regions: the current sheet center, the plasma sheet boundary layers and the lobe. We show that the bulk velocity of all species is the same for most of the magnetic field bipolar signatures associated with these plasma flows. The average speed of the observed plasmoids in the plasma sheet associated with the ion flow bursts is between 350 and 500 km‘s^{-1} and the duration of the events is between 10 and 20 minutes, see Fig. 132. The associated plasmoid length is correspondingly $\sim 9R_J$. The plasmoids are moving approximately with Alfvénic speed. The convection electric field during the plasmoid release is about an order of magnitude higher than the ambient value of the Jovian convection electric field.

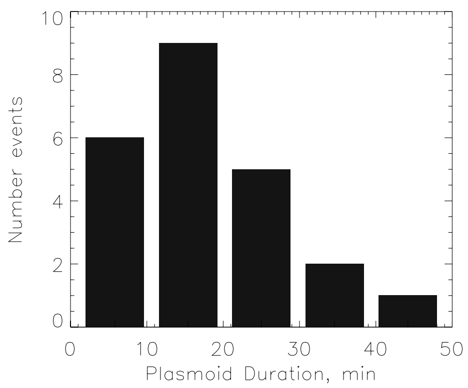

Fig. 132: The occurrence rate of plasmoids versus the duration of the events (23 events), where the panel was constructed by binning these events into 5-R_J-wide intervals.

(E. A. Kronberg, J. Woch, N. Krupp, and A. Lagg)

Comparing Jupiter and Saturn: Dimensionless input rates from plasma sources within the magnetosphere

The quantitative significance for a planetary magnetosphere of plasma sources associated with a moon of the planet can be assessed only by expressing the plasma mass input rate in dimensionless form, as the ratio of the actual mass input to some reference value. Traditionally, the solar wind mass flux through an area equal to the cross-section of the magnetosphere has been used. I have identified another reference value of mass input, independent of the solar wind and constructed from planetary parameters alone, which can be shown to represent a mass input sufficiently large to prevent corotation already at the source location.

The source rate from Enceladus at Saturn has been reported to be an order of magnetitude smaller (in absolute numbers) than that from Io at Jupiter. Both reference values, however, are also smaller at Saturn than at Jupiter, by factors $\sim$ 40 to 60; expressed in dimensionless form, the estimated mass input from Enceladus may be larger than that from Io by factors $\sim$ 4 to 6. The magnetosphere of Saturn may thus, despite a lower mass input in $\mathrm{kg\,s^{-1}}$, intrinsically be more heavily mass-loaded than the magnetosphere of Jupiter. (Vasyliūnas (2008)

(V. M. Vasyliūnas)

Extraterrestrial counterparts/analogs of substorms:similarities and differences

Events corresponding to, analogous to, or similar to magnetospheric substorms have been discussed in connection with a number of objects other than Earth. They include: solar flares and coronal mass ejections at the Sun; events claimed to be scaled versions of terrestrial substorms, in the magnetosphere of Mercury; events similar in some ways to terrestrial substorms, in the magnetospheres of Jupiter, Saturn, and (possibly) Uranus. A systematic intercomparison is encumbered by the variety of observational aspects to a substorm, coupled with the lack of an universally agreed upon definition as well as of a consensus on the essential physical process. The main phenomena of a magnetospheric substorm at Earth can be subsumed under three groups: (1) enhanced energy dissipation (auroral emissions, energetic charged particles), occurring on a dynamical time scale (comparable to or shorter than wave travel times), accompanied by (2) changes of the magnetic field configuration, from stretched-out to more nearly dipolar, (3) fast (order of Alfvén speed or more) plasma bulk flows in the magnetotail. If these substorm or substorm-like events are all regarded as different manifestations of an underlying universal process, the essential steps of the process would seem to be the following: (a) mechanical stresses deform the magnetic field into a configuration of increased energy, (b) the magnetic configuration becomes unsustainable and changes quickly, releasing the energy. The various systems may differ in the mechanical stresses, which are reasonably well understood for planetary magnetospheres but still very uncertain for solar processes. They may also differ in what makes the configuration unsustainable (for planetary magnetospheres, possibly related to the need for return of magnetic flux) and particularly in what sets off the quick change, both highly controversial.

(V. M. Vasyliūnas)

First observation of CO at 345 GHz in the atmosphere of Saturn with the JCMT. New constraints on its origin.

Water and carbon dioxide have been detected in the stratospheres of the outer planets (Feuchtgruber et al. 1997, Coustenis et al. 1998, Burgdorf et al. 2006). Because both species condense at the tropopause (except CO_2 in Jupiter and Saturn), their presence in the stratospheres implies an external origin (interplanetary dust, sputtering from the satellites and/or rings, large meteoritic impacts). Carbon monoxide has been detected in each giant planet. Because this compound does not condense at the tropopause, it can also have an internal origin by means of upwards convective mixing originating from the deep hot atmosphere. The source of CO has been proved to be internal and cometary in Jupiter (Bézard et al. 2002) and Neptune (Lellouch et al. 2005, Hesman et al. 2007), but this is still not clear in the case of Saturn (Noll and Larson 1991). Therefore, constraining the amount of CO in the stratosphere and/or high troposphere of this planet would help solve this question.

We have performed observations of Saturn at submillimetre wavelengths of the CO(3–2) line. At 345 GHz, the atmospheric levels sounded are located between 10 mbar and 1 bar (contribution function analysis), a region overlapping the high troposphere and the low stratosphere. CO lines can be very broad when formed at such pressures. This is the reason why we have recorded the spectrum of Saturn over a wide range of frequencies. The observations were carried out at the JCMT 15 m telescope (Hawaii, USA) in January 2008, with HARP, a 16-receptor heterodyne array receiver. We have recorded 10 sub-bands over a 5.5 GHz band centered on the CO(3–2) frequency.

After filtering out the instrumental ripple and connecting the 10 sub-bands, we have analysed the spectrum with our radiative transfer model (Cavalié et al. 2008). The line has been detected with a peak-to-continuum signal-to-noise (S/N) ratio of 7. The first outcomes on the vertical distribution of CO in the atmosphere of Saturn are: (i) the observed line cannot be attributed to an internal source of CO alone, (ii) we have unambiguously proved that the bulk of observable CO was located in the stratosphere. The best fit model at this stage of the analysis was obtained if (25 ± 6) ppb of CO were located at pressures lower than (15 ± 2) mbar and 0.1 ppb at higher pressures. However, the signature of an internal component may have been filtered out during the data reduction procedure (ripple subtraction). We have derived an upper limit on the tropospheric CO mixing ratio of 1 ppb, based on the amplitude of the ripple (see Fig. 133). New observations either in the (sub)millimetre or in the infrared range are needed to precisely measure the tropospheric CO mixing ratio.

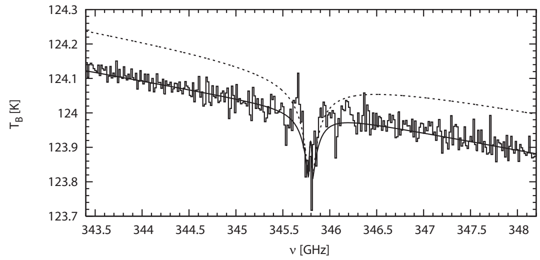

Fig. 133: Comet impact model with an impact time 200 years ago and 4 ppm of CO deposited above 0.1 mbar at the time of the impact. This model is considered with an internal source of 1 ppb of CO (dashed line) and with no internal source (solid line). The value of 1 ppb corresponds to the upper limit fixed on a possible CO internal component filtered out by our data reduction procedure.

We have used a 1D time-dependent transport model of the atmosphere of Saturn to test the external source hypothesis by generating CO mixing ratio vertical profiles. Assuming a permanent and uniform external flux of CO, we retrieve a CO external flux of $(1.5 \pm 0.4) \times 10^6$ cm^{-2}·s^{-1} (diffuse or local source) by modelling the transport in the atmosphere of Saturn. However, such a permanent flux does not give the best agreement with the data. A more likely source of CO to Saturn would be an SL9-like comet which impacted the planet 200 – 350 years ago (see Fig. 133). This would confirm that large comet impacts are important and regular providers of oxygen compounds into the atmospheres of the Outer Planets.

(T. Cavalié and P. Hartogh in collaboration with F. Billebaud, M. Dobrijevic (Université de Bordeaux, Laboratoire d'Astrophysique de Bordeaux, France), T. Fouchet, E. Lellouch, T. Encrenaz (LESIA, Observatoire de Paris, France), G. H. Moriarty-Schieven (Herzberg Institute of Astrophysics, Canada), and J. G. A. Wouterloot (Joint Astronomy Center, Hawaii, USA))

Photochemistry in the Jovian atmosphere

The composition of the troposphere and the stratosphere of Jupiter is being investigated using a one dimensional, steady state photochemical model. This model includes a complete photochemical scheme that allows interaction between hydrocarbons and oxygen compounds, studies in a very detailed way transport processes (molecular and eddy diffusion) and condensation processes, takes into account an influx of external oxygen, and uses updated values obtained by laboratory measurements for reaction rates and photoabsorption cross sections.

The model includes 37 different hydrocarbon and oxygen species that are allowed to vary with vertical transport and with different chemical reactions. The species included are: H (atomic hydrogen), H_2 (molecular hydrogen), CH_4 (methane), C_2H_2 (acetylene), C_2H_4 (ethylene), C_2H_6 (ethane), CH_3C_2H (methylacetylene), C_3H_6 (propene), C_3H_8 (propane), C_4H_2 (diacetylene), H_2O (water), CO (carbon monoxide), H_2CO (formaldehyde), CH_3OH (methanol), O_2 (molecular oxygen), CH_2CO (ketene), CH_3CHO (acetaldehyde), CO_2 (carbon dioxide) and the radicals CH, $^1CH_2$, $^3CH_2$, CH_3 (methyl), C_2H, C_2H_3, C_2H_5, C_3H_2, C_3H_5, C_3H_7, $O(^3P)$, $O(^1D)$, OH, HCO, CH_2OH, CH_3O, HCCO, CH_3CO and C_2H_4OH.

(A. González, and P. Hartogh in collaboration with L. M. Lara (Instituto de Astrofísica de Andalucía, Granada, Spain))

Fine structure in Jupiter's gossamer rings

Dust near Jupiter is produced when interplanetary impactors collide energetically with small inner moons, and is organized into a main ring, an inner halo, and two fainter and more distant gossamer rings. Most of these structures are constrained by the orbits of the moons Adrastea, Metis, Amalthea and Thebe. A faint outward protrusion called the Thebe extension behaves differently and had previously eluded understanding. Dust impacts detected during the Galileo spacecraft's traversal of the outer ring region reveal a gap in the rings interior to Thebe's orbit, a strong excess of submicrometre-sized dust just inside Amalthea's orbit (Fig. 134) and grains on highly inclined paths (Krueger, 2009, in press). Detailed modelling shows that the passage of ring particles through Jupiter's shadow creates the Thebe extension and fully accounts for these Galileo results Hamilton and Krüger (2008). Dust grains alternately charge and discharge when traversing shadow boundaries, allowing the planet's powerful magnetic field to excite orbital eccentricities and, when conditions are right, inclinations as well. Thus, grain dynamics in the gossamer rings is strongly influenced by electromagnetic forces.

(H. Krüger and the Galileo dust team)

Deep convection and the thermal emission of planets

Jupiter and Saturn emit nearly twice the thermal energy they receive from the Sun. Although insolation decreases toward the poles, the large-scale outward heat flux is nearly uniform, with smaller-scale latitudinal undulations that correlate with the zonal jet

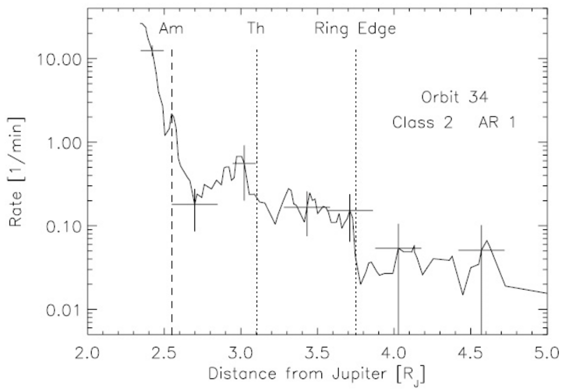

Fig. 134: Dust impact rates (solid curves) measured during Galileo's ring passage on 5 Nov 2002 (smoothed with a boxcar average over 3 data points). Vertical dotted lines indicate the average locations of Amalthea ('Am') and Thebe ('Th') along their slightly eccentric orbits, and the edge of the faint ring extension as seen on images ('Ring Edge'). Uncertainties due to both noise removal and statistical fluctuations within a 10 to 20 minute time interval are indicated by vertical bars. This averaging time interval is indicated by horizontal bars.

streams (see Fig. 135). We have performed numerical simulations of the turbulent 3-D convection in a geometrically thin, uniformly forced layer of Boussinesq fluid that models the deep convection zones of Jupiter and Saturn (Aurnou *et al.* (2008)). Previous studies have shown that such models generate zonal flows comparable to those observed on the gas giants. An analyzes of the simulated patterns of convective heat transfer revealed that deep convection in the gas giants can explain the anomalously uniform large-scale thermal emissions as well as the jet-scale variations. In particular, that convective heat transfer by quasi-geostrophic thermal plumes in the relatively thin spherical shell geometry generates an outward heat flow pattern with a broad equatorial minimum and peaks at the poles. This can compensate the lower insolation at the poles and thereby lead to the observed nearly uniform heat emission of the gas giants. The results suggest an alternative to the hypothesis that insolation controls the large-scale patterns of heat flux and zonal flow on the gas giants. Instead, we propose that the large-scale thermal and zonal flow fields originate deep within the planet's molecular envelopes.

(J. Wicht in collaboration with J. Aurnou, E. King (UCLA), M. Heimpel (University of Alberta, Edmonton), and L. Allen (US Coast Guard Academy, New London))

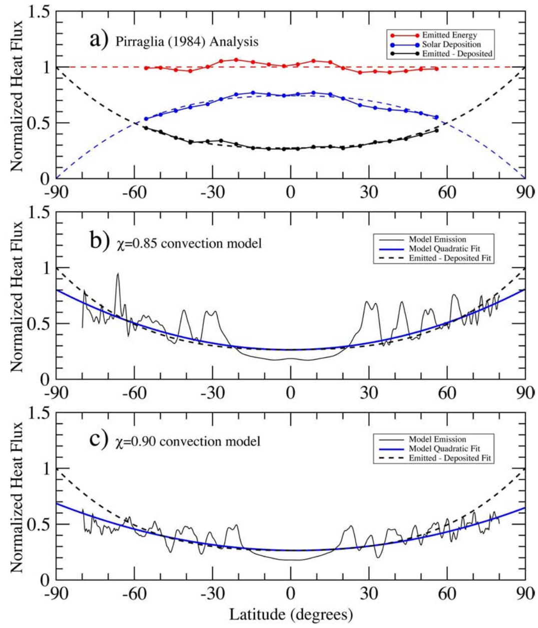

Fig. 135: (a) Normalized Jovian thermal emission profile. The dashed lines are extrapolations that fit the high latitude data from the Pioneer observations. Red lines: net outward thermal emission. Blue lines: deposited solar energy. Black lines: difference between emitted and deposited solar energy. (b) $\chi = 0.85$ and (c) $\chi = 0.90$ model results, where χ is the ratio of inner to outer radius in the simulated shell. The solid black line shows the normalized time averaged outward thermal emission from the outer boundary of the $\chi = 0.85$ ($\chi = 0.90$) convection simulation. The solid blue line is the normalized quadratic fit to the model's emission. The dashed black line shows the emitted—deposited difference profile from (a).

Explaining Saturn's axisymmetric magnetic field

Saturn's magnetic field seems to be very featureless and perfectly axisymmetric and thus differs from all other planetary fields. Convectively driven dynamos tend to show a more complex structure with significant axisymmetric contributions very much like Earth's or Jupiter's magnetic fields. David Stevenson suggested that the possible layering of the planet's dynamo region may be a reason for Saturn's special field geometry. The upper part of the planet's metallic hydrogen core could be stably stratified because of helium depletion: Unlike Jupiter, Saturn has cooled enough for helium droplets to form in it's outer envelope. These droplets rain down to the outer parts of the metallic hydrogen core where Lorentz forces and higher pressures would impede their deeper penetration. We have used 3d numerical dynamo simulations to explore the effects of the upper stable layer. The solutions show that the mostly axisymmetric azimuthal motions in the stable layer can attenuate the non-axisymmetric components (Fig. 136). These components have a strength

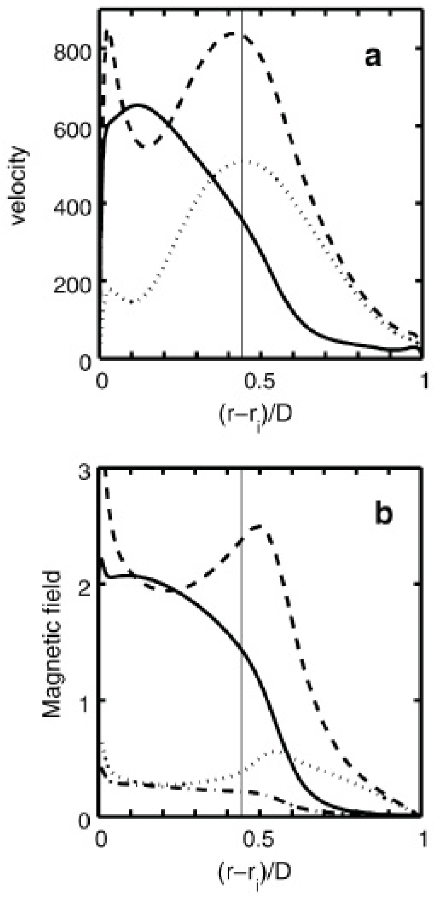

Fig. 136: Variation of components of the velocity (a) and of the magnetic field (b) with radius. rms-values averaged in the angular directions and in time are shown. Full line: poloidal component; broken line: toroidal component; dotted: axisymmetric toroidal or zonal component, dash-dotted: axisymmetric poloidal component. The axisymmetric poloidal velocity is tiny and not shown. The vertical line indicates the nominal radius of neutral stability in the dynamo region. The strong zonal flows in the stable region filter out the non-axisymmetric magnetic field components so that a nearly perfectly axisymmetric poloidal field is left at the upper boundary. The toroidal magnetic field can not leave the dynamo region. r_i is the inner boundary radius and D is the shell thickness.

typical for dipole dominated dynamos in the deeper dynamo regions. However, the differential rotation of the stable layer with respect to the dynamo region hinders the penetration of these components due to a magnetic skin effect. The result is a very axisymmetric exterior magnetic field which is nicely compatible with the observations (Christensen and Wicht (2008)). Our numerical simulations thus confirm the idea by David Stevenson.

(U. Christensen and J. Wicht)

Lunar Research

SIR-2 on Chandrayaan-1 – ready for Science

At 06:22 IST on 22 October 2008, a modified version of a PSLV C11 blasted off into the early morning sky from the Satish Dhawan Space Centre in Andhra Pradesh, approximately 80 km north of Chennai, announcing a new era for the Indian space program. The rocket, carrying the Chandrayaan-1 spacecraft, is the first mission to explore the Moon built by India's national space agency, the Indian Space Research Organization (ISRO). The historic launch, which brings an Indian spacecraft for the first time into interplanetary space, also marks the beginning of the new scientific program, which is geared to bring India from applied space science to more fundamental space exploration (see Fig. 137).

Fig. 137: An Indian PSLV launcher taking off from the Satish Dhawan Space Centre in Andhra Pradesh to carry Chandrayaan-1 into lunar orbit. (Photo courtesy of ISRO)

What seemed to take place in minutes on 22 October 2008 was prepared over years of precise and careful work also at the Max Planck Institute for Solar System Research at Katlenburg-Lindau, Germany, which set out in 2004 to build an instrument to be carried by Chandrayaan-1 as a guest payload to the Moon: The SIR-2 spectrometer.

The SIR-2 experiment (see Fig. 138) is a near-infrared spectrometer covering a wavelength range from 0.9 to 2.4 μm. The purpose of the instrument is to analyze the mineralogical composition of the uppermost layer of the lunar soil. The spectrometer measures the intensity of the solar light, which is reflected from the lunar surface to the instrument sitting on the Chandrayaan-1 spacecraft, which orbits the Moon at an altitude of 100 km. SIR-2 can perform its task with the help of its three components: the telescope, which collects the reflected sunlight, the sensor-radiator unit, which contains the spectrometer and also carries the radiator to cool the experiment, and the electronics box which powers the experiment and controls the data gathering.

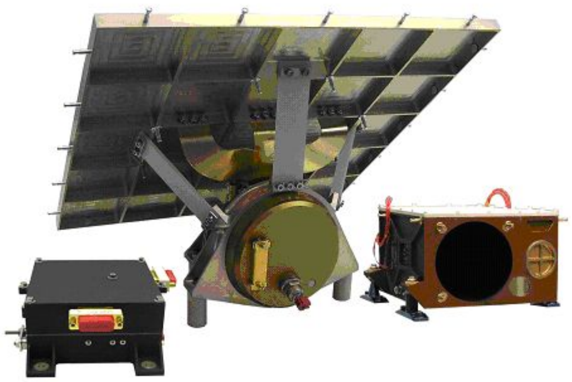

Fig. 138: The SIR-2 instrument consists of three parts: The Electronic Box (left), the Sensor-Radiator Unit (Middle) and the Optical Box (right).

The instrument, which was designed and built at the MPS, in collaboration with the Polish Academy of Science and the University of Bergen in Norway, could profit from the experience the MPS collected with an early technological experiment, which flew to the Moon with the European SMART-1 mission in 2003.

The SIR-2 instrument, (see Fig. 139) which can operate independently on the Chandrayaan-1 spacecraft, will reach its maximum potential in concert with an Indian payload, the Hyper-Spectral-Imager (HySi) experiment sitting on Chandrayaan-1. HySi images the lunar surface in a wavelength range from 0.4 to 0.95 μm, thereby complementing the measuring range of SIR-2. To ensure that the SIR-2 and HySi experiments will be able to join their data in an optimal way, SIR-2 was calibrated as the first foreign science payload ever in November 2007 at the Space Application Center (SAC) in Ahmedabad, where HySi was also calibrated.

After calibration the instrument was shipped by plane to ISRO in Bangalore where SIR-2 was integrated on the Chandrayaan-1 spacecraft (see Fig. 140).

While the experiment was waiting for its launch, a copy of the instrument was travelling in the "Science Express", an exhibition train where Indian visitors could learn more about international cutting-edge research in the natural and biosciences. The train and its exhibition, a collaboration effort between the Indian Department of Science and Technology (DST), the Federal Ministry of Education and Research (BMBF) and the Max Planck Society, was designed to inspire enthusiasm for science among young people all over India (see Figs. 141 and 142).

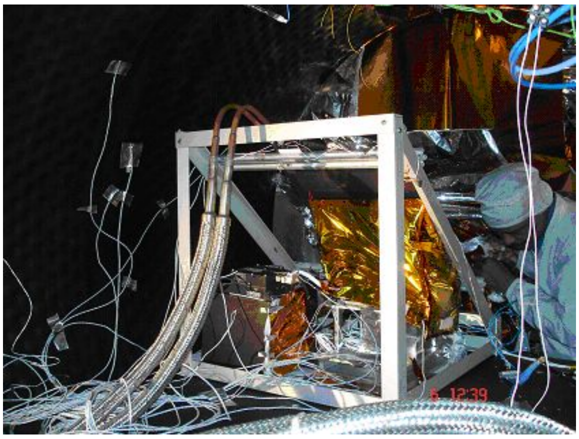

Fig. 139: The SIR-2 instrument at the Space Application Center in Ahmedabad during calibration.

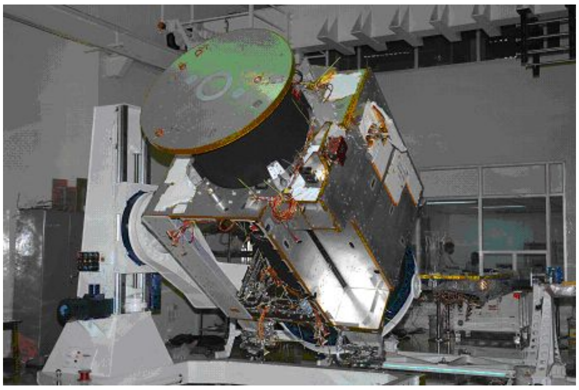

Fig. 140: SIR-2 during integration on the Chandrayaan-1 spacecraft at Bangalore. (Photo courtesy of ISRO).

After a perfect launch Chandrayaan-1 was successfully inserted into lunar orbit on 8 November 2008. The instrument was successfully commissioned in December 2008 at ISRO in Bangalore and started taking its first data in 2009. The Chandrayaan-1 mission is intended to collect data for at least two years. We are now finally ready for Science.

The SIR-2 project at the MPS is supported by the MPG and ESA.

(U. Mall)

Fig. 141: The SIR-2 instrument on display in the Indian Science Express was seen by more than 2.2 million visitors at 57 stops across India.

Fig. 142: The Indian Prime Minister Manmohan Singh and Chancellor Angela Merkel on their way to inspect SIR-2 in the Indian Science Express.

Retrieval simulations of atmospheric gases of Titan in preparation for Herschel

The origin of Titan's atmosphere is poorly understood and its chemistry is rather complicated. In the framework of the *HssO* Herschel KP program one of the goals is performing line scan surveys with PACS (from 55 to 210 μm) to obtain the vertical profiles of important species. Tracing molecules such as CH_4, H_2O, HCN, and CO can help in determining the vertical structure of Titan's atmosphere.

We investigated the possible vertical profile retrievals of temperature and mixing ratio of H_2O with HIFI (Heterodyne Instrument for the Far Infrared), and temperature and mixing ratios of H_2O, HCN, and CO with PACS (Photodetector Array Camera & Spectrometer) for the expected signal-to-noise ratios. In order to model the expected observed emission spectra, a forward model is implemented which accurately takes into account spectroscopy, atmospheric radiative transfer, and instrument characteristics.

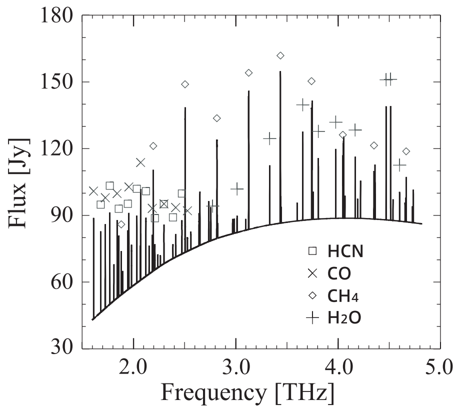

Fig. 143: Synthesized spectrum of the Titan atmosphere with the spectral resolution of the PACS instrument ($\Delta\nu$ = 1 – 4 GHz). The symbols indicate the selection of the lines which we used in the retrieval analysis

Fig. 143 shows model calculations of the synthesized spectrum of Titan's atmosphere with PACS spectral resolutions ($\Delta\nu = 1-4$ GHz). In order to retrieve physical parameters such as the mixing ratio from the spectra, an inversion technique is performed. We report retrieved temperature profiles (from CH_4 lines) and H_2O mixing ratios at 40 – 240 km, and 100 – 180 km, respectively, by using single lines for HIFI. Furthermore, by using a relevant combination of lines for PACS, we demonstrated the possibility of PACS to constrain the temperature and H_2O, HCN, and CO mixing ratios for a set of altitude levels: H_2O, CO and HCN at the stratosphere, and in addition, HCN at the mesosphere. Fig. 144 shows the HCN weighting functions with respect to the mixing ratio, retrieved mixing ratio profile for the simulated observations with their correspond error profiles, and the averaging kernels as an example. Although with PACS's low spectral resolution the information from the line shape of each emission line is unresolved, the multiple-line simulated observation generates as almost as good a sensitivity to the vertical profile of temperature as we can obtain with the high resolution spectroscopy of HIFI. By using a measured spectrum of uniformly mixed species (e.g. CH_4), a retrieved temperature profile successfully allows us to constrain mixing ratio profiles of other gases in Titan's atmosphere.

These results in preparation of Herschel show our technique to be a promising tool for the analysis of

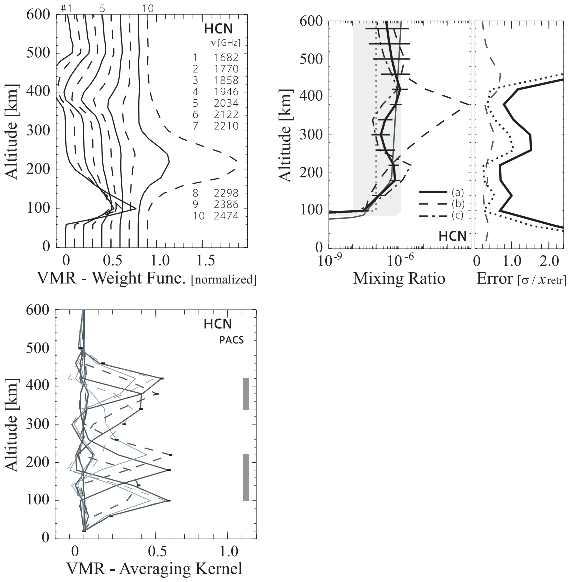

Fig. 144: Example of retrieval simulations for the PACS observations. Upper left: HCN weighting functions with respect to the mixing ratios. Each curve is plotted with an offset of 0.1. Upper right: HCN mixing ratio and errors. Lower left: averaging kernels. Gray bars on the right side indicate the altitude region where the retrieval is satisfactorily obtained.

Titan's atmospheric data.

(M. Rengel, H. Sagawa, and P. Hartogh)

Comets and small bodies

Asteroid Steins imaged by Osiris onboard Rosetta

A series of images of asteroid Steins was taken by Rosetta's Optical, Spectroscopic, and Infrared Remote Imaging System (OSIRIS) in September 2008 during the fly-by maneuver at 800 km distance to the object. The high resolution image around closest approach Fig. 145 shows a long north-south crater chain and a deep crater of approx. 2 km diameter at the north pole.

Asteroid Steins is the first E-type asteroid ever visited by a spacecraft. The size of the body was determined to $6.7 \times 5.9 \times 4.3$ km^3. Spectral coverage in 25 different filters in the wavelength range from 250 to 1000 nm shows little colour variation on the surface of the object.

The fly-by sequence covered nearly 180° in viewing angle including phase angle zero (opposition). Images from opposition to fare-well are mosaicked in Fig. 146. The crater count can lead to determination of the age of the surface of the asteroid.

Credit for all Figures:

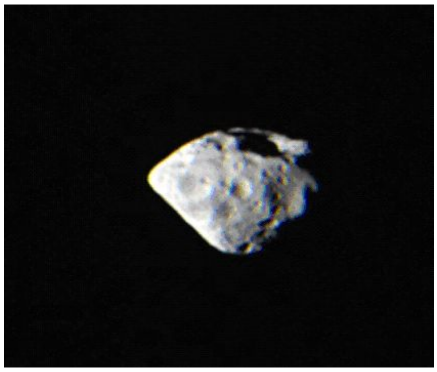

Fig. 145: High resolution image of asteroid Steins taken by the Osiris Wide Angle Camera. The deep crater at the north pole has a diameter of approx. 2 km.)

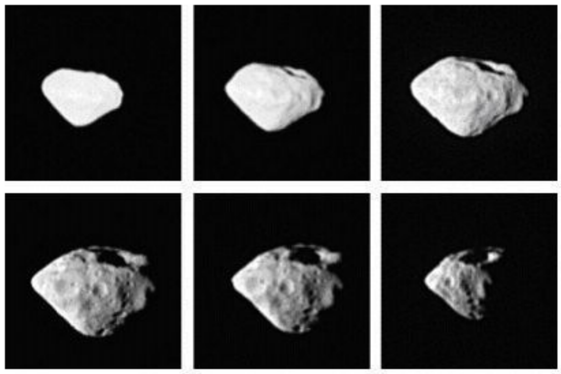

Fig. 146: Set of WAC images from phase angle zero (opposition, upper left) to retreat shows the cratered surface of Steins from different perspectives.

ESA ©2008 MPS for OSIRIS Team MPS/UPD/LAM/IAA/RSSD/INTA/UPM/DASP/IDA

(H. Sierks, S. F. Hviid, R. Moissl, S. Spjuth, C. Tubiana, S. Schroeder, G. Machtoub, I. Büttner, M. Richards, H. U. Keller in collaboration with the Osiris Team)

MIRO Steins fly-by

On 5 September 2008 the Rosetta spacecraft passed the Asteroid Steins in a distance of 800 km. MIRO was powered on for approximately 10 hours centered on the closest approach. The instrument worked perfectly, but the MIRO boresight was significantly displaced from Steins for most of the fly-by due to errors in the spacecraft attitude. This significantly reduced the amount of data collected. The thermal emission from Steins was observed with high signal-to-noise ratio in both millimetre and submillimetre continuum channels. Spectroscopic data with the MPS Chirp Transform Spectrometer was obtained, but no spectral lines were observed. Thermophysical model calculations have been performed indicating that the surface material of Steins has a very low thermal inertia. It has to be < 50 J/(K m^2 s^{0,5}) in order to explain the high temperatures MIRO observed during the fly-by. This value is comparable with what we know from the lunar regolith. Fig. 147 shows the modeled and observed millimetre and submillimetre wave brightness temperatures. On-going work in the data analysis focuses on an improved shape model of Steins. This is essential for retrieving the loss tangent in the regolith.

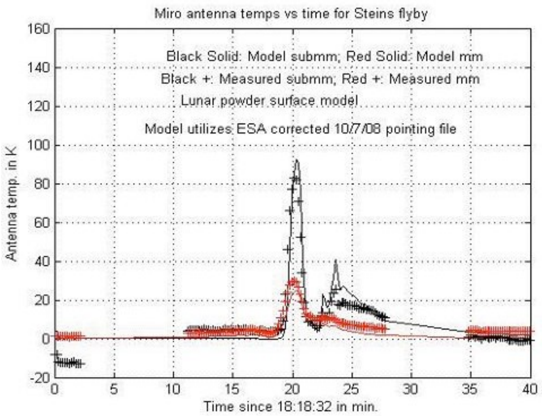

Fig. 147: MIRO mm and submm brightness temperatures during Steins fly-by.

(P. Hartogh and C. Jarchow in collaboaration with the MIRO team)

MIRO: Extension of the Radiation Transfer in the Inner Coma from a 1-D-Model to a 3-D-Model

Up to November 2008 MIRO spectral line observations of the inner coma have been modeled using a simple Haser model. This model is spherical symmetric and hence the coma has been described by a set of spherical shells which grow exponentially in thickness with increasing distance from the nucleus. Within each shell the number density, temperature and expansion velocity is considered to be constant. This model is essentially a one dimensional description of the coma and does not allow to model non-isotropic coma properties like jets, for example. Such a phenomenon requires a three-dimensional coma description and correspondingly a new method to perform the radiation transfer.

Instead of using layers of a given geometry or any other kind of grid description of the coma it appears simpler to leave the radiation transfer equation in its differential form and to use an efficient numerical algorithm to solve this ordinary differential equation with given inital values for the radiation intensity at the start point of the integration. Such an approach does not require any predifined grid - instead the numerical algorithm decides on its own at which locations along the line of sight and at which density (adaptive stepsize) it needs to know the coma properties in order to calculate the absorption coefficient at these locations. So instead of coma properties listed at predefined gridpoints this new approach needs a coma description, which can provide on a fast basis the coma properties at any location in the three dimensional space. Such a description is typically a parameterized model like a series expansion using sperical harmonics or any other kind of appropriate base functions.

A retrieval of the coma properties means then to retrieve the coefficients of such a series expansion. However, using a limb-looking observation geometry instead of the nadir looking geometry facing always the nucleus, even the principles of tomography appear applicable and the possibility to retrieve a xy-cross section through the coma will be investigated in near future.

(C. Jarchow and P. Hartogh)

Project COSAC

COSAC (COmetary SAmpling and Composition experiment) is a gas-chromatograph mass-spectrometer on the Rosetta lander Philae.

Following the successful launch and the commissioning phase several active payload check-outs were performed. COSAC is in good shape.

The main activity in 2008 was centered on active payload checkout No. 8 (PC8). The intention was to upload a newly developed software. It was of clearer structure than the earlier version, allowed to correct the malfunction discovered in the commissioning phase, and had the option of data compression.

Although the software was thoroughly tested on all available ground equipment (i.e. simulators, Ground Reference Model in Cologne, and Flight Spare Unit in Lindau) there was a serious malfunction during the execution of PC8. The true cause is not known but a relation to the software can not be ruled out. Full recovery was achieved in a contingency slot but at the expense of returning to the previous software version.

In order to save the most important additional feature of the new software, the alternative solution for the malfunction discovered during commissioning, another software patch will be uploaded in PC10 in 2009.

(F. Goesmann)

The ROSETTA Lander PHILAE

The biyearly checkouts in flight were continued. The Lander was switched on in addition during Steins fly by and for contingency check outs. All subsystems under MPS responsibility work nominally.

The subsystems under MPS responsibility are:

- Complex landing gear including electronics and damping system
- Mechanical subsystem MSS to separate lander and orbiter and push PHILAE into the landing orbit
- Power subsystem PSS for handling of electrical power generation and distribution
- Harpoons system to anchor the lander on the cometary surface
- Hardware for the command and data management system

In addition the responsibility for the ESS software was taken over in 2008. The ESS manages the communication between orbiter and lander.

(H. Boehnhardt, B. Chares, R. Enge, H. Fischer, O. Küchemann, W. Kühne, R. Roll, M. Sperling, and I. Szemerey)

Surface exploration of small bodies

This project analyses the surface composition and constitution of Transneptunian objects, cometary nuclei and other small objects in the solar system through photometric, spectroscopic and polarimetric measurements.

Using FORS1 at the ESO VLT, the light scattering behaviour of cometary surfaces was explored through measurements of the linear polarization and photometric phase functions over the phase angle range from 0 to about 25 deg. Comets 9P/Tempel 1, 19P/Borrelly and 133P/Elst-Pizarro were observed in 2007/2008. As already found for 2P/Encke for the first time (Boehnhardt et al., 2008, A&A 489, 1337), the polarization light curves of the three comets suggest a light scattering behaviour that is different from other small bodies in the solar system. It is noted that 133P/Elst-Pizarro seems to be closest to F-type asteroids in its polarization and photometric phase functions (Fig. 148). Applying the heuristic albedo-polarization relationships known from asteroid, a geometric albedo of 5-6 percent was obtained which is in good agreement with value found from combined optical and mid-IR measurements of the nucleus. As a by-product the temporal evolution of the dust tail of 133P/Elst-Pizarro was analysed indicating a pre-perihelion on-set of nuclear activity. The photometric results of 9P/Tempel 1 were made available to the StardustNext mission team for inclusion in a comprehensive analysis of rotation motion of the nucleus of this comet in preparation of the forthcoming fly-by of the spacecraft in February 2011. 1 refereed paper published, 3 submitted.

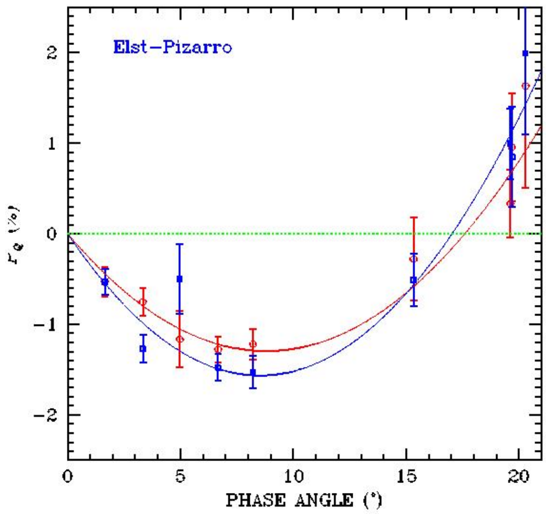

Fig. 148: The polarimetric phase function of the nucleus of comet 133P/Elst-Pizarro. The plot shows the degree of linear polarization (in %; blue/red for the V/R filters) vs. the phase angle.

In an international collaboration (principal investigator: T. Mueller, MPE Garching) the observing program for Open Time Key Program "TNOs are cool was prepared in detail for submission to the ESA's Herschel Observatory, due for launch in spring 2009. The program was granted 378 hours of observing time for the exploration of basic physical properties of Transneptunian Objects (TNOs like Kuiper Belt objects, Centaurs, Scattered Disk SDOs and Detached Disk objects DDOs). The Herschel observations of in total 137 objects aim at the determination of albedo and size, of total mass and density, of thermal properties and at the study of surface albedo variations of these primordial bodies in the outskirts of the planetary system. In support of the New Horizons mission, new observations of the dwarf planet Pluto were performed at the VLT observatory in order to verify the temporal surface ice evolution due to suspected weather phenomena (Protopapa et al., 2008, A&A 490, 365). 3 refereed papers, 1 in press.

(H. Boehnhardt, S. Protopapa, and S. Vincent)

Physical and compositional properties of comets

This program investigates physical properties of the nuclei and of the coma dust as well as of the ice composition of short period and Oort Cloud comets through different measurement and analysis techniques.

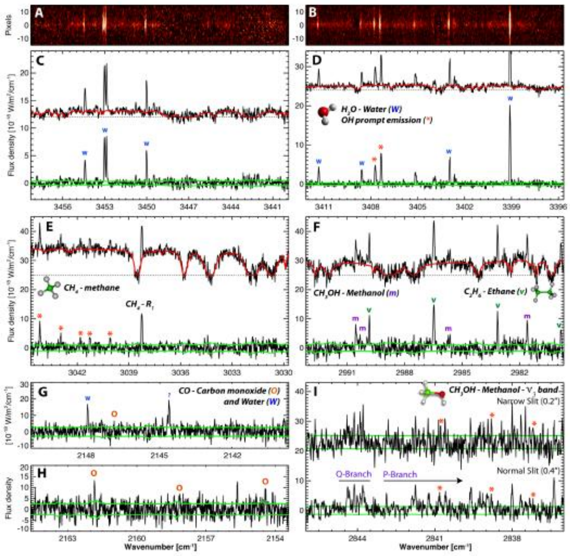

Fig. 149: Detection of parent volatiles in comet 8P/Tuttle in January 2008. The two upper panels show the echellograms of the comet taken with the CRIRES instrument at the VLT Observatory. The central bright dust continuum extends along the x direction (wavelength direction), while gas emissions appear specific wavelength as vertical profiles of different brightness in along-slit direction. The other panels of the figure show extracts of calibrated spectra with lines of several molecules as indicated in the panels (x direction is now in wavenumbers.

The aphelion arc observations of 67P/Churyumov-Gerasimenko, the target comet of ESA's Rosetta mission, were completed in spring 2008. Images of the comet taken at 3.4 AU from the Sun inbound, showed already the presence of the weak dust coma around the nucleus which indicates an even earlier on-set of nucleus activity somewhere between 4.2 and 3.4 AU when approaching the Sun. For a repetitive behaviour of the comet during its next return, Rosetta will be exposed to some nuclear activity during the approach and early mapping phases of the mission as will be the lander Philae when descending to the nucleus at about 3 AU from the Sun. Measurements of the thermal flux of the comet with the Spitzer Observatory and of the reflected sunlight of the nucleus at the VLT Observatory were combined for an analysis of the surface albedo – found to be 0.05 – and of the size – found to be 2.04 km – of the cometary nucleus (Kelley et al., 2009, AJ 137, 4633). The thermal and visible light curves could be phased with only small discrepancies suggesting a shape dominated light curve of the comet. The thermal light curve of the comet at 4.8 AU inbound agrees remarkably well with the post-perihelion one at 4.5 AU pre-perihelion. Similarly, also the visible light curve of the comet did not change significantly over the aphelion arc from about 4.5 AU post- to about 4.5 AU pre-perihelion. 1 refereed paper published, 1 in press.

High dispersion mid IR spectroscopy of the cometary coma is performed using CRIRES at the VLT Observatory in Chile in order to detect parent gas species from supervolatile ices in cometary nuclei. In 2008 periodic comet 8P/Tuttle (Fig. 149) and the Oort Cloud comet C/2007 W1 (Boatini) were successfully observed. For 8P/Tuttle the production rates of H_2O, CO, CH_4, CH_3OH, C_2H_6, and H_2CO were determined (Boehnhardt et al., 2008, ApJ 683, 78L) and a sensitive value of the D/H ratio of water in this comet could be estimated (Villanueva et al., 2009, ApJ 690, L5). The D/H ratio obtained is in agreement with the values for the only 3 other comets published so far and is by a factor of 2.6 higher than that of terrestrial ocean water suggesting that comets – if at all – might not have been the only source for water on Earth. 2 refereed papers published.

(H. Boehnhardt, M. Lippi, C. Tubiana, and J.-B. Vincent)

General studies

Herschel Solar System Observations

MPS is leading the Herschel Key Program for solar system observations with 50 participating scientists from 21 institutes in 10 countries. One unique feature of Herschel is its capability to observe water with extremely high sensitivity. Thus the project is focusing on water and related chemistry. Water is ubiquitous in the Solar System, being present in gaseous form in all planetary and cometary atmospheres, as ice on the surface and subsurface of Mars, comets, most planetary satellites and distant bodies, and in the liquid phase on Earth. Water plays an important or dominant role in the chemistry of planetary and cometary atmospheres. Comets are sources of water for planets through episodic collisions and continuous production of ice-dust grains. This proposal addresses the broad topic of water and its isotopologues in planetary and cometary atmospheres. The nature of cometary activity and the thermodynamics of cometary comae will be investigated by studying water excitation in a sample of comets. The D/H ratio, the key for constraining the origin and evolution of Solar System species (see Fig. 150), will be measured for the first time in a Jupiter-family comet. A comparison with existing and new measurements of D/H in Oort-cloud comets will constrain the composition of pre-solar cometary grains and possibly the dynamics of the protosolar nebula. New measurements of D/H in Giant Planets, similarly constraining the composition of proto-planetary ices, will be obtained. The D/H and other isotopic ratios, diagnostic of Mars' atmosphere evolution, will be accurately measured in H_2O and CO. The role of water vapor in Mars' atmospheric chemistry will be studied by monitoring vertical profiles of H_2O and HDO and by searching for several other species. A detailed study of the source of water in the upper atmosphere of the Giant Planets and Titan will be performed. By monitoring the water abundance, vertical profile, and input fluxes in the various objects, and when possible with the help of mapping observations,the project HSSO will discriminate between the possible sources of water in the outer planets (interplanetary dust particles, cometary impacts, and local sources). In addition to these inter-connected objectives, serendipitous searches will enhance our knowledge of the composition of planetary and cometary atmospheres.

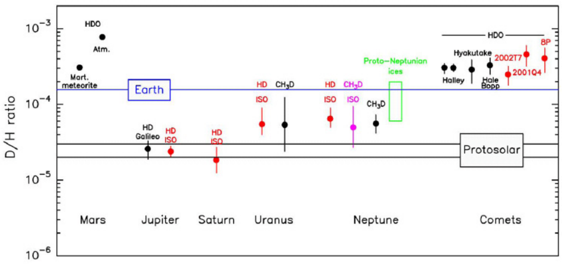

Fig. 150: Herschel will determine several D/H ratios in the solar system for the first time or with much higher accuracy than before.

(P. Hartogh, T. Cavalie, A. Gonzales, C. Jarchow, A. Medvedev, M. Rengel, and H. Sagawa in collaboration with the HssO Team)

Mapping water vapor in the atmospheres of Jupiter and Saturn with Herschel-HIFI and Herschel-PACS

Infrared observations conducted with the Infrared Space Observatory have led to the surprising detection of water vapor in the upper atmospheres of the Outer Planets and Titan (Feuchtgruber et al. 1997, Coustenis et al. 1998). These detections have raised the question of the origin of the oxygen compounds present above the tropospheric cold trap in the reducing atmospheres of the Outer Planets. Indeed, H_2O condense around the tropopause level. Therefore, the observed water vapor must have an external origin. Eligible external sources are of three different kinds: local, diffuse and sporadic sources. The local source is characterized by grains that are sputtered from icy ring particles or satellites, the diffuse source is due to interplanetary dust particles and the sporadic source results into large comet impacts. While the comet supply due to the impact of comet Shoemaker-Levy 9 in 1994 seems to prevail in the atmosphere of Jupiter as shown by infrared (ISO) and submillimetre (SWAS and Odin) observations (Lellouch et al. 2002, Cavalié et al. 2008), local sources could be the major external supplier of water to the atmosphere of Saturn (Prangé et al. 2006). However, the picture remains tentative. Disentangling the various sources is a key objective of the Herschel Guaranteed Time Key Program "Water and related chemistry in the Solar System".

The Herschel Space Observatory will carry 3 instruments: the Heterodyne Instrument for the Far-Infrared (HIFI), the Photodetector Array Camera and Spectrometer (PACS) and the Spectral and Photometric Imaging REceiver (SPIRE). This telescope will enable observing water (among many other molecules) in one of the last unexplored region of the electromagnetic spectrum (55 – 672 μm) with unprecedented sensitivity, spatial and spectral resolution without obscuration by the atmosphere of the Earth (mandatory at most of the observable wavelengths). The telescope will explore a wider frequency range with a better sensitivity than other submillimetre space telescopes like SWAS and Odin, which bands were mostly centered around 550 GHz. It will also have much better sensitivity and spectral resolution than ISO. Therefore, the vertical profile of H_2O will be measurable from very high signal-to-noise ratio observations (S/N$\geq$100) in the upper atmospheres of the Outer Planets.

A means of discriminating the different sources of H_2O is to draw up a very high signal-to-noise 2D-map of its abundance. Fig. 151 shows the different patterns that would result from a local or diffuse source (overabundance at high latitudes) and from a sporadic source (overabundance around the impact location, depending on the impact time). The essential need for performing such observations besides sensitivity is a good spatial resolution. Observations in the band 6 of Herschel-HIFI (spatial resolution of $\sim$13 arcsec) will enable rough mapping of the abundance of water vapor in the atmosphere of Jupiter. The telescope will be used to perform a 13 point map over the jovian disk, with 7 points along the central meridian to look for latitudinal variations. Each point will consist in a spectrally resolved spectrum of the 1669 GHz water line with S/N=100. Besides, the 4512 GHz water line will be used to map both Jupiter and Saturn

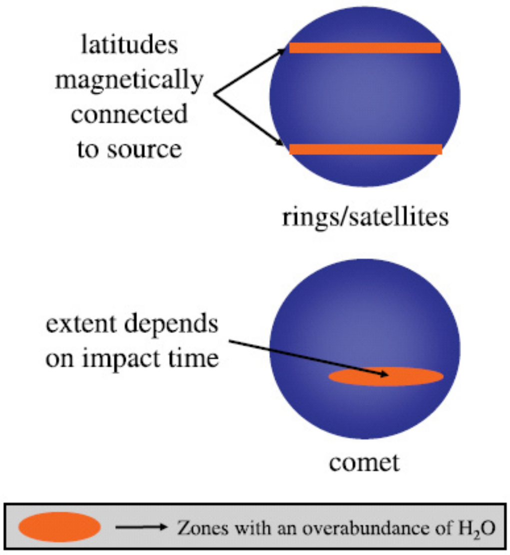

Fig. 151: Different observable patterns in terms of integrated water abundance on a 2D-map as a function of the kind of external source.

with PACS. These observations will result into a 5×5 pixel map covering 47 arcsec×47 arcsec. Each pixel will measure the abundance of water vapor accurately (S/N>100).

(T. Cavalié, P. Hartogh, C. Jarchow, M. Rengel, H. Sagawa, A. González in collaboration with the HssO Team)

Effects of gravity waves in the thermosphere above the turbopause

Vertically propagating internal gravity waves (GWs) are generated in the lower atmosphere of planets, propagate upward carying energy, heat and momentum, and deposit them to the mean flow upon breaking and/or dissipation. GWs play a crucial role in the dynamics and energy budget of the mesosphere and lower thermosphere (MLT). It is known that most of GWs break in the MLT where they contribute to the enhanced eddy diffusion and turbulence just below a certain height called 'turbopause'. Above the turbopause, the molecular diffusion dominates the dynamics. It was widely believed that the role of GWs is insignificant in the upper thermosphere due to the strong damping above the turbopause. Recently, incoherent radars revealed signatures of GWs in the upper atmosphere, and demonstrated that the latter is continuously perturbed by GWs propagating from below. Gross effects of small-scale GWs in the atmosphere are usually studied with general circulation models (GCM) and so-called GW drag parameterizations. Comprehensive GCMs are not yet capable of simulating the thermospheric effects of GWs emanating from the lower atmosphere. There are two major possible reasons for this deficiency: (1) The GCMs do not couple the troposphere and the upper atmosphere. (2) They lack an appropriate GW drag parameterization.

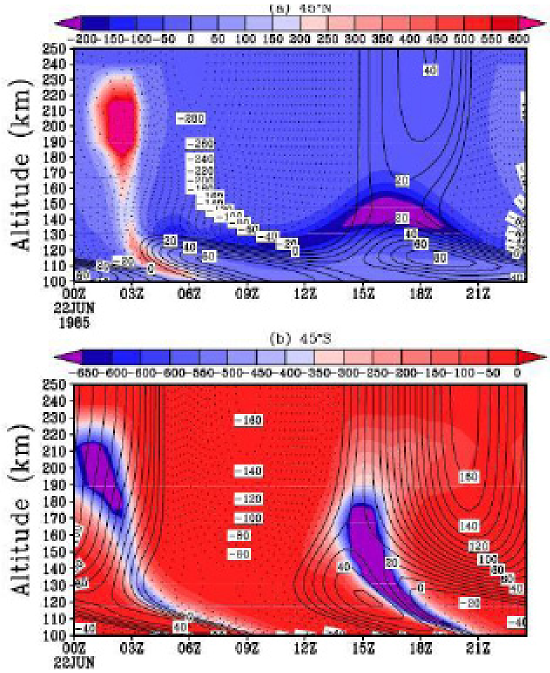

Fig. 152: Diurnal variations of the zonal wind (contours) and of the gravity wave zonal momentum deposition (colour shades). It is seen that effects of GWs vary with local time, and are strong in the upper thermosphere up to 200 – 220 km.

We have developed a novel GW scheme suitable for thermosphere GCMs. Unlike existing parameterizations, it systematically accounts for breaking and dissipation in the upper atmosphere. The scheme was evaluated in a series of off-line tests of increasing complexity, which demonstrated that harmonics with fast horizontal phase velocities can effectively propagate into the upper thermosphere. The parameterization has been implemented into the Coupled Middle Atmosphere-Thermosphere (CMAT) model of the Earth's atmosphere. The results of our simulations suggest that effects of GWs are not only negligible above the turbopause, but are strong and comparable with those of ion friction, at least below 180 – 200 km. In particular, inclusion of GW drag allowed to simulate for the first time the observed separation of the mean winds in the upper thermosphere into the high-latitude easterly (retrograde) and mid- to low latitude westerly (prograde) winter jets (Fig. 152). The contribution of GWs to the momentum budget of the upper thermosphere is highly sensitive to the parameters of GWs. These effects are expected to be extremely important in the upper atmospheres of Mars and Venus.

Further constraints are required to quantify the dynamical coupling of the lower and upper atmospheres of these planets.

(A. S. Medvedev and P. Hartogh in collaboration with E. Yigit and A. Aylward (University College London, UK))

Dawn Framing Camera

Three operational slots in 2008 covered the performance and calibration tests of FC1, the software update of both cameras and the bi-annual check out. During the calibration slot, performed on 22 February the FC1 rendered impressing images showing NGC 3532 (the Wishing Well Cluster) and Eta Carinae (the Homunculus Nebula). The test showed that the camera performance is in line with the design and the ground-based calibration (see Fig. 153).

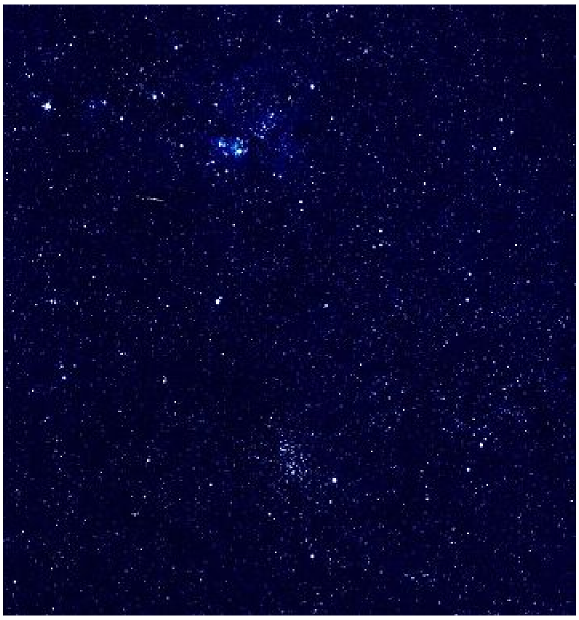

Fig. 153: NGC 3532 (Wishing Well Cluster) and Eta Carinae imaged by the Dawn Framing Camera during instrument checkout.)

The software update was performed on 1 April on both cameras without any incidents. On top of improving the operability of the cameras with a better piece of onboard software, the operation demonstrated that the cameras can be safely updated in flight with the present procedures. The bi-annual checkout performed on 25 August demonstrated the good state of health of both cameras, but was also a ground breaking activity proving that routine operations can be driven remotely by the MPS team from the premises in Lindau. In 2008 the ground operations team at MPS developed and put to work the image calibration pipeline Calliope. The application runs unsupervised and limits the turn-around time of newly received images to a few hours. All the images obtained during the flight ops slots in 2007 and 2008 have been processed through this facility with remarkable success in cleaning and enhancing the images to a scientifically usable level. For the planning of future activities, the first delivery of a multi-mission planning tool, Damocles, aimed at producing command sequences in a reliable and effective manner. Besides, Damocles can be extended by plug-ins, such as the newly developed memory simulator library, that ensures that the operation of the instrument does not exceed the capacity of the mass memory.

(H. Sierks, P. Gutierrez, S. Schroeder, T. Maue, I. Hall, G. Machtoub, and H. U. Keller in collaboration with the Dawn Framing Camera Team)

The Cluster Mission

The Cluster Mission to the Earth's magnetosphere was launched in 2000 from Baikonur and started its initial two-year operation phase in February 2001. A first extension was later granted to last until the end of 2005, followed by a second extension to December 2009. A third extension of 1 – 3 years (depending on spacecraft and instrument health) will be decided on in the middle of 2009.

Each of the four spacecraft carries an identical payload of 11 experiments for measuring plasma and energetic particles, electric and magnetic fields, as well as wave phenomena. During the first 4.5 years, the spacecraft were in a tetrahedron configuration of size varying from 100 to 5000 km, in order to investigate events at different scale sizes (Fig. 154). The separation distances were altered first twice, and then later once a year.

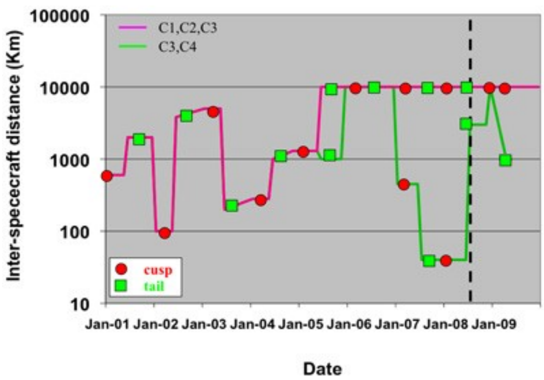

Fig. 154: History of the separations between the Cluster spacecraft over the entire Mission. As of mid-2005, spacecraft 1, 2, 3 have a constant 10 000 km separate (at apogee) while the separation between 3 and 4 is variable from 40 to 10 000 km (green line). Figure curtesy of ESA.

After the manoeuvers in June – July 2005, a totally new concept was implemented: 3 of the 4 spacecraft form a large triangle of size 10 000 km, while the 4th spacecraft is in an orbit such that its distance from one of the others is adjustable from 10's of km to 10 000 km. Furthermore, the orientation of the large triangle can be rotated to be parallel to the geomagnetic tail during the months when the apogee is in the nightside, or perpendicular to the solar wind when the apogee is on the dayside. All these manoeuvers can be achieved with small changes to the spacecrafts' phase within the orbits, with very little fuel consumption. This aspect of the Cluster constellation is referred to as *multi-scaling*. Fig. 155 illustrates the configuration during a tail pass. The increasing southward drift of the apogee means that different regions of the magnetosphere can be attained compared to those in the first years.

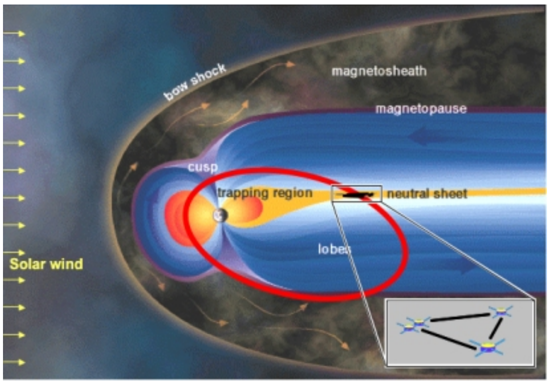

Fig. 155: Cluster orbit in June 2007, showing how the neutral sheet is investigated with three spacecraft in a large horizontal triangle and the 4th spacecraft being very close to one of the others, separated in the north-south direction. Figure curtesy of ESA.

MPS has two major instrument contributions to Cluster: the CIS ion spectrometer (up to ∼40 keV/e) and the RAPID ion and electron imager (from ∼30 keV). These instruments are able to exploit the multi-spacecraft feature of the mission at best with the large separations which approximate the typical ion gyroradii.

MPS also participates in the *Cluster Active Archive*, making available online the high resolution processed data from both the RAPID and EDI instruments. (EDI, or *Electron Drift Instrument*, is the other German-led Cluster experiment, the PI of which was previously located at MPE, Garching.) It is also the home of the *German Cluster Date Centre* that provides access to a subset of the most recent RAPID and EDI data. See separate articles below.

(P. W. Daly, E. Georgescu, E. A. Kronberg, S. Haaland, M. Fränz, and A. Korth)

Comparison of periodic substorms at Jupiter and Earth

In the terrestrial magnetosphere periodic substorms have been observed during magnetic storms. Data from Cluster mission, particularly from particle instruments RAPID and CIS help us to study behaviour of ions during these magnetospheric disturbances (Kronberg *et al.*, 2008). The Energetic Particles Detector and magnetometer measurements on Galileo showed that the Jovian magnetosphere also undergoes quasi-periodic (∼ 3 days) reconfiguration processes which are very similar to the characteristics of a terrestrial substorm. The comparison of the periodic magnetospheric disturbances at Jupiter and Earth shows that they are similar in dynamic features, but have different energy sources, see Fig. 156. It is established that the energy accumulation and subsequent release lead to similar features in the magnetospheres of both planets. The particle data show periodic intensity fluctuations and plasma pressure variations. In addition, recurring signatures of stretching and dipolarization are observed in the magnetic field. Furthermore, the release process is associated with an intensification of auroral emissions. The typical phases for terrestrial substorms like growth, expansion and recovery are also found in the periodic substorms at Jupiter. As a lesson taken from the Jovian magnetosphere it is proposed that under certain conditions periodic magnetospheric substorms at Earth can be driven by mass-loading from the plasmasphere.

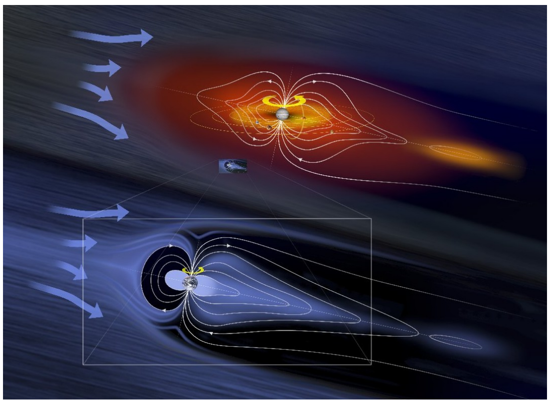

Fig. 156: The comparison of the Jovian and terrestrial magnetospheres: similar dynamic features but different energy sources. At Earth, the well established energy source is the solar wind. At Jupiter, it is believed that internal energy is supplied by the fast planetary rotation and the moon Io which releases ∼ 1000 kg/s of plasma into the magnetosphere.

(E. A. Kronberg, J. Woch, N. Krupp, A. Lagg, P. W. Daly, and A. Korth)

Cluster observations of energetic electrons and electromagnetic fields within a reconnecting thin current sheet in the Earth's magnetotail

Simultaneous Cluster measurements of 3-D electron fluxes, electric and magnetic fields, and waves have been used to study the acceleration of energetic electrons during magnetotail reconnection in a thin current sheet in the magnetotail (Retinò *et al.*, 2008).

Fig. 157 shows RAPID and CIS data together with magnetometer (FGM) and low energy electrons (PEACE). Two consecutive current sheet crossings are observed where the flux of electrons 35—127 keV peaks within an interval of tailward flows. The first crossing shows the signatures of a tailward moving flux rope. The observed magnetic field and density indicate that the flux rope was very dynamic. The second crossing occurs within the ion diffusion region. The flux of electrons is largest within the flux rope where they are mainly directed perpendicular to the magnetic field. At the magnetic separatrices, the fluxes are smaller, but the energy spectra are harder and electrons are mainly field aligned. Reconnection electric fields $E_y \sim 7$ mV/m are observed within the diffusion region, whereas in the flux rope, E_y are much smaller. Waves around lower hybrid frequency do not show a clear correlation with energetic electrons.

Fig. 158 illustrates the interpretation that the field-aligned electrons at the separatrices are directly accelerated by the reconnection electric field in the diffusion region, whereas the perpendicular electrons are trapped within the flux rope and accelerated by a combination of betatron acceleration with nonadiabatic pitch-angle scattering. The observations indicate that thin current sheets during dynamic reconnection are important for *in situ* production of energetic electrons and that simultaneous measurements of electrons and electromagnetic fields within thin sheets are crucial to understand the acceleration mechanisms.

(E. A. Kronberg, P. W. Daly together with A. Retinó *et al.*)

Characteristic ion spectra in the Earth's magnetotail

The German Cluster Data Center plays a major role in the processing and archiving of the Cluster data. Data from two instruments, RAPID and EDI are calibrated, processed and ingested at MPS.

The availability of Cluster data together with support data such as solar wind observations and geomagnetic disturbance indices from several years makes it feasible to perform statistical studies. The Cluster group at

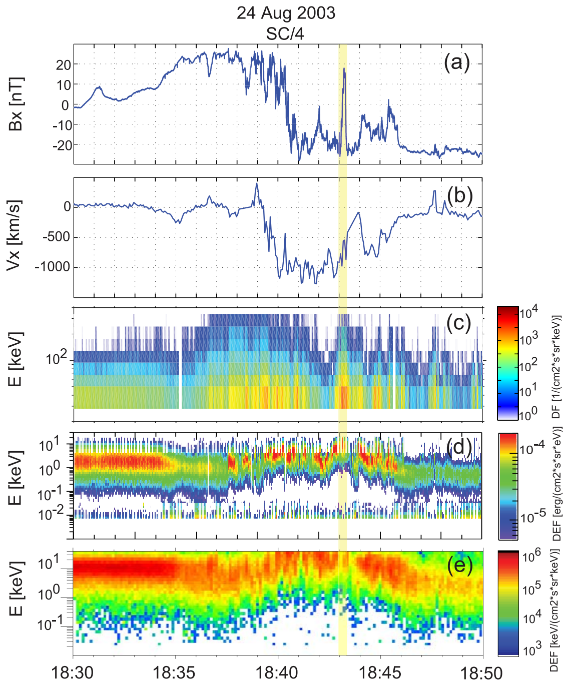

Fig. 157: (a) B_x from FGM sampled at 22 Hz, (b) V_x from CIS/CODIF, (c) RAPID/IES differential flux dF spectrogram in the range 28 – 336.5 keV, (d) combined PEACE/HEEA and PEACE/LEEA differential energy flux dEF spectrogram in the range 10 eV – 26.5 keV, and (e) CIS/CODIF dEF spectrogram in the range 20 eV – 40 keV. RAPID, PEACE and CIS data have 4s time resolution. Vectors are in GSM. The current sheet crossings are shaded yellow. (From Retinò *et al.*, 2008.)

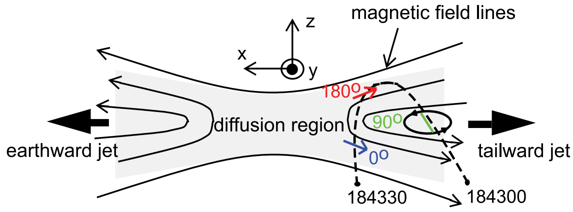

Fig. 158: Cartoon of the current sheet crossings showing the locations and directions of energetic electrons. Cluster trajectory is dashed. (From Retinò *et al.*, 2008.)

MPS has therefore focused on the statistical properties and processes within the nightside magnetosphere.

The magnetotail is one of the most intriguing regions of the Earth's magnetosphere. It mainly acts as a reservoir of magnetic energy entering the magnetosphere via magnetic reconnection at the Earth's dayside magnetopause. In particular during periods of southward directed interplanetary magnetic field, the transfer of energy from the solar wind to the magnetosphere leads to dynamical changes and local plasma instabilities in the magnetotail. The resulting instabilities are manifested locally as plasma heating, fast bursty plasma flow events, and on a larger scale as geomagnetic substorms and storms. On the ground, some of these processes are manifested in the form of aurora. Due to its topology with sharp magnetic field reversals and strong gradients, neither purely classical magnetohydrodynamic or purely kinetic approaches can be used to describe the processes.

To study the large scale behaviour of the energy storage in the magnetotail, we have used a comprehensive dataset from the RAPID and CIS instruments to study characteristic energy spectra during various geomagnetic conditions. Unlike earlier missions, the dataset also contains almost continuous monitoring of the solar wind and interplanetary magnetic field. One of the motivations is to try to distinguish between the reponse to internal processes in the magnetotail and processes directly related to external influences such as changes in the interplanetary magnetic field or rapid changes in the dynamical pressure.

Fig. 159 shows two characteristic energy spectra obtained from RAPID and CIS ion measurements from the magnetotail. The left panel shows a characteristic spectrum during quiet geomagnetic conditions whereas the right panel shows the corresponding spectra during disturbed conditions. We here use the Dst (Distubed Storm Time) index, which is a proxy for the strength of the Earth's ring current to define the geomagnetic activity level. Large negative values indicate a disturbed period with strong ring current, positive values indicate quiet conditions. These two examples show a clear correlation between geomagnetic activity and the spectral slope. During disturbed conditions we see a much harder spectra with a pronounced high energy tail, whereas the quiet time spectra shows a more Maxwellian like shape.

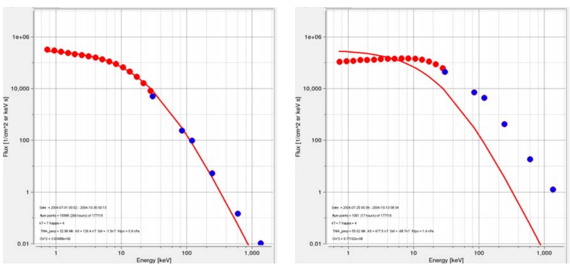

Fig. 159: Characteristic proton spectra in the Earth's magnetotail dring quiet (left panel) and disturbed (right panel) geomagnetic conditions.

The hardening of the spectra indicate non-adiabatic acceleration processes, probably related to the ratio between the particles' gyroradius and the curvature and gradient of the magnetic field. Particles with small gyroradii, such as electrons and low energy protons will mainly behave adiabatically, whereas the more energetic ions with gyroradii comparable or larger than the field curvature will be exposed to stronger magnetic field gradients and cross-tail electric fields. The exact mechanisms for particle acceleration are still debated though.

(S. Haaland, E. A. Kronberg, P. W. Daly, A. Korth, and M. Fränz, in collaboration with L. Degener)

Mass transport in the Magnetotail lobes

The magnetotail and its adjacent boundary layers are embraced by the magnetotail lobes – two regions north and south of the plasma sheet nearly devoid of energetic particles, and with a very low plasma density and comparatively strong, stable magnetic field. The low particle density makes direct plasma measurements difficult. In addition to extremely low count rates obtained with classical particle instrument, spacecraft charging also poses a great challenge. A spacecraft immersed in such a thin plasma will be positively charged due to the loss of photoelectrons caused by incident sunlight, predominantly in the UV range. Composition measurements and moments are therefore not reliable.

To overcome this problem, we have utilized velocity measurments from the Electron Drift Instrument (EDI) combined with density proxies from the Electric Field and Wave (EFW) experiment. EDI emits a beam of electrons which are detected after one (or more) gyrations in the ambient magnetic field. In the absense of strong magnetic field gradients, the displacement of the gyrocenter is a direct measure of the convection velocity. Due to the strong magnetic field and low background plasma density encoutered in the lobes, the EDI technique provides velocity measurements with extremely high precision.

The plasma density is a function of the spacecraft potential, which can be accurately measured by measuring the potential difference between the spacecraft and small boom-mounted spherical probes. Combined with the EDI measurements, we can thus obtain both plasma flow velocity and plasma density. Together with a model of the plasma composition, we are also able to estimate the mass flow.

Fig. 160 shows cross sections of the Earth's magnetotail taken at $X = -10\,\mathrm{Re}$ (Re = Earth radius = ~6370 km) downtail. The left panel shows velocity measurements from the EDI instrument. Each arrow represents the average convection direction and magnitude of the convection velocity. Noteable features are the laminar convection towards the plasma sheet ($Z = 0$), the high velocities near the magnetopause and central plasma sheet as well as some large scale vortices in the lobes. The latter are the magnetospheric manifestations of the large scale plasma circulation, first envisaged by Dungey in the early 1960's. The right panels shows the corresponding electron densities from the EFW instrument. The higher densities in the central plasma sheet as well as the thickening of the plasma sheet towards the flanks are clearly discernible in this plot.

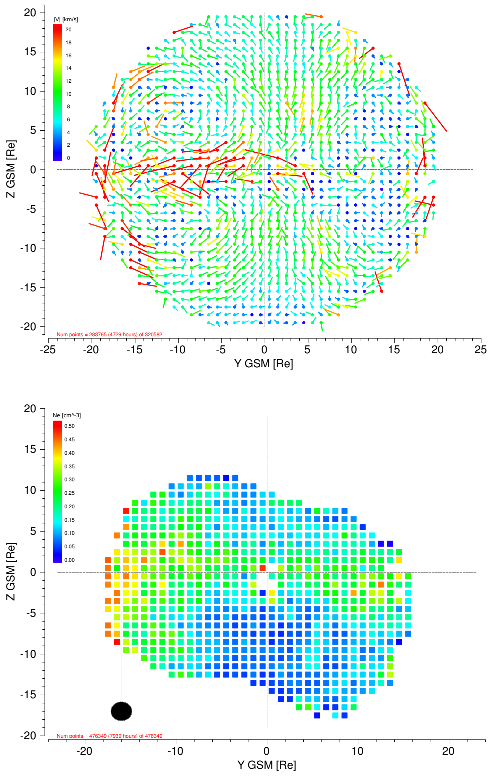

Fig. 160: Cross section of the magnetotail at X = -10 Re. Top : average convection velcocity obtained from the EDI instrument. Bottom panel : average electron density based on EFW probe potential measurements.

One of the interesting outcome of this study was that a substantial part of plasma transfered from the solar wind trough reconnection at the dayside magnetopause escape downtail and does not take part in the full circulation.

(S. Haaland and E. Georgescu)

Cluster Active Archive

The Cluster Active Archive (CAA) is the ESA contribution to the NASA *Living with a Star* Project. It is a repository of processed and validated high-resolution Cluster data, raw data, processing software, calibration data, documentation and other value added products. During the remaining Cluster operation phase (currently until the end of 2009) plus one year, the archive is *active*, meaning it is being regularly populated with new and/or upgraded data, directly from the instrument teams. After that, it will become the long-term archive for the invaluable Cluster data set, making processed data available to the world long after the instrument teams have been dissolved and direct knowledge of the experiments is no longer at hand.

During 2008, MPS has taken over from MPE (Max-Planck-Institut für exterristrische Physik) the responsibility for the archiving of EDI (*Electron Drift Instrument*) data in addition to those of the RAPID experiment. The RAPID data have also been completely reprocessed with improved calibration factors. There are annual user reviews of the entire system and individual instruments, the feedback from which helps to plan additional products and facilitate usage.

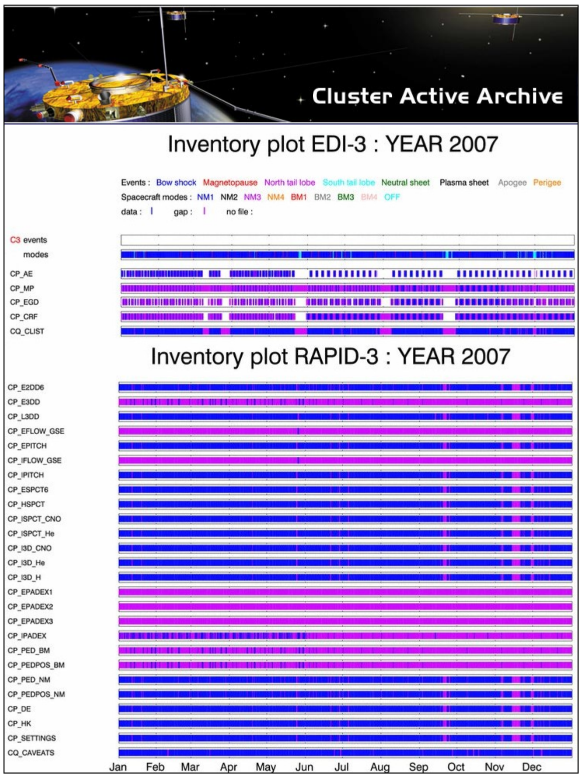

Fig. 161: Inventory plot from CAA showing the availability of the major products for EDI and RAPID on Cluster-3 for the year 2007.

Currently, data from EDI and RAPID are available from 2001 up to 2007 (Fig. 161) for 11 (EDI) and 40 (RAPID) different products, per spacecraft. By 2010, all data up to the end of 2009 will be archived.

(P. W. Daly, E. Georgescu, and E. A. Kronberg)

German Cluster Data Centre

The *Cluster Science Data System* has been planned as an integral part of the Cluster Mission since long before the launch. It was conceived during the days when no one had ever heard of the Internet, as a means by which Cluster investigators could quickly access online a subset of the data from other Cluster instruments. It consists of national data centres in the UK, Sweden, Austria, Hungary, France, and Germany, each processing the data sets for the PI instruments in their respective countries. By mirroring every night, each national data centre has a full set of data for all experiments, for distribution within that country.

The availability of such extensive data sets has made possible many fruitful investigations, such as the statistical studies in the Earth's magnetotail described above on page 118.

The German Cluster Data Centre (GCDC) was originally located at MPE, in Garching, but as of 2008, it is now functioning fully at MPS with new personnel, ingesting validated RAPID and EDI data and regularing mirroring them to the other member data centres (Fig. 162).

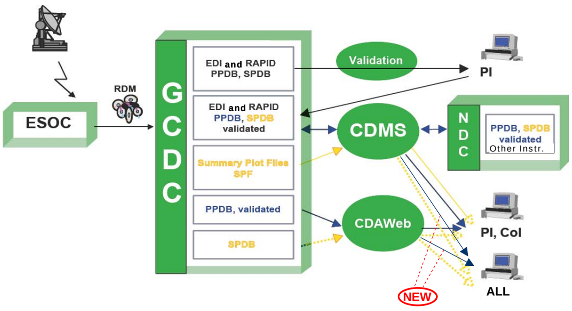

Fig. 162: Data processing chain for the German Cluster Data Centre, from raw data to validated physical parameters distributed to other national data centres.

The CSDS and GCDC complement the more ambitious and modern CAA by providing the most recent data (one or two months old). Recently, the rules have been changed so that the original restrictions to the Cluster community have been removed, and the data are now available to the entire world.

The CSDS data will also be archived at CAA.

(E. Georgescu, S. Haaland, and P. W. Daly)

A QBO-signal in mesospheric water vapor measurements at ALOMAR and in model calculations over a solar cycle

Microwave water vapor measurements between 40 and 80 km over a solar cycle (1996 – 2006) were carried out in high latitudes at ALOMAR (69.29° N, 16.03° E), Norway. Three larger interuptions in the winters of 1996/97 and 2005/06, and from spring 2001 to spring 2002, a few smaller interruptions of monitoring occurred during this period. The observed year-to-year variability is not directly related to the solar activity. The analysis of the observations by the Fast Fourier Transform (FFT) method revealed peaks close to two years, particularly in the upper monitoring domain. Model calculations by means of the real date model LIMA, Leibniz-Institute Middle Atmosphere model, reflect essential patterns of the water vapor variation. The FFT-analysis of the calculated water vapor mixing ratios also showed peaks of around two years. The real period of the QBO during the monitoring period ranged quite close to two years within the time interval considered, with the exception of the years 2001/02 when the period was essentially longer. Although the QBO is a phenomenon occurring in the zonal wind of the tropical stratosphere, we suppose an influence of the QBO on the water vapor distribution of the mesosphere of high latitudes controlled by transport processes. A possible link could be given by the planetary wave activity triggered by the QBO.

(P. Hartogh, C. Jarchow, and L. Song in collaboration with G. Sonnemann, U. Berger, and M. Grygylashvyly (IAP Kühlungsborn, Germany))

Water vapor measurements at ALOMAR over a solar cycle compared with model calculations by LIMA

Water vapor observations were carried out in the mesosphere (40 – 80 km) at ALOMAR (69.29° N, 16.03° E), Norway, from the end of 1995 until the end of 2006 covering nearly one solar cycle (Fig. 163). The monitoring started shortly before the minimum of the solar activity and ended shortly before the next solar minimum so that any bias due to unsymmetrical solar activity was widely reduced. The measurements show a decrease of the mixing ratios at all heights during this period. A similar decline was calculated by the GCM LIMA. Because LIMA uses lower boundaries for the water vapor mixing ratio at the hygropause not changing from year to year, the decreasing tendency must result from altered dynamics. Precisely this assertion has also been confirmed by Randel et al. (2006) and Scherer et al. (2008) who stated a change of the Brewer-Dobson circulation in the tropical stratosphere and a slowdown of the extratropical planetary wave activity. The dependence of the water vapor mixing ratio on the Lyman-α radiation as the most important proxy for solar activity influencing the upper mesosphere/mesopause region is different between summer and winter. The Lyman-α radiation impacts the upper domain (upper mesosphere and above) mainly by dissociation of water vapor forming molecular hydrogen, whereas its influence decreases exponentially with decreasing height. The absorption signal of Lyman-α is transported downward by the downward directed vertical wind in winter. The behaviour is reversed in summer due to the upward flow of humid air in summer. The analysis shows that water vapor is positively correlated with the Lyman-α radiation in the lower mesosphere/stratopause region in winter. This could result from the impact of SSWs which are more frequent and stronger under conditions of high solar activity independent of the phase of the QBO (Sonnemann and Grygalashvyly, 2007). However, when sorting the SSWs according to the phase of the QBO, a significant dependence was discovered. At high solar activity (i.e. larger than the mean amplitude of 10.7 cm-flux), SSWs occurred more often during the west wind phase and at low activity during the east wind phase (Labitzke, 1987). In summer a positive correlation exists at least up to the middle mesosphere. A possible reason is the autocatalytic water vapor production under the condition of high solar activity. But likewise a sudden change of the middle atmospheric dynamics can cause a so-called nonsense correlation. The LIMA calculations exhibit a somewhat different response. The positive correlation in summer reaches up to 75 – 80 km. As the lifetime of water vapor is extremely large at this altitude (from months up to infinity) a slightly enhanced vertical wind in the model can cause such an effect. The differences below 80 km are relatively small, with exception of the wintry values above about 60 to 70 km, so that the agreement between observations and calculations is relatively good.

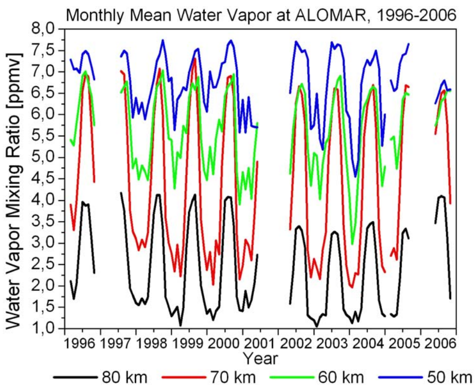

Fig. 163: Water vapour at 4 altitudes observed from ALOMAR over a solar cycle

(P. Hartogh, C. Jarchow, and L. Song in collaboration with G. Sonnemann, U. Berger, M. Grygylashvyly, and F.-J. Lübken (IAP Kühlungsborn, Germany))

A new, high–performance, radiometer for ground–based remote sensing of mesospheric water vapor

A new, high time–resolution radiometer operating at 22.235 GHz for detection of short timescale mesospheric water vapor variations has been installed at ALOMAR in May 2008. The ALOMAR Observatory is situated north of the polar circle (69 16 42 N, 16 00 31 E, elev. 380 m) and has been used for a long time for observations of the polar mesosphere.

The instrument observes the water vapor spectrum in both vertical and horizontal polarization and later averages these in order to get an optimum signal–to–noise ratio. The different polarizations have separate, but identical, signal chains consisting of a cooled HEMT amplifier, an IF stage and a Chirp Transform Spectrometer (CTS) as back–end. Continuous calibration of the signal with two internal loads, a wobbling optical table to reduce standing waves in the optical path and low receiver temperature ensures a time resolution of an order of magnitude better than earlier, similar, instruments.

A first-hand inspection of the retrieved data shows that the improved design is as good as expected. The new system has the ability to resolve atmospheric water vapor dynamics on shorter timescale than ever before observed. An integration time on the order of hours is needed to resolve the weak water vapor emissions and such a time-resolution can be achieved with this instrument. Data-intercomparison between the above described system and an older similar instrument, running at ALOMAR since 1996, is planned.

(K. Hallgren and P. Hartogh)

Radiative transfer and retrieval simulations of spectral shape deviations in planetary atmospheres

(Sub-)Millimeter spectroscopy is a suitable tool for characterizing the chemical taxonomy of planetary and cometary atmospheres. Through rotational transitions of trace gases, it is possible to attain characteristics such as vertical profiles of abundance, temperature, winds, production rates and so forth. In the Earth's middle atmosphere, these rotational transitions at millimeter wavelengths, for instance ozone, water vapor, and chlorine monoxide, are characterized by collisional (or pressure) broadening effects. Since the atmospheric pressure and density decrease approximately exponentially with increasing height, the line shape (or linewidth) yields information about the trace gas content from different layers of the atmosphere.

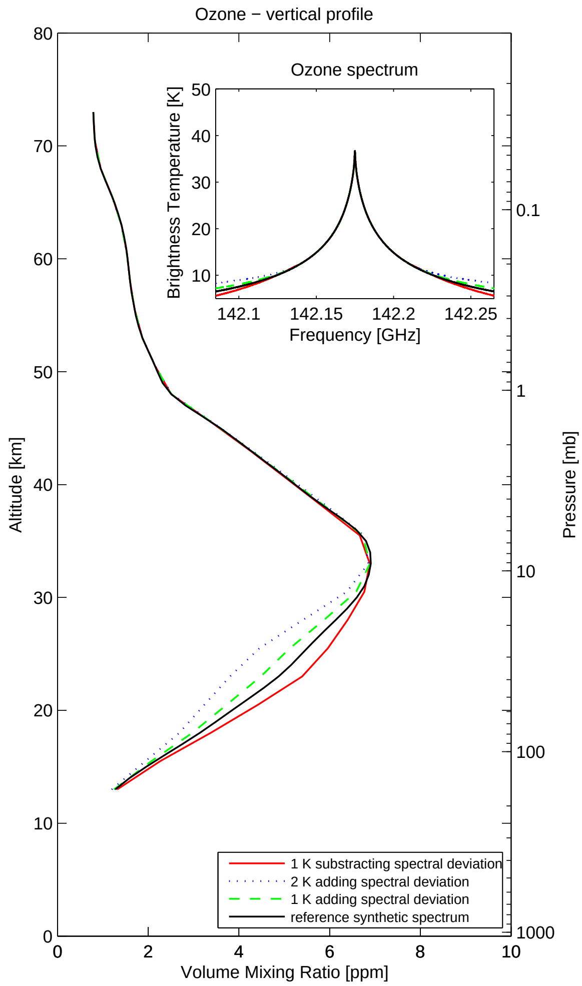

Fig. 164: Effects of small deviations in the spectral intensity at the band edges of a synthetic ozone spectrum into the retrieved vertical profile.

In here, the interpretation of the atmospheric properties can be derived from the measured spectral radiances of its trace gases by fitting synthetic line profiles, obtained with a radiative transfer code, to the observed ones (i.e. the retrieval). On several observation campaigns, unexpected differences have been observed in the spectral amplitude and shape during intercomparison of spectrometers. Thus, we have performed numerical calculations to theoretically demonstrate the importance of spectral accuracy for retrieving the correct physical parameters under observation. This study is performed by means of radiative transfer and retrieval simulations which show how deviations in the spectra might produce considerable changes in the vertical profile of trace gases retrieved in planetary atmospheres. In conclusion these simulations demonstrate that an underestimation of this problem may lead to biased retrieval results (see Fig. 164) and consequently state the need to identify possible sources of deviations or eventually consider these errors in the retrieval algorithm.

(L. Paganini and P. Hartogh)

Progress in the development of Wide Bandwidth SAW Chirp Filters

Dispersive delay lines (DDLs) are key elements in Chirp Transform Spectrometers (CTS) used as real-time backends in heterodyne spectrometers. The so-called reflective array compressor (RAC) design based on the coherent reflection of surface acoustic wave forms propagating on a crystal is the best choice generating large time-bandwidth product impulse responses of DDLs. While long dispersion times have been reported since the mid 1980s, the design and production of large bandwidths is a major challenge, because on the one hand the propagation loss of surface acoustic waves increase with the third power of the center frequency of the DDL and structure sizes of the interdigital transducers (IDTs) and the reflective array get very small. New photo- and electron beam lithographic techniques and improved design tools make it possible to increase the bandwidth step by step. In the last year we improved our DDL design model. Taking advantage of electron beam lithography at the Physikalisch Technische Bundesanstalt (PTB) in Braunschweig we managed to manufacture DDLs not far away from the designed specifications. Deviations from the quadratic phase smaller than 10 degrees RMS could be achieved without any phase compensation. Also for the first time we developed a DDL with a time bandwidth product of > 8000. This device will allow to build a high resolution CTS with large bandwidth at the same time. Finally a new model for controlling the transfer function of the DDL, the duty cycle weighting has been successfully developed and applied.

(X. Li and P. Hartogh in collaboration with F. J. Ahlers, T. Weimann (PTB, Braunschweig, Germany), A. Plessky (GVR, Switzerland), and L. Reindl (University Freiburg,Germany))

V. Selbständige Nachwuchsgruppe Helio- und Asteroseismologie / Independent Junior Research Group of the Max Planck Society "Helio- and Asteroseismology"

The main focus of research is the development of techniques of local helioseismology to study the dynamics of the solar convection zone and the structure of magnetic regions, including sunspots. The Independent Junior Research Group, lead by L. Gizon, is supported by the Max Planck Society, the European Union, and the German Aerospace Center.

Vertical flows in supergranules

Time-distance helioseismology is a method of local helioseismology for peering into the solar interior. In a moving medium, waves travel faster along the flow than against the flow. This principle is used in time-distance helioseismology to infer the existence of subsurface plasma flows from measurements of wave travel times. The travel times are measured from the temporal cross-covariance function between two points at the surface (the cross-covariance function is intimately related to the Green's function between the two points).

We have developed and implemented a linear inversion of the travel times (Jackiewicz, 2008). Two necessary ingredients are the travel-time sensitivity kernels and the noise properties of the measurements. The kernel functions give the linear dependence of travel-time perturbations to subsurface flows; they are computed using the first Born approximation (single-scattering approximation). The inversion produces three-dimensional maps of the solar interior at shallow depths using Optimally Localized Averages (OLA) of the kernel functions. The inversion returns a relatively small cross-talk between the flow components and gives accurate estimates of the noise in the inferred quantities. A compromise – or "trade-off" – is achieved between different observation times, spatial resolutions, and noise levels.

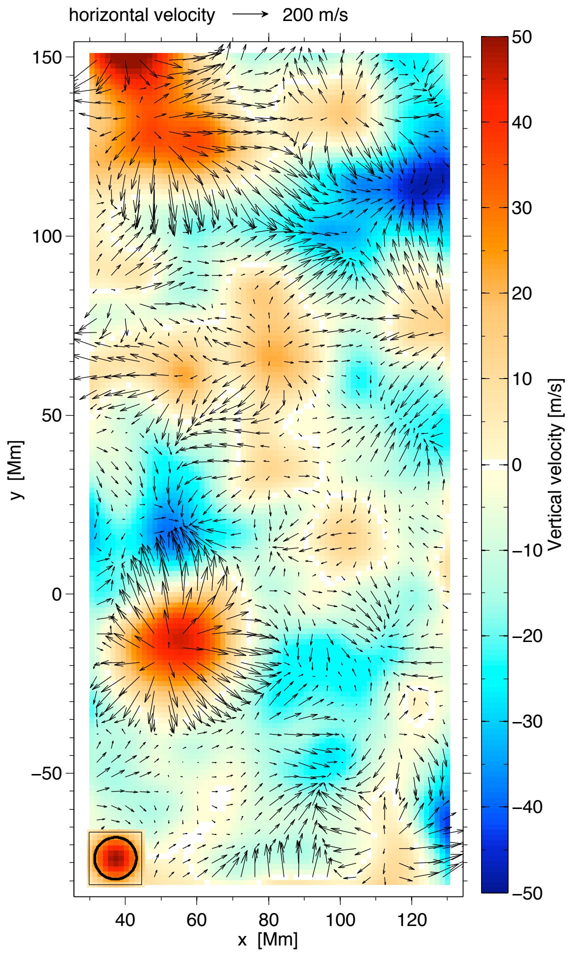

Fig. 165: Map of vector flows at a depth of 1 Mm beneath the photosphere from the time-distance helioseismology inversion. The arrows denote the horizontal flows and the color scale gives the vertical flow velocity counted positive away from the center of Sun. The horizontal spatial resolution is given by the Gaussian function in the bottom corner. This example was computed using a series of two days of full-disk SOHO/MDI Dopplergrams.

As an example of this inversion, in Fig. 165 we show a map of flows near the surface (two day average). The regions of horizontal outflow are identified as supergranular convective cells (Hirzberger *et al.*, 2008). One notices that areas of strong horizontal outflow generally correspond to vertical upflows. Previous inversion studies have not produced consistent maps of the vertical velocity as this one has. The vertical flows in supergranules have a dispersion of about 30 m/s, in agreement with indirect estimates from direct Doppler observations.

(J. Jackiewicz and L. Gizon in collaboration with A. C. Birch (CoRA, Boulder))

Comparative helioseismology of the sunspot in Active Region NOAA 9787

Various methods of helioseismology were used to study the subsurface properties of the sunspot in Active Region NOAA 9787. This sunspot was chosen because it is axisymmetric, shows little evolution during 20 –– 28 January 2002, and was observed continuously by the SOHO/MDI instrument. AR 9787 is visible on helioseismic maps of the far side of the Sun from 15th January, i.e. days before it crossed the East limb.

Oscillations have reduced amplitudes in the sunspot at all frequencies, whereas a region of enhanced acoustic power above 5.5 mHz (above the quiet-Sun acoustic cutoff) is seen outside the sunspot and the plage region. This enhanced acoustic power has been suggested to be caused by the conversion of acoustic waves into magneto-acoustic waves that are refracted back into the interior and re-emerge as acoustic waves in the quiet Sun. Observations show that the sunspot absorbs a significant fraction of the incoming p and f modes around 3 mHz.

Wave travel times and mode frequencies are strongly affected by the sunspot. In most cases, wave packets that propagate through the sunspot have reduced travel times. At short travel correlation distances, however, the sign of the travel-time shifts appears to depend sensitively on how the data are processed and, in particular, on filtering in frequency-wavenumber space.

We carried out two linear inversions for wave speed: one using travel-times and phase-speed filters and the other one using mode frequencies from ring analysis. These two inversions give subsurface wave-speed profiles with opposite signs and different amplitudes (Fig. 166). This strong discrepancy, which had not been noticed before, is a serious issue. Several sources of systematic errors are being investigated. From this study of AR 9787, we conclude that we are currently unable to provide a unified description of the subsurface structure of the sunspot.

(L. Gizon, H. Schunker, R. Cameron, S. M. Hanasoge, J. Jackiewicz, M. Roth, and T. Stahn in collaboration with C. S. Baldner (Yale), R. Bogart (Stanford), S. Zharkov (Sheffield), and others)

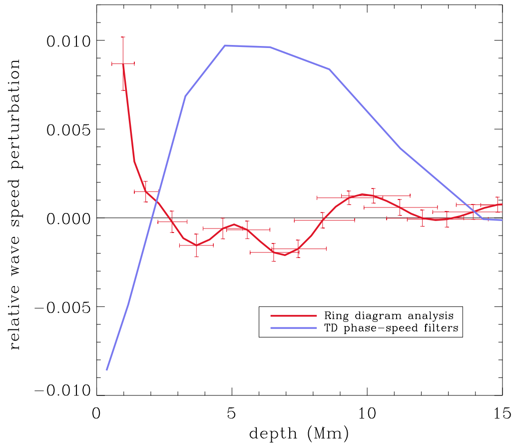

Fig. 166: Comparison of two different helioseismic methods used to infer wave-speed perturbations below AR 9787. The red curve shows the ring-diagram result. The solid blue curve shows the time-distance result (phase-speed filters), after averaging over the area used for ring analysis. Although they are meant to represent the same quantity, these two curves are noticeably different!

Towards understanding the frequency dependence of travel time shifts through sunspots

Helioseismic observations of sunspots show that wave travel times, at fixed horizontal phase speed, depend on the temporal frequency of the waves employed in the data analysis. This frequency variation has been suggested to be consistent with near-surface (vertical length scales of order one Mm or smaller) changes in wave propagation properties relative to the quiet Sun. We investigated this suggestion by employing numerical simulations of acoustic-wave propagation through models with horizontally and vertically inhomogeneous structure. Standard methods of surface-focused helioseismic holography were applied to the resulting simulated wave fields. As seen in Fig. 167, the travel-time shifts measured using holography from the simulations with deep sound-speed perturbations (relative to a plane-parallel quiet-Sun model) do not show a systematic frequency dependence at phase speeds above about 20 km/s. However, shallow sound-speed perturbations, similar to those proposed to model the acoustic scattering properties of sunspots observed with Hankel analysis, produce systematic frequency dependence at these phase speeds. In both cases, positive travel-time shifts can be caused by positive sound-speed perturbations. The details of the travel-time shifts are, however, model dependent.

(R. Cameron in collaboration with A. C. Birch (CoRA), D. C. Braun (CoRA), and S. M. Hanasoge (Stanford))

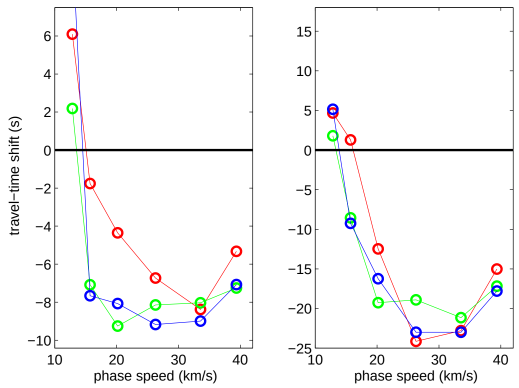

Fig. 167: Travel-time shifts from the SLiM code for shallow (1 Mm, left) and deep (10 Mm, right) sound-speed perturbations ($\delta c > 0$) for three frequency bandpass filters centered at 3 mHz (red), 4 mHz (green), and 5 mHz (blue) as functions of horizontal phase speed. In the deep case, there is no clear dependence of the travel-time shifts on frequency at phase speeds above 20 km/s. In the shallow case, the travel-time shifts at 3 mHz tend to be smaller than those at 4 mHz and 5 mHz.

Wave motion in inclined magnetic fields within sunspot penumbrae

At the surface of the Sun, acoustic waves appear to be affected by the presence of strong magnetic fields in active regions. We study the possibility that the inclined magnetic field in sunspot penumbrae may convert primarily vertically-propagating acoustic waves into elliptical motion (Schunker *et al.*, 2008). We use helioseismic holography to measure the modulus and phase of the correlation between incoming acoustic waves and the local surface motion within two sunspots. These correlations are modeled by assuming the surface motion to be elliptical, and we explore the properties of the elliptical motion on the magnetic-field inclination. We also demonstrate that the phase shift of the outward-propagating waves is opposite to the phase shift of the inward-propagating waves in stronger, more vertical fields, but similar to the inward phase shifts in weaker, more-inclined fields.

(H. Schunker in collaboration with D. C. Braun, C. Lindsey (CoRA) and P. S. Cally (Monash))

Sunspot dynamics: the moat flow

Sunspots are surrounded by the moat flow, a horizontal outflow with an amplitude up to 500 m/s that extends out to about two penumbral radii. We used time-distance helioseismology and the OLA inversion described above to infer the moat flow at different depths in the interior. We used independent measurements of the travel times for five different radial orders, i.e. the ridges f through p_4.

Fig. 168 shows the inferred horizontal flows at different depths: the moat flow is always directed outward from the sunspot in the top 5 Mm. In addition we compared the flow inversions with the motion of the Moving Magnetic Features (MMFs) observed at the surface by SOHO/MDI: the agreement is encouraging.

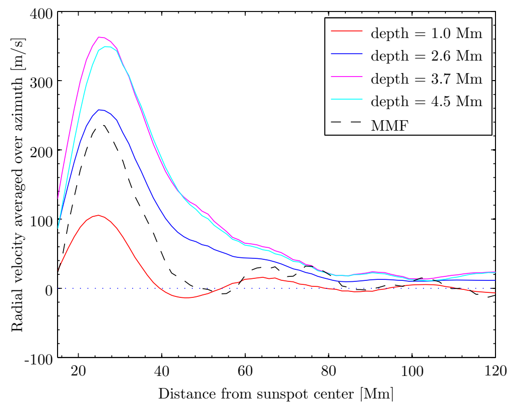

Fig. 168: Azimuthally-averaged horizontal outflow from the sunspot center at different depths (time-distance helioseismology with ridge filtering). The velocity from the MMFs is shown as the dashed line. Note that only the region from the edge of the penumbra outward is shown.

(J. Jackiewicz and L. Gizon)

Acoustic power haloes around active regions

The power of the solar oscillations at high frequencies shows substantial decrements within regions of strong field and curiously, randomly distributed patches of enhancement in the vicinity (Fig. 169). We propose that these enhancements, or haloes, are a consequence of magnetic-field-induced mode mixing (scattering), resulting in the preferential powering of waves that possess strong surface velocity signatures (i.e. scattering from low to high wavenumbers). Evidently, this process can occur in the reverse, and therefore in order to determine if the haloes are indeed caused by mode mixing, we must understand how acoustic waves are scattered by magnetic fields.

Through simulations of the interactions between solar waves and sunspots and models of plage, we have demonstrated that the high to low modal order scattering channels are favored. With increasing frequency and consequently, decreasing wavelength, a growing number of modes are scattered by the sunspot, thereby rendering the enhancements most visible around the high-frequency parts of the spectrum. The haloes obtained from the simulations are on the same order of magnitude but weaker than those observed. We also present observational evidence to support this theory: observations of AR 9787 show that with increasing wavenumber, the extent of the halo effect is seen to increase dramatically, in line with theoretical expectation.

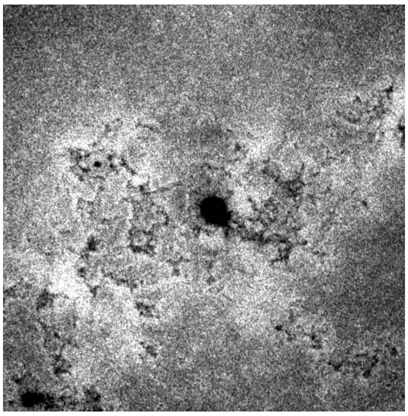

Fig. 169: Power of solar oscillations around Active Region 9787 in the frequency range 5 – 6 mHz measured by SOHO/MDI. The saturated grey scale is such that white corresponds to a power enhancement of 60 % with respect to the quiet Sun and black a power reduction of 40 %. Strong power enhancements (haloes) are seen to envelop the magnetic regions (mostly plage). The size of the image is about 700 Mm on each side.

(S. M. Hanasoge)

Convectively-stable solar background models

The Semi-spectral Linear MHD (SLiM) code developed at MPS computes the propagation of small amplitude waves in a given solar atmosphere (magnetized or not). A prerequisite is a quiet-Sun background reference model. Such a reference model must be solar-like, i.e. it should support modes of oscillation (eigenfrequencies and eigenfunctions) that resemble that of the Sun. It must also be stable against convective instability in order for the SLiM to work.

We have constructed several convectively-stable reference solar models. We begin with a standard solar model (Model S) which we stabilize by modifying the pressure gradient. This adjustment affects the eigenfunctions and eigenfrequencies of the waves. We try to minimize these changes by adjusting the sound speed near the surface by a few percent.

The SLiM code has been used to numerically compute the response of a small region near the solar surface, 145 Mm $\times$ 145 Mm horizontally, and from 2.5 Mm above the surface to 25 Mm below the surface. In order to model the forcing of the waves by convection, we included near-surface random acoustic sources that mimic solar granulation. An ad-hoc damping operator is introduced in the equation to simulate wave attenuation. Fig. 170 shows an azimuthally averaged power spectrum of the surface vertical velocity computed by SLiM for a stabilized atmosphere. The agreement is very good between the frequencies in the original solar model and the stabilized model.

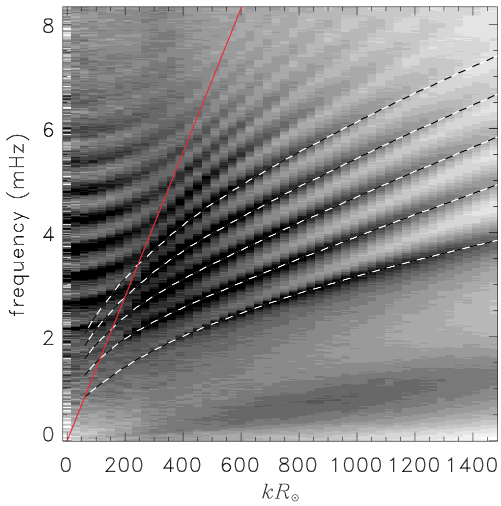

Fig. 170: Power spectrum of solar oscillations simulated by the SLiM code (the grey scale is linear in the logarithm of the power). The white dashed curves show the dispersion relations from a standard solar model (extended Model S). The red line indicates the phase speed above which waves feel the bottom of the simulation box (and should be ignored).

(H. Schunker, R. Cameron, and L. Gizon)

Sunspot models for computational helioseismology

The pressure and density of the plasma inside sunspots are considerably less than that of the surrounding plasma at the same height. Near the surface the fast magneto-acoustic wave speed is several times the value of the quiet-Sun sound speed at the same height. For solar waves, sunspots are not weak perturbations with respect to the quiet-Sun background.

In order to understand the effects of sunspots on solar waves we wish to numerically propagate waves through model sunspots imbedded in a stable reference atmosphere (see above). There are several classes of sunspot models, which were constructed for a variety of reasons, and which are more or less well suited to helioseismic studies. It is useful to examine a number of such models in order be able to test the robustness of the simulation results.

We have considered several semi-empirical models, including an umbral model from Maltby (1986) combined with a penumbral model. This particular model should capture most of the surface properties of the sunspot. The near-surface is particularly important to model well because it is in this layer (top 300 km) that magnetic effects dominate and that mode conversion occurs. Fig. 171 shows a vertical cut through the center of our model sunspot.

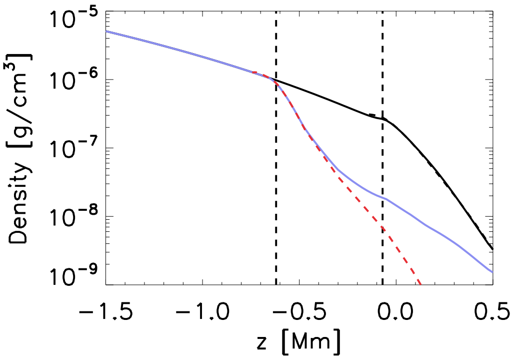

Fig. 171: A semi-empirical sunspot model embedded into a quiet-Sun model. The black curve shows the quiet-Sun density along the axis of the Sunspot, the red dashed curve shows the semi-empirical Maltby model, and the blue curve is the combined atmosphere in which we have embedded the sunspot density changes into the stabilized reference quiet-Sun model.

(R. Cameron and H. Moradi)

Comparing simulations and observations of wave propagation through sunspots

Temporal cross-correlations of SOHO/MDI Dopplergrams were used to image the propagation of solar waves through the sunspot of AR 9787 (Cameron *et al.*, 2008). We used different ridge filters to study separately the f, p_1, and p_2 modes. These cross-correlations were suitably averaged over nine days to reduce stochastic noise.

Three-dimensional numerical MHD simulations of plane wavepackets propagating through various self-similar magnetohydrostatic sunspot models were then performed with SLiM. The initial conditions of the simulations were set up to enable a direct comparison with the observed cross-covariances.

Fig. 172 shows the simulation of the propagation of a p_1 wavepacket (vertical component of wave velocity). The sunspot model has a maximum vertical field of 3 kG at the surface; it is embedded in a Model S background atmosphere, stabilized with respect to convection. At time $t = 0$ the wavepacket is initially located 40 Mm to the left of the sunspot and propagates to the right ($x > 0$). The boundary conditions are periodic in the horizontal directions and there are two sponge layers (not shown here) at the top and at the bottom of the box to avoid the reflection of the waves back into the computational domain.

As shown in Fig. 172, at time $t = 130$ min, the simulation provides a good match in phase and amplitude with the observations. We find that the simulations and the observations agree only when the model sunspot has a peak field strength of 3 kG at the photosphere. The helioseismic observations thus provide a constraint on the magnetic field of the sunspot. This work is a first – but important – step towards the full-

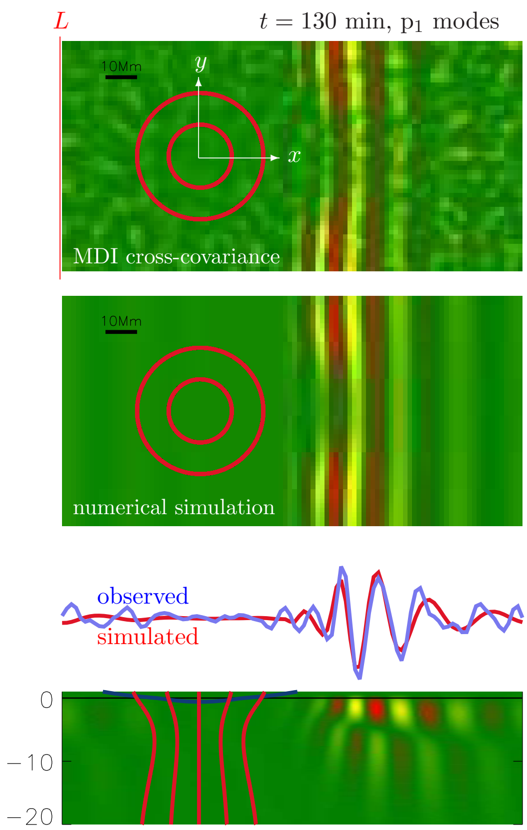

Fig. 172: Comparison between observed and simulated p_1 wavepackets propagating through a sunspot. The top panel shows the observed covariance, C, between the MDI Doppler velocity averaged over the red line (L) at $x = -40$ Mm and the Doppler velocity delayed by $t = 130$ min at any spatial point. The color scale is such that positive values of C are red and negative values are yellow. The two red circles indicate the boundaries of the umbra and penumbra of the sunspot in Active Region 9787. The Doppler observations were filtered to select only the p_1 acoustic modes. To reduce noise, the cross-covariance was averaged over nine days (20 – 28 January 2002) and over angles using the azimuthal symmetry of the sunspot. The middle panel shows the numerical simulation of the vertical component of velocity, v_z. The initial conditions were chosen such that v_z matches the observed cross-covariance in the far field. The bottom panel shows the simulated v_z in the $x-z$ plane through the sunspot. The vertical scale is given in units of Mm. The blue curve shows where the Alfvén speed equals the sound speed.

waveform modeling of sunspots.

It is worth noting that all the sunspot models that we have considered so far (including the model of Fig. 171) need not be deep structures in order to imply the correct travel time shifts.

(R. Cameron and L. Gizon in collaboration with T. L. Duvall Jr. (NASA))

F-mode interaction with thin flux tubes: the scattering matrix

We calculate the scattering effects associated with the interaction of an incoming surface-gravity wave or f mode with a thin magnetic flux tube embedded in a realistically stratified medium (Fig. 173). We find that the dominant scattered wave is an f mode with an amplitude of 1.17% and a phase of 49° relative to the incident wave, compared to the values of 0.13% and 40° estimated from observations. The extent of scattering into high-order acoustic p modes is too weak to be accurately characterized. We recover the result that the amount of scattering is enhanced as (i) the frequency of the incident wave increases and (ii) the flux tube becomes magnetically dominated (Hanasoge *et al.*, 2008).

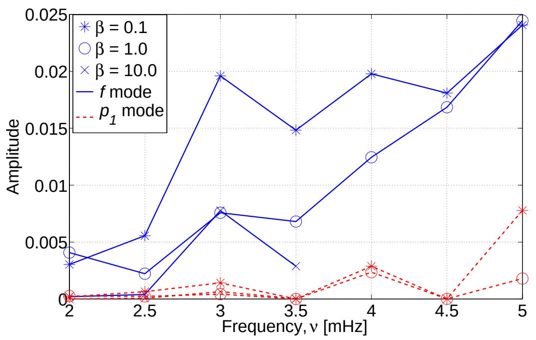

Fig. 173: Amplitudes of f modes (solid lines) and p_1 modes (dashed lines) produced by the scattering of an incoming f mode with a thin flux tube. The scattering amplitudes are shown at various values of plasma-β and wave frequency. The p_1 scattering coefficients are seen to be substantially smaller than the corresponding ones for the f mode.

(L. Gizon in collaboration with S. M. Hanasoge (Stanford), A. C. Birch (CoRA), and T. J. Bogdan (NOAA))

Multiple scattering of waves by stratified flux tubes

We studied the near-field coupling of a pair of flux tubes embedded in a gravitationally stratified environment. The mutual induction of the near-field jackets of the two flux tubes can considerably alter the scattering properties of the system, resulting in sizable changes in the magnitudes of scattering coefficients and interesting trends in the phases. The dominant length scale governing the induction zone turns out to be approximately half the horizontal wave length of the incident mode. Higher-β flux tubes are more strongly coupled than weaker ones, a consequence of the greater role that the near-field jacket modes play in such tubes. It is therefore important to incorporate the effects of multiple scattering when studying mode absorption in plage and interpreting related scattering measurements. That the near-field plays such an important role in the scattering process lends encouragement to the eventual goal of observationally resolving sub-wavelength features of flux tubes using techniques of helioseismology.

(S. M. Hanasoge in collaboration with P. S. Cally (Monash))

A finite-difference code to study non-linear magneto-convection and dynamos

The generation and maintenance of magnetic fields in turbulent plasmas is a phenomenon of interest to many areas of astrophysics. The evolution and interaction of magnetic fields with turbulent convecting plasma is described by the non-linear resistive MHD equations, solutions to which may be non-trivial to extract, depending on the regime of study. In particular, a minimum requirement is the use of precise high-order spatio-temporal schemes to accomplish the computation. To estimate derivatives of various terms, we implement Fast Fourier Transforms along directions where periodicity may apply and sixth-order accurate compact finite differences along directions where the fluid is stratified. Temporal evolution is achieved through the application of a standard fourth-order Runge-Kutta scheme. The code is written according to the MPI 1.0 standard, with the domain distributed along one of the horizontal directions. The code has been validated on a number of tests; some runs with dynamos and isotropic MHD turbulence. Originally written to study linear wave propagation in magnetized solar environments such as sunspots, it has now been extended to compute the fully nonlinear compressible MHD equations.

(S. M. Hanasoge and J. Pietarila Graham)

Observation and modeling of the solar-cycle variation of the meridional flow

We present independent SOHO/MDI observations of the solar-cycle variation of flows near the solar surface and at a depth of about 60 Mm, in the latitude range ±45°. We show that the time-varying components of the meridional flow at these two depths have opposite sign, whereas the time-varying components of the zonal flow are in phase. This is in agreement with previous results. Fig. 174 shows the meridional flow near the surface from SOHO/MDI (time-distance helioseismology) and from GONG (ring-diagram analysis).

We also investigated whether the observations are consistent with a theoretical model of solar-cycle-dependent meridional circulation based on a flux-transport dynamo combined with a geostrophic flow caused by increased radiative loss in the active region belt (the only existing quantitative model). We find that the model and the data are in qualitative agreement, although the amplitude of the solar-cycle variation of the meridional flow at 60 Mm is underestimated by the model (Gizon and Rempel, 2008).

(L. Gizon in collaboration with M. Rempel (HAO, Boulder) and I. González Hernández (NSO, Tucson))

Meridional circulation and global solar oscillations

We investigate the influence of the large-scale meridional circulation on solar p mode frequencies using quasi-degenerate perturbation theory, as proposed by Lavely and Ritzwoller (1992). As input flow we use various (multi-cell) models of stationary meridional circulation obeying the continuity equation. We find that in most cases the meridional circulation leads to negative frequency shifts. Because the meridional circulation is a second order effect, the frequency shifts are tiny (of the order of 0.01 μHz), except for some of the modes for which the shifts may be as big as 1 μHz and potentially detectable. Meridional circulation models with multiple cells have a greater effect on the frequencies (Roth and Stix, 2008).

(M. Roth in collaboration with M. Stix (KIS))

Calculation of spectral darkening and visibility functions for solar oscillations

We performed calculations of spectral darkening and visibility functions for brightness oscillations of the Sun. We used a broad range of the visible and infrared continuum spectrum. The procedure for the calculations of these functions includes the numerical computation of depth-dependent derivatives of the opacity caused by the acoustic modes in the photosphere. We find that opacity effects have to be taken into account because they dominate the violet and infrared part of the spectrum. As a result the visibility functions are negative for those parts of the spectrum. Furthermore, the darkening functions show a wavelength-dependent change of sign for some wavelengths owing to these opacity effects (Nutto *et al.*, 2008).

(M. Roth in collaboration with C. Nutto (KIS), Y. Zhugzhda (IZMIRAN), J. Bruls (KIS), and O. von der Lühe (KIS))

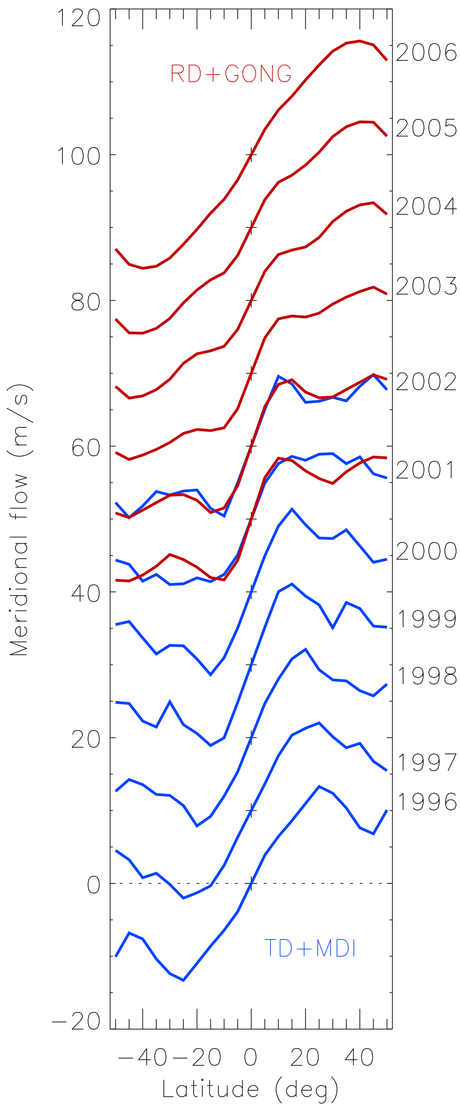

Fig. 174: Anti-symmetric component of the near-surface meridional circulation as a function of latitude during 1996–2006. Each curve corresponds to a different year as indicated on the right. Curves are shifted by multiples of 10 m/s. The blue curves until 2002 show the advection of supergranulation as measured by time-distance helioseismology and MDI full-disk data (2 – 3 months per year) (Gizon and Rempel, 2008). The red curves from 2001 are averages of the meridional flow from the surface down to 7 Mm, inferred by ring-diagram analysis and GONG data (González Hernández et al. 2008). The ring-diagram values are multiplied by a factor of 0.8. Note the local maximum moving towards the equator, from 25° in 1996 to 10° in 2006.

Sub-wavelength resolution imaging of the solar tachocline

We derived expectations for the travel times of waves that interact with thermal anomalies and jets. A series of numerical experiments that involve the dynamic linear evolution of an acoustic wave field in a solar-like stratified spherical shell in the presence of fully three-dimensional time-stationary perturbations are performed. The imprints of these interactions are observed as shifts in the wave travel times, which are extracted from these data through methods of time-distance helioseismology. In situations where at least one of the spatial dimensions of the scatterer was smaller than a wavelength, oscillatory time shifts were recovered from the analyzes, pointing directly to a means of resolving sub-wavelength features (Fig. 175). As evidence for this claim, we presented simulations with spatially localized jets and sound-speed perturbations. We also analyzed one year of SOHO/MDI solar observations to estimate the noise level associated with the time differences. Based on theoretical estimates, Fresnel zone time shifts associated with the (possible) sharp rotation gradient at the base of the convection zone are on the order of 0.01 – 0.1 s, well below the noise level that could be reached with the currently available amount of data (∼ 0.15 – 0.2 s with ten years of data).

(S. M. Hanasoge in collaboration with T. L. Duvall Jr. (NASA))

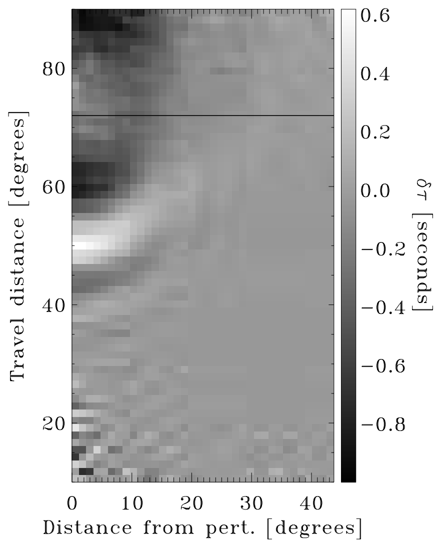

Fig. 175: Simulated travel-time shifts caused by a localized sound-speed perturbation centered at radius $r = 0.55R_\odot$. The vertical axis is the travel distance, also the distance between correlation points. The horizontal axis is the angular distance of the measurement point from the horizontal center of the perturbation. The wavelength of 4 mHz waves at these depths is approximately 70 Mm. The radial size of the perturbation is significantly smaller than the wavelength, a manifestion of which are the variations of the time shifts with travel distance. The horizontal line shows the ray theoretic travel distance for waves whose inner turning point coincides with the radial position of the perturbation.

Dependence of ring-diagram analysis on geometrical mapping

Mapping the solar images onto a local co-moving coordinate system is the first step in any local helioseismology analysis. We considered different types of projections to construct series of mapped GONG Doppler images (tracked data cubes). We then estimated the sub-surface flows from ring diagram analysis (Zaatri *et al.*, 2008). We found that the azimuthal equidistant projection, the transverse cylindrical projection, the gnomonic projection and the stereographic projection produce almost the same velocity fields with standard patch sizes (15° × 15°). The difference between the four projections is more noticeable when larger patches (30° × 30°) are used (Fig. 176).

(M. Roth in collaboration with A. Zaatri (KIS), T. Corbard (OCA, Nice), I. González Hernández (NSO), and O. von der Lühe (KIS))

Fourier analysis of gapped time series

Quantitative helio- and asteroseismology require very precise measurements of the frequencies, amplitudes, and lifetimes of the global modes of stellar oscillation. It is common knowledge that the precision of these measurements depends on the total length, quality, and completeness of the observations. Except in a few simple cases, the effect of the gaps in the data on the measurement precision is poorly understood, in particular in Fourier space where the convolution of the observable with the observation window introduces correlations between different frequencies. We have described and implemented a rather general method to retrieve maximum likelihood estimates of the oscillation parameters, taking into account the proper statistics of the observations (Stahn and Gizon, 2008). Our fitting method applies in complex Fourier space and exploits the phase information. Using numerical simulations, we have demonstrated the existence of cases for which our improved fitting method is less biased and has a much greater precision than when the frequency correlations are ignored (old method). This is especially true for cases where the solar-like oscillations have a low signal-to-noise ratio, where their

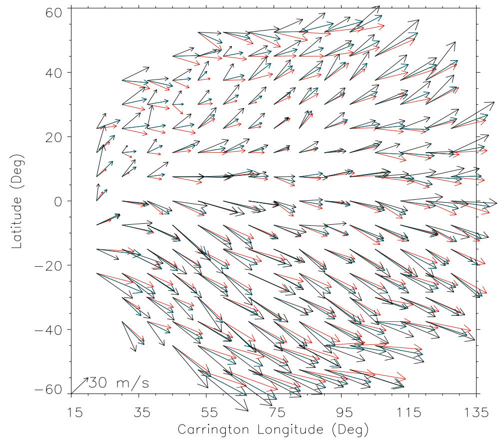

Fig. 176: Daily flow map from ring-diagram analysis of $30^\circ \times 30^\circ$ patches at a depth of 14 Mm. The different colors correspond to different geometrical mappings: transverse equidistant cylindrical (red), azimuthal equidistant (blue), and gnomonic (black).

mode lifetime is significantly shorter than the length of the observation, and for observations with many gaps. Fig. 177 shows an example for solar-like oscillations where the precision on the mode frequency estimate is increased by a very large factor of five, for a duty cycle of 15%. Now that the importance of treating frequency correlations has been demonstrated, we are working on ways to speed up the algorithm in order to take full advantage of this new fitting method.

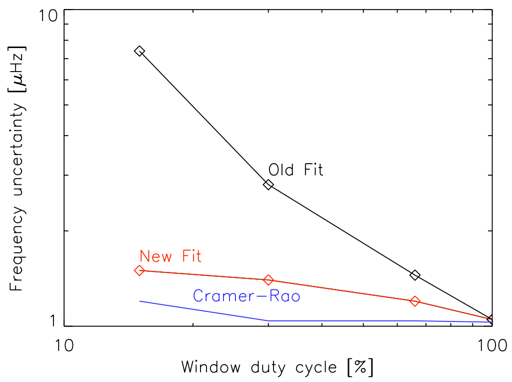

Fig. 177: Uncertainty on estimates of the mode frequency as a function of the window duty cycle as obtained from Monte Carlo simulations using the new fitting method (red) and the old fitting method (black). The blue curve shows the Cramér-Rao lower bounds (formal error bars).

(T. Stahn and L. Gizon in collaboration with T. Hohage (Univ. Göttingen))

PLATO assessment study: ground segment

PLAnetary Transits and Oscillations of stars (PLATO) is one of six medium-class missions in competition for a slot in ESA's Cosmic Vision program. PLATO represents the next technological step beyond the CoRoT and Kepler missions. Its ultimate goal is the detection and, for the first time, the full characterization of many exoplanets, including telluric planets in the habitable zone of Sun-like stars. The characterization of many exoplanetary systems will be achieved thanks to a combination of factors specific to PLATO: the high-precision photometry of a large sample of stars to search for planetary transits, the observation of bright stars that are amenable to high-precision follow-up observations (radial velocities, spectroscopy, Gaia astrometry), and high-cadence long-duration observations for the asteroseismology of planet-host stars (mass, radius, age, rotation, chemical composition).

We led the assessment study of the PLATO ground segment. The role of the PLATO Data Analysis System (PDAS) is to provide ground support for the validation, calibration, and scientific analysis of the PLATO observations. The PDAS will monitor and validate the integrity and quality of the light curves, produce the science-ready calibrated light curves, process the PLATO science data products, and make the PLATO data products available to the science community. The science data products include the transit candidates and their parameters, the asteroseismic mode parameters, the seismically-determined stellar masses and ages. The final PLATO data product is a list of confirmed planetary systems, which will be fully characterized by combining information from the planetary transits, the seismology of the planet-host stars, and the follow-up observations.

The PDAS will remain operational for at least three years after the end of the PLATO space operations phase to enable the confirmation of planets with periods of up to three years. If PLATO is selected, MPS is expected to be the overall leader of the PDAS and thus will play a major role in PLATO.

(L. Gizon)

HELAS Local Helioseismology Network Activity

The European Helioseismology and Asteroseismology Network (HELAS) is a Coordination Action funded by the European Union under the Sixth Framework Programme. The main goals of the HELAS Local Helioseismology Network Activity are to consolidate this field of research in Europe, organize scientific workshops, and facilitate the distribution of observations and data analysis software (Schunker and Gizon, 2008; Schunker *et al.*, 2008).

The MPS hosts the HELAS local helioseismology web site at http://www.mps.mpg.de/

projects/seismo/NA4/, maintained by H. Schunker. The web site now includes outreach material, pre-processed observational data, tools to analyze the observations and modeling tools. The observations are selected from the instruments SOHO/MDI, GONG, MOTH, IVM and SFT. The data analysis software tools consist of ring-diagram, holography, and time-distance codes that operate on the observations provided. A web interface for the computation of travel-time sensitivity kernels was designed by Y. Saidi and is available from the above web site. The modeling tools calculate sunspot models, flux tube models, solar atmospheres, and the SLiM wave propagation simulator. All this is available for download directly from the web site. The HELAS local helioseismology network held a successful international workshop in January 2008 in Freiburg, where the observations of AR 9787 provided on the web site were analyzed by the participants.

(L. Gizon, M. Roth, Y. Saidi, H. Schunker, and the HELAS collaboration)

Book “Helioseismology, Asteroseismology, and MHD Connections”

This Springer volume (Gizon *et al.*, 2008, Fig. 178), reprinted from the journal *Solar Physics*, presents a timely snapshot of the state of helio- and asteroseismology in the era when SOHO/MDI is about to be replaced by SDO/HMI and CoRoT is yielding its first long-duration light curves of thousands of stars. It was inspired by two seminal conferences, HELAS II (organized by MPS in Göttingen in 2007) and SOHO19/GONG 2007, and was open for general submission on the core topics of these conferences. Three papers describing the current status of asteroseismology, global helioseismology, and local helioseismology were specially commissioned for the volume, and these set the context for the other contributions. The talks and posters of the HELAS II conference are available in a separate volume of the *Journal of Physics: Conference Series* (Gizon and Roth, 2008).

(L. Gizon in collaboration with P. S. Cally (Monash) and J. W. Leibacher (NSO))

ERC Starting Grant “Seismic Imaging of the Solar Interior”

The project “Seismic Imaging of the Solar Interior” (SISI) is funded during 2008 – 2012 by the European Research Council (ERC) through a 2007 Starting Grant to L. Gizon. Its aim is to support the scientific analysis and the interpretation of the current and the

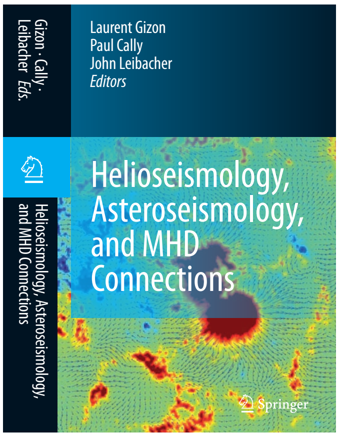

Fig. 178: “Helioseismology, Asteroseismology, and MHD Connections,” ISBN-13: 978-0387894812.

upcoming (SDO/HMI) space data for helioseismology. The broad science objective of SISI is to search for the root causes of solar magnetic activity by establishing physical relationships between internal solar properties and the various components of magnetic activity in the solar atmosphere. One particular goal is to image the subsurface structure of sunspots using SDO data and numerical simulations of the propagation of magneto-acoustic waves. A dedicated supercomputer has been set up at the MPS to address the science objectives of SISI. The SISI compute cluster has 160 CPU cores and over 1 TB of memory, distributed among five identical compute servers (octet quad-core x86-64, 256 GB memory). Compute nodes use a fast InfiniBand communication network that supports the execution of parallel applications based on the MPI standard. The GDC-SDO file servers (see below) are connected to the SISI compute nodes via InfiniBand too.

(L. Gizon)

German Data Center for SDO

The Solar Dynamics Observatory (SDO) is NASA’s most important solar physics mission of this coming decade and will be launched no later than January 2010. The German Data Center (GDC) for SDO, hosted by MPS, will archive, manage, and process all the relevant Level 1 Helioseismic and Magnetic Imager (HMI) data for helioseismology and smaller selected Atmospheric Imaging Assembly (AIA) data sets. This project, funded by the German Aerospace Center (DLR), commenced in August 2007 and will continue until at least the end of 2012. This project is made possible through a close collaboration with Stanford University, USA.

The GDC is now operational (Fig. 179). The GDC has a total online high-density storage capacity of 192 TB (4 Sun Fire servers) supported by 24 AMD CPU cores and extremely fast throughput rates. A preprocessing server (HP Proliant with 8 quad-core AMD processors, 256 GB RAM) will be used to prepare SDO data for scientific analysis. Furthermore, a fast InfiniBand network connects this preprocessing machine to the storage area network described above. The GDC facilities are connected to the SISI compute cluster via the fast network. An additional tape library with 224 slots and LT0-4 tape drives delivers 180 TB of storage capacity. The Data Record Management System (DRMS) is software used to handle all aspects of SDO data management. The Pegasus workflow management system (ISI, Univ. Southern California), along with the CONDOR job scheduler and GLOBUS grid technologies, will be used to automate the GDC data processing workflows.

Fig. 179: German Data Center for SDO. Left: file servers, preprocessing server, network switches, and ERC SISI compute cluster. Right: tape library.

(L. Gizon, R. Burston, and Y. Saidi in collaboration with P. H. Scherrer (Stanford) and E. Deelman (Univ. Southern California))

Helioseismology with Solar Orbiter

Solar Orbiter, ESA's next mission to study the Sun, is one of six medium-class missions in competition for a slot in ESA's Cosmic Vision program. With a launch in 2015, the extended mission would last until 2024. The most interesting aspects of the mission for helioseismology reside in the unique vantage points from which the Sun will be viewed. The spacecraft will use multiple gravity assist manoeuvres at Venus and Earth to reach its science orbit after a cruise phase of about 3.4 years. The orbit design will include two main characteristics, both of which offer novel perspectives for helioseismology. First, Solar Orbiter will make observations away from the ecliptic plane to provide views of the Sun's polar regions. The inclination of the spacecraft's orbit to the ecliptic will incrementally increase at each Venus swing-by manoeuvre to reach at least 30° toward the end of the mission. Second, Solar Orbiter will cover a large range of spacecraft-Sun-Earth angles. In combination with data collected from the ground or near-Earth orbit, Solar Orbiter will thus mark the advent of stereoscopic helioseismology. One important goal is to gain a better understanding of solar activity and variability by probing the solar interior at higher latitudes and larger depths, well beyond what can be achieved with Earth-side observations alone.

(L. Gizon and J. Woch)

Perturbations on spherically symmetric space-times

We linearized the equations of General Relativity about vacuum spherically symmetric background models. The first-order perturbation variables neatly decouple which greatly assists in solving the partial differential equations (Burston and Lun (2008); Burston, 2008). Furthermore, this provides an invaluable tool for learning about how such background models respond to various matter perturbations, i.e. how the modes of oscillation behave. The inclusion of a non-vacuum background model, a highly non-trivial task, would be useful for studying stellar models.

(R. Burston)

Detecting solar g modes with ASTROD

The direct detection of solar internal gravity modes, or g modes, promises to be one of the most important discoveries to probe the deep solar interior. Traditional techniques, that measure motions at the surface of the Sun, are nearing noise levels with still no evidence for individual g modes found.

New technologies propose to search for the signature of solar g modes in the gravitational field of the Sun. There are currently two major efforts to detect low-frequency gravitational effects, the Astrodynamical Space Test of Relativity using Optical Devices (ASTROD) and the Laser Interferometer Space Antenna (LISA).

Given the most recent g mode surface amplitude estimates, both observational and theoretical, it is unclear whether LISA will be capable of successfully detecting these modes. We studied the prospects of detecting g modes using ASTROD for frequencies less than 400 μHz (Burston *et al.*, 2008). We find that ASTROD may be better suited for g-mode detection than LISA as its sensitivity curve is shifted towards lower frequencies with the best sensitivity occurring in the range 100 – 300 μHz (Fig. 180).

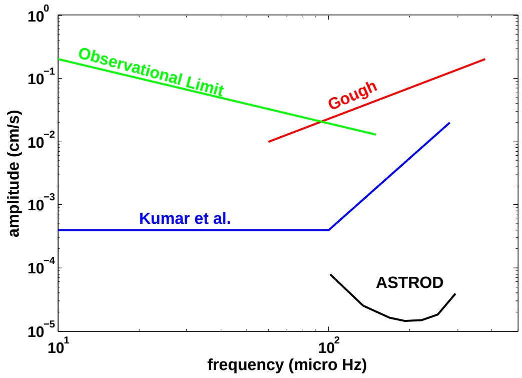

Fig. 180: Comparison of surface radial velocity amplitudes for quadrupole g modes. Shown are theoretical estimates reproduced from Gough (1985) (red curve) and Kumar et al. (1996) (blue curve). The green curve is an observational upper limit from GOLF. The black curve is the ASTROD detection level assuming a one year integration time and a spacecraft orbiting at 0.4 AU.

(R. Burston and L. Gizon in collaboration with T. Appourchaux (IAS) and W.-T. Ni (Purple Mountain Observatory, China))

VI. International Max Planck Research School on Physical Processes in the Solar System and Beyond at the Universities of Braunschweig and Göttingen

Übersicht / Overview

Die “International Max Planck Research School on Physical Processes in the Solar System and Beyond at the Universities of Braunschweig and Göttingen” (Solar System School) wurde 2002 als gemeinsame Inititative des Max-Planck-Instituts für Sonnensystemforschung in Katlenburg-Lindau und der physikalischen Fakultäten der Universität Göttingen (Institut für Astrophysik, Institut für Geophysik) und der Technischen Universität Braunschweig (Institut für Geophysik und Extraterrestrische Physik, Institut für Theoretische Physik) gegründet. Sie bietet in- und ausländischen Studierenden optimal Möglichkeiten, auf dem Gebiet der Physik des Sonnensystems zu promovieren.

Die Schule bietet ein forschungsintensives dreijähriges Promotionsstudium. Voraussetzung ist ein Diplom oder ein Master of Science in Physik oder einem verwandten Fachgebiet. Der Doktorgrad kann an den beteiligten Universitäten Braunschweig oder Göttingen oder an der Heimatuniversität angestrebt werden.

Das Lehrprogramm beinhaltet den gesamten Bereich des Sonnensystems von kleinen Körpern über die Planeten bis zur Sonne. Es ermöglicht eine breite, interdisziplinäre und fundierte wissenschaftliche Ausbildung. Das wissenschaftliche Programm wird durch Kurse in numerischer Physik, Weltraumtechnologie, Projektmanagement, wissenschaftlichem Schreiben und Präsentationstechniken ergänzt. Das Lehrangebot ist in englischer Sprache.

Die Forschungsprojekte der Doktorandinnen und Doktoranden beinhalten kleine Körper im Sonnensystem wie Kometen und Asteroiden, das Innere, die Oberflächen, Atmosphären und Magnetosphären der verschiedenen Planeten, das Innere der Sonne, ihre Atmosphäre von der Photosphäre bis zur Korona, den Sonnenwind und die Heliosphäre. Die Forschungsmethoden reichen von Instrumentierung und Beobachtung über Datenanalyse und Interpretation zu numerischen Simulationen und theoretischer Modellierung. Die Studierenden werden dabei von erfahrenen Wissenschaftlern betreut.

Im Jahr 2008 nahmen insgesamt 65 Doktoranden an der Schule teil, davon haben 12 neu mit ihren Doktorarbeiten begonnen und 16 haben ihre Promotion erfolgreich abgeschlossen. Die Teilnehmer kamen aus insgesamt 26 Ländern. Zwei Drittel der Studierenden sind ausländischer Nationalität. Der Anteil der Frauen beträgt zirka 30 Prozent.

The “International Max Planck Research School on Physical Processes in the Solar System and Beyond at the Universities of Braunschweig and Göttingen” (Solar System School) was founded in 2002 as a joint venture of the Max Planck Institute for Solar System Research with the University of Göttingen (Institute of Astrophysics, Institute of Geophysics) and the Technical University Braunschweig (Institute of Geophysics and Extraterrestrial Physics, Institute of Theoretical Physics).

The School offers graduate students from many countries attractive conditions for education and research on all aspects of solar system science in a 3-year PhD program. A prerequisite is a diploma or masters degree in physics or a related field. The PhD degree can be obtained either from the Universities of Braunschweig or Göttingen or the home university of the student.

The program covers the full range of physics inherent in the rapidly growing field of solar system science from geophysics and planetary science to solar physics, as well as the underlying fundamental physics. It ensures a broad, interdisciplinary, and well-founded education for a career in science. The science program is complemented by training in computational physics, space technology, project management, scientfic writing and presentation and other skills.

High-profile space missions and projects for ground-based instruments, data analysis as well as theoretical and large-scale numerical modeling provide a wide range of research possibilities for PhD students. Re-

Fig. 181: Die Studentinnen und Studenten der Solar System School während eines Seminartags an der Technischen Universität Braunschweig im Februar 2008 / The students of the Solar System School during a seminar day at the Technical University Braunschweig in February 2008

search subjects include the small bodies in the solar system like comets and asteroids, the interiors, surfaces, atmospheres and magnetospheres of the various planets, the interior of the Sun, its atmosphere from the photosphere to the corona, the solar wind and the heliosphere. Methods of research include instrumentation, obvservations, data analysis and theoretical modeling.

In 2008 altogether 65 students took part in the program, from which 12 started with their PhD studies and 16 successfully finished their PhD. The students came from 26 countries. Two thirds were of foreign nationality and one third were female.

http://www.solar-system-school.de

Vorstand / *Chair*

U. Christensen (MPS), J. Blum (Technische Universität Braunschweig), S. Dreizler (Universität Göttingen), K.-H. Glassmeier (Technische Universität Braunschweig), F. Kneer (Universität Göttingen), U. Motschmann (Technische Universität Braunschweig), D. Schmitt (MPS, Koordinator/Coordinator), S. K. Solanki (MPS, Vorsitz/Chair), A. Tilgner (Universität Göttingen)

Lehrveranstaltungen / *Lectures*

Astrobiology Lecture Course Network, WiSe 2007/2008 (Brack et al.)

Einführung in die Physik des Sonnensystems, SoSe 2008 (Christensen et al.)

Wavelet analysis, from the line to the two-sphere, 8 – 9 May 2008 (Antoine)

Time and Self Management, 3 June (Meyer-Ross)

Project Management, 3 – 4 June 2008 (Meyer-Ross)

Dynamo Theory, 5 June 2008 (Schmitt)

Hydrodynamics, 21 – 25 July 2008 (Ferriz Mas)

Integration of Partial Differential Equations, 6 – 9 October 2008 (Wiegelmann)

Introduction to Solar Physics, 24 – 28 November 2008 (Solanki)

Solar System Seminar, 14 seminar days with 39 talks by students and 3 tutorial talks by guests (Schmitt)

Abgeschlossene Dissertationen / *Finished PhDs*

Blanco Rodriguez, Julián: Magnetic activity at the poles of the Sun. Institut für Astrophysik, Universität Göttingen, February 2008.

Bößwetter, Alexander: Wechselwirkung des Mars mit dem Sonnenwind: Hybrid-Simulationen mit besonderem Bezug zur Wasserbilanz. Institut für Theoretische Physik, Technische Universität Braunschweig, December 2008.

Işık, Emre: Magnetic flux generation and transport in cool stars. Universität Göttingen, January 2008.

Lee, Kuang Wu: Collisionless transport of energetic electrons in the solar corona. National Central University, Taiwan, June 2008.

Maltagliati, Luca: Investigation of the Martian atmospheric water cycle by the OMEGA mapping spectrometer onboard Mars Express. Technische Universität Braunschweig, April 2008.

Martinecz, Cornelia: The Venus plasma environment: a comparison of Venus Express ASPERA-4 measurements with 3D hybrid simulations. Technische Universität Braunschweig, November 2008.

Matloch, Lukasz: Modelling of solar mesogranulation. Universität Göttingen, March 2008.

Moissl, Richard: Morphology and dynamics of the Venus atmosphere at the cloud top level as observed by the Venus Monitoring Camera. Technische Universität Braunschweig, July 2008.

Paganini, Lucas: Power spectral density accuracy in Chirp Transform Spectrometers. Universität Freiburg, March 2008.

Roussos, Elias: Interactions of weakly or non-magnetized bodies with solar system plasmas: Mars and the moons of Saturn. Technische Universität Braunschweig, February 2008.

Sánchez-Andrade Nuño, Bruno: Observations, analysis and interpretation with non-LTE of chromospheric structures on the Sun. Institut für Astrophysik, Universität Göttingen, February 2008.

Santos, Jean Carlo: Three dimensional magnetohydrodynamic simulations of solar bright points. INPE, Brazil, February 2008.

Sasso, Clementina: Spectro-polarimetry of the solar chromosphere in the He I 10830 Ålines. Universität Göttingen, March 2008.

Schäfer, Sebastian: Spatial and temporal structure of Alfvén resonator waves at the terrestrial plasmapause. Institut für Geophysik und Extraterrestrische Physik, Technische Universität Braunschweig, December 2008.

Tubiana, Cecilia: Characterization of physical parameters of the ROSETTA target comet 67P/Churyumov-Gerasimenko. Technische Universität Braunschweig, October 2008.

Yelles Chaouche, Lotfi: Observational diagnostics of 3D radiation-MHD simulations of solar and stellar atmospheres. Universität Göttingen, July 2008.

Laufende Dissertationen / *Ongoing PhDs*

MPS:

Akhtar, Naseem: Solar coronal plasma simulation (Büchner/Motschmann).

Angsmann, Anne: Structure and dynamics of the ionosphere of Venus (Fränz/Krupp/Woch/Pätzold).

Attie, Raphael: Explosive events in the transition regions and coronal heating (Solanki/Innes).

Bourouaine, Sofiane: Kinetic models including collisions and wave-particle interactions for magnetic structures in the solar corona (Marsch/Glatzel).

Danilovic, Sanja: The fine structure of photospheric magnetic fields: analysis of high resolution spectropolarimetric observations and MHD simulations (Solanki/Lagg/Kneer).

Dasi Espuig, Maria: Solar variability and Earth climate (Krivova/Solanki).

de Patoul, Judith: Stereoscopy and tomography of coronal structures (Inhester/Wiegelmann/Solanki).

Drahus, Michal: Submillimeter radiative transfer and retrieval simulations of cometary atmospheres in the vicinity of the nucleus (Jarchow/Hartogh/Christensen/Dreizler).

El Maarry, Mohamed Ramy: Geochemistry and geologic evolution of the Martian arctic as inferred from the Phoenix mission (Goetz/Markiewicz/Pack).

Feng, Li: Stereoscopy of the solar corona (Wiegelmann/Inhester/Solanki/Dreizler).

Guo, Jingnan: Particle acceleration by 3D solar magnetic reconnection (Büchner/Marsch/Fang).

Hallgren, Kristofer: Mesospheric water vapour: detection of short term variability by ground-based microwave spectroscopy (Hartogh/Jarchow/Lübken).

Javadi Dogaheh, Setareh: Simulation of solar coronal reconnection (Büchner/Glatzel).

Kadowaki, Masanao: Dynamics of dust in the Martian atmosphere (Hartogh/Takahashi).

Kobel, Philippe: Imaging of photospheric magnetic features and SUNRISE filtergraph instrumentation development (Solanki/Gandorfer/Kneer).

Koch, Christian: Extraction of Mercury's topography and its time dependent variations from laser altimetry data (Christensen/Müller).

Li, Xianyi: Wideband-CTS development (Hartogh/Reindl/Ahlers).

Lippi, Manuela: The composition of comets as inferred from measured production rates of volatiles (Böhnhardt/Blum).

Maneva, Yana: Generation, propagation and dissipation of Alfvénic turbulence in the solar corona and its role in coronal heating and solar wind acceleration (Marsch/Glatzel).

Meling, Martin: Ground- and space-based observation of solar magnetism (Solanki/Gandorfer/Lagg/Dreizler).

Müller, Anna L.: Properties of the Kronian magnetosphere from energetic particle measurements (Krupp/Saur).

Oklay, Nilda: Investigations of solar surface magnetism by high resolution imaging and spectroscopy (Solanki/Gandorfer/Kneer).

Piccialli, Arianna: Investigation of the dynamics of the Venus mesosphere from the Venus Express observations (Titov/Hördt).

Protopapa, Silvia: Surface ice characterization of Pluto and Charon and other Kuiper Belt objects (Böhnhardt/Blum).

Riethmüller, Tino: The SUNRISE filter imager SUFI (Solanki/Gandorfer).

Ruan, Peng: Modeling large-scale coronal structures with advanced models (Wiegelmann/Inhester/Solanki/Marsch/Dreizler).

Saidi, Yacine: Computing and data management systems for helioseismology (Gizon/Appourchaux).

Spjuth, Sofie: Generation of a 3D shape model from OSIRIS images (Sierks/Keller/Glassmeier).

Stahn, Thorsten: Helioseismic probing of solar structure and activity (Gizon/Dreizler/Schmitt).

Tadesse, Tilaye: Nonlinear force-free reconstruction of the coronal magnetic field with advanced numerical methods (Wiegelmann/Inhester/Solanki).

Thalmann, Julia: Evolution of coronal magnetic fields (Wiegelmann/Solanki).

Tian, Hui: Solar transition region and solar wind origin (Marsch/Tu).

Tòthová, Danica: Spectroscopic observations of soft X-ray loops (Innes/Solanki/Kneer).

Vilenius, Esa: Analysis of near infrared data from lunar dayside using the SIR point spectrometer onboard the SMART-1 spacecraft (Mall/Kappas).

Vincent, Jean-Baptiste: From observations and measurements to realistic modeling of cometary nuclei (Böhnhardt/Blum).

Wang, Mingyuan: The Mars ionospheric research based on radar sounding (Nielsen).

Wiese, Manuela Maria: Lunar mineralogy (Mall/Stalder/van den Kerkhof).

Yang, Shangbin: Helicity in flares (Büchner/Zhang).

Yao, Shuo: Interplanetary coronal mass ejections (Marsch/Tu).

Universität Göttingen:

Gui, Bin: Coronal mass ejections and solar energetic particles (Bothmer).

Lutz, Ronny: Key objects in subdwarf B asteroseismology (Dreizler).

Tanriverdi, Vedat: Power spectrum of numerical geodynamos (Tilgner).

Technische Universität Braunschweig:

von Borstel, Ingo: Dust-dust interaction processes studied in dense aerosols using a paul trap (Blum).

Guicking, Lars: Low-frequency waves and the dynamic of the Venusian solar wind interaction region (Glassmeier).

Heyner, Daniel: Mercury's feedback dynamo (Glassmeier/Wicht).

Johansson, Erik: Interaction of extrasolar planets with stellar winds (Motschmann).

Kleindienst, Gero: ULF waves in the Kronian magnetosphere (Glassmeier).

Müller, Joachim: Development of an adaptive grid code for particle-in-cell simulations in plasma physics (Motschmann).

Plaschke, Ferdinand: Dynamic response of the magnetosphere to solar wind variations (Glassmeier).

(D. Schmitt)

VII. Elektroniklabor, Mechanik, Haustechnik, Ausbildung / Electronic Laboratory, Mechanics, Physical Plant, Education

Elektroniklabor

(W. Deutsch, G. Tomasch und Mitarbeiter)

ExoMars

MOMA: Für das Projekt MOMA wurde eine Thermal Vakuum Kammer (Abb. 182) in einem Druckgefäß entwickelt und gebaut um die Umgebungsverhältnisse auf dem Mars zu simulieren. Der Druck in der inneren Kammer ist 10 hPa in einer CO_2 Umgebung mit einem Temperaturbereich von -60° C bis +40° C und in der äußeren Kammer ist ein Druck von 10^{-6} hPa.
(K. Gräbig)

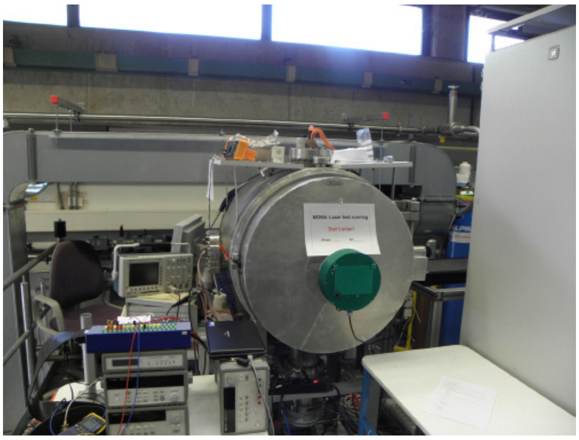

Abb. 182: MOMA Thermal Vakuum Kammer.

Ebenfalls wurde für das Projekt MOMA und SEISmometer eine FPGA Entwicklung in VHDL (Very High Speed Integrated Circuit Hardware Description Language) durchgeführt.
(W. Kühne)

BepiColombo

Eine kommerzielle Dampfphasenlötanlage wurde modifiziert um weltraumtaugliche und jederzeit gut reproduzierbare Lötergebnisse zu erzielen. Entsprechende Lötmusterboards sind an die QA der ESA gesendet worden. Dieses ist der erste Schritt um diesen Prozess durch die ESA für das Projekt BepiColombo und weitere qualifizieren zu lassen.
(A. Loose)

Bela, BepiColombo Laser Alitmeter: Das Projekt wird extern als Industrieauftrag ausgeführt und benötigte vom MPS systemrelevante Mitarbeit um den speziellen Anforderungen eines Weltraumprojektes gerecht zu werden.
(H. Perplies)

SIR2

SIR2 Infrarotspektrometer der Mondmission: Charakterisierung und Verifizierung instrumentspezifischer Eigenschaften vor dem Hintergrund der wissenschaftlichen Datenauswertung.
(H. Perplies)

APS Kamera

Weiterentwicklung der STAR1000 APS Kamera. Erhöhung der Auflösung von 12 auf 14 Bit und Anpassung des Design mit “Rad-Hard Komponenten”. Ein Funktionsmodell des STAR1000 wurde an IAS ausgeliefert.
(St. Werner und R. Enge)

Sunrise

Für das Ballon-Projekt wurden Mechanism Controller entwickelt um Shutter und Filter Wheel in ISLiD betreiben zu können. Die Einheit ist qualifiziert für den Betrieb im Vakuum und Temperaturen von -40° C bis +40° C.

Als Shutter wurde ein kommerzielles System der Firma Nikon modifiziert (Abb. 183). Als Antrieb dient ein Brushless DC Faulhaber Motor, damit ein Betrieb im Vakuum möglich ist. An einem QM wurden Thermal Vakuum Langzeittests mit 500000 Zyklen durchgeführt um die Einheiten zu qualifizieren. Die Shuttereinheiten wurden auch auf ihr Ausgasverhalten durch externe Institutionen untersucht.
(R. Mueller)

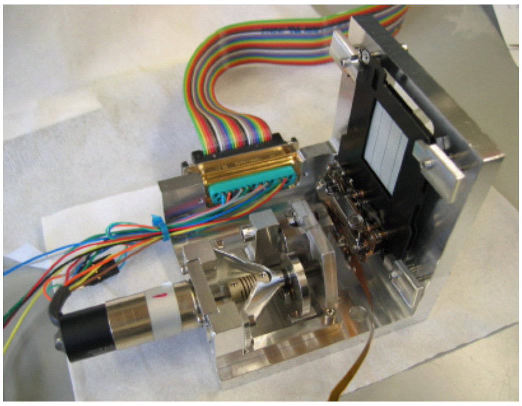

Abb. 183: SUNRISE Shutter.

Entwicklung, Aufbau, Inbetriebnahme und Test einer vakuumtauglichen Power Supply Unit für die SUFI Kamera.
Aufbau, Kalibrierung und Test der Data Storage Subsytem DSS.
(G. Tomasch)

Technologie-Entwicklung im Projekt Sunrise: Windschutz zur thermischen Stabilisierung von Ballon-Gondelsubsystemen

Im Rahmen des Stratosphärenballonprojekts Sunrise wurde ein Verfahren zur Verminderung von Wärmeverlusten beim Ballonaufstieg durch die extrem kalte Tropopausenschicht entwickelt und getestet. Die Tropopause liegt ortsabhängig zwischen 8 und 16 km Höhe. Dort bewirken Lufttemperaturen von -60° C bis -80° C bei erzwungener Konvektion ("Fahrtwind") eine erhebliche Abkühlung von Optik- und Elektronikeinheiten auf Ballongondeln. Dieses kann zum vorübergehenden Ausfall, oder im Extremfall möglicherweise auch zur dauerhaften Beschädigung der Einheiten führen. Kompensation durch elektrisches Heizen erfordert, wie beim Sunrise Testflug 2007 in New Mexico und im Thermalkammertest nachgewiesen, ein Mehrfaches der Leistung, die die Geräte im normalen Betrieb in Flughöhe von 36 km beanspruchen. Der Energie- und Massehaushalt von Ballongondeln kann solche Ressourcen, die nur für den Aufstieg erforderlich wären, nicht vorhalten.
Lösungen durch thermische Isolation, wie z.B. Schaumstoffummantelung und abstrahlarme Oberflächen stehen im Widerspruch zum benötigten Wärmestrahlungsaustausch von Elektronik-Boxen und Radiatoren mit dem kalten Weltraumhintergrund in Flughöhe. Um diese widersprüchlichen Anforderungen für die Aufstiegs- und Flugphase zu lösen, wurde von Sunrise-Mitarbeitern am MPS die Idee eines Windschutzes geboren, der nach dem Aufstieg den thermischen Strahlungsaustausch möglichst nicht behindern soll.
Für einen Versuchsaufbau wurde die gleiche Polyäthylenfolie gewählt, aus der die Ballonhülle besteht. Dieses Material ist weitgehend dehnungs- und reißfest und hat eine Infrarotdurchlässigkeit von ca. 92% für den Wärmehaushalt.
Zum Testen von Schneide-, Kleb- und Handhabungsmethoden und der Beständigkeit bei hohen Luftanströmungsgeschwindigkeiten bis 30 m/s, wurde die Folie auf einen quaderförmigen Rahmen gespannt und für einen Fahrversuch auf ein Pkw-Dach montiert (Abb. 184).

Abb. 184: Ballongondel-Windschutzfolie während eines Anströmversuchs auf Pkw-Dach.

Das Zwischenergebnis war vielversprechend, so dass dem zweiten Schritt eines Testflugs von der schwedischen Weltraum- und Ballonflugbasis ESRANGE auf einer von ESRANGE zur Verfügung gestellten Gondel im Juni 2008 nichts entgegenstand. Die Gondel bestand aus einem würfelförmigen Rahmen mit 70 cm Kantenlänge, der mit der Windschutzfolie bespannt wurde. Im windgeschützten Inneren war auf der Bodenplatte das Qualifikationsmodell des Sunrise Zentralcomputers (ICU), sowie einer Line-of-sight Telemetrie-Einheit (E-Link) von ESRANGE und die Stromversorgung befestigt (Abb. 185). Auf der Gondel oberseite war zum Vergleich eine dem Wind ausgesetzte ICU Dummy Box mit einer Temperaturdatenaufzeichnungseinheit angebracht.

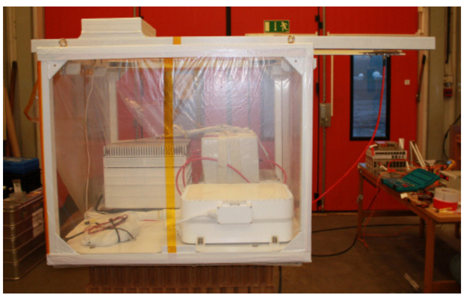

Abb. 185: Sunrise ICU Testfluggondel bei ESRANGE.

Der Flug mit einem 10000 m^3 Stratosphärenballon dauerte 2 Stunden für den Aufstieg und eine Stunde in 30 km Flughöhe. Die dabei gesammelten Messdaten zeigten, dass durch die Windschutzfolie außer der normalen operationellen Leistung keine zusätzliche Heizenergie beim Aufstieg zur Temperierung der Elektronik-Boxen erforderlich war. In Flughöhe wurde das thermale Gleichgewicht nicht negativ beeinflusst, weil genügend Wärme durch die Folie abgestrahlt werden konnte. Die Handhabung und Beständigkeit der mit Kaptonband verstärkten Folie hatte sich als problemlos erwiesen. Damit wurde eine wichtige technologische Vorraussetzung für den im Juni 2009 durchgeführten ersten wissenschaftlichen Sunrise-Flug und auch für zukünftige Ballonmissionen geschaffen.

Abb. 186: Sunrise ICU Testflugballonstart im Juni 2008 von ESRANGE.

Sunrise ist im Juni 2009 erfolgreich geflogen.
(R. Meller)

Mechanik

(B. Chares)

Der Bereich Mechanik unterteilt sich in die mechanische Konstruktion, die Feinmechanikwerkstatt inklusive der Schlosserei und der Lehrwerkstatt für die Ausbildungsberufe Industriemechaniker und Metallbauer. Einer der Schwerpunkte unseres Instituts sind die Entwicklung und Bau von wissenschaftlichen Instrumenten für vorzugsweise Weltraummissionen. Neben dieser direkten Missionsbeteiligung werden Zuarbeiten für Missionsunterhaltungen, Laboraufbauten und Testreihen von Mitarbeitern dieser Bereiche mitentwickelt. Zu den weiteren Aufgaben gehören auch Reparatur- und Instandsetzungsarbeiten (Abb. 187).

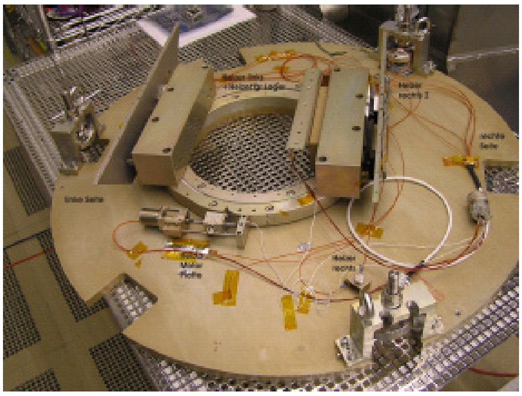

Abb. 187: Instandsetzungsarbeiten an einem Dreh-Schwenktisch für Testeinrichtung im Heizhaus.

Konstruktion

Im Jahr 2008 bestand unsere Konstruktionsabteilung aus 6 Voll- und Teilzeitmitarbeitern. In der Abteilung werden unter Verwendung der CAD Software Pro-Engineer in enger Zusammenarbeit mit Wissenschaftlern mechanische Komponenten für wissenschaftliche Instrumente entwickelt und konstruiert. Für sämtliche Entwicklungsarbeiten werden technische Dokumentationen als Grundlage der Fertigung erstellt. Auch die Fertigungsvergabe im Falle einer Fremdfertigung und die Betreuung dieser liegen in dem Aufgabenbereich der Konstruktion.

Feinmechanik

In der Feinmechanikwerkstatt wurde für sämtliche laufende Projekte und teilweise in Vorbereitung befindliche Projekte mechanische Fertigungsarbeiten geleistet. Für die Planetenabteilung sind folgende Projekte zu nennen. Mit großer Verspätung ist die indische Mondmission "Chandrayaan-1" im Oktober 2008 gestartet. Mit an Bord ist ein Infrarotspektrometer, das mit großem mechanischen Entwicklungs- und

Fertigungsaufwand in unseren Werkstätten mitentwickelt und -gebaut wurde. Die Beteiligungen an der Merkur Mission “BepiColombo”, Mitarbeit an einem Mercury Plasma Particle Experiment, fanden im Jahr 2008 mir einem erfolgreichen Vibrationstest eines Powersupply einen ersten wichtigen Zwischenschritt in der Entwicklungsarbeit (Abb. 188).

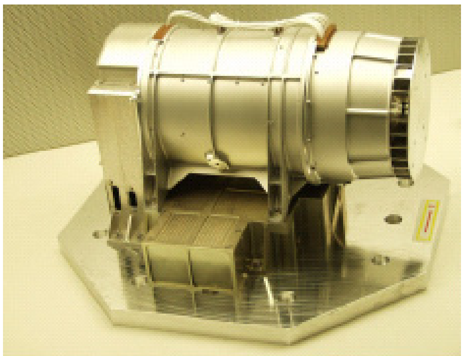

Abb. 188: MSA plus Power Supply in Vorbereitung auf den Vibrationstest.

Institutsbeteiligungen an der geplanten ExoMars Mission der ESA sind ein Instrument zum Detektieren von organischen Molekülen auf dem Mars, genannt MOMA (Abb. 189) und die Entwicklung eines Subsystems für ein Seismometerinstrument (Abb. 190 und Abb. 191).

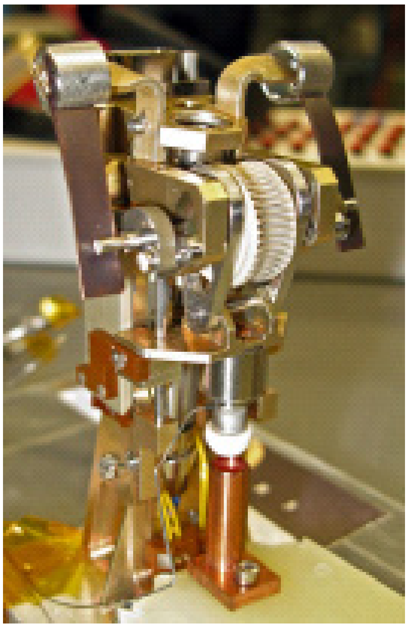

Abb. 189: Tapping Station für das Instrument “MOMA”.

Bei beiden Beteiligungen haben sowohl die Konstruktionsabteilung wie auch die Feinmechanik erhebliche Zuarbeiten geleistet. Für die Sonnenabteilung des MPS ist an erster Stelle Sunrise zu nennen. Das ballongetragene Sonnenobservatorium “Sunrise”, das im

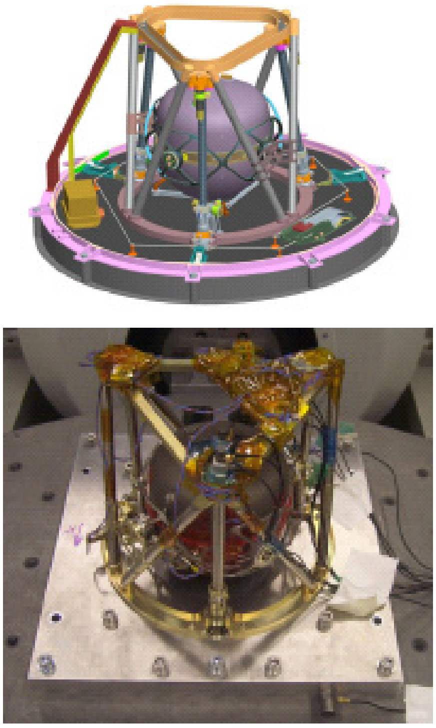

Abb. 190: CAD Darstellung und Vibrationstest des locking device für “Seismometer”, Variante 1.

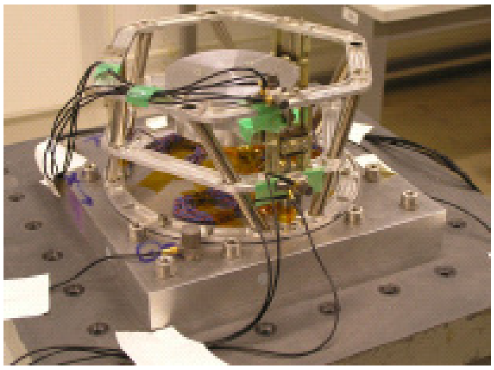

Abb. 191: Locking device für “Seismometer” während eines Vibrationstests, Variante 2.

Jahr 2009 seinen Start vom schwedischen Esrange haben wird, ist im Jahr 2008 aus mechanischer Sicht fertiggestellt worden.

Für die mechanische Arbeiten stehen den Mitarbeitern sowohl konventionelle als auch CNC gesteuerte Maschinen zur Verfügung.

Schlosserei

Neben Wartungs- und Reparaturarbeiten an unseren Test- und Großgeräten werden in der Schlosserei auch Spezialanfertigungen, wie spezielle Schweißkonstruktionen oder besondere Blecharbeiten, für wissenschaftliche Projekte gebaut.

Verwaltung – Teilbereich Haustechnik

(A. Poprawa)

Im Jahr 2008 waren insgesamt 9 Mitarbeiter verschiedener Handwerksberufe beschäftigt. Erfreulich ist es, dass erneut einem jungen Mann eine Ausbildung angeboten werden konnte.

Neben den traditionellen Tätigkeitsfeldern, die in jedem Institut notwendig sind, um die Infrastruktur für wissenschaftliche Forschung sicherzustellen und die bauliche Substanz zu erhalten, haben die Mitarbeiter auch bei Umbaumaßnahmen, Modellen für wissenschaftliche Experimente und der Öffentlichkeitsarbeit ihr Können unter Beweis gestellt.

In verschiedenen Gebäudeteilen wichen die alten Holzdecken einer modernen Brandschutzdecke und diverse Lagerräume wurden durch Nutzungsänderungen zu Testräumen erweitert. Viele Büroräume wurden neu gestrichen, mit neuen Heizkörpern und Regalwänden ausgestattet und erhielten hohe, helle Decken.

Eine weitere Aufgabe, die in letzter Zeit verstärkt wurde, ist der Modellbau für die Öffentlichkeitsarbeit. Bedingt durch die wissenschaftlichen Erfolge steigt die Nachfrage nach Ausstellungen und Führungen, und so wurden verschiedene Modelle angefertigt und im gesamten Bundesgebiet gezeigt. Dazu war es auch notwendig, eine moderne Spritzkabine im Bereich der Malerwerkstatt aufzubauen.

Ausbildung

Rechenzentrum

Im Berichtszeitraum nimmt das Thema Ausbildung weiterhin eine wichtige Bedeutung ein. Insgesamt haben Praktikanten im Rechenzentrum *123* Praktikumswochen absolviert. Es sind teils Schüler-Praktikanten aus Haupt-, Realschulen oder Gymnasien, teils Praktikanten im Rahmen eines Fachhochschul-Studiums, die während ihres 2 bis 22 Wochen langen Aufenthalts im Institut allgemein den Betriebsalltag in einem Rechenzentrum kennen lernen (Schülerpraktikanten), oder anhand von konkreten Projekten praktische Erfahrungen für ihren späteren Beruf erwerben.
Seit dem Jahre 2002 wurde im Rechenzentrum ein Ausbildungsplatz zum Fachinformatiker für Systemintegration eingerichtet. Im Herbst 2003 hat der erste Jugendliche im Rechenzentrum seine 3-jährige Ausbildung als Fachinformatiker, Fachrichtung Systemintegration, begonnen und erfolgreich beendet. Mittlerweile konnte bereits der dritte Jugendliche seine Ausbildung in diesem Beruf beginnen.

(G. Monecke)

Elektroniklabor

Im Bereich Elektronik Lehrwerkstatt lernen acht Elektroniker für Geräte und Systeme. Sie werden in den Grundlagen der Analog- und Digital-Technik ausgebildet und erhalten zusätzlich Betriebsunterricht. Sie werden an allen dafür erforderlichen Messgeräten und Maschinen unterwiesen. Alle jungen Gesellen fanden in den letzten Jahren im Anschluss eine Beschäftigung. Es wurden zahlreiche Schülerpraktika absolviert, sodass sie den ersten Eindruck in dem Beruf des Elektronikers für Geräte und Systeme bekommen konnten. Auch ein Hochschulpraktikant hat im Rahmen seines Studiums die Arbeitswelt eines Elektronikers kennen gelernt.

(O. Matuschek)

Mechanik

Im Jahr 2008 wurden bis zu 16 Lehrlinge gleichzeitig am MPS in dem Beruf Industriemechaniker ausgebildet. In der Schlosserei absolviert derzeit ein Auszubildender seine Ausbildung zum Metallbauer. Die Betreuung der Industriemechaniker erfolgt durch einen Meister als Vollzeittätigkeit. Bei der Betreuung des Metallbauers übt der Meister diese Tätigkeit als Teil seiner Arbeit aus. Den Auszubildenden stehen sowohl herkömmliche als auch wenige CNC-gesteuerte Maschinen zur Verfügung. Damit erhalten sie Grundkenntnisse in allen ihrem Berufsbild entsprechenden Gewerken vermittelt. Außerdem haben im Jahr 2008 noch 15 Schüler- und Studienpraktikanten in unseren Werkstätten ein Praktikum absolviert. Vor der Industrie- und Handelskammer haben folgende Mitarbeiter ihre Facharbeiterprüfung erfolgreich bestanden:

Industriemechaniker 2008: Dennis Hirche, Hendrik Meller, David Römermann, Markus Wolf und Timo Effler.

Hendrik Meller konnte eine Auszeichnung als niedersächsischer Berufsbester der IHK in Empfang nehmen. Weiterhin ist Herr Hendrik Meller als Berufsbester im staatlich anerkannten Ausbildungsberuf "Industriemechaniker Fachrichtung Geräte- und Feinmechanik" auf Bundesebene ausgezeichnet worden.

(B. Chares)

Haustechnik und Verwaltung

Im Bereich der Verwaltung und der Haustechnik wurden im Jahr 2008 insgesamt 5 Auszubildende ausgebildet, davon 4 zu Kaufleuten für Bürokommunikation und 1 Elektroniker für Energie- und Gebäudetechnik. Zwei der Kaufleute absolvieren ihre Ausbildung in Verbindung mit einem weiterführenden berufsbegleitenden Studium zum Bachelor an der VWA Göttingen.

(A. Poprawa)

VIII. Personelle Gliederung / Personnel

Kollegium, wissenschaftliche Mitglieder / Board of directors, scientific members

Direktoren / Directors:

Prof. Dr. Sami K. Solanki
(Geschäftsführender Direktor /Managing director), 01.01.2008 – 31.12.2010
Prof. Dr. Ulrich R. Christensen

Leiter der Selbständigen Nachwuchsgruppe Helio- und Asteroseismologie /
Head, Independent Junior Research Group of the Max Planck Society "Helio- and Asteroseismology":

Dr. Laurent Gizon

Emeritierte wissenschaftliche Mitglieder / Emeritus scientific members:

Prof. Sir Ian Axford, FRS
Dr. Helmut Rosenbauer
Prof. Dr. Vytenis M. Vasyliūnas

Auswärtige wissenschaftliche Mitglieder / External scientific members:

Prof. Dr. Albert A. Galeev, Moskau
Prof. Dr. Johannes Geiss, Universität Bern
Prof. Dr. Karl-Heinz Glaßmeier, Technische Universität Braunschweig
Prof. Dr. Erwin Schopper, Bad Soden

Technischer Geschäftsführer / Technical Manager:

Dr. Iancu Pardowitz (bis 31.03.2008)

Wissenschaftliche und wissenschaftlich-technische Mitarbeiter / Scientific staff

Sonne und Heliosphäre / Sun and Heliosphere

Angestellte auf Planstellen / Permanent staff

Dr. Peter Barthol
Prof. Dr. Jörg Büchner
Dr. Werner Curdt
Dipl.-Ing. Werner Deutsch
Dipl.-Ing. Rainer Enge
Dr. Achim Gandorfer
Dipl.-Ing. Dietmar Germerott
Dr. Bernd Inhester
Dr. Andreas Lagg
Dr. Davina Markiewicz-Innes
Prof. Dr. Eckart Marsch
Dipl.-Ing. Reinhard Meller
Dr. Udo Schühle
Prof. Dr. Manfred Schüssler
Dr. Joachim Woch

Angestellte auf Zeitstellen / Non-permanent staff

Dr. Regina Aznar Cuadrado
Dr. Miroslav Barta (seit 01.11.2008)
Dr. Lokesh Bharti (seit 07.07.2008)
Dr. Juan Manuel Borrero Santiago (seit 01.07.2008)
Dr. Robert Cameron
Dr. Valery Dikarev (bis 31.07.2008)
Dr. Nina Elkina
Dr. Alex Feller
Dr. Johann Hirzberger
Dr. Rene Holzreuter (seit 01.03.2008)
Dr. Volkmar Holzwarth (bis 30.09.2008)
Dr. Emre Isik (21.01.–20.09.2008)
Dr. Jie Jiang (seit 21.07.2008)
Dr. Suguru Kamio (seit 01.12.2008)
Dr. Natalie Krivova
Dr. Maria Madjarska

Dr. Lukasz Matloch (01.04.–30.11.2008)
Dr. Maria Laura Merenda (seit 18.12.2008)
Dr. Anna Pietarila Graham
Dr. Jonathan Pietarila Graham
Dr. Oksana Pleier (seit 15.07.2008)
Dipl.-Ing. Borut Podlipnik
Dipl.-Ing. Hendrik Raasch
Dipl.-Phys. Tino Riethmüller
Dr. Jean Carlo Santos (seit 07.04.2008)
Dr. Clementina Sasso (19.03.–18.09.2008)
Dr. Dieter Schmitt
Dr. Luca Teriaca
Dr. Armin Theissen (bis 31.07.2008)
Dr. Luis Vieira
Dipl.-Ing. Stephan Werner
Dr. Thomas Wiegelmann
Dr. Zhi Xu (bis 31.12.2008)
Dr. Vasily Zakharov (bis 24.09.2008)

Doktoranden und Diplomanden / PhD students

Naseem Akhtar
Raphael Attie
Sofiane Bourouaine
Sanja Danilovic
Espuig Maria Dasi (seit 21.02.2008)
Judith de Patoul (seit 07.01.2008)
Li Feng
Jingnan Guo
Emre Ishik (bis 20.01.2008)
Setareh Javadi Dogaheh
Philippe Kobel
Xiaobo Li
Yana Georgieva Maneva
Martin Meling (bis 30.11.2008)
Maria Laura Merenda (bis 17.12.2008)
Nilda Oklay
Tino Riethmüller
Peng Ruan
Jean Carlo Santos (bis 06.04.2008)
Clementina Sasso (bis 20.01.2008)
Tilaye Asfaw Tadesse (seit 27.02.2008)
Julia Katharina Thalmann
Hui Tian (seit 21.09.2008)
Danica Tòthová
Yang Shangbin (seit 15.02.2008)
Lotfi Yelles Chaouche (bis 04.01.2008)

Planeten und Kometen / Planets and Comets

Angestellte auf Planstellen / Permanent staff

Dr. Hermann Böhnhardt
Dipl.-Ing. Irene Büttner
Dr. Patrick W. Daly
Dipl.-Ing. Arne Dannenberg
Dr. Fred Goesmann
Dr. Paul Hartogh
Dr. Martin Hilchenbach
Dr. Stubbe Hviid
Dr. Christopher Jarchow
Dr. Norbert Krupp
Dipl.-Inf. Oliver Küchemann
Dr. Urs Mall
Dr. Wojcieck Markiewicz
Dipl.-Ing. Henry Perplies
Dr. Reinhard Roll
Dr. Holger Sierks
Dipl.-Ing. Eckhard Steinmetz
Dipl.-Ing. Georg Tomasch
Dr. Johannes Wicht

Angestellte auf Zeitstellen / Non-permanent staff

Dr. Klaus-Michael Aye (bis 29.02.2008)
Dr. Zsofia Bebesi (seit 01.12.2008)
Dr. Ing. Marco Bierwirth (seit 01.04.2008)
Dr. Radoslav Bučík
Dr. Roberto Bugiolacchi (seit 01.08.2008)
Dr. Thibault Jan Cavalié (seit 01.12.2008)
Dr. Borys Dabrowski (seit 01.07.2008)
Prof. Dr. Eduard Dubinin
Dr. Markus Fränz
Edita Georgescu (seit 01.02.2008)
Dr. Walter Goetz
Pablo Gutierrez-Marques
Dr. Nico Hoekzema
Dipl.-Ing. Sebastian Höfner (seit 01.05.2008)
Dr. Kumiko Hori (seit 29.09.2008)
Dr. Reinald Kallenbach
Dr. Jochen Kissel (bis 31.07.2008)
Dipl.-Ing. Ivor Krause
Dr. Elena Kronberg
Dr. Harald Krüger

Dr. Takeshi Kuroda (bis 31.03.2008)
Dr. Ghada Machtoub (seit 10.09.2008)
Dr. Luca Maltagliati (01.05.–31.12.2008)
Dr. Cornelia Martinecz (26.11.–31.12.2008)
Dipl.-Ing. Thorsten Maue
Dr. Alexandre Medvedev
Dr. Richard Moissl (seit 01.10.2008)
Dr. Andreas Nathues
Dr. Kai Nörthemann (seit 01.11.2008)
Dr. Lucas Paganini (seit 01.04.2008)
Dr. Ganna Portyankina (bis 31.01.2008)
Dr. Miriam Rengel (seit 01.01.2008)
Dr. Olaf Roders
Dr. Elias Roussos (07.02.–30.04.2008)
Dr. Hideo Sagawa
Dr. Bruno Sanchez-Andrade Nuno (18.2.-17.5.2008)
Dr. Martin Schrinner (01.02.–31.12.2008)
Dr. Stefan Schröder
Dr. Iouri Skorov (16.06.–31.12.2008)
Dipl.-Ing. Li Song
Dr. Harald Steininger
Dr. Oliver Stenzel
Dipl.-Ing. Istvan Szemerey
Dr. Hellmuth Timpl
Dr. Dmitri Titov
Dr. Johannes Treis (seit 01.02.2008)
Dr. Cecilia Tubiana (seit 01.11.2008)
Dr. Manabu Yamada (seit 27.09.2008)

Doktoranden und Diplomanden / PhD students

Anne Angsmann (seit 01.03.2008)
Megha Upendra Bhatt
Julian Blanco Rodriguez (bis 31.01.2008)
Michal Mateusz Drahus
Prasanta Das (bis 31.07.2008)
Mohamed Ramy El Maarry (seit 26.02.2008)
Armando Enrique Gonzalez Godoy (seit 01.11.2008)
Kristofer Hallgren
Masanao Kadowaki (seit 01.07.2008)
Christian Koch
Xianyi Li
Manuela Lippi
Cornelia Martinecz (bis 25.11.2008)
Richard Moissl (bis 09.07.2008)
Anna Liane Müller (seit 15.01.2008)
Roman Orlik
Arianna Piccialli
Silvia Protopapa
Elias Roussos (bis 27.01.2008)
Bruno Sánchez-Andrade Nuño (bis 10.01.2008)
Piotr Sitek
Sofie Spjuth
Cecilia Tubiana (bis 31.07.2008)
Esa Vilenius (bis 31.05.2008)
Jean-Baptiste Vincent
Mingyuan Wang (bis 30.11.2008)
Piotr Wawer (bis 17.12.2008)
Manuela Maria Wiese

Selbständige Nachwuchsgruppe "Helio- und Asteroseismologie" / Independent Junior Research Group "Helio- and Asteroseismology"

Dr. Raymond Burston
Dr. Shravan Hanasoge (seit 01.10.2008)
Dr. Jason Jackiewicz (bis 20.08.2008)
Dr. Savita Mathur (02.06.–01.09.2008)
Dr. Markus Roth (bis 31.12.2008)
Dr. Hannah Schunker
Dr. Sergei Zharkov (02.10.–31.12.2008)

Doktoranden / PhD students

Yacine Saidi
Thorsten Stahn

Abteilung EDV / Computing department

Leitung /Management: Dr. Iancu Pardowitz

Jens Aigner
Michael Bruns
Lothar Graf
Terrance Ho
Dr. Georg Kettmann
Christine Ludwieg
Daniel Maase (seit 27.06.2008)
Dipl.-Math. Helmut Michels
Godehard Monecke
Adolf Piepenbrink
Jürgen Wallbrecht
Ian Hall (DAWN) (seit 18.08.2008)

Auszubildende / Apprentices:

Daniel Maase (bis 26.06.2008), Lukas Stark (seit 01.09.2008)

Laboratorien / Laboratories

Leitung /Management: Dr. Iancu Pardowitz (bis 31.03.2008)
Ausbilder Elektrotechnik: Olaf Matuschek
Sekretariat: Helga Oberländer

Heiko Anwand (seit 01.04.2008)
Günther Auckthun
Walter Böker
Ulrich Bührke
Andreas Fischer
Dipl.-Ing. Henning Fischer
Klaus-Dieter Gräbig
Dipl.-Ing. Bianca Grauf
Dipl.-Ing. Klaus Heerlein
Jan Heise (seit 01.08.2008)
Manuel-Roland Jünemann (26.01.–31.08.2008)
Heinz Günter Kellner
Tobias Kleindienst
Martin Kolleck
Wolfgang Kühn
Wolfgang Kühne
Dipl.-Ing. Alexander Loose
Olaf Matuschek
Markus Monecke
Dipl.-Ing. Reinhard Müller
Helga Oberländer
Marianne Pulst
Rolf Schäfer
Michael Sperling
Dipl.-Ing. Christoph Stucke (bis 31.03.2008)
Jan Hendrik Wagner (bis 31.08.2008)
Jens Wegner (26.01.–30.04.2008)
Wolfgang Wunderlich

Auszubildende / Apprentices:

Philip Brakel, Nikolai Graf (seit 01.09.2008), Julian Ifland, Manuel-Roland Jünemann (bis 25.01.2008), Tobias Napp, Nicholas Unger, Dustin Vogel, Stefan Wagner, Jens Wegner (bis 25.01.2008), Thomas Wolf (bis 25.01.2008)

Mechanik / Mechanics

Leitung /Management: Bernd Chares
Stellvertreter Feinmechanik: Norbert Meyer
Stellvertreter mechanische Konstruktion: Anita Dullinger
Ausbilder Feinmechanik und Metallbau: Roland Mende
Sekretariat: Beatrix Hartung

Feinmechanik:
Hermann Arnemann, Ernst-Reinhold Heinrichs, Dennis Hirche (seit 26.01.2008), Detlef Jünemann, Fabian Maulhardt (bis 31.12.2008), Hendrik Meller (26.01.–20.08.2008), Roland Mende, Norbert Meyer, David Römermann (26.01.–31.03.2008), Alexander Schmidt (01.03.–31.07.2008), Werner Steinberg, Marcus Wolf (26.01.–31.03.2008)

Schlosserei:
Hans-Joachim Heinemeier

Siebdruck / Laser:
Mathias Schwarz

Dokumentation, Konstruktion / Documentation, mechanical design:
Leitung: Bernd Chares
Dipl.-Ing. Anita Dullinger, Steffen Ebert (bis 29.02.2008), Jan Heinrichs (bis 31.12.2008), Angelika Hilz, Marianne Krause (bis 31.12.2008), Dietmar Oberdorfer, Mona Wedemeier

Auszubildende / Apprentices:
Sascha Adamski, Kevin Brandt (seit 01.09.2008), Dennis Drescher (seit 01.09.2008), André Echtermeyer, Timo Effler (bis 28.01.2008), Christina Fahlbusch, Hauke Fremer (seit 01.09.2008), Nils Henne, Jakob Herbold (seit 01.09.2008), Sven Hilz, Dennis Hirche (bis 25.01.2008), Sascha Kirchhoff, Hendrik Meller (bis 25.02.2008), David Otto, Marius Rinkleff, David Römermann (bis 25.01.2008), Patrick Schenke, Martin Sieber, Peer Strogies, Björn Wemheuer, Sebastian Westphal, Marcus Wolf (bis 25.01.2008)

Verwaltung / Administration

Verwaltungsleiter: Andreas Poprawa
Andrea Macke, Swetlana Alekseenko, Petra Fahlbusch, Aris Thieme (01.05.–31.08.2008),
Christina Thomitzek

Personalbüro / Personell office:
Edith Deisel, Christiane Neu

Buchhaltung / Book-keeping:
Martina Heinemeier, Nadine Teichmann, Andrea Werner

Einkauf / Goods received:
Nadine Ehbrecht, Margitt Elligsen (seit 01.05.2008), Bernhard Vogt

Bibliothek / Library:
Dr. Bernd Inhester (wissenschaftlicher Bibliotheksbeauftragter)
Simone Dietrich (bis 31.03.2008), Andrea Mißling (seit 08.07.2008), Margit Steinmetz

Direktionssekretärinnen / Secretaries of the directors:
Sabine Deutsch, Karin Peschke, Barbara Wieser

Sekretärinnen / Secretaries:
Gerlinde Bierwirth, Carmen Braun (bis 30.06.2008), Jacqueline Bukatz (bis 31.01.2008), Susanne Kaufmann, Julia Müller, Sibylla Siebert-Rust, Ute Spilker, Andrea Vogt, Anja Walowsky, Helga Washausen

Auszubildende / Apprentices:
Jennifer Bartels (Bachelor), Christin Enge (seit 01.09.2008), Jennifer Raabe, Aris Thieme (Bachelor) (seit 01.09.2008)

Technische Dienste / Technical services

Leitung: Andreas Poprawa

Elektro:
Michael Hilz, Mario Reich, Mario Strecker

Auszubildende / Apprentices:
Denis Wirt

Heizung-Sanitär:
Karl-Heinrich Deisel

Tischlerei:
Helge Aue, Martin Heinrich

Gärtner:
Martin Schröter (bis 31.12.2008)

Reinigung / Wäscherei:
Rosemarie Poppe

Küche:
Johannes Kohlrautz, Sylvia Aue, Lilli Dargel, Diana Meyenkoth (bis 31.12.2008), Beate Meyer

it Sonstige Dienste / Other services:
Jürgen Bethe

Baukoordination / Construction coordinator
Margarete Elisabeth Steinfadt (seit 01.11.2008)

Öffentlichkeitsarbeit / Public relations

Dr. Norbert Krupp, Dr. Birgit Krummheuer (seit 01.04.2008), Dr. Bernd Wöbke (bis 30.09.2008)

Redaktion der Instituts-Informationen / Editor of the institute newsletter:
Dr. Martin Hilchenbach

Betreuung der Online Veröffentlichungs- und Vortragsliste / Support of the online publications and presentations list:
Dr. P. W. Daly

Studentische Hilfskräfte und Praktikanten / Student assistant and traineeship:
Jan Koch (01.08.–30.09.2008), Oskar Rene Stangenberg (21.07.–12.09.2008), Stefan Hesse (01.09.–31.12.2008)

IX. Wissenschaftliche Zusammenarbeit und Öffentlichkeitsarbeit / Scientific Collaboration and public relations

Wissenschaftler, die als Gäste längere Zeit am MPS tätig waren / Scientific guests with long-term visits to MPS

(Stipendiaten der MPG, des DAAD, der DFG, der Alexander von Humboldt-Stiftung/Friedrich-Wilhelm-Bessel-Preisträger, Postdocs und Honorarempfänger / Stipend holders of the MPG, the DAAD, the DFG, the Alexander von Humboldt Foundation/Friedrich Wilhelm Bessel Research Award and Postdocs)

Dr. Jaime Araneda, Physics Department, University of Concepción, Chile, 23 June – 8 August 2008. Collaboration with E. Marsch.

Dr. Miroslav Bárta, Astronomical Institute of the Czech Academy of Science, Ondrejov, Czech Republic, 1 November – 31 December 2008. Collaboration with J. Büchner.

Dr. Nikolai Borisov, IZMIRAN, Troitsk, Russia, 16 June – 16 August 2008. Collaboration with M. Fränz.

Dr. Andrzej Czechowski, Space Research Centre, Warsaw, Poland, 31 March – 31 May 2008 and 10 November – 10 December 2008. Collaboration with M. Hilchenbach.

Dr. Nina Elkina, Keldysh Institute of the Russian Academy of Sciences, Moscow, Russia, 1 January – 31 December 2008. Collaboration with J. Büchner.

Dr. Nikolay Ignatiev, Space Research Institute, Moscow, Russia, 14 February – 29 March 2008 and 21 October – 19 December 2008. Collaboration with D. Titov.

Dr. Takeshi Kuroda, Japan Society for the Promotion of Science, Tokyo, Japan, 1 April – 31 December 2008. Collaboration with P. Hartogh.

Kuang-Wu Lee, National Central University, Taipeh, Taiwan, 1 January – 15 February 2008. Collaboration with J. Büchner.

Dr. Shibu Mathew, Udaipur Solar Observatory, India, 1 July – 25 September 2008. Collaboration with S. K. Solanki and N. A. Krivova.

Nozomi Mori, Ochanomizu University, Tokyo, Japan, 1 September – 15 October 2008. Collaboration with D. Schmitt.

Olivier Poch, ENS, Paris, France, 30 February – 4 June 2008. Collaboration with F. Goesmann.

Dr. Anatoly Remizov, Space Research Institute, Russian Academy of Sciences, Moscow, Russia, 15 April – 15 October 2008. Collaboration with M. Hilchenbach and N. Krupp.

Mr. Eugene Shalygin, Kharkiv University, Ukraine, 15 July – 31 August 2008. Collaboration with D. Titov.

Ms. Savindri Pramodya Talgodapitiya, University of St. Andrews, UK, 30 June – 15 September 2008. Collaboration with L. Gizon.

Mingyuan Wang, Shanghai Astronomical Observatory, Shanghai, P. R. China, 1 January – 1 December 2008. Collaboration with E. Nielsen.

Shangbin Yang, National Astronomical Observatory, Bejing, China, 15 February – 31 December 2008. Collaboration with J. Büchner.

Wissenschaftler, die als Gäste nur kurzzeitig am MPS tätig waren / Scientific guests with short-term visits to MPS

Dr. Vincenzo Andretta, INAF-OACN, Napoli, Italy, 23 June – 4 July 2008. Collaboration with L. Teriaca.

Dr. Yoshihiro Asano, Tokyo Institute of Technology, Tokyo, Japan, 28 April – 2 May 2008. Collaboration with P. Daly.

Dr. Stefano Bagnulo, Armagh Observatory, Armagh, Northern Ireland, 1 August – 16 August 2008 and 18 November – 2 December 2008. Collaboration with H. Boehnhardt.

Dr. Dipankar Banerjee, IIA, Bangalore, India, 2 June – 13 June 2008. Collaboration with L. Teriaca.

Prof. Luis Barrera, UMCE, Santiago de Chile, 28 February – 15 March 2008. Collaboration with H. Boehnhardt.

Prof. Alexander Basilevsky, Vernadsky Institute, Moscow, Russia, 1 August – 1 September 2008. Collaboration with D. Titov.

Dr. Aaron C. Birch, Colorado Research Associates, Boulder, CO, USA, 19 April – 3 May 2008 and 2 December – 19 December 2008. Collaboration with L. Gizon.

Samira Biskri, Inst. theor. Phys., University of Louvain, Belgium, 13 July – 27 July 2008. Collaboration with B. Inhester.

Dr. Richard Bogart, Stanford University, Stanford, CA, USA, 7 December – 10 December 2008. Collaboration with L. Gizon.

Prof. Dieter Breitschwerdt, Institute of Astronomy, University of Vienna, Austria, 14 July – 18 July 2008. Collaboration with M. Rengel.

Jean-Philippe Combe, The Bear Fight Center, Winthrop, WA, USA, 10 April – 12 April 2008. Collaboration with U. Mall.

Dr. Bhola N. Dwivedi BHU, Varanasi, India, 3 June – 20 June 2008. Collaboration with W. Curdt.

Ms. Nadezda Evdokimova, Space Research Institute, Moscow, Russia, 10 December – 20 December 2008. Collaboration with D. Titov.

Dr. Shravan Hanasoge, Stanford University, Stanford, CA, USA, 24 September – 29 September 2008. Collaboration with L. Gizon.

Dr. Peter Hoyng, SRON, Utrecht, The Netherlands, 4 February – 8 February 2008, 25 March – 28 March 2008, 21 April – 25 April 2008, 25 August – 29 August 2008, and 27 October – 31 October 2008. Collaboration with D. Schmitt and M. Schrinner.

Dr. Arpad Kis, Geodetic and Geophysical Research Institute of the Hungarian Academy of Sciences, Sopron, Hungary, 22 June – 29 June 2008. Collaboration with P. Daly.

Dr. Gábor Kovács, Createch Kft. 1025 Budapest, Hungary, 27 April – 5 May 2008. Collaboration with U. Mall.

Julius Koza, Slovak Academy of Science, Tatranska Lomnica, Slovakia, 19 November – 5 December 2008. Collaboration with J. Hirzberger and A. Pietarila Graham.

Dr. Maria Loukitcheva, State University, St. Petersburg, Russia, 15 September – 24 September 2008. Collaboration with S. K. Solanki.

Prof. Gottfried Mann Astrophysikalisches Institut, Potsdam, Germany, 8 December – 12 December 2008. Collaboration with E. Marsch.

Dr. Ajay Manglik, National Geophysical Research Institute, Hyderabad, India, 1 October – 29 October 2008. Collaboration with U. Christensen.

Dr. Karen Meech, IFA, Honolulu, Hawaii, USA, 1 September – 9 September 2008. Collaboration with H. Boehnhardt.

Prof. Antonius Otto, University of Alaska, Fairbanks, USA, 5 January – 26 January 2008 and 24 August – 5 September 2008. Collaboration with J. Büchner.

Ms. Natalia Gomez Perez, Carnegie Institution, Washington, USA, 1 May – 31 May 2008. Collaboration with J. Wicht.

Dr. Colin Snodgrass, ESO, Santiago, Chile, 14 September – 8 October 2008. Collaboration with H. Sierks.

Dr. Gerd Sonnemann, IAP Kühlungsborn, Germany, 22 September – 22 October 2008. Collaboration with P. Hartogh.

Prof. Chuanyi Tu, Department of Geophysics, Peking University, Beijing, China, 2 November – 30 November 2008. Collaboration with E. Marsch.

Dr. Sergey Ustyugov, Keldysh Institute of Applied Mathematics, Moscow, Russia, 27 October – 17 November 2008. Collaboration with L. Gizon.

Dr. Lidong Xia, Department of Space Science and Applied Physics, Shandong University, Weihai, China, 2 November – 30 November 2008. Collaboration with E. Marsch.

Dr. Erdal Yiğit, University College London, UK, 12 November – 12 December 2008. Collaboration with P. Hartogh.

Längere Aufenthalte von Wissenschaftlern des MPS an anderen Instituten / Long-term visits of MPS scientists to other institutes

Dr. Lokesh Bharti, Astronomy & Astrophysics Lab., Department of Physics, University College of Science, Mohanlal Sukhadia University, Udaipur, India, 5 December – 27 December 2008.

Dr. Hermann Boehnhardt, Institute for Geophysics and Planetology, Tel Aviv, Israel, 25 May – 1 June 2008.

Prof. Ulrich Christensen, Kauli Institute for Theoretical Physics, Santa Barbara, CA, USA, 22 June – 20 July 2008.

Dr. Laurent Gizon, NorthWest Research Associates, CoRA Division, Boulder, CO, USA, 15 July - 2 August 2008. Institute of Space and Astronautical Science (ISAS/JAXA), Sagamihara, Japan, 17 November – 22 November 2008.

Kristofer Hallgren, ALOMAR, Andoya, Norway, 6 April – 22 April 2008.

Dr. Martin Hilchenbach, CNRS-LPC2E, Orléans, France, 21 September – 29 September 2008 and 22 November – 30 November 2008.

Dr. Johann Hirzberger, Swedish Solar Telescope, La Palma, Spain, 19 June – 5 July 2008.

Dr. Andreas Lagg, NAOJ, Tokyo, Japan, 21 July – 20 October 2008.

Dr. Urs Mall, ISRO Satellite Centre, Bangalore, India, 16 February – 22 February 2008. 20 May – 25 May 2008. 15 September – 20 September 2008. 25 September – 30 September 2008. 20 October – 24 October 2008.

Dr. Hannah Schunker, Colorado Research Associates, Boulder, USA, 5 August – 21 August 2008.

Dr. Holger Sierks, UCLA, Los Angeles, USA, 31 March – 7 April 2008.

Dr. Luca Teriaca, IIA, Bangalore, India, 13 June – 20 June 2008.

Prof. Vytenis Vasyliūnas, Center for Atmospheric Research, University of Massachusetts Lowell, USA, 16 April – 26 April 2008.

Projekte in Zusammenarbeit mit anderen Institutionen / Projects in collaboration with other institutions

Die Art der Zusammenarbeit des MPS mit anderen Institutionen ist im einzelnen ziemlich unterschiedlich. Die folgende Aufzählung soll nur einen kurzen Überblick geben. /The cooperation of MPS with other institutions is extensive and varied. The following list only provides a brief overview.

A Deep Search for Biological Signatures on Mars critically supporting the Herschel mission
P. Hartogh in collaboration with M. Mumma, G. Villanueva, (Goddard Space Flight Center, Greenbelt, USA); R. E. Novak (Iona College, New Rochelle, USA); H. U. Käufl, (European Southern Observatory, Munich, Germany).

Analysis and calibration of historical Ca II spectroheliograms
N. A. Krivova in collaboration with I. Ermolli (INAF Osservatorio Astronomico di Roma, Italy).

A nanoflare model for active region radiance: application of artificial neural networks
D. E. Innes and S. K. Solanki in collaboration with M. Bazarghan, H. Safari (Zanjan University, Iran).

A New Generation Active Region Model
T. Wiegelmann, J. Thalmann, and T. Tadesse in collaboration with P. MacNeice (GSFC, NASA, Washington, USA); D. Spicer (GSFC, NASA, Washington, USA); P. Schuck (NRL, Washington, USA); K. Olson (Drexel University, Philadelphia, USA).

A search for dust clouds near the solar system with the Wilkinson Microwave Anisotropy Probe
H. Krüger and S. K. Solanki in collaboration with D. Schwarz, V. Dikarev (Fakultät für Physik, Universität Bielefeld, Germany); A. V. Krivov (Friedrich Schiller Universität Jena, Germany).

ASTROD I (Astrodynamical Space Test of Relativity using Optical Devices I), *a class-M fundamental physics mission proposal submitted to ESA's Cosmic Vision Programme*
L. Gizon and R. Burston in collaboration with T. Appourchaux (IAS, Orsay, France); W.-T. Ni (Purple Mountain Observatory, Nanjing, China).

Astrophysical spectropolarimetry
A. Gandorfer in collaboration with M. Bianda (IRSOL, Switzerland).

BepiColombo – BELA (Laser Altimeter)
M. Hilchenbach, U. Christensen, R. Kallenbach, R. Roll, H. Fischer, and C. Koch in collaboration with N. Thomas, W. Benz, K. Gunderson, K. Seiferlin (Physikalisches Institut, Universität Bern, Switzerland); T. Spohn, E. Hauber, H. Michaelis, J. Oberst (DLR – Institut für Planetenforschung, Berlin, Germany); G. Beutler (Astronomy Institute, Universität Bern, Switzerland); C. Fallnich (Laser Zentrum Hannover, Germany); D. Giardini (Institute of Geophysics/Swiss Seismological Service, Swiss Federal Institute of Technology, (ETHZ), Zurich, Switzerland); O. Groussin (Department of Astronomy, University of Maryland, College Park, USA); L. Jorda, P. Lamy (Laboratoire d'Astrophysique de Marseille, Marseille, France); L.-M. Lara, J. J. Lopez-Moreno, R. Rodrigo (Instituto de Astrofísica de Andalucía, Granada, Spain); P. Lognonné (Département de Géophysique Spatiale et Planétaire/UMR7096-CNRS, Saint Maur des Fossé, France);; D. Resendes (Instituto Superi-

or Técnico, Universidade Técnica de Lisboa, Lisboa, Portugal).

BepiColombo – MIXS
M. Hilchenbach in collaboration with Fraser (PI) (Leicester, UK).

BepiColombo – MMO (Mercury Magnetospheric Orbiter)
MPPE-MSA: Spektrometer zur Messung von geladenen und neutralen Teilchen in der Merkurmagnetosphäre (Bauphase). N. Krupp, J. Woch, M. Fränz, A. Loose, H. Fischer, and U. Bührke in collaboration with D. Delcourt (Centre d'Etude Terrestre et Planetaire (CETP), Paris, France); Y. Saito (Jaxa/ISAS, Tokio, Japan).

BepiColombo – MPO (Mercury Planetary Orbiter)
PICAM (Planetary Ion CAMera) – Detektoreinheit des Neutral and Charge Particle Analyzers SERENA (Search for Exospheric Refilling and Emitted Natural Abundances). J. Woch, A. Loose, N. Krupp, and M. Fränz in collaboration with S. Orsini (PI) (IFSI, Roma, Italy); K. Torkar (Co-PI) (SRI, Graz, Austria); J.-J. Berthelier (CETP-CNRS, St Maur des Fosses, France); P. Escoubet (ESTEC, Noordwijk, The Netherlands); F. Leblanc (IPSL Verrieres-Le-Buisson, France); D. Nevejans (BIRA, Brusseles, Belgium); K. Szego (KFKI, Budapest, Hungary); O. Vaisberg (IKI, Moscow, Russia).

BepiColombo — MERMAG (Magnetic Field Investigation)
U. Christensen in collaboration with K.-H. Glaßmeier (PI) (Institut für Geophysik und Extraterrestrische Physik, Braunschweig, Germany).

CASSINI – MIMI/LEMMS
Spektrometer zur Messung von geladenen und neutralen energiereichen Teilchen in der Saturnmagnetosphäre (Datenauswertung). N. Krupp, J. Woch, A. Lagg, P. Kollmann, A. Müller, and Z. Bebesi in collaboration with S. M. Krimigis, S. Livi, D. G. Mitchell (Johns Hopkins University, Applied Physics Laboratory, USA); D. Hamilton (University of Maryland, USA); I. Dandouras (CESR, Toulouse, France); T. P. Armstrong (Fundamental Technologies, Kansas, USA).

Chandrayaan-1, ISRO
U. Mall and A. Nathues in collaboration with N. Goswami (PRL, India).

Cluster II – CIS (Cluster Ion Spectrometer)
A. Korth, M. Fränz, P. W. Daly, E. Panov, and E. Kronberg in collaboration with I. Dandouras (PI), CESR (Toulouse, France); MPI für extraterrestrische Physik, (Garching, Germany); Universities of New Hampshire (Washington, Seattle, Berkeley, USA); IFSI/CNR (Frascati, Italy); Lockheed (Palo Alto, USA); SISP (Kiruna, Sweden).

Cluster II – RAPID
Das Teilchen-Spektrometer RAPID. Principle Investigator: P. W. Daly; Co-Investigators: U. Mall, J. Büchner, A. Korth, J. Woch, E. Kronberg, Sir I. Axford, and V. M. Vasyliūnas in collaboration with J. B. Blake, J. F. Fennell, J. Roeder (AC, Los Angeles, USA); Z. Y. Pu, S. Y. Fu (Beijing University, Beijing, China); T. A. Fritz, Q.-G. Zong (BU, Boston, USA); F. Gliem (IDA, Braunschweig, Germany); I. Sandahl, M. Yamauchi (IRF, Kiruna, Sweden); H. Borg (Univ. Umea, Sweden); K. Kecskemety (KFKI, Budapest, Hungary); G. D. Reeves, R. H. W. Friedel (LANL, Los Alamos, USA); D. N. Baker (LASP, Boulder, USA); M. Grande, M. Carter, C. H. Perry, J. Davies, M. Dunlop (RAL, Chilton, UK); M.G.G.T. Taylor (ESTEC, The Netherlands); S. McKenna-Lawlor (SPC, Maynooth, USA); F. Søraas, K. Aarsnes, K. Oksavik (University Bergen, Norway); K. Mursula, P. Tanskanen (University Oulu, Finland); E. T. Sarris (University Thrace, Greece); A.T.Y. Lui (APL, USA).

Cluster Active Archive (CAA)
Archivierung der RAPID-Daten. P. W. Daly and E. Kronberg in collaboration with H. Laakso (ESA); C. H. Perry, J. Davies (RAL, Chilton, UK).

Comparative analysis of plasma environment at Mars and Venus
M. Fränz in collaboration with U. Motschmann, K. H. Glassmeier (TU Braunschweig, Germany).

Comparative helioseismic study of Active Region 9787
L. Gizon, M. Roth, and H. Schunker in collaboration with A. C. Birch, D. C. Braun (CoRA, Boulder, USA); R. Bogart (Stanford University, USA); T. L. Duvall Jr. (NASA GSFC, USA); I. González Hernández, R. Komm (NSO, Tucson, USA); D. Haber (JILA, Boulder, USA); S. Zharkov (University Sheffield, UK), and others.

Contrasts of magnetic features from magneto-convection simulations
M. Schüssler and S. K. Solanki in collaboration with N. Afram, Y. C. Unruh (Imperial College London); A. Vögler (Astronomical Institute Utrecht, The Netherlands).

Coronal MHD-equilibria
T. Wiegelmann and P. Ruan in collaboration with T. Neukirch (University St. Andrews, UK).

COROT additional program (AP)
"Stellar variability and microvariability – III: convection and short term evolution of photospheric active regions". S. K. Solanki and N. A. Krivova in collabo-

ration with Institute of Astronomy, University of Cambridge, UK; School of Physics and Astronomy, University of St. Andrews, UK; Astrophysics Group, Imperial College, London, UK.

Cosmogenic nuclides and past solar activity
M. Schüssler and S. K. Solanki in collaboration with I. G. Usoskin (Sodankylä Geophysical Observatory, Finland); G. A. Kovaltsov (Ioffe Physical-Technical Institute, St. Petersburg, Russia).

DAAD/DST: Detection of waves in the solar Atmosphere
(started in June 2007) L. Teriaca and S. K. Solanki in collaboration with D. Banerjee, G. Gupta (IIA, Bangalore, India).

DAWN
H. Sierks, P. Gutierrez, H. Hartwig, H. U. Keller, A. Nathues, S. Schröder, and U. Christensen in collaboration with R. Jaumann, S. Mottola (DLR/Institut für Planetenforschung, Berlin, Germany); H. Michalik, B. Fiethe (Institut für Datentechnik und Kommunikationsnetze, Braunschweig, Germany); C. Russell, C. Raymond (University of California, Los Angeles, USA); K. C. Patel, E. Miller (Jet Propulsion Laboratory, Pasadena, USA).

Deep Impact at comet 9P/Tempel 1: Exploring the Dust Component
H. Boehnhardt (PI) in collaboration with N. Ageorges, S. Bagnulo, O. Hainaut, E. Jehin, H. U. Kaeufl, F. Kerber, G. LoCurto, E. Pompei, O. Marco, F. Selmann (ESO Garching & Santiago de Chile); L. Barrera (UMCE, Santiago de Chile); T. Bonev (University Sofia, Bulgaria); R. Gredel (MPI Astronomie, Heidelberg, Germany); L. Lara, J. L. Ortiz (Instituto de Astrofísica de Andalucía, Granada, Spain); K. Meech (University Hawaii, Honolulu, USA); E. Pantin (CNRS Paris, France); H. Rauer (DLR Berlin, Germany); G. P. Tozzi (INAF Arcetri Observatory, Florence, Italy).

DFG Schwerpunktprogramm 1176: Climate and Weather of the Sun-Earth-System (CAWSES)
Influence of the mean circulation on gravity wave generation P. Hartogh, A. Medvedev, and T. Kuroda in collaboration with E. Yigit (University College London, UK).

DFG Schwerpunktprogramm 1176: Climate and Weather of the Sun-Earth-System (CAWSES)
Investigation of the solar influence on middle atmospheric water vapour and ozone during the last solar cycle – analysis of the MPS data set P. Hartogh, C. Jarchow, and G. Sonnemann in collaboration with U. Berger and M. Grygalashvyly (Leibniz-Institut für Atmosphärenphysik, Kühlungsborn, Germany).

DFG Schwerpunktprogramm 1176: Climate and Weather of the Sun-Earth-System (CAWSES)
Support proposal for refurbishment and replacement of a microwave spectrometer to be used in the priority programme CAWSES P. Hartogh, C. Jarchow, and K. Hallgren in collaboration with F.-J. Lübken (Leibniz-Institut für Atmosphärenphysik, Kühlungsborn, Germany).

DFG Schwerpunktprogramm 1176: Climate and Weather of the Sun-Earth-System (CAWSES)
N. A. Krivova and S. K. Solanki in collaboration with Freie Universität Berlin, Germany; Institut für Umweltphysik, Universität Bremen, Germany; MPI für Meteorologie, Hamburg, Germany.

DFG-Schwerpunktprogramm 1115 – MAOAM (The Martian Atmosphere: Observing And Modelling)
P. Hartogh, C. Jarchow, T. Kuroda, and A. Medvedev in collaboration with U. Berger, G. Sonnemann, M. Grygalashvyly (IAP Kühlungsborn, Germany); A. Feofilov, A. Kutepov (IAA München, Germany); H. Elbern (Institut für Geophysik und Meteorologie, Köln, Germany); M. Allen (JPL, Pasadena, USA); Gordon Chin (GSFC, Greenbelt, USA).

Diagnostics of magnetoconvection
M. Schüssler, R. Cameron, and S. K. Solanki in collaboration with S. Shelyag (University of Sheffield, UK); A. Vögler (Universität Utrecht, The Netherlands).

Dust dynamics in Jupiter's gossamer rings
H. Krüger in collaboration with D. P. Hamilton (University of Maryland, USA).

EJSM-SWI
P. Hartogh, C. Jarchow, H. Sagawa, M. Rengel, A. Gonzales, T. Cavalie, and A. Medvedev in collaboration with E. Lellouch, P. Drossart, R. Morena, T. Fouchet, J.-M. Krieg, G. Beaudin, A. Maestrini (Observatoire de Paris, France); S. Gulkis, M. Allen, M. Janssen, and I. Mehdi (Caltech-JPL, Pasadena, USA); S. Bolton (Southwest Research Institute, USA); G. Chin (Goddard Space Flight Center, Greenbelt, USA); S. Barabash (IRF, Kiruna, Sweden).

European Solar Telescope (EST)
(The EST design study is a project involving 29 different institutes and companies within Europe. I have only listed the partners we are directly collaborating with, in terms of dedicated work packages.) A. Feller and J. Hirzberger in collaboration with B. Gelly, A. Lopez-Ariste (THEMIS S.L., France); C. Keller, F. Bettonvil (Utrecht University, The Netherlands); R. Volkmer, T. Kentischer (Kiepenheuer Institut für Sonnenphysik, Germany); M. Collados (Instituto de

Astrofísica de Canarias, Spain); G. Scharmer (Royal Swedish Academy of Sciences, Sweden); F. Cavallini (Istituto Nazionale de Astrofisica, Italy); A. Kucera (Astronomical Institute of the Slovak Academy of Sciences); G. Cauzzi (Instituto Nazionale di Astrofisica, Arcetri, Italy); F. Berrilli (Universita'degli Studi di Roma Tor Vergata, Rome, Italy); G. Molodij (Observatoire de Paris, Paris-Meudon, France).

EUROPLANET (European Planetology Network)
Aufbau eines Netzwerks in Europa zur Optimierung der Forschungsaktivitäten im Bereich Planeten. N. Krupp in collaboration with CESR (Toulouse, France); FMI Helsinki (Finland); University Nantes (France); Observatoire Paris (France); University Grenoble (France); Imperial College (London, UK); KFKI (Budapest, Hungary).

Evidence for polar jets as precursors of polar plume formation
S. K. Solanki in collaboration with N.-E. Raouafi, G. J. D. Petrie, A. A. Norton, C. J. Henney (National Solar Observatory, Tucson, USA).

ExoMars – MOMA
F. Goesmann (PI), O. Roders (PM), H. Steininger, E. Steinmetz, and M. Hilchenbach in collaboration with L. Becker (John Hopkins University, Department of Physics and Astronomy, Baltimore, USA); T. Cornish (Applied Physics Laboratory, Baltimore, USA); R. Cotter (Johns Hopkins School of Medicine , Baltimore, USA); C. Szopa (Laboratoire Atmosphéres, Milieux, Observations Spatiales (LATMOS), Paris, France); F. Raulin (Laboratoire Interuniversitaire des Systémes Atmosphériques (LISA), Paris, France).

ExoMars – RAMAN – LIBS
M. Hilchenbach in collaboration with Rull (PI) (Madrid, Spain).

ExoMars – SEIS
U. Christensen and R. Roll in collaboration with P. Lognonné (IPGP, Paris, France).

Galileo – EPD (Energetic Particles Detector)
Spektrometer zur Messung von geladenen energiereichen Teilchen in der Jupitermagnetosphäre (Datenauswertung). N. Krupp, J. Woch, A. Lagg, and E. Kronberg in collaboration with D. J. Williams, R. McEntire (Johns Hopkins University, Applied Physics Laboratory, USA); S. Kasahara (Institute of Space and Astronautical Science, Sagamihara, Kanagawa, Japan).

GBSO – Ground Based Solar Observations
R. Aznar-Cuadrado, S. Danilovic, A. Gandorfer, J. Hirzberger, A. Lagg, M. Meling, T. Riethmüller, C. Sasso, S. K. Solanki, J. Woch, Z. Xu, and V. Zakharov in collaboration with M. Collados (IAC, La Laguna, Tenerife, Spain); A. López Ariste (THEMIS, La Laguna, Tenerife, Spain); D. Fluri, N. Afram (ETH Zürich, Switzerland); K. Puschman, E. Wiehr (Institut für Astrophysik, Universität Göttingen, Germany); S. Stangl (Institut für Physik, Universität Graz, Austria); (Kiepenheuer-Institut für Sonnenphysik, Freiburg, Germany); (Instituto de Astrofísica de Canarias, Spain); (Institute for Solar Physics of the Royal Swedish Society, Stockholm, Sweden).

German Data Center for the Solar Dynamics Observatory (GDC-SDO)
L. Gizon, R. Burston, I. Pardowitz, Y. Saidi, and S. K. Solanki in collaboration with H. Peter (Kiepenheuer-Institut für Sonnenphysik, Freiburg, Germany); G. Mann (Astrophysikalisches Institut Potsdam, Germany).

HELAS (European Helio- and Asteroseismology Network)
L. Gizon, M. Roth, Y. Saidi, and H. Schunker in collaboration with O. von der Lühe (Kiepenheuer-Institut für Sonnenphysik, Freiburg, Germany); P. Pallé (IAC, La Laguna, Tenerife, Spain); M. Thompson (University of Sheffield, UK); J. Christensen-Dalsgaard (University of Aarhus, Denmark); M. Monteiro (Center for Astrophysics, University Porto, Portugal); M. P. Di Mauro (INAF, Rome, Italy); C. Aerts (Katholieke Universiteit Leuven, Belgium); J. Daszyńska-Daszkiewicz (Uniwersytet Wroclawski, Poland); T. Corbard (CNRS, Nice, France).

Helioseismic and Magnetic Imager
J. Borrero in collaboration with S. Tomczyk, D. Elmore, R. Centeno-Elliot, B. Lites (High Altitude Observatory, Boulder, USA); J. Schou, R. Bogart, P. Scherrer (Stanford University, Palo Alto, CA, USA).

Helioseismology of granulation
L. Gizon in collaboration with A. C. Birch, D. C. Braun (CoRA, Boulder, USA); T. L. Duvall Jr. (NASA GSFC, USA).

HIFI–WBS (Heterodyne Instrument for FIRST – Wideband Spectrometer)
P. Hartogh, C. Jarchow, M. Rengel, A. Gonzales, A. Medvedev, and H. Sagawa in collaboration with T. de Graauw, H. J. Aarts, D. A. Beintema, J. Gao, H. Jacobs, W. Jellema, W. Luinge, P. R. Roelfsema, X. Tielens, H. van de Stadt, B. van Leeuwen, N. D. Whyborn, K. J. Wildeman (SRON, Utrecht, The Netherlands); E. Van Dishoeck (Universität Leiden, The Netherlands); R. Güsten, K. Menten (Max-Planck-Institut für Radioastronomie, Bonn, Germany); C. H. Honingh, K. Jacobs, R. Schieder, J. Stutzki (Universität Köln, Germany); A. Emrich (Omnisys, Göteborg, Sweden); S. Torchinsky (Chalmers, Göteborg, Sweden); M. Larsson (Universität Stockholm, Sweden);

C. Rosolen (Arpeges, Observatoire de Paris, Meudon, France); G. Beaudin (LERMA, Meudon, France); E. Caux, A. Cros (CESR, Toulouse, France); P. Cais (Bordeaux Observatory, France); E. Lellouch, T. Encrenaz (DESPA, Paris, France); C. Gry (LAS Marseille, France); N. Maurun (Graal, Montpellier, France); K. Schuster (IRAM, Grenoble, France); F. Boulanger (IAS, Orsay, France); L. T. Little (Kent University, UK); T. Miller (UMIST, UK); T.J.T. Moore (Liverpool-J. Moures, UK); S. Withington (MRAO Cambridge, UK); G. J. White (QMW London, UK); R. Cerrulli, R. Orfei (IFSI Frascati, Italy); V. Natale (CAISMI Florenz, Italy); J. Martin-Pintado (OAN, Alcala, Spain); J.D.G. Puyol (Obs. Yebes, Spain); M. J. Sarna, R. Szczerba (Copernicus AC, Warsaw, Poland); W. R. McGrath, J. C. Pearson, T. C. Gaier (JPL, Pasadena, USA); T. G. Phillips, J. Zmuidzinas (Caltech, Pasadena, USA); A. I. Harris (Maryland University, USA); E. Herbst (Ohio State University, USA); D. A. Neufeld (Johns Hopkins University, USA); N. R. Erickson (FCRAO, Amherst, MA, USA); S. Verghese (Lincoln Lab., MIT, USA); S. Kwok (Calgary University, Canada); D. A. Naylor (Lethbridge University, Canada); F. Lo (IAA, Taiwan); H. Wang (NTU, Taipeh, Taiwan); P. Zimmermann (RPG, Meckenheim, Germany).

Hinode data analysis
A. Lagg, T. Riethmüller, S. Danilovic, S. K. Solanki, and J. Hirzberger in collaboration with National Astronomical Observatory of Japan (NAOJ); S. K. Mathew (Udaipur Observatory, India).

Historical Ca spectroheliograms: making an old resource available for new studies
S. K. Solanki and N. A. Krivova in collaboration with I. Ermolli (Rome Observatory, Italy).

HssO (Herschel Solar System Observations)
M. Rengel, P. Hartogh, T. Cavalie, H. Boehnhardt, A. Gonzalez, H. Sagawa, C. Jarchow, and A. Medvedev in collaboration with M. Banaszkiewicz, M. I. Blecka, S. Szutowicz (Space Research Centre, Polish Academy of Science, Warsaw, Poland); F. P. Bensch (Deutsches Zentrum für Luft- und Raumfahrt (DLR), Bonn, Germany); E. A. Bergin (University of Michigan, Ann Arbor, USA); F. Billebaud (LAB, Observatoire de Bordeaux, France); E. Lellouch, R. Moreno, N. Biver, D. Bockelee-Morvan, R. Courtin, J. Crovisier, T. Encrenaz (LESIA, Observatoire de Paris, France); G. A. Blake (California Institute of Technology, Pasadena, USA); J. Blommaert, L. Decin, B. Vandenbussche, C. Waelkens (Instituut voor Sterrenkunde, Katholieke Universiteit Leuven, Belgium) and others.

Identification and misidentification of different types of kink modes in coronal loops
S. K. Solanki in collaboration with T. J. Wang (Montana State University, Bozeman, USA); M. Selwa (NASA Goddard Space Flight Center, Greenbelt, USA).

Independent Scientist for the ESA ExoMars Mission
D. Titov in collaboration with J. Vago and D. McCoy (ESTEC/ESA, The Netherlands).

Inter-scale coupling in magnetic reonnection
J. Büchner in collaboration with M. Barta, M. Karlicky (Astronomical Institute of the Czech Academy of Science, Ondrejov, Czech Republic).

Inversion of helioseismic traveltimes
J. Jackiewicz and L. Gizon in collaboration with A. C. Birch (CoRA, Boulder, USA); T. Hohage (Göttingen University, Germany).

Investigation of thin current sheets in space and solar plasmas
J. Büchner in collaboration with L. Hau, K. W. Lee (National Central University of Taiwan).

IRIS Interface Region Imaging Spectrograph
T. Wiegelmann in collaboration with A. Title, K. Schrijver (LMSAL, Palo Alto, USA).

ISSI team "Interpretation and modelling of Solar Spectral Irradiance measurements"
N. A. Krivova and S. K. Solanki in collaboration with INAF Osservatorio Astronomico di Roma (Italy); Astrophysics Group, Imperial College (London, UK); PMOD WRC (Davos, Switzerland); LASP, University of Colorado (Boulder, USA); Institut für Umweltphysik, Universität Bremen (Germany); Interferometrics Inc. (Herndon, USA).

ISSI Working Group "Venus Climate"
D. Titov in collaboration with A. Balough, L. Bengtsson, R.-M. Bonnet, S. Koumoutsaris, A.-P. Rossi (ISSI); C. Covey (USA); D. Grinspoon (Museum of Natural History, Denver, USA); S. Lebonnois (LMD, France); S. Limaye (University of Wisconsin, USA); R. Pierrehumbert (USA); P. Read (AOPP, Oxford University, UK); H. Schmidt (MPI Meteorology, Hamburg, Germany); H. Svedhem (ESTEC/ ESA, The Netherlands); M. Yamamoto (Japan).

ISSI Team "Structure and Dynamics of Coronal Plumes and Inter-plume Regions in Solar Coronal Holes"
K. Wilhelm (Team leader), L. Teriaca, and L. Feng in collaboration with L. Abbo, S. Giordano (INAF-Osservatorio Astronomico di Torino, Italy); F. Auchère, A. H. Gabriel, N. Barbey (Institut d'Astrophysique Spatiale, Orsay, France); S. Imada

(National Astronomical Observatory of Japan, Osawa, Japan); A. Llebaria (Laboratoire d'Astrophysique de Marseille, France); W. H. Matthaeus (Bartol Research Institute, Newark, USA); G. Poletto (Osservatorio Astrofisico di Arcetri, Firenze, Italy); N.-E. Raouafi (National Solar Observatory, Tucson, USA); S. T. Suess (NASA Marshall Space Flight Center, Huntsville, USA); Y.-M. Wang, E. O. Hulburt (Center for Space Research, Washington, USA).

Kinetische Plasmaphysik der Sonnenkorona
E. Marsch in collaboration with G. Mann, C. Vocks (Astrophysikalisches Institut Potsdam, Germany).

Kinetische Physik des Sonnenwinds
Forschung auf dem Gebiet der Plasma-Beam Instabilitäten im Sonnenwind und in der Sonnenkorona. Numerische Simulationen zum Zerfall und der parametrischen Entwicklung von Alfvén Wellen großer Amplitude. E. Marsch in collaboration with J. Araneda (Universität Concepción, Chile).

KuaFu – "Space Weather Explorer"
R. Schwenn, U. Schühle, and E. Marsch in collaboration with Chuanyi Tu (PI), J.-S. Wang (Peking University, Beijing, China); E. Donavan (Department of Physics and Astronomy, University of Calgary, Canada); L.-D. Xia (School of Earth and Space Sciences, University of Science and Technology of China, Hefei, Anhui, China); Y.-W. Zhang (China Academy of Space Technology and DFH Satellite Co. Ltd, Beijing, China).

LEO-MIMO
P. Hartogh H. Boehnhardt, C. Jarchow, H. Krüger, T. Kuroda, W. Markiewicz, A. Medvedev, L. Paganini, M. Rengel, H. Sagawa, and D. Titov in collaboration with M. Küppers (European Space Astronomy Centre, Villafranca, Spain); K. Kossacki (Universität Warschau, Institut für Geophysik, Warsaw, Poland).

Local Helioseismology of Small Magnetic Features
L. Gizon in collaboration with T. L. Duvall (NASA, GSFC, Greenbelt, USA); A. C. Birch (CoRA, North West Research Associates, Boulder, USA); S. Hanasoge (Stanford University, USA).

LYman-Alpha Orbiting Telescopes (LYOT) on board SMESE (Small Explorer for the study of Solar Eruptions)
U. Schühle in collaboration with J.-C. Vial (PI) (Institut d'Astrophysique Spatiale, Orsay, France).

MAG (Magnetometer) for Solar Orbiter
E. Marsch in collaboration with T. Horbury (PI) (Imperial College London, UK).

Mars Climate Simulator
O. Stenzel in collaboration with K. Fraedrich and colleagues (Meteorologisches Institut der Universität Hamburg, Germany); R. Greve (Institute of Low Temperature Science, Hokkaido University, Japan).

Mars Express
N. Hoekzema and O. Stenzel in collaboration with K. Gwinner, T. Roatch, H. Hofmann (DLR, Berlin, Germany); G. Neukum (FU, Berlin, Germany); A. Inada (CalTech, Los Angeles, CA, USA); L. Petrova (IKI, Moscow, Russia).

Mars Express – ASPERA-3 (Analyzer of Space Plasmas and EneRgetic Atoms)
M. Fränz, J. Woch, N. Krupp, E. Dubinin, E. Roussos, C. Martinecz, and J. Kleimann in collaboration with R. Lundin (PI), S. Barabash (IRF, Kiruna, Sweden); D. Winningham, R. Frahm (SWRI, San Antonio, USA); P. Wurz (Universität Bern, Switzerland); A. Coates (MSSL, London, UK); M. Grande (RAL, Chilton, UK); J. A. Sauvaud, A. Fedorov (CESR, Toulouse, France); E. Kallio (FMI, Helsinki, Finland); S. Orsini (IFSI, Roma, Italy); C. C. Curtis (UoA, Tuscon, USA).

Mars Express – OMEGA
D. Titov in collaboration with J.-P. Bibring, Y. Langevin, B. Gondet (Institut d'Astrophysique Spatiale (IAS), Orsay, France); P. Drossart (Observatoire de Paris, Meudon, France); N. Ignatiev (Space Research Institute (IKI), Moscow, Russia).

Mars Express – PFS
D. Titov in collaboration with V. Formisano (Institute of Physics of Interplanetary Space (IFSI-INAF), Roma, Italy); N. Ignatiev, A. Fedorova (Space Research Institute (IKI), Moscow, Russia); E. Lellouch, T. Fouchet, Th. Encrenaz (Observatoire de Paris, Meudon, France).

MARSIS
E. Nielsen in collaboration with Department of Physics and Astronomy, University of Iowa (Iowa City, Iowa, USA); Jet Propulsion Laboratory, California Institute of Technology (Pasadena, CA, USA); Istituto di Fisica dello Spazio Interplanetario, Istituto Nazionale di Astrofisica (Rome, Italy); Infocom Department, "La Sapienza" University of Rome (Rome, Italy); School of Earth and Space sciences, Peking University (Beijing, P.R. China).

MARVEL – Mars Volcanic Emission and Life Scout
P. Hartogh in collaboration with M. Allen (JPL, Pasadena, USA); G. Chin (GSFC, Greenbelt, USA).

Measurement of the meridional flow with Fourier–Hankel decomposition
M. Roth in collaboration with L. Krieger

(Kiepenheuer-Institut für Sonnenphysik, Freiburg, Germany).

Micro-turbulent transport
J. Büchner in collaboration with F. Jenko (IPP Garching, Germany).

Millennium – climate simulations for the last millennium using the Earth System Model (ESM)
N. A. Krivova and S. K. Solanki in collaboration with Max-Planck-Institut für Meteorologie (Hamburg, Germany); Freie Universität Berlin (Berlin, Germany).

MPCS – Study of the MarcoPolo Camera System
H. Boehnhardt, A. Nathues, H. Perplies, and G. Tomasch in collaboration with G. Cremonese, V. da-Deppo, S. Marchi, G. Naletto (INAF, Padova, Italy); L. Lara, J. Castro, M. Herranz, J. Ramos, J. Rodrigo (IAA, Granada, Spain); H. Michalik, B. Fiethe, B. Osterloh (IAD, Braunschweig, Germany); S. Mottola, T. Behnke, H. Michaelis, J. Oberst (DLR, Berlin-Adlershof, Germany); G. Alonso, I. Perez-Grande, A. Sanz-Andres (UPM, Madrid, Spain).

NERC consortium: "SOLCLI: Solar Influence on Climate"
N. A. Krivova and S. K. Solanki in collaboration with Astrophysics Group, Imperial College (London, UK).

Nonlinear force-free coronal magnetic fields (NLFFF-consortium)
T. Wiegelmann, J. Thalmann, and T. Tadesse in collaboration with C. J. Schrijver (LMSAL, Palo Alto, USA).

Numerical simulations of coronal loop oscillations
S. K. Solanki in collaboration with L. Ofman, M. Selwa, T. J. Wang (NASA GSFC Greenbelt, USA).

Observations of a flux rope in the solar wind
P. Ruan, A. Korth, E. Marsch, B. Inhester, S. K. Solanki, T. Wiegelmann, and R. Bučik in collaboration with Q.-G. Zong (Center for Atmospheric Research, University of Massachusetts Lowelland, USA); K.-H. Fornacon (Institut für Geophysik und Extraterrestrische Physik, Technische Universität Braunschweig, Germany).

On the common solar signal in different cosmogenic isotope data sets
S. K. Solanki in collaboration with I. G. Usoskin (University of Oulu, Finland); K. Horiuchi (Hirosaki University, Japan); G. Kovaltsov (Ioffe Physical-Technical Institute, St. Petersburg, Russia); E. Bard (Collège de France, Aix-en-Provence, France).

Phobos Grunt
F. Goesmann in collaboration with M. Gerasimov (IKI, Moscow, Russia).

Physical and composition properties of short-periodic and Oort Cloud comets
H. Boehnhardt, M. Drahus, M. Lippi, C. Tubiana, and J.-P. Vincent in collaboration with S. Bagnulo (ESO Santiago de Chile, Armagh Observatory Northern Ireland); L. Barrera (UMCE, Santiago de Chile); D. Harker (University San Diego, USA); M. Kelley (Joint Astronomy Center, USA); S. Kolokolova (University Maryland, College Park, USA); L. Lara (IAA Granada, Spain); M. Mumma, M. DiSanti, B. Bonev (NASA Goddard, Greenbelt, USA); D. Prialnik, E. Beer-Harari (University Tel Aviv, Israel); G. P. Tozzi (INAF Arcetri Observatory, Florence, Italy); D. Wooden (PI) (NASA Ames Res. Center, Moffett Fields, USA); C. Woodward (University Minnesota, USA).

Plasma dynamics in stellar atmospheres
J. Büchner in collaboration with U. Motschmann (Technische Universität Braunschweig, Germany).

PLATO (PLAnetary Transits and Oscillations of stars, a class-M candidate mission of ESA) ground data center assessment study
L. Gizon in collaboration with T. Appourchaux (IAS, Orsay, France); C. Catala (IAP, Paris, France); M. Deleuil (LAM, Marseille, France); N. Walton (IoA, Cambridge, UK), and others.

POLARIS (POLar Investigation of the Sun), a class-M mission submitted to ESA's Cosmic Vision Programme
L. Gizon in collaboration with T. Appourchaux (IAS, Orsay, France), and others.

PROBA II – LYRA (Large Yield Radiometer)
U. Schühle in collaboration with J.-F. Hochedez (PI), A. BenMoussa, D. Berghmans, A. Theissen, V. Delouille, B. Nicula, L. Wauters, R. Van der Linden, A. Zhukov, F. Clette (Royal Observatory of Belgium (ROB), Brussels, Belgium); W. Schmutz, S. Koller, H. Roth, E. Rozanov, I. Rüedi, C. Wehrli (Physikalisch-Meteorologisches Observatorium Davos (PMOD) and World Radiation Center, Davos, Switzerland); K. Haenen, V. Mortet, Z. Remes, M. Nesládek, M. D'Olieslaeger (Institute for Materials Research, Diepenbeek, Belgium); Y. Stockman, J.-M. Defise, J.-P. Halain, P. Rochus (Centre Spatial de Liège (CSL), Angleur, Belgium); D. Gillotay, D. Fussen, M. Dominique, F. Vanhellemont (Belgian Institute for Space Aeronomy, Brussels, Belgium); V. Slemzin, A. Mitrofanov (Lebedev Physical Institute, Moscow, Russia); D. McMullin (Naval Research Laboratory (NRL), Washington, DC, USA); M. Kretzschmar (Istituto Fisica dello Spazio Interplanetario (IFSI), Rome, Italy); R. Petersen, M. Nesládek, M. D'Olieslaeger (IMEC, Division IMOMEC, Diepenbeek, Belgium); J. Roggen (IMEC, Louvain, Belgi-

um); S. Koizumi (Advanced Materials Laboratory, National Institute for Materials Science, Tsukuba, Japan); H. Amano (Department of Materials Science and Engineering, Meijo University, Nagoya, Japan); A. Soltani (Institut d'Electronique, de Microélectronique et de Nanotechnologie, Villeneuve d'Ascq, France).

PROBA II – SWAP (Sun Watcher using APS Detectors)
U. Schühle in collaboration with D. Berghmans, J. F. Hochedez, B. Nicula, G. Lawrence, A. C. Katsyiannis, R. Van der Linden, A. Zhukov, F. Clette (Royal Observatory of Belgium, Solar Physics, Brussels, Belgium); J. M. Defise (PI), J. H. Lecat, P. Rochus, E. Mazy, T. Thibert (Centre Spatial de Liège, Angleur, Belgium); P. Nicolosi, M. G. Pelizzo (University of Padova, Padova, Italy); V. Slemzin (Lebedev Physical Institute, Moscow, Russia).

Propagating waves in polar coronal holes as seen by SUMER & EIS
L. Teriaca and S. K. Solanki in collaboration with D. Banerjee (Indian Institute of Astrophysics, Bangalore, India); G. R. Gupta (Indian Institute of Science, Bangalore, India); S. Imada (National Astronomical Observatory of Japan, Tokyo, Japan); G. Stemborg (Interferometrics, Inc., Herndon, USA).

RAISE – Rapid Imaging Spectrograph Experiment
U. Schühle in collaboration with D. Hassler (PI), D. Slater, C. DeForest, S. McIntosh (Southwest Research Institute, San Antonio, USA); T. Ayres (University of Colorado, Boulder, USA); R. Thomas (NASA GSFC, Greenbelt, USA); H. Michaelis (Institut für Planetenforschung, DLR, Berlin, Germany).

Rosetta – CONSERT (Radio Tomography Project)
E. Nielsen in collaboration with Laboratoire de Planétologie, University of Grenoble, ESA, France.

ROSETTA – COSAC (PHILAE)
F. Goesmann, R. Roll, and H. Boehnhardt in collaboration with F. Raulin (LISA - UMR 7583, Universités Paris 12 & Paris 7, Faculté des Sciences, Créteil, France); U. J. Meierhenrich (Université Nice-Sophia Antipolis L.C.M.B.A. et UMR 6001 CNRS, Nice, France); C. Szopa (Service d'Aéronomie (SA), UMR CNRS 7620, IPSL, Verrières le Buisson, France).

ROSETTA – COSIMA
M. Hilchenbach (PI seit 15. Mai 2005), J. Kissel (PI bis 15. Mai 2005), H. Krüger (Co-I), H. Boehnhardt(Co-I), and H. Fischer (engineer) in collaboration with K. Altwegg (Physikalisches Institut, Universität Bern, Switzerland); B. C. Clark (Lockheed Martin Astronautics, Denver, USA); L. Colangeli (Istituto Nazionale di Astrofisica - Osservatorio Astronomico di Capodimonte, Napoli, Italy); H. Cottin, F. Raulin (LISA, Universites Paris 12 & 7, Creteil Cedex, France); S. Czempiel, J. Eibl, G. Haerendel, H. Höfner, P. Parigger (MPI für extraterrestrische Physik, Garching, Germany); C. Engrand (Centre de Spectrométrie Nucléaire et de Spectrométrie de Masse (CSNSM), Orsay, France); H. M. Fehringer, R. Schulz (ESA/ESTEC, Noordwijk, The Netherlands); B. Feuerbacher (DLR, Köln, Germany); M. Fomenkova (Center for Astrophysics and Space Sciences, University of California, La Jolla, USA); A. Glasmachers (Universität Wuppertal, Lehrstuhl für Messtechnik, Wuppertal, Germany); J. M. Greenberg (Raymond and Beverly Sackler Laboratory for Astrophysics, Leiden, The Netherlands); E. Grün (MPI für Kernphysik, Heidelberg, Germany); H. Henkel, H. von Hoerner, A. Koch (von Hoerner und Sulger, Schwetzingen, Germany); K. Hornung (Universität der Bundeswehr LRT-7, Neubiberg, Germany); E. K. Jessberger, T. Stephan (Institut für Planetologie, Münster, Germany); F. R. Krueger (Ingenieurbüro Krueger, Darmstadt, Germany); G. Kurat (Naturhistorisches Museum, Vienna, Austria); Y. Langevin (Institut d'Astrophysique, Orsay, France); F. Rüdenauer (Institut für Physik, Seibersdorf, Austria); J. Rynö, J. Silén (Finnish Meteorological Institute, Helsinki, Finland); E. R. Schmid, W. Werther (Department of Analytical and Food Chemistry, Universität Wien, Austria); W. Steiger (ARC Seibersdorf Research GmbH Business Field Aerospace Technology, Seibersdorf, Austria); T. Stephan (Univ. of Chicago, Dept. of the Geophys. Sciences, USA); L. Thirkell, R. Thomas, C. Briois (Laboratoire de Phys. & Chim. de L'Environnement, Orléans, France); K. Torkar (Institut für Weltraumforschung, Graz, Austria); M. Trieloff (Mineralogisches Institut der Universität Heidelberg, Germany); N. G. Utterback (Consultant, St. Barbara, USA); K. Varmuza (Institut für Verfahrenstechnik, Umwelttechnik und Techn. Biowissenschaften, TU Wien, Austria); K. P. Wanczek (Institut für Anorganische und Physikalische Chemie, Universität Bremen, Germany); E. Zinner (Laboratory for Space Sciences, Washington University, St. Louis, MO, USA); H. Zscheeg (Abbott Laboratories Vascular Devices Ltd., Beringen, Switzerland).

Rosetta – MIRO (Mirowave Instrument for the Rosetta-Orbiter)
P. Hartogh, C. Jarchow, W. Ip, and I. Mann in collaboration with S. Gulkis, M. Allen, M. Frerking, M. Hofstadter, M. Janssen, T. Spilker (JPL, Pasadena, USA); D. Muhleman (Caltech, Pasadena, USA); G. Beaudin, D. Bockelee-Morvan, J. Crovisier, P. Encrenaz, T. Encrenaz, E. Lellouch (Observatoire de Paris-Meudon, France); D. Despois (Observatoire de Bordeaux, France); H. Rauer (DLR, Berlin, Germany);

P. Schloerb (University of Massachusetts, Amherst, USA).

Rosetta – OSIRIS
H. Sierks, S. F. Hviid, H. U. Keller, R. Kramm, R. Moissl, and C. Tubiana in collaboration with C. Barbieri, F. Angrilli (CISAS, University of Padova, Padova, Italy); P. Lamy, L. Jorda (Laboratoire d'Astrophysique de Marseille, Marseille, France); H. Rickmann (Department of Astronomy and Space Physics, Uppsala, Sweden); R. Rodrigo, L. M. Lara (Instituto de Astrofísica de Andalucía – CSIC, Granada, Spain); D. Koschny (Research and Scientific Support Department, ESTEC, Noordwijk, The Netherlands); M. F. A'Hearn (Department of Astronomy University of Maryland, USA); L. Sabau (Instituto Nacional de Técnica Aersospacial, Torrejon de Ardoz, Spain); M. E. Bailey (Armagh Observatory College Hill, Armagh, Northern Ireland); M. A. Barucci (Observatoire de Paris, Meudon, France); J.-L. Bertaux (Service d'Aéronomie du CNRS, Verrière-le-Buisson, France); J. A. Burns (Cornell University, Ithaca, USA); M. Fulle (Osservatorio Astronomica de Trieste, Trieste, Italy); F. Gliem, H. Michalik (Institut für Datentechnik und Kommunikationsnetze, Braunschweig, Germany); W.-H. Ip (Institute of Space Science, National Central University, Chung Li, Taiwan); E. Kührt (DLR/Institut für Planetenforschung, Braunschweig, Germany); A. Sanz (Universidad Politécnica de Madrid, Madrid, Spain); N. Thomas (Physikalisches Institut der Universität Bern, Bern, Switzerland); G. Cremonese, R. Ragazzoni (INAF, Osservatorio Astronomico, Padova, Italy).

Rosetta – PHILAE (Rosetta Lander)
H. Boehnhardt, R. Roll, B. Chares, R. Enge, H. Fischer, O. Küchemann, W. Kühne, M. Sperling, and I. Szemerey in collaboration with DLR Köln-Wahn, Germany; J. P. Bibring (IAS, Paris, France).

Rosetta – PHILAE – ROMAP
M. Hilchenbach and R. Roll in collaboration with U. Auster (Braunschweig, Germany).

Rosetta – RTOF/ROSINA
Bau der Elektronik für das Massenspektrometer RTOF (Reflection Time-of-Flight). U. Mall and A. Korth in collaboration with H. Balsiger (PI), Universität Bern, Switzerland; BIRA, Brussels, Belgium; CESR, Toulouse, France; IPSL, Saint Maur, France; IDA, Technische Universität Braunschweig, Germany; University of Michigan, Ann Arbor, USA; Southwest Research Institute, San Antonio, USA; Universität Giessen, Germany.

Simulation of flux emergence as seen by Hinode's SP/SOT
L. Yelles Chaouche, S. K. Solanki, M. Schüssler, and A. Lagg in collaboration with M. C. M. Cheung (Lockheed Martin Solar and Astrophysics Laboratory, Palo Alto, USA).

Simulation of the kinetics of space plasmas
J. Büchner in collaboration with M. Palmroth (Finnish Meteorological Institute, Helsinki, Finland).

Simulation of plasma turbulence and magnetic reconnection
J. Büchner in collaboration with M. Ashour-Abdalla (University of California, Los Angeles, USA).

SISI (Seismic Imaging of the Solar Interior, ERC Starting Grant)
L. Gizon in collaboration with P. H. Scherrer (Stanford University, USA).

Slow magnetoacoustic standing waves in a curved solar coronal slab
S. K. Solanki in collaboration with R. Ogrodowczyk (University of Chełm, Poland); K. Murawski (University of Lublin, Poland).

SOFIA–GREAT (SOFIA – German Receiver for Astronomy at THz frequencies)
P. Hartogh and C. Jarchow in collaboration with R. Guesten, K. Menten, P. v. d. Wal (MPI für Radioastronomie, Bonn, Germany); R. Schieder, J. Stutzki (Universität Köln, Germany); H. W. Hübers (DLR-Berlin, Germany); H. P. Röser (Institut für Raumfahrtsysteme, Universität Stuttgart, Germany).

SOHO – CELIAS (Charge, Element and Isotope Analysis System onboard SOHO)
M. Hilchenbach (Lead Co-I STOF), R. Kallenbach, and E. Marsch in collaboration with P. Bochsler (PI), H. Balsiger, A. Bürgi, J. Fischer, P. Wurz, B. Klecker (Physikalisches Institut, Universität Bern, Switzerland); D. Hovestadt (PI hardware phase), B. Klecker (Deputy PI), P. Laeverenz, M. Scholer (MPI für Extraterrestrische Physik, Garching, Germany); F. M. Ipavich (Lead Co-I MTOF), M. A. Coplan, G. Gloeckler, S. E. Lasley, J. A. Paquette (Department of Physics and Astronomy and IPST, University of Maryland, College Park, USA); R. Wimmer-Schweingruber, Karin Bamert (Extraterrestrische Physik, Universität Kiel, Germany); J. Geiss (International Space Science Institute, Bern, Switzerland); F. Gliem (Lead Co-I DPU), K.-U. Reiche (Institut für Datentechnik und Kommunikationsnetze, TU Braunschweig, Germany); D. L. Judge, H. S. Ogawa (Space Science Center, University of Southern California, Los Angeles, USA); G. G. Managadze, M. I. Verigin (Institute for Space Physics, Moscow, Russia); A. B. Galvin, H. Kucharek, M. A. Lee, Y. Litvinenko, E. Möbius (EOS, University of New Hampshire, Durham, USA); M. Neugebauer (Jet Propulsion La-

boratory, Pasadena, USA); K. C. Hsieh (Department of Physics, University of Arizona, Tucson, USA); D. McMullin (Space Science Division, Naval Research Laboratory, Washington, USA); A. Czechowski (Space Research Center, Polish Academy of Sciences, Warsaw, Poland).

SOHO – SUMER
Solar and Heliospheric Observatory – Solar Ultraviolet Measurements of Emitted Radiation. W. Curdt, D. E. Innes, E. Marsch, U. Schühle, S. K. Solanki, T. Wang, L. Teriaca, and M. Madjarska in collaboration with E. Landi, U. Feldman, G. A. Doschek, J. T. Mariska (Naval Research Laboratory (NRL), Washington, USA); P. Lemaire, A. H. Gabriel, J.-C. Vial (Institut d'Astrophysique Spatiale (IAS), Orsay, France); A. I. Poland (GSFC, Greenbelt, USA); M.C.E. Huber (Schweiz); J. Hollandt (PTB, Berlin, Germany); O. Siegmund (SSL, Berkeley, USA); D. Hassler (SWRI, Boulder, USA); P. G. Judge (HAO, Boulder, USA); N. Brynildsen, M. Carlsson, P. Maltby, O. Kjeldseth-Moe (ITA, Oslo, Norway); P. Brekke (ESA/GSFC, Greenbelt, USA); H. P. Warren (HSCA, Cambridge, USA); B. N. Dwivedi (DAP, Varanasi, India); C.-Y. Tu (DG, Peking, China); H. Peter (KIS, Freiburg); J. G. Doyle (Armagh Observatory, Ireland); P. Heinzel (Czech Academy); A. Pauluhn (ISSI Bern, Switzerland). (LASP, Boulder, USA)

SOLAIRE – Solar Atmospheric and Interplanetary Reasearch
E. Marsch (Team leader of the MPS Team). Dieses Research Training Network ist ein Projekt der EU im Rahmen der Marie Curie Actions, umfasst 10 Forschungsgruppen in Europa aus verschiedenen Ländern. Die chinesische Doktorandin Frau J. Guo wird davon finanziert. Beginn von SOLAIRE am 1. Juni 2007, Dauer 4 Jahre.

Solar coronal numerical simulation results comparison with flare magnetic field observations
J. Büchner in collaboration with H. Zhang, X. Li, S. Yang (Chinese Academy of Sciences, Bejing, China).

Solar-C science definition (helioseismology)
L. Gizon in collaboration with T. Sekii (NOAJ, Tokyo, Japan) and others.

Solar–cycle variation of rotation and meridional circulation
L. Gizon in collaboration with M. Rempel (HAO, Boulder, USA); I. González Hernández (NSO, Tucson, USA).

Solar Dynamics Observatory
L. Gizon, S. K. Solanki, and J. Borrero in collaboration with P. H. Scherrer (Stanford University, Palo Alto, USA); S. Tomczyk (High Altitude Observatoy, Boulder, USA); J. Schou (Stanford University, Palo Alto, USA); A. M. Title (Lockheed-Martin Solar and Astrophysics Laboratory, Palo Alto, USA).

Solare Stereoskopie
B. Inhester and T. Wiegelmann in collaboration with ISSI Bern; T. Dudoc de Witt (CNRS, Orleans, France); A. Vouridas (NRL, Washington, USA); J.-F. Hochedez (ROB, Brussels, Belgium); A. Llebaria (LAS, Marseille, France); J. P. Wuelser (LMSAL, Palo Alto, USA); F. Auchere (IAS, Orsay, France).

Solar Flare Telescope
T. Wiegelmann and J. Thalmann in collaboration with T. Sakurai (National Astronomical Observatory, Japan).

Solar infrared spectropolarimetry
A. Lagg, C. Sasso, S. K. Solanki, J. Woch, and Z. Xu in collaboration with M. Collados (Instituto de Astrofísica de Canarias, Tenerife, Spain).

Solar irradiance variations
S. K. Solanki, N. Krivova, and L. Teriaca in collaboration with

Solar Orbiter: EUI
U. Schühle, W. Curdt, L. Teriaca, E. Marsch, J. Büchner, and S. K. Solanki in collaboration with T. Apporchaux, J.-C. Vial, F. Auchere (Institut d'Astrophysique Spatiale, Paris, France); P. Rochus (Centre Spatial de Liege, Liege, Belgium); J.-F. Hochedez (PI), A. BenMoussa (Royal Observatory of Belgium, Brussels, Belgium); J. M. Defise (Centre Spatial de Liege, Liege, Belgium); L. Harra, J. Sun, D. Williams (Mullard Space Science Laboratories, London, UK).

Solar Orbiter: METIS
Multi Element Telescope for Imaging and Spectroscopy instrument. L. Teriaca, U. Schühle and S. K. Solanki in collaboration with E. Antonucci (INAF Osservatorio Astronomico di Torino, Turin, Italy); N. Afram, Y. Unruh (Imperial College, London, UK); J. Harder (University of Colorado, Boulder, USA); T. Wenzler (ETH Zürich, Switzerland).

Solar Orbiter: PHI
S. K. Solanki, W. Curdt, A. Feller, A. Gandorfer, L. Gizon, J. Hirzberger, A. Lagg, U. Schühle, G. Tomasch, S. Werner, and J. Woch in collaboration with V. Martinez Pillet (Instituto de Astrofísica de Canarias, IAC, La Laguna, Spain); T. Appourchaux (Institut d'Astrophysique Spatiale, IAS, Paris, France); M. Sigwarth (Kiepenheuer-Institut für Sonnenphysik, KIS, Freiburg, Germany); G. Scharmer (Institute for Solar Physics, Stockholm, Sweden); M. Carlsson (Institutt for teoretisk astrofysikk, Oslo, Norway).

Solar Orbiter: SPICE (formally EUS)
W. Curdt, U. Schühle, and E. Marsch in collaboration with D. Hassler, C. DeForest, D. Slater (Southwest Research Institute, San Antonio, USA); Davila, Antiochos, Kucera, R. Thomas (GSFC, NASA, Washington, USA); H. P. Warren, Mariska (NRL, Washington, USA); Schrijver (Lockheed, USA); S. Habbal, Roussev (University of Hawaii, USA); T. Zurbuchen (University of Michigan, USA); Longcope (Montana State University, USA); T. Appourchaux, Buchlin, F. Auchere, J.-C. Vial (IAS, Paris, France); Harrison, Young (RAL, Chilton, UK); Mathews (MSSL, London, UK); H. Peter (KIS, Freiburg, Germany); M. Carlsson, V. Hansteen (ITA, Oslo, Norway).

Solis
T. Wiegelmann and J. Thalmann in collaboration with N. E. Raouafi (NSO, Tucson, USA).

Spitzer and ESO observations of Oort Cloud Comets during their sojourns through the Solar Systems
H. Boehnhardt in collaboration with N. Biver (Observatory Paris-Meudon, France); P. Ehrenfreund (University Leiden, The Netherlands); D. Harker (University San Diego, USA); M. Kelley (Joint Astronomy Center, USA); S. Lederer (University San Bernardino, USA); D. Prialnik, E. Beer-Harari (University Tel Aviv, Israel); D. Wooden (PI) (NASA Ames Res. Center, Moffett Fields, USA); C. Woodward (University Minnesota, USA).

Starspot
S. K. Solanki and A. Semenova in collaboration with S. Berdyugina (ETH Zürich, Switzerland); P. Petit (Observatoire Midi-Pyrénées, Toulouse, France).

STEREO – IMPACT/SIT
Suprathermal Ion Telescope. R. Bučik, B. Inhester, U. Mall, B. Podlipnik, P. Ruan, and A. Korth in collaboration with J. Luhmann (University of California, Berkeley, USA); V. Bothmer (Universität Göttingen) und Mitarbeitern folgender Institute: NASA/Goddard Space Flight Centre, Greenbelt, USA; NASA/Jet Propulsion Lab, Pasadena, USA; California Institute of Technology, Pasadena, USA; Los Alamos National Lab, Los Alamos, USA; DESPA, Observatoire de Paris, Meudon, France; University of Michigan, Ann Arbor; Lab for Atmospheric and Space Physics, Univ. of Colorado, Boulder, USA; Universität Kiel; KFKI Research Institute for Particle and Nuclear Physics, Budapest, Hungary; Science Applications International Corporation, San Diego, USA; Centre d'Etude Spatiale des Rayonnements/CRNS, Toulouse, France; ESA/ESTEC, Noordwijk, The Netherlands; University of Maryland, College Park, USA; Space Environment Centre, NOAA, Boulder, USA.

STEREO – SECCHI
Sun Earth Connections Coronal and Heliospheric Investigation. J. De Patoul, L. Feng, B. Inhester, B. Podlipnik, P. Ruan, S. K. Solanki, T. Tadesse, J. Thalmann, and T. Wiegelmann in collaboration with R. Howard (Naval Research Laboratory, Washington D.C., USA); V. Bothmer (Universität Göttingen) und Mitarbeitern folgender Institute: Johns Hopkins University, Laurel, USA; Rutherford Appleton Laboratory, Didcot, Oxfordshire, UK; University College, London, UK; Mullard Space Science Lab, Holmbury, Surrey, UK; NASA/Goddard Space Flight Centre, Greenbelt, USA; University of Birmingham Astrophysics Space Research Group, Birmingham, UK; Universität Kiel, Germany; Centre Spatial de Liege, France; Lockheed Martin Solar Lab, Palo Alto, USA; Institut d'Astrophysique Spatiale, Orsay, France; Royal Observatory of Belgium, Bruxelles, Belgium; Laboratoire d'Astronomie Spatiale, Marseille, France; Observatoire de Paris, France; NASA/Jet Propulsion Labs, Pasadena, USA; University of Michigan, Ann Arbor, USA; Science Applications International Corporation, San Diego, USA.

Structure of sunspots
J. M. Borrero, A. Lagg, S. K. Solanki, S. K. Mathew, N. A. Krivova, and L. Bharti in collaboration with B. Lites (High Altitude Observatory, Boulder, USA).

Structure of the solar chromosphere
S. K. Solanki and A. Lagg in collaboration with M. Loukitcheva (University St. Petersburg, Russia); S. White (University of Maryland, Greenbelt, USA).

SUNRISE
Ballongetragenes 1-m Sonnenteleskop für hochauflösende spektro-polarimetrische Beobachtungen der Sonnenatmosphäre. S. K. Solanki, P. Barthol, A. Gandorfer, M. Schüssler, A. Lagg, and J. Borrero in collaboration with V. Martinez-Pillet (Instituto de Astrofísica de Canarias, Tenerife, Spain), W. Schmidt (Kiepenheuer-Institut für Sonnenphysik, Freiburg, Germany), B. W. Lites (High Altitude Observatory, NCAR, Boulder, USA); Lockheed Martin Solar and Astrophysical Lab, Palo Alto, USA.

Sunspots
A. Lagg, S. K. Solanki, N. A. Krivova, J. Borrero, and L. Bharti in collaboration with V. Martínez Pillet (Instituto de Astrofísica de Canarias, Tenerife, Spain); J. M. Borrero, B. Lites (High Altitude Observatory, Boulder, USA); S. K. Mathew (Udaipur Solar Observatory, India).

Surface exploration of Kuiper Belt Objects and Cometary Nuclei
H. Boehnhardt (PI) and S. Protopapa in collaboration with S. Bagnulo (ESO, Santiago de Chile, Armagh

Observatory, Northern Ireland); A. Barucci (Observatory Paris-Meudon, France); D. Cruikshank (NASA Ames, USA); W. Grundy (University Flagstaff, USA); T. Herbst (MPI für Astronomie, Heidelberg, Germany); K. Muinonen (University Helsinki, Finland); C. Olkin (SWRI Boulder, USA); G. P. Tozzi (INAF Arcetri Observatory, Florence, Italy).

Surface magnetic field effects in local helioseismology
H. Schunker in collaboration with D. C. Braun (CoRA, Boulder, USA); P. S. Cally (Monash University, Victoria, Australia).

SWA (Solar Wind Analyser) for Solar Orbiter
E. Marsch in collaboration with C. Owen (PI) (Mullard Space Science Laboratory (MSSL), UK).

The FeH $F^4\Delta$-$X^4\Delta$ system – Creating a valuable diagnostic tool to explore solar and stellar magnetic fields
S. K. Solanki and A. Lagg in collaboration with N. Afram, S. V. Berdyugina, D. M. Fluri (ETH Zürich, Switzerland).

The intensity oscillations in the chromospheric emissions
M. Loukitcheva and S. K. Solanki in collaboration with S. White (University of Maryland, College Park, USA).

Three-dimensional reconnection
J. Büchner in collaboration with B. Scott (IPP Garching, Germany).

Three–dimensional sensitivity kernels for ring–diagram analysis
L. Gizon in collaboration with A. C. Birch (CoRA, Boulder, USA); B. W. Hindman, D. A. Haber (JILA, Boulder, USA).

TNOs are cool
H. Boehnhardt, P. Hartogh and M. Rengel in collaboration with T. Mueller (MPE, Garching, Germany); E. Lellouch, A. Barucci, J. Crovisier, A. Delsanti, A. Dorresoundiram, S. Fornasier, D. Hestroffer (Observatoire Paris-Meudon, France); J. Stansberry, M. Mueller, D. Trilling (Univ. Arizon, Phoenix, USA); E. Dotto (Obs. Rome, Rome, Italy); R. Duffard, P. Gutierres, L. Lara, R. Moreno, J.-L. Ortiz, P. Sanz, A. Thirosin (IAA, Granada, Spain); O. Groussin (LAM, Marseille, France); O. Hainaut (ESO, Garching, Germany); A. Harris (DLR, Berlin-Adlershof, Germany) J. Horner (Open Univ, Milton Keynes, Great Britain); D. Jewitt, P. Lacerda (Univ. Hawaii, Honolulu, USA); M. Kidger (ESAC, Villafranca Spain); C. Kiss (Konkoly Obs, Budapest, Hungary); T. Lim, B. Swinyard (RAL, Didcot, Great Britain); N. Thomas (Univ. Bern, Bern, Switzerland).

Topology of coronal magnetic fields
T. Wiegelmann in collaboration with E. Priest, S. Régnier (University St. Andrews, UK).

Toroidal versus poloidal and radial magnetic fields in Sun-like stars: a rotation threshold
S. K. Solanki in collaboration with P. Petit, B. Dintrans, J.-F. Donati, M. Aurière, F. Lignières, J. Morin, F. Paletou, R. Fares (Université de Toulouse, CNRS, France); J. Ramirez, C. Catala (LESIA, Observatoire de Paris-Meudon, France).

Travel–time sensitivity kernels for vector flows
L. Gizon in collaboration with A. C. Birch (CoRA, Boulder, USA).

Ulysses – DUST
H. Krüger (PI) and J. Kissel in collaboration with N. Altobelli, C. Polanskey (Jet Propulsion Laboratory, Pasadena, USA); B. Anweiler, D. Linkert, G. Linkert, R. Srama (MPI für Kernphysik, Heidelberg, Germany); E. Grün, R. Srama (MPI für Kernphysik, Heidelberg and Hawaii Institute of Geophysics and Planetology, Honolulu, USA); S. F. Dermott, B. A. Gustafson (University of Florida, Gainesville, USA); A. Flandes (Instituto de Geofísica, UNAM, Mexico); A. L. Graps (INAF-Istituto di Fisica dello Spazio Interplanetario, CNR - ARTOV, Rome, Italy); D. P. Hamilton (University of Maryland, College Park, USA); M. S. Hanner (Jet Propulsion Laboratory, Pasadena, USA); M. Horany (Laboratory for Atmospheric and Space Physics, Univ. of Colorado, Boulder, USA); M. Landgraf (ESA/ESOC, Darmstadt, Germany); B. A. Lindblad (Lund Observatory, Lund, Sweden); I. Mann (Institut für Planetologie, Universität Münster, Germany); J.A.M. McDonnell (Planetary and Space Science Research Institute, Milton Keynes, UK); G. E. Morfill (MPI für Extraterrestrische Physik, Garching, Germany); G. Schwehm (ESTEC, Noordwijk, The Netherlands).

Ulysses – SWICS (Solar Wind Ion Composition Spectrometer)
J. Woch and M. Fränz in collaboration with L. Rodriguez (Royal Observatory of Belgium, Brussels, Belgium); R. von Steiger (ISSI, Bern, Switzerland).

Understanding the WMAP Results: Low-order multipoles and dust in the vicinity of the solar system
V. Dikarev, O. Preuß, S. K. Solanki, and H. Krüger in collaboration with A. Krivov (Universität Jena, Germany).

Venus Express – ASPERA-4 (Analyzer of Space Plasmas and EneRgetic Atoms)
M. Fränz, J. Woch, N. Krupp, E. Dubinin, E. Roussos, C. Martinecz, and J. Kleimann in collaboration

with S. Barabash (PI), R. Lundin (IRF, Kiruna, Sweden); D. Winningham, R. Frahm (SWRI, San Antonio, USA); P. Wurz (Universität Bern, Switzerland); A. Coates (MSSL, London, UK); M. Grande (RAL, Chilton, UK); C. C. Curtis (UoA, Tuscon, USA); J. A. Sauvaud, A. Fedorov (CESR, Toulouse, France); E. Kallio (FMI, Helsinki, Finland); S. Orsini (IFSI, Rome, Italy).

Venus Express Scientific Support
D. Titov in collaboration with H. Svedhem, O. Witasse (ESTEC-ESA, Noordwijk, The Netherlands); R. Hoofs, D. Meritt, M. Almeida (ESAC-ESA, Madrid, Spain).

Venus Express-VeRa (Venus Radio Science)
D. Titov in collaboration with M . Paetzold, S. Tellmann (Rheinisches Institut für Umweltforschung Cologne, Germany); B. Haeusler (University of Bundeswehr, Munich, Germany).

Venus Express – VIRTIS
D. Titov in collaboration with P. Drossart (Observatoire de Paris, Meudon, France); G. Piccioni, D. Grassi (Institute for Space Astrophysics (IAS-INAF), Rome, Italy).

Venus Express – VMC (Venus Monitoring Camera)
D. Titov in collaboration with H. Michalik, B. Fiethe, C. Dierker, B. Osterloh (Institut für Datentechnik und Kommunikationsnetze (IDA), TU Braunschweig, Germany); R. Jaumann, Th. Behnke, Th. Roatsch, K.-D. Matz, F. Scholten (Institut für Planetenforschung); N. Ignatiev, D. Belyaev, I. Khatuntsev (Space Research Institute (IKI), Moscow, Russia); E. Shalygin (Kharkov University, Ukraine); A. Basilevsky (Vernadsky Institute for Analytical Chemistry and Geochemistry (GEOKHI), Moscow, Russia); S. Limaye (University of Wisconsin, USA).

VESPER – Venus Atmosphere Chemistry and Dynamics Orbiter
P. Hartogh and C. Jarchow in collaboration with G. Chin (GSFC, Greenbelt, USA); M. Allen (JPL, Pasadena, USA).

VUV spectroscopy for Solar-C
L. Teriaca, S. K. Solanki, U. Schühle, and W. Curdt in collaboration with T. Shimizu (ISAS/JAXA, Tokio, Japan); T. Watanabe, S. Tsuneta (NAOJ, Tokio, Japan).

WASPAM / CAWSES
P. Hartogh, C. Jarchow, and L. Song in collaboration with G. Hansen (NILU, Tromsö, Norway); U. P. Hoppe (FFI, Kjeller, Norway); M. Gausa (ALOMAR, Andenes, Norway); U. von Zahn, F. J. Lübken, U. Berger, G. Sonnemann (IAP Kühlungsborn, Germany); G. Nedoluha, M. Stevens (NRL, Washington, USA); P. Espy (British Antarctic Survey, Cambridge, UK); Y. Kasai (NICT, Applied Research and Standards Department, Tokyo, Japan).

Wave propagation in inclined magnetic fields
H. Schunker in collaboration with D. C. Braun (CoRA, Boulder, USA); P. Cally (Monash University, Australia).

Projektförderungen durch das Bundesministerium für Wirtschaft und Technologie (BMWI) und andere Institutionen / Project grants provided by BMWI and other institutions

BMWI / DLR: ASTEX (DLR-Studie zu Near-Earth Asteroid Mission), BepiColombo-BELA, BepiColombo MMO MPPE-MSA, BepiColombo MPO SERENA-PICAM, Cassini MIMI-LEMMS, Cluster Active Archive (50%), Cluster-CIS, DAWN, ExoMars-SEIS, German Data Center for the Solar Dynamics Observatory (GDC-SDO), HIFI/WBS, Mars Express ASPERA-3, MOMA, Phoenix, RAPID, Rosetta/COSAC, Rosetta/COSIMA, Rosetta/MIRO, Rosetta/OSIRIS, Rosetta/PHILAE (Rosetta lander), Rosetta/RTOF, SOHO-SUMER, SOHO-LASCO, STEREO (SECCHI), SUNRISE, ULYGAL (Galileo EPD and Ulysses EPAC/GAS+SWICS).

DFG: DFG-Projekt: Evolution of Coronal Magnetic Fields, DFG Schwerpunktprogramm 1115 “Mars und die terrestrischen Planeten” – Plasma induced atmospheric escape on Mars.

ESA: Chandrayaan-1, Cluster Active Archive (50%), Exomars - MOMA, Venus Express/ASPERA-4, Venus Express/VIRTIS, VEXCEL.

EU: ChroMag, EST, EuroPlaNet, HELAS, SISI, Solaire.

JPL: DAWN, Project Herschel Guaranteed Time Key Programme, entitled: “Water and Related Chemistry in the Solar System” (PI: P. Hartogh), ROSETTA/OSIRIS.

NASA: RAISE.

Mitgliedschaften in wissenschaftlichen Gremien / Memberships in scientific councils

Boehnhardt, H.: Member of the Science Study Definition team for ESA’s Marco Polo Mission Study.

Christensen, U.: Göttinger Research Council; Kommission für Geowissenschaftliche Hochdruckforschung der Bayerischen Akademie der Wissenschaften; Executive Committee der International Association of Seismology and Physics of the Earth's Interior (IASPEI); Lichtenberg-Kommission der Göttinger Akademie der Wissenschaften; EGU Award & Medal Committee.

Curdt, W.: German JOSO representative.

Gandorfer, A.: THEMIS science council; ESA Solar Orbiter payload working group.

Gizon, L.: Chairman, Local Helioseismology Network Activity, European Helio- and Asteroseismology Network (HELAS, EU FP-6), 01.04.2006 – 31.03.2010; Member, HELAS Board; Member, Organizing Committee, IAU Div. II Comm. 12 "Solar Radiation and Structure"; Member, SOLAR-C Science Definition Team; Member, PLATO Assessment Study Team.

Hartogh, P.: Alomar Scientific Advisory Commitee; International Comission on Planetary Aeronomy.

Krupp, N.: Member of the science defintion team for the Europa Jupiter System Mission (EJSM).

Marsch, E.: Co-Chair of the Joint Science and Technology Definition Team für das ESA/NASA Programm HELEX (Heliophysical Explorers: Solar Orbiter and Sentinels); Mitglied (seit 2001) im Gutachterausschuss Extraterrestrik des DLR.

Rengel, M.: JCMT reviewer, International Time Allocation Committee (ITAC) for the James Clerk Maxwell Telescope (JCMT) participate in assessing observing proposals, in connection with the ITAG.

Roth, M.: HELAS Board Member; HELAS Project Scientist.

Solanki, S. K.: Stellvertretender Vorsitzender und Mitglied des Senatsausschusses des DLR; Mitglied des Berufungsausschusses und des Dreierausschusses des Senats des DLR; Vorsitzender und Mitglied des Programmausschusses Extraterrestrik des DLR; Mitglied der Programmkommission des DLR; Mitglied der Perspektivenkommission der Chemisch-Physikalisch-Technischen Sektion der MPG; Mitglied des wissenschaftlichen Beirats des High Altitude Observatory in Boulder, Colorado/USA, und des Istituto Ricerche Solari Locarno (IRSOL); Stellvertretender Vorsitzender und Mitglied des Beirats der Gesellschaft für Wissenschaftliche Datenverarbeitung Göttingen.

Schlegel, K.: Past President der URSI (International Union of Radio Sciences).

Titov, D.: Chair of the C3 Sub-commission of COSPAR; Vice-President of ICPAE (International Commission on Planetary Atmospheres and their Evolution); Member of the Science and Technology Definition Team for the NASA Flagship mission to Venus.

Gutachtertätigkeiten / Review reports

Gutachtertätigkeiten für wissenschaftliche Zeitschriften/Reviews for scientific journals
(Die folgende Aufstellung soll nur eine kurze Übersicht über die Gutachtertätigkeiten von Wissenschaftlern des MPS für wissenschaftliche Zeitschriften geben. Angeführt sind die Namen der Gutachter (alphabetisch) und die Zeitschriften./*In the following the names of the reviewers and the journals.*)

Gutachter / Reviewers:

H. Boehnhardt, U. Christensen, W. Curdt, P. W. Daly, M. Fränz, A. Gandorfer, L. Gizon and the SNWG Helio- and Asteroseismology, P. Hartogh, M. Hilchenbach, J. Hirzberger, B. Inhester, N. Krivova, E. Kronberg, H. Krüger, N. Krupp, A. Lagg, E. Marsch, E. Nielsen, A. Pietarila Graham, M. Rengel, J. C. Santos, K. Schlegel, U. Schühle, S. K. Solanki, L. Teriaca, D. Titov, V. Vasyliūnas, J. Wicht, T. Wiegelmann, K. Wilhelm, J. Woch.

Zeitschriften / Journals:

Advances in Geosciences (5), Advances in Space Research (5), Annales Geophysicae (6), Applied Optics (2), Astra (1), Astronomy and Astrophysics (20), Astrophysical Journal (8), Astrophysical Journal Letters (8), Atmospheric Chemistry and Physics (ACP)(2),Earth Planets and Space (1), Earth & Planetary Science Letters (2), Eos (1), Geophysical Journal International (1), Geophysical Research Letters (10), Icarus (6), IEEE (1), IEEE J. = Selected Topics in Signal Processing (1), Journal of Atmospheric and Solar-Terrestrial Physics (1), Journal of Geophysical Research (19), Monthly Notices of the Royal Astronomical Society (2), Nature (2), New Astronomy Reviews (1), Physical Review Letters (2), Physics of Plasmas (2), Physics of the Earth and Planetary Deep Interiors (3), Planetary and Space Science (11), Proceedings RAS (1), Proceedings of 5th Solar Polarization Workshop (1), Publications of the Astronomical Society of Japan (PASJ) (1), Science (4), Solar Physics (13), Space Science Reviews (3), Springer Astrophysics (2), SPW5 proceedings (1), The Rosetta Mission (ESA book) (3),

Gutachtertätigkeiten anderer Art /
Other types of reviews:

Boehnhardt, H.: Advisor for application to the German-Israeli Foundation for Scientific and Technical development; Advisor for the ESO study team of

METIS, the infrared spectrograph and imager for the Extremely Large Telescope; Advisor for MAPIS, the study team of the visnir spectrometer for ESA's MarcoPolo Mission; DLR Gutachterausschuss Extraterrestrik; Leibniz-Antrag.

Christensen, U.: Reviewing board Institute de Physique du Globe, Paris, France; Reviewing panel Sonderforschungsbereich (Collaborative Research Center), Universität Kiel.

Goesmann, F.: External examiner for a PhD thesis (Open University, Milton Keynes, UK).

Lagg, A.: Leibniz-Antrag.

Marsch, E.: Gutachten für ein Advanced Fellowship Proposal für das Science Technology Facility Council (STFC) in United Kingdom (1). Promotionsgutachten (3).

Rengel, M.: Memberships in Scientific Councils: JCMT reviewer: International Time Allocation Committee (ITAC) for the James Clerk Maxwell Telescope (JCMT) participate in assessing observing proposals, in connection with the ITAG. Mitarbeit bei Beobachtungsproposals: 2 approved Herschel Key Programs (co-I for for guaranteed time proposal, associated scientist for open time proposal); 1 approved ESO observing time proposals (PI); 1 approved SMA observing time proposal (Co-I), 1 approved CARMA observing time proposal (Co-I).

Schlegel, K.: 1 Gutachten für die University of Lancaster; 1 Gutachten für die University of Tromsö; 1 Gutachten für die NSERC-Canada.

Solanki, S. K.: Deutsche Forschungsgemeinschaft (3).

Wiegelmann, T.: Grant Proposal Reviewer for Academy of Science of the Czech Republic (1).

Herausgebertätigkeiten / Editorships

Aznar Cuadrado, R.: Living Reviews in Solar Physics.

Boehnhardt, H.: Earth, Moon, and Planets, Editorial board member. Co-editor, The solar system beyond Neptune. Co-editor, The Rosetta Book.

Christensen, U.: Phys. Earth Planet. Int. (Editorial board).

Daly, P.: ISSI SR-008, Multi-Spacecraft Analysis Methods Revisited.

Gizon, L., Leibacher, J., and Cally, P.: Editors, "Helioseismology, Asteroseismology, and MHD Connections", Springer, ISBN 978-0-387-89481-2, 2008.

Gizon, L. and Roth, M.: Editors, "Proceedings of the Second HELAS International Conference", Journal of Physics: Conference Series, Volume 118, 2008.

Hartogh, P.: Atmospheric Chemistry and Physics. Advances in Geosciences. Planetary and Space Science. ACP Special Issue on MIPAS.

Marsch, E.: Living Reviews in Solar Physics.

Solanki, S. K. : 'Editor in chief' der elektronischen, referierten Review-Zeitschrift "Living Reviews in Solar Physics" http://solarphysics.livingreviews.org. Editorial Board "Solar Physics" .

Titov, D.: Guest Editor of the Venus Express Special Issue of JGR.

Wilhelm, K.: Co-editor: ISSI Editor Group "Observing Photons in Space" (with about 40 authors). Mitarbeit an Landolt-Börnstein VI 4a.

Tätigkeiten als Convener bei wissenschaftlichen Tagungen / Convenorships during scientific meetings

Büchner, J.: Convenor, COSPAR, Montreal, Canada, 2008; Convenor, EGU, Vienna, Austria, April 2008.

Christensen, U.: Co-Convenor, Mercury-Session, EGU, Vienna, Austria, April 2008. Lead Convenor for ISSI Workshop on Planetary Magnetism, Bern, Switzerland, September 2008.

Gizon, L.: Convenor, Session IS61 – ST9/SM25 Synergies in terrestrial and solar seismology, EGU, General Assembly, Vienna, Austria, 17 April 2008.

Hartogh, P.: Convenor, AOGS Busan, Korea, June 2008.

Krüger, H.: Convenor, session 'Comets, asteroids and TNOs' at EPSC, Münster, Germany, September 2008.

Titov, D.: Convenor, COSPAR, Montreal, Canada, 2008; Convenor, EGU, Vienna, Austria, April 2008.

Wicht, J.: Convenor, EGU, Vienna, Austria, April 2008.

Organisation von Workshops und Tagungen / Workshop and scientific meetings organisation

Boehnhardt, H.: ESO INAF workshop on "Future ground-based solar system research: Synergies with space probes and space telescopes", Elba, Italy, 9 – 12 September 2008.

Gizon, L.: Chairman, Scientific Organizing Committee, Second HELAS Workshop on Local Helioseismology, Freiburg, Germany, 7 – 11 January 2008. Member of Scientific Organizing Committee, SOHO XXI/GONG 2008 "Solar-stellar dynamos as revealed by helio- and asteroseismology", Boulder, CO, USA, 11 – 15 August 2008. Chairman, First PLATO Ground Data Center Assessment Study Meeting, Katlenburg-Lindau, Germany, 27 – 28 October 2008.

Hilchenbach, M.: COSIMA Workshop, Nördlingen, Germany, 27 – 29 October 2008. COSIMA II Workshop, Nördlingen, Germany, 29 – 30 October 2008.

Krupp, N.: Cassini MAPS workshop, MPS, Katlenburg-Lindau, Germany, April 2008.

Roth, M.: Chairman, Local Organizing Committee, Second HELAS Workshop on Local Helioseismology, Freiburg, Germany, 7 – 11 January 2008.

Solanki, S. K.: 37th COSPAR Scientific Assembly, Session E23 "Photospheric Magnetic Field and Coronal Response", Montreal, Canada, 18 – 25 July 2008. Solar eclipse 2008: "Solar magnetism, corona and space weather", Jiuquan City, China, 29 July – 1 August 2008. 3rd International Symposium on KuaFu Project, Kunming, Yunnan, China, 21 – 26 September 2008. Evershed Centenary Meeting "Magnetic Coupling Between the Interior and the Atmosphere of the Sun", Bangalore, India, 2 – 5 December 2008.

Titov, D.: ESLAB Conference on Comparative Planetology, Frascati, Italy, 10 – 14 November 2008. Venus Express Workshop, La Thuile, Italy, 3 – 8 March 2008.

Wiegelmann, T.: NLFFF-5 Workshop, Katlenburg-Lindau, Germany, 30 June – 2 July 2008.

Öffentlichkeitsarbeit / Public relations

Dr. B. Krummheuer und Dr. N. Krupp (Verantwortliche für die Presse- und Öffentlichkeitsarbeit des MPS)

Die Presse- und Öffentlichkeitsarbeit am MPS setzt sich zusammen aus der Erstellung von Pressenotizen, dem Beantworten von Journalisten-Anfragen, der Organisation und Durchführung von Besuchen von Radio- und Fernsehteams, Führungen durch das Institut, öffentlichen Vortragsreihen, Ausstellungen sowie der Teilnahme an speziellen, öffentlichen Veranstaltungen.
Zur Steigerung des überregionalen Bekanntheitsgrads des Instituts hat 2008 besonders die Pressearbeit im Zusammenhang mit der Marslandung der NASA-Raumsonde Phoenix und mit der Teilnahme an der indischen Mondmission Chandrayaan beigetragen.

TV- und Hörfunkauftritte / Media coverage

Der Besuch von Radio- und TV-Teams am MPS hat sich 2008 weiter gesteigert. Eine Übersicht befindet sich in der Tabelle auf Seite 174.

Pressenotizen / Press releases

2008 hat das MPS 19 Pressemitteilungen herausgegeben. Diese wurden insgesamt in mehr als 400 Fällen von regionalen und überregionalen Medien aufgegriffen.

2008 wurden die folgenden Pressemitteilungen herausgegeben:

- Raumsonde Cassini enthüllt neue Rätsel der Eismonde des Saturn. 21. Februar 2008.
- Der leuchtende Schleier der Liebesgöttin. 25. Februar 2008.
- Ringe um Rhea. 6. März 2008.
- Mädchen erkunden die Weltraum-Labors (Einladung zum Girls' Day). 18. April 2008.
- Staubige Begleiter durch Licht und Schatten. 30. April 2008.
- Deutsche Technik auf dem Mars. 22. Mai 2008.
- Ein Blick in die Schaufel der Phoenix-Sonde. 30. Mai 2008.
- Turbulente Winde und dichte Wolkendecken. 30. Mai 2008.
- Deutsche Mars-Kamera findet Hinweise auf Eis. 2. Juni 2008.
- Mars-Sonde Phoenix: Es muss Eis sein. 20. Juni 2008.
- Erstes Tagebuch einer Sonneneruption. 11. August 2008.
- Eine nächtliche Reise zu Planeten, Kometen und zur Sonne. 22. August 2008.
- Eine Kamera navigiert durchs All. 28. August 2008.
- Es brodelt unterm Sonnenfleck. 1. September 2008.
- Erste Bilder des Asteroiden Steins. 6. September 2008.
- Max-Planck fliegt zum Mond (Abb. 192). 20. Oktober 2008.
- Max-Planck-Institut für Sonnensystemforschung ist "Ausgewählter Ort im Land der Ideen 2009" (Abb. 193). 25. November 2008.
- In einem neuen Licht betrachtet. 3. Dezember 2008.
- Das Teleskop am Kran. 19. Dezember 2008.


Indien schießt Sonde zum Mond

Die Mission dient der Wissenschaft, doch das Raumfahrtprogramm ist zugleich Symbol nationaler Stärke

Abb. 192: Die Pressemitteilung zur MPS-Beteiligung an der indischen Mondmission Chandrayaan wurde von mehr als 120 Medien aufgegriffen. Die Abbildung zeigt den Artikel aus der Süddeutschen Zeitung vom 23.10.2009.

Von besonders vielen Medien wurden die Pressemitteilungen "Staubiger Begleiter durch Licht und Schatten" (mehr als 30 Medien), "Deutsche Technik auf dem Mars" (mehr als 90 Medien), "Deutsche Mars-Kamera findet Hinweise auf Eis" (mehr als 30 Medien), "Erstes Tagebuch einer Sonneneruption" (mehr

Landkreis Northeim

Mittwoch, 26. November 2008

Preis für Sonnenforschung

Lindauer Institut zum zweiten Mal als „Ort im Land der Ideen" ausgezeichnet

HINTERGRUND

Schirmherr ist Horst Köhler

Abb. 193: Auch die Mission SUNRISE stieß in Medien und Öffentlichkeit auf großes Interesse. Unter anderem erhielt das MPS für dieses Projekt die Auszeichnung "Ausgewählter Ort im Land der Ideen 2009".

als 30 Medien) und "Max-Planck fliegt zum Mond" (mehr als 120 Medien) aufgegriffen.

Erich-Regener-Vortragsreihe / Erich-Regener lecture series

Die öffentliche Vortragsreihe "Erich-Regner-Vorträge" wurde 2008 erfolgreich fortgesetzt. Die Vorträge waren stets gut besucht.

- 21. Februar 2008.
  Prof. Dr. Gerhard Haerendel (MPI für extraterrestrische Physik, Garching): Das Unsichtbare sichtbar machen – Plasmawolkenexperimente im Weltraum.
- 10. April 2008.
  Dr. Walter Goetz (MPS): Die Geologie des Mars: Erkenntnisse aus früheren und Ausblick auf zukünftige Mssionen.
- 9. Juni 2008.
  Prof. Dr. Peter Schuster (Universität Wien): Leben – Ein Produkt von Evolution oder Design?
- 21. August 2008.
  Prof. Dr. Gudrun Wolfschmidt (Universität Hamburg, Geschichte der Naturwissenschaften): Sonnenphysik im 2. Weltkrieg.
- 7. Oktober 2008.
  Dr. Michael Küppers (ESA, Villanueva de la Canada/Madrid): Klein, aber oho – Rosetta begegnet einem aussergewöhnlichen Asteroiden.
- 9. Dezember 2008.
  Dr. Jürgen Hamel (Berlin): 1609 – oder: Kepler, Galilei, das Fernrohr und die Folgen. Das Internationale Jahr der Astronomie 2009.

Institutsführungen, Ausstellungen und spezielle Events / Guided tours, exhibitions, and special events

Ein wesentlicher Bestandteil der Öffentlichkeitsarbeit am MPS sind Führungen durch das Institut. Die Besuchergruppen kommen nicht nur aus der Umgebung, sondern reisen zum Teil auch aus anderen Bundesländern an. Die Besucher umfassen Erwachsene, Jugendliche, Schüler und Kindergartenkinder. 2008 wurden am MPS 14 Führungen für insgesamt mehr als 350 Personen durchgeführt.

Spezielle Veranstaltungen

Im Berichtszeitraum hat das Institut an mehreren, öffentlichkeitswirksamen Veranstaltungen teilgenommen.

Am 24. April 2008 hat das Institut etwa 30 Mädchen (und Jungen) zum Girls' Day eingeladen. Die Teilnehmer waren zwischen elf und 15 Jahren alt. Sie hatten an diesem Tag die Gelegenheit, speziell die Werkstätten und Labore des Instituts näher kennen zulernen und sich dort an einigen praktischen Übungen zu versuchen. Zudem konnten sie sich im Rahmen eines Mit-Mach-Vortrages über das Sonnensystem informieren.

Vom 28. Juni bis zum 4. Juli 2008 war das MPS mit einem Stand beim Wissenschaftssommer in Leipzig vertreten. Der Stand trug den Titel "Planetare Dynamos" und informierte im Rahmen des Jahres der Mathematik darüber, wie mathematische Methoden am MPS zum Einsatz kommen, um den Geo-Dynamo der Erde und anderer Planeten zu erforschen. Für die Besucher gab es zahlreiche Experimente zum Ausprobieren, die in das Phänomen des Magnetismus einführten. Zudem wurde der Geo-Dynamo der Erde anhand einer riesigen, aufgeschnittenen Erdkugel (1,2 Meter Durchmesser) erläutert. Poster ermöglichten zudem einen Einblick in das Innere anderer Planeten des Sonnensystems. Der Stand des MPS war während der gesamten Ausstellungszeit außerordentlich gut besucht. Besonders die Experimente erfreuten sich großer Beliebtheit. Nach Angaben der Veranstalter besuchten den Wissenschaftssommer in Leipzig zwischen 70000 und 100000 Gäste pro Woche. Über die Veranstaltung wurde in überregionalen Medien ausführlich berichtet.

Am 4. Juli fand am MPS das Kinderuni-Seminar "Unser Sonnensystem" mit 16 Schülern statt.

Am 6. September fand am MPS der Astronomietag statt. Von 17 bis 23 Uhr hatten Besucher die Gelegenheit, sich über die Forschung am Institut zu informieren. Neben zahlreichen Informationsständen gab es ein umfangreiches Vortragsprogramm. Ein besonderer Publikumsmagnet war dabei ein Kindervortrag über das Sonnensystem. Zudem gab es Filme, ein spezielles Bastel- und Spielprogramm für Kinder und mehrere Planetenwegwanderungen. Insgesamt besuchten etwa 1000 Gäste an diesem Tag das MPS (Abb. 194).

Abb. 194: Der Kindervortrag über das Sonnensystem, gehalten von Prof. Sami K. Solanki, füllte den Hörsaal des Max-Planck-Instituts für Sonnensystemforschung.

Tag der Aufnahme	**Radio Sender**	**TV Sender**	**Sende-datum/zeit**	**Projekt Thema**
10.03.08		Sat 1 Regional	11.03.08: 17.30	Cassini Rhea Roussos, Krüger, Krupp
07.05.08	SWR2		09.05.08	Ulysses, Woch, Krupp, Krüger
07.05.08	Deutschlandfunk		10.06.2009: 16:35	Ulysses, Woch, Krupp, Krüger
09.05.08	Radio Frei Erfurt		25.05.08: 18.00 26.05.08: 11.00	Ulysses, Krupp
15.05.08		Sat 1 Regional	23.05.08: 17.30	Phoenix, Goetz, Markiewich
21.05.08		ZDF heute-Nachrichten	26.05.08: 17.00, 19.00, 21.45	Phoenix, Goetz, Markiewich
23.05.08	NDR			Phoenix, Christensen, Goetz, Markiewicz
23.05.08	Bayrischer Rundfunk			Phoenix, Christensen, Goetz, Markiewicz
		NDR “Hallo Niedersachsen”	26.05.08: 18.00, 19.30	Phoenix, Goetz, Markiewich
26.05.08	Nordwest-Radio		26.05.08: 6.40, abends	Phoenix, Christensen, Goetz, Markiewicz
26.05.08	Radio FFN		26.05.08	Phoenix, Christensen, Goetz, Markiewicz
26.05.08	MDR		26.05.08	Phoenix, Christensen, Goetz, Markiewicz
28.05.08	Deutschland-Radio		28.05.08	Phoenix, Christensen, Goetz, Markiewicz
03.06.08	Nordwest-Radio		03.06.08	Phoenix, Christensen, Goetz, Markiewicz
		NDR “DAS forscht”	20.06.08: 11.00	Phoenix,
01.08.08	NDR		01.08.08	Phoenix, Christensen, Goetz, Markiewicz
01.08.08	Deutschland-Radio		01.08.08	Phoenix, Christensen, Goetz, Markiewicz
01.08.08	Hit Radio Antenne Niedersachsen		01.08.08	Phoenix, Christensen, Goetz, Markiewicz
01.08.08	NDR2		01.08.08	Phoenix, Christensen, Goetz, Markiewicz
01.08.08		ARD Tagesschau	01.08.08: 20.00	Phoenix, Christensen, Goetz, Markiewicz
	NDR Logo		12.08.08	Sonneneruptionen, Wiegelmann, Thalmann
	NDR Radio		06.09.08	Astronomietag
	Deutschland-Radio		Forschung-Aktuell 04.09.08	Rosetta, Sierks
		NDR “Hallo Niedersachsen”	22.10.08: 18.00 + 19.30	SIR2, Chandrayaan 1
		RTL	24.10.08	SIR2, Chandrayaan 1
		RTL	30.10.08: 18.00	SIR2, Chandrayaan 1
		NDR “das Magazin”	11.11.08	Phoenix, Keller
	NDR1, NDR2, NDR info		11.11.08	Phoenix, Keller

X. Projektvorschläge, Lehrtätigkeit, Vorträge und Veröffentlichungen / Proposals, Teaching, Talks, and Publications

Projektvorschläge / Proposals

Applications of Nano-tube technology to space instrumentations
submitted to ERC FP7. M. Fraenz with F. Leblanc and U. Vohrer.

CARMA
1 approved CARMA observing time proposal (Co-I). M. Rengel.

ESO
5 ESO proposals (PI or co-I) got observing time granted. H. Boehnhardt.

ESO
1 approved ESO observing time proposal. (PI) M. Rengel.

GM-VIS-NIR Spektrometer
submitted to DLR. U. Mall.

Gravity wave drag in the thermosphere
submitted to DFG. P. Hartogh with A. Medvedev.

Herschel Key Programs
2 approved Herschel Key Programs (co-I for guaranteed time proposal, associated scientist for open time proposal). M. Rengel.

HGF – Alliance, Planetary, Evolution, and Life
submitted to Helmholtz Gesellschaft. U. Christensen with T. Spohn (DLR, Berlin) and others.

HIFI WBS Aufstockungsantrag
submitted to DLR. P. Hartogh

Interstellar Dust inside and outside the heliosphere
submitted to DFG. H. Krüger.

Investigations of the solar influence on middle atmospheric water vapour and ozone during the last solar cycle; analysis of the MPS data set
submitted to DFG. P. Hartogh with C. Jarchow.

MAPIS – The MarcoPolo visible-near-IR spectrometer
submitted to ESA. H. Boehnhardt and the MAPIS team.

Mars Riometer System
submitted to FP7, EC. E. Nielsen with F. Honary, S. Marple, V. Romano, G. de Franceschi, L. Alfonsi, L. Spogli, E. Zuccheretti, T. Ulich, C.-F. Fnell, M. Hapgood, P. Janhunen, J. Borg.

MPCS – The MarcoPolo Camera system
submitted to ESA. H. Boehnhardt and the MPCS team.

Phase II German Data Center for the SDO
funded by DLR Bonn; 2008 – 2012, PI: L. Gizon (527 kEUR, granted).

Polarimetric and Helioseismic Imager for Solar Orbiter
submitted to ESA. J. Woch with S. K. Solanki, A. Gandorfer, J. Hirzberger, A. Feller, L. Gizon, A. Lagg, U. Schuehle, et al.

Rosetta MIRO
submitted to DLR. P. Hartogh with H. Boehnhardt.

Seismic Imaging of the Solar Interior (SISI)
European Research Council (ERC) Starting Grant 2008 – 2012, PI: L. Gizon (500 kEUR, granted).

Simulacoes numericas em tres dimensoes de eventos solares geoefetivos
submitted to Conselho Nacional de Desenvolvimento Cientifico e Tecnologico (CNPq-Brazil). J. C. Santos with J. Büchner.

SMA
1 approved SMA observing time proposal (Co-I). M. Rengel.

SOLIVAR-3
submitted to DFG, SPP 1176 – CAWSES. N. A. Krivova with S. K. Solanki.

SOPHI
submitted to ESA. A. Gandorfer with S. K. Solanki, J. Woch et al.

SPP Planetary Magnetism
submitted to DFG. J. Wicht with M. Hohlschneider (Universität Potsdam), M. Mandea (GFZ), H. Luehr (GFZ), S. Gilder (LMU München).

Technische Untersuchungen für das Visible-Near Infrared Spektrometer (VIS-NIR) im Hinblick auf die geplante LEO Mission
submitted to DLR (AZA). U. Mall.

Lehrtätigkeiten / Teaching

Von Mitgliedern des MPS wurden an mehreren, inländischen und ausländischen Universitäten verschiedene Vorlesungen gehalten: /
MPS scientists have lectured at a number of German and foreign universities:

Georg-August-Universität zu Göttingen

Dr. Hermann Boehnhardt, Prof. Dr. Jörg Büchner, Prof. Dr. Ulrich Christensen, Dr. Laurent Gizon, Prof Dr. E. Marsch, Dr. Dieter Schmitt, Prof. Dr. Manfred Schüssler, Prof. Dr. Sami K. Solanki, and Dr. Dmitry Titov
SS 2008: Einführung in die Physik des Sonnensystems

Prof. Dr. Jörg Büchner
WS 2007/2008: Introduction into Heliophysics
SS 2008: Numerical Solution of Partiell Differential Equations
WS 2008/2009: Introduction into the Physics of the Sun, the Solar Wind and Space Weather

IMPRS Vorlesungen / IMPRS lectures

Astrobiology Lecture Course Network, 30 October 2007 – 18 March 2008 (A. Brack et al.)

Einführung in die Physik des Sonnensystems, SoSe 2008, Seminarraum Astrophysik (H. Boehnhardt, J. Büchner, U. Christensen, L. Gizon, E. Marsch, D. Schmitt, M. Schüssler, S. Solanki, D. Titov)

Retreat, 1 – 5 May 2008 (D. Schmitt)

Wavelet analysis, from the line to the two-sphere, 8 – 9 May 2008 (J.-P. Antoine, Institut de Physique Théorique, UniversitĆatholique de Louvain, 1348 Louvain-la-Neuve, Belgium)

Hydrodynamics, 21 – 25 July 2008 (Antonio Ferriz Mas)

Integration of Partial Differential Equations, 6 – 9 October 2008 (T. Wiegelmann)

Introduction to Solar Physics, 24 – 28 November 2008 (S. Solanki)

Weitere Lehrtätigkeiten oder Kurse / Other lectures or courses

Dr. Andreas Lagg
A He 10830 lecture: some aspects from an observer's viewpoint, National Astronomical Observatory of Japan, 26 August 2008.

Dr. Dieter Schmitt
Geomagnetic dynamo theory, International School of Space Science, L'Aquila, Italy, 7 – 11 April 2008.

Dr. Dmitry Titov
Lecture course "Physics of planets" at Lulea Technical University, Kiruna, Sweden, 2008.

Prof. Vytenis Vasyliūnas
Energy conversion in planetary magnetospheres, Heliophysics II Summer School, Boulder, Colorado, USA, 23 – 31 July 2008.

Tee-Seminare / Tea Seminars

Leitung/Organizers: Dr. W. Curdt, Dr. C. Jarchow und Dr. W. Markiewicz

In den Seminaren wird von Wissenschaftlern des MPS, aber auch von Gästen in unregelmäßigen Zeitabständen über laufende Arbeiten vorgetragen.

MPS scientists, as well as guests to the Institute, report on their current work in the informal seminars.

Dr. Tra-Mi Ho, ESTEC, Netherlands Cometary Emission Morphology. 7 January 2008.

Dr. Mag Selwa, GSFC Greenbelt, USA, 3-D numerical simulations of coronal loops oscillations. 9 January 2008.

Prof. Antonius Otto, University of Alaska, Fairbanks, USA, Kelvin-Helmholtz Modes and Magnetic Reconnection: Plasma Transport across Magnetic Boundaries. 17 January 2008.

Prof. Dr. Thorsten Hohage, Uni Göttingen, Germany, Regularization of Inverse Problems. 29 February 2008.

Dr. René Holzreuter, Institut für Astronomie, ETHZ Zürich, Switzerland, A short walk through the Second Solar Spectrum. 5 March 2008.

Dr. Kaufmann, MacKenzie Univ., Sao Paulo, Brazil, Solar burst broadband coherent synchrotron radiation at microwaves produced by bunched high energy electron beams. 17 March 2008.

Dr. Jean-Phillipe Combe, Bear Fight Center, Winthrop, WA, USA, Remote mineralogy analysis of planetary surfaces by reflectance imaging spectrometry: Examples for the surface of the Moon. 11 April 2008.

Prof. Carsten Denker, AIP Potsdam, Germany, Perspectives for High-Resolution Imaging Spectropolarimetry. 21 April 2008.

Dr. Roberto Bugiolacchi, University College London, UK, Stratigraphy and composition of lava flows in Mare Nubium and Mare Imbrium. 29 May 2008.

Dr. Eberhard Wiehr, retired from Institut für Astrophysik, Göttingen, Germany, Small-scale intergranular structures as tracers for magnetic regions. 12 June 2008.

Prof. Per Helander, MPI for Plasma Pysics, Stellarator Theory Division, Greifswald, Germany, 'Runaway' acceleration of electrons in tokamaks and elsewhere. 24 June 2008.

Dr. Arpad Kis, Geodetic and Geophysical Research Institute of the Hungarian Academy of Sciences, Hungary, Energetic ions and low frequency waves in front of the Earth's bow shock. 25 June 2008.

Dr. Hakan Smith, Centre for Fusion, Space and Astrophysics, Warwick University, Coventry, UK, Runaway electrons in tokamak disruptions. 30 July 2008.

Dr. Stefano Bagnulo, Armagh Observatory, UK, Polarimetry with large telescopes. 12 August 2008.

Dr. Murthy Gudipati, Jet Propulsion Laboratory, California Institute of Technology, USA, Organic Chemistry in Planetary Water-Ices. 1 September 2008.

Dr. Gianna Cauzzi, INAF-Arcetri Astrophysical Observatory, Italy, Observing the dynamic solar chromosphere with IBIS. 16 September 2008.

Dr. Nagaraju Krishnappa, Indian Institute of Astrophysics, Bangalore, India, Potentiality of H-alpha as a chromospheric magnetic diagnostic: observational point of view. 18 September 2008.

Dr. Geronimo Villanueva, NASA-Goddard Space Flight Center, Greenbelt, MD, USA, Is Mars a Dead Planet? 19 September 2008.

Dr. Shibu Mathew, Udaipur Solar Observatory, India, A 20 cm space coronograph on Aditya I. 22 September 2008.

Dr. Pedro Lacareda, University of Hawaii, USA, The comet domain. 22 September 2008.

Dr. Jiansen He, School of Earth and Space Sciences, Peking University, China, Electron trapping around a magnetic null pair during magnetic reconnection. 29 September 2008.

Dieter H. Nickeler, Astronomical Institute, Ondrejov, Czech Republic, Stationary stagnation point flows in the vicinity of a 2-D magnetic null point. 10 November 2008.

Dr. Julius Koza, Astronomical Institute, Tatranska Lomnica, Slovakia, Dynamic fibrils in H-alpha and Ly-alpha. 2 December 2008.

Prof. Gottfried Mann, AIP Potsdam, Germany, Electric circuits and electron acceleration in the solar atmosphere. 11 December 2008.

Nadezda Evdokimova, Space Research Institute (IKI), Moscow, Russia, Ice, frost and bound water retrieved from mapping spectrometer OMEGA/Mars Express data: a link to the seasonal water cycle. 11 December 2008.

IMPRS Solar System Seminars

Leitung: Dr. Dieter Schmitt

The Solar System Seminars (S^3) takes place every second Wednesday afternoon from 13:00 to 16:30. It consists of up to three talks by students on their PhD projects (each 20 min talk plus 10 min discussion), an extended coffee break for further discussion and a tutorial talk (60 min).

Manuela Lippi:
Gas emission from active comets.
Silvia Protopapa:
Surface ice spectroscopy of Pluto and Charon resolved.
Nilda Oklay:
Small-scale magnetic structures in the photosphere as seen with spectropolarimetric eyes.
16 January 2008.

Peng Ruan:
Modeling large-scale coronal structures.
Li Feng:
3-D reconstructions of coronal loops from SECCHI/STEREO images.
Yana Maneva:
The importance of wave-particle interactions in the corona and solar wind.
Setareh Javadi:
Solar coronal bright point modeling.
31 January 2008.

Visiting the Technical University Braunschweig
13 February 2008.

Lars Guicking:
Venus: Solar wind interaction and Venus Express magnetometer observations.
Joachim Müller:

Adaptive mesh refinement applied to Plasma Simulation Codes.
Erik Johansson:
Close-in extrasolar planets and hybrid simulations of their interaction with the stellar wind.

Lotfi Yelles Chaouche:
Comparison of the thin flux tube approximation with 3-D MHD simulations.
Sofiane Bourouaine:
Coronal loop model including ion kinetics.
Arianna Piccialli:
Cyclostrophic wind in Venus mesosphere.
20 February 2008.

Sanja Danilovic:
MHD simulations vs. Hinode/SP data.
Raphael Attie:
Explosive events in the not-so-quiet sun.
Philippe Kobel:
Statistical classification: Application to Solar Bright Points and Faculae.
23 April 2008.

Hui Tian:
Magnetic structure of the solar transition region.
Manuela Wiese:
From spectra to lunar geology.
7 May 2008.

Julia Thalmann:
Magnetic field extrapolation of flaring active regions.
Richard Moissl:
Morphology and dynamics of the Venus atmosphere at cloud top level.
20 May 2008

Esa Vilenius:
Data reduction of near infrared spectrometers SIR and SIR-2.
Xianyi Li:
Development of large time bandwidth product SAW chirp filters.
Gero Kleindienst:
ULF waves in the Kronian magnetosphere.
18 June 2008.

Jingnan Guo:
Particle acceleration in solar flares.
Tino Riethmüller:
Stratification of sunspot umbral dots from the inversion of Hinode/SP data.
Nilda Oklay:
Spectropolarimetric investigations of the deep photospheric layers of solar magnetic structures.
2 July 2008.

Yana Maneva:
Shaping of particles' distributions in coronal holes and fast solar wind – theory and simulations.
Danica Tothova:
Signatures of shock acceleration and plasma heating.
Mingyuan Wang:
Ionospheres of weakly magnetized planets in stellar winds – the case of Mars.
29 October 2008.

Manuela Lippi:
High resolution spectroscopy of comets in the mid-infrared.
Shangbin Yang:
Evidences for magnetic helicity exchange between two neighbouring emerging active regions.
Anna Müller:
Energetic particle injections in the Kronian magnetosphere.
Daniel Heyner:
A Hermean feedback dynamo.
12 November 2008.

Anne Angsmann:
Structure and dynamics of the upper ionosphere of Venus.
Judith de Patoul:
3-D reconstruction of solar polar plumes from STEREO/SECCHI images using the Hough transform.
Ferdinand Plaschke:
The magnetopause: A membrane under tension?
3 December 2008.

Ramy El Maarry:
Aqueous alteration products and the role of impact events: insights from Phoenix.
Thorsten Stahn:
Attempting a global fit for oscillation parameters of alpha Cen A.
Kristofer Hallgren:
Ground based observations of short term water vapor variability in the upper mesosphere.
17 December 2008.

MPS-Kolloquien / MPS Colloquia

Leitung: Dr. Hermann Böhnhardt

Zu diesen Kolloquien werden meistens nur auswärtige Wissenschaftler eingeladen, um möglichst allgemein über ihr Arbeitsgebiet zu berichten.

Colloquia are usually given by external scientists invited to the Institute to report fairly broadly on their field of research.

Prof. Dr. Thomas Klinger, MPI, Plasma Physics Greifswald, Germany: Magnetic field geometry and plasma inclusion – History, physics and praxis of praxis of the nuclear fusion project Wendelstein 7-X. 16 January 2008.

Prof. Dr. Dina Prialnik, University of Tel Aviv, Israel: Modelling icy bodies in the solar system. 23 January 2008.

Prof. Dr. Karl-Heinz Glassmeier, Technical University Braunschweig, Germany: Turbulence, waves and oscillations of the terrestrial magnetospheric system. 20 February 2008.

Prof. Dr. Conny Aerts, University of Leuven, Netherlands: Recent highlights in asteroseismology: A biased selection. 27 February 2008.

Prof. Dr. Luis Barrera, University Santiago de Chile: South American archaeoastronomy in Inka and Rapa Nui (Easter Island) cultures. 12 March 2008.

Prof. Dr. Michel Blanc, Observatoire Midi-Pyrenees, France: The new face of the Saturn system and the fascinating world of Titan: highlights of the CASSINI-HUYGENS mission. 2 April 2008.

Prof. Dr. Tom Krimigis, Academy of Athens, Greece: Particles and fields at Mercury: MESSENGER's first flyby. 3 April 2008.

Prof. Dr. Claude Catala, Observatoire de Paris-Meudon, France: PLATO: PLAnetary Transits and Oscillations of stars. 12 June 2008.

Prof. Dr. Thomas Reiter, DLR Köln, Germany: The mission Astrolab – fascination space. 4 July 2008.

Prof. Dr. Hartmut Grassl, Zentrum für Marine und Atmosphärische Wissenschaften, Germany: The dampening of anthropogenic climate change. 14 August 2008.

Prof. Dr. Harald Hiesinger, University of Münster, Germany: The Moon – A Stepping Stone for the Exploration of the Solar System. 27 August 2008.

Dr. Fernando Comeron, European Southern Observatory Garching, Germany: Between planets and stars – The lightest bodies formed in isolation. 1 October 2008.

Prof. Dr. Humberto Campins, University of Florida, Orlando, USA: Comet-Asteroid Transition Objects. 26 November 2008.

Dr. Tetsuya Tokano, University Köln, Germany: Variation in Titan's Rotation Caused by the Atmosphere. 17 December 2008.

Vorträge 2008 / Talks 2008

Betreuung der Online-Veröffentlichungs- und Vortragsliste: P. W. Daly

Aasnes, A., **M. Taylor**, C. P. Escoubet, H. Laakso, A. Masson, J. Davies, P. Daly, A. N. Fazakerley, and C. Perry: Electron acceleration observed in a near-Earth magnetotail reconnection event. 37th COSPAR Scientific Assembly, Montreal, Canada, July 13-20, 2008. (Oral)

Abramenko, V., V. Yurchyshyn, and T. Wiegelmann: A proxy for horizontal electric currents in the solar photosphere. AGU Fall Meeting, San Francisco, USA, December 15-19, 2008. (Poster)

Agarwal, J., M. Mueller, M. V. Sykes, W. T. Reach, H. Boehnhardt, and E. Gruen: The dust trail of comet 67P/Churyumov-Gerasimenko near aphelion. Asteroids, Comets, Meteors 2008, Baltimore, USA, July 13-18, 2008. (Poster)

Angsmann, A., E. Dubinin, M. Fränz, C. Martinecz, J. Woch, S. Barabash, M. Pätzold, and T. L. Zhang: Structure and dynamics of the ionopause of Venus. European Planetary Science Congress 2008, Münster, Germany, September 22-26, 2008. (Oral)

Araneda, J., **E. Marsch**, and A. Vinas: Proton core heating and beam formation via parametrically unstable Alfvén-cyclotron waves. Frühjahrstagung des DPG Fachverbands Extraterrestrische Physik (EP) und der AEF e.V., Freiburg, Germany, March 3-7, 2008. (Oral)

Armstrong, T., J. Manweiler, D. Hamilton, S. M. Krimigis, N. Krupp, C. Paranicas, and D. Mitchell: Energy spectra, angular distributions, and compositions of energetic ions in saturn's inner magnetosphere. 37th COSPAR Scientific Assembly, Montreal, Canada, July 13-20, 2008. (Oral)

Arridge, C. S., H. J. McAndrews, N. Andre, E. J. Bunce, K. C. Hansen, T. W. Hill, R. E. Johnson, G. H. Jones, S. Kempf, K. K. Khurana, N. Krupp, W. S. Kurth, J. S. Leisner, C. Paranicas, E. Roussos, C. T. Russell, P. Schippers, E. C. Sittler, H. T. Smith, and M. F. Thomsen: Mapping magnetospheric regions at Saturn: a mini Jovian analogue? Saturn after Cassini-Huygens Symposium, Imperial College London, UK, July 28 - August 1, 2008. (Oral)

Asano, Y., I. Shinohara, A. Retino, P. Daly, E. Kronberg, Y. Khotyaintsev, A. Vaivads, C. J. Owen, A. N. Fazakerley, R. Nakamura, W. Baumjohann, T. Nagai, T. Takada, Y. Miyashita, M. Fujimoto, E. A. Lucek, and H. Rème: Electron acceleration in the near-Earth magnetotail in substorms. AGU Fall Meeting, San Francisco, USA, December 15-19, 2008.

Attie, R. and D. Innes: Explosive events in the not-so-quiet Sun. European Solar Physics Meeting (ESPM), Freiburg, Germany, September 8-12, 2008. (Oral)

Aurnou, J., M. Heimpel, A. King, and J. Wicht: Convective heat transfer and the pattern of thermal emission on the Gas Giants. AGU Fall Meeting, San Francisco, USA, December 15-19, 2008. (Poster)

Bárta, M., J. Büchner, and M. Karlicky: Multi-scale MHD numerical approach to the current sheet filamentation. Fifth International Cambridge Workshop on Magnetic Reconnection, Bad Honnef, Germany, August 18-22, 2008. (Oral)

Bárta, M., J. Büchner, and M. Karlicky: Multi-scale numerical modelling of the current sheet fragmentation. 37th COSPAR Scientific Assembly, Montreal, Canada, July 13-20, 2008. (Oral)

***Barucci, M. A.**, M. Yoshikawa, D. Koschny, H. Boehnhardt, et al.*: Science of Marco Polo: A near-Earth object sample return mission. 37th COSPAR Scientific Assembly, Montreal, Canada, July 13-20, 2008. (Oral)

Barucci, M. A., M. Yoshikawa, P. Michel, J. Kawaguchi, H. Yano, J. R. Brucato, I. A. Franchi, E. Dotto, M. Fulchignoni, S. Ulamec, H. Boehnhardt, M. Coradini, S. F. Green, J.-L. Josset, D. Koschny, M. Muinonen, J. Oberst, and the Marco Polo Science Team: MARCO POLO: A near Earth object sample return mission. 39th Lunar and Planetary Science Conference, League City, Texas, USA, March 10-14, 2008. (Oral)

Berchem, J., R. Richard, C. P. Escoubet, J. M. Bosqued, M. Taylor, K. Trattner, F. Pitout, H. Laakso, A. Masson, M. Dunlop, I. Dandouras, H. Rème, A. N. Fazakerley, and P. Daly: Global simulation of the cusps response to an abrupt change in the IMF direction: comparison with Cluster observations. 37th COSPAR Scientific Assembly, Montreal, Canada, July 13-20, 2008. (Oral)

Berdichevsky, D., D. Reames, C.-C. Wu, R. Schwenn, R. Lepping, R. MacDowall, C. Farrugia, J.-L. Bougeret, A. Ng, and C. Lazarus: Exploring the global shock scenario at multiple points between Sun and Earth: the launch of solar transients on January 1 and September 23, 1978. 35th COSPAR Scientific Assembly, Paris, France, July 13-20, 2008.

Blanc, M., M. Fujimoto, R. T. Pappalardo, S. Sasaki, L. Zelenyi, Y. Alibert, N. André, S. Atreya, R. Beebe, W. Benz, A. Coradini, A. Coustenis, V. Dehant, M. Dougherty, P. Drossart, O. Grasset, L. Gurvits, P. Hartogh, H. Hussmann, Y. Kasaba, M. Kivelson, K. Khurana, N. Krupp, P. Louarn, J. Lunine, M. McGrath, D. Mimoun, O. Moussis, J. Oberst, T. Okada, O. Prieto-Ballesteros, D. Prieur, P. Regnier, M. R. Serote, J. Schubert, C. Sotin, T. Spilker, Y. Takahashi, T. Takashima, F. Tosi, D. Turrini, and T. V. Hoolst: The LAPLACE original proposal. European Geosciences Union General Assembly, Vienna, Austria, April 13-18, 2008. (Oral)

Boehnhardt, H.: A lander for ESA's Marco Polo mission. ESA Cosmic Vision workshop - Marco Polo, Cannes, France, June 5-6, 2008. (Oral)

Boehnhardt, H.: The 2008 Heidelberg Christmas Comet Cocktail Recipe. Instituts-Kolloquium, Heidelberg, Germany, December 16, 2008. (Oral)

Boehnhardt, H. and H. U. Käufl: Future Ground-Based Solar System Research - A Conference summary. Future Ground-Based Solar System Research – Synergies with Space Probes and Space Telescopes, Portoferraio, Elba, Italy, September 8-12, 2008. (Oral)

Boehnhardt, H., A. Nathues, A. W. Harris, W. Goetz, C. Gritzneer, C. Jentsch, S. Schaeff, N. Schmitz, F. Weischede, and A. Wiegand: ASTEX – An in-situ exploration mission to two near-Earth asteroids. EGU General Assembly, Vienna, Austria, April 14-18, 2008. (Oral)

Boehnhardt, H., A. Nathues, A. W. Harris, and the ASTEX Study Team: ASTEX – An in-situ exploration mission to two near-Earth asteroids. DPG General Assembly, Freiburg, Germany, March 3-7, 2008. (Poster)

Boehnhardt, H., A. Nathues, A. W. Harris, and the ASTEX team: ASTEX – a study of a lander and orbiter mission to two near-Earth asteroids. Asteroids, Comets, Meteors 2008, Baltimore, USA, July 13-18, 2008. (Oral)

Boehnhardt, H., G. P. Tozzi, S. Bagnulo, K. Muinonen, A. Nathues, and L. Kolokolova: Imaging and polarimetry of the nucleus of comet 2P/Encke. Asteroids, Comets, Meteors 2008, Baltimore, USA, July 13-18, 2008. (Oral)

Boehnhardt, H., G. P. Tozzi, M. Sterzik, K. Muinonen, S. Bagnulo, and L. Kolokolova: Polarimetry in planetary science – A step forward with the VLT and a need for E-ELTs. Future Ground-Based Solar System Research – Synergies with Space Probes and Space Telescopes, Portoferraio, Elba, Italy, September 8-12, 2008. (Oral)

Bourouaine, S. and E. Marsch: Coronal loop modeling including ion kinetics. Solar Cycle 24, NAPA, California, USA, December 8-12, 2008.

Bourouaine, S. and E. Marsch: Multi-strand coronal loop and filter-ratio analysis. Solar Cycle 24, NAPA, California, USA, December 8-12, 2008, (Oral)

Bourouaine, S., C. Vocks, and E. Marsch: Coronal loop model including ion kinetics. Frühjahrstagung des DPG Fachverbands Extraterrestrische Physik (EP) und der AEF e.V., Freiburg, Germany, March 3-7, 2008. (Poster)

Brandt, P. C., C. P. Paranicas, D. G. Mitchell, E. C. Roelof, B. H. Mauk, S. M. Krimigis, and N. Krupp: Global energetic particle dynamics in Saturn's magnetosphere. AGU Fall Meeting, San Francisco, USA, December 15-19, 2008. (Oral)

Brucato, J., M. A. Barucci, D. Agnolon, R. Binzel, H. Boehnhardt, and the Marco Polo Science Study TEam: The Marco Polo Mission: A European opportunity to return samples from a near-Earth object for laboratory studies. Future Ground-Based Solar System Research – Synergies with Space Probes and Space Telescopes, Portoferraio, Elba, Italy, September 8-12, 2008. (Oral)

Büchner, J.: 3D reconnection in solar wind acceleration and flare eruptions. Fifth International Cambridge Workshop on Magnetic Reconnection, Bad Honnef, Germany, August 18-22, 2008. (Invited Lecture)

Büchner, J.: Anomalous resistivity in collisionless space plasmas. 5th Annual General Meeting of the Asia Oceania Geosciences Society, Busan, South Korea, June 20, 2008. (Oral)

Büchner, J.: From DC current heating to 3D reconnection – the modes of magnetic energy conversion in the chromosphere and corona investigated by means of numerical RMHD simulations based on Hinode observations. 2nd Hinode Science Meeting, Boulder, USA, September 29 – October 3, 2008. (Oral)

Büchner, J.: Influence of turbulence on solar magnetic reconnection. The Seventh International Workshop on Nonlinear Waves and Turbulence in Space Plasmas, Beaulieu, France, April 25, 2008. (Invited Lecture)

Büchner, J.: Magnetic reconnection at Sun and in Space. INPE Seminario Geofisica Espacial, Sao Jose dos Campos, Brazil, February 28, 2008. (Invited Colloquium Talk)

Büchner, J.: Magnetic reconnection at the Sun and in Space. Colloquium, Department of Physics and Astronomy, National Central University, Shuanglian, Taiwan, June 23, 2008. (Invited Lecture).

Büchner, J.: Magnetische Rekonnexion in Weltraumplasmen. Physikalisches Kolloquium, Ruhr-Universität Bochum, Germany, January 14, 2008. (Invited Lecture)

Büchner, J.: Magnetic reconnection at the Sun – observations and numerical simulation results. Modelling of astrophysical plasmas, Krakow, Poland, October 5-11, 2008, (Invited Lecture). (Oral).

Büchner, J.: Modelling 3D solar magnetic reconnection. International Workshop on the 2008 Total Solar Eclipse, Jiuquan, Gansu, China, July 31, 2008. (Invited Lecture)

Büchner, J.: Modelling current sheets and 3D solar magnetic reconnection. 37th COSPAR Scientific Assembly, Montreal, Canada, July 13-20, 2008. (Oral)

Büchner, J.: Numerical simulation of solar magnetic reconnection. Postgraduate school on "Computational Methods in Astrophysics", Bochum, Germany, March 13, 2008. (Invited Review Lecture)

Büchner, J.: Numerical simulation of the coronal response to the photospheric magnetic fiel evolution. 5th Annual meeting of the Asia Oceanic Geosciences Society, Busan, Korea, June 17, 2008. (Oral)

Büchner, J.: Numerical simulation of the non-force free coronal response to the photospheric magnetic field evolution and Hinode observations. 37th COSPAR Scientific Assembly, Montreal, Canada, July 13-20, 2008. (Oral)

Büchner, J.: Reconnection and dissipation in the Sun and its corona. 2nd International Workshop on Laboratory, Space, and Astrophysical Plasmas, Asia Pacific Center for Theoretical Physics, Pohang, South Korea, June 23, 2008. (Invited Lecture)

Büchner, J.: Signatures of reconnection in the solar corona. Dynamical Processes in Space Plasmas, Ein Bokek, Israel, May 11-19, 2008. (Invited Lecture)

Büchner, J.: Simulation of observable signatures of reconnection. 5th Annual Meeting of the Asia Oceanic Geosciences Society, Busan, Korea, June 17, 2008. (Invited Lecture)

Büchner, J.: Sites and signatures of reconnection in the solar corona. First SMESE workshop on coronal mass ejections and flares, Paris, France, March 10-12, 2008. (Oral)

Büchner, J.: The coronal response to the photospheric magnetic field evolution. 5th Annual General Meeting of the Asia Oceania Geosciences Society, Busan, South Korea, June 17, 2008. (Oral).

Büchner, J., J. C. Santos, and S. Javadi: Hinode related solar coronal plasma simulation. Hinode / SOLAR-C Meeting, MPI for Solar System Research Katlenburg-Lindau, Germany, January 30 – February 1, 2008. (Oral)

Bučík, R., R. Gomez-Herrero, B. Inhester, A. Korth, U. Mall, G. M. Mason, M. Mierla, and N. Srivastava: STEREO observations of solar energetic particles: a case study. European Geosciences Union General Assembly, Vienna, Austria, April 13-18, 2008. (Poster)

Bučík, R., R. Gomez-Herrero, A. Korth, U. Mall, and G. M. Mason: STEREO observations of energetic ion composition in the corotating interaction regions during the solar flares in May 2007. STEREO/Ulysses/SOHO/ACE energetic particle investigations meeting, Kiel, Germany, October 6-8, 2008. (Oral)

Bučík, R., R. Gomez-Herrero, A. Korth, U. Mall, and G. M. Mason: STEREO observations of source population for CIRs near weak SEP events. 21st European Cosmic Ray Symposium, Kosice, Slovakia, September 9-12, 2008. (Poster)

Bučík, R., R. Gomez-Herrero, A. Korth, U. Mall, and G. M. Mason: STEREO observations of suprathermal ion composition in CIRs around small SEP events. STEREO SWG & Science Workshop, Meudon, France, April 20-22, 2008.

Bučík, R., R. Gomez-Herrero, A. Korth, U. Mall, and G. M. Mason: The suprathermal ion telescope for STEREO mission. STEREO/Ulysses/SOHO/ACE energetic particle investigations meeting, Kiel, Germany, October 6-8, 2008. (Oral)

Burston, R., L. Gizon, Y. Saidi, and S. Solanki: German Data Center for the Solar Dynamics Observatory. 12th European Solar Physics Meeting, Freiburg, Germany, September 8-12, 2008. (Poster)

Burston, R., R. Lapole, L. Gizon, and A. Birch: Travel-time sensitivity kernels for weak magnetic field. 12th European Solar Physics Meeting, Freiburg, Germany, September 8-12, 2008. (Poster).

Cameron, R.: Helioseismology of sunspots. European Geosciences Union General Assembly, Vienna, Austria, April 13-18, 2008. (Oral)

Cameron, R.: Solar surface magnetoconvection simulations. International workshop of the 2008 solar total eclipse: Solar magnetism, corona and space weather – Chinese Space Solar Telescope Science, Jiuquan, Gansu, China, July 28 – August 1, 2008.

Christensen, U.: Modeling of planetary dynamos. Colloquium, Department of Geology and Geophysics, Yale University, New Haven, CT, USA, March 5, 2008, invited. (Oral)

Christensen, U. R.: Dynamo scaling laws. ISSI Workshop on Planetary Mangnetism, Bern, Switzerland, September 1-5, 2008, invited. (Oral)

Christensen, U. R.: Lessons from planetary dynamos. ISSI Workshop on the origin and dynamics of solar magnetism, Bern, Switzerland, January 24, 2008, invited. (Oral)

Christensen, U. R.: Planetary dynamos. European Geosciences Union General Assembly, Vienna, Austria, April 13-18, 2008, invited. (Oral)

Christensen, U. R.: Scaling laws for dynamos - from planets to rapidly rotating stars. KITP Conference on Magnetic Fields in Experiments, Geophysics and Astrophysics, Santa Barbara, CA, USA, July 14-18, 2008, invited. (Oral)

Christensen, U. R.: Tides and interior structure. BepiColombo Geodesy and Geophysics Working Group Workshop, Institute of Physics of Interplanetary Space, Rom, Italy, October 20-22, 2008. (Oral)

Curdt, W.: The solar corona: New insights from spectroscopic observations. LASP (Laboratory for Atmospheric and Space Physics), Boulder, CO, USA, May 29, 2008. (Oral)

Curdt, W., H. Tian, B. N. Dwivedi, and E. Marsch: The redshifted network contrast of transition region emission. ESPM-12, Freiburg, Germany, September 8-12, 2008. (Poster)

Curdt, W., H. Tian, L. Teriaca, U. Schühle, and P. Lemaire: The Lyman-alpha profile and centre-to-limb variation of the quiet Sun. ESPM-12, Freiburg, Germany, September 8-12, 2008. (Poster)

Czechowski, A., M. Hilchenbach, K. C. Hsieh, S. Grzedzielski, and J. Kota: Combining the HSTOF ENA observations with Voyager ion data to image the forward heliosheath. AGU Fall Meeting, San Francisco, USA, December 15-19, 2008. (Poster)

Daly, P.: RAPID calibration report. 8th CAA Cross-calibration meeting, Kinsale, Ireland, October 28-30, 2008. (Oral)

Daly, P.: Status Report on the RAPID Instrument on Cluster. CIS/RAPID-Cluster/HIA-Double Star Joint Team Meeting, Venice, Italy, October 14-17, 2008. (Oral)

Daly, P. W.: RAPID Report to SWT 48. Cluster Science Working Team Meeting #48, Tenerife, Spain, March 10, 2008. (Oral)

Daly, P. W. and E. Kronberg: The RAPID Products in the Cluster Active Archive. 15th Cluster Workshop and CAA school, Tenerife, Spain, March 11-15, 2008. (Oral)

D'Amicis, R., A. Mura, S. Orsini, M. Hilchenbach, K. C. Hsieh, D. Telloni, R. Bruno, and E. Antonucci: Numerical studies on neutral solar wind flux at Solar Orbiter's perihelion. 37th COSPAR Scientific Assembly, Montreal, Canada, July 13-20, 2008. (Poster)

De Groof, A., D. Berghmans, J.-M. Defise, B. Nicula, and U. Schühle: SWAP onboard PROBA2: an innovative EUV imager designed for space weather. 12th European Solar Physics Meeting ESPM12, Freiburg, Germany, September, 8-12, 2008. (Poster).

De Lucas, A., R. Schwenn, E. Marsch, A. Dal Lago, A. L. Clua de Gonzalez, and W. D. Gonzalez Alarcon: A statistical analysis of shock wave extension in the inner heliosphere as observed by the two Helios probes. 37th COSPAR Scientific Assembly, Montreal, Canada, July 13-20, 2008. (Oral)

Delcourt, D., Y. Saito, J. M. Illiano, J. J. Berthelier, D. Fontaine, N. Krupp, M. Fränz, M. Godefroy, H. Fischer, S. Yokota, and the MMO MSA Team (continued): The Mass Spectrum Analyzer onboard Bepi Colombo MMO: scientific objectives and prototype results. European Geosciences Union General Assembly, Vienna, Austria, April 13-18, 2008. (Oral)

Deng, X., P. Decreau, M. Ashour-Abdalla, M. Zhou, S. Li, Y. Pang, E. Lucek, M. Andre, A. Fazakerley, I. Dandouras, J. Pickett, P. Daly, N. Cornilleau-Wehrlin, and D. Pontin: Observations of 3-D reconnection and dynamics of electron scale thin current sheets with small satellite separation. AGU Fall Meeting, San Francisco, USA, December 15-19, 2008.

DeRosa, M. L., C. J. Schrijver, G. Barnes, K. D. Leka, B. W. Lites, M. J. Aschwanden, T. Amari, A. Canou, J. M. McTiernan, S. Régnier, J. K. Thalmann, G. Valori, M. S. Wheatland, T. Wiegelmann,

M. C. M. Cheung, P. A. Conlon, M. Fuhrmann, B. Inhester, and T. Tadesse: Nonlinear force-free magnetic field modeling of the solar corona: a critical assessment. AGU Fall Meeting, San Francisco, USA, December 15-19, 2008. (Poster)

Dialynas, K., P. C. Brandt, S. M. Krimigis, B. H. Mauk, D. G. Mitchell, D. C. Hamilton, N. Krupp, A. M. Rymer, and H. T. Smith: Global neutral gas distribution at Saturn and Jupiter derived from ENA images. AGU Fall Meeting, San Francisco, USA, December 15-19, 2008. (Oral)

Dubinin, E.: Solar wind interaction with Venus, Mars and comets. Mutual lessons. Venus Express Science workshop, La Thuile, Italy, March 3-8, 2008. (Oral)

Dubinin, E., M. Fraenz, and J. Woch: Plasma environment on Mars. DFG Colloquium "Mars and Terrestrial planets", Münster, Germany, February 28-29, 2008. (Oral)

Dubinin, E., R. Modolo, M. Fraenz, J. Woch, F. Duru, F. Akalin, D. Gurnett, G. Chanteur, S. Barabash, and R. Lundin: Plasma environment of Mars as observed by simultaneous ASPERA-3 and MARSIS observations on MEX. EPSC 2008, Münster, Germany, September 21-26, 2008. (Oral)

Dubinin, E., R. Modolo, **M. Fraenz**, J. Woch, F. Duru, F. Akalin, D. Gurnett, R. Lundin, S. Barabash, J. Winningham, R. Frahm, J. Plaut, and G. Picardi: Structure and dynamics of solar wind/Mars interaction on Mars from ASPERA-3 and MARSIS observations. COSPAR 2008, Montreal, Canada, July 13-20, 2008. (Oral)

Dubinin, E., R. Modolo, M. Fränz, D. Gurnett, J. Woch, R. Lundin, and S. Barabash: Structure and dynamics of the solar wind/ionosphere interface on Mars. ASPERA-3 and MARSIS observations on MEX. European Geosciences Union General Assembly, Vienna, Austria, April 13-18, 2008. (Oral)

El Maarry, M. R.: Overview of the preliminary results from the Phoenix Lander on Mars. ESTEC student Planetary Workshop, ESA, Noordwijk, Netherlands, October 9-10, 2008. (Oral).

El Maarry, M. R.: Preliminary results from the Phoenix Lander Mission on Mars: primary phase. Cairo University, Cairo, Egypt, December 27, 2008, (Invited Talk) (Oral).

Espy, P., P. Hartogh, M. Clilverd, and K. Holmen: A microwave radiometer for the remote sensing of nitric oxide and ozone in the middle atmosphere. 5th General Meeting of the Asia Oceania Geosciences Society (AOGS 2008), Busan, Korea, June 16-20, 2008. (Oral).

Facsko, G., G. Erdos, M. Tatrallyay, I. Dandouras, and P. Daly: Study of hot flow anomalies using Cluster multi-spacecraft measurements. 37th COSPAR Scientific Assembly, Montreal, Canada, July 13-20, 2008. (Oral)

Facskó, G., P. Kovács, K. Kecskeméty, M. Tátrallyay, G. Erdõs, P. W. Daly, and I. Dandouras: Turbulent processes and boundary layer behavior in the hot diamagnetic cavies based on Cluster measurements. European Geosciences Union General Assembly, Vienna, Austria, April 13-18, 2008. (Poster)

Feng, L., B. Inhester, S. K. Solanki, and T. Wiegelmann: Stereoscopic reconstructions of coronal loops. European Geosciences Union General Assembly, Vienna, Austria, March 13-17, 2008. (Oral)

Feng, L., B. Inhester, S. K. Solanki, and T. Wiegelmann: Stereoscopic reconstructions of coronal loops and polar plumes. STEREO SWG #18 and 7th SECCHI Team Meeting, Paris, France, April 22-24, 2008. (Oral)

Feng, L., B. Inhester, S. K. Solanki, T. Wiegelmann, and B. Podlipnik: Stereoscopic reconstruction of polar plumes. 2008 Joint AGU Assembly, Fort Lauderdale, USA, May 27-30, 2008. (Oral)

Feng, L., J. de Patoul, B. Inhester, S. K. Solanki, and **T. Wiegelmann**: Stereoscopic reconstructions of polar plumes from EUVI/SECCHI images. AGU Fall Meeting, San Francisco, USA, December 15-19, 2008. (Oral)

Fineschi, S. and **S. K. Solanki**: UV instrumentation. SOLAR-C Science Definition Meeting, Tokyo, Japan, November 18-21, 2008. (Invited Talk)

Fränz, M.: Magnetic field influence on the atmospheres of Mars and Venus. DFG Roundtable: Planetary Magnetism, Potsdam, Germany, April 24, 2008. (Oral)

Fränz, M., E. Dubinin, C. Martinecz, E. Roussos, and J. Woch: Plasma boundaries at Mars and Venus. 37th COSPAR Scientific Assembly, Montreal, Canada, July 13-20, 2008. (Oral).

Fränz, M., A. Angsmann, E. Dubinin, C. Martinecz, J. Woch, S. Barabash, R. Lundin, and A. Fedorov: Ion density and transport in the upper ionospheres of Mars and Venus. European Planetary Science Congress 2008, Münster, Germany, September 22-26, 2008. (Oral)

Fränz, M., E. Dubinin, J. Kleimann, C. Martinecz, E. Roussos, J. Woch, S. Barabash, R. Lundin, R. A.

Frahm, and J. D. Winningham: The plasma environment of Mars as mapped by the ASPERA-3 experiment. Chapman Conference on the Solar Wind Interaction with Mars, San Diego, USA, January 22-25, 2008. (Oral)

Fränz, M., E. Dubinin, C. Martinecz, E. Roussos, J. Woch, A. Coates, S. Barabash, R. Lundin, and T. L. Zhang: Plasma boundaries at Mars and Venus. European Geosciences Union General Assembly, Vienna, Austria, April 13-18, 2008. (Oral)

Fränz, M., E. Dubinin, C. Martinecz, E. Roussos, J. Woch, A. J. Coates, S. Barabash, R. Lundin, and T. L. Zhang: Plasma boundaries at Mars and Venus. 37th COSPAR Scientific Assembly, Montreal, Canada, July 13-20, 2008. (Oral)

Georgescu, E.: EDI Final Report for the 1st Phase of CAA. CAA Final Review - 1st Phase, ESTEC, Noordwijk, Netherlands, May 20, 2008. (Oral)

Georgescu, E., H. Vaith, R. Torbert, A. Rochel, and J. Gloag: EDI contribution to cross-calibration. 7th CAA Cross-Calibration Meeting, Tenerife, Spain, March 9, 2008. (Oral)

Georgescu, E., H. Vaith, R. Torbert, A. Rochel, and J. Gloag: Magnetic field cross-calibration using CAA. 15th Cluster Workshop, Tenerife, Spain, March 11-15, 2008. (Poster)

Georgoulis, M. K. and T. Wiegelmann: Magnetic helicity and free magnetic energy: their relation and predictive power in eruptive solar magnetic configurations. AGU Fall Meeting, San Francisco, USA, December 15-19, 2008. (Poster)

Gizon, L.: Current diagnostic capability of helioseismology and future direction. Solar-C Science Definition Meeting, ISAS/JAXA, Sagamihara, Kanagawa, Japan, November 18-21, 2008, invited. (Oral)

Gizon, L.: Helioseismology of sunspots. Thüringer Landessternwarte Tautenburg, Tautenburg, Germany, June 25, 2008, invited. (Oral)

Gizon, L.: Imaging the solar interior in three dimensions. 1st Middle East and Africa Regional IAU Meeting, Cairo, Egypt, April 5-10, 2008, invited review. (Oral)

Gizon, L.: PLATO Data Center. Plenary Meeting of the PLATO Payload Consortium, ESTEC, Noordwijk, The Netherlands, November 28, 2008, invited. (Oral)

Gizon, L.: Possible contribution from Max Planck Institute for Solar System Research. PLATO Payload Consortium: Kick-off meeting, ESTEC, Noordwijk, The Netherlands, June 2, 2008. (Oral)

Gizon, L.: Report on the HELAS-II Conference. 5th HELAS Mid-Term Review and Board Meeting, European Commission, Brussels, Belgium, May 19-20, 2008. (Oral)

Gizon, L.: Scientific and technical interests in PLATO. German PLATO meeting, DLR - Institut für Planetenforschung, Berlin-Adlershof, Germany, April 30, 2008. (Oral)

Gizon, L.: Solar interior and helioseismology. 12th European Solar Physics Meeting, Freiburg, Germany, September 8-12, 2008, invited review. (Oral)

Gizon, L.: Sunspot seismology. ISSI Workshop on the Origin and Dynamics of Solar Magnetism, International Space Science Institute, Berne, Switzerland, January 21-25, 2008, invited review. (Oral)

Gizon, L.: The Sound of the Sun. Sitzung der Chemisch-Physikalisch-Technischen Sektion des Wissenschaftlichen Rates der Max-Planck-Gesellschaft, Berlin, Germany, February 14-15, 2008, invited. (Oral)

Gizon, L.: Tomography of the solar interior. Physik-Kolloquium, Friedrich-Alexander-Universität Erlangen-Nürnberg, Erlangen, Germany, October 20, 2008, invited. (Oral)

Gombosi, T. I., T. P. Armstrong, C. Arridge, M. Blanc, K. Khurana, S. M. Krimigis, N. Krupp, A. Persoon, and M. Thomsen: Magnetospheric configuration. Saturn after Cassini-Huygens Symposium, Imperial College London, UK, July 28 – August 1, 2008. (Oral)

Gómez-Pérez, N., J. Wicht, and M. Heimpel: Effects of external imposed magnetic fields on 3-dimensional self-sustained numerical dynamos. AGU Fall Meeting, San Francisco, USA, December 15-19, 2008. (Poster)

Grygalashvyly, M., P. Hartogh, A. Medvedev, and G. R. Sonnemann: The Doppler-Sonnemann Effect (DSE) on the photochemistry on Mars. 5th General Meeting of the Asia Oceania Geosciences Society (AOGS 2008), Busan, Korea, June 16-20, 2008. (Oral).

Guo, J., **J. Büchner**, E. Marsch, P. Chen, C. Fang, and W. Gan: Numerical simulations of the energetic particles accelerated by reconnection electric field. Frühjahrstagung des DPG Fachverbands Extraterrestrische Physik (EP) und der AEF e.V., Freiburg, Germany, March 3-7, 2008. (Poster)

Guo, J., J. Büchner, A. Otto, and J. C. Santos: Simulation of particle acceleration in numerical 3D reconnection MHD fields. Fifth International Cambridge

Workshop on Magnetic Reconnection, Bad Honnef, Germany, August 18-22, 2008. (Poster)

Haberreiter, M., J. Fontenla, W. Curdt, and H. Tian: Modeling the UV/EUV spectrum with SRPM. ESPM-12, Freiburg, Germany, September 8-12, 2008. (Poster)

Hallgren, K., P. Hartogh, and C. Jarchow: A new, high-performance, radiometer for ground-based remote sensing of mesospheric water vapor. AOGS 2008, Busan, Korea, June 16-20, 2008. (Oral)

Hallgren, K., P. Hartogh, and C. Jarchow: The new, high performance, heterodyne spectrometer at ALOMAR observatory. Cawses SPP, Berlin, Germany, September 10-11, 2008.

Hanasoge, S. M.: Numerical models of MHD wave interactions for sunspot seismology. Evershed Meeting, Indian Institute of Astrophysics, Bangalore, India, December 2-5, 2008, invited. (Oral).

Hartogh, P.: HssO science preparation status. HIFI Science Day, Sterrewacht Leiden, Netherlands, September 22, 2008. (Oral).

Hartogh, P.: Mars modeling work packages of MPS. HGF-Meeting, Berlin-Adlershof, Germany, May 16, 2008. (Oral).

Hartogh, P.: Microwave Instrument for a Moon Orbiter (MIMO). 5th General Meeting of the Asia Oceania Geosciences Society (AOGS 2008), Busan, Korea, June 16-20, 2008. (Oral).

Hartogh, P.: MIMO optimiertes Backend Design. LEO-Meeting EADS, Friedrichshafen, Germany, July 22, 2008. (Oral).

Hartogh, P.: MIMO science and development status. 4. Lunar Exploration Orbiter Wissenschaftlermeeting, DLR Adlershof, Germany, November 13-14, 2008. (Oral).

Hartogh, P.: MIMO science requirements and design status. Lunar Exploration Orbiter Meeting, DLR Adlershof, Germany, February 27-28, 2008. (Oral).

Hartogh, P.: Recent science results of WASPAM. ASAC-Meeting, Kühlungsborn, Germany, June 2-5, 2008. (Oral).

Hartogh, P.: Recent science results of WASPAM. ASAC-Meeting, Kühlungsborn, Germany, May 26, 2008. (Oral).

Hartogh, P.: Reduction of insertion loss by chirped SAW transducers. SAW-DDL Meeting, Academia Sinica, Institute for Acoustics, China, November 3-4, 2008. (Oral).

Hartogh, P.: Science requriements for submm Instruments on Laplace and Tandem. WBS Meeting, ESTEC, Noordwijk, Netherlands, July 1, 2008. (Oral).

Hartogh, P.: Sub-mm investigations of Jupiter's and Europa's atmospheres. Europa-Jupiter International Science Workshop, Frascati, Italy, April 21-22, 2008. (Oral).

Hartogh, P.: Submillimeter wave instrument. Outer Planets Flagship Mission Instrument Workshop, Monrovia, CA, USA, June 2-5, 2008. (Oral).

Hartogh, P.: Summary of the MAOAM results. DFG-SPP 1115 Workshop, Münster, Germany, February 29, 2008. (Oral).

Hartogh, P. and C. Jarchow: Submm flux calibration using an optically thick line in the Martian atmosphere. Herschel Calibration Workshop, Madrid, Spain, February 6-8, 2008. (Oral).

Hartogh, P. and E. Lellouch: Planetary science with Herschel. Future Ground-based Solar System Research: Synergies with Space Probes and Space Telescopes, Elba, Italy, September 8-12, 2008, invited. (Oral).

He, J., H. Tian, E. Marsch, and C. Tu: Comparison of solar wind origin in a coronal hole and a quiet-Sun region. 5th Annual Meeting AOGS, Busan, Korea, June 16-20, 2008. (Oral)

Hilchenbach, M.: Cometary grains: In-situ analysis as a tool for studying the history of the building blocks of comet nuclei? 37th COSPAR Scientific Assembly, Montreal, Canada, July 13-20, 2008. (Oral)

Hilchenbach, M.: In-situ analysis of cometary grains: A tool for studying the history of the building blocks of comet nuclei. AOGS, Busan, Korea, June 16-20, 2008, invited. (Oral)

Hilchenbach, M.: Merkur - Besuche beim Götterboten. Volkshochschule Buxtehude, Buxtehude, Germany, May 15, 2008. (Oral)

Hilchenbach, M.: Merkur - Besuche beim Götterboten. Helmholtz Gymnasium, Bielefeld, Germany, June 10, 2008. (Oral)

Hilchenbach, M.: Remote sensing and evolution of Hermean's regolith due to cometary matter impacts. AOGS, Busan, Korea, June 16-20, 2008. (Poster)

Hilchenbach, M., A. Czechowski, and K. C. Hsieh: Is the forward heliosheath thin? HSTOF ENA and Voyager 1 ion data. 37th COSPAR Scientific Assembly, Montreal, Canada, July 13-20, 2008. (Oral)

Holzwarth, V.: Magnetic activity of cool stars – from the convection zone to the astrosphere. Pysikalisch-Meteorologisches Observatorium, Davos, Switzerland, March 12, 2008. (Oral)

Irwin, P. G. J., B. N. Ellison, L. N. Fletcher, B. Alderman, P. Hartogh, R. de Kok, N. Teanby, and S. B. Calcutt: Oxford RAL Terahertz-Infrared Sensor ORTIS. Outer Planet Flagship Mission Instrument Workshop, Monrovia, CA, USA, June 3-5, 2008. (Poster).

Jackiewicz, J. and L. Gizon: Mass flows around sunspots. GONG 2008 / SOHO XXI Meeting, Boulder, Colorado, USA, August 11-15, 2008, contributed talk. (Oral)

Jackman, C. M., C. S. Arridge, N. Krupp, E. J. Bunce, D. G. Mitchell, W. S. Kurth, H. J. McAndrews, M. K. Dougherty, C. T. Russell, N. Achilleos, A. J. Coates, D. L. Talboys, and G. H. Jones: A multi-instrument view of tail reconnection at Saturn. Saturn after Cassini-Huygens Symposium, Imperial College London, UK, July 28 – August 1, 2008. (Oral)

Javadi, S., **J. Büchner**, and J. C. Santos: Influence of photospheric plasma motion on the pressure and temperature enhancement and the generation of electric currents. Frühjahrstagung des DPG Fachverbands Extraterrestrische Physik (EP) und der AEF e.V., Freiburg, Germany, March 3-7, 2008. (Poster)

Jing, J., T. Wiegelmann, Y. Suematsu, M. Kubo, and H. Wang: Changes of magnetic structure in 3D associated with the X3.4 flare of Dec 13, 2006. 2008 Joint AGU Assembly, Fort Lauderdale, USA, May 27-30, 2008. (Poster)

Jockers, K. and S. Szutowicz: HCN and CN in comet 2P/Encke, a three-dimensional view on comet Encke's outgassing. European Planetary Science Congress 2008, Münster, Germany, September 21-26, 2008, ePSC2008-A-00492.

Jones, G. H., E. Roussos, N. Krupp, S. M. Krimigis, D. Young, T. Denk, M. S. Tiscareno, J. A. Burns, D. F. Strobel, and S. Kempf: A debris disk surrounding Saturn's moon Rhea. AGU Fall Meeting, San Francisco, USA, December 15-19, 2008. (Oral)

Kallenbach, R., M. Hilchenbach, C. Koch, and U. Christensen: Studies of the tidal elevation of planetary surfaces by laser altimetry. 37th COSPAR Scientific Assembly, Montreal, Canada, July 13-20, 2008. (Oral)

Käufl, H. U., H. Boehnhardt, and the METIS team: METIS, a mid infrared multi-mode instrument for the E-ELT. Future Ground-Based Solar System Research – Synergies with Space Probes and Space Telescopes, Portoferraio, Elba, Italy, September 8-12, 2008. (Oral)

Keller, H. U., M. Küppers, and E. Kührt: Comet nucleus sample return: exciting, feasible, and timely. IPEWG, Okinawa, Japan, January 14-16, 2008. (Oral)

Keller, H. U., W. J. Markiewicz, S. F. Hviid, W. Goetz, M. T. Mellon, M. E. Maarry, M. B. Madsen, P. Smith, W. Pike, A. Zent, M. H. Hecht, D. Ming, and U. Staufer: Physical properties of the ice soil at the Phoenix landing site. AGU Fall Meeting, San Francisco, USA, December 15-19, 2008.

Keller, H. U., C. T. Russell, H. Sierks, and Dawn Science Team: DAWN – The mission to the largest of the small bodies. IPEWG, Okinawa, Japan, January 14-16, 2008. (Oral)

Kellett, S., N. Sergis, E. Bunce, C. Arridge, S. Cowley, T. Krimigis, E. Roelof, D. Hamilton, D. Mitchell, N. Krupp, M. Dougherty, and A. Coates: The Saturnian ring current as revealed through combined plasma, energetic particle and magnetic field measurements. Inertial or pressure gradient driven? AGU Fall Meeting, San Francisco, USA, December 15-19, 2008. (Oral)

Kelley, M. S., D. H. Wodden, C. E. Woodward, D. E. Harker, H. Boehnhardt, and C. Tubiana: Preperihelion observations of comet 67P/Churyumov-Gerasimenko with Spitzer. Future Ground-Based Solar System Research – Synergies with Space Probes and Space Telescopes, Portoferraio, Elba, Italy, September 8-12, 2008. (Poster)

Khurana, K., M. Dougherty, C. Paranicas, N. Krupp, C. Russell, D. Mitchell, and C. S. Arridge: The effect of ring current region plasma anomalies on the structure of Saturn's magnetosphere. 37th COSPAR Scientific Assembly, Montreal, Canada, July 13-20, 2008. (Oral)

Khurana, K. K., M. K. Dougherty, C. T. Russell, C. Paranicas, D. G. Mitchell, C. S. Arridge, and N. Krupp: Sources of rotational signals in Saturn's magnetosphere. Cassini MAPS workshop, Max-Planck-Institut für Sonnensystemforschung, Katlenburg-Lindau, Germany, April 2-4, 2008. (Oral)

Khurana, K. K., M. K. Dougherty, C. T. Russell, C. Paranicas, D. G. Mitchell, C. S. Arridge, and N. Krupp: Tilting of Saturns current sheet by asymmetric lift of Saturns magnetosphere. Saturn after Cassini-Huygens Symposium, Imperial College London, UK, July 28 – August 1, 2008. (Oral)

Khurana, K. K., D. G. Mitchell, C. S. Arridge, M. K. Dougherty, C. T. Russell, C. Paranicas, and N. Krupp: The mystery of rotational signals from Saturns magnetosphere revealed. European Geosciences Union General Assembly, Vienna, Austria, April 13-18, 2008. (Oral)

Koch, C., U. R. Christensen, and R. Kallenbach: Analysis of global static and time-dependent topography from laser altimeter records using a rectangular-grid method. EPSC 2008, Münster, Germany, September 21-26, 2008. (Oral)

Koch, C., U. R. Christensen, and R. Kallenbach: Extraction of the tidal amplitude from synthetic topography data of the BepiColombo laser altimeter in the polar regions of Mercury. EPSC 2008, Münster, Germany, September 21-26, 2008. (Poster)

Koch, Ch., U. R. Christensen, and R. Kallenbach: Extraction of tidal Love number and forced libration amplitude of Mercury from synthetic laser altimetry records. European Geosciences Union General Assembly, Vienna, Austria, April 13-18, 2008. (Poster)

Koch, C., R. Kallenbach, U. Christensen, and M. Hilchenbach: Study of the interior structure of planetary bodies by laser altimetry. 5th Annual General Assembly of the Asia Oceania Geosciences Society, Busan, South Korea, June 16-20, 2008. (Oral).

***Koschny, D.**, M. A. Barucci, M. Yoshikawa, H. Boehnhardt, et al.*: Marco-Polo – A mission to return a sample from a near-Earth object. Asteroids, Comets, Meteors 2008, Baltimore, USA, July 13-18, 2008. (Oral)

Krivova, N. A.: Long term variations of solar activity. Colloquium, Leibniz-Institut für Atmosphären Physik, Kühlungsborn, Germany, December 11, 2008, invited. (Oral)

Krivova, N. A.: Variations of solar total and spectral irradiance. EMS-2009: European Meteorological Society Annual Meeting / European Conference on Applied Climatology, Amsterdam, The Netherlands, September 29 – October 3, 2008, invited. (Oral)

Krivova, N. A. and S. K. Solanki: Reconstructions of solar irradiance variations. European Geosciences Union General Assembly, Vienna, Austria, April 13-18, 2008, invited. (Oral)

Krivova, N. A., S. K. Solanki, L. Balmaceda, M. Dasi, L. Vieira, Y. C. Unruh, D. Siegel, and I. Ermolli: Models of solar total and spectral irradiance variability of relevance for climate studies. Schwerpunktkolloquim "Climate and Weather of the Sun-Earth-System (CAWSES)", Berlin, Germany, September 10-11, 2008. (Oral)

Kronberg, E., P. Daly, and I. Dandouras: RAPID/IIMS & CIS/CODIF cross-calibration. 7th CAA Cross-Calibration Meeting, Tenerife, Spain, March 9, 2008. (Oral)

Kronberg, E., P. Daly, I. Dandouras, and A. Barthe: RAPID status report. 8th CAA Cross-Calibration Meeting, Kinsale, Ireland, October 28-30, 2008. (Oral)

Kronberg, E., P. Daly, I. Dandouras, S. Haaland, and E. Georgescu: RAPID/IIMS & CIS/CODIF cross-calibration. CIS/RAPID-Cluster/HIA-Double Star Joint Team Meeting, Venice, Italy, October 14-17, 2008.

Kronberg, E., P. Daly, and S. Mühlbachler: RAPID Final Report for the 1st Phase of CAA. CAA Final Review - 1st Phase, ESTEC, Noordwijk, Netherlands, May 20, 2008. (Oral)

Kronberg, E., S. Haaland, P. Daly, M. Fränz, E. Georgescu, A. Aasnes, and L. Degener: Spectral characteristics of the tail plasma sheet. CIS/RAPID-Cluster/HIA-Double Star Joint Team Meeting, Venice, Italy, October 14-17, 2008. (Oral)

Kronberg, E., A. Kis, B. Klecker, P. Daly, and E. Lucek: Multipoint observations of ions in the energy range 30-160 keV upstream of Earths bow shock. 15th Cluster Workshop and CAA school, Tenerife, Spain, March 11-15, 2008. (Poster)

Kronberg, E., A. Kis, B. Klecker, P. Daly, E. Lucek, and I. Dandouras: Multipoint observations of ions in the energy range 30-225 keV upstream of Earth's bow shock. 37th COSPAR Scientific Assembly, Montreal, Canada, July 13-20, 2008. (Oral)

Kronberg, E., S. Mühlbachler, and P. Daly: RAPID visualization tool. 15th Cluster Workshop and CAA school, Tenerife, Spain, March 11-15, 2008. (Oral)

Kronberg, E., J. Woch, N. Krupp, A. Lagg, and K. H. Glassmeier: Substorms at Jupiter? Ninth International Conference on Substorms, Schloss Seggau, Austria, May 5-9, 2008. (Oral)

Krüger, H.: Deep Impact – Einschlag auf einem Kometen. Volkshochschule Soest/Astronomischer Arbeitskreis, Soest, Germany, November 27, 2008. (Oral)

Krüger, H.: Dust released from the Jovian moons: a tool for direct surface composition analysis. Europa-Jupiter International Science Workshop, Frascati, Italy, April 21-22, 2008. (Oral)

Krüger, H.: Kometen – Boten aus der Frühzeit des Sonnensystems. Volkshochschule Mosbach/Baden, Binau, Germany, February 29, 2008. (Oral)

Krüger, H.: Kometen – Boten aus der Frühzeit des Sonnensystems. 11. Göttinger Woche Wissenschaft und Jugend, Haupt- und Realschule Lindau, Germany, June 17, 2008. (Oral)

Krüger, H.: Level 1 data processing software for Rosetta/Cosima. Cosima Technical Team Meeting, Nördlingen, Germany, October 29, 2008. (Oral)

Krüger, H.: Staubteilchen – Boten ferner Welten. Volkshochschule Mosbach, Binau/Mosbach(Baden), Germany, October 24, 2008. (Oral)

Krüger, H.: The dust environment of Jupiter as seen by Galileo. European Planetary Science Congress, Münster, Germany, September 21-26, 2008. (Oral)

Krüger, H.: Ulysses interstellar dust measurements – an update. Ulysses Science Working Team Meeting 60, Pasadena, CA, USA, November 11-13, 2008. (Oral)

Krüger, H., N. Altobelli, M. Landgraf, and E. Grün: Interstellar dust measurements from Ulysses' third solar orbit. 37th Cospar Scientific Assembly, Montreal, Canada, July 13-20, 2008. (Oral)

Krüger, H., C. Briois, C. Engrand, H. Fischer, M. Hilchenbach, J. Kissel, P. Martin, J. Rynö, T. Stephan, L. Thirkell, R. Thomas, and K. Varmuza: An automatic pipline processing software for secondary ion time-of-flight mass spectra of Rosetta/COSIMA. 37th Cospar Scientific Assembly, Montreal, Canada, July 13-20, 2008. (Poster)

Krüger, H., D. P. Hamilton, R. Moissl, and E. Grün: Galileo in-situ dust measurements and the sculpting of Jupiter's gossamer rings by its shadow. European Plaenetary Science Congress, Münster, Germany, September 21-26, 2008. (Oral)

Krüger, H., D. P. Hamilton, R. Moissl, and E. Grün: Galileo in-situ dust measurements and the significance of planetary shadowing in shaping Jupiter's gossamer ring structure. 37th Cospar Scientific Assembly, Montreal, Canada, July 13-20, 2008. (Oral)

Krüger, H., M. Landgraf, and E. Grün: In-situ interstellar dust measurements in the solar system. Cosmic Dust – Near and Far, Heidelberg, Germany, September 8-12, 2008. (Poster)

Krupp, N.: The Jovian environment. ISSI/Europlanet workshop on exchange processes in icy moons, Bern, Switzerland, November 17-21, 2008. (Oral)

Krupp, N., A. Lagg, E. C. Roelof, J. Woch, and K. K. Khurana: Global flows of energetic ions in the Jovian magnetosphere: Galileo EPD measurements 1996-2003. European Geosciences Union General Assembly, Vienna, Austria, April 13-18, 2008. (Oral)

Krupp, N., E. Roussos, T. Armstrong, C. Paranicas, D. Mitchell, S. Krimigis, G. H. Jones, K. Dialynas, N. Sergis, and D. Hamilton: Discovery of a transient radiation belt at Saturn. AGU Fall Meeting, San Francisco, USA, December 15-19, 2008. (Poster)

Krupp, N., E. Roussos, A. Lagg, A. Müller, D. Mitchell, and J. Saur: Electron distributions during high latitude orbits. Cassini MAPS workshop, Max-Planck-Institut für Sonnensystemforschung, Katlenburg-Lindau, Germany, April 2-4, 2008. (Oral)

Kuroda, T. and P. Hartogh: Simulation of the water cycle on Mars for the Herschel mission. 5th General Meeting of the Asia Oceania Geosciences Society (AOGS 2008), Busan, Korea, June 16-20, 2008. (Oral).

Kuroda, T., A. S. Medvedev, P. Hartogh, and M. Takahashi: Study of the semiannual oscillations in the Martian atmosphere with a general circulation model. 5th General Meeting of the Asia Oceania Geosciences Society (AOGS 2008), Busan, Korea, June 16-20, 2008. (Oral).

Lagg, A.: A He 10830 lecture: some aspects from an observer's viewpoint. Special NAOJ Lecture, National Astronomical Observatory of Japan, Tokyo, Japan, August 26, 2008.

Lagg, A.: Chromospheric magnetic field measurements. ISSI Workshop on Solar Magnetism, Bern, Switzerland, January 21-25, 2008, invited. (Oral)

Lagg, A.: Chromospheric magnetic field measurements in the He 10830 Å line. SSP seminar at the National Astronomical Observatory of Japan, Tokyo, Japan, August 22, 2008. (Oral)

Lagg, A.: Measurement of the magnetic canopy: First application of HeLIX+ to He 10830 observations. SSP seminar, National Astronomical Observatory, Tokyo, Japan, October 17, 2008, invited talk. (Oral)

Lagg, A.: Stokes polarimetry in He 10830: the key to understand chromospheric magnetism? Kyoto University, Kyoto, Japan, October 14, 2008, invited talk. (Oral)

Lagg, A., R. Ishikawa, L. Merenda, T. Wiegelmann, S. Tsuneta, and S. K. Solanki: Internetwork horizontal magnetic fields in the quiet Sun chromosphere: results from a joint Hinode/VTT study. Hinode 2 – Beyond Discovery – Toward Understanding, Boulder, Colorado, USA, Sepember 29 – October 3, 2008. (Poster)

Lellouch, E., J. Crovisier, T. Müller, P. Hartogh, H. Boehnhardt, and two Herschel key program teams: Small bodieswith Herschel. Future Ground-Based Solar System Research – Synergies with Space Probes and Space Telescopes, Portoferraio, Elba, Italy, September 8-12, 2008. (Oral)

Lellouch, E., S. Vinatier, M. Allen, S. Gulkis, P. Hartogh, R. Moreno, I. Mehdi, A. Maestini, and J.-M. Krieg: Science case for a sub-millimeter sounder on the TSSM mission. Outer Planet Flagship Mission Instrument Workshop, Monrovia, CA, USA, June 3-5, 2008. (Poster).

Lellouch, E., S. Vinatier, P. Hartogh, G. Beaudin, and R. Moreno: The case for a submillimeter sounder on the TSSM Titan Orbiter. TandEM (Titan and Enceladus Mission), Meudon, France, February 17-19, 2008. (Oral).

Limaye, S., I. Khatuntsev, **W. J. Markiewicz**, D. Titov, and R. Moissl: Cloud level circulation on Venus from Venus Monitoring Camera on Venus Express. 37th COSPAR Scientific Assembly, Montreal, Canada, July 13-20, 2008.

Limaye, S., **W. J. Markiewicz**, R. Moissl, and D. Titov: Small scale waves on Venus at high latitudes. 40th Annual Meeting of the Division for Planetary Sciences of the American Astronomical Society, Ithaca, NY, USA, October 10-15, 2008.

Limaye, S., **W. J. Markiewicz**, D. Titov, G. Piccione, K. H. Baines, and M. Robinson: State of the Venus atmosphere from Venus Express at the time of MESSENGER FLy-By. 37th COSPAR Scientific Assembly, Montreal, Canada, July 13-20, 2008.

Lippi, M., M. J. Mumma, G. L. Villanueva, M. A. DiSanti, B. Bonev, and H. Boehnhardt: The volatile composition of the periodic comet 8P/Tuttle as measured with CCRIRES at ESOs VLT observatory. Future Ground-Based Solar System Research – Synergies with Space Probes and Space Telescopes, Portoferraio, Elba, Italy, September 8-12, 2008. (Poster)

Lippi, M., M. J. Mumma, G. L. Villanueva, M. A. DiSanti, B. Bonev, and H. Boehnhardt: The volatile composition of the periodic comet 8P/Tuttle as measured with CRIRES at ESO's VLT Observatory. Asteroids, Comets, Meteors 2008, Baltimore, USA, July 13-18, 2008. (Poster)

Lognonné, P., W. T. Pike, D. Mimoun, D. Mance, D. Giardini, U. R. Christensen, A. van den Berg, R. Roll, S. Calcutt, J. M. Smit, and the SEIS team: The ExoMars-Humbold SEIS experiment. European Geosciences Union General Assembly, Vienna, Austria, April 13-18, 2008. (Oral)

de Lucas, A., R. Schwenn, E. Marsch, A. Dal Lago, and A. C. de Gonzalez: A statistical analysis of shock wave extension in the inner heliosphere as observed by the two Helios probes. Latin American School on International Heliophysical Year, Sao Paulo, Brazil, February 14-20, 2008. (Poster)

de Lucas, A., R. Schwenn, E. Marsch, A. Dal Lago, A. L. Clúa de Gonzalez, and W. Gonzalez: A statistical analysis of shock wave extension in the inner heliosphere as observed by the two Helios probes. 37th COSPAR Scientific Assembly, Montreal, Canada, July 13-20, 2008. (Oral)

Lundin, R., S. Barabash, M. Holmström, H. Nilsson, M. Yamauchi, M. Fränz, and E. M. Dubinin: Solar forcing and the comet-like escape of ionospheric plasma from Mars. European Geosciences Union General Assembly, Vienna, Austria, April 13-18, 2008. (Oral)

Maneva, Y., J. Araneda, and E. Marsch: Sample title of talk. Space Plasma Physics: school and workshop, Sozopol, Bulgaria, August 31 – September 7, 2008. (Oral)

Markiewicz, W. J., H. U. Keller, K. J. Kossacki, M. T. Mellon, H. F. Stubbe, B. J. Bos, R. Woida, L. Drube, K. Leer, M. B. Madsen, W. Goetz, M. R. E. Maarry, and P. Smith: Sublimation of exposed snow queen surface water ice as observed by the Phoenix Mars Lander. AGU Fall Meeting, San Francisco, USA, December 15-19, 2008.

Markiewicz, W. J., D. Titov, H. U. Keller, R. Moissl, S. Limaye, N. Ignatiev, R. Jaumann, H. Michalik, and N. Thomas: A few highlights from Venus Monitoring Camera on Venus Express. 40th Annual Meeting of the Division for Planetary Sciences of the American Astronomical Society, Ithaca, NY, USA, October 10-15, 2008.

Markiewicz, W. J., D. Titov, S. Limaye, R. Moissl, N. Ignatiev, A. T. Basilevsky, E. V. Shalygin, M. A. Kreslavsky, I. Khatuntsev, H. U. Keller, R. Jaumann, N. Thomas, and H. Michalik: Morphology and dynamics of the Venus upper cloud layer. 37th COSPAR Scientific Assembly, Montreal, Canada, July 13-20, 2008.

Marsch, E.: Coronal circulation - plasma flows and mass supply. The Third International Symposium on Kuafu Project (ISKP-III), Kunming, Yunnan, China, September 14-19, 2008. (Oral)

Marsch, E.: Solar wind acceleration. 5th Annual Meeting AOGS, Busan, Korea, June 16-20, 2008. (Oral)

Marsch, E.: The heliophysical explorers sentinels and Solar Orbiter – science programme and relations with Kuafu. The Third International Symposium on Kuafu Project (ISKP-III), Kunming, Yunnan, China, September 14-19, 2008. (Oral)

Marsch, E.: Turbulence in the solar wind – generation, evolution, and dissipation. 2nd Laboratory, space, and astrophysical plasma workshop at the POSCO International Center, POSTECH, Pohang, Korea, June 21-22, 2008, invited. (Oral)

Marsch, E.: Turbulenz im Sonnenwind – Quellen, Entwicklung und Dissipation. Geophysikalisch-Meteorologisches Kolloquium, Universität Köln, Köln, Germany, November 10, 2008, invited. (Oral)

Marsch, E.: Turbulenz im Sonnenwind - Anregung, Entwicklung und Dissipation. Physikalisches Kolloquium der Ruhr-Universität Bochum, Bochum, Germany, June 2, 2008. (Oral)

Marsch, E., J. Araneda, and A. F.-Vinas: Proton heating and beam formation via parametrically unstable Alfvén-cyclotron waves. 37th COSPAR Scientific Assembly, Montreal, Canada, July 13-20, 2008. (Oral)

Marsch, E., H. Tian, C. Tu, J. He, G. Q. Zhou, and L. Xia: Sizes and heigts of magnetic structures in the solar transition region as observed in ultraviolet emission lines at different temperatures. 37th COSPAR Scientific Assembly, Montreal, Canada, July 13-20, 2008. (Oral)

Martinecz, C., A. Boesswetter, M. Fränz, E. Roussos, N. Krupp, J. Woch, E. Dubinin, U. Motschmann, S. Wiehle, S. Simon, S. Barabash, R. Lundin, T. L. Zhang, H. Lammer, H. Lichtenegger, and Y. Kulikov: The plasma environment of Venus: comparison of Venus Express ASPERA-4 measurements with 3D hybrid simulations. European Planetary Science Congress 2008, Münster, Germany, September 22-26, 2008. (Oral)

Martinecz, C., M. Fränz, J. Woch, N. Krupp, E. Dubinin, E. Roussos, S. Barabash, T. L. Zhang, U. Motschmann, and A. Boesswetter: The plasma environment of Venus: comparison of Venus Express ASPERA-4 measurements with 3D hybrid simulations. European Geosciences Union General Assembly, Vienna, Austria, April 13-18, 2008. (Poster)

Martínez, G. M., J. S. Jacinto, B. Vargas Cardenas, H. Aguirre Marquez, and R. Schwenn: Mexican Coronagraph "Mextli" Project. 37th COSPAR Scientific Assembly, Montreal, Canada, July 13-20, 2008. (Oral)

Mason, G. M., M. I. Desai, U. Mall, R. Bučík, K. Simunac, and R. A. Leske: In-situ observations of CIRs on STEREO and ACE during 2007-2008. 8th SECCHI Team Meeting, Naval Research Laboratory, Washington DC, USA, October 22-24, 2008. (Oral)

Medvedev, A. S. and P. Hartogh: The Role of the meridional transport in the Martian atmosphere on the formation of the variable hygropause. 5th General Meeting of the Asia Oceania Geosciences Society (AOGS 2008), Busan, Korea, June 16-20, 2008. (Oral).

Medvedev, A. S., P. Hartogh, and C. Jarchow: The role of the meridional transport in the Martian atmosphere on the formation of the variable hygropause. AOGS 2008, Busan, Korea, June 16-20, 2008.

Medvedev, A. S., A. Kutepov, A. Feofilov, and P. Hartogh: Additional radiative cooling of the mesosphere due to gravity wave-induced temperature fluctuations. 5th General Meeting of the Asia Oceania Geosciences Society (AOGS 2008), Busan, Korea, June 16-20, 2008. (Oral).

Medvedev, A. S., T. Kuroda, P. Hartogh, and M. Takahashi: Detection and modelling of the semiannual oscillations in the atmosphere of Mars. Third International Workshop on the Mars atmosphere, Williamsburg, Virginia, USA, November 10-13, 2008.

Medvedev, A. S., T. Kuroda, P. Hartogh, and M. Takahashi: Semiannual oscillations in the atmosphere of Mars. 2008 Joint AGU Assembly, Fort Lauderdale, USA, May 27-30, 2008. (Oral)

Medvedev, A. S., A. A. Kutepov, A. G. Feofilov, and P. Hartogh: Additional radiative cooling of the mesosphere due to gravity wave-induced temperature fluctuations. AOGS 2008, Busan, Korea, June 16-20, 2008.

Mitchell, D. G., J. F. Carbary, N. Krupp, S. M. Krimigis, D. C. Hamilton, C. Paranicas, P. Brandt, G. B. Hospodarsky, W. S. Kurth, and M. K. Dougherty: Energetic particle acceleration at Saturn. Cassini MAPS workshop, Max-Planck-Institut für Sonnensystemforschung, Katlenburg-Lindau, Germany, April 2-4, 2008. (Oral)

Mitchell, D. G., W. S. Kurth, G. B. Hospodarsky, D. A. Gurnett, N. Krupp, J. Saur, B. A. Mauk, J. F. Carbary, S. M. Krimigis, P. C. Brandt, M. K. Dougherty, J. T. Clarke, J. D. Nichols, J. Gerard,

D. Grodent, W. R. Pryor, E. J. Bunce, and F. J. Crary: Coordinated measurements of auroral processes at Saturn from the Cassini spacecraft and HST. AGU Fall Meeting, San Francisco, USA, December 15-19, 2008. (Oral)

Moissl, R., S. S. Limaye, I. Khatuntsev, **W. J. Markiewicz**, and D. Titov: Results on atmospheric dynamics at the Venus cloud tops from digital and manual wind tracking in VMC images. 40th Annual Meeting of the Division for Planetary Sciences of the American Astronomical Society, Ithaca, NY, USA, October 10-15, 2008.

Mueller, T. G., E. Lellouch, H. Boehnhardt, and Co-authors: Herschel Open Time Key Programme: TNOs are cool: A survey of the Transneptunian region. Asteroids, Comets, Meteors 2008, Baltimore, USA, July 13-18, 2008. (Poster)

Müller, A., N. Krupp, J. Saur, D. G. Mitchell, S. M. Krimigis, and B. H. Mauk: Das azimuthale Geschwindigkeitsprofil der Saturnmagnetosphäre. DPG Frühjahrstagung, Freiburg, Germany, March 3-6, 2008. (Oral).

Müller, A., N. Krupp, J. Saur, D. G. Mitchell, S. M. Krimigis, and B. H. Mauk: Injections at Saturn. Europlanet Workshop on Jupiter's and Saturn's aurora, Liege, Belgium, April 10-11, 2008. (Oral)

Müller, A., N. Krupp, J. Saur, D. G. Mitchell, S. M. Krimigis, and B. H. Mauk: The azimuthal velocity profile of the Kronian magnetosphere. Cassini PSG, JPL, Pasadena, CA, USA, January 29-31, 2008. (Oral)

Müller, A. L., J. Saur, N. Krupp, D. G. Mitchell, S. M. Krimigis, B. H. Mauk, and C. Paranicas: Azimuthal plasma flow determined from injection events. Cassini MAPS workshop, Max-Planck-Institut für Sonnensystemforschung, Katlenburg-Lindau, Germany, April 2-4, 2008. (Oral)

Müller, T. G., E. Lellouch, H. Boehnhardt, and the project team: Herschel Open Time Key Programme: TNOs are cool: A survey of the Transneptunian region. Future Ground-Based Solar System Research – Synergies with Space Probes and Space Telescopes, Portoferraio, Elba, Italy, September 8-12, 2008. (Poster)

Nathues, A., H. Boehnhardt, A. W. Harris, W. Goetz, C. Gritzner, C. Jentsch, N. Schmitz, S. Schaeff, F. Weischede, and A. Wiegand: ASTEX – an in-situ exploration mission to two near-Earth asteroids. Asteroids, Comets, Meteors 2008, Baltimore, USA, July 13-18, 2008. (Poster)

Nesis, A., R. Hammer, H. Schleicher, and M. Roth: Velocity pattern evolution within the photosphere. 12th European Solar Physics Meeting, Freiburg, Germany, September 8-12, 2008. (Poster)

Noir, J., F. Hemmerlin, J. Wicht, S. M. Baca, and J. Aurnou: Laboratory models of librationally-driven flow in planetary core and sub-surface oceans. AGU Fall Meeting, San Francisco, USA, December 15-19, 2008. (Poster)

Nykyri, K., A. Otto, E. Adamson, E. Kronberg, B. Lavraud, and P. Daly: Simultaneous measurements of the high-energy particle properties at a cusp diamagnetic cavity and surrounding magnetosheath: evidence for local acceleration mechanism? AGU Fall Meeting, San Francisco, USA, December 15-19, 2008.

Paganini, L.: The importance of power spectral accuracy in microwave spectroscopy. Institute of Applied Physics, University of Bern, Switzerland, October 17, 2008, invited. (Oral).

Paganini, L. and P. Hartogh: On the identification of nonlinear processes in chirp transform spectrometers. 5th General Meeting of the Asia Oceania Geosciences Society (AOGS 2008), Busan, Korea, June 16-20, 2008. (Oral).

Pagaran, J., M. Weber, K. Bramstedt, J. Burrows, N. Krivova, S. K. Solanki, and L. Floyd: Variability of UV-vis-IR solar irradiance from GOME and SCIAMACHY for use in GCMs. International Workshop on Solar Variability, Earth's Climate and the Space Environment, Bozeman, Montana, USA, June 1-6, 2008. (Oral)

Pagaran, J., M. Weber, J. Burrows, N. Krivova, S. K. Solanki, and L. Floyd: Variability of solar irradiance from the UV to the NIR from GOME and SCIAMACHY for use in atmospheric models. 37th COSPAR Scientific Assembly, Montreal, Canada, July 13-20, 2008. (Poster)

Panov, E. V., J. Büchner, M. Fränz, A. Korth, S. P. Savin, I. Dandouras, and K.-H. Fornacon: Magnetopause transport by ion-cyclotron resonant wave-particle interaction. European Geosciences Union General Assembly, Vienna, Austria, April 13-18, 2008. (Oral)

Paranicas, C., D. G. Mitchell, S. M. Krimigis, D. C. Hamilton, E. Roussos, N. Krupp, G. H. Jones, R. E. Johnson, J. F. Cooper, and T. P. Armstrong: Satellite surface weathering. Cassini MAPS workshop, Max-Planck-Institut für Sonnensystemforschung, Katlenburg-Lindau, Germany, April 2-4, 2008. (Oral)

Pietarila, A., R. Cameron, and S. Solanki: Expansion of magnetic flux concentrations with height: a comparison of Hinode SOT data and MHD simulations. Hinode 2 – Beyond Discovery – Toward Understanding, Boulder, USA, September 29 – October 3, 2008. (Poster)

Pietarila, A., J. Hirzberger, V. Zahkarov, and S. Solanki: Fibrils in Ca II K. ESPM-12, Freiburg, Germany, September 8-12, 2008. (Poster)

Pietarila Graham, J., S. Danilovic, and M. Schüssler: How well do Zeeman measurements reflect the turbulent solar magnetic field? ESPM-12, Freiburg, Germany, September 8-12, 2008. (Poster)

Pietarila Graham, J., S. Danilovic, M. Schüssler, and A. Vögler: The solar surface dynamo. Second Hinode Science Meeting, Boulder, CO, USA, September 29 – October 3, 2008, invited Keynote. (Oral)

Protopapa, S., H. Boehnhardt, T. M. Herbst, D. P. Cruikshank, W. M. Grundy, F. Merlin, and C. B. Olkin: Spectra of Pluto and Charon resolved up to 5mu: Implications for surface properties. Asteroids, Comets, Meteors 2008, Baltimore, USA, July 13-18, 2008. (Poster)

Radioti, A., D. Grodent, J.-C. Gérard, B. Bonfond, E. Roussos, N. Krupp, C. Paranicas, D. Mitchell, T. Krimigis, and J. T. Clarke: Correlation of auroral emissions with particle injections in the magnetosphere of Saturn. Cassini MAPS workshop, Max-Planck-Institut für Sonnensystemforschung, Katlenburg-Lindau, Germany, April 2-4, 2008. (Oral)

Radioti, A., A. T. Tomas, D. Grodent, J.-C. Gerard, B. Bonfond, J. Gustin, N. Krupp, and J. Woch: Jupiter's diffuse auroral emissions – Comparison of HST and Galileo data. European Geosciences Union General Assembly, Vienna, Austria, April 13-18, 2008. (Oral)

Reardon, K. P., **G. Cauzzi**, L. Teriaca, M. Pitterle, and W. Curdt: Chromospheric counterparts of UV explosive events. ESPM-12, Freiburg, Germany, September 8-12, 2008. (Oral)

Rengel, M.: A new peculiar Class 0 object in Lupus 3. Astro Colloquium, Astrophysikalisches Institut und Universitäts-Sternwarte (AIU), Jena, Germany, December 17, 2008, invited. (Oral)

Rengel, M.: How comets can help in studies of planet formation? – Missions. JENAM 2008 (Joint European and National Astronomy Meeting), Vienna, Austria, September 8-12, 2008. (Oral)

Rengel, M., **P. Hartogh**, and C. Jarchow: Venusian mesospheric temperature, CO abundance, and winds from HHSMT CO spectral-line observations in support of Venus Express mission. ELBA 2008, Future Ground based Solar System Research: Synergies with Space Probes and Space Telescope, Isola d'Elba, Livorno, Italy, September 8-12, 2008. (Poster)

Rengel, M., P. Hartogh, and C. Jarchow: Vertical thermal structure and winds in Venus' mesosphere from HHSMT. European Geosciences Union General Assembly, Vienna, Austria, April 14-18, 2008. (Poster)

Rengel, M., M. Küppers, H.-U. Keller, P. Gutierrez, and S. Hviid: The terminal velocity of the deep impact dust ejecta. Astro-Kolloquium, Astrophysikalisches Institut und Universitäts-Sternwarte Jena, Jena, Germany, May 7, 2008, (Invited).

Rengel, M., H. Sagawa, and P. Hartogh: Retrieval of atmospheric gases from Herschel observations of the outer planets, Titan, and Enceladus. Asia Oceania Geosciencies Society 5th Meeting, Busan, Korea, June 16-20, 2008. (Oral)

Retino, A., R. Nakamura, A. Vaivads, K. Keika, Y. Asano, Y. Khotyaintsev, W. Baumjohann, M. Volwerk, E. Panov, M. Bavassano-Cattaneo, P. Daly, E. Kronberg, C. Owen, E. Lucek, and N. Cornilleau-Wehrlin: The microphysics of the dipolarization/jet braking region in the near-Earth magnetotail: Cluster multi-point observations. AGU Fall Meeting, San Francisco, USA, December 15-19, 2008.

Retino, A., R. Nakamura, A. Vaivads, Y. Khotyaintsev, D. Sundkvist, K. Tanaka, S. Kasahara, M. Fujimoto, J. Eastwood, F. Mozer, M. Andre, W. Baumjohann, P. Daly, E. Kronberg, M. Bavassano-Cattaneo, C. Owen, and N. Cornilleau-Wehrlin: In-situ observations of magnetic reconnection and associated energetic particle acceleration in near-Earth space. AGU Fall Meeting, San Francisco, USA, December 15-19, 2008, invited. (Oral)

Roatsch, T., A. T. Basilevsky, E. V. Shalygin, D. Titov, **W. J. Markiewicz**, F. Scholten, M. A. Kreslavsky, and R. Jaumann: Geologic interpretation of the NIR images taken by the Venus Monitoring Camera. 37th COSPAR Scientific Assembly, Montreal, Canada, July 13-20, 2008.

Roatsch, T., K.-D. Matz, R. Jaumann, G. Neukum, **W. J. Markiewicz**, C. Porco, and C. Russell: Multi-mission image processing and archiving at DLR. 37th COSPAR Scientific Assembly, Montreal, Canada, July 13-20, 2008.

***Romstedt, J.**, M. A. Barucci, M. Yoshikawa, D. Koschny, H. Boehnhardt, et al.*: Planetary protection issues for the Marco Polo NEO sample return mission. 37th COSPAR Scientific Assembly, Montreal, Canada, July 13-20, 2008. (Oral)

Roth, M.: Data assimilation and helioseismology. GONG 2008 / SOHO XXI Meeting, Boulder, Colorado, USA, August 11-15, 2008, invited talk. (Oral)

Roth, M., O. von der Lühe, P. Pallé, M. Thompson, M. Monteiro, L. Gizon, C. Aerts, and J. Christensen-Dalsgaard: HELAS Midterm Review. HELAS Midterm Review bei der Europäischen Kommission, Brussels, Belgium, May 19, 2008. (Oral)

Roth, M. and M. Stix: Meridional circulation and global solar oscillations. 12th European Solar Physics Meeting, Freiburg, Germany, September 8-12, 2008. (Oral)

Rothkaehl, H., K. Kudela, R. Bučík, and O. Grigoryan: The response of ionospheric plasma to the physical processes in radiation belts regions. 37th COSPAR Scientific Assembly, Montreal, Canada, July 13-20, 2008. (Oral)

Roussos, E., M. Fränz, E. Dubinin, J. Woch, C. Martinecz, S. Barabash, R. Lundin, A. J. Coates, and ASPERA-3 Team: The origin of energetic electron asymmetries in the induced magnetosphere of Mars. European Geosciences Union General Assembly, Vienna, Austria, April 13-18, 2008. (Poster)

Roussos, E., N. Krupp, T. P. Armstrong, D. G. Mitchell, C. Paranicas, S. M. Krimigis, A. Müller, and G. H. Jones: SEP events at Saturn and the effective shielding of the inner magnetosphere by the icy moons. Cassini MAPS workshop, Max-Planck-Institut für Sonnensystemforschung, Katlenburg-Lindau, Germany, April 2-4, 2008. (Oral)

Roussos, E., N. Krupp, A. Lagg, C. Paranicas, T. P. Armstrong, D. G. Mitchell, K. Dialynas, N. Sergis, and S. M. Krimigis: Access of solar wind MeV ions in Saturn's innermost magnetosphere. European Geosciences Union General Assembly, Vienna, Austria, April 13-18, 2008. (Oral)

Ruan, P., **T. Wiegelmann**, B. Inhester, and T. Neukirch: A MHS model in the solar corona. AGU Fall Meeting, San Francisco, USA, December 15-19, 2008. (Poster)

Ruan, P., T. Wiegelmann, B. Inhester, S. Solanki, and L. Feng: Modeling large scale coronal structures. European Geosciences Union General Assembly, Vienna, Austria, April 13-18, 2008. (Poster)

Santos, J. and J. Büchner: Plasma motion, electric currents and magnetic field topology near EUV bright points. Fifth International Cambridge Workshop on Magnetic Reconnection, Bad Honnef, Germany, August 18-22, 2008. (Oral)

Saur, J., B. H. Mauk, D. G. Mitchell, N. Krupp, K. K. Khurana, S. Livi, S. M. Krimigis, P. T. Newell, D. J. Williams, P. C. Brandt, A. Lagg, E. Roussos, and M. K. Dougherty: Anti-planetward auroral electron beams at Saturn. Saturn after Cassini-Huygens Symposium, Imperial College London, UK, July 28 – August 1, 2008. (Oral)

Savin, S., L. Zelenyi, E. Amata, V. Budaev, J. Büchner, J. Blecki, J. L. Rauch, A. Skalsky, and S. Romanov: New scenario of the plasma flow braking: formation of coherent accelerated structures versus thermalization. 37th COSPAR Scientific Assembly, Montreal, Canada, July 13-20, 2008. (Poster)

Schad, A., M. Roth, and J. Timmer: Analysis of long solar oscillation time series. 12th European Solar Physics meeting, Freiburg, Germany, September 8-12, 2008. (Poster)

Schad, A., M. Roth, and J. Timmer: Analysis of long solar oscillation time series. GONG 2008 / SOHO XXI Meeting, Boulder, Colorado, USA, August 11-15, 2008, contributed talk. (Oral)

Schlegel, K., H. Lühr, M. Rother, and K. Yumoto: Night-time sudden commencements observed with CHAMP and bround-based magnetometers. ISEA 12 – International Symposium on Equatorial Aeronomy, Crete, Greece, May 18-24, 2008. (Poster)

Schlegel, K., M. Rother, H. Lühr, and H. Vo: Validation of CHAMP electron density and electron temperature data with corresponding data from the Arecibo incoherent scatter facility. Frühjahrstagung Arbeitsgemeinschaft Extraterrestrische Forschung e.V., Freiburg, Germany, March 3-7, 2008. (Oral)

Schmitt, D.: Der Sternenhimmel im Sommer. 11. Göttinger Woche Wissenschaft und Jugend, Realschule Seesen, Realschule Lindau, Hainberg-Gymnasium Göttingen, Germany, June 30, July 1, July 2, 2008. (Oral)

Schmitt, D.: Geomagnetic dynamo theory. International School of Space Science, L'Aquila, Italy, April 7-11, 2008, invited lecture. (Oral)

Schühle, U. and L. Teriaca: Design of a Lyman-α detector and imager for SMESE-LYOT. First SMESE Workshop: "Coronal mass ejections and flares: new insights with the SMESE project", Institut d'Astrophysique de Paris, France, March 10-12, 2008. (Poster)

Schunker, H.: Properties of surface velocities within penumbral magnetic fields. ISSI Workshop on the Origin and Dynamics of Solar Magnetism, International Space Science Institute, Berne, Switzerland, January 21-25, 2008, invited. (Oral)

Schunker, H., R. Cameron, and L. Gizon: Sunspots, random waves, and the SLiM code. GONG 2008 / SOHO XXI Meeting, Boulder, Colorado, USA, August 11-15, 2008, contributed talk. (Oral)

Schunker, H., R. Cameron, and L. Gizon: The seismic effects of a sunspot. 12th European Solar Physics Meeting, Freiburg, Germany, September 8-12, 2008. (Poster)

Schüssler, M.: MHD simulation: from the convection zone to the corona and beyond. 12th European Solar Physics Meeting, Freiburg, Germany, September 8-12, 2008, invited review. (Oral)

Schüssler, M.: MHD simulations of sunspot structure. Solar Group Seminar, Institute for Astrophysics, Univ. of Göttingen, Germany, June 25, 2008. (Oral)

Schüssler, M.: Solar surface dynamo action. 10000 MHD days, Astrophys. Inst. Potsdam, Germany, September 1, 2008. (Oral)

Schwenn, R.: Sonnenstürme brausen durchs Sonnensystem – wie funktioniert das Weltraumwetter? Vortragsreihe, Altenwohnstift Göttingen, Germany, November 7-8, 2008.

Schwenn, R.: Space weather – why should we care? Latin American School on International Heliophysical Year, Sao Paulo, Brazil, February 14-20, 2008, invited Review.

Schwenn, R.: Space weather and solar-terrestrial relations. 4th El Leoncito Summer School on Solar Physics, El Leoncito and La Punta Universizy, San Luis, Argentina, November 24-29, 2008.

Schwenn, R.: Storms in space – when the Sun goes wild. Seminar, Weihai University, China, September 22, 2008.

Sergis, N., C. S. Arridge, S. M. Krimigis, D. G. Mitchell, A. Rymer, D. C. Hamilton, N. Krupp, E. C. Roelof, and M. Dougherty: Detection, structure, avriation and pressure balance in the Saturnian plasma sheet. Combined MIMI, CAPS and MAG measurements. Saturn after Cassini-Huygens Symposium, Imperial College London, UK, July 28 – August 1, 2008. (Oral)

Sergis, N., C. S. Arridge, S. M. Krimigis, D. G. Mitchell, A. M. Rymer, D. C. Hamilton, N. Krupp, E. C. Roelof, M. K. Dougherty, and A. J. Coates: Structure, variation and pressure balance in the Saturnian plasma sheet. Combined MIMI, CAPS and MAG measurements from Cassini. AGU Fall Meeting, San Francisco, USA, December 15-19, 2008. (Oral)

Sergis, N., S. M. Krimigis, D. Hamilton, D. G. Mitchell, E. C. Roelof, and N. Krupp: Energy content of suprathermal (>3 keV) ions in the Kronian magnetosphere measured by the Magnetospheric Imaging Instrument (MIMI) on Cassini: Magnetic field perturbation. European Geosciences Union General Assembly, Vienna, Austria, April 13-18, 2008. (Oral)

Sergis, N., S. M. Krimigis, D. C. Hamilton, D. G. Mitchell, E. C. Roelof, and N. Krupp: Energy content of suprathermal (>3 keV) ions in the Kronian magnetosphere, based on 3.5 years of Cassini/MIMI measurements: Magnetic field perturbation. Cassini MAPS workshop, Max-Planck-Institut für Sonnensystemforschung, Katlenburg-Lindau, Germany, April 2-4, 2008. (Oral)

Slavin, J. A., M. H. Acuña, B. J. Anderson, S. Barabash, M. Benna, S. A. Boardsen, M. Fränz, G. Gloeckler, G. C. Ho, and H. Korth: MESSENGER and Venus Express observations of the near-tail of Venus: Magnetic flux transport, current sheet structure, and flux rope formation. European Geosciences Union General Assembly, Vienna, Austria, April 13-18, 2008. (Oral)

Snodgrass, C., A. Fitzsimmons, H. Boehnhardt, and T. Lister: The October 2007 outburst of 17P/Holmes. Asteroids, Comets, Meteors 2008, Baltimore, USA, July 13-18, 2008. (Oral)

Solanki, S. K.: Das Licht der Sonne Ursprung und Einfluss auf die Erde. Akademie-Vorlesung im Schloss, Braunschweig, Germany, October 28, 2008, invited talk.

Solanki, S. K.: Exploring our fiery star, the Sun. Bernard Price lecture of the SAIEE (South African Institute of Electrical Engineering), Johannesburg, South Africa, October 12, 2008, invited talk.

Solanki, S. K.: Exploring our fiery star, the Sun. Bernard Price lecture of the SAIEE (South African Institute of Electrical Engineering), George, South Africa, October 13, 2008, invited talk.

Solanki, S. K.: Exploring our fiery star, the Sun. Bernard Price lecture of the SAIEE (South African Institute of Electrical Engineering), Port Elizabeth, South Africa, October 14, 2008, invited talk.

Solanki, S. K.: Exploring our fiery star, the Sun. Bernard Price lecture of the SAIEE (South African Institute of Electrical Engineering), Durban, South Africa, October 15, 2008, invited talk.

Solanki, S. K.: Exploring our fiery star, the Sun. Bernard Price lecture of the SAIEE (South African Institute of Electrical Engineering), Capetown, South Africa, October 16, 2008, invited talk.

Solanki, S. K.: Global climate change: is the Sun to blame? CAWSES Meeting "Solar Variability, Earths Climate and the Space Environment", Bozeman, Montana, USA, June 1-8, 2008, public lecture.

Solanki, S. K.: Ist die Sonne am Klimawandel schuld? Wohnstift Charlottenburger Strasse Göttingen, Germany, March 8, 2008, invited talk.

Solanki, S. K.: Long-term solar activity reconstruction: Grand Minima and Maxima. CAWSES Meeting "Solar Variability, Earths Climate and the Space Environment", Bozeman, Montana, USA, June 1-8, 2008, invited talk.

Solanki, S. K.: Magnetic fields on multiple scales. SDO Science Teams Meeting, Napa, California, USA, March 25-28, 2008, invited talk.

Solanki, S. K.: Present and future solar space missions. JENAM 2008 – "New Challenges to European stronomy", Vienna, Austria, September 7-12, 2008, invited talk.

Solanki, S. K.: Quiet Sun magnetism. ISSI Workshop on the Origin and Dynamics of Solar Magnetism, Bern, Switzerland, January 21-25, 2008, invited.

Solanki, S. K.: Solar activity. International Workshop of 2008 Solar Total Eclipse: Solar magnetism, Corona and Space Weather Chinese Space Solar Telescope Science, Jiuquan, China, July 28 – August 1, 2008, invited general public lecture.

Solanki, S. K.: Solar chromospheric magnetic fields: terra incognita. Seminar University of Kyoto, Kyoto, Japan, November 16, 2008, invited talk.

Solanki, S. K.: Solar surface magnetic field-based irradiance models. CAWSES Meeting "Solar Variability, Earths Climate and the Space Environment", Bozeman, Montana, USA, June 1-8, 2008, invited talk.

Solanki, S. K.: The Solar Orbiter Mission. International Workshop of 2008 Solar Total Eclipse: Solar magnetism, Corona and Space Weather Chinese Space Solar Telescope Science, Jiuquan, China, July 28 – August 1, 2008, invited talk.

Solanki, S. K.: The Suns magnetic field and its possible role in the Earths climate change. Seminar Udaipur Solar Observatory, Udaipur, India, December 8, 2008, invited talk.

Solanki, S. K.: The Suns magnetic field and its possible role in the Earths climate change. Seminar Indian Institute of Astrophysics, Bangalore, India, December 11, 2008, invited talk.

Solanki, S. K.: The Sun's photospheric magnetic field. 1st Middle East and Africa Regional IAU Meeting, Cairo, Egypt, April 5-10, 2008, invited talk.

Solanki, S. K.: Unser Sonnensystem: von Planeten, Raketen und der heißen Sonne. Kinder-Uni, Göttingen, Germany, June 18, 2008.

Solanki, S. K. and N. Krivova: Solar irradiance and activity reconstructions on timescales up to millenia. SORCE's Past, Present, and Future Role in Earth Science Research, Science Meeting 2008, Santa Fé, New Mexico, USA, February 5-7, 2008, invited review.

Solanki, S. K., A. Pietarila, and A. Lagg: Measurement of chromospheric magnetic fields. SOLAR-C Science Definition Meeting, Tokyo, Japan, November 18-21, 2008, invited talk.

Sonnemann, G. R., L. Hartogh, P. Song, and M. Grygalashvyly: Microwave water vapor measurements at ALOMAR over a solar cycle and calculations by means of the real date model LIMA. 5th General Meeting of the Asia Oceania Geosciences Society (AOGS 2008), Busan, Korea, June 16-20, 2008. (Oral).

Stahn, T. and L. Gizon: Fourier analysis of gapped time-series. Wroclaw HELAS Workshop "Interpretation of Asteroseismic Data", Wroclaw, Poland, June 23-27, 2008. (Poster)

Staiger, J., M. Roth, H. Wöhl, H. Schleicher, and K. Puschmann: Local helioseismology with GFPI at the vacuum tower telescope, Tenerife. 12th European Solar Physics Meeting, Freiburg, Germany, September 8-12, 2008. (Poster)

Stenzel, O. J., R. Greve, B. Grieger, H. U. Keller, K. Fraedrich, E. Kirk, and F. Lunkeit: Results from the Mars Climate Simulation Project. 5th Colloquium of the DFG SPP 1115 "Mars and the Terrestrial Planets", Münster, Germany, February 28-29, 2008. (Oral)

Stenzel, O. J., N. M. Hoekzema, W. J. Markiewicz, and H. U. Keller: Improvements to the Albedo Method. HRSC CO-I Team Meeting, Pescara, Italy, April, 21, 2008. (Oral)

Stenzel, O. J., N. M. Hoekzema, W. J. Markiewicz, and H. U. Keller: Lookup tables – a possible way to implement operational dust correction. MEX HRSC Co-I Team Meeting, Münster, Germany, September 18-19, 2008. (Oral)

Szego, K., Z. Bebesi, Z. Dobe, M. Fränz, A. Fedorov, S. Barabash, A. J. Coates, and T. L. Zhang: The ion flow below the magnetic barrier at Venus. European Geosciences Union General Assembly, Vienna, Austria, April 13-18, 2008. (Oral)

Tachihara, K., **M. Rengel**, Y. Nakajima, N. Yamaguchi, P. Andre, R. Neuhaeuser, T. Onishi, Y. Fukui, and A. Mizuno: A new peculiar Class 0 object in Lupus 3. JENAM 2008 (Joint European and National Astronomy Meeting) – "New Challenges to European Astronomy", Vienna, Austria, September 8-12, 2008. (Oral)

Tadesse, T. and T. Wiegelmann: NLFF coronal magnetic field extrapolation in spherical coordinates for part of a sphere. NLFFF5-meeting, Lindau, GERMANY; June 30 – July 02, 2008. (Oral)

Tadesse, T. and T. Wiegelmann: Nonlinear force-free reconstruction in spherical coordinates for active regions using Optimization method. Workshop: A Next Generation Coronal Active Region Model, Philadelphia, USA, October 22-23, 2008. (Oral)

Teriaca, L.: Are there velocities in polar plumes below 1.1 solar radii? Solar Activity during the Onset of Solar Cycle 24, Napa, California, USA, December 8-12, 2008, contributed. (Oral)

Teriaca, L.: Results from the Hinode/SUMER campaigns. Second Hinode science meeting, Boulder, Colorado, USA, September 29 – October 3, 2008, invited talk. (Oral)

Teriaca, L., W. Curdt, U. Schühle, and **S. K. Solanki**: UV spectrometer for Solar C. SOLAR-C Science Definition Meeting, Tokyo, Japan, November 18-21, 2008. (Oral)

Thalmann, J. and **T. Wiegelmann**: Evolution of two flaring active regions with CME association. AGU Fall Meeting, San Francisco, USA, December 15-19, 2008. (Poster)

Thalmann, J. and T. Wiegelmann: Sequences of NLFFF-extrapolations for flaring ARs. NLFFF5-meeting, Lindau, Germany, June 30 – July 02, 2008. (Oral)

Thalmann, J. and T. Wiegelmann: Using Solis Vector-SpectroMagnetograph data for coronal magnetic field extrapolation. Workshop: A Next Generation Coronal Active Region Model, Philadelphia, USA, October 22-23, 2008. (Oral)

Thalmann, J. K. and T. Wiegelmann: Evolution of the coronal magnetic field of NOAA active region 10540. European Geosciences Union General Assembly, Vienna, Austria, April 13-18, 2008. (Poster)

Thalmann, J. K. and T. Wiegelmann: Magnetic field extrapolation of flaring active regions. NLFFF Consortium Meeting 5, Katlenburg-Lindau, Germany, June 30 – July 2, 2008. (Oral)

Thalmann, J. K. and T. Wiegelmann: Magnetic field extrapolation of flaring active regions. IXth Hvar Astrophysical Colloquium – Solar Minimum Meeting, Hvar, Croatia, September 22-26, 2008. (Oral)

Tian, H., **W. Curdt**, E. Marsch, and J. He: Cool and hot components of a coronal bright point. ESPM-12, Freiburg, Germany, September 8-12, 2008. (Poster)

Tian, H., **E. Marsch**, C.-Y. Tu, J.-S. He, and G.-Q. Zhou: Signature of mass supply to quiet coronal loops. Frühjahrstagung des DPG Fachverbands Extraterrestrische Physik (EP) und der AEF e.V., Freiburg, Germany, March 3-7, 2008. (Poster)

Tu, C., H. Tian, **J. He**, and E. Marsch: A model of the solar wind driven by supergranular circulation. 37th COSPAR Scientific Assembly, Montreal, Canada, July 13-20, 2008. (Oral)

Tubiana, C., H. Boehnhardt, M. Drahus, L. Barrera, J. L. Ortiz, G. Schwehm, R. Schulz, and J. Stuewe: 67P/Churyumov-Gerasimenko: Photometry and spectroscopy of the ROSETTA target comet in the aphelion arc. Future Ground-Based Solar System Research – Synergies with Space Probes and Space Telescopes, Portoferraio, Elba, Italy, September 8-12, 2008. (Poster)

Tubiana, C., H. Boehnhardt, M. Drahus, L. Barrera, J. L. Ortiz, G. Schwehm, R. Schulz, J. Stuewe, and J. B. Vincent: 67P/Churyumov-Gerasimenko: The Rosetta target comet in the aphelion arc. Asteroids, Comets, Meteors 2008, Baltimore, USA, July 13-18, 2008. (Poster)

Unruh, Y. C., N. A. Krivova, S. K. Solanki, and J. W. Harder: Irradiance variations on rotational timescales: a comparison between SORCE measurements and the SATIRE model. SORCE's Past, Present, and Future Role in Earth Science Research, Science Meeting 2008, Santa Fé, New Mexico, USA, February 5-7, 2008. (Oral)

Vasyliūnas, V. M.: Birkeland currents in mirror fields: Physical origin of the Knight relation. 9th International Conference on Substorms, Schloss Seggau, Austria, May 5-9, 2008. (Poster)

Vasyliūnas, V. M.: Do electric fields drive ionospheric plasma flows? Seminar, Center for Atmospheric Research, University of Massachusetts, Lowell, Massachusetts, USA, April 25, 2008. (Oral)

Vasyliūnas, V. M.: Energy conversion in planetary magnetospheres. Heliophysics Summer School: Year 2, Boulder, Colorado, USA, July 23-30, 2008, invited lecture. (Oral)

Vasyliūnas, V. M.: Extraterrestrial counterparts/analogs of substorms: similarities and differences. 9th International Conference on Substorms, Schloss Seggau, Austria, May 5-9, 2008, (invited talk). (Oral)

Vasyliūnas, V. M.: Maximum intensity of magnetic storms. The First Korean Winter School on Space Physics, Gyeongju, Korea, February 21-22, 2008, invited paper. (Oral)

Vasyliūnas, V. M.: Origin of the camshaft field: what can and what cannot work. Cassini MAPS Workshop, Max-Planck-Institut für Sonnensystemforschung, Katlenburg-Lindau, Germany, April 2-4, 2008. (Oral)

Vasyliūnas, V. M.: Reinterpreting the Burton-McPherron-Russell equation for predicting Dst: Implications for the energy input of storms and substorms. Storm-Substorm Workshop, Gyeongju, Korea, February 18-19, 2008. (Oral)

Vasyliūnas, V. M.: Understanding the magnetosphere: the counter-intuitive simplicity of cosmic electrodynamics. AGU Fall Meeting, San Francisco, USA, December 15-19, 2008, Van Allen lecture, invited. (Oral)

Vasyliūnas, V. M. and P. Song: Do electric fields drive ionospheric plasma flows? 12th International Symposium on Equatorial Aeronomy, Crete, Greece, May 18-24, 2008. (Oral)

Vieira, L. A., N. A. Krivova, S. K. Solanki, and L. Balmaceda: A multi-millennial reconstruction of the total solar irradiance from the carbon radioisotope production rate. 2008 Joint AGU Assembly, Fort Lauderdale, USA, May 27-30, 2008. (Poster)

Vieira, L. E. A. and L. A. da Silva: Longitudinal anomaly in the lower stratospheric temperature in southern hemisphere: effects of particle precipitation in the southern hemisphere magnetic anomaly? International Astronomical Union (IAU) Symposium 257 on "Universal Heliophysical Processes", Ioannina, Greece, September 15-19, 2008. (Oral)

Villanueva, G. L., M. J. Mumma, B. P. Bonev, M. A. DiSanti, E. L. Gibb, H. Boehnhardt, and M. Lippi: Measurement of the D/H in comet 8P/Tuttle: On the origin of Earth's water. Asteroids, Comets, Meteors 2008, Baltimore, USA, July 13-18, 2008. (Oral)

Vincent, J.-B., H. Boehnhardt, L. M. Lara, and I. Bertini: Coma structures analysis for comet Schwassmann-Wachmann 3, components B and C. Asteroids, Comets, Meteors 2008, Baltimore, USA, July 13-18, 2008. (Oral)

Vincent, J.-B., H. Boehnhardt, L.-M. Lara, and I. Bertini: Imaging and analysis of coma structures for comet Schwassmann-Wachmann 3, fragment C. Future Ground-Based Solar System Research – Synergies with Space Probes and Space Telescopes, Portoferraio, Elba, Italy, September 8-12, 2008. (Poster)

Wang, H., J. Jing, C. Tan, and T. Wiegelmann: Study of magnetic channel structure in AR 10930. 2008 Joint AGU Assembly, Fort Lauderdale, USA, May 27-30, 2008. (Oral)

Whittaker, I. C., M. Grande, G. Guymer, B. Pintér, S. Barabash, A. Federov, C. Mazelle, J. Sauvaud, R. Lundin, C. Russell, Y. Futaana, M. Fränz, T. L. Zhang, H. Andersson, K. Brinkfeldt, A. Grigoriev, M. Holmström, M. Yamauchi, K. Asamura, W. Baumjohann, H. Lammer, A. J. Coates, D. O. Kataria, D. R. Linder, C. C. Curtis, K. C. Hsieh, B. R. Sandel, H. Gunell, H. E. Koskinen, E. Kallio, P. Riihelä, T. Säles, W. Schmidt, J. Kozyra, N. Krupp, J. Woch, J. Luhmann, S. McKenna-Lawlor, J. J. Thocaven, S. Orsini, R. Cerulli-Irelli, M. Mura, M. Milillo, M. Maggi, E. Roelof, P. Brandt, K. Szego, J. D. Winningham, R. A. Frahm, J. Scherrer, J. Sharber, P. Wurz, and P. Bochsler: The effect of fast and slow solar wind on the Venusian upper atmosphere. AGU Fall Meeting, San Francisco, USA, December 15-19, 2008. (Oral)

Wicht, J.: Numerical models of planetary dynamos. ISSI Workshop on Planetary Magnetism, Bern, Switzerland, September 1-5, 2008. (Oral)

Wicht, J. and J. Aubert: Towards understanding geomagnetic field reversals. European Geosciences Union General Assembly, Vienna, Austria, April 13-18, 2008. (Oral)

Wicht, J. and A. Jonkers: Simulated geomagnetic reversals: How realistic are they and what can we learn? AGU Fall Meeting, San Francisco, USA, December 15-19, 2008. (Oral)

Wiegelmann, T.: Nonlinear force-free evolution of AR 8210. Workshop: A Next Generation Coronal Active Region Model, Philadelphia, USA, October 22-23, 2008, invited. (Oral)

Wiegelmann, T. and T. Neukirch: A first step towards a nonlinear and self-consistent modelling of the interface region between photosphere, chromosphere and corona. AGU Fall Meeting, San Francisco, USA, December 15-19, 2008. (Oral)

Wiegelmann, T., T. Neukirch, P. Ruan, and B. Inhester: Optimization approach for the computation of magnetohydrostatic coronal equilibria. European Geosciences Union General Assembly, Vienna, Austria, April 13-18, 2008. (Poster)

Wiegelmann, T. and J. Thalmann: H-alpha preprocessing of Hinode vector magnetograms. NLFFF5-meeting, Lindau, Germany, June 30 – July 02, 2008, invited. (Oral)

Wiegelmann, T. and J. Thalmann: How to compute the magnetic vector potential from NLFFF-models? Workshop: A Next Generation Coronal Active Region Model, Philadelphia, USA, October 22-23, 2008, invited. (Oral)

Wiegelmann, T. and J. Thalmann: NLFFF-extrapolations of Hinode cases with optimization method. NLFFF5-meeting, Lindau, Germany, June 30 – July 02, 2008, invited. (Oral)

Wiegelmann, T., J. Thalmann, B. Inhester, and the NLFFF-consortium: Nonlinear force-free models. 37th COSPAR Scientific Assembly, Montreal, Canada, July 13-20, 2008, invited review talk. (Oral)

Wiegelmann, T. and J. K. Thalmann: A brief summary about nonlinear force-free coronal magnetic field modelling for SDO. SDO Science Teams Meeting, Napa, CA, USA, March 25-28, 2008, invited. (Oral)

Wiegelmann, T., J. K. Thalmann, and B. Inhester: Nonlinear force-free extrapolation of coronal magnetic fields. CSTR Group Meeting, Newark, NJ, USA, April 1, 2008, invited. (Oral)

Wiegelmann, T., J. K. Thalmann, B. Inhester, L. Feng, and P. Ruan: Solar coronal magnetic fields:Source of Space weather. NJIT, Newark, NJ, USA, March 31, 2008, invited colloquium talk. (Oral)

Wiegelmann, T., J. K. Thalmann, B. Inhester, and the NLFFF consortium: Nonlinear force-free field modeling for SDO. SDO Science Teams Meeting, Napa, CA, USA, March 25-28, 2008, invited. (Oral)

Wiegelmann, T., J. K. Thalmann, C. J. Schrijver, M. L. DeRosa, and T. R. Metcalf: How to include H-Alpha Images to estimate the chromospheric and coronal magnetic field from photospheric vector-magnetograms? European Geosciences Union General Assembly, Vienna, Austria, April 13-18, 2008. (Oral)

Wilhelm, K., **B. N. Dwivedi**, and W. Curdt: Spectroscopic diagnostics of polar coronal plumes observed from space. Magnetic Coupling between the Interior and the Atmosphere of the Sun "Centenary Commemoration of the Discovery of the Evershed Effect", Bangalore, India, December 2-5, 2008. (Poster)

Wooden, D. H., M. S. Kelley, C. E. Woodward, D. E. Harker, H. Boehnhardt, C. Tubiana, and D. Prialnik: Comet 67P/Churyumov-Gerasimenko: Nuclear properties and heliocentric-distance dependent activity. Asteroids, Comets, Meteors 2008, Baltimore, USA, July 13-18, 2008. (Poster)

Yamauchi, M., **R. Lundin**, I. Dandouras, G. Stenberg, P. W. Daly, H. Frey, Y. Enihara, H. Nilsson, H. Rème, M. André, P.-A. Lindquvist, E. Kronberg, and A. Balogh: Sudden formation of bi-directional ion beam and associated large-scale configuration change in the equatorial ring current at 19 MLT and L=4. European Geosciences Union General Assembly, Vienna, Austria, April 13-18, 2008. (Poster)

Zaatri, A. and M. Roth: Meridional flow measurements: comparisons between ring diagram analysis and Fourier-Hankel analysis. 12th European Solar Physics Meeting, Freiburg, Germany, September 8-12, 2008. (Poster)

Zacharias, P., H. Peter, and J. Büchner: Spectral analysis of a 3D MHD bright point model. DPG Tagung 2008, Freiburg im Breisgau, Freiburg, Germany, March 4, 2008. (Poster)

Veröffentlichungen 2008 / Publications 2008

Betreuung der Online-Veröffentlichungs- und Vortragsliste: P. W. Daly

Afram, N., S. V. Berdyugina, D. M. Fluri, S. K. Solanki, and A. Lagg: The FeH $F^4\Delta$-$X^4\Delta$ system. Creating a valuable diagnostic tool to explore solar and stellar magnetic fields. Astron. & Astrophys. **482**, 387–395 (2008), doi:10.1051/0004-6361:20079300.

Amit, H. and U. R. Christensen: Accounting for magnetic diffusion in core flow inversions from geomagnetic secular variation. Geophys. J. Int. **175**, 913–924 (2008), doi:10.1111/j.1365-246X.2008.03948.x.

André, N., M. Blanc, S. Maurice, P. Schippers, E. Pallier, T. I. Gombosi, K. C. Hansen, D. T. Young, F. J. Crary, S. Bolton, E. C. Sittler, H. T. Smith, R. E. Johnson, R. A. Baragiola, A. J. Coates, A. M. Rymer, M. K. Dougherty, N. Achilleos, C. S. Arridge, S. M. Krimigis, D. G. Mitchell, N. Krupp, D. C. Hamilton, I. Dandouras, D. A. Gurnett, W. S. Kurth, P. Louarn, R. Srama, S. Kempf, H. J. Waite, L. W. Esposito, and J. T. Clarke: Identification of Saturn's magnetospheric regions and associated plasma processes: Synopsis of Cassini observations during orbit insertion. Rev. Geophys. **46**, RG4008 (2008), doi:10.1029/2007RG000238.

Andretta, V., P. J. D. Mauas, A. Falchi, and L. Teriaca: Helium Line Formation and Abundance during a C-Class Flare. Astrophys. J. **681**, 650–663 (2008), doi:10.1086/587933.

Antonucci, E., V. Andretta, S. Cesare, A. Ciaravella, G. Doschek, S. Fineschi, S. Giordano, P. Lamy, D. Moses, G. Naletto, J. Newmark, L. Poletto, M. Romoli, S. K. Solanki, D. Spadaro, L. Teriaca, and L. Zangrilli: METIS, the Multi Element Telescope for Imaging and Spectroscopy: An Instrument Proposed for the Solar Orbiter Mission. In: Proc. International Conference on Space Optics (ICSO 2008) (2008), on CD.

Apatenkov, S. V., V. A. Sergeev, O. Amm, W. Baumjohann, R. Nakamura, A. Runov, F. Rich, P. Daly, A. Fazakerley, I. Alexeev, J. A. Sauvaud, and Yu. Chotyaintsev: Conjugate observation of sharp dynamical boundary in the inner magnetosphere by Cluster and DMSP spacecraft and ground network. Ann. Geophys. **26**, 2771–2780 (2008).

Araneda, J. A., E. Marsch, and A. F.-Viñas: Proton Core Heating and Beam Formation via Parametrically Unstable Alfven-CyclotronWaves. Phys. Rev. Lett. **100**, 125003 (2008), doi:10.1103/PhysRevLett.100.125003.

Arvidson, R. E., S. W. Ruff, R. V. Morris, D. W. Ming, L. S. Crumpler, A. S. Yen, S. W. Squyres, R. J. Sullivan, J. F. Bell, III, N. A. Cabrol, B. C. Clark, W. H. Farrand, R. Gellert, R. Greenberger, J. A. Grant, E. A. Guinness, K. E. Herkenhoff, J. A. Hurowitz, J. R. Johnson, G. Klingelhoefer, K. W. Lewis, R. Li, T. J. McCoy, J. Moersch, H. Y. McSween, S. L. Murchie, M. Schmidt, C. Schroeder, A. Wang, S. Wiseman, M. B. Madsen, W. Goetz, and S. M. McLennan: Spirit Mars Rover Mission to the Columbia Hills, Gusev Crater: Mission overview and selected results from the Cumberland Ridge to Home Plate. J. Geophys. Res. **113**, E12S33 (2008), doi:10.1029/2008JE003183.

Aschwanden, M. J., L. F. Burlaga, M. L. Kaiser, C. K. Ng, D. V. Reames, M. J. Reiner, T. I. Gombosi, N. Lugaz, W. Manchester, I. I. Roussev, T. H. Zurbuchen, C. J. Farrugia, A. B. Galvin, M. A. Lee, J. A. Linker, Z. Mikić, P. Riley, D. Alexander, A. W. Sandman, J. W. Cook, R. A. Howard, D. Odstrčil, V. J. Pizzo, J. Kóta, P. C. Liewer, J. G. Luhmann, B. Inhester, R. W. Schwenn, S. K. Solanki, V. M. Vasyliūnas, T. Wiegelmann, L. Blush, P. Bochsler, I. H. Cairns, P. A. Robinson, V. Bothmer, K. Kecskemety, A. Llebaria, M. Maksimovic, M. Scholer, and R. F. Wimmer-Schweingruber: Theoretical Modeling for the Stereo Mission. Space Sci. Rev. **136**, 565–604 (2008), doi:10.1007/s11214-006-9027-8.

Åsnes, A., R. W. H. Friedel, B. Lavraud, G. D. Reeves, M. G. G. T. Taylor, and P. Daly: Statistical properties of tail plasma sheet electrons above 40 keV. J. Geophys. Res. **113**, A03202 (2008), doi:10.1029/2007JA012502.

Åsnes, A., M. G. G. T. Taylor, A. L. Borg, B. Lavraud, R. W. H. Friedel, C. P. Escoubet, H. Laakso, P. Daly, and A. N. Fazakerley: Multispacecraft observation of electron beam in reconnection region. J. Geophys. Res. **113**, A07S30 (2008), doi:10.1029/2007JA012770.

Attie, R. and D. E. Innes: Explosive Event in the Quiet Sun Seen by XRT-EIS and SUMER. In: First Results From Hinode, eds. S. A. Matthews, J. M. Davis, and L. K. Harra, ASP Conference Series, p. 155, Astronomical Society of the Pacific, San Francisco (2008).

Aubert, J., J. Aurnou, and J. Wicht: The magnetic structure of convection-driven numerical dynamos. Geophys. J. Int. **172**, 945–956 (2008), doi:10.1111/j.1365-246X.2007.03693.x.

Aurnou, J., M. Heimpel, L. Allen, E. King, and J. Wicht: Convective heat transfer and the pattern of thermal emission on the gas giants. Geophys. J. Int. **173**, 793–801 (2008), doi:10.1111/j.1365-246X.2008.03764.x.

Auster, H. U., K. H. Glassmeier, W. Magnes, O. Aydogar, W. Baumjohann, D. Constantinescu, D. Fischer, K.-H. Fornaçon, E. Georgescu, P. Harvey, O. Hillenmaier, R. Kroth, M. Ludlam, Y. Narita, R. Nakamura, K. Okrafka, F. Plaschke, I. Richter, H. Schwarzl, B. Stoll, A. Valavanoglou, and M. Wiedemann: The THEMIS Fluxgate Magnetometer. Space Sci. Rev. **141**, 235–264 (2008), doi:10.1007/s11214-008-9365-9.

Bamert, K., R. Kallenbach, J. le Roux, M. Hilchenbach, C. Smith, and P. Wurz: Evidence for Iroshnikov-Kraichnan-Type Turbulence in the Solar Wind Upstream of Interplanetary Traveling Shocks. Astrophys. J. **675**, L45–L48 (2008), doi:10.1086/529491.

Barthol, P., A. M. Gandorfer, S. K. Solanki, M. Knölker, V. Martinez Pillet, W. Schmidt, A. M. Title, and the SUNRISE Team: SUNRISE: High resolution UV/VIS observations of the Sun from the stratosphere. Adv. Space Res. **42**, 70–77 (2008), doi:10.1016/j.asr.2007.09.024.

Barucci, M. A., H. Boehnhardt, D. P. Cruikshank, and A. Morbidelli (eds.): The Solar System Beyond Neptune. The University of Arizona Space Science Series, University of Arizona Press, Tucson, USA (2008).

Barucci, M. A., H. Boehnhardt, D. P. Cruikshank, and A. Morbidelli: The Solar System Beyond Neptune: Overview and Perspectives. In: The Solar System Beyond Neptune, eds. M. A. Barucci, H. Boehnhardt, D. P. Cruikshank, and A. Morbidelli, The University of Arizona Space Science Series, The University of Arizona Press, Tucson, USA (2008).

Basilevsky, A. T., E. V. Shalygin, D. V. Titov, W. J. Markiewicz, F. Scholten, and M. A. Kreslavsky: Geologic Analysis of the Surface Thermal Emission Images Taken by the Venus Monitoring Camera, Venus Express Initial Results. In: 39th Lunar and Planetary Science Conference, (Lunar and Planetary Science XXXIX), held March 10-14, 2008 in League City, Texas, p. 1526, Lunar and Planetary Institute (2008).

Bazarghan, M., H. Safari, D. E. Innes, E. Karami, and S. K. Solanki: A nanoflare model for active region radiance: application of artificial neural networks. Astron. & Astrophys. **492**, L13–L16 (2008), doi:10.1051/0004-6361:200810911.

Bhardwaj, A., P. Hartogh, Y. Kasaba, and C. Y. R. Wu: Advances in Planetary Sciences: AOGS 2007 (based on the Forth Annual Meeting of the AOGS, Bangkok, Thailand). Planet. Space Sci. **56**, 1675 (2008), doi:10.1016/j.pss.2008.08.002.

Bloomfield, D. S., A. Lagg, and S. K. Solanki: The nature of running penumbral waves revealed. In: Proc. IAU Symposium 247 "Waves & Oscillations in the Solar Atmosphere: Heating and Magneto-Seismology", eds. R. Erdélyi and C. A. Mendoza-Briceno, pp. 55–58, International Astronomical Union (2008), doi:10.1017/S1743921308014658.

Boehnhardt, H., M. J. Mumma, G. L. Villanueva, M. A. DiSanti, B. P. Bonev, M. Lippi, and H. U. Käufl: The Unusual Volatile Composition of the Halley-Type Comet 8P/Tuttle: Addressing the Existence of an Inner Oort Cloud. Astrophys. J. **683**, L71–L74 (2008), doi:10.1086/591446.

Boehnhardt, H., G. P. Tozzi, S. Bagnulo, K. Muinonen, A. Nathues, and L. Kolokolova: Photometry and polarimetry of the nucleus of comet 2P/Encke. Astron. & Astrophys. **489**, 1337–1343 (2008), doi:10.1051/0004-6361:200809922.

Bonev, T., H. Boehnhardt, and G. Borisov: Broadband imaging and narrowband polarimetry of comet 73P/Schwassmann-Wachmann 3, components B and C, on 3, 4, 8, and 9 May 2006. Astron. & Astrophys. **480**, 277–287 (2008), doi:10.1051/0004-6361:20078527.

Bonev, T., K. Jockers, and N. Karpov: A dynamical model with a new inversion technique applied to observations of Comet WM1 (LINEAR). Icarus **197**, 183–202 (2008), doi:10.1016/j.icarus.2008.04.009.

Borrero, J. M., B. W. Lites, and S. K. Solanki: Evidence of magnetic field wrapping around penumbral filaments. Astron. & Astrophys. **481**, L13–L16 (2008), doi:10.1051/0004-6361:20079002.

Borrero, J. M. and S. K. Solanki: Are there field-free gaps near $\tau = 1$ in sunspot penumbrae? Astrophys. J. **687**, 668–677 (2008), doi:10.1086/591220.

Bourouaine, S., E. Marsch, and C. Vocks: On the efficiency of nonresonant ion heating by coronal Alfven waves. Astrophys. J. **684**, L119–L122 (2008), doi:10.1086/592243.

Bourouaine, S., C. Vocks, and E. Marsch: Coronal loop model including ion kinetics. Astrophys. J. **676**, 1346–1355 (2008), doi:10.1086/527554.

Bourouaine, S., C. Vocks, and E. Marsch: Multi-ion kinetic model for coronal loop. Astrophys. J. **680**, L77–L80 (2008), doi:10.1086/589741.

Brandenburg, A., K.-H. Raedler, and M. Schrinner: Scale dependence of alpha effect and turbulent diffusivity. Astron. & Astrophys. **482**, 739–746 (2008), doi:10.1051/0004-6361:200809365.

Brandl, B. R., R. Lenzen, E. Pantin, A. Glasse, J. Blommaert, L. Venema, F. Molster, R. Siebenmorgen, H. Boehnhardt, E. van Dishoeck, P. van der Werf, T. Henning, W. Brandner, P.-O. Lagage, T. J. T. Moore, M. Baes, C. Waelkens, C. Wright, H. U. Käufl, S. Kendrew, R. Stuik, and L. Jolissaint: METIS: the mid-infrared E-ELT imager and spectrograph. In: Ground-based and Airborne Instrumentation for Astronomy II, eds. I. S. McLean and M. M. Casali, *Proceedings of the SPIE*, vol. 7014, p. 70141N (2008), doi:10.1117/12789241.

Büchner, J.: Ab Initio Vlasov Code Simulation of Micro-Turbulence, Phase Space Structure Formation and the Resulting Anomalous Transport and Particle Acceleration in Collisionless Astrophysical Plasmas, I: The 2D2V Code. In: High Peformance Computing in Science and Engineering, eds. S. Wagner, M. Steinmetz, A. Bode, and M. Brehm, pp. 19–28, Springer, Berlin-Heidelberg (2008), doi:10.1007/978-3-540-69182-2.

Bučík, R., R. Gomez-Herrero, A. Korth, U. Mall, and G. M. Mason: Energetic ions from corotating interaction regions during small solar events in May 2007. In: Proceedings of 21st European Cosmic Ray Symposium, eds. P. Kiraly, K. Kudela, M. Stehlik, and A. W. Wolfendale, Košice, Slovakia (2008).

Bučík, R., A. Korth, U. Mall, and G. Mason: Simulations of events in time-of-flight telescope for suprathermal ions in heliosphere. In: Astroparticle, Particle and Space Physics, Detectors and Medical Physics Applications, Proceedings of the 10th Conference, eds. M. Barone, A. Gaddi, C. Leroy, L. Price, P.-G. Rancoita, and R. Ruchti, pp. 852–857, World Scientific Publishing Co. Pte. Ltd., Singapore (2008).

Bučík, R., K. Kudela, and D. Smith: Simulations of hard X ray and gamma ray response in CsI(Tl) scintillator detector. In: Proc. of the 30th International Cosmic Ray Conference, eds. R. Caballero, J. C. D'Olivo, G. Medina-Tanco, L. Nellen, F. A. Sánchez, and J. F. Valdés-Galicia, vol. 1 (SH), pp. 3–6, Universidad Nacional Autónoma de México, Mexico City, Mexico (2008).

Burston, R., L. Gizon, T. Appourchaux, W.-T. Ni, and the ASTROD I ESA Cosmic Vision 2015-2025 Team: Detecting solar g modes with ASTROD. J. Phys.: Conf. Ser. **118**, 012043 (2008), doi:10.1088/1742-6596/118/1/012043.

Burston, R. B.: 1+1+2 Electromagnetic perturbations on non-vacuum LRS class II space-times: Decoupling scalar and 2-vector harmonic amplitudes. Class. Quantum Grav. **25**, 075002 (2008), doi:10.1088/0264-9381/25/7/075002.

Burston, R. B.: 1+1+2 Gravitational perturbations on LRS class II space-times: Decoupling gravito-electromagnetic tensor harmonic amplitudes. Class. Quantum Grav. **25**, 075004 (2008), doi:10.1088/0264-9381/25/7/075004.

Burston, R. B.: 1+1+2 gravitational perturbations on LRS class II spacetimes: II. Decoupling gravito-electromagnetic 2-vector and scalar harmonic amplitudes. Class. Quantum Grav. **25**, 235004 (2008), doi:10.1088/0264-9381/25/23/235004.

Burston, R. B. and A. W. C. Lun: 1+1+2 Electromagnetic perturbations on general LRS spacetimes: Regge-Wheeler and Bardeen-Press equations. Class. Quantum Grav. **25**, 075003 (2008), doi:10.1088/0264-9381/25/7/075003.

Cameron, R., L. Gizon, and T. L. Duvall, Jr.: Helioseismology of sunspots: Confronting observations with three-dimensional MHD simulations of wave propagation. Solar Phys. **251**, 291–308 (2008), doi:10.1007/s11207-008-9148-1.

Cameron, R. and M. Schüssler: A robust correlation between growth rate and amplitude of solar cycles: consequences for prediction methods. Astrophys. J. **685**, 1291–1296 (2008), doi:10.1086/591079.

Cao, X., Z. Y. Pu, H. Zhang, V. M. Mishin, Z. W. Ma, M. W. Dunlop, S. Y. Fu, L. Xie, C. J. Xiao, X. G. Wang, Q. G. Zong, Z. X. Liu, M. V. Kubyshkina, T. I. Pulkkinen, H. U. Frey, A. Korth, M. Fraenz, E. Lucek, C. M. Carr, H. Reme, I. Dandouras, A. N. Fazakerley, G. D. Reeves, R. Friedel, K. H. Glassmeier, and C. P. Escoubet: Multispacecraft and ground-based observations of substorm timing and activations: Two case studies. J. Geophys. Res. **113**, A07S25 (2008), doi:10.1029/2007JA012761.

Chang, J., J. H. Adams, Jr., H. S. Ahn, G. L. Bashindzhagyan, K. E. Batkov, M. Christl, A. R. Fazely, O. Ganel, R. M. Gunashingha, T. G. Guzik, J. Isbert, K. C. Kim, E. N. Kouznetsov, Z. W. Lin, M. I. Panasyuk, A. D. Panov, W. K. H. Schmidt, E. S. Seo, N. V. Sokolskaya, J. W. Watts, J. P. Wefel, J. Wu, and V. I. Zatsepin: Resolving electrons from protons in ATIC. Adv. Space Res. **42**, 431–436 (2008), doi:10.1016/j.asr.2007.06.012.

Chang, J., J. H. Adams, Jr., H. S. Ahn, G. L. Bashindzhagyan, M. Christl, O. Ganel, T. G. Guzik, J. Isbert, K. C. Kim, E. N. Kuznetsov, M. I. Panasyuk, A. D. Panov, W. K. H. Schmidt, E. S. Seo, N. V. Sokolskaya, J. W. Watts, J. P. Wefel, J. Wu, and

V. I. Zatsepin: An excess of cosmic ray electrons at energies of 300-800 GeV. Nature **456**, 362–365 (2008), doi:10.1038/nature07477.

Chen, L. J., N. Bessho, B. Lefebvre, H. Vaith, A. Fazakerley, A. Bhattacharjee, P. A. Puhl-Quinn, A. Runov, Y. Khotyaintsev, A. Vaivads, E. Georgescu, and R. Torbert: Evidence of an extended electron current sheet and its neighboring magnetic island during magnetotail reconnection. J. Geophys. Res. **113**, A12213 (2008), doi:10.1029/2008JA013385.

Chen, L.-J., A. Bhattacharjee, P. A. Puhl-Quinn, H. Yang, N. Bessho, S. Imada, S. Mühlbachler, P. W. Daly, B. Lefebvre, Y. Khotyaintsev, A. Vaivads, A. Fazakerley, and E. Georgescu: Observation of energetic electrons within magnetic islands. Nature Physics **4**, 19–23 (2008), doi:10.1038/nphys777.

Chen, P. F., D. E. Innes, and S. K. Solanki: SOHO/SUMER observations of prominence oscillation before eruption. Astron. & Astrophys. **484**, 487–493 (2008), doi:10.1051/0004-6361:200809544.

Cheung, M. C. M., M. Schüssler, T. D. Tarbell, and A. M. Title: Solar Surface Emerging Flux Regions: A Comparative Study of Radiative MHD Modeling and Hinode SOT Observations. Astrophys. J. **687**, 1373–1387 (2008), doi:10.1086/591245.

Christensen, U. R.: A sheet-metal geodynamo. Nature **454**, 1058–1059 (2008), doi:10.1038/4541058a.

Christensen, U. R. and J. Wicht: Models of magnetic field generation in partly stable planetary cores: Applications to Mercury and Saturn. Icarus **196**, 16–34 (2008), doi:10.1016/j.icarus.2008.02.013.

Coates, A. J., R. A. Frahm, D. R. Linder, D. O. Kataria, Y. Soobiah, G. Collinson, J. R. Sharber, J. D. Winningham, S. J. Jeffers, S. Barabash, J. A. Sauvaud, R. Lundin, M. Holmstrom, Y. Futaana, M. Yamauchi, A. Grigoriev, H. Andersson, H. Gunell, A. Fedorov, J. J. Thocaven, T. L. Zhang, W. Baumjohann, E. Kallio, H. Koskinen, J. U. Kozyra, M. W. Liemohn, Y. Ma, A. Galli, P. Wurz, P. Bochsler, D. Brain, E. C. Roelof, P. Brandt, N. Krupp, J. Woch, M. Fraenz, E. Dubinin, S. McKenna-Lawlor, S. Orsini, R. Cerulli-Irelli, A. Mura, A. Milillo, M. Maggi, C. C. Curtis, B. R. Sandel, K. C. Hsieh, K. Szego, A. Asamura, and M. Grande: Ionospheric photoelectrons at Venus: Initial observations by ASPERA-4. Planet. Space Sci. **56**, 802–806 (2008), doi:10.1016/j.pss.2007.12.008.

Curdt, W., H. Tian, B. N. Dwivedi, and E. Marsch: The redshifted network contrast of transition region emission. Astron. & Astrophys. **491**, L13 (2008), doi:10.1051/0004-6361:200810490.

Curdt, W., H. Tian, L. Teriaca, U. Schühle, and P. Lemaire: The Ly-α profile and center-to-limb variation of the quiet Sun. Astron. & Astrophys. **492**, L9 (2008), doi:10.1051/0004-6361:200810868.

Curdt, W., K. Wilhelm, L. Feng, and S. Kamio: Multi-spacecraft observations of polar coronal plumes. Astron. & Astrophys. **481**, L61–L64 (2008), doi:10.1051/0004-6361:20079065.

Czechowski, A., M. Hilchenbach, K. C. Hsieh, S. Grzedzielski, and J. Kota: Imaging the heliosheath using HSTOF energetic neutral atoms and Voyager 1 ion data. Astron. & Astrophys. **487**, 329–335 (2008), doi:10.1051/0004-6361:200809555.

Daly, P. W., S. J. Schwartz, and B. Lefebvre: Plasma kinetics. In: Multi-Spacecraft Analysis Methods Revisited, eds. G. Paschmman and P. W. Daly, no. SR-008 in ISSI Scientific Report, pp. 75–80, International Space Science Institute, Bern (2008).

Dammasch, I. E., W. Curdt, B. N. Dwivedi, and S. Parenti: The redshifted footpoints of coronal loops. Ann. Geophys. **26**, 2955–2959 (2008).

Dandouras, I., P. Garnier, D. G. Mitchell, E. C. Roelof, P. C. Brandt, N. Krupp, and S. M. Krimigis: Titans exosphere and its interaction with Saturns magnetosphere. Phil. Trans. R. Soc. A **367**, 743–752 (2008), doi:10.1098/rsta.2008.0249.

Danilovic, S., A. Gandorfer, A. Lagg, M. Schüssler, S. K. Solanki, A. Vögler, Y. Katsukawa, and S. Tsuneta: The intensity contrast of solar granulation: comparing Hinode SP results with MHD simulations. Astron. & Astrophys. **484**, L17 (2008), doi:10.1051/0004-6361:200809857.

Daum, P., J. A. Wild, T. Penz, E. E. Woodfield, H. Rème, A. N. Fazakerley, P. W. Daly, and M. Lester: Global MHD simulation of flux transfer events at the high-latitude magnetopause observed by the Cluster spacecraft and the SuperDARN radar system. J. Geophys. Res. **113**, A07S22 (2008), doi:10.1029/2007JA012749.

De Groof, A., D. Berghmans, B. Nicula, J.-P. Halain, J.-M. Defise, T. Thibert, and U. Schühle: CMOS-APS detectors for solar physics: lessons learned during the SWAP pre-flight calibration. Solar Phys. **249**, 147–163 (2008), doi:10.1007/s11207-008-9175-y.

Desai, M. I., G. M. Mason, R. Müller-Mellin, A. Korth, U. Mall, J. R. Dwyer, and T. T. von Rosenvinge: The spatial distribution of upstream ion events from the

Earth's bow shock measured by ACE, Wind, and STEREO. J. Geophys. Res. **113**, A08103 (2008), doi:10.1029/2007JA012909.

Dikarev, V., O. Preuss, S. K. Solanki, H. Krüger, and A. Krivov: Understanding the WMAP results: low-order multipoles and dust in the vicinity of the solar system. Earth, Moon and Planets **102**, 555–561 (2008), doi:10.1007/s11038-007-9172-4.

Doressoundiram, A., H. Boehnhardt, S. C. Tegler, and C. Trujillo: Color Properties and Trends of the Transneptunian Objects. In: The Solar System Beyond Neptune, eds. M. A. Barucci, H. Boehnhardt, D. P. Cruikshank, and A. Morbidelli, The University of Arizona Space Science Series, The University of Arizona Press, Tucson, USA (2008).

Drolshagen, G., V. Dikarev, M. Landgraf, H. Krag, and W. Kuiper: Comparison of meteoroid flux models for near earth space. Earth, Moon and Planets **102**, 191–197 (2008), doi:10.1007/s11038-007-9199-6.

Dubinin, E., G. Chanteur, M. Fraenz, R. Modolo, J. Woch, E. Roussos, S. Barabash, R. Lundin, and J. D. Winningham: Asymmetry of plasma fluxes at Mars. ASPERA-3 observations and hybrid simulations. Planet. Space Sci. **56**, 832–835 (2008), doi:10.1016/j.pss.2007.12.006.

Dubinin, E., G. Chanteur, M. Fraenz, and J. Woch: Field-aligned currents and parallel electric field potential drops at Mars. Scaling from the Earth aurora. Planet. Space Sci. **56**, 868–872 (2008), doi:10.1016/j.pss.2007.01.019.

Dubinin, E., M. Fraenz, J. Woch, E. Roussos, J. D. Winningham, R. Frahm, A. Coates, F. Leblanc, R. Lundin, and S. Barabash: Access of solar wind electrons into the Martian magnetosphere. Ann. Geophys. **26**, 3511–3524 (2008).

Dubinin, E., M. Fraenz, J. Woch, D. Winningham, R. Frahm, R. Lundin, and S. Barabash: Suprathermal electron fluxes on the nightside of Mars: ASPERA-3 observations. Planet. Space Sci. **56**, 846–851 (2008), doi:10.1016/j.pss.2007.12.010.

Dubinin, E., R. Modolo, M. Fraenz, J. Woch, G. Chanteur, F. Duru, F. Akalin, D. Gurnett, R. Lundin, S. Barabash, J. D. Winningham, R. Frahm, J. J. Plaut, and G. Picardi: Plasma environment of Mars as observed by simultaneous MEX-ASPERA-3 and MEX-MARSIS observations. J. Geophys. Res. **113**, A10217 (2008), doi:10.1029/2008JA013355.

Dubinin, E., R. Modolo, M. Fraenz, J. Woch, F. Duru, F. Akalin, D. Gurnett, R. Lundin, S. Barabash, J. J. Plaut, and G. Picardi: Structure and dynamics of the solar wind/ionosphere interface on Mars. MEX-ASPERA-3 and MEX-MARSIS observations. Geophys. Res. Lett. **35**, L11103 (2008), doi:10.1029/2008GL033730.

Echer, E., A. Korth, Q. G. Zong, M. Fränz, W. D. Gonzalez, F. L. Guarnieri, S. Y. Fu, and H. Reme: Cluster observations of O+ escape in the magnetotail due to shock compression effects during the initial phase of the magnetic storm on 17 August 2001. J. Geophys. Res. **113**, A05209 (2008), doi:10.1029/2007JA012624.

El Maarry, M. R., O. Gasnault, M. J. Toplis, D. Baratoux, J. M. Dohm, H. E. Newsom, W. V. Boynton, and S. Karunatillake: Gamma-ray constraints on the chemical composition of the martian surface in the Tharsis region: A signature of partial melting of the mantle? Journal of Volcanology and Geothermal Research **185**, 116–122 (2008), doi:10.1016/j.jvolgeores.2008.11.027.

Encrenaz, T., T. Fouchet, R. Melchiorri, P. Drossart, B. Gondet, Y. Langevin, J.-P. Bibring, F. Forget, L. Maltagliati, D. Titov, and V. Formisano: A study of the Martian water vapor over Hellas using OMEGA and PFS aboard Mars Express. Astron. & Astrophys. **484**, 547–553 (2008), doi:10.1051/0004-6361:20079288.

Escoubet, C. P., J. Berchem, J. M. Bosqued, K. J. Trattner, M. G. G. T. Taylor, F. Pitout, H. Laakso, A. Masson, M. Dunlop, I. Dandouras, H. Rème, A. N. Fazakerley, and P. Daly: Effect of a northward turning of the interplanetary magnetic field on cusp precipitation as observed by Cluster. J. Geophys. Res. **113**, A07S13 (2008), doi:10.1029/2007JA012771.

Facskó, G., K. Kecskeméty, G. Erdős, M. Tátrallyay, P. W. Daly, and I. Dandouras: A statistical study of hot flow anomalies using Cluster data. Adv. Space Res. **41**, 1286–1291 (2008), doi:10.1016/j.asr.2008.02.005.

Farrugia, C. J., F. T. Gratton, V. K. Jordanova, H. Matsui, S. Mühlbachler, R. B. Torbert, K. W. Ogilvie, and H. J. Singer: Tenuous solar winds: Insights on solar wind-magneto sphere interactions. J. Atmos. Solar-Terr. Phys. **70**, 371–376 (2008), doi:10.1016/j.jastp.2007.08.032.

*Fedorov, A., C. Ferrier, J. A. Sauvaud, S. Barabash, T. L. Zhang, C. Mazelle, R. Lundin, H. Gunell, H. Andersson, K. Brinkfeldt, Y. Futaana, A. Grigoriev, M. Holmstrom, M. Yamauchi, K. Asamura, W. Baumjohann, H. Lammer, A. J. Coates, D. O. Kataria, D. R. Linder, C. C. Curtis, K. C. Hsieh, *B. R. Sandel, J.-J. Thocaven, M. Grande, H. Koskinen, E. Kallio, T. Sales, W. Schmidt, P. Riihela, J. Kozyra, N. Krupp, J. Woch, J. Luhmann, S. McKenna-Lawlor, S. Orsini, R. Cerulli-Irelli, A. Mura, A. Milillo, M. Maggi, E. Roelof, P. Brandt, C. T. Russell, K. Szego, J. D. Winningham, R. A. Frahm, J. Scherrer, J. R. Sharber, P. Wurz, and P. Bochsler*: Comparative analysis of Venus and Mars magnetotails. Planet. Space Sci. **56**, 812–817 (2008), doi:10.1016/j.pss.2007.12.012.

Foing, B. H., G. D. Racca, J. L. Josset, D. Koschny, D. Frew, M. Almeida, J. Zender, D. Heather, S. Peters, A. Marini, L. Stagnaro, S. Beauvivre, M. Grande, B. Kellett, J. Huovelin, A. Nathues, U. Mall, P. Ehrenfreund, P. McCannon, and The SMART 1 Sci & Technol Working Team: SMART-1 highlights and relevant studies on early bombardment and geological processes on rocky planets. Physica Scripta **T130**, 014026 (2008), doi:10.1088/0031-8949/2008/T130/014026.

Förster, M., S. Haaland, G. Paschmann, J. M. Quinn, R. B. Torbert, H. Vaith, and C. A. Kletzing: High-latitude plasma convection during Northward IMF as derived from in-situ magnetospheric Cluster EDI measurements. Ann. Geophys. **26**, 2685–2700 (2008).

Futaana, Y., S. Barabash, M. Yamauchi, S. McKenna-Lawlor, R. Lundin, J. G. Luhmann, D. Brain, E. Carlsson, J.-A. Sauvaud, J. D. Winningham, R. A. Frahm, P. Wurz, M. Holmström, H. Gunell, E. Kallio, W. Baumjohann, H. Lammer, J. R. Sharber, K. C. Hsieh, H. Andersson, A. Grigoriev, K. Brinkfeldt, H. Nilsson, K. Asamura, T. L. Zhang, A. J. Coates, D. R. Linder, D. O. Kataria, C. C. Curtis, B. R. Sandel, A. Fedorov, C. Mazelle, J.-J. Thocaven, M. Grande, H. E. J. Koskinen, T. Sales, W. Schmidt, P. Riihela, J. Kozyra, N. Krupp, J. Woch, M. Fränz, E. Dubinin, S. Orsini, R. Cerulli-Irelli, A. Mura, A. Milillo, M. Maggi, E. Roelof, P. Brandt, K. Szego, J. Scherrer, and P. Bochsler: Mars Express and Venus Express multi-point observations of geoeffective solar flare events in December 2006. Planet. Space Sci. **56**, 873–880 (2008), doi:10.1016/j.pss.2007.10.014.

Galli, A., P. Wurz, P. Bochsler, S. Barabash, A. Grigoriev, Y. Futaana, M. Holmstrom, H. Gunell, H. Andersson, R. Lundin, M. Yamauchi, K. Brinkfeldt, M. Fraenz, N. Krupp, J. Woch, W. Baumjohann, H. Lammer, T. L. Zhang, K. Asamura, A. J. Coates, D. R. Linder, D. O. Kataria, C. C. Curtis, K. C. Hsieh, B. R. Sandel, J. A. Sauvaud, A. Fedorov, C. Mazelle, J. J. Thocaven, M. Grande, E. Kallio, T. Sales, W. Schmidt, P. Riihela, H. Koskinen, J. Kozyra, J. Luhmann, S. McKenna-Lawlor, S. Orsini, R. Cerulli-Irelli, A. Mura, A. Milillo, M. Maggi, E. Roelof, P. Brandt, C. T. Russell, K. Szego, D. Winningham, R. Frahm, J. Scherrer, and J. R. Sharber: First observation of energetic neutral atoms in the Venus environment. Planet. Space Sci. **56**, 807–811 (2008), doi:10.1016/j.pss.2007.12.011.

Garnier, P., I. Dandouras, D. Toublanc, E. C. Roelof, P. C. Brandt, D. G. Mitchell, S. M. Krimigis, N. Krupp, D. C. Hamilton, O. Dutuit, and J.-E. Wahlund: The lower exosphere of Titan: Energetic neutral atoms absorption and imaging. J. Geophys. Res. **113**, A10216 (2008), doi:10.1029/2008JA013029.

Georgescu, E., H. U. Auster, T. Takada, J. Gloag, H. Eichelberger, K.-H. Fornaçon, P. Brown, C. Carr, and T. L. Zhang: Modified gradiometer technique applied to Double Star (TC-1). Adv. Space Res. **41**, 1579–1584 (2008), doi:10.1016/j.asr.2008.01.014.

Gizon, L., P. Cally, and J. Leibacher: Preface. Solar Phys. **251**, 1–2 (2008), doi:10.1007/s11207-008-9248-y.

Gizon, L. and M. Rempel: Observation and modeling of the solar-cycle variation of the meridional flow. Solar Phys. **251**, 241–250 (2008), doi:10.1007/s11207-008-9162-3.

Gizon, L. and M. Roth: Abstract book. J. Phys.: Conf. Ser. **118**, 011003 (2008), doi:10.1088/1742-6596/118/1/011003.

Gizon, L. and M. Roth: Foreword. J. Phys.: Conf. Ser. **118**, 011001 (2008), doi:10.1088/1742-6596/118/1/011001.

Gizon, L. and M. Roth: Interactive conference picture. J. Phys.: Conf. Ser. **118**, 011002 (2008), doi:10.1088/1742-6596/118/1/011002.

Gizon, L. and M. Roth (eds.): Proceedings of the Second HELAS International Conference: Helioseismology, Asteroseismology and MHD Connections, *Journal of Physics: Conf. Ser.*, vol. 118 (2008).

Gizon, L. and M. Roth: Special session. J. Phys.: Conf. Ser. **118**, 011004 (2008), doi:10.1088/1742-6596/118/1/011004.

Glassmeier, K.-H., H.-U. Auster, D. Constantinescu, K.-H. Fornaçon, Y. Narita, F. Plaschke, V. Angelopoulos, E. Georgescu, W. Baumjohann, R. Nakamura, W. Magnes, C. W. Carlson, S. Frey, J. P. McFadden, T. Phan, I. Mann, I. J. Rae, and J. Vogt: Magnetospheric quasi-static response to the dynamic magnetosheath: A THEMIS case study.

Geophys. Res. Lett. **35**, L17S01 (2008), doi:10.1029/2008GL033469.

Goetz, W., K. Leer, H. P. Gunnlaugsson, P. Bartlett, B. Basso, J. Bell, P. Bertelsen, C. S. Binau, P. C. Chu, S. Gorevan, M. F. Hansen, S. F. Hviid, K. M. Kinch, G. Klingelhoefer, A. Kusack, M. B. Madsen, D. W. Ming, R. V. Morris, E. Mumm, T. Myrick, M. Olsen, S. W. Squyres, J. Wilson, and A. Yen: Search for magnetic minerals in Martian rocks: Overview of the Rock Abrasion Tool (RAT) magnet investigation on Spirit and Opportunity. J. Geophys. Res. **113**, E05S90 (2008), doi:10.1029/2006JE002819.

Graham, J. P., D. D. Holm, P. D. Mininni, and A. Pouquet: Three regularization models of the Navier-Stokes equations. Phys. Fluids **20**, 035107 (2008), doi:10.1063/1.2880275.

Gunasingha, R. M., A. R. Fazely, J. H. Adams, Jr., H. S. Ahn, G. L. Bashindzhagyan, K. E. Batkov, J. Chang, M. Christl, O. Ganel, T. G. Guzik, J. Isbert, K. C. Kim, E. N. Kouznetsov, M. I. Panasyuk, A. D. Panov, W. K. H. Schmidt, E. S. Seo, N. V. Sokolskaya, J. W. Watts, J. P. Wefel, J. Wu, V. I. Zatsepin, and Z. W. Lin: A detailed FLUKA-2005 monte-carlo simulation for the ATIC detector. Adv. Space Res. **42**, 417–423 (2008), doi:10.1016/j.asr.2007.03.079.

Gunell, H., U. V. Amerstorfer, H. Nilsson, C. Grima, M. Koepke, M. Fränz, J. D. Winningham, R. A. Frahm, J.-A. Sauvaud, A. Fedorov, N. V. Erkaev, H. K. Biernat, M. Holmström, R. Lundin, and S. Barabash: Shear driven waves in the induced magnetosphere of Mars. Plasma Phys. Control. Fusion **50**, 074018 (2008), doi:10.1088/0741-3335/50/7/074018.

Guo, Y., M. D. Ding, T. Wiegelmann, and H. Li: 3D Magnetic Field Configuration of the 2006 December 13 Flare Extrapolated with the Optimization Method. Astrophys. J. **679**, 1629–1635 (2008), doi:10.1086/587684.

Gurnett, D. A., R. L. Huff, D. D. Morgan, A. M. Persoon, T. F. Averkamp, D. L. Kirchner, F. Duru, F. Akalin, A. J. Kopf, E. Nielsen, A. Safaeinili, J. J. Plaut, and G. Picardi: An overview of radar soundings of the martian ionosphere from the Mars Express spacecraft. Adv. Space Res. **41**, 1335–1346 (2008), doi:10.1016/j.asr.2007.01.062.

Guzik, T. G., J. H. Adams, Jr., H. S. Ahn, G. L. Bashindzhagyan, K. E. Batkov, J. Chang, M. Christl, A. R. Fazely, O. Ganel, R. M. Gunasingha, J. Isbert, K. C. Kim, E. N. Kouznetsov, M. I. Panasyuk, A. D. Panov, W. K. H. Schmidt, E. S. Seo, N. V. Sokolskaya, J. W. Watts, J. P. Wefel, J. Wu, and V. I. Zatsepin: Enhancing the ATIC charge resolution. Adv. Space Res. **42**, 424–430 (2008), doi:10.1016/j.asr.2007.08.017.

Haaland, S., G. Paschmann, M. Förster, J. Quinn, R. Torbert, H. Vaith, P. Puhl-Quinn, and C. Kletzing: Plasma convection in the magnetotail lobes: statistical results from Cluster EDI measurements. Ann. Geophys. **26**, 2371–2382 (2008).

Hamilton, D. P. and H. Krüger: The sculpting of Jupiter's gossamer rings by its shadow. Nature **453**, 72–75 (2008), doi:10.1038/nature06886.

Hanasoge, S. M., A. C. Birch, T. J. Bogdan, and L. Gizon: f-mode interactions with thin flux tubes: the scattering matrix. Astrophys. J. **680**, 774–780 (2008), doi:10.1086/587455.

Hartogh, P. and P. J. Espy (eds.): MIPAS (Michelson Interferometer for Passive Atmosphere Sounding): Potential of the experiment, data processing and validation of results. ACP- Special Issue, European Geosciences Union (2008).

He, J.-S., C.-Y. Tu, and E. Marsch: Modeling of Solar Wind in the Coronal Funnel with Mass and Energy Supplied at 5 Mm. Solar Phys. **250**, 147–158 (2008), doi:10.1007/s11207-008-9214-8.

Heber, B., M. Bird, H. Krüger, N. Krupp, J. Woch, and M. Gaida: Über die Sonnenpole, Rückblick auf die Mission ULYSSES - Over the Poles of the SUN, Looking back at the Ulysses Mission. Countdown, Aktuelles aus der DLR Raumfahrtagentur/Topics from DLR Space Agency **4/08**, 20–27 (2008).

Hecht, M. H., J. Marshall, W. T. Pike, U. Staufer, D. Blaney, D. Braendlin, S. Gautsch, W. Goetz, H.-R. Hidber, H. U. Keller, W. J. Markiewicz, A. Mazer, T. P. Meloy, J. M. Morookian, C. Mogensen, D. Parrat, P. Smith, H. Sykulska, R. J. Tanner, R. O. Reynolds, A. Tonin, S. Vijendran, M. Weilert, and P. M. Woida: Microscopy capabilities of the Microscopy, Electrochemistry, and Conductivity Analyzer. J. Geophys. Res. **113**, E00A22 (2008), doi:10.1029/2008JE003077.

Heyminck, S., R. Güsten, P. Hartogh, H.-W. Hübers, J. Stutzki, and U. U. Graf: GREAT: a first light instrument for SOFIA. In: Ground-based and Airborne Instrumentation for Astronomy II, eds. I. S. McLean and M. M. Casali, *Proceedings of the SPIE*, vol. 7014, SPIE–The International Society for Optical Engineering. (2008), doi:10.1117/12.788273.

Hirzberger, J., L. Gizon, S. K. Solanki, and T. L. Duvall, Jr.: Structure and evolution of supergranulation from local helioseismology. Solar Phys. **251**, 417–437 (2008), doi:10.1007/s11207-008-9206-8.

Holzwarth, V.: Flow instabilities of magnetic flux tubes III. Toroidal flux tubes. Astron. & Astrophys. **485**, 351–361 (2008), doi:10.1051/0004-6361:200809564.

Hori, K. and S. Yoshida: Non-local memory effects of the electromotive force by fluid motion with helicity and two-dimensional periodicity. Geophys. Astrophys. Fluid Dynamics **102**, 601–632 (2008), doi:10.1080/03091920802260466.

Howard, R. A., J. D. Moses, A. Vourlidas, J. S. Newmark, D. G. Socker, S. P. Plunkett, C. M. Korendyke, J. W. Cook, A. Hurley, J. M. Davila, W. T. Thompson, O. C. St Cyr, E. Mentzell, K. Mehalick, J. R. Lemen, J. P. Wuelser, D. W. Duncan, T. D. Tarbell, C. J. Wolfson, A. Moore, R. A. Harrison, N. R. Waltham, J. Lang, C. J. Davis, C. J. Eyles, H. Mapson-Menard, G. M. Simnett, J. P. Halain, J. M. Defise, E. Mazy, P. Rochus, R. Mercier, M. F. Ravet, F. Delmotte, F. Auchere, J. P. Delaboudiniere, V. Bothmer, W. Deutsch, D. Wang, N. Rich, S. Cooper, V. Stephens, G. Maahs, R. Baugh, D. McMullin, and T. Carter: Sun Earth Connection Coronal and Heliospheric Investigation (SECCHI). Space Sci. Rev. **136**, 67–115 (2008), doi:10.1007/s11214-008-9341-4.

Hu, Q., B. Dasgupta, D. P. Choudhary, and J. Büchner: A practical approach to coronal magnetic field extrapolation based on the principle of minimum dissipation rate. Astrophys. J. **679**, 848–853 (2008), doi:10.1086/587639.

Inada, A., M. Garcia-Comas, F. Altieri, K. Gwinner, F. Poulet, G. Bellucci, H. U. Keller, W. J. Markiewicz, M. I. Richardson, N. Hoekzema, G. Neukum, and J.-P. Bibring: Dust haze in Valles Marineris observed by HRSC and OMEGA on board Mars Express. J. Geophys. Res. **113**, E02004 (2008), doi:10.1029/2007JE002893.

Innes, D. E.: SUMER-Hinode Observations of Microflares: Excitation of Molecular Hydrogen. In: First Results From Hinode, eds. S. A. Matthews, J. M. Davis, and L. K. Harra, ASP Conference Series, p. 174, Astronomical Society of the Pacific, San Francisco (2008).

Innes, D. E.: SUMER-Hinode observations of microflares: excitation of molecular hydrogen. Astron. & Astrophys. **481**, L41–L44 (2008), doi:10.1051/0004-6361:20078977.

Innes, D. E., R. Attie, H. Hara, and M. S. Madjarska: EIS/ Hinode Observations of Doppler Flow Seen through the 40-Arcsec Wide-Slit. Solar Phys. **252**, 283–292 (2008), doi:10.1007/s11207-008-9271-z.

Isbert, J., J. H. Adams, Jr., H. S. Ahn, G. L. Bashindzhagyan, K. E. Batkov, M. Christl, A. R. Fazely, O. Ganel, R. M. Gunashingha, T. G. Guzik, J. Chang, K. C. Kim, E. N. Kouznetsov, Z. W. Lin, M. I. Panasyuk, A. D. Panov, W. K. H. Schmidt, E. S. Seo, N. V. Sokolskaya, J. W. Watts, J. P. Wefel, J. Wu, and V. I. Zatsepin: Temperature effects in the ATIC BGO calorimeter. Adv. Space Res. **42**, 437–441 (2008), doi:10.1016/j.asr.2007.12.014.

Jackiewicz, J., L. Gizon, and A. C. Birch: High-resolution mapping of flows in the solar interior: Fully consistent OLA inversion of helioseismic travel times. Solar Phys. **251**, 381–415 (2008), doi:10.1007/s11207-008-9158-z.

Jackiewicz, J., L. Gizon, and A. C. Birch: The forward and inverse problems in time-distance helioseismology. J. Phys.: Conf. Ser. **118**, 012033 (2008), doi:10.1088/1742-6596/118/1/012033.

Jackman, C. M., C. S. Arridge, N. Krupp, E. J. Bunce, D. G. Mitchell, H. J. McAndrews, M. K. Dougherty, C. T. Russell, N. Achilleos, G. H. Jones, and A. J. Coates: A multi-instrument view of tail reconnection at Saturn. J. Geophys. Res. **113**, A11213 (2008), doi:10.1029/2008JA013592.

Jaumann, R., T. Spohn, H. Hiesinger, E. K. Jessberger, G. Neukum, J. Oberst, J. Helbert, U. Christensen, H. U. Keller, U. Mall, P. Hartogh, K.-H. Glassmeier, H.-U. Auster, A. Moreira, M. Werner, M. Pätzold, H. Palme, R. Wimmer-Schweingruber, M. Mandea, F. Flechtner, V. Lesur, B. Häusler, R. Srama, S. Kempf, A. Hördt, K. Eichentopf, E. Hauber, H. Hoffmann, U. Köhler, E. Kührt, H. Michaelis, M. Pauer, F. Sohl, T. Denk, and S. van Gasselt: German Lunar explaration orbiter (LEO): providing a globally covered, highly resolved, integrated, geological, geochemical, and geophysical data base of the moon. In: 39th Lunar and Planetary Science Conference, (Lunar and Planetary Science XXXIX), held March 10-14, 2008 in League City, Texas., 2008LPI....39.1253J, pp. 1253–1254 (2008).

Jing, J., T. Wiegelmann, Y. Suematsu, M. Kubo, and H. Wang: Changes of Magnetic Structure in Three Dimensions Associated with the X3.4 Flare of 2006 December 13. Astrophys. J. **676**, L81–L84 (2008), doi:10.1086/587058.

Jones, G. H., E. Roussos, N. Krupp, U. Beckmann, A. J. Coates, F. Crary, I. Dandouras, V. Dikarev, M. K. Dougherty, P. Garnier, C. J. Hansen, A. R. Hendrix, G. B. Hospodarsky, R. E. Johnson, S. Kempf, K. K. Khurana, S. M. Krimigis, *H. Krüger, W. S. Kurth, A. Lagg, H. J. McAndrews, D. G. Mitchell, C. Paranicas, F. Postberg, C. T. Russell, J. Saur, M. Seiß, F. Spahn, R. Srama, D. F. Strobel, R. Tokar, J.-E. Wahlund, R. J. Wilson, J. Woch, and D. Young*: The Dust Halo of Saturns Largest Icy Moon, Rhea. Science **319**, 1380–1384 (2008), doi:10.1126/science.1151524.

Kallio, E., T. L. Zhang, S. Barabash, R. Jarvinen, I. Sillanpaa, P. Janhunen, A. Fedorov, J.-A. Sauvaud, C. Mazelle, J.-J. Thocaven, H. Gunell, H. Andersson, A. Grigoriev, K. Brinkfeldt, Y. Futaana, M. Holmstrom, R. Lundin, M. Yamauchi, K. Asamura, W. Baumjohann, H. Lammer, A. J. Coates, D. R. Linder, D. O. Kataria, C. C. Curtis, K. C. Hsieh, B. R. Sandel, M. Grande, H. E. J. Koskinen, T. Sales, W. Schmidt, P. Riihela, J. Kozyra, N. Krupp, J. Woch, J. G. Luhmann, S. McKenna-Lawlor, S. Orsini, R. Cerulli-Irelli, A. Mura, A. Milillo, M. Maggi, E. Roelof, P. Brandt, C. T. Russell, K. Szego, J. D. Winningham, R. A. Frahm, J. R. Scherrer, J. R. Sharber, P. Wurz, and P. Bochsler: The Venusian induced magnetosphere: A case study of plasma and magnetic field measurements on the Venus Express mission. Planet. Space Sci. **56**, 796–801 (2008), doi:10.1016/j.pss.2007.09.011.

Kamio, S., H. Hara, T. Watanabe, and W. Curdt: Velocity Structure of Bright Points in a Coronal Hole. In: First Results from Hinode, eds. S. A. Matthews, J. M. Davis, and L. K. Harra, *Astron. Soc. Pacific Conf. Ser.*, vol. 397, p. 35 (2008).

Keller, H. U., W. Goetz, H. Hartwig, S. F. Hviid, R. Kramm, W. J. Markiewicz, R. Reynolds, C. Shinohara, P. Smith, R. Tanner, P. Woida, R. Woida, B. J. Bos, and M. T. Lemmon: Phoenix Robotic Arm Camera. J. Geophys. Res. **113**, E00A17 (2008), doi:10.1029/2007JE003044.

Keller, H.-U., B. Grieger, M. Küppers, S. E. Schröder, Y. V. Skorov, and M. G. Tomasko: The properties of Titan's surface at the Huygens landing site from DISR observations. Planet. Space Sci. **56**, 728–752 (2008), doi:10.1016/j.pss.2007.11.020.

Kleint, L., A. Feller, and M. Bianda: Combination of two Fabry-Perot etalons and a grating spectrograph for imaging polarimetry of the Sun. In: Ground-based and Airborne Instrumentation for Astronomy II, eds. I. S. McLean and M. M. Casali, *Proceedings of the SPIE*, vol. 7014, pp. 701 414–701 414–9 (2008), doi:10.1117/12.787923.

Koch, Ch., U. R. Christensen, and R. Kallenbach: Simultaneous Determination of global Topography, tidal Love number and libration amplitude of Mercury by Laser altimetry. Planet. Space Sci. **56**, 1226–1237 (2008), doi:10.1016/j.pss.2008.04.002.

Korokhin, V. V., V. G. Kaydash, Y. G. Shkuratov, D. G. Stankevich, and U. Mall: Prognosis of TiO2 abundance in lunar soil using a non-linear analysis of Clementine and LSCC data. Planet. Space Sci. **56**, 1063–1078 (2008), doi:10.1016/j.pss.2008.02.001.

Kossacki, K. J. and W. J. Markiewicz: Small-scale trench in the north polar region of Mars: Evolution of surface frost and ground ice concentration. Icarus **199**, 75–85 (2008), doi:10.1016/j.icarus.2008.09.003.

Krivova, N. A. and S. K. Solanki: Models of solar irradiance variations: current status. J. Astrophys. Astron. **29**, 151–158 (2008), doi:10.1007/s12036-008-0018-x.

Kronberg, E., J. Woch, N. Krupp, and A. Lagg: Mass release process in the Jovian magnetosphere: Statistics on particle burst parameters. J. Geophys. Res. **113**, A10202 (2008), doi:10.1029/2008JA013332.

Kronberg, E. A., J. Woch, N. Krupp, A. Lagg, P. W. Daly, and A. Korth: Comparison of periodic substorms at Jupiter and Earth. J. Geophys. Res. **113**, A04212 (2008), doi:10.1029/2007JA012880.

Krüger, H.: Deep Impact - Einschlag auf einem Kometen. Astronomie und Raumfahrt im Unterricht **103**, 13–16 (2008).

Krüger, H. and E. Grün: Interstellar Dust Inside and Outside the Heliosphere. Space Sci. Rev. **143**, 347–356 (2008), doi:10.1007/s11214-008-9431-3.

Kudela, K., R. Bučík, and P. Bobík: On transmissivity of low energy cosmic rays in disturbed magnetosphere. Adv. Space Res. **42**, 1300–1306 (2008), doi:10.1016/j.asr.2007.09.033.

Kuroda, T., A. Medvedev, P. Hartogh, and M. Takahashi: Semiannual oscillations in the atmosphere of Mars. Geophys. Res. Lett. **35**, L23202 (2008), doi:10.1029/2008GL036061.

Kuznetsov, S. N., B. Yu. Yushkov, K. Kudela, and R. Bučík: CORONAS-F measurements of high-energy solar proton spectra. In: Proc. of the 30th International Cosmic Ray Conference, eds. R. Caballero, J. C. D'Olivo, G. Medina-Tanco, L. Nellen, F. A. Sánchez, and J. F. Valdés-Galicia, vol. 1 (SH), pp. 71–74, Universidad Nacional Autónoma de México, Mexico City, Mexico (2008).

Lee, K. W., J. Büchner, and N. Elkina: Collisionless transport of energetic electrons in the solar corona at current-free double layers. Astron. & Astrophys. **478**, 889–895 (2008), doi:10.1051/0004-6361:20078419.

Leer, K., P. Bertelsen, C. S. Binau, L. D. Olsen, L. Drube, T. V. Falkenberg, M. P. Haspang, M. B. Madsen, M. Olsen, H. Sykulska, S. Vijendran, W. T. Pike, U. Staufer, D. Parrat, M. Lemmon, M. H. Hecht, C. T. Mogensen, M. A. Gross, W. Goetz, J. Marshall, D. Britt, P. Smith, C. Shinohara, P. Woida, R. Woida, R. Tanner, R. Reynolds, and A. Shaw: Magnetic properties experiments and the Surface Stereo Imager calibration target onboard the Mars Phoenix 2007 Lander: Design, calibration, and science goals. J. Geophys. Res. **113**, E00A16 (2008), doi:10.1029/2007JE003014.

Loukitcheva, M. A., S. K. Solanki, and S. White: ALMA as the ideal probe of the solar chromosphere. Astrophys. Space Sci. **313**, 197–200 (2008), doi:10.1007/s10509-007-9626-1.

Luhmann, J. G., D. W. Curtis, P. Schroeder, J. McCauley, R. P. Lin, D. E. Larson, S. D. Bale, J.-A. Sauvaud, C. Aoustin, R. A. Mewaldt, A. C. Cummings, E. C. Stone, A. J. Davis, W. R. Cook, B. Kecman, M. E. Wiedenbeck, T. von Rosenvinge, M. H. Acuna, L. S. Reichenthal, S. Shuman, K. A. Wortman, D. V. Reames, R. Mueller-Mellin, H. Kunow, G. M. Mason, P. Walpole, A. Korth, T. R. Sanderson, C. T. Russell, and J. T. Gosling: STEREO IMPACT Investigation Goals, Measurements, and Data Products Overview. Space Sci. Rev. **136**, 117–184 (2008), doi:10.1007/s11214-007-9170-x.

Lundin, R., S. Barabash, M. Holmstrom, H. Nilsson, M. Yamauchi, M. Fraenz, and E. Dubinin: A comet-like escape of ionospheric plasma from Mars. Geophys. Res. Lett. **35**, L18203 (2008), doi:10.1029/2008GL034811.

Madjarska, M. S. and J. G. Doyle: Small-scale flows in SUMER and TRACE high-cadence co-observations. Astron. & Astrophys. **482**, 273–278 (2008), doi:10.1051/0004-6361:200809349.

Mailyan, B., C. Munteanu, and S. Haaland: What is the best method to calculate the solar wind propagation delay? Ann. Geophys. **26**, 2383–2394 (2008).

Maltagliati, L., D. V. Titov, T. Encrenaz, R. Melchiorri, F. Forget, M. Garcia-Comas, H. U. Keller, Y. Langevin, and J.-P. Bibring: Observations of atmospheric water vapor above the Tharsis volcanoes on Mars with the OMEGA/MEx imaging spectrometer. Icarus **194**, 53–64 (2008), doi:10.1016/j.icarus.2007.09.027.

Marsch, E.: An effective Dirac equation for a binary of two fermions. J. Phys. A: Math. Theor. **41**, 185301 (2008), doi:10.1088/1751-8113/41/18/185301.

Marsch, E., H. Tian, J. Sun, W. Curdt, and T. Wiegelmann: Plasma flows guided by strong magnetic fields in the solar corona. Astrophys. J. **685**, 1262–1269 (2008).

Martinecz, C., M. Fränz, J. Woch, N. Krupp, E. Roussos, E. Dubinin, U. Motschmann, S. Barabash, R. Lundin, M. Holmström, H. Andersson, M. Yamauchi, A. Grigoriev, Y. Futaana, K. Brinkfeldt, H. Gunell, R. A. Frahm, J. D. Winningham, J. R. Sharber, J. Scherrer, A. J. Coates, D. R. Linder, D. O. Kataria, E. Kallio, T. Sales, W. Schmidt, P. Riihela, H. E. J. Koskinen, J. U. Kozyra, J. Luhmann, C. T. Russell, E. C. Roelof, P. Brandt, C. C. Curtis, K. C. Hsieh, B. R. Sandel, M. Grande, J.-A. Sauvaud, A. Fedorov, J.-J. Thocaven, C. Mazelle, S. McKenna-Lawler, S. Orsini, R. Cerulli-Irelli, M. Maggi, A. Mura, A. Milillo, P. Wurz, A. Galli, P. Bochsler, K. Asamura, K. Szego, W. Baumjohann, T. L. Zhang, and H. Lammer: Location of the bow shock and ion composition boundaries at Venus-initial determinations from Venus Express ASPERA-4. Planet. Space Sci. **56**, 780–784 (2008), doi:10.1016/j.pss.2007.07.007.

Martinez Pillet, V., A. G. Kosovichev, J. T. Mariska, T. J. Bogdan, M. Asplund, G. Cauzzi, J. Christensen-Dalsgaard, L. E. Cram, W. Gan, L. Gizon, P. Heinzel, M. G. Rovira, and P. Venkatakrishnan: Commission 12: Solar Radiation and Structure: Reports on Astronomy 2006-2009. In: Transactions IAU 4, Issue 27A, ed. K. van der Hucht, pp. 104–123, Cambridge University Press, Cambridge (2008), doi:10.1017/S1743921308025362.

Mason, G. M., A. Korth, P. H. Walpole, M. I. Desai, T. T. Von Rosenvinge, and S. A. Shuman: The Suprathermal Ion Telescope (SIT) for the IMPACT/SEP Investigation. Space Sci. Rev. **136**, 257–284 (2008), doi:10.1007/s11214-006-9087-9.

Mecheri, R. and E. Marsch: Drift instabilities in the solar corona within the multi-fluid description. Astron. & Astrophys. **481**, 853–860 (2008), doi:10.1051/0004-6361:20079221.

Mendis, D. A. and W. I. Axford: Revisiting Iapetus following recent Cassini observations. J. Geophys. Res. **113**, A11217 (2008), doi:10.1029/2008JA013532.

Metcalf, T., M. Derosa, C. Schrijver, G. Barnes, A. van Ballegooijen, T. Wiegelmann, M. Wheatland, G. Valori, and J. McTiernan: Nonlinear Force-Free Modeling of Coronal Magnetic Fields. II. Modeling a Filament Arcade and Simulated Chromospheric and Photospheric Vector Fields. Solar Phys. **247**, 269–299 (2008), doi:10.1007/s11207-007-9110-7.

Mierla, M., J. Davila, W. Thompson, B. Inhester, N. Srivastava, M. Kramar, O. C. St. Cyr, G. Stenborg, and R. A. Howard: A Quick Method for Estimating the Propagation Direction of Coronal Mass Ejections Using STEREO-COR1 Images. Solar Phys. **252**, 385–396 (2008), doi:10.1007/s11207-008-9267-8.

Mierla, M., R. Schwenn, L. Teriaca, G. Stenborg, and B. Podlipnik: Analysis of the Fe X and Fe XIV line width in the solar corona using LASCO-C1 spectral data. Astron. & Astrophys. **480**, 509 – 514 (2008), doi:10.1051/0004-6361:20078329.

Morgan, D. D., D. A. Gurnett, D. L. Kirchner, J. L. Fox, E. Nielsen, and J. J. Plaut: Variation of the Martian electron density from Mars Express radar soundings. J. Geophys. Res. **113**, A09303 (2008), doi:10.1029/2008JA013313.

Mothe-Diniz, T., J. M. Carvano, S. J. Bus, R. Duffard, and T. H. Burbine: Mineralogical analysis of the Eos family from near-infrared spectra. Icarus **195**, 277–294 (2008), doi:10.1016/j.icarus.2007.12.005.

Mura, A., S. Orsini, A. Milillo, E. Kallio, A. Galli, S. Barabash, P. Wurz, A. Grigoriev, Y. Futaana, H. Andersson, R. Lundin, M. Yamauchi, M. Fraenz, N. Krupp, J. Woch, K. Asamura, A. J. Coates, C. C. Curtis, K. C. Hsieh, B. R. Sandel, A. Fedorov, M. Grande, H. Koskinen, J. U. Kozyra, J. G. Luhmann, S. McKenna-Lawlor, R. Cerulli-Irelli, R. D'Amicis, M. Maggi, S. Massetti, E. C. Roelof, P. C. Brandt, D. J. Winningham, R. A. Frahm, and J. R. Sharber: ENA detection in the dayside of Mars: ASPERA-3 NPD statistical study. Planet. Space Sci. **56**, 840–845 (2008), doi:10.1016/j.pss.2007.12.013.

Nilsson, H., M. Waara, O. Marghitu, M. Yamauchi, R. Lundin, H. Reme, J.-A. Sauvaud, I. Dandouras, E. Lucek, L. M. Kistler, B. Klecker, C. W. Carlson, M. B. Bavassano-Cattaneo, and A. Korth: An assessment of the role of the centrifugal acceleration mechanism in high altitude polar cap oxygen ion outflow. Ann. Geophys. **26**, 145–157 (2008).

Nilsson, H., M. Waara, O. Marghitu, M. Yamauchi, R. Lundin, H. Rème, J.-A. Sauvaud, I. Dandouras, E. Lucek, L. M. Kistler, B. Klecker, C. W. Carlson, M. B. Bavassano-Cattaneo, and A. Korth: Transients in oxygen outflow above the polar cap as observed by the Cluster spacecraft. Ann. Geophys. **26**, 3365–3373 (2008).

Nuño, B. S.-A., N. B. Gonzalez, J. B. Rodriguez, F. Kneer, and K. G. Puschmann: Fast events and waves in an active region of the Sun observed in H alpha with high spatial resolution. Astron. & Astrophys. **486**, 577–587 (2008), doi:10.1051/0004-6361:20079231.

Nutto, C., M. Roth, Y. Zhugzhda, J. Bruls, and O. von der Lühe: Calculation of spectral darkening and visibility functions for solar oscillations. Solar Phys. **251**, 179–188 (2008), doi:10.1007/s11207-008-9132-9.

Ogrodowczyk, R., K. Murawski, and S. K. Solanki: Slow magnetoacoustic standing waves in a curved solar coronal slab. Astron. & Astrophys. **495**, 313–318 (2008), doi:10.1051/0004-6361:200809377.

Ohtsuki, S., N. Iwagami, H. Sagawa, M. Ueno, Y. Kasaba, T. Imamura, K. Yanagisawa, and E. Nishihara: Distributions of the Venus 1.27-μm O_2 airglow and rotational temperature. Planet. Space Sci. **56**, 1391–1398 (2008), doi:10.1016/j.pss.2008.05.013.

Paganini, L., P. Hartogh, and L. Reindl: An improved method for nonlinearity detection applied to a new 400-MHz bandwidth Chirp transform spectrometer. Transactions on Systems, Signals & Devices **3**, 1–15 (2008).

Panov, A. D., V. I. Zatsepin, N. V. Sokolskaya, J. H. Adams, Jr., H. S. Ahn, G. L. Bashindzhagyan, J. W. Watts, J. P. Wefel, J. Wu, O. Ganel, T. G. Guzik, R. M. Gunashingha, J. Isbert, K. C. Kim, M. Christl, E. N. Kouznetsov, M. I. Panasyuk, E. S. Seo, J. Chang, W. K. H. Schmidt, and A. R. Fazely: Measuring the deposited energy by the scintillation calorimeter in the ATIC experiment. Instrum. Exp. Tech. **51**, 665–681 (2008), doi:10.1134/S0020441208050047.

Panov, E. V., J. Büchner, M. Fränz, A. Korth, S. P. Savin, H. Rème, and K.-H. Fornaçon: High-latitude Earths magnetopause outside the cusp: Cluster observations. J. Geophys. Res. **113**, A01220 (2008), doi:10.1029/2006JA012123.

Paranicas, C., D. G. Mitchell, S. M. Krimigis, D. C. Hamilton, E. Roussos, N. Krupp, G. H. Jones, R. E. Johnson, J. F. Cooper, and T. P. Armstrong: Sources and losses of energetic protons in Saturn's magnetosphere. Icarus **197**, 519–525 (2008), doi:10.1016/j.icarus.2008.05.011.

Paschmann, G. and P. W. Daly (eds.): Multi-Spacecraft Analysis Methods Revisited. No. SR-008 in ISSI Scientific Report, International Space Science Institute, Bern (2008).

Pérez-Suárez, D., R. C. Maclean, J. G. Doyle, and M. S. Madjarska: The structure and dynamics of a bright point as seen with Hinode, SoHO and TRACE. Astron. & Astrophys. **492**, 575–583 (2008), doi:10.1051/0004-6361:200809507.

Petit, P., B. Dintrans, M. Aurière, C. Catala, J.-F. Donati, R. Fares, T. Gastine, F. Lignières, J. Morin, F. Paletou, J. Ramirez, S. K. Solanki, and S. Théado: Magnetic geometries of Sun-like stars: impact of rotation. In: SF2A-2008: Proc. Annual Meeting French Society of Astronomy and Astrophysics, eds. F. C. C. Charbonnel and R. Samadi, Société Française d'Astronomie et d'Astrophysique (2008).

Petit, P., B. Dintrans, J.-F. Donati, S. K. Solanki, M. Aurière, F. Lignières, J. Morin, F. Paletou, J. Ramirez, C. Catala, and R. Fares: Toroidal vs. poloidal magnetic fields in Sun-like stars: a rotation threshold. Mon. Not. Roy. Astron. Soc. **388**, 80–88 (2008), doi:10.1111/j.1365-2966.2008.13411.x.

Petrova, E. V., V. P. Tishkovets, and K. Jockers: Rebuttal to comment on Modeling of opposition effects with ensembles of clusters: Interplay of various scattering mechanisms by Elena V. Petrova, Victor P. Tishkovets, Klaus Jockers, 2007 [Icarus 188, 233245]. Icarus **194**, 853–856 (2008), doi:10.1016/j.icarus.2007.10.018.

Piccialli, A., D. V. Titov, D. Grassi, I. Khatuntsev, P. Drossart, G. Piccioni, and A. Migliorini: Cyclostrophic winds from the Visible and Infrared Thermal Imaging Spectrometer temperature sounding: A preliminary analysis. J. Geophys. Res. **113**, E00B11 (2008), doi:10.1029/2008JE003127.

Protopapa, S., H. Boehnhardt, T. M. Herbst, D. P. Cruikshank, W. M. Grundy, F. Merlin, and C. B. Olkin: Surface characterization of Pluto and Charon by L and M band spectra. Astron. & Astrophys. **490**, 365–375 (2008), doi:10.1051/00046361.

Radioti, A., J.-C. Gerard, D. Grodent, B. Bonfond, N. Krupp, and J. Woch: Discontinuity in Jupiters main auroral oval. J. Geophys. Res. **113**, A01215 (2008), doi:10.1029/2007JA012610.

Raouafi, N.-E., G. J. D. Petrie, A. A. Norton, C. J. Henney, and S. K. Solanki: Evidence for polar jets as precursors of polar plume formation. Astrophys. J. **682**, L137–L140 (2008), doi:10.1086/591125.

Rengel, M., P. Hartogh, and C. Jarchow: HHSMT observations of the Venusian mesospheric temperature, winds, and CO abundance around the MESSENGER flyby. Planet. Space Sci. **56**, 1688–1695 (2008), doi:10.1016/j.pss.2008.07.014.

Rengel, M., P. Hartogh, and C. Jarchow: Mesospheric vertical thermal structure and winds on Venus from HHSMT CO spectral-line observations. Planet. Space Sci. **56**, 1368–1384 (2008), doi:10.1016/j.pss.2008.07.004.

Retinò, A., R. Nakamura, A. Vaivads, Y. Khotyaintsev, T. Hayakawa, K. Tanaka, S. Kasahara, M. Fujimoto, I. Shinohara, J. P. Eastwood, M. Andre, W. Baumjohann, P. W. Daly, E. A. Kronberg, and N. Cornilleau-Wehrlin: Cluster observations of energetic electrons and electromagnetic fields within a reconnecting thin current sheet in the Earth's magnetotail. J. Geophys. Res. **113**, A12215 (2008), doi:10.1029/2008JA013511.

Riethmüller, T. L., S. K. Solanki, and A. Lagg: Stratification of sunspot umbral dots from inversion of Stokes profiles recorded by Hinode. Astrophys. J. **678**, L157–L160 (2008).

Riethmüller, T. L., S. K. Solanki, V. Zakharov, and A. Gandorfer: Brightness, distribution, and evolution of sunspot umbral dots. Astron. & Astrophys. **492**, 233–243 (2008), doi:10.1051/0004-6361:200810701.

Rodriguez, L., N. Krupp, J. Woch, and M. Fränz: Elemental Abundances of Energetic Particles within Magnetic Clouds Detected by Ulysses. Astrophys. J. **673**, 621–628 (2008), doi:10.1086/523999.

Roth, M. and M. Stix: Meridional circulation and global solar oscillations. Solar Phys. **251**, 77–89 (2008), doi:10.1007/s11207-008-9232-6.

Rothkaehl, H., K. Kudela, R. Bučík, and O. Grigoryan: The response of ionospheric plasma to the physical processes in the radiation belt regions. In: COST 724 final report: Developing the scientific basis for monitoring, modeling and predicting Space Weather, pp. 227–235, OPOCE (2008).

Roussos, E., M. Fraenz, E. Dubinin, C. Martinecz, J. Woch, U. Motschmann, J. D. Winningham, R. Frahm, S. Barabash, and R. Lundin: Energetic electron asymmetries at Mars: ASPERA-3 observations. Planet. Space Sci. **56**, 836–839 (2008), doi:10.1016/j.pss.2007.12.009.

Roussos, E., G. H. Jones, N. Krupp, C. Paranicas, D. G. Mitchell, S. M. Krimigis, J. Woch, A. Lagg, and K. Khurana: Energetic electron signatures of Saturn's smaller moons: Evidence of an arc of material at Methone. Icarus **193**, 455–464 (2008), doi:10.1016/j.icarus.2007.03.034.

Roussos, E., N. Krupp, T. P. Armstrong, C. Paranicas, D. G. Mitchell, S. M. Krimigis, G. H. Jones, K. Dialynas, N. Sergis, and D. C. Hamilton: Discovery of a transient radiation belt at Saturn. Geophys. Res. Lett. **35**, L22106 (2008), doi:10.1029/2008GL035767.

Roussos, E., J. Müller, S. Simon, A. Bösswetter, U. Motschmann, N. Krupp, M. Fränz, J. Woch, K. K. Khurana, and M. K. Dougherty: Plasma and fields in the wake of Rhea: 3-D hybrid simulation and comparison with Cassini data. Ann. Geophys. **26**, 619–637 (2008).

Ruan, P., A. Korth, E. Marsch, B. Inhester, S. Solanki, T. Wiegelmann, Q.-G. Zong, R. Bučík, and K.-H. Fornaçon: Multiple-spacecraft study of an extended magnetic structure in the solar wind. J. Geophys. Res. **114**, A02 108 (2008), doi:10.1029/2008JA013769.

Ruan, P., T. Wiegelmann, B. Inhester, T. Neukirch, S. K. Solanki, and L. Feng: A first step in reconstructing the solar corona self-consistently with a magneto-hydrostatic model during solar activity minimum. Astron. & Astrophys. **481**, 827–834 (2008), doi:10.1051/0004-6361:20078834.

Rucker, H. O., M. Panchenko, K. C. Hansen, U. Taubenschuss, M. Y. Boudjada, W. S. Kurth, M. K. Dougherty, J. T. Steinberg, P. Zarka, P. H. M. Galopeau, D. J. McComas, and C. H. Barrow: Saturn kilometric radiation as a monitor for the solar wind? Adv. Space Res. **42**, 40–47 (2008), doi:10.1016/j.asr.2008.02.008.

Santos, J. C., J. Büchner, M. S. Madjarska, and M. V. Alves: On the relation between DC current locations and an EUV bright point: A case study. Astron. & Astrophys. **490**, 345–352 (2008), doi:10.1051/0004-6361:200809975.

Santos, J. C., J. Büchner, and H. Zhang: Inferring plasma flow velocities from photospheric vector magnetic field observations for the investigation of flare onsets. Adv. Space Res. **42**, 812–821 (2008), doi:10.1016/j.asr.2007.05.082.

Savin, S., E. Arnata, L. Zelenyi, V. Budaev, G. Consolini, R. Treumann, E. Lucek, J. Safrankova, Z. Nemecek, Y. Khotyaintsev, M. Andre, J. Büchner, H. Alleyne, P. Song, J. Blecki, J. L. Rauch, S. Romanov, S. Klimov, and A. Skalskya: High energy jets in the Earth's magnetosheath: Implications for plasma dynamics and anomalous transport. JETP Lett. **87**, 593–599 (2008), doi:10.1134/S0021364008110015.

Schad, A., M. Roth, B. Schelter, O. von der Lühe, and J. Timmer: Cross-spectral analysis of solar oscillation time series. J. Phys: Conf. Ser. **118**, 012091 (2008), doi:10.1088/1742-6596/118/1/012091.

Schippers, P., M. Blanc, N. Andre, I. Dandouras, G. R. Lewis, L. K. Gilbert, A. M. Persoon, N. Krupp, D. A. Gurnett, A. J. Coates, S. M. Krimigis, D. T. Young, and M. K. Dougherty: Multi-instrument analysis of electron populations in Saturn's magnetosphere. J. Geophys. Res. **113**, A07208 (2008), doi:10.1029/2008JA013098.

Schrijver, C. J., M. L. Derosa, G. Barnes, B. Lites, T. Tarbell, J. McTiernan, G. Valori, T. Wiegelmann, M. S. Wheatland, T. Amari, P. Demoulin, M. Fuhrmann, K. Kusano, S. Regnier, and J. K. Thalmann: Nonlinear force-free field modeling of a solar active region around the time of a major flare and coronal mass ejection. Astrophys. J. **675**, 1637–1644 (2008), doi:10.1086/527413.

Schröder, S. E. and H.-U. Keller: The reflectance spectrum of Titan's surface at the Huygens landing site determined by the Descent Imager/Spectral Radiometer. Planet. Space Sci. **56**, 753–769 (2008), doi:10.1016/j.pss.2007.10.011.

Schunker, H., D. C. Braun, C. Lindsey, and P. S. Cally: Physical properties of wave motion in inclined magnetic fields within sunspot penumbrae. Solar Phys. **251**, 341–359 (2008), doi:10.1007/s11207-008-9142-7.

Schunker, H. and L. Gizon: HELAS local helioseismology activities. Communications in Asteroseismology **156**, 93–105 (2008).

Schunker, H., L. Gizon, and M. Roth: HELAS: local helioseismology data website. J. Phys.: Conf. Ser. **118**, 012087 (2008), doi:10.1088/1742-6596/118/1/012087.

Schüssler, M. and A. Vögler: Strong horizontal photospheric magnetic field in a surface dynamo simulation. Astron. & Astrophys. **481**, L5–L8 (2008), doi:10.1051/0004-6361:20078998.

Sergeev, V., M. Kubyshkina, I. Alexeev, A. Fazakerley, C. Owen, W. Baumjohann, R. Nakamura, A. Runov, Z. Vörös, T. L. Zhang, V. Angelopoulos, J.-A. Sauvaud, P. Daly, J. B. Cao, and E. Lucek: Study of near-Earth reconnection events with Cluster and Double Star. J. Geophys. Res. **113**, A07S36 (2008), doi:10.1029/2007JA012902.

Skorov, Y. V., H. U. Keller, and A. V. Rodin: Optical properties of aerosols in Titan's atmosphere. Planet. Space Sci. **56**, 660–668 (2008), doi:10.1016/j.pss.2007.11.013.

Smith, P. H., L. Tamppari, R. E. Arvidson, D. Bass, D. Blaney, W. Boynton, A. Carswell, D. Catling, B. Clark, T. Duck, E. DeJong, D. Fisher, W. Goetz, P. Gunnlaugsson, M. Hecht, V. Hipkin, J. Hoffman, S. Hviid, H. U. Keller, S. Kournaves, C. F. Lange, M. Lemmon, M. Madsden, M. Malin, W. J. Markiewicz, J. Marshall, C. McKay, M. Mellon, D. Michelangeli, D. Ming, R. Morris, N. Renno, *W. T. Pike, U. Staufer, C. Stoker, P. Taylor, J. Whiteway, S. Young, and A. Zent*: Introduction to special section on the Phoenix Mission: Landing Site Characterization Experiments, Mission Overviews, and Expected Science. J. Geophys. Res. **113**, E00A18 (2008), doi:10.1029/2008JE003083.

Snekvik, K., R. Nakamura, N. Östgaard, S. Haaland, and A. Retinó: The Hall current system revealed as a statistical significant pattern during fast flows. Ann. Geophys. **26**, 3429–3437 (2008).

Solanki, S. K., T. Wenzler, and D. Schmitt: Moments of the latitudinal dependence of the sunspot cycle: A new diagnostic of dynamo models. Astron. & Astrophys. **483**, 623–632 (2008), doi:10.1051/0004-6361:20054282.

Sonnemann, G. R., P. Hartogh, M. Grygalashvyly, L. Song, and U. Berger: The quasi 5-day signal in the mesospheric water vapor concentration at high latitudes in 2003 — A comparison between observations at ALOMAR and calculations. J. Geophys. Res. **113**, D04101 (2008), doi:10.1029/2007JD008875.

Srama, R., T. Stephan, E. Grün, N. Pailer, A. Kearsley, A. Graps, R. Laufer, P. Ehrenfreund, N. Altobelli, K. Altwegg, S. Auer, J. Baggaley, M. J. Burchell, J. Carpenter, L. Lolangeli, F. Esposito, S. F. Green, H. Henkel, M. Horanyi, A. Jäckel, S. Kempf, N. McBride, G. Moragas-Klostermeyer, H. Krüger, P. Palumbo, A. Srowig, M. Trieloff, P. Tsou, Z. Sternovsky, O. Zeile, and H.-P. Röser: Sample return of interstellar matter (SARIM). Experimental Astronomy **23**, 303–328 (2008), doi:10.1007/s10686-008-9088-7.

Stahn, T. and L. Gizon: Fourier analysis of gapped time series: Improved estimates of solar and stellar oscillation parameters. Solar Phys. **251**, 31–52 (2008), doi:10.1007/s11207-008-9181-0.

Štverák, Š., P. Trávníček, M. Maksimovic, E. Marsch, A. N. Fazakerley, and E. E. Scime: Electron temperature anisotropy constraints in the solar wind. J. Geophys. Res. **113**, A03103 (2008), doi:10.1029/2007JA012733.

Subramanian, S., M. S. Madjarska, R. C. Maclean, J. G. Doyle, and D. Bewsher: Magnetic topology of blinkers. Astron. & Astrophys. **488**, 323–329 (2008), doi:10.1051/0004-6361:20079315.

Svedhem, H., O. Witasse, and D. Titov: Exploring Venus - Answering the big questions with Venus Express. ESA Bulletin **29**, 2–9 (2008).

Svenes, K. R., B. Lybekk, A. Pedersen, and S. Haaland: Cluster observations of near-Earth magnetospheric lobe plasma densities — a statistical study. Ann. Geophys. **26**, 2845–2852 (2008).

Tarcea, N., T. Frosch, P. Roesch, M. Hilchenbach, T. Stuffler, S. Hofer, H. Thiele, R. Hochleitner, and J. Popp: Raman Spectroscopy – A Powerful Tool for in situ Planetary Science. Space Sci. Rev. **135**, 281–292 (2008), doi:10.1007/s11214-007-9279-y.

Taylor, M. G. G. T., B. Lavraud, C. P. Escoubet, S. E. Milan, K. Nykyri, M. W. Dunlop, J. A. Davies, R. H. W. Friedel, H. Frey, Y. V. Bogdanova, A. Åsnes, H. Laakso, P. Trávnícek, A. Masson, H. Opgenoorth, C. Vallat, A. N. Fazakerley, A. D. Lahiff, C. J. Owen, F. Pitout, Z. Pu, C. Shen, Q. G. Zong, H. Rème, J. Scudder, and T. L. Zhang: The plasma sheet and boundary layers under northward IMF: A multi-point and multi-instrument perspective. Adv. Space Res. **41**, 1619–1629 (2008), doi:10.1016/j.asr.2007.10.013.

Teriaca, L., W. Curdt, and S. K. Solanki: SUMER observations of the inverse Evershed effect in the transition region above a sunspot. Astron. & Astrophys. **491**, L5–L8 (2008), doi:10.1051/0004-6361:200810209.

Teriaca, L., T. Wiegelmann, A. Lagg, S. K. Solanki, W. Curdt, T. Sekii, and the HINODE/SOT Team: Loop morphology and flows and their relation to the magnetic field. In: First Results from Hinode, eds. S. Matthews, J. M. Davis, and L. K. Harra, *Astron. Soc. Pacific Conf. Ser.*, vol. 397, p. 196 (2008).

Thalmann, J. K. and T. Wiegelmann: Evolution of the flaring active region NOAA 10540 as a sequence of nonlinear force-free field extrapolations. Astron. & Astrophys. **484**, 495–502 (2008), doi:10.1051/0004-6361:200809508.

Thalmann, J. K., T. Wiegelmann, and N.-E. Raouafi: First nonlinear force-free field extrapolations of SOLIS/VSM data. Astron. & Astrophys. **488**, L71–L74 (2008), doi:10.1051/0004-6361:200810235.

Thomas, N., C. Alexander, and H. U. Keller: Loss of the surface layers of comet nuclei. Space Sci. Rev. **138**, 165–177 (2008), doi:10.1007/s11214-008-9332-5.

Tian, H., W. Curdt, E. Marsch, and J. He: Cool and hot components of a coronal bright point. Astrophys. J. **681**, L121–L124 (2008), doi:10.1086/590410.

Tian, H., E. Marsch, C.-Y. Tu, L.-D. Xia, and J.-S. He: Sizes of transition-region structures in coronal holes and in the quiet Sun. Astron. & Astrophys. **482**, 267–272 (2008), doi:10.1051/0004-6361:20079235.

Tian, H., C.-Y. Tu, E. Marsch, J.-S. He, and G.-Q. Zhou: Signature of mass supply to quiet coronal loops. Astron. & Astrophys. **478**, 915–919 (2008), doi:10.1051/0004-6361:20078813.

Tian, H., C.-Y. Tu, L.-D. Xia, and J.-S. He: Radiance and Doppler shift distributions across the network of the quiet Sun. Astron. & Astrophys. **489**, 1297–1306 (2008), doi:10.1051/0004-6361:200809923.

Tian, H. and L.-D. Xia: Network oscillations at the boundary of an equatorial coronal hole. Astron. & Astrophys. **488**, 331–337 (2008), doi:10.1051/0004-6361:200810124.

Tian, H., L.-D. Xia, and S. Li: Long-period oscillations in solar coronal bright points. Astron. & Astrophys. **489**, 741–745 (2008), doi:10.1051/0004-6361:200810146.

Titov, D. V., F. W. Taylor, and H. Svedhem: Introduction to the special section on Venus Express: Results of the Nominal Mission. J. Geophys. Res. **113**, E00B19 (2008), doi:10.1029/2008JE003202.

Titov, D. V., F. W. Taylor, H. Svedhem, N. I. Ignatiev, W. J. Markiewicz, G. Piccioni, and P. Drossart: Atmospheric structure and dynamics as the cause of ultraviolet markings in the clouds of Venus. Nature **456**, 620–623 (2008), doi:10.1038/nature07466.

Tschimmel, A., N. I. Ignatiev, D. V. Titov, E. Lellouch, T. Fouchet, M. Giuranna, and V. Formisano: Investigation of water vapor on Mars with PFS/SW of Mars Express. Icarus **195**, 557–575 (2008), doi:10.1016/j.icarus.2008.01.018.

Tsurutani, B. T., O. P. Verkhoglyadova, A. J. Mannucci, A. Saito, T. Araki, K. Yumoto, T. Tsuda, M. A. Abdu, J. H. A. Sobral, W. D. Gonzalez, H. McCreadie, G. S. Lakhina, and V. M. Vasyliūnas: Prompt penetration electric fields (PPEFs) and their ionospheric effects during the great magnetic storm of 30–31 October 2003. J. Geophys. Res. **113**, A05311 (2008), doi:10.1029/2007JA012879.

Tu, C.-Y., R. Schwenn, E. Donovan, E. Marsch, J.-S. Wang, L.-D. Xia, Y.-W. Zhang, and the Kuafu working team: Space weather explorer – The KuaFu mission. Adv. Space Res. **41**, 190–209 (2008), doi:10.1016/j.asr.2007.04.049.

Tubiana, C., L. Barrera, M. Drahus, and H. Boehnhardt: Comet 67P/Churyumov-Gerasimenko at a large heliocentric distance. Astron. & Astrophys. **490**, 377–386 (2008), doi:10.1051/0004-6361:20078792.

Unruh, Y. C., N. A. Krivova, S. K. Solanki, J. W. Harder, and G. Kopp: Spectral irradiance variations: comparison between observations and the SATIRE model on solar rotation time scales. Astron. & Astrophys. **486**, 311–323 (2008), doi:10.1051/0004-6361:20078421.

Usoskin, I. G., K. Horiuchi, S. K. Solanki, G. A. Kovaltsov, and E. Bard: On the common solar signal in different cosmogenic isotope data sets. J. Geophys. Res. **114**, A03 112 (2008), doi:10.1029/2008JA013888.

Vasyliūnas, V. M.: Comparing Jupiter and Saturn: dimensionless input rates from plasma sources within the magnetosphere. Ann. Geophys. **26**, 1341–1343 (2008).

Vieira, L. E. A., L. Alves da Silva, and F. L. Guarnieri: Are changes of the geomagnetic field intensity related to changes of the tropical Pacific sea-level pressure during the last 50 years? J. Geophys. Res. **113**, A08226 (2008), doi:10.1029/2008JA013052.

Wang, H., J. Jing, C. Tan, T. Wiegelmann, and M. K. Kubo: Study of Magnetic Channel Structure in Active Region 10930. Astrophys. J. **687**, 658–667 (2008), doi:10.1086/592082.

Wang, T. J., S. K. Solanki, and M. Selwa: Identification of different types of kink modes in coronal loops: principles and application to TRACE results. Astron. & Astrophys. **489**, 1307–1317 (2008), doi:10.1051/0004-6361:200810230.

Wedemeyer-Böhm, S., A. Lagg, and Å. Nordlund: Coupling from the photosphere to the chromosphere and the corona. Space Sci. Rev. **144**, 317–350 (2008), doi:10.1007/s11214-008-9447-8.

Wicht, J., S. Stellmach, and H. Harder: From fundamental cartesian model to 3d simulations of field reversals. In: Geomagnetic field variations, eds. K.-H. Glassmeier, H. Soffel, and J. Negendank, Springer Monograph, Springer (2008).

Wiegelmann, T.: Nonlinear force-free modeling of the solar coronal magnetic field. J. Geophys. Res. **113**, A03S02 (2008), doi:10.1029/2007JA012432, review article.

Wiegelmann, T., J. K. Thalmann, C. J. Schrijver, M. L. DeRosa, and T. R. Metcalf: Can We Improve the Preprocessing of Photospheric Vector Magnetograms by the Inclusion of Chromospheric Observations? Solar Phys. **247**, 249–267 (2008), doi:10.1007/s11207-008-9130-y.

Wilhelm, K., W. Curdt, I. E. Dammasch, and D. M. Hassler: Comment on "Energy levels and spectral lines of NeVIII". Eur. Phys. J. D **47**, 325–325 (2008), doi:10.1140/epjd/e2008-00057-7.

Yigit, E., A. Aylward, and A. S. Medvedev: Parameterization of the effects of vertically propagating gravity waves for thermosphere general circulation models: sensitivity study. J. Geophys. Res. **113**, D19106 (2008), doi:10.1029/2008jd010135.

Zaatri, A., T. Corbard, M. Roth, I. G. González Hernández, and O. von der Lühe: Comparison of geometrical mapping for ring diagram analysis. J. Phys.: Conf. Ser. **118**, 012090 (2008), doi:10.1088/1742-6596/118/1/012090.

Zakharov, V., J. Hirzberger, T. L. Riethmüller, S. K. Solanki, and P. Kobel: Evidence of convective rolls in a sunspot penumbra. Astron. & Astrophys. **488**, L17–L20 (2008), doi:10.1051/0004-6361:200810266.

Zhang, H., Q.-G. Zong, T. A. Fritz, S. Y. Fu, S. Schaefer, K. H. Glassmeier, P. W. Daly, H. Rème, and A. Balogh: Cluster observations of collisionless Hall reconnection at high-latitude magnetopause. J. Geophys. Res. **113**, A03204 (2008), doi:10.1029/2007JA012769.

Zhang, Z., T. Hagfors, E. Nielsen, G. Picardi, A. Mesdea, and J. J. Plaut: Dielectric properties of the Martian south polar layered deposits: MARSIS data inversion using Bayesian inference and genetic algorithm. J. Geophys. Res. **113**, E05004 (2008), doi:10.1029/2007JE002941.

Zong, Q.-G., H. Zhang, T. A. Fritz, M. L. Goldstein, S. Wing, W. Keith, J. D. Winningham, R. Frahm, M. W. Dunlop, A. Korth, P. W. Daly, H. Rème, A. Balogh, and A. N. Fazakerley: Multiple cusps during an extended northward IMF period with a significant B-y component. J. Geophys. Res. **113**, A01210 (2008), doi:10.1029/2006JA012188.

Zong, Q.-G., H. Zhang, S. Y. Fu, Y. F. Wang, Z. Y. Pu, A. Korth, P. W. Daly, and T. A. Fritz: Ionospheric oxygen ions dominant bursty bulk flows: Cluster and Double Star observations. J. Geophys. Res. **113**, A07S23 (2008), doi:10.1029/2007JA012764.

Max-Planck-Institut für
Sonnensystemforschung
Max-Planck-Straße 2
37191 Katlenburg-Lindau
Tel: 05556-979-0
Fax: 05556-979-240
E-Mail: presseinfo@mps.mpg.de